Operations Research/Computer Science Interfaces Series

Carlos Ocampo-Martinez
Rudy R. Negenborn *Editors*

Transport of Water versus Transport over Water

Exploring the Dynamic Interplay of Transport and Water

Springer

Operations Research/Computer Science Interfaces Series

Volume 58

More information about this series at http://www.springer.com/series/6375

Carlos Ocampo-Martinez • Rudy R. Negenborn
Editors

Transport of Water versus Transport over Water

Exploring the Dynamic Interplay of Transport and Water

Springer

Editors
Carlos Ocampo-Martinez
Universitat Politècnica de Catalunya
Inst. de Robòtica i Informàtica
Industrial (CSIC-UPC)
Barcelona, Spain

Rudy R. Negenborn
Maritime and Transport Technology
Delft University of Technology
Delft, The Netherlands

ISSN 1387-666X
Operations Research/Computer Science Interfaces Series
ISBN 978-3-319-16132-7 ISBN 978-3-319-16133-4 (eBook)
DOI 10.1007/978-3-319-16133-4

Library of Congress Control Number: 2015938918

Springer Cham Heidelberg New York Dordrecht London

Printed on acid-free paper

Springer International Publishing AG Switzerland is part of Springer Science+Business Media (www.springer.com)

Preface

This book is the result of our efforts to bring together ideas and researchers from the fields of transport of water and transport over water. These two domains of research have fascinated us for many years, due to the high societal importance of water and transport systems in many parts of the world (e.g., low-lying countries, countries with dry climates, densely populated areas). The efficient function of such systems is therefore crucial. As we started to understand more and more from the different aspects of those domains, we realized that many of the problems encountered are in the literature addressed from rather mono-disciplinary perspectives, even though the underlying problems are in fact of a multi-disciplinary nature.

In summer 2013, we discussed the idea for bringing about this multi-disciplinary nature in a book. We hereby considered a systems and control perspective for structuring this: Considering a basic system that is meant for transport of water, with its sensors and actuators for measuring and controlling flows of waters, with on top of that a system for transport over water, with its own sensors and actuators specifically meant for arranging moves of cargo and people over water. We subsequently invited key researchers working on different aspects of transport of water and transport over water, in particular at the operational control level, and challenged them to present their research lines to the wider community and discuss how their research lines relate to this systems-and-control-based framework.

The result of this effort is this book, featuring no less than 22 chapters presenting the various angles considered, besides the introductory chapter, which gives more details on the ideas leading to this book and the questions asked to be answered by the researchers. In total 54 researchers contributed to this book, coming from 11 countries and representing 31 research groups.

We greatly acknowledge the efforts that the researchers and reviewers have made in preparing the contributions of this book. With timely responses to set deadlines and appropriate addressing of reviewers' comments, this book is available for further discussion and as source for further research early 2015.

We also thank the Transport Institute at Delft University of Technology for its support. The Transport Institute has as mission to bring together researchers and students from different backgrounds to identify the solutions that result in safer,

cleaner, and more efficient transport and improved accessibility. After reading the various chapters of this book, it will be clear that by supporting this book, the Transport Institute is indeed contributing to realization of this mission. Finally, we acknowledge the financial support from the Spanish project "ECOCIS: Economic Operation of Critical Infrastructure Systems" (reference DPI-2013-48243-C2-1-R) and "ShipDrive: A Novel Methodology for Integrated Modeling, Control, and Optimization of Hybrid Ship Systems" (project 13276) of the Dutch Technology Foundation STW.

Since this book is devoted to providing new insights into the world of management, monitoring and control of transport, and use of water, we hope that readers of diverse nature (engineers, researchers, students) will find inspiration in this book, and that it will bring to a new generation of researchers new ideas and lines of research to pursue in innovative and almost unexplored directions related to an integrated framework in which water and transport are the main components.

Feedback, comments, or ideas are of course welcome. Feel free to contact us via: http://transportoverwater.net/, where the complete information about this book is presented and where new developments regarding the topic of the book will be announced.

Barcelona, Spain — Carlos Ocampo-Martinez
Delft, The Netherlands — Rudy R. Negenborn
December 2014

Contents

Contributors

L. Alfonso UNESCO-IHE Institute for Water Education, Delft, The Netherlands

S. Axelsson Blekinge Institute of Technology, Karlskrona, Sweden

G. Belaud UMR G-Eau, SupAgro, Montpellier, France

R. Bittner Max Planck Institute for Dynamics of Complex Technical Systems, Magdeburg, Germany

J. Blesa Institut de Robòtica i Informàtica Industrial (CSIC-UPC), Technical University of Catalonia, Barcelona, Spain

M. Burger TBA, Delft, The Netherlands

C. Burt Irrigation Training and Research Center (ITRC), California Polytechnic State University, San Luis Obispo, California

B. Carlsson Blekinge Institute of Technology, Karlskrona, Sweden

G. Cembrano Advanced Control Systems Group, CSIC-UPC, and CETaqua, Water Technology Centre, Barcelona, Spain

K. Chuquet Voies Navigables de France, Lille, France

B. De Schutter Delft University of Technology, Delft, The Netherlands

D. Dorchies UMR G-EAU, Montpellier, France

C. Dorée Compagnie Nationale du Rhône, Département Ouvrages Hydroélectriques et Fluviaux, Lyon, France

M. Drijver CIG Maritime Technology, Groningen, The Netherlands

E. Duviella Institut Mines Telecom, Mines Douai, Doaui, France

J. Froese Jacobs University Bremen GmbH, Bremen, Germany

M. Godjevac Delft University of Technology, Delft, The Netherlands

J. Harmsen TNO, Delft, The Netherlands

V. Hassani Department of Marine Technology, Norwegian Marine Technology Research Institute (MARINTEK) and Centre for Autonomous Marine Operations and Systems (AMOS), Norwegian University of Science and Technology, Trondheim, Norway

R.G. Hekkenberg Delft University of Technology, Delft, The Netherlands

K. Horváth Institut Mines Telecom, Mines Douai, Doaui, France

N. Jean-Baptiste EDF—Direction Production Ingénierie Hydraulique, CIH—Département CC Lyon, Lyon, France

J.M. Lemos INESC-ID/IST/Universidade de Lisboa, Lisbon, Portugal

X. Litrico LyRE, R&D center of Lyonnaise des Eaux, Bordeaux, France

J. Maes University of Antwerp, Antwerp, Belgium

J.M. Maestre Department of Engineering of Systems and Automatics, University of Seville, Seville, Spain

P.-O. Malaterre UMR G-EAU, Montpellier, France

E. Mostert Department of Water Management, Delft University of Technology, Delft, The Netherlands

R.R. Negenborn Department of Maritime and Transport Technology, Delft University of Technology, Delft, The Netherlands

C. Ocampo-Martinez Institut de Robòtica i Informàtica Industrial (CSIC-UPC), Universitat Politècnica de Catalunya, Barcelona, Spain

E. Osekowska Blekinge Institute of Technology, Karlskrona, Sweden

A. Padilla Universidad de La Frontera, Temuco, Chile

A.M. Pascoal Laboratory of Robotics and Systems in Engineering and Science, Instituto Superior Técnico, University of Lisbon, Lisbon, Portugal

M. Petreczky Institut Mines Telecom, Mines Douai, Doaui, France

V. Puig Institut de Robòtica i Informàtica Industrial (CSIC-UPC), Universitat Politècnica de Catalunya, Barcelona, Spain

L. Rajaoarisoa Institut Mines Telecom, Mines Douai, Doaui, France

E. Revestido Herrero Universidad de Cantabria, Santander, Spain

A. Sadowska Delft Center for Systems and Control, Delft University of Technology, Delft, The Netherlands

I. Sampaio INESC-ID/IST/Universidade de Lisboa, Lisbon, Portugal

C.C. Sun Advanced Control Systems Group, Institut de Robòtica i Informàtica Industrial, CSIC-UPC, Barcelona, Spain

C. Sys University of Antwerp, Antwerp, Belgium

M. Tefferi UNESCO-IHE Institute for Water Education, Delft, The Netherlands

X. Tian Department of Water Management, Delft University of Technology, Delft, The Netherlands

M. Tomás-Rodríguez School of Engineering and Mathematical Sciences, City University London, London, UK

T. Vanelslander University of Antwerp, Antwerp, Belgium

E. van Hassel University of Antwerp, Antwerp, Belgium

A. van Loenen Deltares, Delft, The Netherlands

J. van Meijeren TNO, Delft, The Netherlands

P.-J. van Overloop Water Resources Management, Delft University of Technology, Delft, The Netherlands

A.W. Veenstra Eindhoven Technical University, Eindhoven, the Netherlands

F.J. Velasco Universidad de Cantabria, Santander, Spain

A. Verbraeck Delft University of Technology, Delft, The Netherlands

M. Xu Deltares, Delft, The Netherlands

J.I. Yuz Universidad Técnica Federico Santa María, Valparaiso, Chile

About the Editors

Carlos Ocampo-Martinez
Dr. Ocampo-Martinez received his electronic engineering degree and his M.Sc. degree in industrial automation from the National University of Colombia, Campus Manizales, in 2001 and 2003, respectively. In 2007, he received his Ph.D. degree in Control Engineering from the Technical University of Catalonia (Barcelona, Spain). After his Ph.D. studies, he was with the ARC Centre of Complex Dynamic Systems and Control (University of Newcastle, Australia) as a postdoctoral fellow and with the Spanish National Research Council (CSIC) at the Institut de Robòtica i Informàtica Industrial (CSIC-UPC) in Barcelona as a *Juan de la Cierva* research fellow. Since 2011, he is assistant professor in automatic control and model predictive control at the Technical University of Catalunya, Automatic Control Department (ESAII). Currently, he is Deputy Director of the Institut de Robòtica i Informàtica Industrial (CSIC-UPC), a Joint Research Center of UPC and CSIC.

He has over 90 peer-reviewed scientific publications in journals and prestigious conferences and congresses around the world. He is the author of the book *Model Predictive Control of Wastewater Systems* (Springer, 2011). Moreover, he is Senior Member of the IEEE Control Systems Society and vice-chair of the IFAC Technical Committee 8.3 on "Modelling and Control of Environmental Systems" since 2014. His main research interests are focused on constrained model predictive control, large-scale systems management (partitioning and non-centralized control), and industrial applications (mainly related to the key scopes of water and energy).

Rudy Negenborn
Dr. Negenborn obtained his M.Sc. degree in computer science/intelligent systems from Utrecht University, the Netherlands, in 1998. He received his Ph.D. degree in distributed control for transport systems from Delft University of Technology, the Netherlands, in 2007. Currently, he is assistant professor in automatic control & coordination of transport technology at the Section Transport Engineering & Logistics of Department Maritime & Transport Technology.

Dr. Negenborn's research interests include multi-agent systems, distributed control, model predictive control, simulation of large-scale transport systems,

and applications in (waterborne) networked transport systems. Current research lines he is leading are developing control theoretical approaches for efficient and sustainable operation of future container terminals, interterminal transport systems in port areas, and intermodal/synchromodal transport networks at national and European scale. He has over 100 peer-reviewed academic publications and is on the editorial board of the series on "Intelligent Systems, Control and Automation: Science and Engineering". Dr. Negenborn has co-organized several international conferences (including IEEE control conferences and maritime systems & logistics conferences) and was guest editor of a special journal issue on control of water systems. In addition, he is editor of the books *Intelligent Infrastructures*, *Distributed Model Predictive Control Made Easy*, and *Transport of Water versus Transport over Water*.

Chapter 1
Perspectives on Transport *of* Water *versus* Transport *over* Water

R.R. Negenborn and C. Ocampo-Martinez

Abstract This chapter discusses the characteristics of transport *of* water, transport *over* water, and their relations. A framework is proposed aimed at integration of operational control and management approaches related to both fields. Providing this framework enables discussing how solutions presented in the literature related to either one, or both fields, could in the future be merged into a unified control methodology. This methodology will enable balancing the transport of and over water objectives, while respecting operational constraints. The main features of the unified framework are discussed and an overview of the main points that need to be addressed in order to relate ongoing research to this framework is provided. A brief summary of the main topics investigated, problems and methodologies proposed of a survey of 22 research directions related to this framework is subsequently presented, including references to further, more detailed information. As such, this chapter serves as the introduction to the book "Transport of Water Versus Transport over Water: Exploring the Dynamic Interplay Between Transport and Water".

1.1 Introduction

Transport systems have been around for centuries for bringing goods and people from one place to another. Whereas initially transport took place mostly over roads, soon alternative modes of transport started being used: transport over water, transport over rail, and transport through the air. Nowadays, transport using these different modalities is common practice. The trend is to move towards intermodal

R.R. Negenborn (✉)
Department of Maritime and Transport Technology, Delft University of Technology, Delft, The Netherlands
e-mail: r.r.negenborn@tudelft.nl

C. Ocampo-Martinez
Institut de Robòtica i Informàtica Industrial (CSIC-UPC), Technical University of Catalonia, Barcelona, Spain
e-mail: cocampo@iri.upc.edu

C. Ocampo-Martinez, R.R. Negenborn (eds.), *Transport of Water versus Transport over Water*, Operations Research/Computer Science Interfaces Series 58,
DOI 10.1007/978-3-319-16133-4_1

transport, in which commodity does not use one type of modality, but multiple types of modalities, chosen in such a way that costs, time of arrival and sustainability objectives are balanced.

Water is a particular kind of good, the availability of which is crucial for the survival of humanity. Mankind has long been developing transport systems to effectively move water from sources (springs) to places where it is consumed or disposed (as drinking water, for feeding cattle, for use in agriculture, for hygienic purposes, or for ensuring safety). Originally relying on the transport systems created by nature herself (rivers), at some point people started creating their own canal systems and storage locations for water. Transport of water systems were born.

The book *Transport of Water versus Transport over Water* explores the dynamic interaction between two vibrant areas of research: transport systems on the one hand and water systems on the other. Water systems and transport systems are two classes of systems that have received over the years a significant amount of attention. Initially, the research in these areas focused on how to design such water and transport systems. More recently, a strong research line is emerging with a focus on how to obtain the best performance for a given water or transport system, after it has been designed.

Of particular interest is the consideration of transport systems that transport water directly (such as river, canal, irrigation systems, among others) and systems that use water to transport goods (typically using vessels). Transport over water of goods, using a system for transport of water, poses challenging design and control problems. The objectives and relevant constraints for the different types of systems can be different. It is the question how these can be considered simultaneously.

For both water and transport systems, at an operational level, approaches have been proposed in the literature aimed at optimizing system performance at a day to day, hour to hour, or even minute to minute time scale. Nevertheless, approaches that consider the interaction between these two types of systems are lacking. However, at such fast time scales, to interplay between the two types of systems cannot be ignored. It thus becomes important to explore to what extent transport and water systems interact at an operational time scale, and how the dynamics of both systems can be aligned in the best way possible using operational control techniques. Many approaches are possible.

In short, design and control of systems for transport of water (e.g., river systems, open canal networks) have gained increasing attention due to changes in local land-use, climate changes, and the need for energy savings. In order to take into account a variety of different objectives, methods for control of systems for transport of water are being proposed. Besides the safety objective typically considered, navigation is another objective that is often relevant for such systems. At the same time and for the same reasons, design and control of systems for transport over water (e.g., navigation systems, vessels, barges) are gaining increasing attention. As the volume of goods to be transported in the near future is expected to continue to rise, and as transport over water is the most environmentally friendly mode of transport, the need for innovative transport over water systems is apparent. In order to obtain the best performance, such transport systems should take into account the particular

dynamics and behavior of the underlying water transport systems, which facilitate that transport over water.

The remainder of this chapter is structured as follows. In Sect. 1.2 we propose the unified framework merging transport of water and transport over water. In Sect. 1.3, the objectives of this framework are outlined while Sect. 1.4 shows what aspects need to be considered in order to achieve these objectives and detail the framework. Next, in Sect. 1.5, a categorization of a range of different problems treated by research community to transport of and transport over water is provided, highlighting the most relevant methods to cope with them. Section 1.6 explains the way in which the approaches considered by the research community have been organized in the book "Transport of Water Versus Transport over Water". Finally, in Sect. 1.7 the main conclusions of the chapter are provided.

1.2 Unified Interdisciplinary Framework

The management of transport of water systems and transport over water systems involves important cross relations given by the interdependency of their dynamics when facing the fulfilment of overall control objectives. A simplified bottom-up framework that captures the main aspects for control of interacting water and transport systems can be seen as the composition of (see Fig. 1.1):

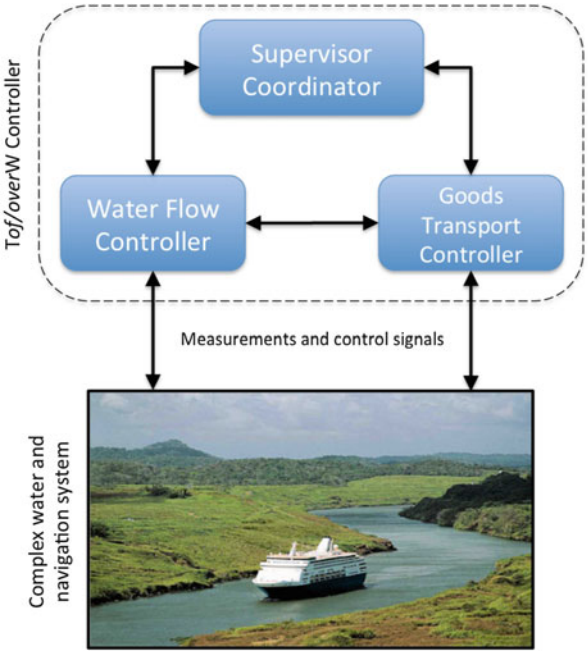

Fig. 1.1 Control framework and its interaction with the complex water system

1. The control of a first layer consisting of the water flowing through its infrastructure (without consideration for transport dynamics).
2. The control of a second layer consisting of a transport flow (without consideration for water dynamics).
3. The control of the interactions between both layers (water flow and transport flow).

On top of this, additional logistics-oriented layers can be considered, which determine from where to where transport flows are supposed to take place.

The considerations on the design of such a unifying framework is lacking in the literature. In fact, bridging the gap between both worlds could give rise to management policies that improve each system separately while optimizing further the performance of the overall complex and mixed infrastructure. The complexity in achieving the development of such a unifying framework lies in the truly interdisciplinary nature of the aspects needed to be considered. Expertise is amongst others required from the domains of mechanical engineering, civil engineering, hydrodynamics, automatic control, computer science, operations research, system identification, computer science, transport engineering, maritime systems, and ship design.

1.3 Overall Objectives of the Framework

This framework aims at stimulating discussion between researchers working on state of the art approaches for transport of water on the one hand and researchers working on state of the art approaches for transport over water on the other hand. As such, it aims at bringing together the different domains of expertise required to develop the unifying framework. Besides this, the main contribution of the framework as a whole is to present novel perspectives ultimately leading to the management of the envisioned unified management framework taking the recent advances form both worlds as a baseline. The framework:

- is devoted to become a reference for control-oriented engineers who manage water systems with either or both purposes in mind (transport of water, transport of goods over water);
- aims at promoting the topics of transport and water control;
- highlights the possible twofold nature of water projects, where water either acts as primary object of study or as a means.

1.4 Pieces of the Framework Puzzle

In order to achieve the objectives set out, a large number of research groups has been invited to prepare a chapter addressing in which way they work on transport of water, transport over water, and the interaction between these two domains.

This has resulted in the chapters with a common structure, addressing the following aspects:

1. Introduction of the research in either transport of water, transport over water, or the combination, including exposition of relevant theoretical and application-based contributions.
2. Description and discussion of the specific case study or case studies, including overall description and presentation of main results and insights obtained.
3. Views on the nature of the unified framework, addressing questions such as:
   - How does the presented research take into account transport of water?
   - How does the presented research take into account transport over water?
   - What would be the benefit of the presented approach within a combined framework?
4. Proposal of working directions that deserve future research attention either on the presented and discussed approach or on the rising research coming from the unified network.
5. Concluding remarks regarding findings obtained so far.

When surveying the range of contributions presented in the literature, the different aspects of transport of and transport over water that have been considered so far and that need to be considered in the future become clear. This will aid researchers in their pursuit for developing methods that are better suited for providing an efficient operation of both types of systems.

1.5 Summarizing the Outcomes

In total, we have surveyed 22 main research lines on transport of water, transport over water, and their interplay. The book "Transport of Water Versus Transport over Water" contains the details of each of these research lines, presented by the key researchers developing those. Many of these lines address specific problem with a focus either more on the transport of water domain or more on the transport over water domain. Some of the lines focus more explicitly on a problem directly related to both domains. When surveying the research lines, it becomes clear that the following are the main problems being addressed:

- **Problems with a focus on transport of water**
  - Improving **water quality**; removing algae for efficient water transport; effectively transporting sediment through water transport systems [2]
  - Optimally handing **water quantity**; avoiding too much or too little water (avoiding floods and droughts); delivering water at the right time at the right place [15, 19]
- **Problems with a focus on transport over water**

  - Increasing safety of **navigation** in transport over water; improving ship manoeuvring; keeping ships efficiently at specific positions via dynamic positioning [5–7, 16]
  - Enhancing **sustainability**; decreasing energy consumption of transport over water systems; determining optimal power configuration for vessels [6, 11]
  - Improving the **logistics** of transport over water; estimating the travel times accurately; modeling the traffic in transport over water systems [3, 8, 11, 13]

- **Problems of a more generalized nature**
  - Addressing the tradeoffs at different **space scales**; modeling whole networks at macroscopic perspective; modeling transport of and over water at smaller microscale scales [2, 9, 13]
  - Taking into account explicitly **uncertainties**; modeling and preparing for variations in currents, winds, social influences, system understanding [1, 7, 9, 11, 18, 20, 21]
  - Benefitting from the interaction between **humans and automated systems** [9, 18]
  - Increasing the **cooperation** in transport of and over water systems; reactivating the transport over water market [11, 20, 22]

- **Problems focusing on the interaction**
  - **Balancing conflicting objectives** of optimal delivery of water versus optimal navigation over water [15]
  - **Designing** the interactions among ship-waterway physics, river-wetland connections, river-waterway-canal interaction [7, 8, 13]

The methods that are used to address these problems are a clear indication of the multidisciplinary nature of the domain considered:

- **Modeling (for control)**: Closed-loop identification, data assimilation, Kalman filters, probabilistic maps, potential fields, dynamical models, hydraulic models, LTV models [2, 12, 14, 16]
- **Different control techniques**:
  - **Centralized**: Uncertain control, delay-aware control, multi-objective control, nonlinear iterative control, predictive control, (automatically tuned) PI, nonlinear MPC, event-driven control, decentralized PI, optimization-based control, fault tolerant control [2, 4, 12, 15, 17, 21]
  - **Distributed**: single level, multi-level/hierarchical [10, 17, 18]
- **Operations research techniques** (planning): scheduling, routing, mixed-integer optimization [3, 21]
- **Integrated control and scheduling** [3, 20]
- **Economical analysis** [8, 22]
- **Proposal validation**: Virtually in simulation studies, physical lab experiments, gaming for education [7, 15, 22]

Details on all the above mentioned problems and methods, as well as their relation to the common framework of transport of water and transport over water are found in the provided references.

1.6 Outline of the Book

The book "Transport of Water Versus Transport over Water" categorizes the approaches investigated in the literature in two parts: the first part considers those chapters mainly focusing on the modeling, management and control of infrastructures related to the transport *of* water (water networks, rivers, irrigation canals). The second part collects contributions focusing on the transport of goods and/or navigation activities, i.e., systems related to the transport *over* water. Within both parts, research lines have been ordered in such a way that earlier chapters consider more integrated approaches among both fields of transport (*of* and *over*) while, as that integration decreases, chapters are becoming more related to either *of* or *over* fields. This organization allows the reader to identify and distinguish the proposed approaches and how the respective research lines treat and contribute to the unified framework discussed.

As mentioned before, each research lines offers its own discussion of the integrated framework in the light of the particular approach presented and discussed according to the field. Hence, many ideas arise for actually shaping the details of the proposed integrated framework naturally arise—the methodologies applied to one field (*of* or *over*) require new perspectives from the complementary field for the unified framework to be applicable. This leads to many interesting new research directions.

1.7 Concluding Remarks

Methodologies and relevant approaches related to transport *of* water and transport *over* water have experienced a fast evolution over the past years via separated ways, although closely related by the common element of water. Moreover, case studies are everyday more challenging and complex, implying smart solutions to management problems mainly taking into account the possible interactions between systems and the consequent difficulties to cope with them.

The book "Transport of Water versus Transport over Water" provides contributions from recognized water-field researchers that also work in "real-world" applications related to diverse sectors of the water field. Research lines investigated are structured following a common format: starting with the problem formulation and description (according to the particular topic—of water, over water), where the proposed approach is discussed and exemplified by means of a water case study. Next the explicit linking between transport *of* water and transport over water

is presented and discussed for the particular proposed approach. Then, the open topics and directions of new/future research lines are proposed and, finally, the most relevant conclusions are drawn. The transport of/over water linking sections is what distinguishes this book: the link is shown, contextualized and highlighted.

The book will be useful for engineers facing complex applications and willing to use recent methods of identification and control in solving them. In addition, applied researchers looking for areas in which to contribute in reducing the theory/application gap and exploring practical issues. Both will take great benefit from the framework and approaches presented in this book.

Acknowledgements This research has been partially funded by the Transport Institute at Delft University of Technology—bringing together researchers and students from different backgrounds to identify the solutions that result in safer, cleaner and more efficient transport and improved accessibility. Moreover, this research has been partially funded the Maritime Project "ShipDrive: A Novel Methodology for Integrated Modeling, Control, and Optimization of Hybrid Ship Systems" (project 13276) of the Dutch Technology Foundation STW, and the Spanish project "ECOCIS: Economic Operation of Critical Infrastructure Systems" (reference DPI-2013-48243-C2-1-R).

References

1. Alfonso L, Tefferi M. Effects of uncertain control in transport of water in a river-wetland system of the Low Magdalena River, Colombia. In: Ocampo-Martinez C, Negenborn RR, editors. Transport of water versus transport over water: Exploring the dynamic interplay between transport and water, Chap. 8. New York: Springer; 2015.
2. Belaud G, Litrico X. Transport of water versus particular transport in open-channel networks. In: Ocampo-Martinez C, Negenborn RR, editors. Transport of water versus transport over water: Exploring the dynamic interplay between transport and water, Chap 6. New York: Springer; 2015.
3. Burger M, De Schutter B. Effects of water flow on energy consumption and travel times of micro-ferries for energy-efficient transport over water. In: Ocampo-Martinez C, Negenborn RR, editors. Transport of water versus transport over water: Exploring the dynamic interplay between transport and water, Chap. 12. New York: Springer; 2015.
4. Dorchies D, Malaterre P-O. Automatic tuning of PI controllers for water level regulation of a multi-pool open-channel hydraulic system. In: Ocampo-Martinez C, Negenborn RR, editors. Transport of water versus transport over water: Exploring the dynamic interplay between transport and water, Chap. 9. New York: Springer; 2015.
5. Froese J. Safe and efficient port approach by vessel traffic management in waterways. In: Ocampo-Martinez C, Negenborn RR, editors. Transport of water versus transport over water: Exploring the dynamic interplay between transport and water, Chap. 15. New York: Springer; 2015.
6. Godjevac M, Drijver M. Performance evaluation of an inland pusher. In: Ocampo-Martinez C, Negenborn RR, editors. Transport of water versus transport over water: Exploring the dynamic interplay between transport and water, Chap. 20. New York: Springer; 2015.

7. Hassani V, Pascoal AM. Wave filtering and dynamic positioning of marine vessels using a linear design model: Theory and experiments. In: Ocampo-Martinez C, Negenborn RR, editors. Transport of water versus transport over water: Exploring the dynamic interplay between transport and water, Chap. 17. New York: Springer; 2015.
8. Hekkenberg RG. Technological challenges and developments in European inland waterway transport. In: Ocampo-Martinez C, Negenborn RR, editors. Transport of water versus transport over water: Exploring the dynamic interplay between transport and water, Chap. 16. New York: Springer; 2015.
9. Horváth K, Rajaoarisoa L, Duviella E, Blesa J, Petreczky M, Chuquet K. Enhancing inland navigation by model predictive control of water levels: The Cuinchy-Fontinettes case. In: Ocampo-Martinez C, Negenborn RR, editors. Transport of Water versus Transport over Water: Exploring the dynamic interplay between transport and water, Chap. 13. New York: Springer; 2015.
10. Lemos JM, Sampaio I. Distributed LQG control for multiobjective control of water canals. In: Ocampo-Martinez C, Negenborn RR, editors. Transport of water versus transport over water: Exploring the dynamic interplay between transport and water, Chap. 4. New York: Springer; 2015.
11. Maes J, Sys C, Vanelslander T. City logistics by water: Good practices and scope for expansion. In: Ocampo-Martinez C, Negenborn RR, editors. Transport of water versus transport over water: Exploring the dynamic interplay between transport and water, Chap. 21. New York: Springer; 2015.
12. Malaterre P-O, Jean-Baptiste N, Dorée C. Data assimilation to improve models used for the automatic control of rivers or canals. In: Ocampo-Martinez C, Negenborn RR, editors. Transport of water versus transport over water: Exploring the dynamic interplay between transport and water, Chap. 3. New York: Springer; 2015.
13. Osekowska E, Axelsson S, Carlsson B. Potential fields in modeling transport over water. In: Ocampo-Martinez C, Negenborn RR, editors. Transport of water versus transport over water: Exploring the dynamic interplay between transport and water, Chap. 14. New York: Springer; 2015.
14. Padilla A, Bittner R, Yuz JI. Closed-loop identification and control of inland vessels. In: Ocampo-Martinez C, Negenborn RR, editors. Transport of water versus transport over water: Exploring the dynamic interplay between transport and water, Chap. 18. New York: Springer; 2015.
15. Puig V, Ocampo-Martinez C, Negenborn RR. Model predictive control for combined water supply and navigability/sustainability in river systems. In: Ocampo-Martinez C, Negenborn RR, editors. Transport of water versus transport over water: Exploring the dynamic interplay between transport and water, Chap. 2. New York: Springer; 2015.
16. Revestido Herrero E, Tomás-Rodríguez M, Velasco FJ. Nonlinear iterative control of manoeuvring models for transport over water. In: Ocampo-Martinez C, Negenborn RR, editors. Transport of water versus transport over water: Exploring the dynamic interplay between transport and water, Chap. 19. New York: Springer; 2015.
17. Sadowska A, van Overloop PJ, Burt C, De Schutter B. Hierarchical MPC-based control of an irrigation canal. In: Ocampo-Martinez C, Negenborn RR, editors. Transport of water versus transport over water: Exploring the dynamic interplay between transport and water, Chap. 10. New York: Springer; 2015.
18. Sun CC, Puig V, Cembrano G. Coordinating model predictive control of transport and supply water systems. In: Ocampo-Martinez C, Negenborn RR, editors. Transport of water versus transport over water: Exploring the dynamic interplay between transport and water, Chap. 7. New York: Springer; 2015.
19. Tian X, Negenborn RR, van Overloop PJ, Maestre JM, Mostert E. Model predictive control for incorporating transport of water and transport over water in the dry season. In: Ocampo-Martinez C, Negenborn RR, editors. Transport of water versus transport over water: Exploring the dynamic interplay between transport and water, Chap. 11. New York: Springer; 2015.

20. van Hassel E. Reactivation of the small inland waterway network. In: Ocampo-Martinez C, Negenborn RR, editors. Transport of water versus transport over water: Exploring the dynamic interplay between transport and water, Chap. 22. New York: Springer; 2015.
21. van Loenen A, Xu M. Forecasting and predictive control of the Dutch canal network. In: Ocampo-Martinez C, Negenborn RR, editors. Transport of water versus transport over water: Exploring the dynamic interplay between transport and water, Chap. 5. New York: Springer; 2015.
22. Veenstra AW, van Meijeren J, Harmsen J, Verbraeck A. Fostering cooperation in inland waterway networks: A gaming and simulation approach. In: Ocampo-Martinez C, Negenborn RR, editors. Transport of water versus transport over water: Exploring the dynamic interplay between transport and water, Chap. 23. New York: Springer; 2015.

Part I
Transport of Water

Chapter 2
Model Predictive Control for Combined Water Supply and Navigability/Sustainability in River Systems

V. Puig, C. Ocampo-Martinez, and R.R. Negenborn

Abstract In this chapter, a methodology for the optimal management of combined water supply and navigability/sustainability in river systems based on model predictive control (MPC) is proposed. A control-oriented modeling methodology for this type of systems is presented as well. MPC is used to generate flow-control strategies from the sources to both the farmers and urban consumers in order to meet future demands with appropriate flows, optimizing operational goals such as network safety volumes in dams and smooth operations of actuators (valves, gates and pumps). At the same time, the generated flow-control strategies should allow maintaining the appropriate river water levels that, in turn, allows to preserve the ecological flows and the navigability of the downstream part of the river. The case study of the Guadiana river is used to show and verify the proposed optimal management methodology.

2.1 Introduction

Water management is a subject of increasing concern. Limited water supplies, conservation and sustainability policies, as well as the infrastructure complexity for meeting consumer demands with quality levels make water management a challenging problem. Water systems, which are quite often of large-scale nature, comprise:

- Supplies, where raw water is drawn from superficial or underground sources, such as rivers, reservoirs or boreholes;

V. Puig (✉) • C. Ocampo-Martinez
Institut de Robòtica i Informàtica Industrial (CSIC-UPC), Universitat Politècnica de Catalunya, Barcelona, Spain
e-mail: vpuig@iri.upc.edu; cocampo@iri.upc.edu

R.R. Negenborn
Delft University of Technology, Delft, The Netherlands
e-mail: r.r.negenborn@tudelft.nl

C. Ocampo-Martinez, R.R. Negenborn (eds.), *Transport of Water versus Transport over Water*, Operations Research/Computer Science Interfaces Series 58,
DOI 10.1007/978-3-319-16133-4_2

- Production facilities, where water is treated to meet consumer-use standards;
- Transport systems, natural or artificial open-flow canals carrying water from the sources to the treatment locations and to the distribution areas;
- Distribution areas, including consumer demands, storage tanks and pressurized pipe networks, to which water must be supplied with appropriate pressure levels
- Control elements in all the above-mentioned subsystems, such as gates, valves, and pumps.

Water supply, treatment, transport and distribution are often operated separately by different authorities and/or utilities. Planning and management of these subsystems have different goals and time scales. Additionally, hydraulics involved differ considerably from one to another, in particular, between large and spatially-distributed open canals and pressurized water sections for distribution to consumers. In many water systems, network operation is carried out based on heuristic approaches, operator judgment, among other approaches, which may be quite complex for large-scale interconnected systems. Decision support systems, which are based on mathematical network and operation models, may efficiently contribute to the optimal management of water networks by computing control strategies ahead in time, which optimize management goals [3]. Optimization and optimal control techniques provide an important contribution to strategy computation in water systems management, as reported in [1, 14].

Many modern water systems are operated through centralized or distributed telemetry and telecontrol systems but supervised by expert humans. Over the past few years, Model Predictive Control (MPC) has proven to be one of the most effective and accepted control strategies for large-scale complex systems [11, 17]. The objective of using this technique for controlling water systems is to compute, in a predictive way, the manipulated inputs in order to achieve the optimal performance of the network according to a given set of control objectives and predefined performance indices. As shown in [9, 22], MPC controllers are suitable to be used in the global/supervisory control of networks related to the urban water cycle. Figure 2.1 shows a conceptual scheme for a hierarchical structure considered on the control of such networks. Here, the MPC, as the global control law, determines the references (set-points) for the local controllers placed at different elements of the networked system. These references are computed according to measurements taken from sensors distributed around the network. The management level provides the MPC with its operational objectives, which are reflected in the controller design as the performance indices to be enhanced, which can be either minimized or maximized, depending on the case. Finally, water systems control requires the use of a supervisory system to monitor the performance of the different control elements in the networks (e.g., valves and gates) and to take appropriate correcting actions in the case where a malfunction is detected, to achieve a proper fault-tolerant control.

In this chapter, a methodology based on MPC for the optimal management of water supply in river systems combined with navigability and sustainability features is proposed. A control-oriented modeling approach for these systems is also presented. MPC is used to generate flow-control strategies from the sources to both

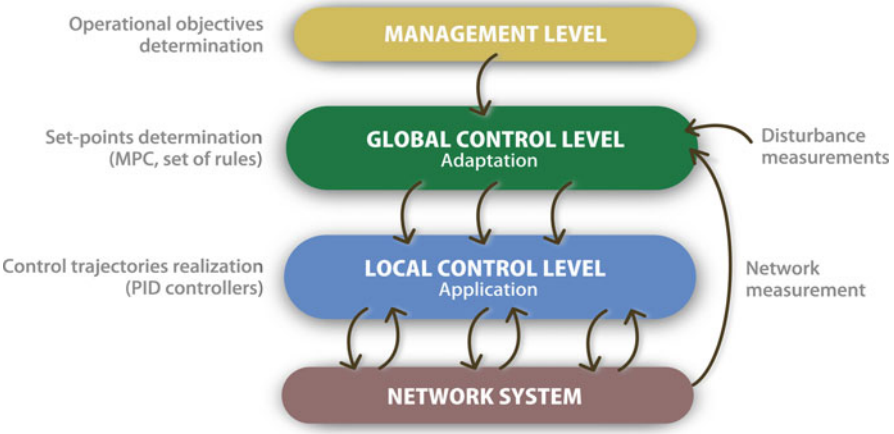

Fig. 2.1 Hierarchical structure for RTC system based on MPC (taken from [14])

the farmers and urban consumers to meet future demands with appropriate flows, optimizing operational goals such as network safety volumes in dams and control input smoothness in actuators. Simultaneously, the generated flow-control strategies should allow maintaining the appropriate water levels in the river, allowing in turn to preserve the ecological flows and the navigability at the downstream portion of the river.

Regarding the case study through which the proposed methodology is illustrated, a brief description is going to be presented next. The Guadiana River is an international river defining a long stretch of the Portuguese–Spanish border, separating Extremadura and Andalucia (Spain) from Alentejo and Algarve (Portugal), see Fig. 2.2. The basin of the river extends from the eastern portion of Extremadura to the southern provinces of the Algarve; the river and its tributaries flow from east to west, then south through Portugal to the border towns of Vila Real de Santo António (Portugal) and Ayamonte (Spain), where it flows into the Gulf of Cádiz. With a course that covers a distance of 829 km, it is the fourth-longest in the Iberian peninsula, and its hydrological basin extends over an area of approximately 68,000 km^2 (the majority of which lies within Spain).

The Guadiana ecosystem has Mediterranean hydrological characteristics, including high variation in intra- and inter-annual discharge, large floods and severe droughts. This variability is a consequence of considerable variation in rainwater supply, averaged around an annual mean of 400–600 mm. There are over thirty dams on the river basin, the largest of which is the Alqueva Dam, near Moura, in the Beja District, responsible for the largest reservoir in Western Europe (see Fig. 2.3). The Alqueva reservoir occupies an area of 250 km^2, with a capacity for 4,150 hm^2. For the most part, the Guadiana is navigable until Mértola (a distance of 68 km), see Fig. 2.4.

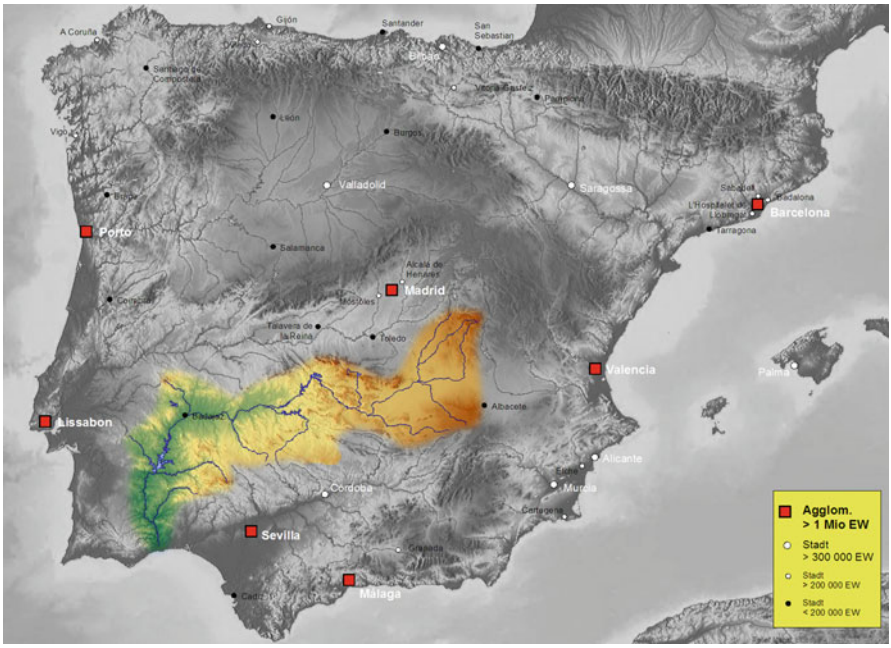

Fig. 2.2 Guadiana basin

Fig. 2.3 Alqueva dam

Fig. 2.4 Ship navigation in the Guadiana river

The chapter is organized as follows. In Sect. 2.2, the control-oriented modeling methodology is described and the predictive control strategy applied to water supply systems is presented and discussed for the mentioned case study: the Guadiana river. Section 2.3 highlights and motivates some discussion about the approach proposed in this chapter within the *transport of water* framework and its relation/connection with the *transport over water*. Finally, in Sect. 2.4, the main conclusions are drawn.

2.2 Proposed Approach and Case Study

2.2.1 Control-Oriented Modeling Methodology

Several modeling techniques dealing with the operational control of water systems have been presented in the literature, see [1, 10], among others. Here, a flow control-oriented modeling approach is outlined, which follows the principles presented by the authors in [13, 14]. Natural extensions to include pressure features in the system model can be found in [5, 6, 20, 24]. A water system generally contains storing elements, which store the water coming from the network sources, a network of pressurized/unpressurized pipes and a number of sinks. Valves, gates and/or pumping stations are elements that allow to manipulate the water flow according to a specific policy and to supply water requested by the network users. These flows are chosen by a global management strategy.

The water system model can be considered as composed of a set of constitutive elements, which are presented and discussed below. Some of these elements follow the description reported in [15] for flow networks, but will be included here for the proper completeness of the discussion.

Tanks and Dams

Water dams/reservoirs provide the entire water system with the storage capacity of water while water tanks at distribution level additionally provide at appropriate elevation levels to supply water with adequate pressure service to consumers. The mass balance expression relating the stored volume v, the manipulated inflows q_{in}^{j} and outflows q_{out}^{h} (including the demand flows as outflows) for the i-th tank can be written as the discrete-time difference equation

$$v_i(k+1) = v_i(k) + \Delta t \left(\sum_j q_{\text{in}}^{j}(k) - \sum_h q_{\text{out}}^{h}(k) \right), \tag{2.1}$$

where Δt denotes the sampling time and k denotes the discrete-time instant. The physical constraint related to the range of admissible water in the i-th dam/tank is expressed as

$$\underline{v}_i \leq v_i(k) \leq \overline{v}_i, \quad \forall\ k, \tag{2.2}$$

where $\underline{v}_i$ and $\overline{v}_i$ denote the minimum and the maximum admissible storage capacity, respectively. As this constraint is physical, it is impossible to send more water to a tank than it can store, or drawing more water than the stored amount. Although $\underline{v}_i$ might correspond with an empty dam/tank, in practice this value can be set as nonzero in order to maintain an emergency stored volume enough to supply for facing extreme circumstances. Moreover, there will be restrictions in the amount of flow that can be extracted from the dam/tank depending on the volume stored according to the discharge curves.

For simplicity purposes, the dynamic behavior of these elements is described as a function of the volume. However, in most of the cases the measured variable is the water level (by using level sensors), which implies the computation of the water volume taking into account the element geometry.

Actuators

Several types of control actuators are considered: valves, gates and pumps (more precisely, complex pumping stations). It is assumed that the MPC controller provides the flow set-point to a local controller that is responsible to establish the required flow through the actuator by using a closed-loop control system with a PID

or a PLC. The manipulated flows through the actuators represent the manipulated variables, denoted as q_u. All considered actuators have lower and upper physical limits, which are taken into account as system constraints. As in (2.2), they are expressed as

$$\underline{q_{u_i}} \leq q_{ui}(k) \leq \overline{q_{ui}}, \quad \forall\ k, \tag{2.3}$$

where $\underline{q_{u_i}}$ and $\overline{q_{ui}}$ denote the minimum and the maximum flow capacity, respectively.

Nodes

These elements correspond to the network points where water flows are merged or split. Thus, the nodes represent mass balance relations, being modeled as equality constraints related to inflows (from other dams/tanks through gates/valves or pumps) and outflows, these latter being represented not only by manipulated flows but also by demand flows. The expression of the mass conservation in these elements can be written as

$$\sum_j q_{\text{in}}^j(k) \ = \ \sum_h q_{\text{out}}^h(k). \tag{2.4}$$

From now on and with some abuse of notation, node inflows and outflows are denoted by q_{in} and q_{out}, respectively, despite they can be manipulated flows and hence denoted by q_u, if correspond.

River/Canal Reaches

In the proposed control-oriented methodology, a single river/canal reach can be approximated by using the IDZ model introduced in [7] used the Laplace transform

$$Y_{dns}(s) = G_1(s)Q_{ups}(s) + G_2(s)Q_{dns}(s), \tag{2.5}$$

where $Y_{dns}(s)$ is the water level at the control point, and $Q_{ups}(s)$, $Q_{dsn}(s)$ are the upstream and downstream flows, respectively. Moreover, $G_1(s) = e^{-\tau_d s}/A_d s$ and $G_2(s) = -1/A_d s$ with τ_d being the downstream transport delay and A_d the downstream backwater area.

Taking into account the linearized relation between Q_{dns} and Y_{dns} in the control point, the following relation can be established:

$$Q_{dns}(s) = \beta Y_{dns}(s), \tag{2.6}$$

where β is a constant varying with the operating point. Combining (2.5) and (2.6), the following first order plus time delay (FOPTD) model is obtained:

$$G(s) = \frac{Q_{dns}(s)}{Q_{ups}(s)} = \frac{Ke^{-\tau_d s}}{Ts+1}, \tag{2.7}$$

with $K = 1$ and $T = A_d/\beta$. This model can be represented in discrete time, using a sampling time Δt, in terms of the Z-transform as follows:

$$G_d(z) = \frac{Q_{dns}(z)}{Q_{ups}(z)} = \frac{b_0 z^{-d}}{z - a_1}, \tag{2.8}$$

where $d = \tau_d / T_s$, $b_0 = 1 - a_1$ and $a_1 = e^{-\frac{T_s}{T}}$. Alternatively, it can be written as a difference equation as

$$q_{dns}(k+1) = a_1 q_{dns}(k) + b_0 q_{ups}(k-d). \tag{2.9}$$

Urban and Irrigation Demands

Urban and irrigation demands are considered as measured disturbance of the system at a given time instant. The demand in urban areas can be anticipated by a forecasting algorithm that is integrated within the MPC closed-loop architecture [16, 23]. In [16], the demand forecasting algorithm uses a two-level scheme composed by (a) a time-series model to represent the daily aggregate flow values, and (b) a set of different daily flow demand patterns according to the day type to cater for different consumption during the weekends and holidays periods. Every pattern consists of 24 hourly values for each daily pattern. This algorithm runs in parallel with the MPC algorithm. The daily series of hourly-flow predictions are computed as a product of the daily aggregate flow value and the appropriate hourly demand pattern. On the other hand, irrigation demand is typically planned in advance with farmers. Pre-established flows for irrigation are established in the irrigation areas for determined periods of the year.

2.2.2 MPC Problem Formulation for Water Supply Systems

Water supply and distribution infrastructures are quite complex multivariate systems. In order to improve their performance, predictive control [8, 17] provides suitable techniques to compute optimal control strategies ahead in time for all the flow and pressure control elements of a water system. The optimal strategies are computed by optimizing a mathematical function describing the operational goals in a given time horizon and using a representative model of the network dynamics, as well as demand forecasts.

In many water systems, a supervision sampling time and control interval of the order of 1h is used, which is based on the scanning time of the telemetry system and on the dynamics of water distribution. Water consumption in urban areas is usually managed on a daily basis, because proper hourly 24-h-ahead demand predictions may, in general, be available and common transport time delays between supply locations and the consumer sites allow operators to follow daily water request patterns. Therefore, this horizon is appropriate for evaluating the effects of different control strategies on the water network, with respect to operational goals. However, other horizons may also be appropriate for different utilities.

Operational Goals

In most water systems, the regulated elements, namely pumps, gates and retention devices, are typically controlled locally, i.e., they are controlled by a remote station according to the measurements of sensors connected only to that station. However, a global real-time control system may require the use of an operational model of the system dynamics in order to compute, ahead in time, optimal control strategies for the actuators based on the current state of the system provided by supervisory control and data acquisition (SCADA) sensors, the current disturbance measurements and appropriate disturbance predictions. The computation procedure of an optimal global control law should take into account all the physical and operational constraints of the dynamical system, producing set-points though which given control objectives are achieved.

The immediate control goal of a water supply system is to meet the demands at consumer sites with appropriate flows, according to the requirements from the users. Predictive control techniques may be used to compute strategies which achieve this, while also optimizing the system performance in terms of different operational criteria. Regarding those criteria, some of them are discussed next.

- *Cost reduction*: The main economic costs associated with drinking water production are due to treatment processes, water acquisition or use costs and, most importantly, to electricity costs for pumping. Delivering this drinking water to appropriate pressure levels through the network involves important electricity costs in booster pumping as well as elevation from underground sources. In a specific case, this objective can be mathematically formulated as the minimization of

$$J_1(k) = (\alpha_1 + \alpha_2(k))\, q_u(k), \tag{2.10}$$

  where α_1 corresponds to a known vector related to the economic costs of the water depending on the selected water source, and $\alpha_2(k)$ is a vector of suitable dimensions associated to the economic cost of the flow through certain actuators

(pumps only) and their control cost (pumping). Note the k-dependence of α_2 since the pumping cost has different values according to the variable electric tariffs along a day.

- *Operational safety*: This criterion refers to maintaining appropriate water storage volumes in dams and tanks of the network for emergency handling. Therefore, this objective may be achieved by minimizing the following expression:

$$J_2(k) = \begin{cases} (v(k) - v^{\text{safe}})^T \ (v(k) - v^{\text{safe}}) & \text{if} \quad v(k) \leq v^{\text{safe}} \\ 0 & \text{otherwise,} \end{cases} \tag{2.11}$$

  where v^{safe} is a term which determines the safety volume to be considered for the control law computation.
- *Demand management*: This criterion refers to the fact that, although urban demands must be fully satisfied, irrigation demands allow some degree of slackness. Therefore, this objective may be achieved by minimizing the following expression:

$$J_3(k) = \begin{cases} (q(k) - d(k))^T \ (q(k) - d(k)) & \text{if} \quad q(k) \leq d(k) \\ 0 & \text{otherwise,} \end{cases} \tag{2.12}$$

  where $d(k)$ is the irrigation flow demanded for irrigation while $q(k)$ is the flow served.
- *Minimum-flow management*: This criterion refers to the need of enforcing that the generated flow strategies allow maintaining the appropriate water flows (or levels) in the river that allows to preserve the ecological flows and the navigability of the downstream portion of the river. This is achieved by means of the following objective expression:

$$J_4(k) = \begin{cases} (q(k) - q^{\text{safe}})^T \ (q(k) - q^{\text{safe}}) & \text{if} \quad q(k) \leq q^{\text{safe}} \\ 0 & \text{otherwise,} \end{cases} \tag{2.13}$$

  where q^{safe} is a term which determines the safety flow to be considered for the control law computation.
- *Control action smoothness*: The operation of actuators usually requires smooth flow set-point variations for equipment conservation. To obtain such smoothing effect, control signal variation between consecutive time intervals (slew rate) is then penalized. The penalty term to be minimized is

$$J_5(k) = \Delta q_u(k)^T \ \Delta q_u(k), \tag{2.14}$$

  where $\Delta q_u(k) \triangleq q_u(k) - q_u(k-1)$.

Multi-objective Performance Function

The multi-objective performance function $\mathcal{J}(k)$ that gathers the aforementioned control objectives may be written as

$$\mathcal{J}(k) = \sum_{j=1}^{n_J} \gamma_j J_j(k), \tag{2.15}$$

where a set of n_J control objectives are considered and, in turn, a *multi-objective* open-loop optimization problem is stated. The prioritization of the control objectives is performed by using the order of the mathematical cost function associated to each objective, and also a set of appropriate weights γ_j. These weights are selected off-line by means of trial and error procedures, taking into account the priority of each objective within the cost function. More sophisticated tuning methodologies for tuning multi-objective control problems based on lexicographic minimizers [12], goal programming [4], or Pareto-front computations [21] may be also considered.

Non-linear MPC Strategy

Collecting the control-oriented model and operational goals described in previous subsections, the MPC design follows the traditional procedures presented in [2, 8, 17], which involves solving an optimization problem over a prediction horizon H_p, where a cost function is minimized subject to a set of physical and operational constraints. Once the minimization is performed, a vector of control actions is obtained. Only the first component of that vector is considered and applied over the plant. The procedure is repeated for the next time instant taking into account the feedback measurements coming from the system, following the classic receding-horizon strategy.

Given a general nonlinear dynamic model of the water system obtained applying the proposed control-oriented modeling methodology presented above

$$x(k+1) = g(x(k), u(k)), \tag{2.16}$$

being $x(k) \in \mathbb{R}^n$ the mapping of states and $u(k) \in \mathbb{R}^m$ the control signals, where $g : \mathbb{R}^n \times \mathbb{R}^m \to \mathbb{R}^n$ is an arbitrary system state function and $k \in \mathbb{Z}_+$, the MPC is based on the solution of the open-loop optimization problem

$$\min_{\{u(k)\}_{i=0}^{H_p-1}} \sum_{i=0}^{H_p-1} \mathcal{J}\left(u(k+i|k), x(k+i|k)\right), \tag{2.17a}$$

subject to

$$Hu(k+i) \leq b, \tag{2.17b}$$

$$H_{eq}u(k+i) = b_{eq}, \tag{2.17c}$$

$\forall\, i \in [0, H_p{-}1]$, where $\mathcal{J}(\cdot)$ is the cost function, H_p denotes the *prediction horizon*, and H, H_{eq}, b, b_{eq} are matrices with suitable dimensions. In sequence (2.17a), $x(k+i|k)$ denotes the prediction of the state at time $k+i$ performed at k , starting from $x(0|k) = x(k)$. In particular, constraints (2.17c) are related to elements with static dynamics, where an equality condition must hold. The optimal solution of (2.17) is given by the sequence

$$u(0|k)^*, u(1|k)^*, \ldots, u(H_p - 1|k)^*,$$

and then the receding horizon philosophy sets

$$u_{\text{MPC}}(x(k)) \triangleq u(0|k)^*, \tag{2.18}$$

disregarding the computed inputs from $k = 1$ to $k = H_p - 1$, with the whole process repeated at the next time instant $k \in \mathbb{Z}_+$. Expression (2.18) is known in the MPC literature as *the MPC law*.

In order to manage the uncertainty of the system disturbances over the prediction horizon, the stochastic paradigm can be used, which leads to include explicit models of uncertainty/disturbances in the design of control laws and by transforming hard constraints into probabilistic constraints. The stochastic approach is a classic one in the field of optimization, but due to the advances in technology which improve computation capacity and the flexibility of the MPC framework to incorporate models and constraints within an optimal control problem, a renewed attention has been given to the stochastic programming [19], as a powerful tool for robust control design, leading to stochastic MPC approaches.

2.2.3 Case Study: Guadiana River

Description

As discussed in the introduction, the Guadiana has its source in Spain and flows into the Atlantic Ocean on the Portugal coast. It runs through the central south part of Spain from east to west most of its length to turn to the south direction when it is passing through Portugal. The hydrologic basin of Guadiana covers up to 67,733 km^2, from which 55,512 m^2 belongs to Spain (81.9 %). The annual average sources to the basin is about 3,884 hm^3. The global basin has 87 reservoirs with higher capacity of 1 hm^3 and a total storage capacity of more than 9,000 m^3.

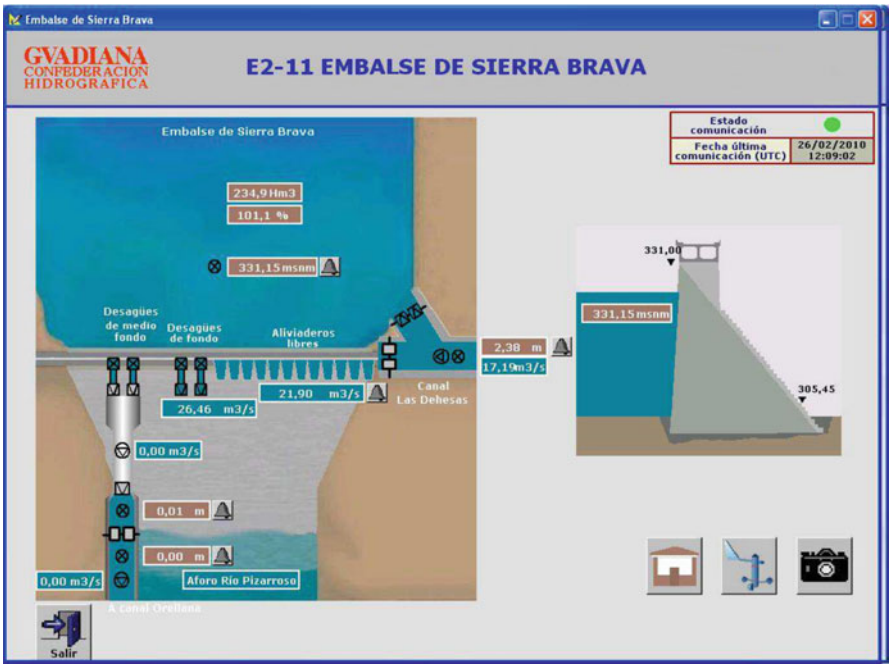

Fig. 2.5 Screen of the SCADA system

In the Guadiana catchment, the climatic conditions are characterized, in a general sense, by high temperature in summer and moderate in winter, and by a very irregular pluviometry, which is typical of the Mediterranean areas. This climatology configures a catchment that presents scarce and irregular rainfall, and sudden strong precipitation and frequent dry years. Agricultural and farming demand represents about the 90 % of the water use while the remaining demand is domestic or industrial.

Currently, the monitoring and control of the Guadiana catchment is by the Automatic Hydrological Information System of the Guadiana Water Authority that, by means of a SCADA system (see Fig. 2.5 for a sample of a SCADA screen), allows to know the current state of the water resources and river flows and operate dams and control elements. Currently, there are 144 control points: 86 in rivers sections, 48 in dams and 10 in canals plus 150 meteorological stations.

This chapter considers just the central part of this basin, where the Guadiana River is highly regulated by 16 dams linked by canals and pipes. The total capacity of these reservoirs is about 7,800 hm^3, which regulate the river flow and supply to all the demands and the important irrigation zones of the basin. A bilateral agreement (*Convenio de Albufeira*) between Spain and Portugal establishes a minimum flow at specific sections of the river during normal precipitation years. This regulation takes into account the restrictions of ecological flows for summer periods and the

operational rules for the reservoirs in rainy episodes. All these restrictions will be part of the optimization problem. The conceptual model of the Guadiana central portion is shown in Fig. 2.6. In this figure, blue lines define the stretches rivers and the open canals, while in black lines define the pressurized pipes.

Results

In this section, control results are presented for representative selected elements. The control results have been obtained under the following considerations:

- The selected scenario lasts 16 months, with a sampling time of 1 day.
- The operational control strategy aim to guarantee the preservation of a minimum volume of water at the dams/reservoirs and the smooth behavior of the actuators (gates) while satisfying the consumer demands and the *Convenio of Albufeira*.
- The maximum available flow to deliver through all outlets of the reservoirs is limited by the total volume of water according to the corresponding discharge curve.

The control objectives of the multi-objective optimization associated to the MPC problem are defined in Sect. 2.2.2. The prediction horizon used for the MPC controller is one month (30 days). Optimization problems have been solved using the CONOPT3 solver in GAMS. The computer used to run the simulations is a PC Intel® Core™ running both cores at 2.8 GHz with 4 GB of RAM. Computation time of each MPC iteration is less than 1 min.

The MPC controller is implemented by means of the tool presented in Fig. 2.7. This is general-purpose decision-support tool that has been developed to allow the user to implement optimal/predictive control techniques in large-scale water systems. An important feature of this tool compared to other existing tools is the application of a unified approach to the complete water system including supply, production, transport and distribution and, therefore pressurized and open-canal dynamics, simultaneously. The modeling and predictive control problem solution algorithm in this tool is designed for real-time decision support, in connection with the SCADA system using the OPC protocol. The hydraulic modeling relies on the control-oriented methodology described in Sect. 2.2.1, whose parameters are estimated on-line using recursive parameter estimation and real data from network sensors. Demand forecasting models, based on time-series analysis, are also dynamically updated. The real-time calibration using recursive parameter estimation methods contributes to deal with hydraulic uncertainty. This modeling choice, as well as the optimization method selection allow to deal with quite large-scale systems. Another distinguishing feature of the tool is its capability to accommodate complex operational goals.

Some results illustrating the performance of the proposed approach and developed tool in the Guadiana are presented in the following. Figure 2.8 shows the urban demand E2-07 supplied from the river. Figure 2.9 shows the resulting flow through gate V2-07 of a dam upstream of this demand, which is manipulated to

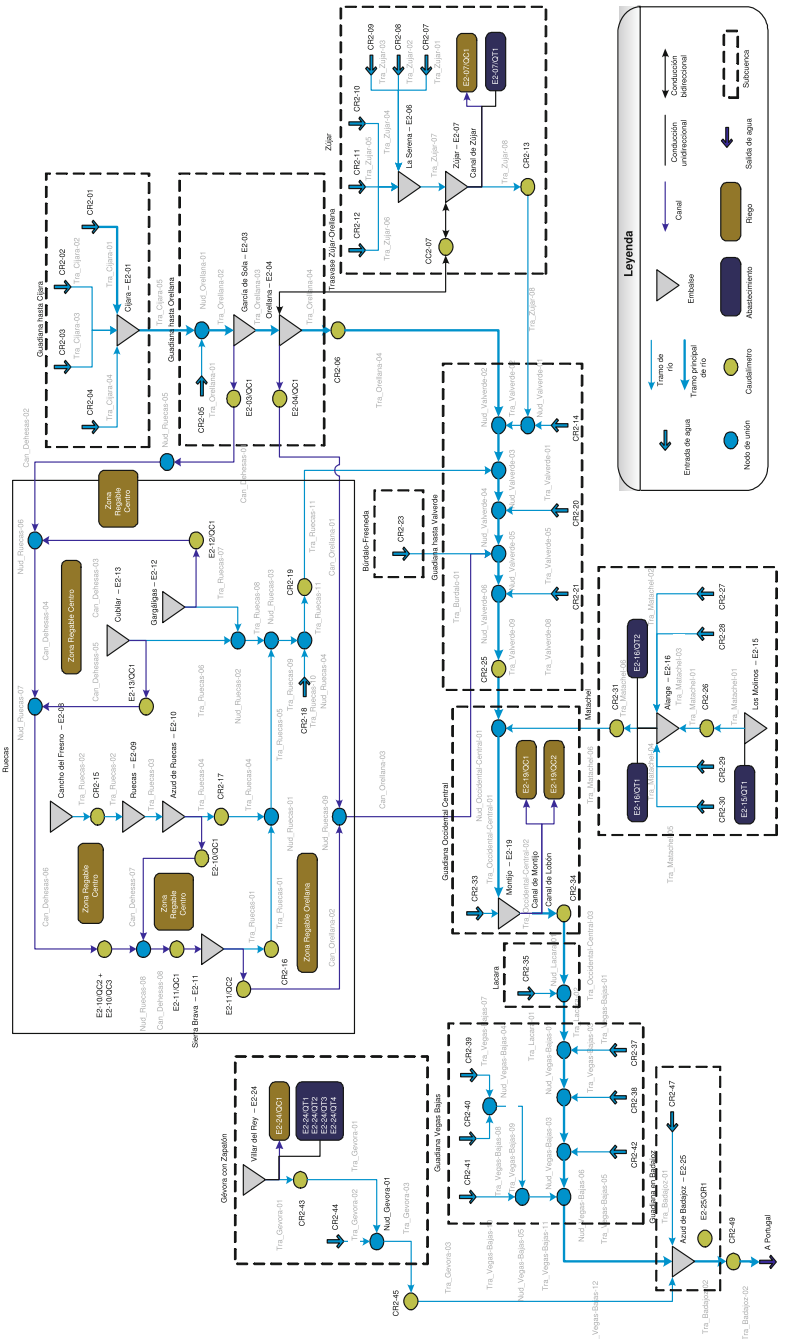

Fig. 2.6 Conceptual scheme of the Guadiana river portion used as case study

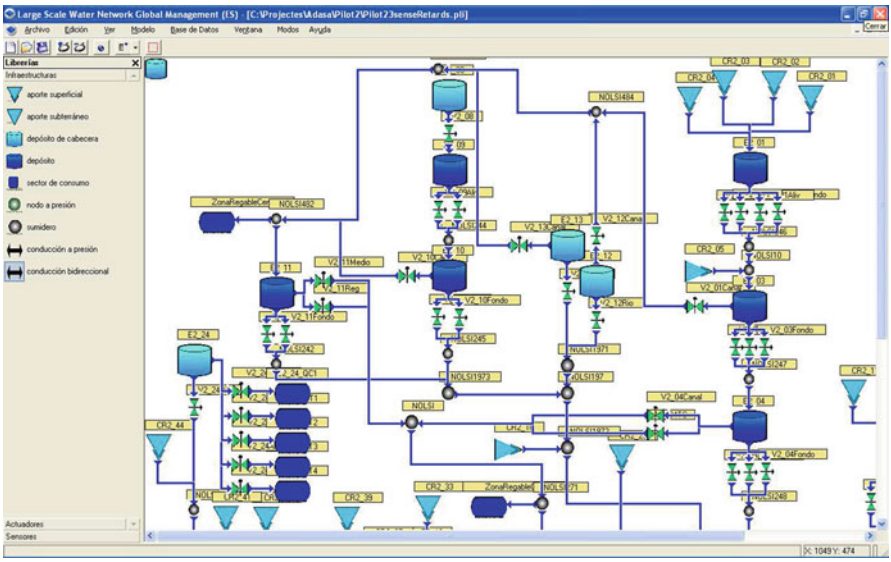

Fig. 2.7 Screen of the MPC design software tool

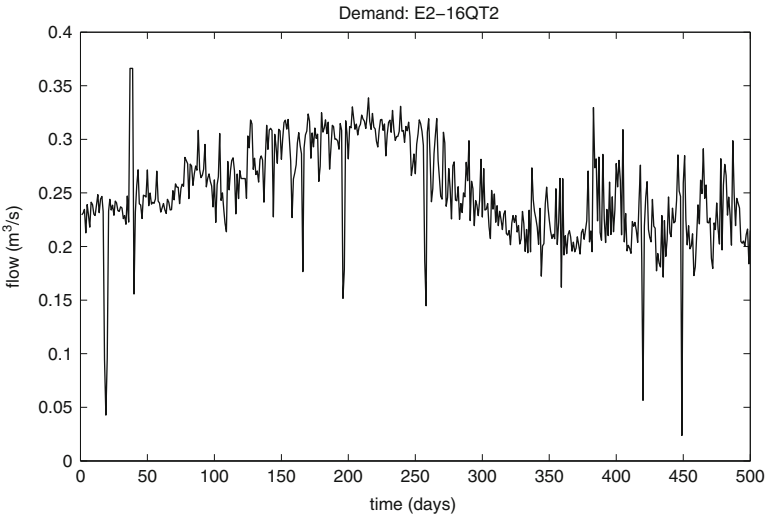

Fig. 2.8 Water demand E2-07

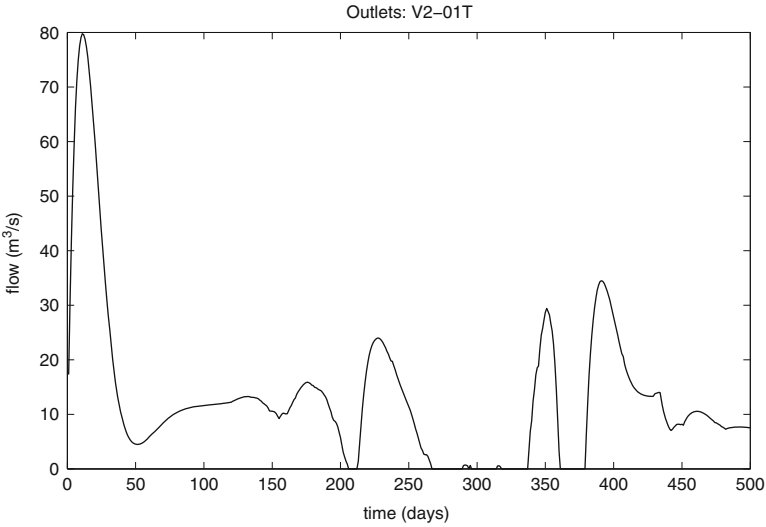

Fig. 2.9 Flow through gate V2-07

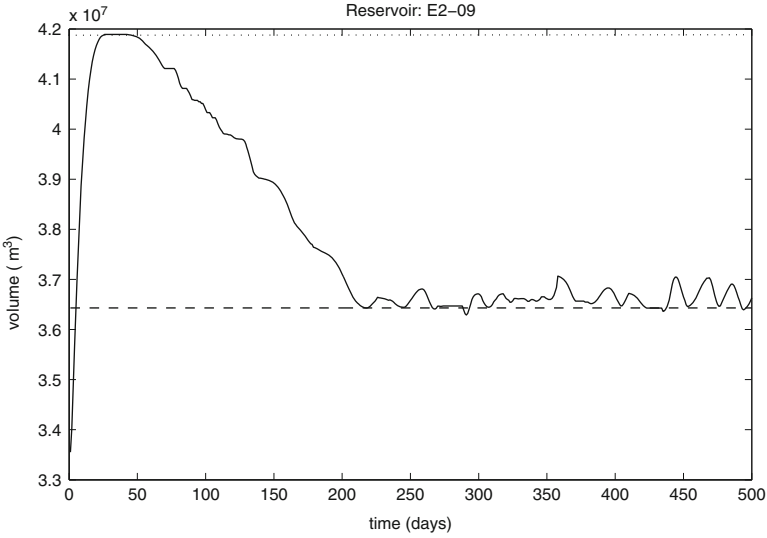

Fig. 2.10 Volume evolution of dam E2-07

satisfy it while fulfilling the rest of objectives such as the minimizing the river flow and maintaining the dam volume up to the safety volume. This can be seen in Fig. 2.10 for the volume evolution of dam E2-07, where the control strategy guarantees that the dam volume surpasses the safety volume most of the time, being able to vary freely but without getting empty. On the other hand, Fig. 2.10 shows that the minimum flow (2 m^3/s) established by the Convenio of Albufeira to preserve sustainability and downstream navigability of the river is satisfied (Fig. 2.11).

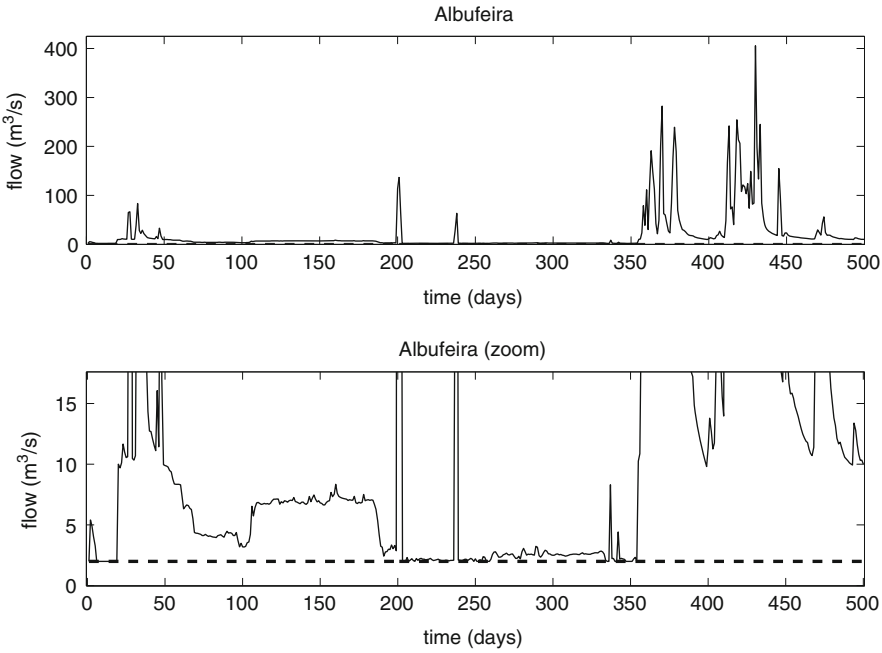

Fig. 2.11 Albufeira flow

2.3 Linking Transport *of* and Transport *over* Water

As discussed along this chapter, an important characteristic of the Guadiana catchment is the strong seasonal variations as consequence of the inter-annual regularity of drought and rainy periods. This distinctive condition of the river implies that its flow needs to be regulated by means of dams in order to adapt it to the needs of the ecological and navigability flows,[1] hydroelectric generation and water supply demands. In drought periods, a great part of the Guadiana river tributaries have no water flow and show significant levels of eutrophication.[2] Until recently, the bilateral relationships between Spain and Portugal in water aspects were based on sharing water for hydroelectric generation. However, since November 1998, the Convenio de Albufeira agreement establishes a minimum flow at specific sections of the Guadiana river during normal precipitation years. This implies that integrated water resource management in all the Guadiana catchment is needed to manage in a efficient way the stored water in dams allowing to supply the required flows and

[1]For the most part, the Guadiana is navigable until Mértola, a distance of 68 km away from the sea.

[2]Eutrophication or hypertrophication is defined as the ecosystem response to the addition of artificial or natural substances, mainly phosphates, through detergents, fertilizers, or sewage, to an aquatic system [18].

keep the minimum flows at the specific sections of the Guadiana river. Nowadays, all this management is carried out using empirical rules and "historic" strategies, which come from years of operational experience and empirical results. While these may generally be adequate, the best operational policies may be quite complex to be determined for large-scale interconnected systems as the Guadiana catchment. Thus, decision-support systems for operational control as the one proposed in this chapter, based on mathematical models of network operation and optimal control techniques, provide useful guidance for efficient management of water networks at different levels (namely, as for the integrated water resources/watershed planning and management with medium or long-term horizons) and with contradictory goals (water supply and ecological/navigability flow preservation) specially in drought periods of scarce water resources.

2.4 Conclusions

In this chapter, a methodology based on MPC for the optimal management of combined water supply systems with navigability/sustainability features in river systems has been proposed. First, a control-oriented modeling approach for this type of systems has been introduced. Then, MPC is introduced as a means of generating flow control strategies from the sources to the consumer to meet future demands with appropriate flows, optimizing operational goals such as network safety volumes in dams and control input smoothness in actuators (valves, gates and pumps). At the same time, the resultant flow-control strategies allow maintaining the appropriate levels in the river, allowing in turn to preserve the ecological flows and the navigability of the downstream portion of the river. The case study of Guadiana river has been used to illustrate the proposed management methodology. A decision support tool that implements the proposed methodology is described and some illustrative results in a real scenario are presented.

Acknowledgements This research has been partially funded by CDTI (MCyT) project HIDROPTIM IDI-20100722, the Spanish project ECOCIS (DPI-2013-48243-C2-1-R), the DGR of Generalitat de Catalunya (SAC group Ref. 2014 SGR 374), and the Maritime Project "ShipDrive: A Novel Methodology for Integrated Modeling, Control, and Optimization of Hybrid Ship Systems" (project 13276) of the Dutch Technology Foundation STW. The authors thank *Confederación Hidrográfica del Guadiana* for providing the case study as well as for sharing their hydrological management expertise.

References

1. Brdys M, Ulanicki B. Operational control of water systems: Structures, algorithms and applications. London: Prentice Hall International; 1994.
2. Camacho EF, Bordons C. Model predictive control. 2nd ed. London: Springer; 2004.

3. Cembrano G, Quevedo J, Puig V, Pérez R, Figueras J, Verdejo JM, Escaler I, Ramón G, Barnet G, Rodríguez P, Casas M. Plio: A generic tool for real-time operational predictive optimal control of water networks. Water Sci Technol. 2011;64(2):448–59.
4. Chen A, Xu X. Goal programming approach to solving network design problem with multiple objectives and demand uncertainty. Expert Syst Appl. 2012;39(4):4160–70.
5. Kang D. Real-time optimal control of water distribution systems. Procedia Eng. 2014;70: 917–23.
6. Koppel T, Vassiljev A. Estimation of real-time water fluxes in water distribution system on the basis of pressure measurements. Adv Eng Softw. 2013;66:19–23.
7. Litrico X, Fromion V. Modeling and control of hydrosystems. Berlin: Springer; 2009.
8. Maciejowski JM. Predictive control with constraints. Great Britain: Prentice Hall; 2002.
9. Marinaki M, Papageorgiou M. Optimal real-time control of sewer networks. Secaucus: Springer; 2005.
10. Mays LW. Urban stormwater management tools. New York: McGrawHill Professional Publishing; 2004.
11. Ocampo-Martinez C, Barcelli D, Puig V, Bemporad A. Hierarchical and decentralised model predictive control of drinking water networks: Application to the Barcelona case study. IET Control Theory Appl. 2012;6(1):62–71.
12. Ocampo-Martinez C, Ingimundarson A, Puig V, Quevedo J. Objective prioritization using lexicographic minimizers for MPC of sewer networks. IEEE Trans Control Syst Technol. 2008;16(1):113–21.
13. Ocampo-Martinez C, Puig V, Cembrano G, Creus R, Minoves M. Improving water management efficiency by using optimization-based control strategies: The Barcelona case study. Water Sci Technol Water Supply. 2009;9(5):565–75.
14. Ocampo-Martinez C, Puig V, Cembrano G, Quevedo J. Application of predictive control strategies to the management of complex networks in the urban water cycle [applications of control]. IEEE Control Syst Mag. 2013;33(1):15–41.
15. Ocampo-Martinez C, Puig V, Grosso JM, S. Montes de Oca. Multi-layer decentralized model predictive control of large-scale networked systems, chapter. In: DMPC made easy. Berlin: Springer; 2013.
16. Quevedo J, Puig V, Cembrano G, Blanch J. Validation and reconstruction of flow meter data in the Barcelona water distribution network. Control Eng Pract. 2010;11(6):640–51.
17. Rawlings JB, Mayne DQ. Model predictive control: Theory and design. Madison: Nob Hill Publishing; 2009.
18. Schindler D, Vallentyne J. Algal bowl: Overfertilization of the World's freshwaters and estuaries. Edmonton: University of Alberta Press; 2004.
19. Shapiro A, Dentcheva D, Ruszczynski A. Lectures on stochastic programming: Modeling and theory. Philadephia: Society for Industrial and Applied Mathematics and Mathematical Programming Society; 2009.
20. Sitzenfrei R, von Leon J. Long-time simulation of water distribution systems for the design of small hydropower systems. Renew Energy. 2014;72:182–7.
21. Toro R, Ocampo-Martinez C, Logist F, Van Impe J, Puig V. Tuning of predictive controllers for drinking water networked systems. In: Proceedings of the IFAC world congress, Milano, 2011.

22. Van Overloop PJ. Model predictive control on open water systems. Delft: Delft University Press; 2006.
23. Wang Y, Ocampo-Martinez C, Puig V, Quevedo J. Gaussian-process-based demand forecasting for predictive control of drinking water networks. In: Proceedings of the 9th international conference on critical information infrastructures security, Limassol, 13–15 October 2014.
24. Xu Y, Zhang XY. Research on pressure optimization effect of high level water tank by drinking water network hydraulic model. Procedia Eng. 2012;31:958–66.

Chapter 3
Data Assimilation to Improve Models used for the Automatic Control of Rivers or Canals

P.-O. Malaterre, N. Jean-Baptiste, and C. Dorée

Abstract The dams and the hydropower plants on the Rhône River, managed by the Companie Nationale du Rhône (CNR), are controller in real-time by Model Predictive Controllers (MPC) since the early 2000s. The control objectives and constraints are manyfold: optimize electrical production, allow navigation, protect the banks from erosion, prevent or reduce the damages during flood events, supply water to industries, cities and irrigation districts. In case the outputs of the embedded model used by MPC do not fit the field measurements, some questions are raised on: how to interpret this, and what can be done to solve this problem? We will present recent developments, carried out and illustrated on the Rhône River allowing to address these issues. The framework we will use is the one of Kalman filtering. We will see that this framework is very powerful to solve the above described problems. But, in some cases the obtained solution is not the one we would expect. The conditions of success can be expressed and checked from some mathematical tests, and linked to some physical properties (number and location of sensors, uncertainties of the measurements and of the model, hydraulic configuration of the hydraulic system).

3.1 Introduction

Irrigation is well-known for being responsible of more than 70 % of the fresh water withdrawal, in average in the world. But irrigated lands also contribute for more that 40 % of the world food production with less than 20 % of the cultivated area. Recent

P.-O. Malaterre (✉)
UMR G-eau, Irstea, Montpellier, France
e-mail: p-o.malaterre@irstea.fr

N. Jean-Baptiste
EDF—Direction Production Ingénierie Hydraulique, CIH—Département CC Lyon, Lyon, France
e-mail: nelly.jean-baptiste@edf.fr

C. Dorée
Compagnie Nationale du Rhône, Département Ouvrages Hydroélectriques et Fluviaux, Lyon, France
e-mail: c.doree@cnr.tm.fr

C. Ocampo-Martinez, R.R. Negenborn (eds.), *Transport of Water versus Transport over Water*, Operations Research/Computer Science Interfaces Series 58,
DOI 10.1007/978-3-319-16133-4_3

FAO figures indicate that for 2030, the food production will have to be increased by more that 80 % to fulfill demand, but with no more than 12 % additional water extraction, due to the lack of availability of other new resources. Therefore, high levels of efficiencies of water uses are increasingly expected from the managers of irrigation canals or rivers used for irrigation.

Hydropower production is also getting more attention in the present context of energy shortage, global change and greenhouse effect. The power production must be optimized while respecting hydraulic constraints on the rivers. The water levels are constrained within minimum and maximum values, and maximum rate of change for navigation purposes in particular.

River transportation is also gaining more attention from the mid-1990s, with a continuous increase in the volume of goods transported. The planning law on the implementation of the French Grenelle Environment Forum in 2009, confirmed the shift of freight from road transport to alternative modes, as a mean to reduce greenhouse gas emissions. The Rhône-Saône bassin is the second in France (after the Seine with about 3.9 M t-km) in terms of transportation of goods, with more than 1.28 M t-km. The project of Seine-North Europe 2020 is also a good illustration of this dynamic. River transportation generates specific disturbances (from locks maneuvers) and gives additional constraints to the river or canal managers, in terms or minimum water depth at certain locations, limitation of wave generated by hydraulic devices operations, and possible optimisation of flow conditions for boats consumption reduction. The operation of these locks (Fig. 3.1) is done using advanced remote and automated control procedures, and taken into account in the overall management of the hydraulic system (Fig. 3.2).

In a general control engineering context, the water management objectives include (1) to understand the behavior of natural (e.g., rivers) or manmade (e.g., irrigation canals) hydraulic systems, (2) to predict the behavior of the system over a future time horizon, and (3) to correct this behavior, if it is not considered as fully satisfactory. This latter corrective action has been done during millenniums through structural static changes (e.g., dams or weirs construction, river recalibration, sediment removal). The first hydromechanical devices based on floats and counter weights used extensively on irrigation canals world wide (e.g., AMIL, AVIS, AVIO or Mixte gates) have been built by the Neyrpic company created in 1917 in Grenoble, France. Since the early 1970s, this action over hydraulic systems is also done using dynamic operational devices and procedures (e.g., gates or weirs movements, using sensors and actuators). This is particularly true for irrigation canals where control gates can be manipulated in order to distribute water to users, at the right location, proper time and good quantity. These new technics for the automatic management of open-surface hydraulic systems promoted the development of advanced control algorithms, numerical simulation models and SCADA (Supervisory Control And Data Acquisition) technologies for their implementation. Different approaches have been developed during the latest decades [12]. Advanced techniques such as ℓ_1, LQG (Linear Quadratic Guaussian) or MPC (Model Predictive Control) proved their ability to control such complex MIMO (multi-input, multi-output) systems, taking into account different constraints, based on a hydraulic model and maximizing a given criteria.

Fig. 3.1 Lock on the Rhône river

Hydraulic models can be used in different manners, either just to test and validate controllers prior to implementation, to tune the controller parameters off-line, or used on-line, in real-time, to calculate the control action variables u, using measured variables z obtained from the real system, in order to achieve some objectives for some controlled variables y [12].

When a hydraulic system is under automatic control, whatever the control objectives are (supply of water, transportation, etc), detailed information on its hydraulic state must be available. This is also true for advanced remote manual control. Usually, the only known quantities are the measurements performed on the hydraulic system, at limited locations, with limited precision, and with possible sensor, data processing or communication failures. Detection of sensor drifts or breakdowns, or problems of actuators and estimation of unknown perturbations are also important issues. At present, no field implementation of real time estimation of the complete hydraulic state of a canal or river has been realized. Only data reconciliation for daily volumes, where dynamic effects can be neglected, has been carried out [5]. The main causes are the noisy character of the measurements, the size of the systems, the non-linearity of the cross-structure equations and open-channel dynamics and the lack of availability of corresponding robust and generic tools.

This chapter will describe a methodology and a mathematical framework to address this problem and to cope with some specific issues. In particular, the

Fig. 3.2 Operation of locks on the Rhône

convergence towards zero of the reconstruction error will be studied, and its link with the given problem to solve (configuration of the hydraulic network, location and number of sensors, measurement noise, etc). In order to illustrate them, they will be applied and tested on a case study: the Rhône river. This case study will be described in Sect. 3.2. The hydraulic model will be presented in Sect. 3.2.1. The mathematical framework that will be used to solve the problem is the Kalman filter presented in Sect. 3.2.2. This includes a mathematical test to check the convergence of the Kalman filter (or more precisely of the estimation error towards zero), called "a-posteriori" since it can be checked **after** the design of the Kalman filter. But, this test does not show the links between the convergence property and the problem setup, and is done after the Kalman design, which needs calculation efforts. We are then looking for an a-priori test, done **before** any Kalman design, keeping the links with the original problem setup. This test will be found and presented in Sect. 3.2.3. Then, the methodology and algorithms are tested on four different scenarii in Sect. 3.2.4, covering some of the more classical and interesting problems. Section 3.3 will give remarks on the use of such methodology and algorithms to feed the original problems of transport of water or transport over the water. Finally, before the conclusion, Sect. 3.4 will list some pending issues to be solved before this can be used in a generic operational tool, as well as some still opened scientific questions.

3.2 Case Study

The Rhône river is equipped, in its French portion, with 19 hydropower plants (Fig. 3.3) and 19 dams (Fig. 3.4) representing a total of 3 Giga Watts of installed power. They are spread over the 530 km of the Rhône river reaches, from the French-Switzerland boarder down-to the Mediterranean sea (Fig. 3.5). This represents 25 % of the French hydroelectricity production. The CNR is also managing 14 large gauge locks (Fig. 3.1) on the downstream part of the Rhône river, allowing communication within 29 industrial ports. The 19 hydropower plants along the Rhône river have always the same general pattern, with two convergent reaches, a linear branch and two diversion reaches. Among the two convergent or divergent reaches, one is the natural river equipped with hydraulic gates (Fig. 3.4), and the other one is the hydropower plant by-pass equipped with turbines. CNR was using PID type control algorithms during the end of the last century, and modernized progressively all 19 plants using Model Predictive Controllers (MPC) at the very beginning of this new century. Most of these 19 systems are now controlled, in real time, using predictive controllers based on a full Saint-Venant embedded model (named CRUE simulation model from CNR). The choice made for this MPC controller was to use a full Saint-Venant model, assuming that a good model was required in order to take several hydraulic effects that occur during normal or exceptional events (backwater

Fig. 3.3 Power generation on the Rhône river—Vallabrègues plant

Fig. 3.4 Dam gates on the Rhône river—Vallabrègues plant

effects, flooding to lateral major beds, tributaries inflows, change of bathymetry due to sedimentation, etc). Using such an advanced model have nevertheless some drawbacks: more data is required to set up the model (bathymetry, geometry of cross and lateral devices, friction coefficients, etc), more CPU time is required for its calculation, and with some hydraulic scenarios it can have numerical difficulties to be run (Fig. 3.5).

A portion of the Rhône River, between two hydropower plants managed by the Compagnie Nationale du Rhône (CNR), is selected for this study (Fig. 3.6).

3.2.1 The Open Channel Hydraulic Model

In order to be well founded, a state estimation must be based on a proper modeling of the physical system. Irstea (National Research Institute of Science and Technology for Environment and Agriculture) is developing methodologies and software tools (dedicated to academic partners, consultant companies and canal or river managers) allowing accurate hydrodynamic modeling [1]. The numerical tests carried out hereafter are run on the SIC^2 software developed by Irstea [2]. This model is based on the 1D Saint-Venant equations describing the dynamic behavior of water (flows and elevations) in an open-channel (3.1).

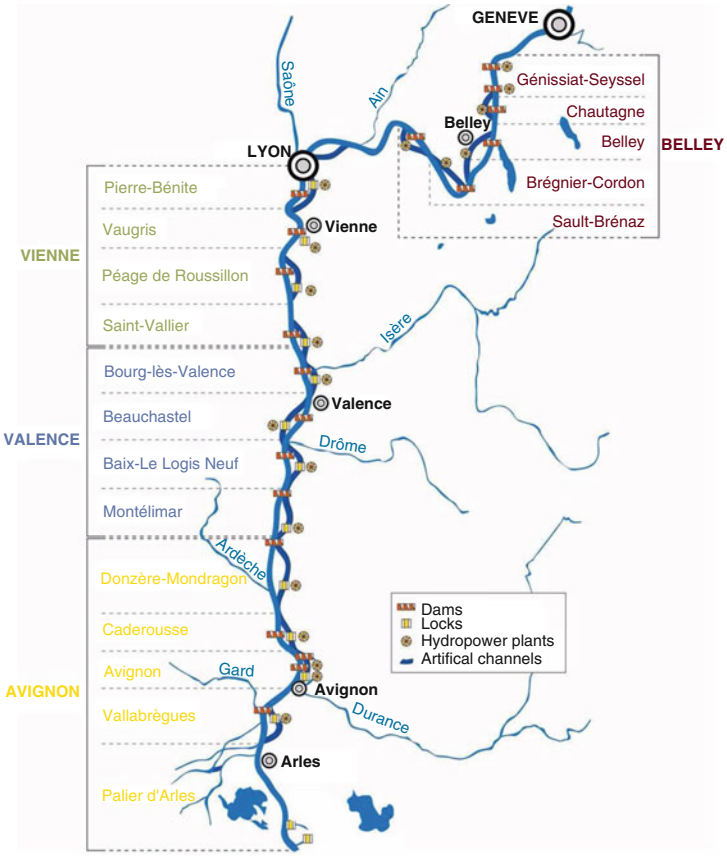

Fig. 3.5 Rhône river and its 19 hydropower plants

The 1D Saint-Venant equations are two hyperbolic, first-order, non-linear, partial-derivative equations:

$$\begin{cases} \frac{\partial S}{\partial t} + \frac{\partial Q}{\partial x} = q \\ \frac{\partial Q}{\partial t} + \frac{\partial \frac{Q^2}{S}}{\partial x} + g.S\frac{\partial Z}{\partial x} + g.S.J = q.\frac{Q}{S}, \end{cases} \tag{3.1}$$

where Q is the discharge (m^3/s), S the wetted cross-area (m^2), Z the water elevation (m), J the friction slope, q is the lateral inflow or outflow discharge linear rate (m^2/s), x the longitudinal abscissa (m) and t the time (s). The friction slope J is usually obtained from the Manning-Strickler formula: $J = \frac{n^2 Q^2}{S^2 R^{\frac{4}{3}}}$, where n is the Manning's coefficient ($K = \frac{1}{n}$ is called the Strickler coefficient) and R is the hydraulic radius (m) ($R = \frac{S}{P}$, where P is the wetted perimeter).

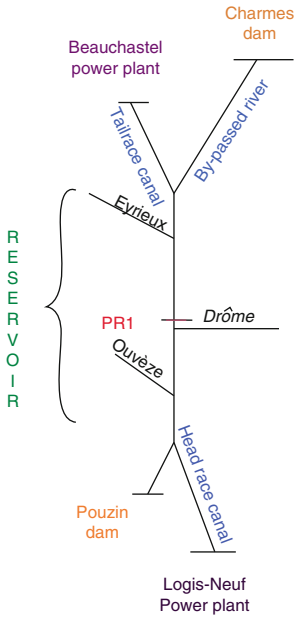

Fig. 3.6 Portion of the Rhône river between two hydropower plants

These equations are completed by external and internal boundary conditions such as upstream and lateral inflows, downstream rating curves and weir or gate equations. The equation of the flow through a gate structure is usually taken as:

$$Q = C_d \sqrt{2g} L u \sqrt{z_{up} - z_{dn}},$$

where C_d is the gate discharge coefficient, L the gate width, u the gate opening (m) and z_{up} (resp. z_{dn}) the water level upstream (resp. downstream) of the gate (m). More complex equations are usually used to handle different flow conditions (freeflow/submerged, open-flow/pipe-flow) in a continuous way [2].

Having no known analytical solution (in the general case), they are solved numerically, after being discretized in time (Δt time step) and space (Δx space step) through the implicit Preissmann finite difference scheme [3, 10]

$$\begin{cases} f(x,t) = \frac{\Theta}{2}(f_{i+1}^{n+1} + f_i^{n+1}) + \frac{1-\Theta}{2}(f_{i+1}^{n} + f_i^{n}) \\ \frac{\partial f}{\partial x} = \Theta \frac{f_{i+1}^{n+1} - f_i^{n+1}}{\Delta x} + (1-\Theta) \frac{f_{i+1}^{n} - f_i^{n}}{\Delta x} \\ \frac{\partial f}{\partial t} = \frac{f_{i+1}^{n+1} - f_{i+1}^{n} + f_i^{n+1} - f_i^{n}}{2\Delta t}, \end{cases} \tag{3.2}$$

The gate structure equation (3.2) is linearized and introduced at the proper locations in the numerical scheme. The double sweep method is used to solve the system of discretized equations and iterations are processed to solve the non-linear terms [3].

3.2.2 Kalman Filter Framework

Since the original work of Luenberger [9], state observers proved to be useful and are widely used in estimation and other engineering applications. It has been used in some cases for hydraulic systems [11]. In this line, the Kalman filter has dominated the applications in signal processing and control areas. It provides a minimum variance recursive algorithm to optimally estimate the unknown states of a dynamic linear system with Gaussian uncertainties. This type of filter is a set of mathematical equations which estimates the state vector at every time step [7, 8].

Linear State Space Model

The first step is to design an approximate linear model of the true system in state space form:

$$\begin{cases} x_k = Ax_{k-1} + Bu_{k-1} \\ y_k = Cx_k, \end{cases} \tag{3.3}$$

where A (state transition model), B (control-input model) and C (observation model) are real constant matrices of appropriate dimensions. They could also be varying depending on the current state estimate used for the linearization (A_k, B_k, C_k), leading to the extended Kalman filter framework.

The A matrix is obtained as $A = A_1^{-1}A_2$, where A_1 and A_2 are constructed from the discretization of the Saint-Venant equations (3.1), using the Preissmann implicit numerical scheme (3.2). The full non-linear model SIC^2 presented in the previous section and the linear state space model are therefore based on some similar principle, except that SIC^2 is using the double sweep algorithm, non-linear iterations and discretization updates, whereas the linear state space model is obtained by a simple matrix inversion and multiplication. This leads to a discrete-time state-space representation of the desired form [11].

The A_1 and A_2 matrices have both the following block diagonal structure:

$$A_2 = \begin{pmatrix} \lambda^{(up)} & & & & & & & & & & & \\ a_{11}^{(1)} & a_{12}^{(1)} & a_{13}^{(1)} & a_{14}^{(1)} & & & & & & & & \\ a_{21}^{(1)} & a_{22}^{(1)} & a_{23}^{(1)} & a_{24}^{(1)} & & & & & & & & \\ & & a_{11}^{(2)} & a_{12}^{(2)} & a_{13}^{(2)} & a_{14}^{(2)} & & & & & & \\ & & a_{21}^{(2)} & a_{22}^{(2)} & a_{23}^{(2)} & a_{24}^{(2)} & & & & & & \\ & & & & \cdots & \cdots & \cdots & \cdots & & & & \\ & & & & \cdots & \cdots & \cdots & \cdots & & & & \\ & & & & & & \cdots & \cdots & \cdots & & & \\ & & & & & & & a_{11}^{(n)} & a_{12}^{(n)} & a_{13}^{(n)} & a_{14}^{(n)} & \\ & & & & & & & a_{21}^{(n)} & a_{22}^{(n)} & a_{23}^{(n)} & a_{24}^{(n)} & \\ & & & & & & & & & & & \lambda^{(dn)} \end{pmatrix} \tag{3.4}$$

The x state vector is composed of hydraulic variables (discharges Q and water levels Z) at each calculation cross section, relative to some reference state (this is why we use the notation with δ variables). The parameters $\lambda^{(up,dn)} \in [0, \ldots, 1]$ depend on the choice of the discretization of the boundary conditions. In our example we used a time step $\Delta t = 300\,\mathrm{s}$ and a space step $\Delta x \approx 150\,\mathrm{m}$. This leads to a number of states $n_x \approx 300$.

$$x = \begin{pmatrix} \delta Q_1 \\ \delta Z_1 \\ \delta Q_2 \\ \delta Z_2 \\ \delta Q_3 \\ \delta Z_3 \\ \cdots \\ \cdots \\ \cdots \\ \delta Q_n \\ \delta Z_n \end{pmatrix}. \tag{3.5}$$

Since the state vector x includes explicitly the discharges at calculation cross sections, and since the control input variables u are, for example, the discharge boundary conditions upstream, downstream and at some intermediate tributaries, the B matrix is obtained easily by putting, for each column corresponding to a variable of the vector u, nil values at all lines except at locations where a discharge boundary conditions is imposed. Following the same principle, boundary conditions in terms of water elevation, or relationships between water elevations and discharges (rating curves) can also be imposed. For the same reason, the C matrix is also easily obtained, since measurements y are usually water elevations or discharges, that is to say components of the state vector x. In the following examples the number of input variables u is 7 (2 upstream discharges, three tributaries, one downstream discharge, one downstream rating curve) leading to a size of a B matrix of $n_x \times 7$. The size of the C matrix depends on the number of measurements. For the Scenario 4, presented hereafter, with three water level measurement this size is $3 \times n_x$.

In practice, a linear model is not a perfect representation of the reality and the measurements are not perfectly precise. This is the reason why noise is added to the process model and to the measurements. The linear stochastic difference equations become:

$$x_k = Ax_{k-1} + Bu_{k-1} + \eta_{k-1}, \tag{3.6}$$

with measurement equation:

$$y_k = Cx_k + \epsilon_k^o. \tag{3.7}$$

The random variables η_k and ϵ_k^o are assumed to be independent to each other, white, and with normal probability distributions:

$$\begin{aligned} P(\eta) &\sim N(0, Q) \\ P(\epsilon^o) &\sim N(0, R). \end{aligned} \tag{3.8}$$

The Q and R matrices can be time varying. In our simulations we took these matrices as time invariant and diagonal $R = diag(\sigma^2)$ with $\sigma = 2\,\text{cm}$ for water level measurements (in our scenarios we did not use discharge measurements), and $Q = diag(\sigma^2)$ with $\sigma_Z = 0.1\,\text{cm}$ for water level states and $\sigma_Q = 2\,\text{m}^3\text{s}^{-1}$ for discharge states.

Kalman Filter Equations

The equations for the Kalman filter are divided into two groups: time update equations and measurement update equations. The time update equations (3.9) project forward in time the current state X_{k-1}^a and error covariance estimates P_{k-1}^a to obtain the a priori estimates for the next time step X_k^b and P_k^b. The measurement update equation in (3.10) incorporate new measurements into the a priori estimate X_k^b to obtain an improved a posteriori estimate X_k^a. The a superscript stands for "analyzed" and b for "background" according to standard terminologies. The T superscript hereafter stands for the transpose operator. In the Kalman filter sections we will use the capital X and Y variable instead of the previous x and y since they can represent different variants of these variables (analyzed, background, true).

Discrete Kalman filter time update equations:

$$\begin{aligned} X_k^b &= AX_{k-1}^a + Bu_{k-1} \\ P_k^b &= AP_{k-1}^a A^T + Q. \end{aligned} \tag{3.9}$$

Discrete Kalman filter measurement update equations:

$$\begin{aligned} K_k &= P_k^b C^T (CP_k^b C^T + R)^{-1} \\ X_k^a &= X_k^b + K_k(Y_k - CX_k^b) \\ P_k^a &= (I - K_k C)P_k^b. \end{aligned} \tag{3.10}$$

These equations are simple matrix calculations, requiring little CPU time even for 300×300 matrices. The calculation can even be further reduced by using the asymptotic K_k matrix (obtained solving a Riccati equation) without loss of performance (this has been tested and verified, but not presented in this chapter).

Conditions for the Convergence of the Estimation Error of the Kalman Filter Towards 0

The analysis error of the Kalman filter can be written (where the t superscript stands here for "true" but unknown state vector):

$$\epsilon^a_{k+1} = X^a_{k+1} - X^t_{k+1}. \tag{3.11}$$

By using (3.10) into (3.11) we get:

$$\epsilon^a_{k+1} = X^b_{k+1} + K_{k+1}(Y_{k+1} - C_{k+1}X^b_{k+1}) - X^t_{k+1}. \tag{3.12}$$

Knowing the propagation of the model (3.6) and the relation of the Kalman filter (3.10), it is then possible to write (3.12) such as:

$$\begin{aligned}
\epsilon^a_{k+1} &= A_k X^a_k + B_k U_k + K_{k+1}(Y_{k+1} - C_{k+1}X^b_{k+1}) - A_k X^t_k - B_k U_k - \eta_k \\
&= A_k X^a_k + K_{k+1}(C_{k+1}X^t_{k+1} + \epsilon^o_{k+1} - C_{k+1}A_k X^a_k - C_{k+1}B_k U_k) - A_k X^t_k - \eta_k \\
&= A_k X^a_k + K_{k+1}(C_{k+1}A_k X^t_k + C_{k+1}B_k U_k + C_{k+1}\eta_k + \epsilon^o_{k+1} - C_{k+1}A_k X^a_k \\
&\quad - C_{k+1}B_k U_k) - A_k X^t_k - \eta_k \\
&= A_k X^a_k + K_{k+1}(C_{k+1}A_k X^t_k + C_{k+1}\eta_k + \epsilon^o_{k+1} - C_{k+1}A_k X^a_k) - A_k X^t_k - \eta_k \\
&= A_k(X^a_k - X^t_k) - K_{k+1}C_{k+1}A_k(X^a_k 0 - X^t_k) + K_{k+1}C_{k+1}\eta_k + K_{k+1}\epsilon^o_{k+1} - \eta_k \\
&= (A_k - K_{k+1}C_{k+1}A_k)\epsilon^a_k + K_{k+1}C_{k+1}\eta_k + K_{k+1}\epsilon^o_{k+1} - \eta_k.
\end{aligned} \tag{3.13}$$

The calculation of the mean value of the expression (3.13) gives the asymptotic value of the Kalman filter reconstruction error:

$$\begin{aligned}
E[\epsilon^a_{k+1}] &= E[(A_k - K_{k+1}C_{k+1}A_k)\epsilon^a_k + K_{k+1}C_{k+1}\eta_k + K_{k+1}\epsilon^o_{k+1} - \eta_k] \\
&= (A_k - K_{k+1}C_{k+1}A_k)E[\epsilon^a_k] + K_{k+1}C_{k+1}E[\eta_k] + K_{k+1}E[\epsilon^o_{k+1}] + E[\eta_k].
\end{aligned} \tag{3.14}$$

The hypothesis of the Kalman filter impose that the model and the measurement noises have a nil mean values. These hypothesis allow to simplify the relation (3.14) such as:

$$E[\epsilon^a_{k+1}] = (A_k - K_{k+1}C_{k+1}A_k)E[\epsilon^a_k]. \tag{3.15}$$

Moreover, (3.15) is equivalent to:

$$E[\epsilon^a_{k+1}] = (A_k - K_{k+1}C_{k+1}A_k)(A_{k-1} - K_k C_k A_{k-1}) \ldots (A_0 - K_1 C_1 A_0)E[\epsilon^a_0]. \tag{3.16}$$

In the case of an unbiased estimation, then we want to have the estimated error value converging towards 0, meaning $E[\epsilon^a_{k+1}] = 0$, or at least $E[\epsilon^a_{k+1}] \to 0$.

This means, either:

- the initial state is unbiased, meaning:

$$E[\epsilon_0^a] = 0, \tag{3.17}$$

- or

$$\lim_{k\to\infty} (A_k - K_{k+1}C_{k+1}A_k)(A_{k-1} - K_kC_kA_{k-1})\dots(A_0 - K_1C_1A_0) = 0. \tag{3.18}$$

The first condition (3.17) is satisfied when the initial "true" state (X_0^t) is perfectly known and the background state error ϵ_0^b is unbiased. These hypothesis are too strong and not realistic. This is why we will focus on the second condition (3.18) allowing to write a sufficient condition for the convergence of the filter:

$$\exists N \in \mathcal{N}, \forall k \geq N, \quad (A_{k-1} - K_kC_kA_{k-1}) \text{ Schur}^1 \Rightarrow E[\epsilon_k^a] \to 0. \tag{3.19}$$

In the time invariant case, when A, B, C, Q and R matrices are constant, this condition is easy to check, and the sufficient condition becomes

$$(A - KCA) \text{ Schur} \Rightarrow E[\epsilon_k^a] \to 0. \tag{3.20}$$

3.2.3 A-Priori Condition for Convergence

Theorem

The above condition, is a sufficient a-posteriori condition, that can be checked after the calculation of the Kalman filter gain K. But this calculation depends on the model and observation matrices (A, B and C) and on the covariance matrices of the model and observation errors (Q and R). We are looking for an a-priori condition, directly on the (A, B, C, Q and R), without calculation of the Kalman gain K. This will save calculation efforts and link the convergence properties directly to the model, observation and error characteristics.

In the time invariant case (A, B, C, Q and R matrices constant), by using the (3.10) the invariant covariance matrix P^b (if a solution exists) must satisfy the following stationary Riccati equation:

$$P^b = AP^bA^T + Q - AP^bC^T(R + CP^bC^T)^{-1}CP^bA^T. \tag{3.21}$$

[1] A square matrix A is said to be *Schur* stable if all its eigenvalues are strictly inside the unit circle on the complex plane. If A is the dynamical matrix of a discrete-time system, this correpsonds to a stable system. In continuous time the equivalent is a Hurwitz matrix.

From (3.10), we obtain P^a allowing to calculate the constant optimal gain:

$$K = P^a C^T R^{-1}, \tag{3.22}$$

and P^a and P^b matrices are linked by the following equation:

$$(P^a)^{-1} = (P^b)^{-1} + C^T R^{-1} C. \tag{3.23}$$

For this stationary systems, we have the following fundamental theorem [4]:

Theorem 3.1.
Given a pair (A, C) *detectable,*
Given a matrix Q*, factorizable in* $Q = \Gamma\Gamma^T$*, such as the pair* (A, Γ) *is stabilizable,*[2]
Given a matrix R *definite positive,*
Then the algebraic Riccati equation (3.21) has one and only one solution, positive P^b *and the matrix* $(A - KCA)$ *where* $K = P^a C^T R^{-1}$*, is an asymptotic stability matrix.*

Application

In other terms, for a detectable (A, C) stationary systems, since the matrix R represent observation noises, it is always positive. The condition is then to impose a matrix Q such that the pair (A, Γ) (with $Q = \Gamma\Gamma^T$) is stabilizable. We choose therefore to study the stabilizability of (A, Γ) for the Q we selected for the selected examples. We also do the same for a variation of Γ, in order to prospect the influence of the choice of Q on stabilizability of (A, Γ) and therefore on the convergence properties of the analyzed state error. This variation of Γ, is obtained by scaling the Q matrix with a multiplicative scalar λ, such as $Q_\lambda = \lambda Q = \lambda\Gamma\Gamma^T = (\sqrt{\lambda}\Gamma)(\sqrt{\lambda}\Gamma)^T = \Gamma_\lambda\Gamma_\lambda^T$ with $\Gamma_\lambda = \sqrt{\lambda}\Gamma$.

We observe that the pair (A, Γ_λ) of Example of scenario 3 with 8 water level measurements is not observable (Fig. 3.7) for the same conditions that when Q_λ is such that the gain K_λ does not lead to $(A - K_\lambda CA)$ Schur (Fig. 3.8). We can also observe from Fig. 3.8 that there is an optimal λ for which the largest eigenvalue is smaller. This is the value that gives the fastest convergence of the analyzed state error towards 0. In our example it is obtained for $\lambda = 10^1$. It comes out that this value gives a Q covariance matrix on the model errors that is more realistic than the initial one. What we also observe from Fig. 3.8 is that for small values of λ, meaning small Q_λ covariance matrix coefficients, meaning small model errors, the Kalman filter does not provide good convergence properties. Since the influence of

[2] A system is stabilizable when its non-controlable part (if any) is stable. The stabilizability and the detectability are two dual concepts.

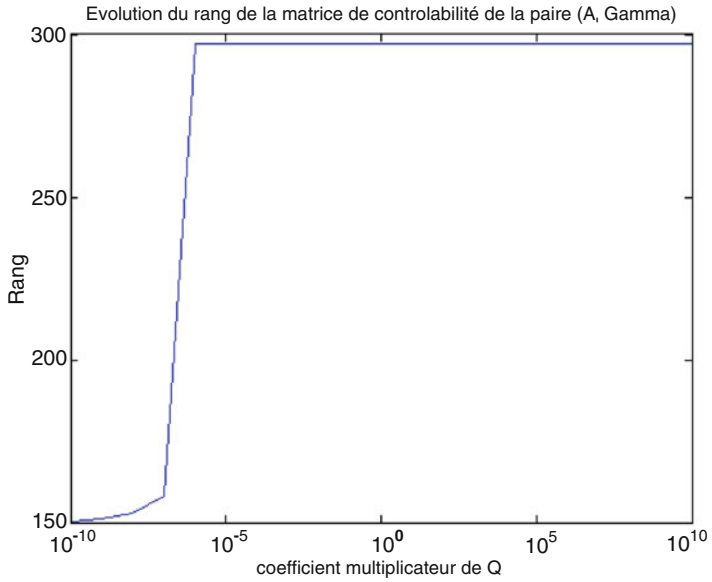

Fig. 3.7 Evolution of the rank from the pair (A, Γ_λ) for Example of scenario 3

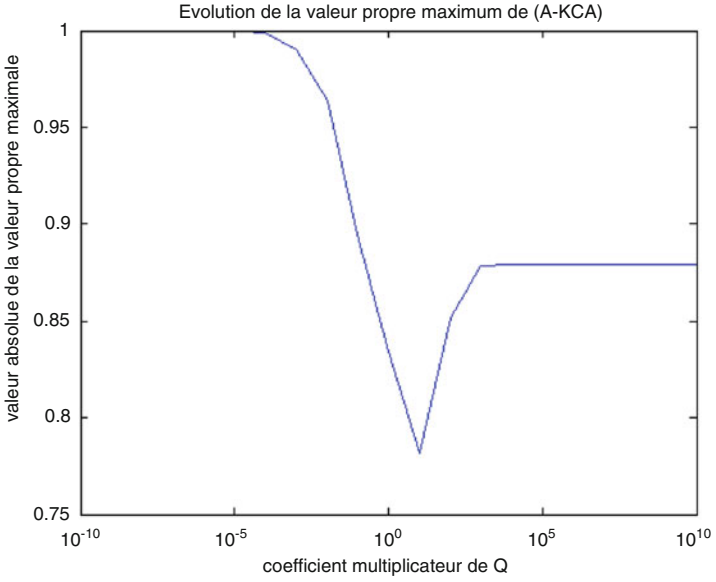

Fig. 3.8 Evolution of the largest eigenvalue of $(A - K_\lambda CA)$ for Example of scenario 3

the Q and R matrices are in fact acting in opposition, this can also be expressed as saying that for large observation errors (large R matrices), the Kalman filter does not provide good convergence properties. The analyzed state error will maybe converge towards something, but not towards 0.

We could also check the influence on the number and locations of the measurements on these convergence properties. For the Scenario 3 (reconstruction of unknown inflows simultaneously at two tributaries) we could observe that with only one water level measurement, the reconstruction error obtained from the Kalman filter never converges towards 0. With two measurements the reconstruction error from the Kalman filter converges only in the configurations when the measurements were not on the same upstream or downstream side on the two tributaries. For more than three measurements, the reconstruction error obtained from the Kalman filter always converged towards 0. This methodology can be used to look for the optimal location of sensors, and evaluate quantitatively the improvement provided by any additional sensor.

3.2.4 Test on Four Scenarios

A Kalman filter is designed and used to reconstruct unmeasured data on four scenarios, representative of real field situations. In these scenarios, the first three ones are based on twin experiences. This means that a first simulation is run to generate data. White noises are then added to the data. The second simulation is then done using the Kalman filter to reconstruct data and detect faults. For this latest phase, incomplete or wrong data can be given depending on the scenario.

During the three first scenarios that have been selected, the upstream hydropower plant is supposed to follow the discharge schedule as depicted on Fig. 3.9 showing $\pm 100\,\mathrm{m^3 s^{-1}}$ discharge variations around an initial value of $1{,}683\,\mathrm{m^3 s^{-1}}$. The other inflows are supposed to stay constant during the simulation: $10\,\mathrm{m^3 s^{-1}}$ at Charmes dam, $1\,\mathrm{m^3 s^{-1}}$ at Eyrieux, $5\,\mathrm{m^3 s^{-1}}$ at Drôme, $1\,\mathrm{m^3 s^{-1}}$ at Ouvèze, $999\,\mathrm{m^3 s^{-1}}$ at Logis-Neuf downstream power plant and $701\,\mathrm{m^3 s^{-1}}$ at Pouzin dam. In the fourth real scenario, upstream, downstream and inflow conditions are taken from the measurement database of CNR.

Scenarios 1: Convergence of the Filter from a Wrong Initial State

The first scenario aims at reconstructing the complete state vector x_k at any time instant k from an unknown (or false) initial state x_0. This is a realistic scenario, since when the Kalman filter is initialized, the real initial state vector x_0 is not known. An approximation can be guessed since the state vector components have physical meanings (water elevations and discharges along the system). But this guess is an approximation of the reality. We choose, in our twin experiences, a x_0 state vector corresponding to the correct initial steady state, and then we added errors of 0.1 m + white noise on water elevations and $100\,\mathrm{m^3 s^{-1}}$ + white noise on discharges. The whites noises are those described in the previous section. This initial

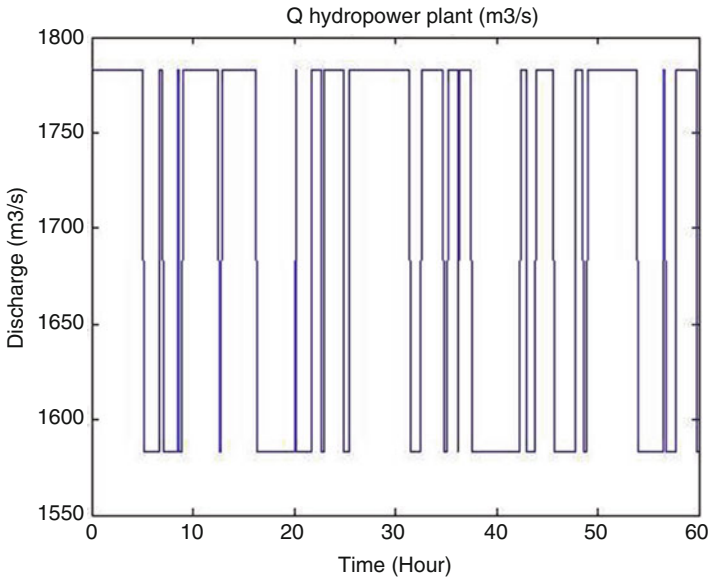

Fig. 3.9 Pumping flow at Beauchastel hydropower plant

state is really far from the true one: 0.1 m on the whole Rhône River corresponds to a very large volume difference to be cleared.

We can observe (Fig. 3.10) that the state $n°116$ corresponding to the water elevation at location PR1 (Fig. 3.6) is converging very quickly towards the real value (in less than 1 h). The convergence error is then kept minimum even in the presence of the white noise, at all calculation cross sections (this error is displayed at sections $n°25$, $n°116$ and $n°151$ on Fig. 3.11). The convergence rate is slower upstream of the system (water level at section $n°25$) compared to the downstream end of the system (water level at section $n°151$). This also implies larger bounds on the error. This is due to the fact that less measurement points are located at the upstream side of the system.

Scenarios 2: Fault Detection

The second scenario aims at detecting and correcting a sensor fault. In this scenario we suppose that the water level sensor at location PR1 (Fig. 3.6) has a drift of 7 cm from time 4 to 10 h. We can see on Fig. 3.12 that the re-estimation state at the sensor location is very close to the real value, despite the wrong measurement. The high frequencies changes on the graphs are due to the white noise added to the measurements. This sensor can then be detected as in default, and removed from the Kalman filter inputs. We observed in this case that the state reconstruction is even slightly improved (Fig. 3.13).

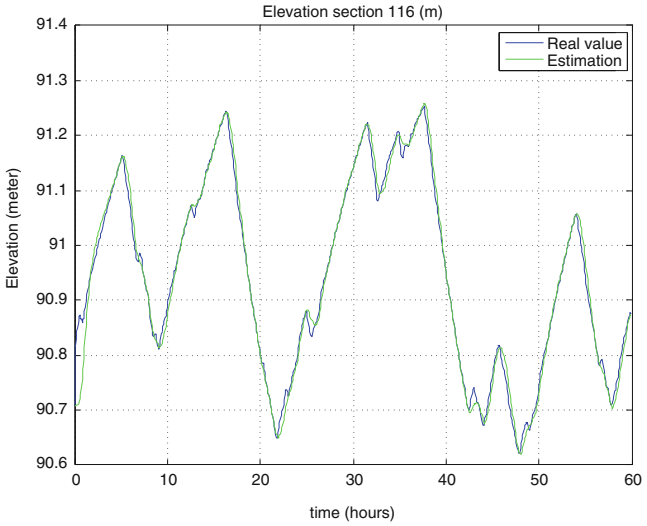

Fig. 3.10 Scenario 1. Convergence of state at section 116

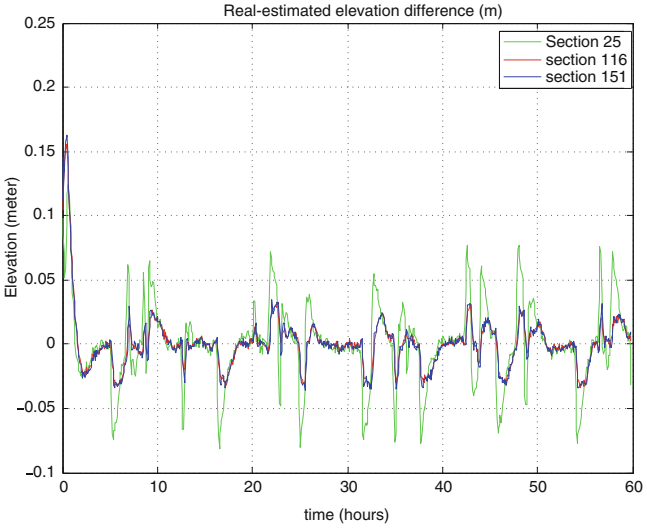

Fig. 3.11 Scenario 1. Convergence error of state at sections 25, 116 and 151

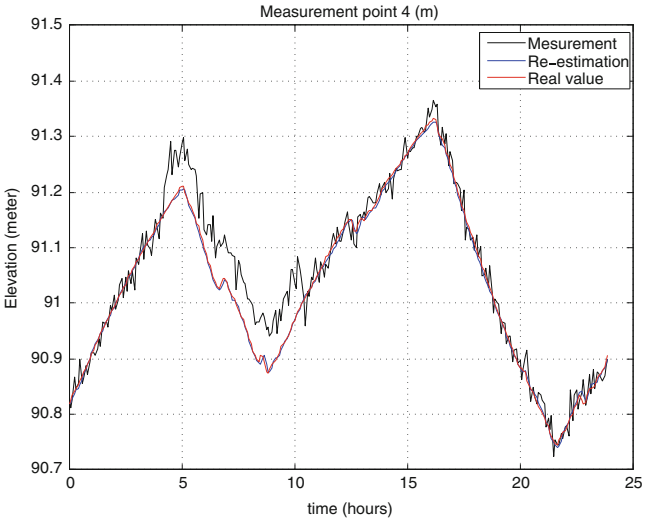

Fig. 3.12 Scenario 2. State estimation at sensor location

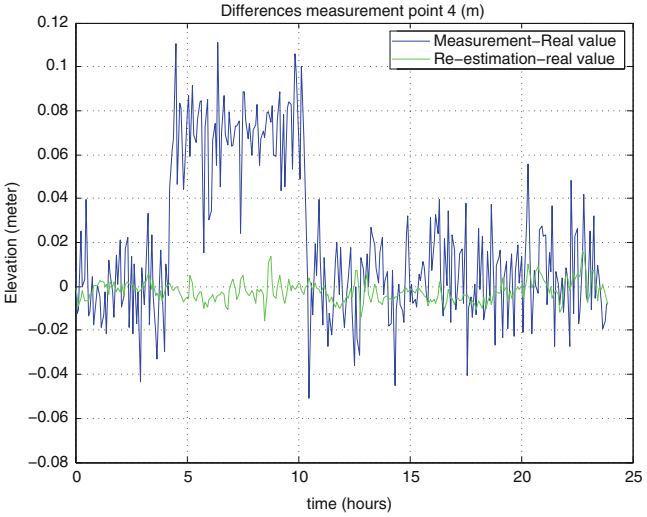

Fig. 3.13 Scenario 2. State estimation error at sensor location

Scenarios 3: Reconstruction of Unknown Inflows

The third scenario aims at reconstructing unknown inflows at Eyrieux (node 3) and Ouvèze (node 6) tributaries. We can observe on Fig. 3.14 that the inflows are correctly reconstructed.

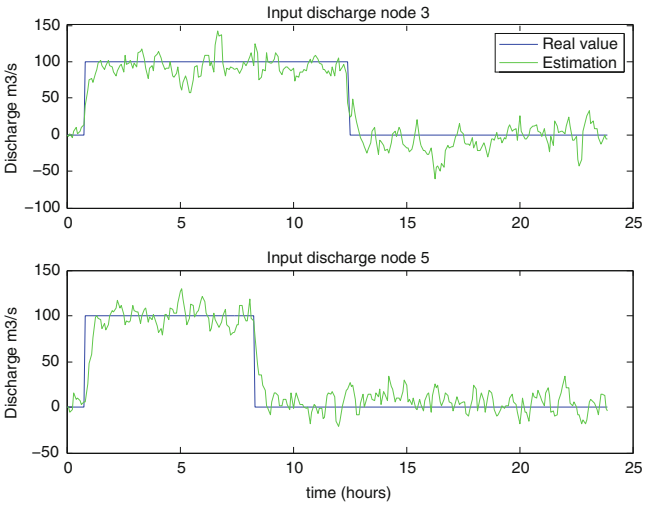

Fig. 3.14 Scenario 3. Differentiated inflow estimation

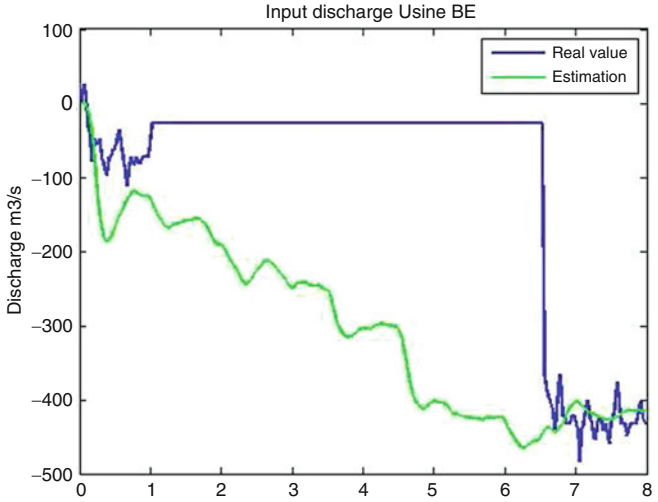

Fig. 3.15 Scenario 4. Reconstruction of inflow at upstream plant

Scenarios 4: Test on Real Field Data with a Sensor Failure

The fourth scenario using real data aims at reconstructing unknown upstream flows following sensors breakdowns. This is a realistic scenario, since even thought most sensors are redundant on the Rhône river, they can have simultaneous failures. This event really happened on the field in March 2009 (Fig. 3.15, sensor failure between time 1 h and 6h30). We can observe that the missing discharge measurement at

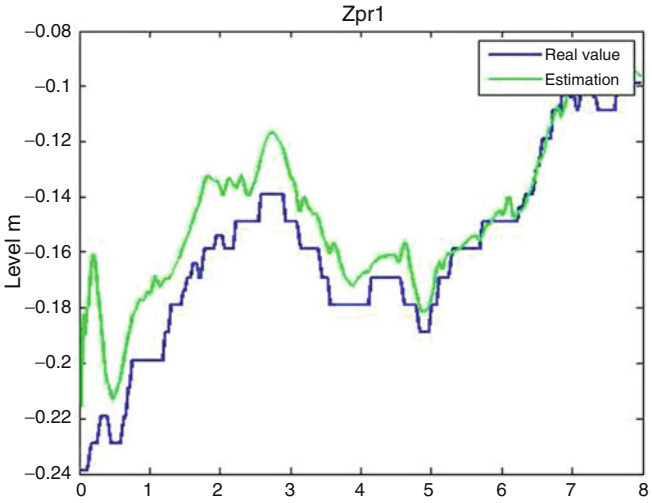

Fig. 3.16 Scenario 4. Reconstruction of water elevation at PR1

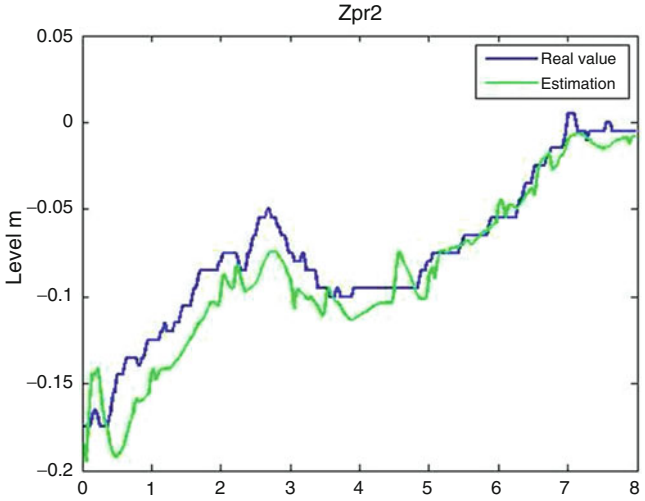

Fig. 3.17 Scenario 4. Reconstruction of water elevation at PR2

the upstream power plant (obtained using several water level and turbine position sensors located at this plant) is correctly reconstructed (Fig. 3.15), at least before and after the sensor failure, when the measured data is available for comparison, along with the water measurements at PR1 (Fig. 3.16) and PR2 (Fig. 3.17). This has been done using only three water level measurements at the upstream confluence, at PR1 and at PR2 (Fig. 3.6). We can observe that when the discharge measurement at the upstream power plant is functioning again after time 6h30 (Fig. 3.15) the estimated

values (discharge at the upstream plant, water levels at location PR1 and PR2) are very close to the measured ones. This validates the filter and lets us think that the estimated values of the discharge at the upstream plant is correct during the period when the sensors where in default.

3.3 Transdisciplinary Discussion

The specificities of considering the transport "of" or the transport "over" water are mainly appearing at the steps of the definition of the control algorithm, objectives, constraints, measurement points, and inputs and outputs of the controllers. What has been presented in this chapter is quite generic, and can be considered as an algorithmic and data processing layer placed before the control algorithms, and used to detect sensor problems, to reconstruct unknown states, inputs, or parameters [13]. The classical variables considered for the transport **of** water are mainly and usually water levels and discharges, sometimes volumes inside pools or reaches. We can think that in the case of transport **over** the water, the classical variables are water levels, change in water levels over time and velocities of the flow. This means that the soft sensors developed using data assimilation technics will rather focus on the first or the second list of variables depending on the application. When using the Saint-Venant 1D model used in what we presented in this chapter, this is not an important issue, since the model, either the linear or the non-linear one are encompassing all these variables. The classical variables used are water levels and discharges, but all other variables can be obtained from these basic ones.

3.4 Open Topics

The algorithm presented here are based on linear Kalman filters. This Data Assimilation technic proved to be efficient in many cases, as illustrated in this chapter and in cited publications. The advantage of this technic is also to provide simple mathematical tests to evaluate if the data assimilation is providing good results or not. These tests are based on the convergence of the reconstruction error between the true (unknown) state X^t and the estimated state X^a. If these tests are not satisfied, then we know that the Kalman filter in itself will converge as usual (K_k, P_k^a and P_k^b matrices are converging towards some bounded values), along with the estimated reconstruction error $X_k^a - X_k^t$, but towards a solution that is not satisfactory in the sense that this reconstruction error is not converging towards 0, within the linear assumption. On the other side, if these tests are satisfied (either the a-posteriori one, or the a-priori one) we can expect satisfactory results, meaning a reconstruction error converging towards 0. But this is true only if the assumption made on the model and measurement noises are valid. If the non-linearities are strong, then the reconstruction error can still present permanent errors. In this case, more advanced

technics can be tested and used. The simplest extension of this work is extended Kalman filter, where the estimated state is propagated using the full non-linear model instead of the simplified linear one. Another more advanced technic is to use a full non-linear technic such as 4D-Var. This has been tested and compared with Kalman filter in some more difficult configurations as presented in [13] (these results obtained with 4D-Var were not available yet for the chapter but were presented at the oral presentation at the HIC2014 conference and also at an internal Irstea seminar [6]). The verification of the well-posedness of the problem and of the convergence of the 4D-Var algorithm are also possible using the Hessian. We have been also using Monte-Carlo particle filter methods also handling non-linear features, with good results [14]. But this method, along with others in the family of ensemble based methods (ensemble Kalman filter, Unscented Kalman filter), are based on many simulations, which can be a problem in some cases for real-time control applications. Indeed in usual contextes, the control time step can be of a few minutes (e.g., 100 s at the Compagnie Nationale du Rhône, 15 min at the Société du Canal de Provence). An other issue is the number and location of the variables that can be estimated using a given number and locations of measurements. We have already tested some combinations, such as hydraulic states (elevations Z and discharges Q), tributaries inflows or outflows, and cross device discharge coefficients. We are also working at estimating friction coefficients and bathymetry. But this is true that there are limits to the results we can expect from these algorithms, if we ask too much with too little measurements (both spatially and in time sampling). Fortunately, there are mathematical tools allowing to verify the convergence properties prior to any implementations, as the one presented in this chapter. One classical approach is also to generate and configure different algorithms (e.g., different Kalman filters or different 4D-Var problems) more focussed on one or several limited aspects, instead of trying to generate a complete algorithm detecting and correcting everything all together.

3.5 Conclusions and Future Research

In this chapter, we have proposed an approach allowing to estimate, in real time, the hydraulic state of a river reach from measurements. One can understand that this knowledge of the hydraulic state is of first importance in the current context of water resources management. The results are very good with both approaches. The Kalman filter is converging very quickly and requires few CPU time. This makes it compatible with real time control constraints, even for large systems with several hundreds of state variables. This filter can handle all type of scenarios: initialization, sensor fault, reconstruction of unmeasured inflows of tributaries. The method can be extended to the estimation of physical parameters related to the current state of the river or canal such as friction parameters. Another advantage of the Kalman filtering approach is the possibility to study its mathematical properties using well based mathematical criteria.

References

1. Baume J-P, Sau J, Malaterre P-O. Modeling of irrigation channel dynamics for controller design. In: Proceedings of the Ieee international conference on systems, man and cybernetics (SMC98), San Diego, California, 11–14 Oct 1998.
2. Baume J-P, Malaterre P-O, Belaud G, Le Guennec B. Métodos Numéricos em Recursos Hidricos 7, ABRH (Associacao Brasileira de Recursos Hidricos), chapter. SIC: a 1D hydrodynamic model for river and irrigation canal modeling and regulation. Brazilla: Coppetec Fundacao; 2005.
3. Cunge JA, Holly FM, Verwey A. Practical aspects of computational river hydraulics. London: Pitman Advanced Publishing Program; 1980.
4. de Larminat P. Automatique, Commande des systèmes linéaires. 2nd ed. Paris: Hermès; 1996.
5. Deltour J-L, Canivet E, Sanfilippo F, Sau J. Data reconciliation on the complex hydraulic system of canal de provence. J Irrig Drain Eng. 2005;131(3):291–7.
6. Gejadze I, Malaterre P-O. Prise en compte d'incertitudes paramétriques dans un modèle hydraulique 1D pour résoudre un problème inverse 4D-var avec l'adjoint. In: Séminaire mesure, Irstea Antony, 15–16 Sept 2014.
7. Jean-Baptiste N. Assimilation de données pour l'estimation de l'état hydraulique d'un aménagement hydroélectrique du Rhône équipé de la commande prédictive. Ph.D. thesis. Toulouse, France: Université Paul Sabatier; 2011.
8. Jean-Baptiste N, Malaterre P-O, Dorée C, Sau J. Data assimilation for real-time estimation of hydraulic states and unmeasured perturbations in a 1D hydrodynamic model. J Math Comput Simul. 2011;81(10):2201–14.
9. Luenberger DG. Computational methods for resolution of mass spectra. Anal Chem. 1966;38(6):715–20.
10. Malaterre P-O. Modélisation, analyse et commande optimale LQG d'un canal d'irrigation. Ph.D. thesis. Paris, France: LAAS - CNRS - ENGREF - Cemagref; 1994.
11. Malaterre P-O. PILOTE: linear quadratic optimal controller for irrigation canals. ASCE J Irrig Drain Eng. 1998;124(4):187–94.
12. Malaterre P-O, Rogers DC, Schuurmans J. Classification of canal control algorithms. ASCE J Irrig Drain Eng. 1998;124(1):3–10.
13. Malaterre P-O, Dorchies D, Baume J-P. Estimation of offtake discharge and cross-device parameters using data assimilation for the automatic control of an irrigation canal. In: Proceedings of the hydroinformatics conference, New York, 17–21 Aug 2014.
14. Sau J, Malaterre P-O, Baume J-P. Sequential Monte Carlo hydraulic state estimation of an irrigation canal - estimation de l'état hydraulique d'un canal d'irrigation par une méthode Monte Carlo séquentielle. Compte Rendu de l'Académie des Sciences - Mécanique. 2010;338:212–9.

Chapter 4
Distributed LQG Control for Multiobjective Control of Water Canals

J.M. Lemos and I. Sampaio

Abstract This chapter addresses distributed LQG control of multipurpose open water channels, used both for water delivery and vehicle transportation. The use of a local control agent structure of the so called local upstream control type ensures that the water level is kept close to a desired level, even in the presence of disturbances caused by water turnout at side offtakes, so as to ensure navigability. Local control agents are modified LQG controllers coupled with a nonlinear compensation of the nonlinearities induced by the gates nonlinear models. The coordination among local controllers is achieved through an algorithm based on game theory that drives the local decisions to a Nash equilibrium. Experimental results in a large scale pilot canal are included to demonstrate the control concepts proposed.

4.1 Introduction

Several open water channels may be used both as water delivery channels, e.g., as a means to carry water for irrigation, and/or as a navigation mean. Depending on the operational objectives, different control structures may be employed on these systems. While on a water delivery canal dedicated to irrigation the main purpose might be to save water, implying the use of distant upstream control or of its variants [1], other choices are preferred if the major aim is to ensure a desired water level to allow navigation and simultaneously use part of the water for irrigation. In this last case, local upstream control [1] might be an option since it yields a fast rejection of disturbances induced by water turnout at side offtakes.

On the other way, the complexity of large scale water channel systems [2], together with requirements on reliability and quality of service specifications, provide a strong motivation to consider fault tolerant control methods for this type of systems. The idea consists of exploring the redundancy in their sensors and

J.M. Lemos (✉)
INESC-ID/IST/Universidade de Lisboa, R. Alves Redol 9, 1000-029 Lisboa, Portugal

I. Sampaio
INESC-ID/IST/Universidade de Lisboa, Lisbon, Portugal
e-mail: jlml@inesc-id.pt; inesgcsampaio@gmail.com

C. Ocampo-Martinez, R.R. Negenborn (eds.), *Transport of Water versus Transport over Water*, Operations Research/Computer Science Interfaces Series 58,
DOI 10.1007/978-3-319-16133-4_4

actuators to reconfigure the control system such as to allow the plant operation to continue, perhaps with some graceful degradation, when a sensor or actuator fails. Furthermore, instead of using a centralized controller, where a single processing unit receives all the information and sends the commands to all the actuators, there is a growing trend to consider a network of distributed control agents that negotiate among themselves in order to reach a consensus on the value of the different manipulated variables.

The concept of fault tolerant control (FTC) has been the subject of intense research in the last 20 years [3–5]. This activity yielded a rich bibliography that, of course, cannot be covered here and that comprises aspects such as fault detection and isolation and fault tolerant control design. In what concerns distributed control an important concept is "integrity", namely the capacity of the system to continue in operation when some part of it fails [6]. Other type of approach models the failures as disturbances that are estimated and compensated by the controller [7].

No attempt is made here to review the extensive bibliography that exists, on one side, on the control of water delivery canals, and on the other side on reconfigurable and fault tolerant control. Instead, we just point out a few references that provide a framework for the approach followed here. In what concerns water delivery canal systems, a topic that receives attention due to their immediate economic impact related to water saving is leak detection [8]. Other aspects found in the literature are control loop monitoring [9], and reconfiguration to mitigate fault effects [10], which is the issue considered in this work. Reconfiguring the controller in face of a plant fault falls in the realm of hybrid systems and raises issues related to stability that must be taken into account [11].

This chapter describes a fault tolerant distributed controller for a multi-use water channel. Although, due to its dimensions, the channel may not be used for navigation, it is operated as if it could be.

4.2 Case Study

Hereafter we present a case study that illustrates the type of control proposed. The canal used is a pilot facility that has the advantage of illustrating through experimental results the performance of the algorithms described. The canal is first described, together with the faults considered. Then, the distributed controller proposed is explained, including:

- The plant model used for control design;
- The local controllers;
- The coordination algorithm.

4.2.1 Canal and Fault Description

The work reported in this chapter was performed at the experimental canal of *Núcleo de Hidráulica e Controlo de Canais* (Universidade de Évora, Portugal), described in [12]. The canal has four stretches with a length of 35 m, separated by three undershoot gates, with the last stretch ended by an overshoot gate. In this work only the first three gates are used. The maximum nominal design flow is $0.09\,\mathrm{m^3 s^{-1}}$. There are water off-takes downstream from each branch made of orifices in the channel walls, that are used to generate disturbances corresponding to water usage.

Water level sensors are installed downstream of each pool. The water level sensors allow to measure values between 0 and 900 mm, a value that corresponds to the canal bank. For stretch number i, $i = 1, \ldots, 4$, the downstream level is denoted y_i and the opening of gate i is denoted u_i. stretch number i ends with gate number i.

Each of the actual gate positions $u_{r,i}$, $i = 1, 2, 3$ are manipulated by a command signal u_i. However, the PLCs that command gate motors are programmed such that $u_{r,i}$ only moves in response to u_i if $|u_i - u_{r,i}| \geq 0.5$ mm. This dead zone nonlinearity has two types of implications. First of all, it limits the controller achievable precision when tracking a reference and may even induce small amplitude oscillations. Furthermore, when comparing the signals u_i and $u_{r,i}$ in order to detect a fault, this difference must be taken into consideration.

Following [2], in order to compensate for a nonlinearity, instead of using as manipulated variable the gate positions $u_{r,i}$, the corresponding water flows q_i crossing the gates are used. These are related by

$$q_i = C_{ds} W u_{r,i} \sqrt{2g(h_{ups,i} - h_{dwns,i})}, \tag{4.1}$$

where C_{ds} is the discharge coefficient, W is the gate width, $g = 9.8$ m/s is the gravity acceleration, $h_{ups,i}$ is the water level immediately upstream of the gate and $h_{dwns,i}$ is the water level immediately downstream of the gate. This approach corresponds to represent the canal by a Hammerstein model and to compensate the input nonlinearity using its inverse. The linear controller computes the flow crossing the gates, that is considered to be a virtual command variable v_i and the corresponding gate position is then computed using (4.1). The discharge coefficient is not estimated separately, but instead is considered to be incorporated in the static gain of the linear plant model.

The faults to be considered consist of either manipulated variable or sensor isolated faults. Manipulated variable faults consist of the blockade of gate number 2. When a fault occurs, the position of gate 2 remains constant and does not change anymore in response to the corresponding command signal. Sensor faults consist of the signal issued by the y_2 becoming stuck at its maximum value. It is assumed that no multiple faults occur. Furthermore, since the focus of the work is on controller reconfiguration and not on fault isolation, we consider the simplified situation in which the fault type is a priori known.

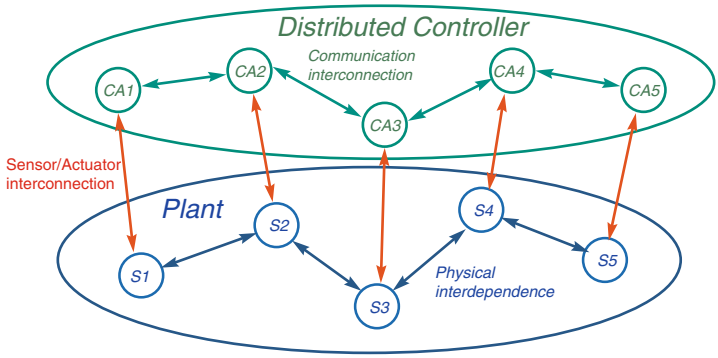

Fig. 4.1 Graphs representing the interrelation of a distributed process with a distributed controller

4.2.2 Distributed LQG Control

In distributed control the plant model is assumed to be represented by a graph (see Fig. 4.1) with nodes associated to physical agents that have bonds among them that reflect physical interdependencies and are associated to edges. Correspondingly, the distributed controller is described by a graph whose edges are local control agents and whose edges are associated to communication interconnection links. The distributed controller network and the graph network that represents the plant are interconnected by sensors and actuators. A local control agent (or control agent for short) is a software entity that has the following three components:

- A feedback controller that, given the data from the sensors and the local decision unit, computes the sinal commands to the actuators.
- A communication unit, that is able to interchange data with other (neighbor) control agents; this data is made of sensor measures and of (possibly potential) decisions about the local manipulated variable.
- A local decision unit, provided with a coordination algorithm, that is able to modify the value of the manipulated variables computed by the local controller on the basis of pure local feedback.

Each of these elements is described hereafter in this section for the water channel considered.

Around an equilibrium point, the plant is represented by linear state-space models written as

$$x(k+1) = Ax(k) + Bv(k), \tag{4.2}$$

$$y(k) = Cx(k), \tag{4.3}$$

where $k \in \mathbb{N}$ denotes discrete time, $x \in \mathbb{R}^n$ is the full canal state, $y \in \mathbb{R}^p$ is the output, with p the number of outputs, $v \in \mathbb{R}^p$ is the manipulated variable and

$A \in \mathbb{R}^{n\times n}$, $B \in \mathbb{R}^{n\times 3}$ and $C \in \mathbb{R}^{3\times n}$ are matrices. Assuming operation around a constant equilibrium point, and no fault conditions, these matrices are identified by constraining the model to have the following structure:

$$A = \begin{bmatrix} A_{11} & \underline{0} & \underline{0} \\ \underline{0} & A_{22} & \underline{0} \\ \underline{0} & \underline{0} & A_{33} \end{bmatrix}, \quad B = \begin{bmatrix} B_{11} & B_{12} & \underline{0} \\ B_{21} & B_{22} & B_{23} \\ \underline{0} & B_{32} & B_{33} \end{bmatrix},$$

$$C = \begin{bmatrix} C_1 & \underline{0} & \underline{0} \\ \underline{0} & C_2 & \underline{0} \\ \underline{0} & \underline{0} & C_3 \end{bmatrix}. \tag{4.4}$$

The block matrices in (4.4) have dimensions that match the state x_i associated to each stretch such that $x = [x_1' \; x_2' \; x_3']'$.

In the presence of a fault, the matrices have the structure

$$A = \begin{bmatrix} A_{11}^F & \underline{0} \\ \underline{0} & A_{33}^F \end{bmatrix}, \quad B = \begin{bmatrix} B_{11}^F & B_{13}^F \\ B_{31}^F & B_{22}^F \end{bmatrix},$$

$$C = \begin{bmatrix} C_1^F & \underline{0} \\ \underline{0} & C_3^F \end{bmatrix}. \tag{4.5}$$

The superscript F enhances the fact that the matrix blocks are estimated assuming that a fault has occurred and that they are different from the ones in (4.4). This structure is imposed to reflect the decomposition of the canal model in subsystems, each associated to a different pool. Furthermore, it is assumed that each stretch interacts directly only with its neighbors, and only through the input.

From the global multivariable model (4.2) and (4.3), each stretch i is represented by the state model with accessible disturbance d_i

$$x_i(k+1) = A_{ii}x_i(k) + B_{ii}v_i(k) + d_i(k), \tag{4.6}$$

where

$$d_1(k) = B_{12}v_2(k), \tag{4.7}$$

$$d_2(k) = B_{21}v_1(k) + B_{23}v_3(k), \tag{4.8}$$

and

$$d_3(k) = B_{32}v_2(k). \tag{4.9}$$

Augmenting each local model $\mathcal{S}_i$ with a parallel integrator yields the augmented state-space local model

$$\bar{x}_i(k+1) = \bar{A}_{ii}\bar{x}_i(k) + \bar{B}_{ii}v_i(k), \tag{4.10}$$

$$y = \bar{C}\bar{x}(k), \tag{4.11}$$

where $\bar{x}_i$ is the augmented state of the local model, given by

$$\bar{x}(k) = \begin{bmatrix} x_i(k) \\ x_{I,i}(k) \end{bmatrix}, \tag{4.12}$$

with $x_{I,i}$ the state of the integrator added to the local model $\mathcal{S}_i$, and

$$\bar{A}_{ii} = \begin{bmatrix} A_{ii} & \underline{0} \\ -T_s C_i & 1 \end{bmatrix}, \quad \bar{B}_{ii} = \begin{bmatrix} B_{ii} \\ 0 \end{bmatrix}, \quad \bar{C}_i = \begin{bmatrix} C_i & \underline{0} \end{bmatrix}. \tag{4.13}$$

Since this realization is not observable, only x_i is estimated, using the estimator that depends only on variables available locally for control agent $\mathcal{C}_i$

$$\hat{x}_i(k|k-1) = A_{ii}\hat{x}_i(k-1|k-1) + B_{ii}u_i(k-1), \tag{4.14}$$

$$\hat{x}_i(k|k) = \hat{x}_i(k|k-1) + M_{p,i}[y_i(k) - C_i\hat{x}_i(k|k-1)], \tag{4.15}$$

where the $M_{p,i}$ are kalman gains, that depend on the solution of an algebraic Riccati equation. The manipulated variable is then given by

$$v_i(k) = -K_{x,i}\hat{x}_i(k|k) - K_{I,i}x_{I,i}(k), \tag{4.16}$$

where

$$K_i = [K_{x,i} \;\; K_{I,i}] \tag{4.17}$$

is obtained by solving a LQ problem that consists of minimizing the steady state quadratic cost

$$J_i = \sum_{k=1}^{\infty} \bar{x}_i^T(k) Q_i \bar{x}_i(k) + \bar{u}_i^T(k)\rho_i \bar{u}_i(k), \tag{4.18}$$

with

$$Q_i = \begin{bmatrix} C_i^T C_i & \underline{0} \\ \underline{0} & 1 \end{bmatrix}, \tag{4.19}$$

and $\rho_i > 0$ a design parameter, and is given by the expression

$$K_i = (I + \frac{1}{\rho_i}\bar{B_{ii}}^T P_{ii}\bar{B_{ii}})^{-1}\frac{1}{\rho_i}\bar{B}_{ii}^T P_i \bar{A}_{ii}, \tag{4.20}$$

in which P_i is the positive definite solution of the algebraic Riccati equation

$$P_i = \bar{A}_{ii}^T P_i [I + \bar{B}_{ii}\frac{1}{\rho_i}\bar{B}_{ii}^T P_i]^{-1}\bar{A}_{ii} + Q_i. \tag{4.21}$$

When using distributed control, each gate is manipulated by a SISO controller that selects its moves so as to drive the corresponding water level to the reference value. In addition, there is a correction to achieve a coordinated action. The coordination among controllers is performed by the following algorithm.

Coordination Algorithm

At the beginning of each sample time, compute $v_{i,0}(k)$ *by solving a LQG problem associated to model (4.6) and assuming* $d_i(k) = 0$.
For $j = 1$ *up to* $j = N_c$ *recursively perform the following cycle*

1. *For* $i = 1, 2, 3$, *compute* $d_{i,j-1}(k)$ *using (4.7)–(4.9) with* $v_i(k)$ *replaced by* $v_{i,j-1}(k)$;
2. *For* $i = 1, 2, 3$, *compute* $v_{i,j}(k)$ *by solving a LQG problem associated to model (4.6)*;

Apply to the plant the control given by

$$v_i(k) = v_{i,j}(k). \tag{4.22}$$

4.2.3 Controller Reconfiguration

In response to a fault that inhibits the action of one of the local control agents (either missing communication links, or a sensor or actuator fault) the strategy proposed consists in the reconfiguration of the distributed controller network that consists in the activation of new communication links, together with the redefinition of the control objectives that will probably suffer some degradation.

Assume, as an example, the situation shown in Fig. 4.2 in which the actuator associated to the local control agent CA3 fails. After the moment in which this fault is detected, the local agents CA2 and CA4, that are neighbors to CA3, no longer negotiate with this agent, but start negotiating directly among themselves the value of their respective manipulated variables. Furthermore, the control objectives that depend directly on CA3 may no longer be attainable. For instance, if the plant is

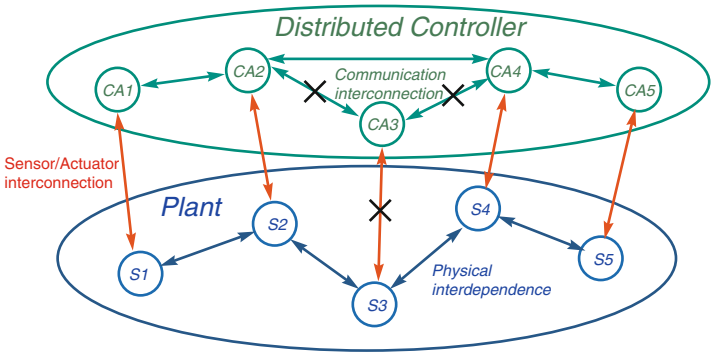

Fig. 4.2 Graph reconfiguration in response to a fault

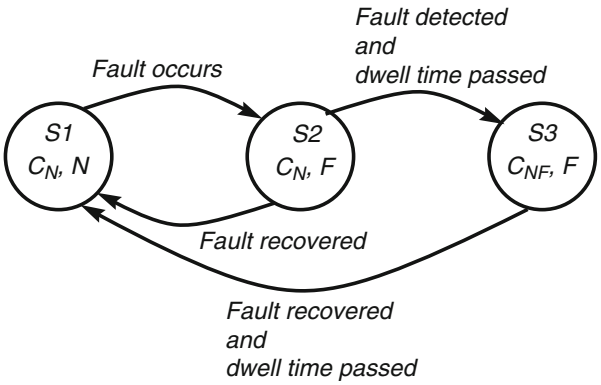

Fig. 4.3 Discrete states in controller reconfiguration

a water channel and the actuators associated to the control agents are gates, it is no longer possible to control with precision the level associated to the gate that corresponds to CA3.

Actuator Faults

Figure 4.3 shows a discrete state diagram that explains how controller reconfiguration is performed when an actuator fault occurs in the water channel considered in this chapter. For simplicity, only the occurrence of faults in gate 2 are considered. State $\mathcal{S}_1$ corresponds to the situation in which all gates are working normally with a controller $\mathcal{C}_N$ that matches this situation. When a fault occurs, the system state switches to $\mathcal{S}_2$, in which gate 2 is faulty (blocked) but the controller used is still the one designed for the no fault situation.

When the fault is detected, the state switches to $\mathcal{S}_3$, in which a controller $\mathcal{C}_F$ designed for the faulty situation is connected to the canal. When the fault is recovered (gate 2 returns to normal operation), the state returns to $\mathcal{S}_1$. A dwell time condition is imposed to avoid instability that might arise due to fast switching [13]. This means that, once a controller is applied to the plant, it will remain so for at least a minimum time period (called dwell time).

When distributed control is used, the controller designed for normal operation (shown in Fig. 4.4), $\mathcal{C}_N$, consists of three SISO LQG controllers $\mathcal{C}_1$, $\mathcal{C}_2$ and $\mathcal{C}_3$, each regulating a stretch and such that each individual controller negotiates the control variable with its neighbors. This means that, in states $\mathcal{S}_1$ and $\mathcal{S}_2$, $\mathcal{C}_1$ negotiates with $\mathcal{C}_2$, $\mathcal{C}_2$ negotiates with $\mathcal{C}_1$ and with $\mathcal{C}_3$ and $\mathcal{C}_3$ negotiates with $\mathcal{C}_2$. The controller for the faulty condition (shown in Fig. 4.5) is made just of two SISO controllers that control stretches 1 and 3 and negotiate with each other.

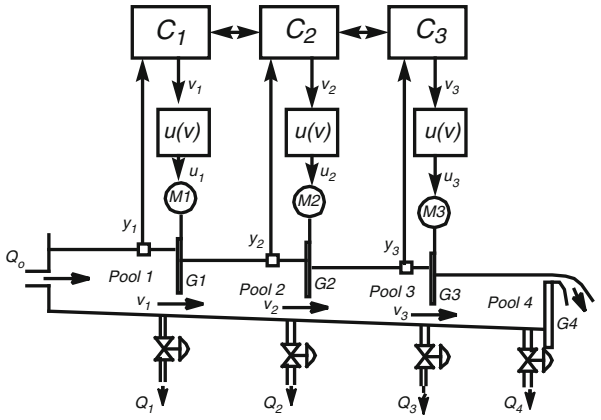

Fig. 4.4 Distributed controller in normal (no fault) operation

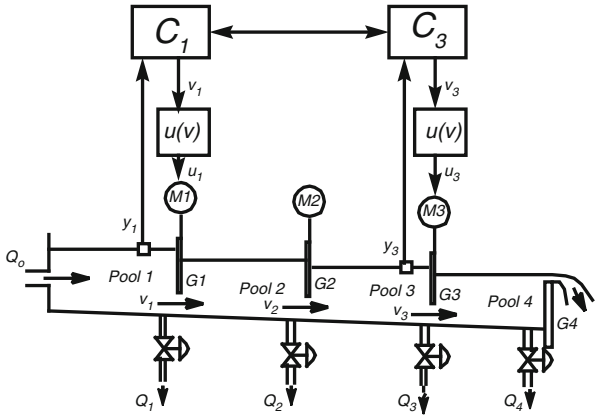

Fig. 4.5 Distributed controller after a fault is detected

A bumpless transfer algorithm is used in order to ensure the continuity of the manipulated variable command applied to the gates when there are switching among controllers.

For actuator faults, the fault detection algorithm operates as shown in the block diagram of Fig. 4.6. For each gate i, $i = 1, 2, 3$, define the error $\tilde{u}_i$ between the command of the gate position u_i and the actual gate position $u_{r,i}$ by

$$\tilde{u}(k) = u_i(k) - u_{r,i}(k). \tag{4.23}$$

A performance index Π is then computed from this error by

$$\Pi(k) = \gamma\Pi(k-1) + (1-\gamma)|\tilde{u}(k)|. \tag{4.24}$$

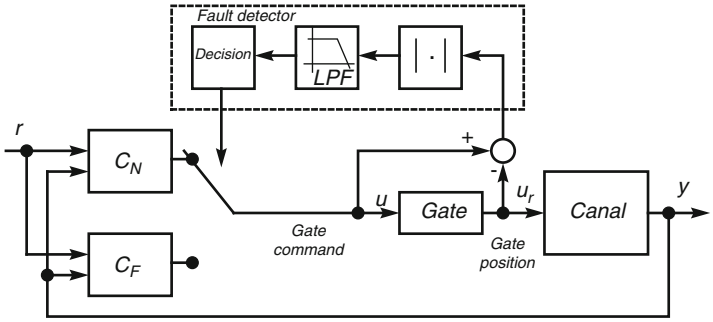

Fig. 4.6 Structure of local controllers

If $\Pi(k) \geq \Pi_{max}$, where Π_{max} is a given threshold, it is then decided that a fault has occurred.

Figure 4.7 shows results obtained with the distributed LQG controller and reconfiguration structure just described. At the time instant marked by a red vertical line, a fault occurs that forces gate 2 to become stuck. Shortly after, at the instant marked by the yellow vertical line, this fault is detected, and the controller is reconfigured as explained. From this moment on, there is no warranty on the value of the level J_2, but J_1 and J_3 continue to be controlled. The effect of coordination is apparent in the setpoint decrease of stretch 1, close to time 5,300 s. Gate 1 opens to allow the water in stretch 1 to be drained, but gate 3 also opens despite the water level upstream of gate 3 remaining very little disturbed. Therefore, the opening of gate 3 is not due to a feedback effect. Instead, it is due to the coordination between controllers 1 and 3.

Sensor Faults

The sensor fault considered consists of the sensor of level J_2 to become constant and equal to the maximum variable of this variable (800 mm). The sensor fault is detected by building an error signal between the measured signal and its estimate computed from the level sensor in the middle of the pool. An indicator variable is then obtained in a similar way as for actuator fault detection. When a sensor fault is detected, the signal used for feedback is the reconstruction obtained from the level sensor in the middle of the pool.

Figure 4.8 shows an example of sensor reconfiguration of a distributed LQG controller applied to the water channel in response to a fault in the sensor level of J_2. After the time instant marked by the first vertical yellow line, the sensor fault has been detected (shortly after its occurrence). The second vertical yellow line marks the end of the fault, in which the sensor returns to the normal condition. When the fault is active, the controller uses as feedback signal a reconstructed signal obtained by filtering the measures from other sensors. Although there is a degradation in

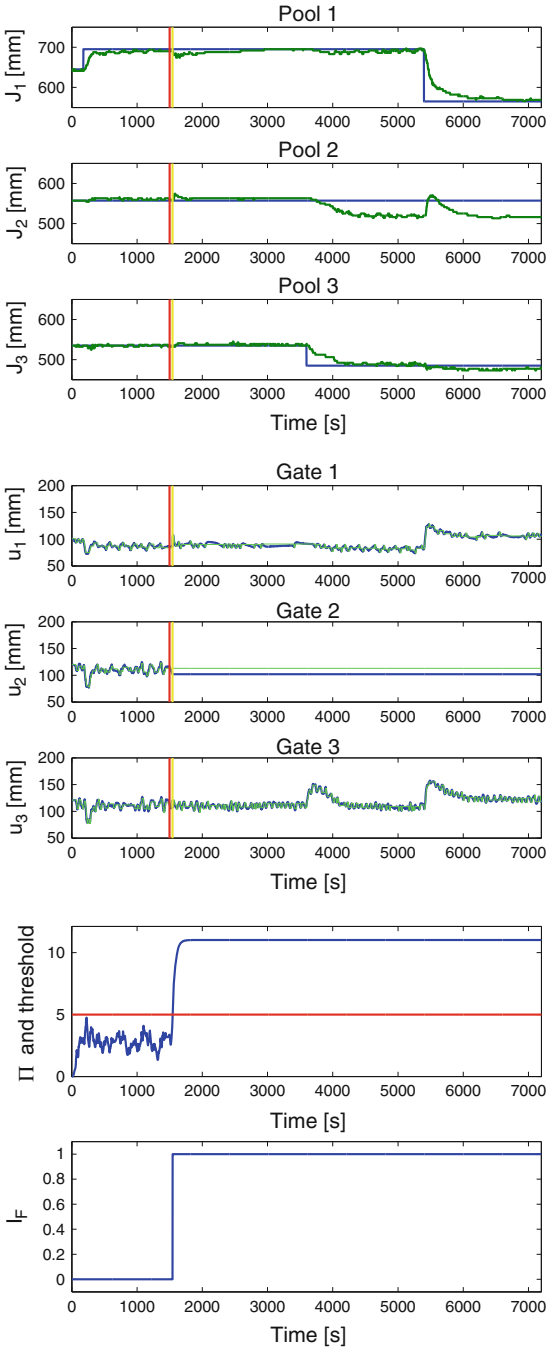

Fig. 4.7 Distributed LQG controller. Reconfiguration after a fault in gate 2. Stretch levels (*above*), gate positions (*middle*) and fault detection variables (*below*)

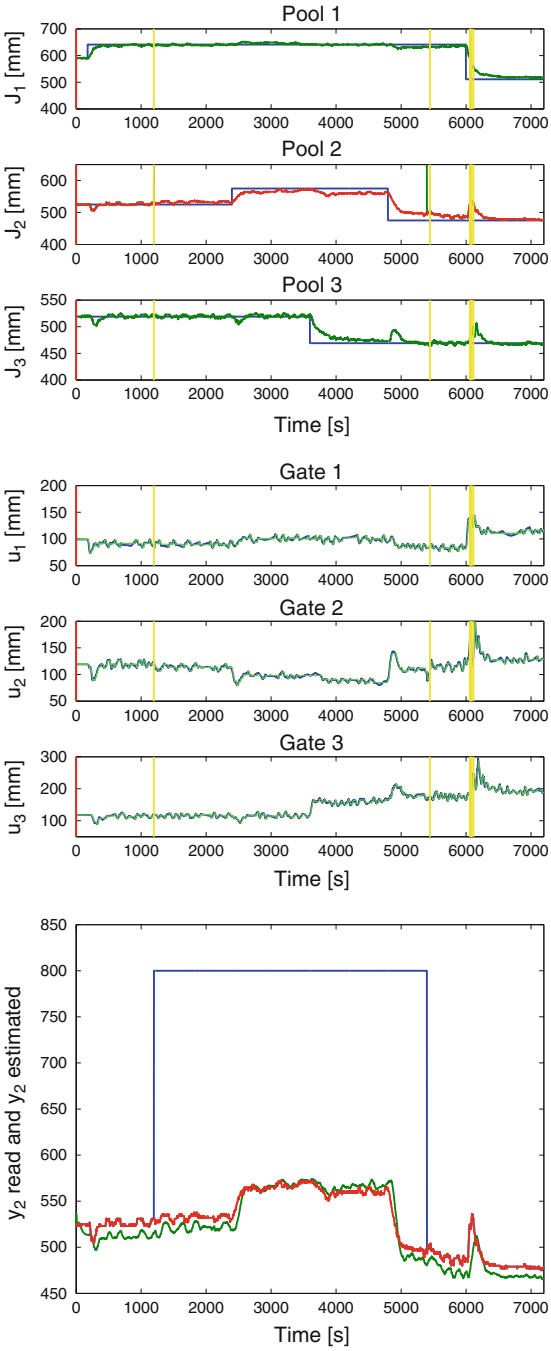

Fig. 4.8 Distributed LQG controller. Reconfiguration after a fault in the sensor that measures y_2. Stretch levels (*above*), gate positions (*middle*) and reconstructed variables (*below*)

control performance in stretch 2, the results are still acceptable. In case nothing would have been done to accommodate the fault, gate 2 would open completely because it would "see" a very high level. Furthermore, this would completely mix-up the coordination procedure, leading ultimately to a serious process failure. The pair of yellow lines just after 6,000 s corresponds to a false alarm of short duration.

4.3 Linking Transport of and Transport over Water

The first feature of the solution proposed that is to be highlighted is the use of distributed control. Distributed control provides the technical means to operate very large open channel water networks, that might even comprise regions with different operating rules or legislations. This chapter proposes a distributed control system in which local controllers negotiate their decisions with their neighbors using an algorithm based on a cooperative game approach.

The other aspect is concerned with the type of signals used for the local feedback loops. In distant upstream control the upstream gate of each canal stretch is operated such as to deliver only the desired amount of water to the stretch that follows it, taking into consideration the farmer needs of irrigation. As a consequence, there is no guarantee on the value of the water level along the pool, that most of the time can be insufficient to allow navigation. Opposite, in local upstream control, the control objective consists of imposing a water level close to the gate that ends the pool. This choice causes an increase in the volume of water accumulated along the pool, thereby providing conditions for navigation and, simultaneously, the ability to respond quickly to the local demand of water caused by side-taking extraction for irrigation use. For this propose, the controller that manipulates the downstream gate uses as feedback signal the measurement issued by a level sensor located upstream the gate and close to it. If available, the measure of the water flow that passes through the side-take for irrigation may also be used with advantage as a feedforward signal in order to reject this disturbance faster and improve the level regulation performance.

The price to pay for using local upstream control is that this structure is not efficient in what concerns water usage, and a lot of water is lost. This fact suggests the use of other structures in order to mitigate the water losses, while ensuring the water level required to allow navigation along the canal.

4.4 Open Topics

The discussion on the previous section suggests that, to solve the dual objective of saving water and allowing navigation, mixed control structures ought to be considered. The hybrid systems supervisor considered in this chapter to embed fault tolerant features in the controller can be extended to include more discrete

states in such a way that different control strategies are followed at different times, according to the prevailing objective at a given time interval, of allowing navigation or delivering water. A dwell time condition for each state of the supervisor, together with adequate corresponding controllers, ensures stability of the overall system.

The approach that was followed in this chapter allows to impose the water depth in a finite number of points along the canal, typically at points that are close to the gates that end each pool, where the sensors are located. An improved strategy might be to invert the system dynamics in order to steer the part of the plant state given by the water depth along the canal so that it is close to a specified profile. This problem might be solved using the techniques of Flat Systems [14, 15], either using an approximate lumped parameter model, or directly the Saint-Venant equations [15]. Flat systems provide a nominal path for the manipulated variables that, if applied to the plant under ideal circumstances (perfect model, no disturbances), drives its state according to a specified profile. To tackle the deviations with respect to the nominal profile caused by non-ideal effects, a regulation controller is then used. In addition, an adaptation mechanism can be added to this structure. Employing this technique allows to take advantage of all the machinery of control for robotics in order to yield the adequate spatial profile for the water level.

4.5 Conclusions and Future Research

A recent trend in computer controlled system is the consideration of the so called Cyber-Physical Systems (CPS). These engineering systems are made of physical parts and computational parts, that include communication, simulation and control elements. These parts interact through feedback loops in a synergetic way such that they modify their individual dynamics and cooperate to achieve a common goal. The traditional bottom-up approach to the design of water channel networks is no longer able to provide adequate answers to the operation of multi-use systems of this type. Instead, the approach based on CPS concepts provides a more powerful framework that integrates aspects like communication, cooperation and distributed decision and control with robust and fault-tolerant features.

Although far from complete, this chapter provides an example of using a number of key elements of CPS to manage multiuse water channel networks that comprise:

- The use of distributed control achieved through the cooperation of local control agents that negotiate through a communication network in order to reach a consensus;
- Embedding fault tolerant features;
- The ability of the controller to reconfigure in response to different operating conditions.

Controller reconfiguration was made by a supervisor implemented through a discrete state machine. While only the response to mitigate the effect of specific

sensor and actuator faults was considered, the supervisor might be extended in a simple way to tackle changes of operating objectives that are either automatically or human triggered.

Acknowledgements This work was supported by national funds through FCT—Fundação para a Ciência e a Tecnologia, Portugal, under contracts PTDC/EMS-CRO/2042/2012 (project *ORCHESTRA—Distributed Optimization and Control of Large Scale Water Delivery Systems*) and PEst-OE/EEI/LA0021/2013.

References

1. Litrico X, Fromion V. Modeling and control of hydrosystems. New York: Springer; 2009.
2. Cantoni M, Weyer E, Li Y, Ooi SK, Mareels I, Ryan M. Control of large-scale irrigation networks. Proc IEEE. 2007;95(1):75–91.
3. Zhang Y, Jiang J. Bibliographical review on reconfigurable fault-tolerant control systems. In: Proceedings of 5th IFAC symposium on fault detection, supervision and safety of technical systems, Washington, DC; 2003. pp. 265–76.
4. Åstrom K, Albertos P, Blanke M, Isidori A, Schaufelberger W, Sanz R, editors. Control of complex systems. Berlin: Springer; 2001.
5. Blanke M, Staroswiecki M, Wu NE. Concepts and methods in fault-tolerant control. In: Proceedings of 2001 American Control Conference; 2011. pp. 2606–20.
6. Campo P, Morari M. Achievable closed-loop properties of systems under decentralized control: conditions involving the steady-state gain. IEEE Trans. Autom. Control. 1994;39(5):932–43.
7. Zhao Q, Jiang J. Reliable state feedback control design against actuator failures. Automatica. 1998;34(10):1267–72.
8. Weyer E, Bastin G. Leak detection in open water channel. In: Proceedings of 17th IFAC world congress, Seoul, Korea; 2008. pp. 7913–8.
9. Zhang PZ, Weyer E. A reference model approach to performance monitoring of control loops with applications to irrigation channels. Int J Adapt Control Signal Process. 2005;19(10):797–818.
10. Choy S, Weyer E. Reconfiguration scheme to mitigate faults in automated irrigation channels. In: Proceedings of 44th IEEE conference on decision and control, Sevilla, Spain; 2005. pp 1875–80.
11. Koutsoukos X, Antsaklis PJ, Stiver JA, Lemmon MD. Supervisory control of hybrid systems. Proc IEEE. 2000;88(7):1026–49.
12. Lemos JM, Machado F, Nogueira N, Rato L, Rijo M. Adaptive and non-adaptive model predictive control of an irrigation channel. Netw Heterog Media. 2009;4(2):303–24.
13. Liberson D, Morse AS. Basic problems in stability and design of switched systems. IEEE Control Syst. 1999:19(5):59–70.
14. Fliess M, Lévine J, Martin Ph, Rouchon P. Flatness and defect of nonlinear systems: introductory theory and examples. Int J Control. 1995;61(6):1327–61.
15. Martin Ph, Murray RM, Rouchon P. Flat systems, ch. 8. In: Bastin G, Gevers M, editors. European control conference 1997 – plenary courses and mini-courses; 1997. pp. 211–264.

Chapter 5
Forecasting and Predictive Control of the Dutch Canal Network

A. van Loenen and M. Xu

Abstract Everywhere in the world where canal systems have been constructed, often the main purpose was transportation. But for most canal systems it was inevitable that they also started to play a role in the hydrology of the regions the canals crossed. In normal situations the canals have a drainage function, but in dry periods the systems can provide fresh water. An important goal for the operators is to maintain water levels on setpoint for navigation purposes. Their target is to minimize operating costs, while giving operation for navigation the highest priority. Thereby they have to take into account that the control structures have a limited operating range. A short-term optimization approach for the operational management of the canal system can increase efficiency of the water management, thereby decreasing operation costs. For the Twente Canal system, located in the eastern part of The Netherlands, such an short-term optimization approach was implemented in the operational system. This advisory module calculates the optimal operation of the available structures, given expected fluxes and system boundaries. The approach is based on Model Predictive Control and integrates observations from a gauge network and forecasted fluxes to calculate the best use of pumps and gates. The approach anticipates future lateral inflow and lock operation. The future lateral inflow in the canal sections is calculated by a rainfall-runoff model, which uses observed and forecast precipitation and evaporation. Future lock operation is estimated based on the expertise of the operators. Both have a large impact on the water balance and contain related uncertainties. The short-term optimization is implemented in the Operational Monitoring System for regulated water systems under authority of the National Water Authority (Rijkswaterstaat). This monitoring system advises operating staff on the operation of the related hydraulic structures.

A. van Loenen (✉) • M. Xu
Deltares, Delft, The Netherlands
e-mail: arnejan.vanloenen@deltares.nl; min.xu@deltares.nl

C. Ocampo-Martinez, R.R. Negenborn (eds.), *Transport of Water versus Transport over Water*, Operations Research/Computer Science Interfaces Series 58,
DOI 10.1007/978-3-319-16133-4_5

5.1 Introduction of the Research

5.1.1 Goal of the Research

Everywhere in the world where canal systems have been constructed, often the main purpose was transportation. But for most canal systems it was inevitable that they also started to play a role in the hydrology of the regions the canals crossed: the canals were used to drain the region, or to supply it with fresh water. In those situations where the effect of the lock operation on the water volume resulted in low water levels, transportation could be hindered or even halted. This is also the case when the lateral outflow is larger than the lateral inflow. In those situations measures were necessary to refill the canal system. The Netherlands also contains several of those canal systems. The canals were given dimensions suitable for standard bulk vessels. Characteristic for most of the water control structures in these systems are the limited control options: pumps can be switched on or off and gates have only a limited number of settings. These options are sufficient for manual control. Despite increases in road and railroad transportation in the past century, navigation has remained the main function of many of the bigger canal systems in The Netherlands. In the past decades the ships became wider and tonnage increased. But also the importance of the canal systems for the local water management increased. The canals were being used to dispose surplus water, but in dry periods the canal systems proved valuable in providing water. That transportation and water management are strongly related, can be seen at the canal locks, where gates, pumps and the locks themselves are clustered together (see Fig. 5.1). Especially the first development had an impact on the infrastructure of the canal system. Bridges proved a constraint for vessel height and therefore cargo volume. Locks needed to be increased, alongside with pumping capacity to refill the canal. The second development resulted in the fact that lock operators had to take more factors into account than just navigation. Based on expert knowledge and experience, the operators are able to keep water levels within the constraints. An optimization approach was expected to improve water management efficiency, by balancing the requirements from navigation and water management. An important side effect is that knowledge and experience on the operation of the canal system is translated into practical decision algorithms.

5.1.2 Scientific Field

Over the last decades, the optimization approach has received an increasing attention on controlling irrigation systems, such as [1, 2]. As forecasting systems are applied more and more, model predictive control is becoming a hot topic in operational water management. MPC originated in the industrial field in 1970s. It is an advanced control method that uses an internal (prediction) model to predict future system dynamics and solves an optimization problem to achieve optimal

Fig. 5.1 All the structures of Lock Eefde, seen from the air. The lock itself is on the *right*. The two buildings on the *left* contain the discharge gates. The first white building from the *left* is the pumping station

control actions. Constraints can be explicitly taken into account. MPC has a large application in irrigation canals and rivers [3–5]. MPC is an online control method that is computationally expensive. In the development of MPC in operational water management, the internal model was first intensively researched to reduce the computational burden. This resulted in highly simplified ID and IDZ models [6, 7]. On the other hand, model accuracy is another consideration. Xu [8] applied a model reduction method on the full hydraulic model in MPC that balanced model accuracy and computation time. Current development of MPC in operational water management is to speed up the optimization by providing analytic gradients of the objective function using adjoin methods [9]. Based on this method, Xu [10] analyzed advantages and disadvantages of sequential and simultaneous MPC. In this research, the application of Twente Canal control is implemented in the open-source software package RTC-Tools [11], which contains both traditional feedback control and MPC. RTC-Tools contains both hydrological and multiple hydraulic models to simulate and control water systems. It can be seamlessly integrated in the Flood Early Warning System Delft-FEWS, which is a widely-used platform for flood forecasting [12]. The implementation of RTC-Tools for Twente Canals is used as an advice module for the operators and does not control structures directly.

5.1.3 Contents

In this chapter we describe a study focused on optimization of the water management of a canal system, while taking into account the transportation function. The study took place at the Twente Canals system, in the eastern part of The Netherlands. The operation of the canal system is aimed at facilitating transportation over water; the water management of the canal system supports this operation. Because of this focus on transportation over water, the operation can result in high operation costs, which can be decreased by implementing Model Predictive Control (MPC). An important aspect of this study is that it takes the lock operation for transportation as a boundary: there is no information on the characteristics of the transport taking place, and the transport cannot be influenced. The study has resulted in an optimization module, which has been implemented in the operational water management system. The optimization module gives an hourly advice to the operators.

In this chapter we will first describe some relevant characteristics of the canal system. Next, we will describe the optimization approach, optimization goals, the model of the canal systems, and the optimization boundaries. In a separate paragraph we will describe the cost function and solution method. Next the results of the study will be presented, and its implementation of the operational water management system. The chapter will end with a transdisciplinary discussion into the unified framework, and suggestions for further research. It is noted that part of this text is based on [13].

5.2 Specific Case Study Discussion

5.2.1 Current Conditions

History

The Twente Canal System is named after the region in The Netherland where it was constructed. The canal system connects the three main cities of the region Twente (Almelo, Hengelo and Enschede) with the national network of rivers and canals. The total length of the canal system is 65 km. The main goal for constructing the canals was a better supply of resources for the textile industry, which was then the main economical factor in the region (see Fig. 5.2). The construction started in 1930 and was mainly by manual labor. Construction finished in 1938 [14]. Although the textile industry collapsed in the 1970s, the transportation function of the canal system remained important for the region. Nowadays the canals are mainly used for transport of sand, gravel, salt, fodder and containers. But the canal is also used for recreation, drinking water supply, irrigation and drainage. In 2010 the total traffic volume was 6 megaton, daily about 20 ships navigate the canals.

Fig. 5.2 The main purpose of many canals was transportation. Picture taken in Hengelo, 1935 (picture originates from http://mijnstadmijndorp.nl)

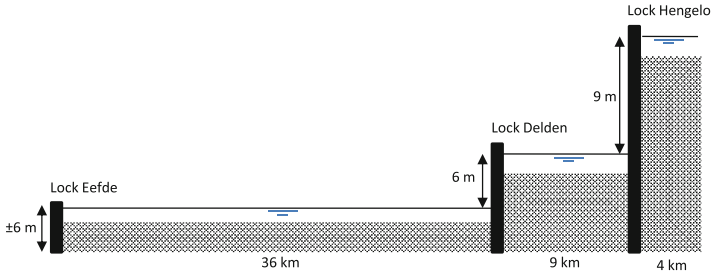

Fig. 5.3 Longitudinal cross-section of the canal system

Dimensions

The total length of the canal system is 65 km. Unique for the Netherlands is the large total level difference between Zutphen and Enschede: 21 m. To bridge this difference, the Twente Canal has three locks. The lock at Eefde bridges approximately 6 m, depending on the water level in the River IJssel. The lock at Delden also bridges 6 m and the lock at Hengelo 9 m. A longitudinal cross-section of the canal system is presented in Fig. 5.3. Because of this level difference, the water volume lost in each lock operation is about 15.000 m^3 for Eefde and 10.000 m^3 for Hengelo and Delden. Especially for the relatively small canal section upstream of Hengelo this will for every lock operation result in a water level decrease of about 5 cm. The largest compartment is between Eefde and Delden, which is 36 km.

Between Delden and Hengelo the canal stretches for 9 km and between Hengelo and Enschede 5 km. All canal sections are between 50 and 53 m wide. The water depth is between 3.3 and 5 m. Each lock has a length of 140 m and a width of 12 m.

Operation Structures

The gates of the lock contain paddles to fill or empty the chamber. Since this is not sufficient for draining the canals, the locks at Eefde and Delden are provided with additional gates. Lock Eefde has three additional gates with a total discharge capacity of 175 m^3/s. These gates can be opened up to any desired height. Lock Delden has two gates with a total capacity of 10 m^3/s. Each of these gates can have four opening positions, therefore limiting the operation space. During extreme inflows in the canal system, the paddles can be used to provide an extra discharge capacity of 34 m^3/s. Lock Hengelo has no additional discharge structures. In this lock the paddles provide the only discharge option.

The large volume of water lost during each lock operation cannot always be compensated by the inflow of streams in the canals. In dry periods the canals are used for supplying fresh water to the region, so the net water balance is negative. Therefore each of the locks is provided with a number of pumps. Locks Delden and Eefde are each equipped with three gasoline pumps (with capacities ranging from 1.2 to 5.5 m^3/s). The pumps are not provided with gears, since these were not thought to be necessary for manual operation and would also require high maintenance costs. The downside was that the operators need to take the limited operation space into account. Lock Hengelo is equipped with three electrical pumps with a capacity of 1.4 m^3/s: this canal section is very small and lateral inflow low, so the water volume lost during every lock operation has to be compensated directly.

Lock Operation

The locks, pumps and gates are operated by the lock operators, whose primary goal is safe and quick passage of cargo vessels. Operating the gates and the pumps is therefore mainly aimed at keeping the water level at setpoint. Limits to the water levels have been defined as upper- and lower thresholds (see Fig. 5.4). If the water level crosses those thresholds, the operators will receive an alarm signal. 24 h per day one operator is on standby duty.

The operators need to take the limitations of the water control structures into account. At Lock Eefde and Lock Delden the pumps are operated by the lock operators. At Lock Eefde the pumps are not used frequently. Here the actual operation is outsourced to a local contractor, resulting in extra costs for starting and stopping pump operations. Because the locks are not operated during the night, the gate and pump settings should be sufficient for a safe nightly operation.

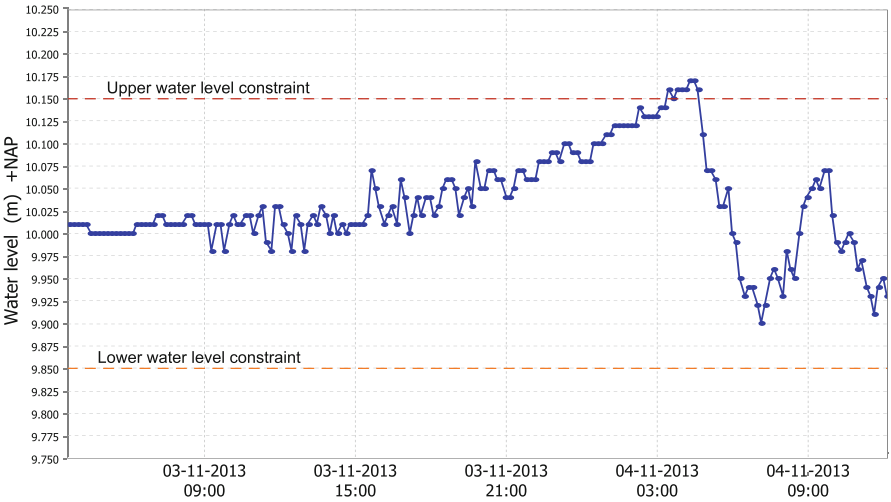

Fig. 5.4 If a threshold crossing occurs during the night, the operator on duty receives an alarm signal and has to go to the lock to change the settings (data originates from the operational water management system)

Table 5.1 Elements in the water balance for each canal section

Inflow	Outflow
Upstream lock operation*	Lock operation*
Upstream gate operation**	Gate operation**
Pumping**	Upstream pumping**
Lateral inflow	Leakage
Precipitation	Seepage
	Lateral outflow

Canal Water Balance

For the water management of the canal system the operators keep a strict administration of the water balance. The operation of pumps and gates depends mainly on actual and anticipated inflows in the canal sections, and the expected lock operation. The water balance of each canal section is made up of the posts in Table 5.1.

The elements marked with single asterisk (*) are the result of the lock operation. They are regarded as a set value but can be a large part of the water balance, since each lock operation results in a discharge of 10.000 m^3. With a number of lock operations varying between 5 and 25 per day (see Fig. 5.5) this is a large volume of fresh water.

The cells marked with double asterisk (**) are totally defined by the actions of the operators. A discharge upstream will result in an increased inflow in a canal compartment. The lock operator of the downstream compartment will need to take this into account. Another important (variable) part of the water balance is the lateral inflow from several streams discharging in the canal system (see Fig. 5.6 for an overview of the catchments). The water authority administering these laterals is

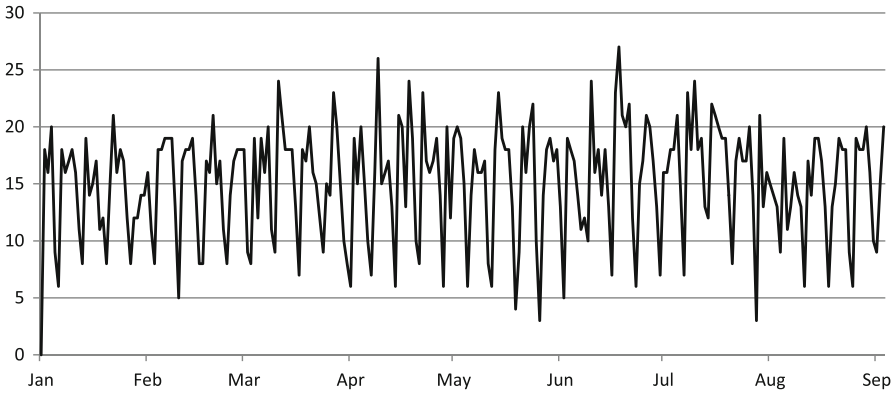

Fig. 5.5 Number of vessels daily passing Lock Delden in 2013 (numbers registered by gate operators)

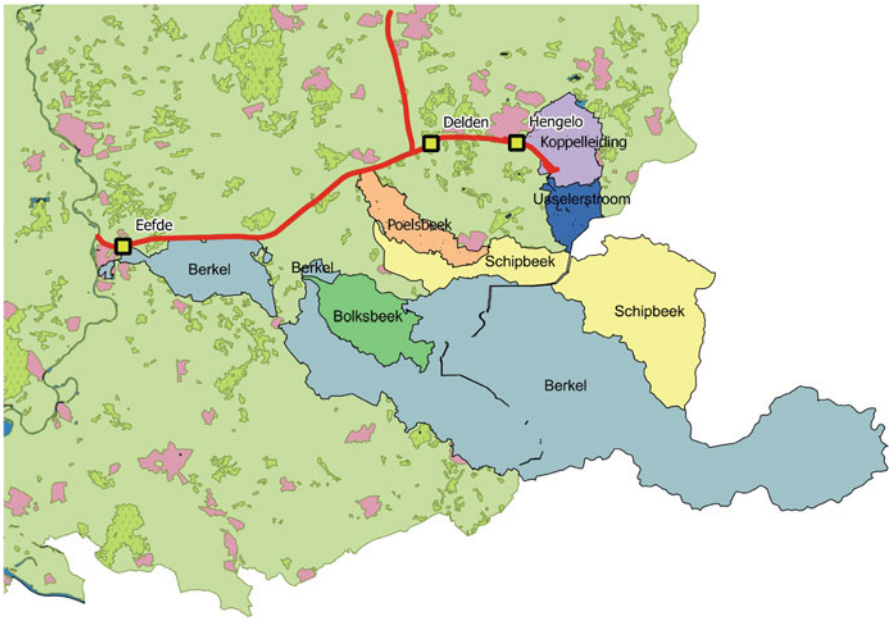

Fig. 5.6 Catchments of the main streams that discharge into the canal

Waterboard Vechtstromen. They provide flow measurement data of these laterals for the operation of the canals. Flow forecasts for the laterals are calculated within the operational water management system. A regression formula using measured and forecast precipitation and evaporation gives an indication of the expected inflow from the laterals [15] see Fig. 5.7.

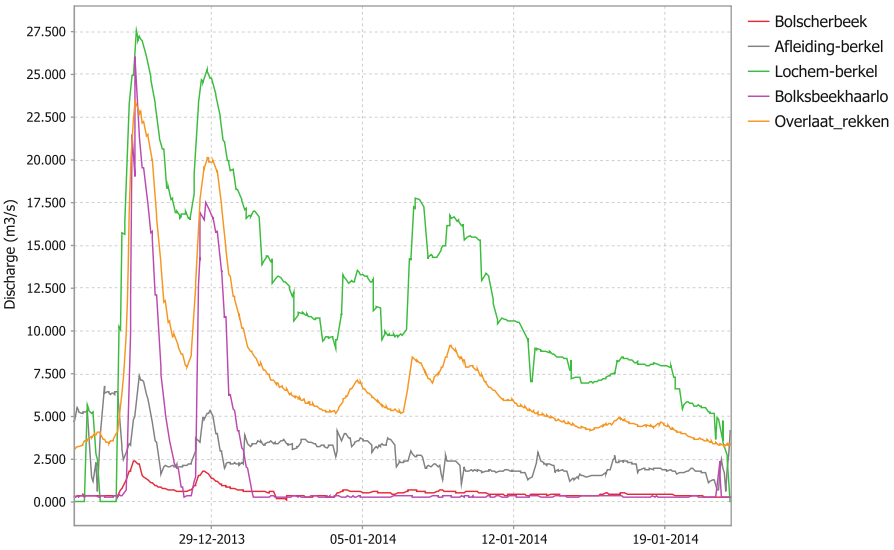

Fig. 5.7 Contributions of several streams to the inflow in the canal compartment upstream of Lock Eefde

The final terms in the water balance (leakage, seepage and lateral outflow) are unknown. It is known though that these terms are relatively small and (except for rain) invariable. Therefore, for these factors at this moment a constant value is applied when calculating the water balance.

5.2.2 Optimization Approach

In contrast with traditional operation, the optimization approach uses a hydraulic model to predict future system behavior and applies an optimization algorithm to calculate optimal operation of hydraulic structures. In the operation of Twente Canal, the optimization module only provides advice for operators instead of replacing manual operation. In the following sections, two components of the optimization approach are elaborated, namely prediction model and objectives.

Model Schematization

Figure 5.8 shows how the Twente Canal system is schematized in the optimization module. The canal sections in the Twente Canal are modeled as reservoirs, which are connected through hydraulic structures. Each reservoir has a summed lateral inflow. This is the inflow calculated through a rainfall runoff model. There are both

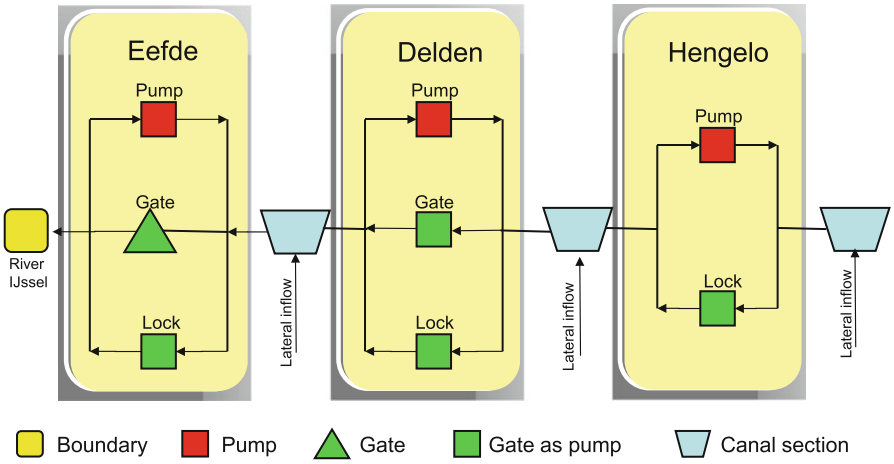

Fig. 5.8 Schematic model of the water system and its structures

pumps and gates at each location to maintain water levels. Pumps at each location are lumped as one pump. The maximum pumping capacity can vary based on pump availabilities, which are user-configurable in the advice module. Each location has a lock to let ships pass, but which are not used for water management. In extreme situations though, the paddles in the locks can be opened for flood control if the use of the gates is not sufficient. Lock operation, and its effect on the water balance, is defined as a fixed boundary. The mathematical formulation of the model can be described by a diffusive wave model. It is a simplified version of the Saint-Venant equations, where the inertia and the advection terms are neglected in the momentum equation. The expression is as follows:

$$\begin{aligned} \frac{\partial A}{\partial t} + \frac{\partial Q}{\partial x} &= q_{lat}, \\ gA\frac{\partial h}{\partial x} &= -g\frac{Q|Q|}{C^2AR}, \end{aligned} \tag{5.1}$$

where the A is the cross-sectional area, Q is the mean discharge, q_{lat} is the lateral flow discharge on unit length, h is the water level, g is the gravitational acceleration, C is the chezy friction coefficient, R is the hydraulic radius, which equals A/P (P is the wetted perimeter), x is the space and t is the time.

The discretization of (5.1) uses fully explicit scheme [11]. Substituting discharges from the momentum equation into the continuity equation, we can calculate water levels. Because the canal is only discretized by one calculation node, discharge between two nodes is replaced by hydraulic structure formulas. For pumps, it is pump discharge. For gates, it is categorized into four flow conditions (in Twente Canal, the flow through gates is free weir flow due to large head difference

between upstream and downstream, see (5.2). The work in [16] lists gate equations in other flow conditions):

$$Q = c_w W_s \frac{2}{3}\sqrt{\frac{2}{3}g}(h_1 - z_s)^{\frac{3}{2}}, \tag{5.2}$$

where c_w is lateral contraction coefficient, W_s is crest width, h_1 is upstream water level, z_s is gate crest level.

Optimization Goals and Boundaries

The short-term optimization aims at the following goals:

1. Keeping water level at setpoint.
2. Preventing water levels from crossing thresholds.
3. Minimizing pumping costs.
4. Prevent frequent changing structure settings.
5. Limit changing structure settings to office hours.

The mathematical formulation of the optimization module is described as follows:

$$\begin{aligned} J = \min_U \{ \sum_{k=1}^{n_t} [& \sum_{i=1}^{n_s} (W_{h,i}^k (h_i^k - h_{sp,i}))^2 + \sum_{j=1}^{n_c} (W_{u,j}^k u_j^k)^2 \\ & + \sum_{i=1}^{n_s} (W_{upper,i}^k \max(h_i^k - h_{upper,i}, 0))^2 \\ & + \sum_{i=1}^{n_s} (W_{lower,i}^k \min(h_i^k - h_{lower,i}, 0))^2] \} \end{aligned} \tag{5.3}$$

$$\textit{subject to:} \begin{cases} h_i^k = f(h_i^{k-1}, u_j^{k-1} \\ u_{min} \le u_j^k \le u_{max} \end{cases} \qquad \begin{pmatrix} i = 1, \cdots, n_s \\ j = 1, \cdots, n_c \\ k = 1, \cdots, n_t \end{pmatrix}$$

where h is the water level state, h_{sp} is the water level setpoint, h_{upper} is the water level upper bound, h_{lower} is the water level lower bound, u is the control input, W_h, W_{upper}, W_{lower} and W_u are weighing factors on water level deviation from setpoints, upper bounds and lower bounds, and control inputs, respectively, f is the diffusive wave model, n_t, n_s and n_c are the number of prediction steps, states and control inputs, respectively. Control inputs are restricted to minimum and maximum physical constraints of (u_{min}, u_{max}). Moreover, U is the vector of control inputs over the prediction horizon.

Optimization goals 1 and 2 are realized through the first, third and fourth terms of (5.3). The Twente Canal is used for both ship transport and water management. Ships need a minimum water depth to travel, while water in a canal also should not exceed a maximum depth because of bridge heights. These ranges are depicted in Fig. 5.4. Therefore, two objectives need to meet a consensus in formulating a water level range in each reach. Water levels are maintained to a setpoint, but can vary within the range.

Once the water level exceeds the range, a warning signal is generated. However, MPC tries to keep the water level around the bound as much as possible. In order to maintain the water level to either the upper bound or the lower bound during extreme conditions, it is necessary to assign relatively large weighing factors for both terms which provides highest importance to the objective. Optimization goals 3 and 4 are realized through the second term of (5.3). Pumping has a direct link to energy cost. It is necessary to consider energy saving by minimizing the pump usage. This is realized by assigning pump discharges to the control inputs. If possible, Optimization tries to minimize the pump discharge, thus, minimize the energy cost. Since adjustment of the gates requires manual effort, an advice to change the gate settings every time step will quickly be ignored by the operators. Therefore, rate of change is assigned to the objective of controlling gate opening.

The last optimization goal is realized through setting of constraints. This optimization problem is used to provide advice to operators for manual adjustments. A practical consideration is the office hour. Since operators only work during the day, it is undesirable that operators have to drive to the station at night for operation. The optimization should be able to avoid operation at night while water levels can still be controlled well. This is realized by using the rate of change constraints for both pumps and gates, and setting both minimum and maximum changing rate to zero at night.

The optimization problem is solved through ipopt [17], which is an open source algorithm for nonlinear optimization. In RTC-Tools, it uses an adjoint method to calculate the gradient [11].

Optimization Implementation

The optimization provides advices on the operation of hydraulic structures over a prediction horizon of 2 days with a control time step of 1 h. The optimization module implemented in RTCTools is seamlessly integrated in Delft-FEWS [12] and the control results are shown in Figs. 5.9, 5.10, and 5.11 for the locks of Hengelo, Delden and Eefde. The red vertical line indicates the current time (T0) in consideration. Left hand side of the line represents historical measurements and manual operations, while right hand side is forecasting.

The first sub-figure shows the rainfall (bar) and corresponding runoff (line). The forecast runoff is generated from the rainfall-runoff model. The forecasts contain certain rainfall events. These are the external inputs (disturbances) to the

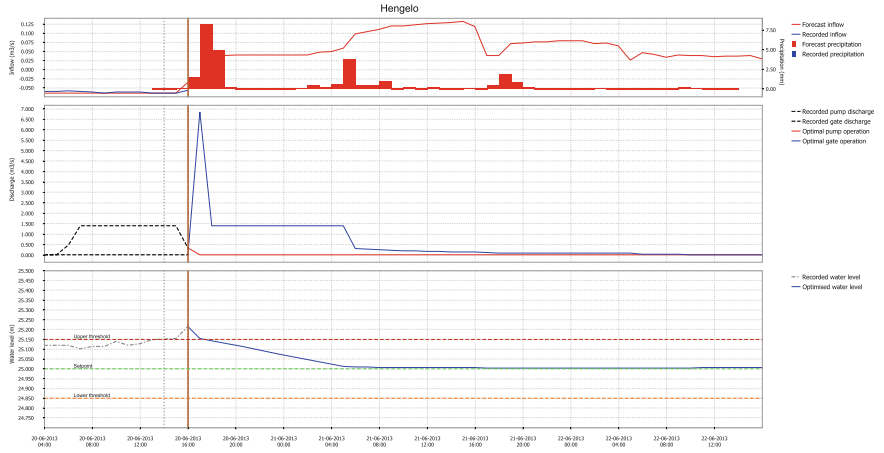

Fig. 5.9 Control results at Lock Hengelo

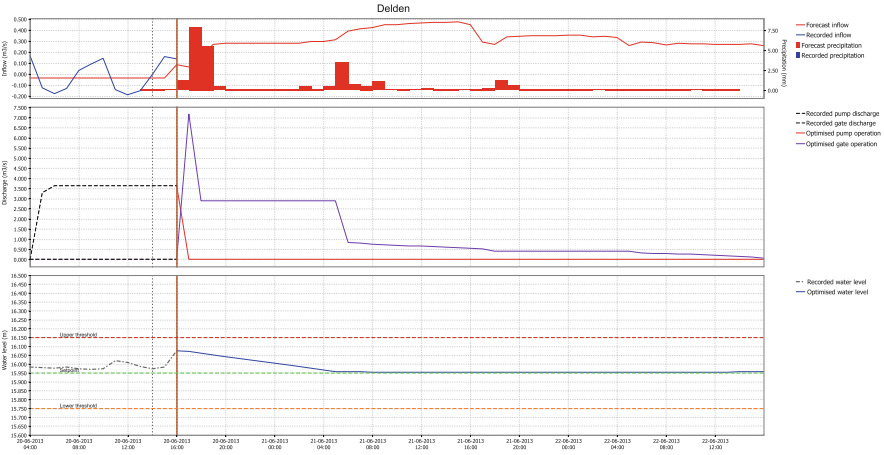

Fig. 5.10 Control results at Lock Delden

optimization model, which directly influence the operations of hydraulic structures. It is noticed that the forecasting accuracy of the rainfall-runoff model needs to be improved.

The second and third sub-figures show the optimal operations of hydraulic structures and controlled water level in each canal section, respectively. The combination of rainfall and high water levels (above the upper bounds) at Hengelo indicates that the pump operation which takes place before T0 is a wrong operation. This is a manual operation without the advice of MPC. Due to the prediction of rainfall, MPC suggests stopping the pumps and opening the gates to discharge water downstream. The water level at Eefde is below the setpoint. However, the optimization recognizes rainfall and water coming upstream and it opens the gates instead of pumping water in.

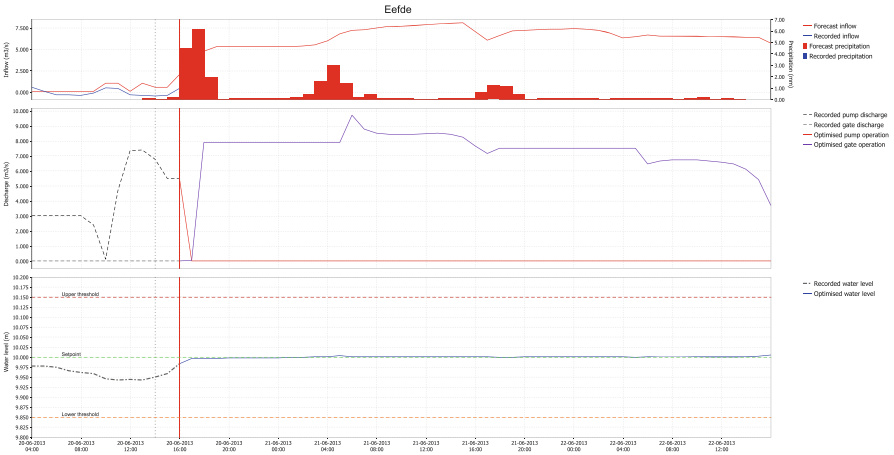

Fig. 5.11 Control results at Lock Eefde

It is noticed that there is no operation (adjustment) of hydraulic structures at night periods due to the setting of office hours from 18:00 to 07:00 in the optimization. The proposed operations can control the water levels to the setpoints (green dashed line) very well. This guarantees the objectives of both navigation and water management.

From Optimal Operation to Control Advice

The optimization algorithm calculates continuous solutions and is not able to calculate a solution for pumps and gates with limited operation space, such as in the Twente Canal system. Therefore a postprocessing module is in development, which calculates the best settings for the individual structures, based on the optimal solution and the structure characteristics.

5.3 Transdisciplinary Discussion into the Unified Framework

In the research presented, the transport of water serves the transport over water. From that perspective the presented optimization approach could be integrated in the unified framework as the water flow controller. Although in this research the transport over water formed the boundaries and goals for the transport of water, the presented approach offers ample opportunities to integrate both into a unified framework. There does not seem a prospect that vessel loading will be influenced

by water system conditions. Shipping companies will not load their vessels with just two layers of containers because of water management purposes. The presented approach will support the unified framework in that the management of the water system under view will be optimized, while taking into account the constraints being given by the transport over water.

These constraints are formed by the maximum and minimum allowed water levels, making it possible for certain vessel classes to navigate the canal. Maximum water levels are based on the level of the bridges crossing the canals: at these levels vessels carrying three levels of containers can still pass the bridges. The minimum allowed water levels are based on the maximum draught of vessels passing the canals. Since no information is available on the freight of the vessels that will pass the canals, these water level boundaries are fixed. Here is an opportunity for further research.

In the unified framework, constraints and goals can be set based on data of actual navigation requirements. The economic balance will always favor to both optimal transport over water and optimal transport of water. Therefore, if an integration in an unified framework would take place, the transport over water will still set some constraints and goals for the transport of water. But if detailed information on vessel location, loading and routes were available, the fixed constraints and goals can be released and dynamically changed depending on actual requirements for transport over water. For instance, during summer there is a period with some severe rainstorms. The rainstorms cause a large rise of water levels in the canals. Normally the operators would release the surplus to get back to target level. After the rainstorms, the dry weather takes over and because of lock operations, pumping is required to keep water levels at target level.

If the system has knowledge on actual vessels in the canal, and vessels that will enter the canal, the maximum level can be dynamically altered depending on the loads of these vessels. If is known that these vessels are all loaded with less than three layers of containers, water levels can be allowed to rise higher than the current maximum water level. Thus keeping as much water in the system as possible, and so decreasing pump operation.

Obviously, a lot of research needs to be done to get into this situation. First of all, since the economic importance of transport over water greatly overrides a small optimization of water management, it is important that navigation is not disturbed. A system as described does need forecasts, since water levels cannot be altered within a short time frame. Since information about a future situation is inherently uncertain, the system needs to be able to take a level of uncertainty into account.

It is expected that the implementation of the presented short-term approach will improve efficiency of the operational water management, although no functions have been integrated to measure this performance improvement. First of all, the overall pump operation is expected to decrease. Because of the large capacity of these pumps (up to 5.5 m^3/s), a decrease in pump operation will directly lead to lower operation costs see Fig. 5.12. Furthermore, the optimized water management is expected to have the water levels in the canals to deviate less from the target levels. An integration of the presented approach in the unified framework is expected to further increase system performance since constraints become more flexible.

Fig. 5.12 One of the gasoline pumps at Lock Eefde, with a capacity of 5.5 m^3/s

5.4 Open Topics

5.4.1 Dealing with Uncertainty

The approach presented in this research calculates an optimal use of pumps and gates for the near-future, based on forecasts of inflow and downstream water level, expected lock operation, and using a simple reservoir model. All these components contribute to an uncertainty in the output of the optimization. The forecast inflows and water levels, which are the model forcing of the routing model, are known to be uncertain. Especially the future inflow in the Twente Canal system is relatively uncertain. Also expected lock operation at this moment is set as a constant factor, while Fig. 5.5 shows that lock operation is very variable, and thus the influence of lock operation in the near future on the water balance can vary. The last relevant source of uncertainty is the routing model used in the optimization approach. This model is a simple schematization of reality and will never fully correspond with reality. In the current implementation of the optimization module these uncertainties are not taken into account. There are two ways of dealing with this uncertainty: (1) decrease the uncertainty and (2) visualize the uncertainty so the operator is aware of the uncertainty in the control advise and makes decisions based on the optimization advice and his own experience and expert judgement. The uncertainty

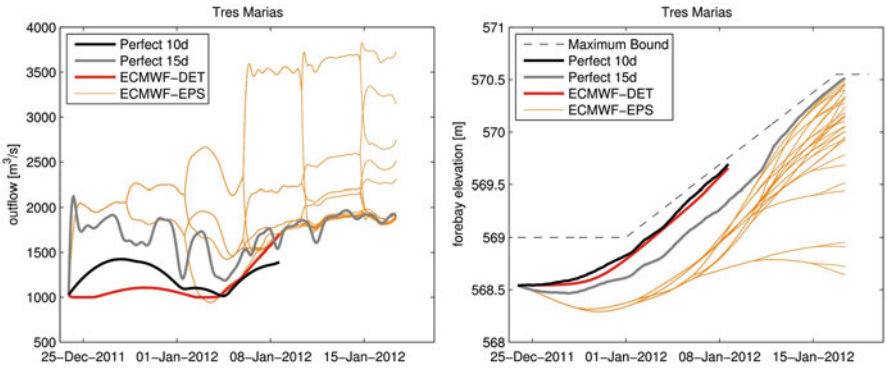

Fig. 5.13 Deterministic and stochastic optimization results for optimized reservoir operation of Tres Marias Hydropower reservoir in the Sao Fransico River [20]

caused by the hydrological forecasting can be decreased by implementing a better forecasting model, since the current model uses a simple regression algorithm. The hydraulic model can be improved by adding more computation points, this is especially important for gate and lock elements whose operation is calculated based on water levels directly upstream and downstream. Uncertainty on lock operation can be decreased by connecting to vessel tracking systems. This aspect perfectly fits the initiative to develop a unified framework in which transport over water is connected to transport of water. The uncertainty of the input can be visualized by applying the optimization approach to multiple input options. It is necessary to consider ensemble weather forecasting and apply ensemble model predictive control or more practically tree-based model predictive control to improve decision making [18, 19] Fig. 5.13. The current optimization approach takes approximately 10 s for one optimization calculation. It is expected that a tree-based approach will increase the computational burden, but can still take place within usable limits.

5.4.2 Implementation in the Operational Monitoring System

The short-term optimization is implemented in the Operational Monitoring System for regulated water systems under authority of the National Water Authority (Rijkswaterstaat). The operators are not academic hydrologists, but lock operators experienced and educated in safe passage of vessels through canal locks. There is not much knowledge on optimization approaches, application constraints and forecasting systems. The Operational Monitoring System is specifically designed to present only relevant information, required for operational control, to the operators. In general this information consists of actual data on lateral inflows, water levels, pump operation, and water balances of canal sections. The information is presented in clear displays (see Fig. 5.14). Graphs are hardly used, since operation focuses on the current situation.

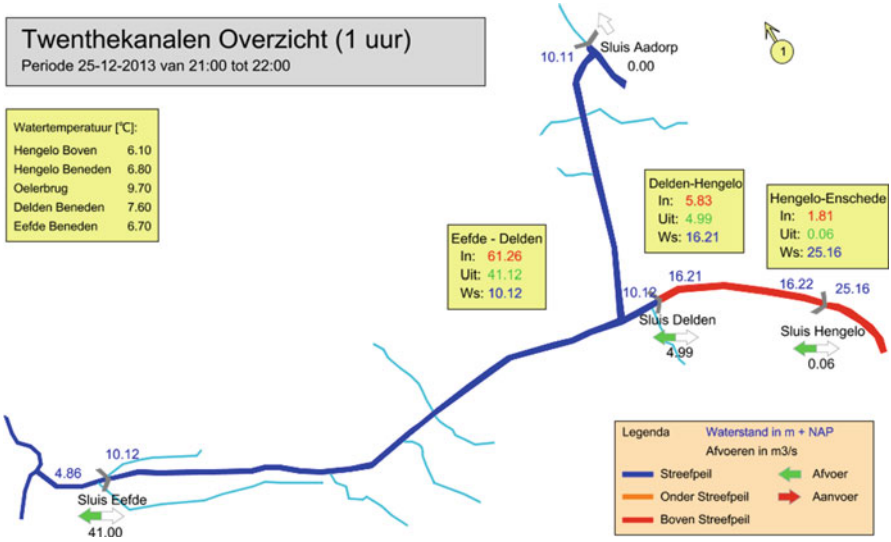

Fig. 5.14 One of the standard displays of the Operational Monitoring System

The control strategy, as calculated by the optimization module, also needs to be presented to the operators in a clear and basic manner. Implementing forecast information in displays such as Fig. 5.14 needs to be well-thought, and can be considered an unique scientific discipline. In the current implementation, the design of the display has been discussed thoroughly with the operators. In the display the actual advice for each lock is presented in a small table. The table only contains the advice for the upcoming 4 h, thereby taking into account the operational use of the Operational Monitoring System where the system is consulted every few hours. The content of the table is thus refreshed after every run of the optimization module.

5.5 Conclusions and Further Research

In this chapter an optimization approach was presented that advises lock operators on the best operation of water control structures. The system takes transportation over water as a fixed constraint, which defines the goals for the water management. The optimization algorithm also takes other targets into account, such as limited operation periods, a minimum pump operation and a minimum of structure setting changes, therefore mimicking the operational rules of the operators.

In almost all cases, the objectives for water transport can be guaranteed with the calculated optimal operation strategy. However, the current optimization generates continuous solutions. Hydraulic structures normally can only be adjusted to minimum and maximum operation, such as pump on and off, gate opening at different

stages. This is also the case in the Twente Canal system. Post processing has been proposed to consider this issue as a first improvement, but in a later research, the application of mixed integer optimization should be studied.

The implementation and actual use of the system show that the approach of the system fits well to the practice of water management in the Twente Canals. Extra attention has been spend to the presentation of the relatively complex control forecast to the gate operators.

Future research will further aim at improving the data on actual and forecast lock operation. Since the lock operation is an important term in the water balance, knowledge on past and future lock operations will greatly improve the water balance. The near-future fluxes can greatly affect the control forecast, and is therefore a source of uncertainty. Further research could focus on applying tree-based optimization to give the operators insight in the operation space.

In the proposed unified framework, the presented optimization approach can well be considered to be the water flow controller. It already optimizes water flow, while considering transport over water as a given input. Future research could focus on applying flexible constraints as given by the transport over water. Currently those constraints are based on the assumption that there are always vessels with three layers of containers, or with maximum draught, in the canal system. Based on information on actual or expected vessels, constraints to the water levels can be set dynamically, thus further integrating transport over water with transport of water.

References

1. Reddy JM, Dia A, Oussou A. Design of control algorithm for operation of irrigation canals. J Irrig Drain Eng. 1992;118(6):852–867.
2. Clemmens AJ, Schuurmans J. Simple optimal downstream feedback canal controllers theory. J Irrig Drain Eng. 2004;130(1):26–34.
3. van Overloop PJ. Model predictive control on open water systems. Delft: IOS Press; 2006.
4. Negenborn RR, van Overloop PJ, Keviczky T, de Schutter B. Distributed model predictive control of irrigation canals. Netw Heterog Media, 4(2):359–380, 2009.
5. Barjas Blanco T, Willems P, Chang PK, Haverbeke N, Berlamont J, de Moor B. Flood regulation using nonlinear model predictive control. Control Eng Pract. 2010;18(10):1147–1157.
6. Schuurmans J, Bosgra OH, Brouwer R. Open-channel flow model approximation for controller design. Appl Math Model. 1995;19:525–530.
7. Litrico X, Fromion V. Simplified modeling of irrigation canals for controller design. J Irrig Drain Eng. 2004;130:373–383.
8. Xu M. Real-time control of combined water quantity and quality in open channels. PhD thesis, Delft University of Technology, Delft; 2013.
9. Schwanenberg D, Verhoeven GF, van den Boogaard H. Nonlinear model predictive control of flood detention basins in operational flood forecasting. In: 9th International Conference on Hydroinformatics, Tianjin; 2010.
10. Xu M, Schwanenberg D. Comparison of sequential and simultaneous model predictive control of reservoir systems. In: 10th International Conference on Hydroinformatics, Hamburg; 2012.
11. Schwanenberg D, Becker B, Xu M. The open RTC-Tools software framework for modeling real-time control in water resources systems. J Hydroinformatics. 2014;17:130–148.

12. Werner M, Schellekens J, Gijsbers P, van Dijk M, van den Akker O, Heynert K. The Delft-FEWS flow forecasting system. Environ Model Softw. 2013;40:65–77.
13. van Loenen A, Xu M, Engel R. Short-term optimization of a canal network for navigation and water management. In: 11th International Conference on Hydroinformatics, New York; 2014.
14. Heitling WH, Lensen L. De Twenthekanalen; succes van een mislukking. Zutphen: Terra; 1984. ISBN 9062551866 (in Dutch) 1984.
15. de Bruine EP. Water balance and SOBEK model Twente Canals. Subreport water balances (in Dutch). Rotterdam: Witteveen+Bos; 2010.
16. Delft Hydraulics WL. In: Sobek User Guide and Technical Reference Manual; 2004.
17. Wachter A, Biegler LT. On the implementation of a primal-dual interior point filter line search algorithm for large-scale nonlinear programming. Math Program. 2006;106(1):25–57.
18. Raso L, Schwanenberg D, Schruff T, Failache Gallo N. Tree-based model predictive control for optimizing hydro power production and floods. In: 10th International Conference on Hydroinformatics, Hamburg; 2012.
19. Raso L, van de Giesen N, Stive P, Schwanenberg D, van Overloop PJ. Tree structure generation from ensemble forecasts for real time control Hydrol Process. 2013;27:75–82.
20. Schwanenberg D, Fan F, Naumann S, Kuwajima J, Montero R. Short-term reservoir operation for flood mitigation under meteorological and hydrological forecast uncertainty. In: Water Resources Management (draft); 2014.

Chapter 6
Transport of Water versus Particular Transport in Open-Channel Networks

G. Belaud and X. Litrico

Abstract Hydraulic performance has largely benefited from recent advances in canal control. Nonetheless, taking account of water quality criteria at the same time is more challenging due to longer delay times for particular transport than for wave transport, and to poorly quantified interactions between flow and substratum. This chapter is first illustrated with a typical situation where both water quality and discharge are expected to be controlled. Different approaches of modeling are then introduced, leading to the definition of different delay times that must be considered in the perspective of real-time control. Open-loop and closed-loop control strategies of water quality in open-channels are finally presented and discussed. Research perspectives are suggested regarding combined hydraulic and water quality control.

6.1 Introduction

Hydraulic control of canals has largely been developed in the past 20 years, with many successful applications to real systems, allowing improvement performance regarding hydraulic criteria.

Canals do not only transport water. They also convey different types of elements, some of them being passive, some of them being undesirable when they arrive at check structures or delivery points. This is the case for some dissolved pollutants, floating debris, oil pollution, sediments or phytoplanctonic algae (also called drift). Controlling such transport raises new difficulties compared to water control.

Salinity control appears as one of the simplest problems, although it may be important in some contexts. Problems usually appear in drainage systems in coastal areas when sea level becomes higher than freshwater level. It is rather simple to monitor salt concentration thanks to conductimeters. Based on that, [16] presented

G. Belaud (✉)
UMR G-Eau, SupAgro, Montpellier, France
e-mail: gilles.belaud@supagro.fr

X. Litrico
LyRE, R&D center of Lyonnaise des Eaux, Bordeaux, France
e-mail: xavier.litrico@lyonnaise-des-eaux.fr

C. Ocampo-Martinez, R.R. Negenborn (eds.), *Transport of Water versus Transport over Water*, Operations Research/Computer Science Interfaces Series 58,
DOI 10.1007/978-3-319-16133-4_6

control methods using either Proportional Integral (PI) or Model Predictive Control for the control of inflow within polders, with both salinity and water level objectives. Compared to hydraulic control, one needs to consider salt transport and dilution, which are well described thanks to the advection-diffusion process. These are also the processes involved in accidental chemical pollutions.

Sediment transport is another type of problem involving particular transport. It may not be a problem if sediments are transported to the cultivated plots, but irrigation networks are usually not able to achieve that. Indeed, channel networks are composed of pools, the size of which decrease from upstream to downstream due to water distribution along the network. With decreasing transport capacity, sediment particles tend to get deposited in upstream portions of the canals. The presence of backwater due to control structures, with large canal depths and low velocity, also decreases the sediment transport capacity and then favour sediment deposition: achieving high hydraulic performance may be contradictory with the objective of minimizing sediment deposition. In this case, the transported class is far from being conservative since most of the particle inflow may be stored in the pools, causing in turn bed aggradation. Also, since sediments are not distributed homogeneously in a canal section, concentrations may evolve at each canal bifurcation [1].

The case of algae cumulates these features. Their growth leads to different management problems, such as clogging of drip emitters, canal roughness variation, and possible toxin release. The interaction between flow and vegetation is difficult to predict accurately, which is a real issue when designing hydraulic management strategies which take into account the disturbances due to algae.

The objective of this chapter is to illustrate operational control methods in which the interplay between transport of water and transport of particles are considered. The case of algae management is used to introduce key issues related to this interplay. Section 6.2 introduces the issues of particle management in open-channel networks and models derived to simulate the involved processes. Section 6.2.4 presents the methods developed to control the transport of particles. Section 6.3 discusses the specific issues related to particle transport management, the interplay with flow control and open topics in this field.

6.2 Case Study: The Management of Algae Transport

Dealing with particular transport implies different time scales. Longer term strategies should prevent the apparition of disturbances by choosing appropriate hydraulic conditions. For example, avoiding sediment deposition requires maintaining sufficient velocities throughout the canals. These conditions may be far from being optimal regarding hydraulic control. Another option is to use transient phenomena in order to eliminate regularly the accumulated particles or vegetation. These events require adapted control procedures, in which both transport of water and transport of particle must be considered. After presenting these strategies, models describing the involved processes are described.

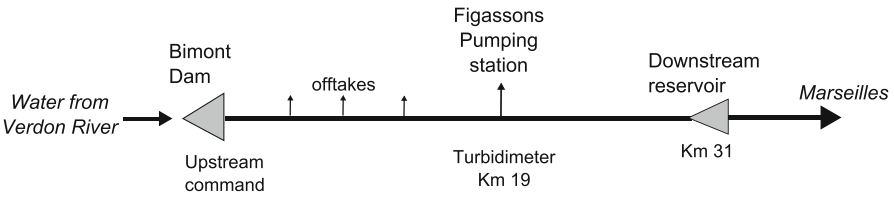

Fig. 6.1 Sketch of the studied portion of the Canal de Provence (Branche Marseille-Nord)

6.2.1 Flushing-Flow Strategies

Flushing-flows consist in increasing flow during a certain time so that shear stress is increased and attached material is moved. This is being practiced in some sewer networks [4] in order to entrain deposited sediments. This results in a turbidity cloud which transported towards the downstream end of the network. This principle has been applied on the Canal de Provence, Branche de Marseille-Nord, in order to detach algal mats fixed on the concrete canal banks. This branch of the Canal de Provence, located in South-Eastern France, is a strategic infrastructure that supplies treatment plants for the city of Marseille, industries and farmers all along its 31 km (Fig. 6.1). The normal discharge in the branch is between 1 and 2 m^3/s, out of a conveyance capacity of 3.5 m^3/s. The canal is lined with concrete. Check structures are controlled from the SCADA located at Aix-en-Provence. To perform a flush, a flow increase is obtained by releasing water from a dam during a few hours. In this case the released volume is stored in another reservoir at the end of the branch. These flushes allow the canal managers to maintain a constant algal population. Biological analyses have demonstrated that the same flushes should be performed every 2–3 weeks [6].

Turbidity is monitored at different measuring stations (upstream, downstream and intermediate). For each flush, the intensity must be sufficient to detach enough material. Since pumping stations and farmers are located all along the branch, this intensity should not be too large in order to keep the turbidity under an acceptable level. The operation must be done at a time when it disturbs a minimum of end-users. All these constraints justify the necessity to develop models able to simulate the effect of a flush on the transported material.

6.2.2 Process Modeling

In open-channel networks, the hydraulic variables are usually calculated by solving the one-dimensional Saint Venant's equations. The control structures between pools and at each water delivery point are taken into account via stage-discharge-opening relationships.

For the transport of particles, a specific equation is needed in order to calculate the evolution of the concentrations throughout the system. Molecular diffusion,

turbulent diffusion and dispersion due to velocity gradients are represented in a unique diffusion term. For non-conservative transport, an exchange term is required in the advection-diffusion equation written in a generic form as follows:

$$\frac{\partial UC}{\partial t} + \frac{\partial (U\ A\ C)}{\partial x} - \frac{\partial}{\partial x}\left[A\ D\ \frac{\partial C}{\partial x}\right] - A\ E = 0, \tag{6.1}$$

in which A is the wetted area (m^2), x the distance along the network (m), Q the discharge (m^3/s), D the diffusion coefficient (m^2/s), C the particle concentration (usually in kg/m^3) and E the exchange rate ($kg/m^3/s$). The resolution of (6.1) needs two boundary conditions, given for instance by particle upstream input and zero-diffusion at the downstream end. At bifurcations, the proportions of materials passing to each downstream branch should depend on the type of material, whether they are floating (vegetation) or moving preferentially near the bed (like sand particles).

In the case of a flush, the exchange rate becomes essential, since it represents the effect of the hydrodynamic perturbation on the material attached to the canal bed or bank. For sediment, it is common to consider that this rate is a power function of the difference between actual bottom shear stress and a threshold shear stress [15]. By similarity with cohesive erosion models, the same type of relation is considered for attached algae [6]:

$$E = \frac{1}{\alpha} B \left(\frac{\tau_0 - \tau_{0,c}}{\tau_{0,c}}\right) \quad \text{if} \quad \tau_0 > \tau_{0,c} \tag{6.2}$$

$$E = 0 \quad \text{otherwise}, \tag{6.3}$$

with α time constant, $\tau_{0,c}$ critical bottom shear stress, τ_0 bottom shear stress, B fixed biomass per unit bed area. Based on field sampling during flushes, it was shown that the turbidity was proportional to the drift algae concentration, with high correlation coefficient.

The coefficients of the above relations can be calibrated thanks to the monitoring of a limited number of flushes. This set of equations can be used for direct simulation, providing essential information for management such as delay times and turbidity dynamics during the flush. An illustration of flush flow simulation is provided in Fig. 6.2, showing flow and turbidity simulation and measurements at different monitoring stations. We can observe the increase of peak turbidity from upstream to downstream, due to algae detachment in response to flow increase.

6.2.3 Simplified Linear Models

The above models have the advantage to provide detailed hydraulic variables and concentrations at any calculation section. The counterpart is the calculation time which limits their use for real-time control (RTC). For RTC, it can be sufficient

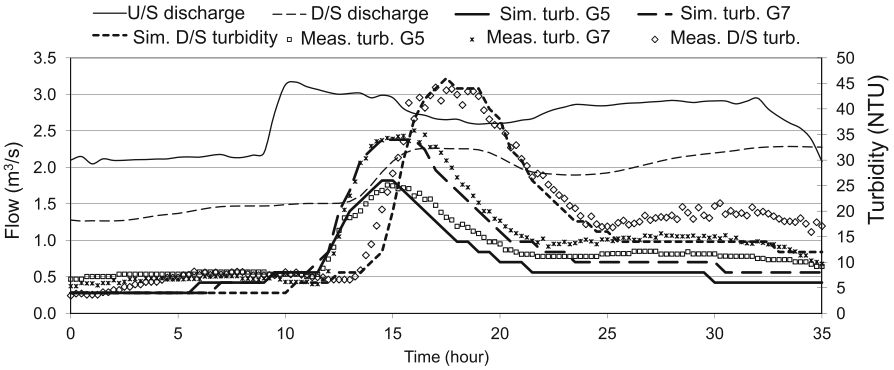

Fig. 6.2 Simulation of turbidity, Branche Marseille-Nord, flush performed in 2007

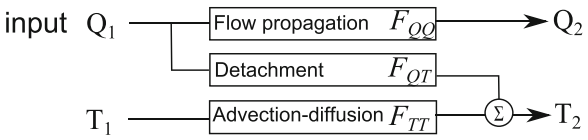

Fig. 6.3 Transfer functions between upstream and downstream variables (discharge and turbidity)

to write the transfer functions between the input variables (for example the flow entering a canal, or a gate position) and the controlled variables (for example, a water level at a given section). Linear transfer functions are preferable since they are computed very quickly, they can give explicit stability conditions, and under some conditions they can be inverted in order to compute the input that should be applied to obtain a desired response.

In this study case, the input variable is the head discharge, released from a barrage, and the output variable is the concentration at the downstream end of the canal. If the incoming turbidity is not negligible, this turbidity is superimposed to the one generated in the canal. For a canal reach, the downstream response uses three transfer functions (Fig. 6.3):

- F_{QT}, that gives the response of turbidity to the discharge increase;
- F_{QQ}, that gives the downstream discharge variation in response to upstream discharge variation;
- F_{TT}, that propagates the upstream turbidity.

It is useful to have intermediate turbidity variations. To do so, we need to split the canal at the intermediate location, and to calculate the transfer function for each portion of the canal.

Linear models can be derived from the full nonlinear systems of equations. To this end, we first linearize the Saint-Venant and advection-diffusion equations. Thanks to Laplace transforms of the time domain equations, we can obtain explicitly the response at any location, as a function of the input variables. Using approximate transfer functions (first or second order with delay), we obtain simplified transfer

functions that can be used for RTC. Based on the approach described in [10], polynomial transfer functions with delay can be derived [8]:

$$F_{QQ} = \frac{e^{-\tau_Q s}}{1 + K_Q s}, \tag{6.4}$$

$$F_{TT} = \frac{e^{-\tau_T s}}{1 + K_T s}, \tag{6.5}$$

$$F_{QT} = \frac{G_D}{1 + K_D s}\left(F_{QQ} - F_{TT}\right), \tag{6.6}$$

with s the Laplace variable. The first two transfer functions have different delays (τ_Q and τ_T) corresponding to hydraulic propagation and advection-diffusion. The time constants K_Q and K_T represent the hydraulic attenuation and the diffusion. These coefficients can be obtained from the properties described in the full nonlinear equations. The time constant K_D expresses the sensitivity of the attached material to the discharge increase. The gain G_D of F_{QT} is sensitive the quantity of material that can be detached during the flush. It also includes the linear correspondence between algal concentration and turbidity. This gain can hardly be defined by a deterministic approach.

Equation (6.6) cannot be inverted analytically in the time domain. A more compact form was proposed in [7]:

$$F_{QT} = \frac{s\gamma_0 e^{-\tau_D s}}{(1 + K_{D_1} s)(1 + K_{D_2} s)} \quad \text{if} \quad dQ_u/dt > 0, \tag{6.7}$$

$$= 0 \quad \text{otherwise}, \tag{6.8}$$

in which Q_u is the upstream discharge. In the time domain, the differential equation which gives the turbidity is

$$K_{D_1} K_{D_2} \frac{d^2 Tb_d}{dt^2} + (K_{D_1} + K_{D_2}) \frac{dTb_d}{dt} + Tb_d(t) = \gamma_0 \frac{dQ_u}{dt}(t - \tau_D). \tag{6.9}$$

This quasi-linear model is easy to implement under calculation tools or spreadsheets, so that the four parameters K_{D_1}, K_{D_2}, τ_D and γ_0 representing the turbidity response to a flush can be easily identified from field measurements. Among these parameters, the first three ones are expected to remain constant for all flushes, while the gain γ_0 will vary with the attached biomass. Adjusting this gain can be done thanks to the expertise of the manager (as done at the Canal de Provence, see Sect. 6.2.4), or in real-time using appropriate controllers (see Sect. 6.2.4). Illustrations of the model performance are presented in [7].

6.2.4 Real-Time Control of Particular Transport

Open-Loop Control

In order to design a flush, one needs to define how much water should be released, at what time and for how much time. The higher is the released discharge, the larger is the shear stress increase and the more biomass is detached.

Yet, impacts must be considered: the hydraulic disturbance affects the water quality for some time, and it also causes undesirable water level fluctuations. In practice, most of these disturbances should occur during the night, when water demand is the lowest, so that pumping stations can be stopped if the turbidity is excessive.

Hydraulic disturbances can be anticipated using Saint Venant's equations-based models. It is not simple, however, to determine the flow release that is necessary to achieve a given downstream discharge objective, as the inversion of the Saint-Venant's equations is an ill-posed problem [5]. There are also some physical limitations, mainly due to the attenuation during flow propagation. Linear models offer an alternative for hydraulic inversion, such as a first-order with delay derived from Saint-Venant's equations with offtakes [13].

For water quality management, the inversion of the system of three equations is again an ill-posed problem. Here, the objective is to reach a given turbidity which guarantees that attached material has been removed from the canal banks. It is also expected not to overcome this targeted turbidity in order to avoid clogging problems at the hydraulic devices.

The linear transfer function (6.9) can be used to compute the upstream discharge $Q_u(t)$ from the desired downstream turbidity. Practical curves can be derived from the model, such as the flush duration or the amplitude of the discharge increase. For the flushes performed at the Canal de Provence, the following principles are used:

- the gain of the model is adapted with experience, based on the gain obtained for previous flushes
- discharge must be increased by about 60 % in order to reach the threshold that will initiate algal detachment
- then, the discharge is increased linearly until the maximum is reached, as defined by the discharge-turbidity transfer function.

These concepts have been used to design the feedforward controller which calculates a priori the command u_r to apply (see Sect. 6.2.4, Fig. 6.4).

Closed-Loop Control

Most of the operational control methods of irrigation canals are based the well-known linear PI controller. The calibration of the controller parameters must fulfil two contradictory objectives: reactiveness and stability. This calibration is

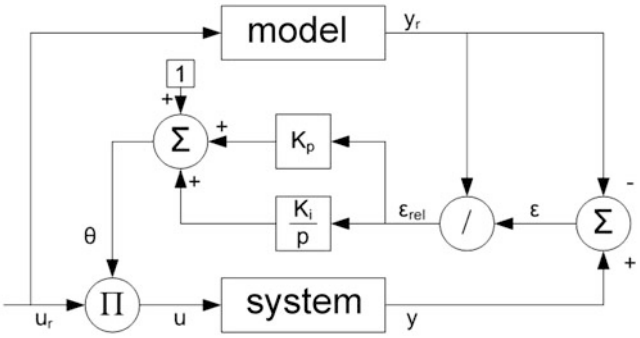

Fig. 6.4 Adaptive control as implemented at SCP (Branche Marseille Nord)

usually done by trial-and-error method. Due to the delay between action (upstream discharge) and system response (downstream turbidity), one may be tempted to increase reactiveness by increasing the proportional gain of the controller. This may cause undesired oscillations. When dealing with water quality, the delay is much larger than for hydraulic transfer, so the risk of instability is larger. The issue of delay times is discussed in the next section.

A second big issue is the large uncertainty when defining the transfer function gain between discharge and turbidity F_{QT}. When only hydraulic transfer is considered, the gain between upstream and downstream discharge is close to unity. It is a bit smaller if withdrawals are larger than supplies from intermediate tributaries, and larger than unity in the opposite case. Monitoring systems are usually installed at stations where large flow changes are likely to occur, so that the transfer function gains can be quite correctly estimated. Regarding quality control, there are cases where the situation is similar, for example when dilution is the main process governing the evolution of a solute concentration. This is the case for salinity control, as described in [16], in which it is shown that PI controller is able to maintain a desired salt concentration. The case of sediment or algae flushes is far more complex, since the downstream response to a discharge increase is mostly due to the interaction between the substrate and the flow, so that the flux of particles is far from being conserved between upstream and downstream sections. In the extreme case, one can have clear water at the upstream control section (concentration is 0), while downstream concentration can be large, due to internal erosion processes. In this case, the exchange process is a predominant term in (6.1), which will determine the gain of the transfer function. To date, there is no universal model which is able to predict with a good accuracy the erosion rate of non-cohesive sediment. This is even worse for cohesive sediments and algal biofilms, for which chemical and biological properties increase the complexity of the cohesion processes. For efficient flushes, another problem is that the material which can be eroded decreases with time during the flush, so that the gain of the transfer function is likely to decrease.

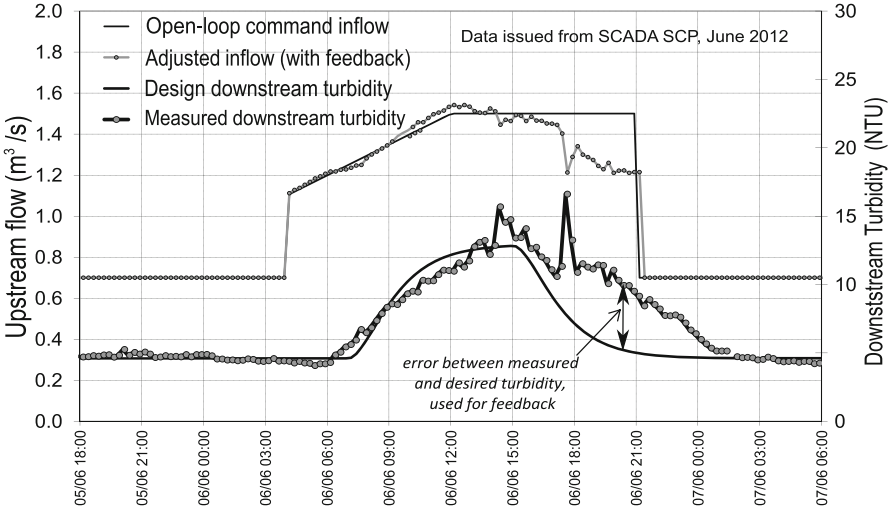

Fig. 6.5 Flush performed in June 2012, Branche de Marseille Nord (Canal de Provence), between Bimont dam and Figassons pumping station (km 19)

Adaptive control, which was designed to control systems with slowly varying gains, looks adequate for the real time control of flushes expected to cause erosion. This was implemented at the Canal de Provence and applied in routine since 2012. The controller is presented in Fig. 6.4. The initial command inflow (u_r) is given by the open-loop controller. During the flush, the relative error on the downstream turbidity is used to adapt the proportional and integral gains of a PI controller that will adjust the released flow by multiplying the initial command u_r. The correction θ takes account of the error of the transfer function (inaccurate initial gain), and to the adaptation process itself (decrease of erodible material during the flush). A speed of adaptation is also defined, which conditions the stability of the controller.

Figure 6.5 shows the performance of the flush performed in June 2012, with data extracted from the SCADA of the Canal de Provence, stations Bimont (upstream dam) and Figassons (control point 19 km further, with pumping station). Four curves are presented: open-loop flow command (u_r), adapted flow u, expected turbidity at downstream section, which is the result of the open-loop transfer function applied to u_r, and measured turbidity. One can see that the model response of the model was very good, in terms of delay and attenuation, during the first 13 h after the start of the flush. During this period, almost no correction was necessary (θ close to 1). Then, observed turbidity is greater than the expected one. This leads to decrease the command inflow. The flush is stopped after a regular decrease of the turbidity is observed, and the initial turbidity is recovered after about 3 h.

6.3 Discussion

6.3.1 Managing the Transport of Particles: What's New for Hydraulic Control?

Controlling the transport of particles in regulated open-channel networks open new perspectives for canal control. The example of algal management illustrates some of these perspectives, some parallels that can be drawn between the control of hydraulic variable and the control of quality variables, but also some new issues raised by the interplay between both problems. These perspectives are discussed below.

Does Quality Management Require a New Control Framework?

We have seen in the above example that the framework developed for hydraulic control can be extended to water quality control. Following the classification introduced by [11], Table 6.1 summarizes the framework which was applied to design the control of water quality during flushes, in parallel with the one used for hydraulic control.

Does the Superposition of Various Dynamics Makes the Control Problem More Complex?

A main issue with canal control is the delay between an action, for example a gate movement, and the expected result of this action. When you release water at the

Table 6.1 Summary of the control frameworks for hydraulic and quality

	Hydraulic control	Water quality control
Controlled variables	Flow, water level	Turbidity, concentration
Control action variables	Gate position, flow	
Process modeling	Saint-Venant's equations (SVE)	Advection-dispersion, SVE
Main uncertainties in transfer functions	Withdrawals, ungauged supplies	Erodible material, interplay between hydrodynamics and substrate
Real-time modeling	Linear models based on linearization of above equations, e.g. first or second-order with delay equations	
Control logics	Feedforward and feedback, upstream and downstream control	
Performance objectives	Satisfactory flow distribution, limited level fluctuations	Limitation of risks regarding quality and particle load, of hydraulic disturbances
	Limitation of operation and maintenance costs	

head of a canal, it will take time for the wave to arrive at a downstream section, and it will take more time to obtain the discharge which has been released, due to attenuation during flow propagation. These times do not only depend on the canal cross section characteristics, but also on the control structures which cause a backwater, and feedback between flow variation and level variation [14]. In practice, managers must consider the delays when planning gate operations in order to satisfy a delivery schedule. The optimal delay (or "response time") is the one which will ensure that the released volume is delivered to the targeted offtake [2]. This time is about 8 h for the Branche de Marseille Nord, between Bimont Dam and Figassons.

Regarding quality, one needs to consider other delays, such as the travel time of particles (denotes T_p) or the travel time of a turbidity cloud. During a flush performed with an upstream flow release, the discharge increase will cause erosion in the upstream section, then the corresponding turbidity is transported at the bulk velocity. The hydraulic wave also propagates downstream, more rapidly than the particles of water causing erosion. The superposition of all these phenomena makes it difficult to calculate the delay times between flow release and turbidity response. This turbidity response is also characterized by a time of arrival, greater than the travel time of surface waves (T_{sw}), and a peak time, which in our study case corresponds to the travel time of particles. The definitions of these times are summarized in Table 6.2. They can be easily obtained by simulation, as illustrated by Fig. 6.6 for the Branche de Marseille Nord. The travel time of particles is much larger than the others. These hydraulic times can be related to the parameters of the simplified transfer functions:

- The delay τ_Q is close to T_{sw};
- $\tau_Q + K_Q$ corresponds to the travel time of long waves T_{lw} [2];
- similarly, $\tau_T + K_T$ corresponds to the travel time of particles T_p. In our case, it also corresponds to $\tau_D + K_{D_1} + K_{D_2}$.

A second key issue is the uncertainty inherent to the erosion processes:

- The existence of a threshold before erosion can occur is likely to increase these delays.
- There may be a large spatial variability of the material likely to be flushed. If, for example, no algae or no sediment were present in the downstream reaches, then no material would be detached and entrained when the wave arrives. This also delays the response.

Table 6.2 Definition and calculation of hydraulic times, for a reach between abscissas x_1 and x_2

Travel time of particles	$T_p = \int_{x_1}^{x_2} \frac{dx}{U}$	U mean flow velocity
Travel time of surface waves	$T_{sw} = \int_{x_1}^{x_2} dx/\left(U + \sqrt{gA/B}\right)$	g gravity constant, B top width, A flow area
Travel time of long waves	$T_{lw} = dV/dQ$	V volume of the reach, Q mean discharge in reach

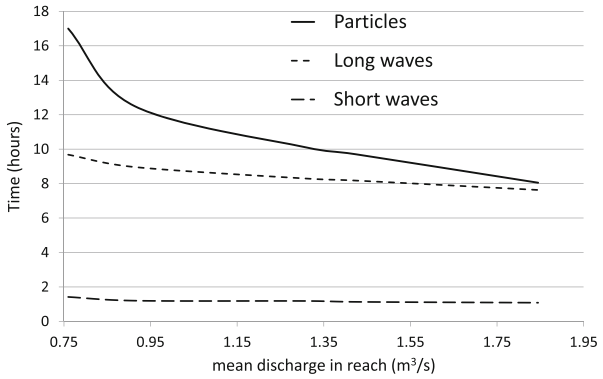

Fig. 6.6 Delay times, Branche de Marseille Nord, between Bimont Dam to Figassons. The x-axis corresponds to the mean discharge in the reach. Simulations are done with SIC

The superposition of all these aspects makes it difficult to identify the main processes that need to be considered when managing the canal system.

6.3.2 Estimating the Performance of Control Strategies

Managing algal issues by hydraulic methods has been innovative, and the evaluation of the strategy is a frequent question. Two time scales must be considered to start addressing this issue.

On the short term, we must evaluate the performance of a flush. To do so, standard hydraulic criteria could be used, such as Mean Absolute Error or Integral of Absolute Error [3] or released volume, which, in some cases, may be lost if it is not stored downstream. Since the primary objective of the flush is to detach fixed material, it makes more sense to build an indicator reflecting the efficiency of the flush. To do so, it is preferable to use the integral of turbidity at the downstream end, I_T, which can be calculated explicitly as a function of the flush parameters (discharge increment and duration) [7]. Then the open-loop model was build by maximizing I_T with the constraint that turbidity does not overcome a given threshold. For example, for the flush of Fig. 6.5, I_T is equal to 90 NTU.hr, which 1.38 times the value initially used for the design of the flush. This indicator indicates that the flush has been as efficient as expected. It also suggests that the initial biomass was under-estimated.

In this case, no hydraulic performance indicator is considered. This was not a problem since flushes were performed during the night when water demand was the lowest. However, in some other cases, water level fluctuations may be an issue for gravity offtakes. This would lead to build multiple criteria in order to take account of both turbidity and hydraulic objectives. These objectives are antagonistic, since larger detachment efficiency will implies larger hydraulic disturbances. The design

of the control method and the performance evaluation then requires writing the optimization problem with an aggregated performance measure, and constraints with both turbidity and hydraulic variables. The performance measure may be written as a weighted combination of I_T and hydraulic performance indicators, such as normalized errors on water levels, with weighing factors set by experience of the manager.

On the long term, the performance must be measured with more integrative criteria. Regarding the issue of algae development, since it is hardly feasible to get direct measurements of biomass, indirect estimations of the performance can be obtained by registering the disturbances caused by algae, such as filters clogging, increase of water levels due to increased bottom friction, etc.

6.3.3 A Unified Framework for Transport of and over Water?

The example of algae management illustrates the idea that multiple (and sometimes antagonistic) objectives may be searched while controlling hydraulic structures. In this study case, a unified framework was applied for both quantity and quality management, with three main components: building appropriate models for each of the considered processes, defining performance indicators, and then designing appropriate controllers.

The interplay results from the fact that the same hydraulic variables are involved. For instance, the flow velocity needs to be increased in order to detach algae, keeping the water levels high enough so that algae present on the banks remain in water during the flushes. This increase of velocity therefore causes an increase of discharge, and thus an excess of flow passing through the system. Regarding transport over water, flow velocity is also a key variable that will be used to express the fluxes of boats, while water levels must remain within a desired range. We can see some evident parallels with the issues of flushing flows.

Therefore, we think that a unified framework can be applied for the control of waterways regarding transport of water and transport over water. This supposes to develop appropriate models for each of the processes, and then controllers using either hydraulic variables, or other variables that can be measured in real time such as turbidity or transport loads. Performance indicators must be properly designed and weighed, in case multiple objectives need to be achieved at the same time.

6.3.4 Open Topics

Understanding and managing the interplay between hydraulic control and water quality requires improving our representation of the involved processes. Among these processes, the effect of hydrodynamics on the biological substrate is the one which introduces the most uncertainty in the exchange term of

advection-dispersion (6.1). Local studies, with fluid mechanics tools, can give an insight on the basic processes, the key variables, the thresholds required to obtain the detachment of an algal filament, ... Nevertheless, at the scale of the studied system, we are not able to go into such detailed representations, and it is reasonable to choose integrative variables such as mean biomass and mean critical shear stress. Based on that, (6.2) seems appropriate to represent the exchange term. Still, the time constant and the critical shear stress depend on the biological substrate.

Also, large uncertainties remain however on the transfer function between discharge and turbidity. Turbidity response is directly proportional the detachable biomass which a key state variable. As physical sampling is hardly feasible in an operational context, indirect measurement methods based on a combination of sensors could be a solution. Conversely, the vegetation growth may dramatically increase the roughness, causing overflowing in some extreme cases. Although laboratory-scale studies have brought an inside on this issue [9], the link between global biomass and hydraulic properties still need to be explored. There is room today for many fruitful interactions between hydrobiology and fluid mechanics [12]. While most of the studies are performed in river contexts, some issues are very specific to regulated open-channels, such as the flow variations imposed by gate operations, or the way detached material are transported from upstream to downstream, passing or not check structures and bifurcations.

The control structures give also the chance to manage vegetation and water quality at the same time as water volumes. This leads to consider multiple management objectives and constraints, to consider new performance criteria, and to develop new methods able to address the specific issues of water quality control. For real time control during a flush, adaptive control was a way to deal with large uncertainties on initial biomass, and re-estimate this biomass in real time. Other frameworks may be worth studying, such as model predictive control (as used in [16] for salinity control), with data assimilation for real-time estimation of biomass, and performance criterion aggregating quality and hydraulic performance.

6.4 Conclusions and Future Research

With the diversification of uses of the hydraulic infrastructures, which is pushed by integrated water management objectives, it is necessary to adapt the hydraulic management strategies of these systems with adapted indicators and rules. We have shown a study case in which hydraulic management is expected to control complex water quality aspects: in order to control the fixed algae populations, flushes are performed regularly in a multi-purpose open-channel network, a strategic infrastructure for agriculture, industries and domestic water in South-Eastern France; during a flush, water quality is controlled in real-time thanks to advanced automatic command methods.

This example has illustrated issues linked to the interplay between concurrent objectives. The complexity of the management is largely increased by the superposition of different processes, with multiple delays and attenuation dynamics between action and system response. These issues have raised new questions about modeling (comprehensive models and simplified more adapted to real-time control), and about management methods able to address uncertainty and multi-objective criteria. Some of these questions will be raised by the interplay between transport of water and over water.

Further research will continue the efforts to characterize the links between hydraulic management and water quality, with an increased focus on aquatic plants which, like algae, are subject to withdraw nutrients from the water bodies but also cause very large friction. This requires considering larger time scales, with seasonal evolution of biomass and impact of hydraulic control on nutrient cycles.

Acknowledgements The case presented in this chapter was studied under project "Algequeau" supported by the French National Research Agency. The Societe du Canal de Provence is gratefully acknowledged for providing field data and implementing the real-time control strategies. The authors are also very thankful to Dr Ophelie Fovet who was a key actor of the project.

References

1. Belaud G, Baume J-P. Maintaining equity in a surface irrigation network affected by silt deposition. J Irrig Drain Eng. 2002;128(5):316–325.
2. Belaud G, Litrico X, Clemmens AJ. Response Time of a Canal Pool for Scheduled Water Delivery. J Irrig Drain Eng. 2013;139(4):300–308.
3. Clemmens AJ, Kacerek TF, Grawitz B, Schuurmans W. Test cases for canal control algorithms. J Irrig Drain Eng. 1998;124(1):23–30.
4. Creaco E, Bertrand-Krajewski J-L. Numerical simulation of flushing effect on sewer sediments and comparison of four sediment transport formulas. J Hydraul Res. 2009;47(2):195–202.
5. Cunge JA, Holly FM, Vervey A. Practical aspects of computanional river hydraulics. Boston: Pitman; 1980.
6. Fovet O, Belaud G, Litrico X, Charpentier S, Bertrand C, Dollet P, Hugodot C. A model for fixed algae management in open-channels using flushing flows. River Res Appl 2012;28(7):960–972.
7. Fovet O, Litrico X, Belaud G. Turbidity management during flushing-flows: a model for open-loop control. Adv Water Res. 2012;39:7–17.
8. Fovet O, Litrico X, Belaud G, Genthon O. Adaptive control of algae detachment in regulated canal networks. J Hydroinformatics 2013;15(2):321–334.
9. Labiod C, Godillot R, Caussade B. The relationship between stream periphyton dynamics and near-bed turbulence in rough open-channel flow. Ecol Model. 2007;209:78–96.
10. Litrico X, Fromion V. Frequency modeling of open channel flow. J Hydraul Eng 2004;130(8):806–815.
11. Malaterre P-O, Rogers DC, Schuurmans J. Classification of canal control algorithms. J Irrig Drain Eng. 1998;124(1):3–10.
12. Nepf H. Hydrodynamics of vegetated channels. J Hydraul Res. 2012;50(3):262–279.

13. Rabbani T, Munier S, Dorchies D, Malaterre P-O, Bayen A, Litrico X. Flatness-based control of open-channel flow in an irrigation canal using SCADA [applications of control]. Control Syst IEEE. 2009;29(5):22–30.
14. Strelkoff T, Deltour J-L, Burt C, Clemmens AJ, Baume J-P. Influence of canal geometry and dynamics on controllability. J Irrig Drain Eng. 1998;124(1):16–22.
15. Wu W. Computational river dynamics. London: Taylor & Francis; 2008.
16. Xu M. Real-time control of combined water quantity & quality in open channels. PhD thesis, TU Delft; 2013.

Chapter 7
Coordinating Model Predictive Control of Transport and Supply Water Systems

C.C. Sun, V. Puig, and G. Cembrano

Abstract Transport and supply water networks are two types of systems which have received a significant amount of attention in the recent years. Issues on how to obtain the best performance for a given transport or supply water systems, or how to coordinate interactions between them are still open and need more research. This chapter presents a hierarchical Model Predictive Control (MPC) scheme with a supervisor that coordinates transport and supply water systems. First, a two-level hierarchical control structure resulting from a functional decomposition of water network is briefly presented. Inside each hierarchy, an MPC controller is used. In the two-level hierarchy, a supervisory coordinating mechanism is used to generate control strategies which consider objectives at different time scales. The first level, in charge of managing the transport system, works in a daily scale in order to achieve the global management policies for the transport over water (e.g., navigation, vessels and barges) in different rivers and balance management of different reservoirs. The second level, in charge of managing the supply system, works in a hourly scale and manipulates actuator (pumps and valves) set-point to satisfy the local water supplying objectives (e.g., minimizing economic cost, handling emergency storage and smoothing actuator operation). The results of the modeling will be applied to the Catalunya Regional Water Network and based on an aggregate model.

C.C. Sun
Advanced Control Systems Group, Institut de Robòtica i Informàtica Industrial, CSIC-UPC, Barcelona, Spain
e-mail: csun@iri.upc.edu

V. Puig (✉)
Advanced Control Systems Group, SIC-UPC, Barcelona, Spain
e-mail: vicenc.puig@upc.edu

G. Cembrano
Advanced Control Systems Group, CSIC-UPC, and CETaqua, Water Technology Centre, Barcelona, Spain
e-mail: cembrano@iri.upc.edu

C. Ocampo-Martinez, R.R. Negenborn (eds.), *Transport of Water versus Transport over Water*, Operations Research/Computer Science Interfaces Series 58,
DOI 10.1007/978-3-319-16133-4_7

7.1 Introduction

From a functional perspective, a regional water network can be structurally organized into two separate systems:

- Transport system, composed by water sources, open channels, large reservoirs and also natural aquifers.
- Supply system, which links water treatment and desalinization plants with reservoirs distributed all over the city.

Both of the partitions of a regional water network must be operated at different time scale because of the different dynamics they present according to their specified objectives. In general, these systems are normally separately operated. The coordinated operation of supply and transport systems in a regional network is one of the main motivations for the research reported in this chapter.

In recent literature, there is a renewed interest in hierarchical MPC either from industrial practice or from academia [10, 11]. This is specially the case when a system is composed of subsystems with multiple time scales as the case of the regional water networks. A straightforward task of designing and implementing a single centralized control unit is too difficult as discussed in [3], because the required long prediction horizon and short control time steps might lead to an optimization problem of high dimension and under large uncertainty radius. A way to cope with this problem is to apply a hierarchical control based on decomposing the original control task into a sequence of different, simpler and hierarchically structured subtasks, handled by dedicated control systems operating at different time scales [1].

This chapter proposes a temporal hierarchical MPC scheme for complex transport and supply water systems. The proposed strategy will coordinate the MPC controllers for the transport and supply systems by means of a temporal hierarchical sequence of optimization problems with constraints going from one level of the hierarchy to the other. Case study and results are described in Sect. 7.2. Interdisciplinary discussion about the unified framework and some open topics are explained in Sects. 7.3 and 7.4, respectively. Finally, conclusions and future research are provided in Sect. 7.5.

7.2 Case Study: Catalunya Regional Water Network

The Catalunya Regional Water Network in Fig. 7.1 lies within the Catalunya Inland Basins, from which the Metropolitan area of Barcelona is fed and where most of the population is concentrated. It composed by river *Llobregat*, *Ter* and the related components. According to definition of functional decomposition, the Catalunya Regional Water Network can be separated into two systems. The transport system, composed by rivers *Llobregat*, *Ter* and all the connected elements, lies at the two side of Fig. 7.1. The supply system, composed by metropolitan areas and also treatment, desalination plants inside them, lies in the center.

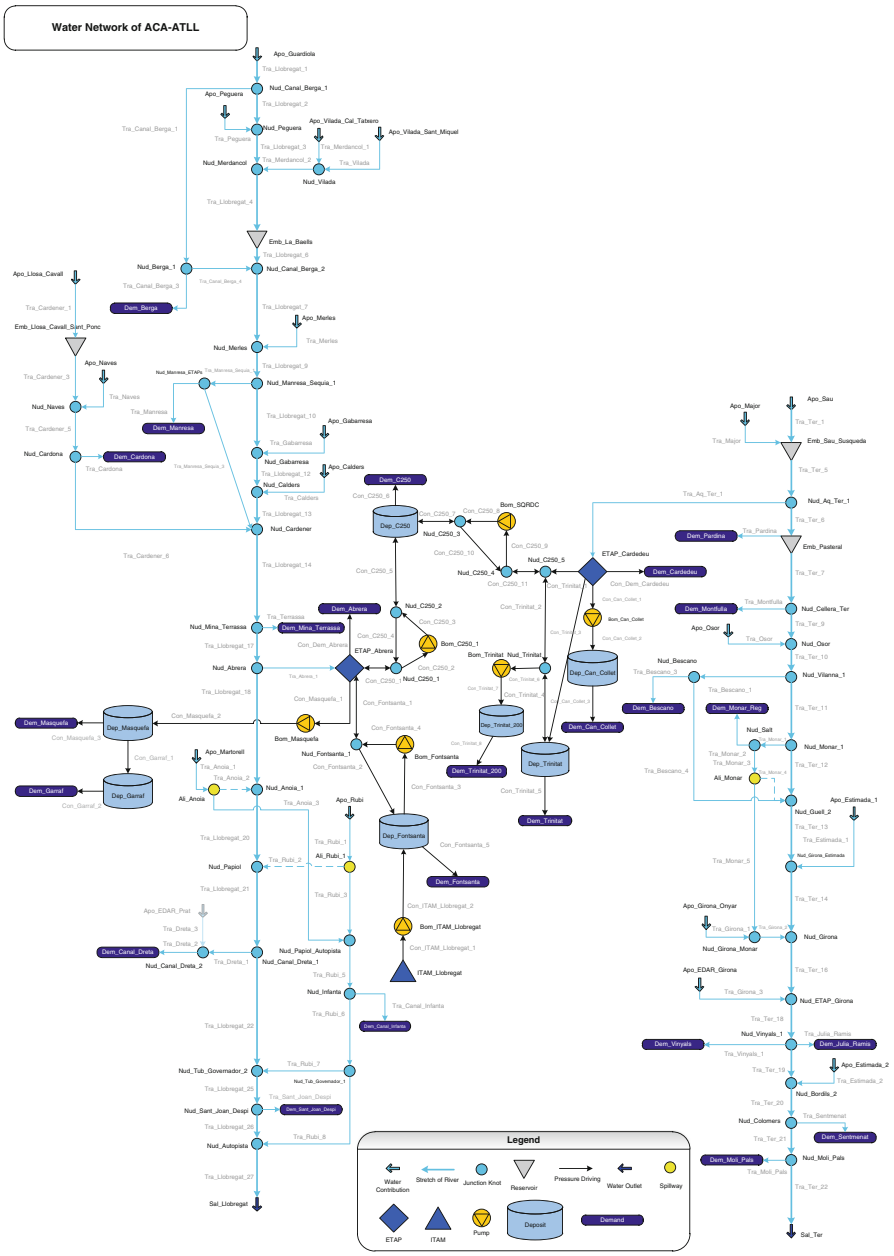

Fig. 7.1 Aggregate diagram of Catalunya regional water network

7.2.1 Operational Goals of the Transport System

The goal of a water transport system is basically to maintain the river water levels while providing water to the supply system and satisfying irrigation demands.

The control problem of the transport system is typically operated within a 30-day horizon, at daily time scale and operational goals should be achieved are:

- *Operational safety* (J_{safety}): This criterion refers to maintain appropriate water storage levels in dams and reservoirs for emergency-handling.
- *Demand management* (J_{demand}): This is especially important in the transport system when urban and irrigation demands exist since urban demands must be fully satisfied while irrigation demands allow some degree of slackness.
- *Balance management* ($J_{balance}$): This is necessary for keeping rivers or reservoirs to be used in a balanced way and escaping water deficit problem in a longer time.
- *Minimizing waste* (J_{mwaste}): Taking into account that the river water eventually goes to the sea, this term ties to avoid unnecessary water release from reservoirs (that is release water that does not meet any demand and is eventually wasted).
- *Transport water levels* (J_{level}): Water sources such as boreholes, reservoirs and rivers are usually subject to operational constraints to maintain certain water levels which are needed for transporting over water and maintaining ecological flows.
- *Control actions smoothness* ($J_{smoothness}$): The operation of transport over water usually requires smooth flow set-point variations for best process operation.

7.2.2 Operational Goals of the Supply System

The immediate control goal of water supply system is to meet the demands at consumer sites with appropriate flows and optimized costs according to users' needs.

The supply network is typically operated with a 24 h horizon, at hourly time scale. The main operational goals to be achieved in the supply network are:

- *Cost reduction* (J_{cost}): Water cost is related to treatment, which have different prices at different sources, and due to different source elevations, which implies electrical pumping costs affected by power tariffs which may vary in a day.
- *Operational safety* (J_{safety}): This criterion refers to maintain appropriate water storage levels in dams and reservoirs of the network for emergency-handling.
- *Control actions smoothness* ($J_{smoothness}$): The operation of water treatment plants and main valves/pumps usually requires smooth flow set-point variations for best process operation.

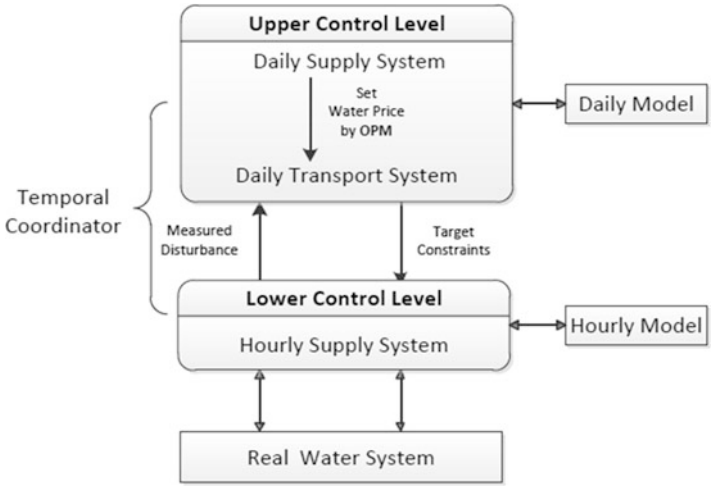

Fig. 7.2 Temporal hierarchical coordinating structure

7.2.3 Temporal Hierarchical Coordinating Technique

The general principle of a pure temporal hierarchical controller is that: decision of a higher level has a wider temporal extent than that of a lower level, and the higher level decision units process more aggregated information than the lower ones [2].

In this chapter, transport system could be assumed as the upper level, while supply systems could be considered as the lower level. This temporal hierarchical coordinating structure is proposed in Fig. 7.2. In the upper level, the daily model of the supply system is used in order to estimate the aggregated prices (which include both water and electricity costs) by means of the *optimal path method* (OPM) in [4, 6]. Detailed algorithms for this temporal coordination mechanism will be provided in detail in the following section.

7.2.4 MPC of the Transport System

State Space Model

State space model of transport system includes two kind of states and control variables. First kind of state variables represent reservoirs and the managed variables correspond to actuator flows:

$$x(k+1) = A\,x(k) + B\,u(k) + B_p\,[d(k) - \varepsilon(k)], \quad k \in \mathbb{Z} \tag{7.1}$$

where $x(k) \in \mathbb{R}^{n_x}$ are reservoir volumes, $u(k) \in \mathbb{R}^{n_u}$ are actuator flows, $d(k) \in \mathbb{R}^{n_d}$ represents disturbance demands, $\varepsilon(k) \in \mathbb{R}^{n_d}$ is slack variable for violated demands and $\varepsilon(k)$ is introduced to control the amount of demand which has not been satisfied.

The second kind of state and control variables represent river flows with delays. For simplicity and brevity, consider river reach model as a transport delay [7]:

$$q_{out_i} = q_{in_i}(k - \tau_d), \tag{7.2}$$

where τ_d represents delay values.

For time delays associated with flows within the network, the following auxiliary state equations are introduced:

$$x_{j,1}(k+1) = q_j(k), \tag{7.3}$$

$$x_{j,i+1}(k+1) = x_{j,i}(k), i = 1, \cdots, \tau_d, \tag{7.4}$$

where $x_{j,i}(k) \in \mathbb{R}^{n'_x}$ represent flows, $q_j(k) \in \mathbb{R}^{n'_u}$ means flow as part of control variables and $\tau_d \in \mathbb{Z}$ is number of delays.

Combining (7.3), (7.4) with (7.1), state space representation (7.1) becomes

$$\tilde{x}(k+1) = \tilde{A}\,\tilde{x}(k) + \tilde{B}\,\tilde{u}(k) + \tilde{B}_p\,[d(k) - \varepsilon(k)], \quad k \in \mathbb{Z}, \tag{7.5}$$

where

$$\tilde{x}(k) = \begin{bmatrix} x(k) \\ x_{j,i}(k) \end{bmatrix}, \quad \tilde{u}(k) = \begin{bmatrix} u(k) \\ q_j(k) \end{bmatrix},$$

and $\tilde{x}(k) \in \mathbb{R}^{\tilde{n}_x}$, $\tilde{u}(k) \in \mathbb{R}^{\tilde{n}_u}$.

All the variables are subject to the following inequality constraints:

$$\tilde{x}_{min} \le \tilde{x}(k) \le \tilde{x}_{max}, \tag{7.6}$$

$$\tilde{u}_{min} \le \tilde{u}(k) \le \tilde{u}_{max}, \tag{7.7}$$

$$\varepsilon_{min} \le \varepsilon(k) \le \varepsilon_{max}, \tag{7.8}$$

where $\tilde{x}_{min}$, $\tilde{x}_{max}$ are physical limitations of reservoirs, $\tilde{u}_{min}$, $\tilde{u}_{max}$ are physical limitations of the river flows and ε_{min} lies between zero and the related demand.

Besides that, the balance at every node should be satisfied, where E, E_d, $E_{\tilde{x}}$ are matrices which parameters can be obtained from topology of the water network:

$$E\,\tilde{u} + E_d\,d - E_d\,\varepsilon + E_{\tilde{x}}\,\tilde{x} = 0.$$

Control Objectives

Operational goals of the transport system lead to the following function:

$$J = J_{safety} + J_{demand} + J_{mwaste} + J_{balance} + J_{level} + J_{smothness} \tag{7.9}$$

$$= \varepsilon_{\tilde{x}}(k)^{\top} W_{\tilde{x}} \varepsilon_{\tilde{x}}(k) + \varepsilon(k)^{\top} W_f \varepsilon(k) \tag{7.10}$$

$$+ (\tilde{u}_{i\ldots j}(k) - \tilde{u}_s(k))^{\top} W_{\tilde{w}} (\tilde{u}_{i\ldots j}(k) - \tilde{u}_s(k)) \tag{7.11}$$

$$+ (\left(0 \ \ldots 0 \ \ \frac{1}{x_{i,max}} \ \ 0 \ldots 0 \ \ \frac{-1}{x_{j,max}} \ \ 0 \ldots \ 0\right) \tilde{x}(k))^{\top} w_{\tilde{m}} \tag{7.12}$$

$$\times (\left(0 \ \ldots 0 \ \ \frac{1}{x_{i,max}} \ \ 0 \ldots 0 \ \ \frac{-1}{x_{j,max}} \ \ 0 \ldots \ 0\right) \tilde{x}(k))$$

$$+ \Delta\tilde{u}(k)^{\top} W_{\tilde{u}} \Delta\tilde{u}(k), \tag{7.13}$$

where

$$\varepsilon_{\tilde{x}}(k) = \tilde{x}(k) - \tilde{x}_r,$$

$$\tilde{u} = \Theta\Delta\tilde{u} + \Pi\tilde{u}(k-1),$$

$$\Delta\tilde{u}(k) = \tilde{u}(k) - \tilde{u}(k-1),$$

and $W_{\tilde{x}}$, W_f, $W_{\tilde{w}}$, $W_{\tilde{x}}$, $w_{\tilde{m}}$, $W_{\tilde{u}}$ are weights which decide the priorities (established by the water network authorities) for all the objective terms.

Water storage in reservoirs should be kept above a given level (named as water safety level) which is used as emergency supply for drought period. Any situation below the emergency level should be penalized using soft constraints:

$$\tilde{x} \geq \tilde{x_r} - \varepsilon_{\tilde{x}}, \tag{7.14}$$

$$\varepsilon_{\tilde{x}} \geq 0, \tag{7.15}$$

where $\tilde{x_r}$ is the water safety level and $\varepsilon_{\tilde{x}}$ is the slack to $\tilde{x_r}$.

7.2.5 MPC of the Supply System

Basic state-space model is used for the supply system [9].

Control Objectives

Operational goals of the supply system will lead to the following function:

$$J = J_{safety} + J_{smothness} + J_{cost} \tag{7.16}$$

$$= \varepsilon_{\tilde{x}}(k)^{\top} W_{\tilde{x}} \varepsilon_{\tilde{x}}(k) + \Delta\tilde{u}(k)^{\top} W_{\tilde{u}} \Delta\tilde{u}(k) + W_a(a_1 + a_2(k))\tilde{u}(k), \tag{7.17}$$

where

$$\begin{aligned} \varepsilon_{\tilde{x}}(k) &= \tilde{x}(k) - \tilde{x}_r, \\ \tilde{u} &= \Theta\Delta\tilde{u} + \Pi\tilde{u}(k-1), \\ \Delta\tilde{u}(k) &= \tilde{u}(k) - \tilde{u}(k-1), \end{aligned}$$

and $W_{\tilde{x}}$, $W_{\tilde{u}}$, W_a are weights which establish the priorities for the objective terms and the vectors a_1 and a_2 contain the cost of water treatment and pumping, respectively.

7.2.6 Temporal Hierarchical Coordinating Technique

Optimal Path Method

When optimizing the transport system, the whole supply system will be simplified into a virtual demand with unitary price after considering both the treatment and electricity costs. In order to determine this unitary price, OPM is used [4].

There are three steps for realizing OPM:

- Step 1. *Searching Exhaustive Paths*: Find all possible paths from sources to demands detecting closed cycles to avoid infinite loops.
- Step 2. *Choosing Optimal Path*: Find optimal path from the all paths set obtained in Step 1.
- Step 3. *Calculating the source price*: Calculate the source price by the total cost and the water consumption in the optimal path obtained in Step 2.

Searching exhaustive paths: In order to search optimal economical paths from sources to demands, it is necessary to determine all possible paths between them [5]. Before that, a node-arc representation method for a regional water network is provided, where a node represents a source, reservoir, demand or junction and an arc represents a transfer or trade [4].

In a regional water network, all flow paths can be obtained from node-arc incidence matrices because water always flows from upstream sources to downstream. In a node-arc incidence matrix, a node is represented by a row and an arc is represented by a column. In a row of the matrix, entry arcs are represented by $+1$ and leaving arcs are represented by -1. In a column, an element of $+1$ and an element of -1 represent the ending and starting nodes, respectively, of this arc.

Table 7.1 shows the node-arc incidence matrix for the network in Fig. 7.3. On the other hand, the node-arc incidence matrix that defines the relationship of the direction between nodes and arcs is transformed into a flow path matrix that defines

Table 7.1 Node-arc incidence matrix for the network of Fig. 7.1

Node	Arc 1	Arc 2	Arc 3	Arc 4	Arc 5	Arc 6
1	−1	−1	−1	0	0	0
2	+1	0	0	−1	0	−1
3	0	+1	0	+1	−1	0
4	0	0	+1	0	+1	+1

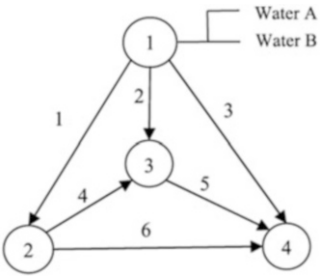

Fig. 7.3 A hypothetical network system

all flow paths of the network. The flow path matrix A is a set of binary parameters $a_{s,r}$ that describe all flow paths in a water network

$$A = \begin{pmatrix} a_{1,1} & a_{1,2} & a_{1,3} & \ldots\ldots & a_{1,p} \\ a_{2,1} & a_{2,2} & a_{2,3} & \ldots\ldots & a_{2,p} \\ a_{3,1} & a_{3,2} & a_{3,3} & \ldots\ldots & a_{3,p} \\ \vdots & \vdots & \vdots & \ddots\ddots & \vdots \\ a_{n,1} & a_{n,2} & a_{n,3} & \ldots\ldots & a_{n,p} \end{pmatrix}.$$

In this matrix A, which is the target matrix in this section, p denotes number of paths and n denotes total number of arcs (or flow actuators) in a water network. A column represents a flow path and a row represents an arc in the network. The connection parameters $a_{s,r}$ is binary $(0, 1)$ and is used to describe the connection between source nodes and receiving nodes. The connection parameters are assigned equal to 1 for linking arcs s in a flow path r, while other arcs are assigned 0.

Choosing optimal path: The objective of this step is to find the optimal flow through each path. The optimal flow path problem can be formulated as a linear optimization problem as follows:

$$min_x c^T Ax \qquad \text{subject to} \qquad \begin{array}{l} Ax \le b \\ A_{eq}x = b_{eq} \\ l_b \le x \le u_b \end{array} \tag{7.18}$$

where c, x, b, b_{eq}, l_b and u_b are vectors and A and A_{eq} are matrices. The meaning of these vectors and equations is described in the following.

Optimal path solution x***:*** The vector x contains the optimal flow through each path that minimize the total operational cost. This cost is measured by the

operational cost of each actuator, and the actuators involved in each path according to the flow path matrix A. The cost function can be expressed as $c^T Ax$, where Ax provides the total flow through each actuator.

Operational cost c**:** The daily cost of each actuator is calculated as the mean cost value:

$$c(i) = \sum_{k=1}^{24} \frac{\text{cost}(i,k)}{24}, \tag{7.19}$$

where i represents the actuator and index k represents the instant time.

Actuator constraints $Ax \leq b$**:** Inequality constraints are related to actuator operational limits. One actuator can be involved in different paths, and each path can require a different constant flow through it. So, it is necessary to guarantee that the total flow for each actuator does not go beyond its upper limit.

As explained in the previous section, A, whose row dimension is the number of actuators and column dimension is the number of paths, is a matrix formed by ones and zeros that indicates which actuators are used in each path. The product of this matrix with the solution vector x gives as a result the flow that goes through each actuator. Vector b contains the maximum actuator flow.

Demand constraints $A_{eq}x = b_{eq}$**:** The total volume of water from sources to each demand sector must be equal to its demand. This can be expressed by using equality constraints related to demands and by introducing matrix A_{eq} that indicates which demand sector is supplied from which path. The row dimension of matrix A_{eq} is number of demand sectors while column dimension is number of paths.

Path capacity constraints l_b ***and*** u_b**:** They are used to restrict the flow in each path by establishing the interval of possible values due to operational limits of the actuators involved in the path. The upper limit u_b is given by the minimal of the actuator upper bounds involved the path, while the lower limit l_b is the maximal of the actuator lower bounds in the path.

Calculating the source price: From the optimal flow path calculation, the source price for the transport layer (including both the production and transportation cost) can be obtained as indicated in Algorithm 7.1 in lines 23 and 24. The economical unitary costs for the sources, C_{s1} and C_{s2}, are calculated by weighted averaging the optimal flow paths linking each source with the supply demands. The detailed calculations for every step of OPM are described in Algorithm 7.1.

Coordinating Mechanism

As shown in Fig. 7.2, the transport and supply systems are coordinated by interchanging the following information:

- Measured disturbance (d_s): which provides the daily demands to the transport layer by aggregating the hourly demands in the supply layer.

Algorithm 7.1 Optimal path method

1: $x := [x_1, x_2, \ldots, x_p]$;
{optimization vector}
2: $l_b := [min_{x_1}, min_{x_2}, \ldots, min_{x_p}]$;
{lower bounds of x}
3: $u_b := [max_{x_1}, max_{x_2}, \ldots, max_{x_p}]$;
{upper bounds of x}
4: $Source := [s_1, s_2]$;
{source matrix}
5: $b_{eq} := [d_1, d_2, \ldots, d_m]$;
{demand node matrix}
6: $Actuator := [a_1, a_2, \ldots, a_n]$;
{actuator matrix}
7: build $0-1$ exhaustive path matrix
8: $Path := [s_1, a_{11}, a_{21}, \ldots, d_1; \ldots; s_2, a_{12}, a_{22}, \ldots, d_m]$
{number of row is p}
9: build $0-1$ actuator and path matrix
10: $A := [a_{11}, a_{21}, \ldots, a_{p1}; \ldots; a_{n1}, a_{n2}, \ldots, a_{pn}]$
11: $b := [max_{a_1}, max_{a_2}, \ldots, max_{a_n}]$
{maximum flow column for all the actuators}
12: build $0-1$ demand and path matrix
13: $A_{eq} := [d_{11}, d_{21}, \ldots, d_{p1}; \ldots; d_{m1}, d_{m2}, \ldots, d_{mp}](24)(3600)$
14: Build cost matrix contain electrical and water cost
15: $c := [c_1; c_2; \ldots; c_n]$;
16: Set objective function
17: $f_{obj} = c^T Ax$;
18: Optimizing the problem
19: $x = linprog(f_{obj}, A, b, A_{eq}, b_{eq}, l_b, u_b, x_0, option)$
{x_0 is provided}
20: Calculating the flow through each actuator;
21: $flow = Ax$
22: Calculating the source price by weighted averaging the optimal flow paths linking sources and demands;
23: $C_{s1} = c_{s1}^T (A[s1, :]x(s1))/flow[s1]$
24: $C_{s2} = c_{s2}^T (A[s2, :]x(s2))/flow[s2]$

- Target constraint (T_d): which expresses management policies from the transport system to the supply system in the form of control constraints.

Measured disturbance: In the topology of the transport system, the whole supply system is simplified as one aggregated demand. Measured disturbance for the transport system is obtained by aggregating the hourly demands in the supply layer.

$$d_s(k) = \sum_{m=1}^{24} d_t(k, m), \tag{7.20}$$

where d_t is the hourly demand vector at the supply system corresponding to the k-th day, while $d_s(k)$ could be considered as the demand for the transport system.

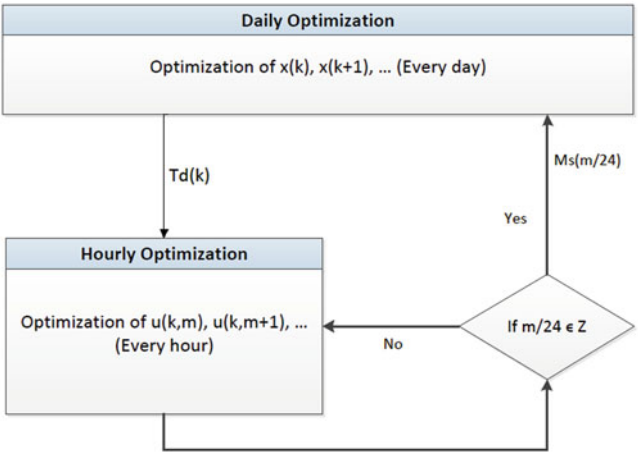

Fig. 7.4 Upper and lower layer optimizations of multi-layer MPC

Target constraints: The goal for the temporal coordination algorithm is transferring management policies from the transport to the supply system for overall controlling of transport over water network and supply water network. In order to achieve this coordination, the following constraint is added to the MPC controller in the supply system:

$$\sum_{m=1}^{24} u(k,m) \leq T_d(k), \tag{7.21}$$

where u is the shared control vector between transport and supply systems.

This constraint is introduced to enforce the amount of water decided to be transferred from the transport to the supply system is satisfying the management policies in the transport layer. Structure of the temporal coordinator is shown at Fig. 7.4.

Formulation of Temporal Coordination Problem

The goal for the temporal coordination algorithm is transferring management policies from the transport to the supply layer. In order to achieve this coordination, the constraint (7.21) is added to the supply hierarchical MPC. Algorithm 7.2 shows how this constraint, that establishes a daily limitation, is generated and adapted at every time iteration of the lower layer MPC that operates at a hourly scale. Algorithm 7.2 takes into account the following facts when generating the constraint (7.21):

- after the application of n hourly control actions $u_s(m)$ corresponding to the k-th day, the total remaining water for this day will be: $T_d(k) - \sum_{m=1}^{n} u(m)$.
- when limiting the control actions in the prediction horizon L, there is a part of control actions $u(m)$ that corresponds to hours of the current day k that should be limited by $T_d(k)$, while the control actions correspond to hours of the next day $k+1$ that should be limited by $T_d(k) - \sum_{m=1}^{n} u(m)$.
- the generated constraints are added as additional constraints of the BOP problem associated to the supply MPC.

7.2.7 Results for the Transport System

There are three scenarios in practical use, which are:

- *Scenarios 1*: More initial water in Llobregat than in Ter.
- *Scenarios 2*: More initial water in Ter than in Llobregat.
- *Scenarios 3*: Initial water in both rivers are similar.

According to reality use, for the first two scenarios, when water in one river is adequate while in another river limited, management policies will be set to ask water from only one of the rivers. For the Scenario 3, when water is abundant in both of rivers, according to the balance management control objectives, water consumption in both of the rivers will be proportional to their supplying capacity.

Table 7.2 provides detailed results and also the improvement of water usages in the two rivers achieved by the proposed multi-hierarchical MPC scheme. In this table, *Source* means outside sources flow into rivers, *Fixed Demand* means fixed demands which can not choose water source while *Variable Demand* is the demand which can receive water from more than one river. *BD*, abbreviation of *Balanced Demand*, is water volume that has been consumed from each of the reservoirs and *PB*, abbreviation of *Proportion of Balanced demand*, is the proportion of *BD* for the two reservoirs. *PR*, abbreviation of *Proportion of Reservoir capacity*, is the proportion of storage capacities of the two reservoirs. The similar values for *PB* and *PR* is what the multi-hierarchical scheme wants to reach. And *SA*, abbreviation of *Supplying Ability*, is the ability of water supply and transport over water in days of the whole water network before meeting a deficit problem at the hypothesis of no rain and no water flow in from outside. The comparisons prove that, after using the proposed MPC scheme, the proportion of water usage from two rivers (58.93 %, which is ratio of Llobregat/Ter) is much closer to the proportion of their storage capacities (53.48 %). And what is more, the Catalunya Regional Water Network can transport over water and supply water 65 days longer than that without balance management, which is a good improvement regarding the sustainable usage of water resource in the long term perspective.

Algorithm 7.2 Temporal multi-level coordinator

$L := 24$ hours
$I := 24N$ hours
$T_s := 1$ hour
{start creating new constraints for lower-layer BOP }
for $i := 1$ to I **do**
  $d := floor(i/24)$
  $t := rem(i, 24)$
  if $t == 0$ **then**
    Update BOP by adding the following constraints:
    $u(1|k) \leq T_d(d) - \sum_{j=i-L+1}^{i-1} u_s(j|k)$;
    $\sum_{j=2}^{L} u(j|k) \leq T_d(d+1)$;
  end if
  if $t == 1$ **then**
    Update BOP by adding the following constraints:
    $\sum_{j=1}^{L} u(j|k) \leq T_d(d+1)$;
  end if
  if $t == 2$ **then**
    Update BOP by adding the following constraints:
    $\sum_{j=1}^{L-1} u(j|k) \leq T_d(d+1)$;
    $u(L|k) \leq T_d(d+2)$;
  end if
  if $t \geq 3$ **then**
    Update BOP by adding the following constraints:
    $\sum_{j=1}^{L-t+1} u(j|k) \leq T_d(d+1) - \sum_{j=i-L+1}^{i-1} u_s(j|k)$;
    $\sum_{j=L-t+2}^{L} u(j|k) \leq T_d(d+2)$;
  end if
  Solve BOP to obtain $u(j|k), u(j+1|k), \ldots$ with the new constraints added
  $u_s(i|k) := u(1|k)$;
end for
{end of loop}

Figure 7.5 is one of the examples of one river reach. The plot shows that, after controlling transport water levels, water flow at this reach could meet the water level needed by transporting over water during the whole optimization process.

Table 7.2 Balancing comparison of Scenarios 3

Sc.	Multi-hierarchical MPC control scheme						
Es.	Source	Fixed demand	Variable demand	BD	PB	PR	SA
L.	3,008	2,981	724	697	58.93 %	53.48 %	242 Days
T.	3,532	3,518	1,196	1,182			
Sc.	Model predictive control						
Es.	Source	Fixed demand	Variable demand	BD	PB	PR	SA
L.	3,008	2,981	7.6	−19.4	−1.02 %	53.48 %	177 Days
T.	3,532	3,518	1,914	1,900			

7.2.8 *Results for Coordination*

During the coordination process, management policies at the transport system are transferred to the supply system establishing the set-points for the shared actuators. Figures 7.6 and 7.7 show the amount of water consumed by the supply system from different rivers for satisfying the same demands before and after coordination, respectively. The two figures prove that average levels of water consumption from two rivers are much closer after balance management.

Figure 7.8 shows source flow comparisons between multi-hierarchical MPC and centralized MPC, which proves the similarity between the two kinds of controllers.

Table 7.3 provides detailed numerical results and compares the obtained control results in terms of economical and computational performance over 4 days among the multi-hierarchical and centralized MPC control techniques:

- *Current Control*: Control the supply system of Catalunya Regional Water Network using heuristic strategies by human operators.
- *Multi-hierarchical Model Predictive Control Scheme*:
  Control transport-supply system of Catalunya Regional Water Network using Multi-hierarchical Model Predictive Control techniques with temporal hierarchical coordinator between the transport and supply systems.
- *Centralized Model Predictive Control*:
  Control the transport-supply system of Catalunya Regional Water Network using centralized Model Predictive Control techniques without coordination.

In the Table 7.3, *Wat.*, abbreviation of *Water*, means water cost during the day, while *Ele.*, abbreviation of *Electricity*, shows electricity cost, *Tot.*, abbreviation of *Total*, means the total cost which include both water and electricity, where the indices representing costs are given in economic units (e.u.) instead of Euro due to confidentiality restrictions, and *Comp.*, abbreviation of *Computation time*, which means the needed computing time for that optimizing process in seconds. The row of *Proportion* is the improved proportion to the current control. From this table, the result shows that, Multi-hierarchical MPC technique with temporal coordination is much better than the current controller but is a little worse than centralized MPC technique regarding economical cost, especially of electricity cost.

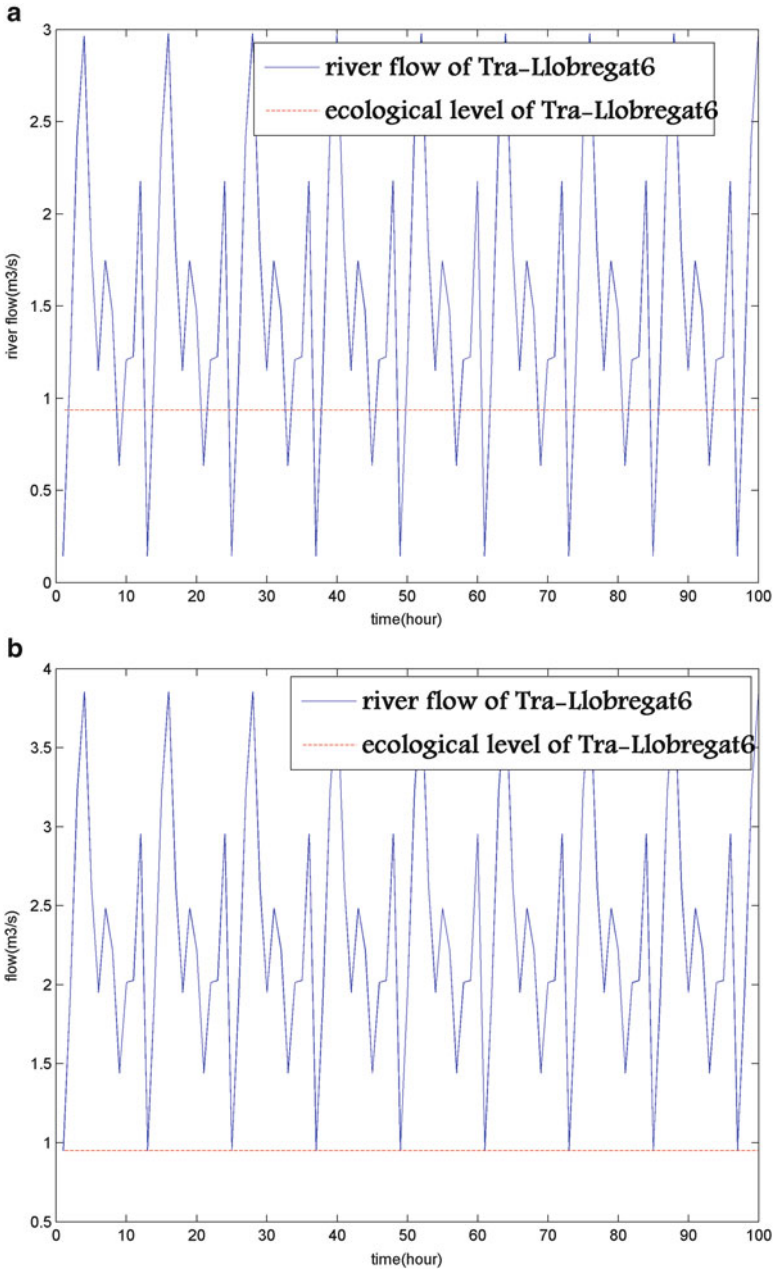

Fig. 7.5 River flow with ecological level before and after control in river Llobregat. (**a**) Before control. (**b**) After control

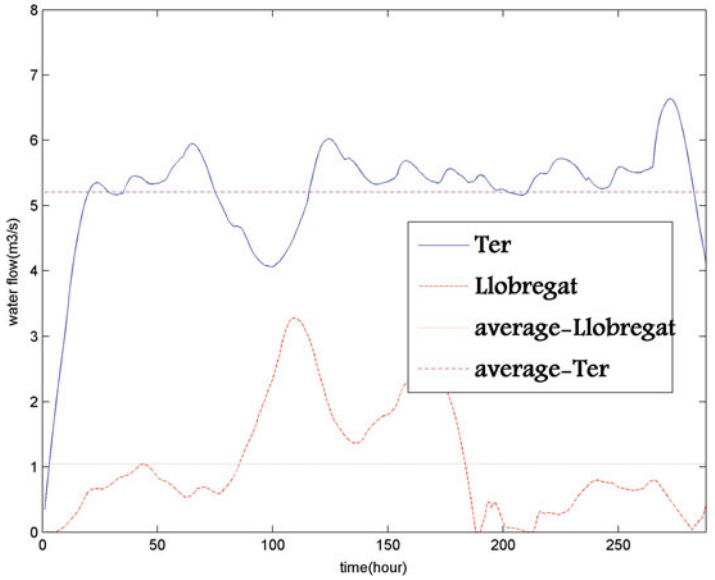

Fig. 7.6 Flows from the two rivers before using temporal coordination with x-time and y-flow axis

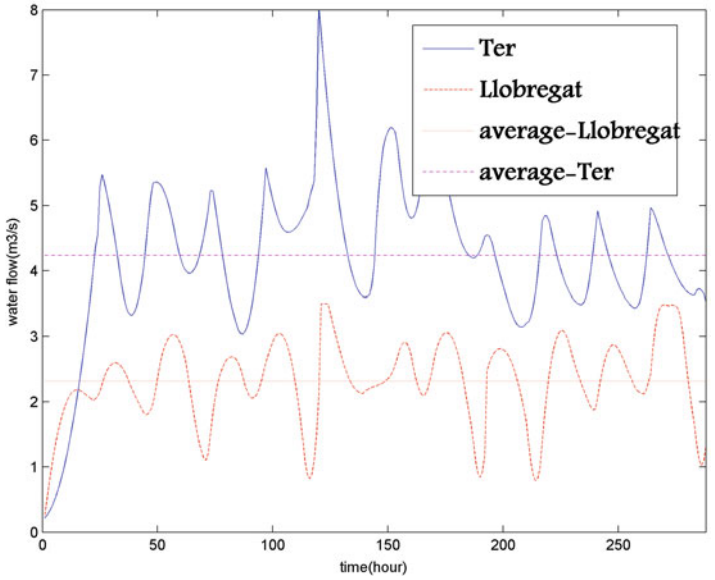

Fig. 7.7 Flows from the two rivers after using temporal coordination with x-time and y-flow axis

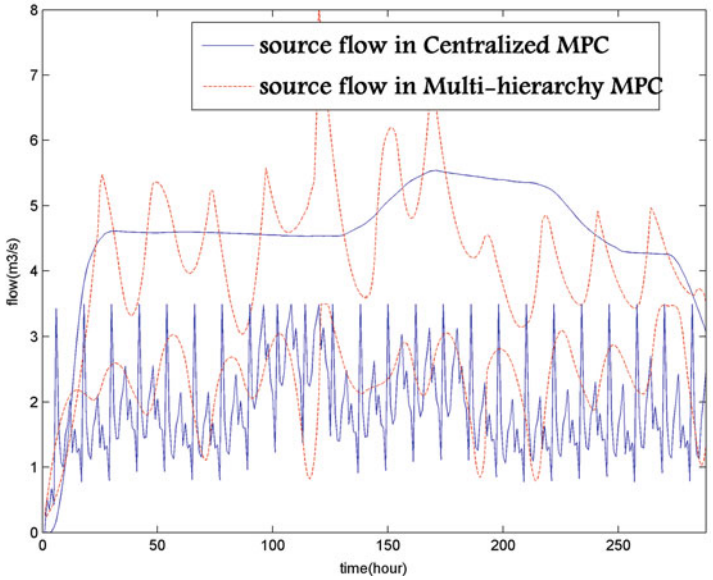

Fig. 7.8 Source flows comparison between multi-hierarchical MPC and centralized MPC

Table 7.3 Closed-loop performance results (all values in e.u.)

Define day	Current control				Multi-hierarchical MPC				Centralized MPC			
	Ele.	Wat.	Tot.	Comp.(s)	Ele.	Wat.	Tot.	Comp.(s)	Ele.	Wat.	Tot.	Comp.
1st	240	100	340	23	213	44	257	32	141	40	181	58
2nd	239	106	345	21	237	47	284	27	170	39	209	57
3rd	246	94	340	19	238	48	286	34	171	41	212	61
4th	264	110	374	21	253	66	319	29	168	42	210	62
Proportion					−5 %	−50 %	−18 %	45 %	−34 %	−61 %	−42 %	183 %

The explanation is that while introducing multi-hierarchical control scheme, which simplifies the whole supply system into a virtual demand, the optimization of electricity price for the actuators becomes invalid. On the other hand, computation time is much improved after introducing multi-hierarchical control scheme, which is also necessary for the large scale water systems. Besides that, scalability is also improved after introducing the proposed multi-hierarchical MPC scheme.

7.3 Interdisciplinary Discussion into the Unified Framework

Transport of water is part of the master planning of communities, counties and municipalities. Limited water supplies, conservation and sustainable policies, as well as the infrastructure complexity for meeting consumer demands with appropriate flow pressure and quality levels make water management a challenging control problem. Decision support systems provide useful guidance for operators in complex networks, as reported in [8, 12].

Transport over water, which has the advantages of less investment and low cost, has been developed as the main bearer of large, bulky freight. In reality, plenty of natural conditions, like seasonal fluctuations of water level, water forms complex, could impact easily transportation ability of inland waterways, which affect both the play of navigation and also economical interests. Stability of river flows and adequate water levels of open channels in transport water networks are critical control factors in the operational control models.

This chapter takes into account *transport of water* from the dams to the consumers while at the same time considers the *transport over water* by keeping some ecological flows in the rivers. The transport system works in a daily time scale in order to achieve the global management policies for the transport over water in different rivers and balance management of different reservoirs. The supply system works in a hourly time scale and manipulates actuator set-points to satisfy the local water supplying objectives. For each water system, an MPC controller is provided to produce optimized control sequence for different control objectives. A supervisor coordinating mechanism that coordinates transport and supply water systems for sustainable and ecological benefits is used to generate control strategies which consider objectives at different time scales. OPM is used to generate unitary source prices for the transport water system. The results of this control scheme after being applied to the Catalunya Regional Water Network in Sect. 7.2 shows that, comparing with the separated control strategies, this unified framework which deals with both short term objectives and long term objectives provides sustainable and ecological results, which even has economical benefits in the long term perspective.

7.4 Open Topics

Besides advantages and benefits of the unified control scheme proposed in this chapter, there still exist topics which need more research and verification, which are:

T1: How to manage the priorities when long term objectives have conflicts with short term objectives?
T2: How to choose the control strategies between multi-hierarchical and centralized MPC with coordination when computation load is not a problem?
T3: In reality, how to deal with uncertainties for the complex water system, which affect both transport and supply systems?

7.5 Conclusions and Future Research

In this chapter, a multi-hierarchical MPC scheme with temporal coordination for complex transport and supply water systems is proposed. The need of multi-hierarchical scheme derives from the fact that different networks in the transport

over water and supply systems are operated according to different management goals, with different time horizon. While the management of the transport network is mainly concerned with long term safe-yield and ecological issues, the supply hierarchical must achieve economic goals in the short term (hourly strategy), while meeting demands and operational constraints. The use of the multi-hierarchical modeling and the temporal hierarchical MPC coordination techniques proposed in this chapter makes it possible to realize communication and coordination between the two separated systems in order to let individual operational goals affect to each other, and finally, obtain short-term strategies which can effectively consider long-term objectives as well.

Acknowledgements The authors thank ACA, ATLL and ADASA for providing the case study as well as for sharing their hydrological management expertise. This research has been partially funded by CDTI (MCyT) project HIDROPTIM IDI-20100722, the DGR of Generalitat de Catalunya (SAC group Ref. 2009/SGR/1491), the AGAUR by an FI grant and by EFFINET grant FP7-ICT-2012-318556 of the European Commission.

References

1. Brdys M, Tatjewski P. Iterative algorithms for multilayer optimizing control. London: Imperial College Press; 2005.
2. Brdys M, Ulanicki B. Operational control of water systems: structures, algorithms and applications. London: Prentice Hall; 1994.
3. Brdys MA, Grochowski M, Gminski T, Konarczak K, Drewa M. Hierarchical predictive control of integrated wastewater treatment systems. Control Eng Pract. 2008;16(6):751–767.
4. Cheng W, Hsu N, Cheng WM, Yeh W. A flow path model for regional water distribution optimization. Water Resour Res. 2009;45:W09411.
5. Danielson GH. On finding simple paths and circuits in a graph. IEEE Trans. Circuit Theory. 1968;CT-15:294–295.
6. de Oca Armeaga, SM. Hierarchical multilayer and decentralized MPC control of the Barcelona water network. Master Thesis, Universitat Politecnica de Catalunya, 2011.
7. Evans R, Li L, Mareels I, Okello N, Pham M, Qiu W, Saleem SK. Real-time optimal control of river basin networks. Preprints of the 18th IFAC World Congress, Milano, Italy; 2011. p. 11459–11464.
8. Nitivattananon V, Sadowski EC, Quimpo RG. Optimization of water supply system operation. J Water Res Plan Manage. 1996;122(5):374–384.
9. Ocampo-Martinez C, Puig V, Cembrano G, Quevedo J. Application of predictive control strategies to the management of complex networks in the urban water cycle. IEEE Control Syst Mag. 2013;33(1):15–45.
10. Scattolini R. Architectures for distributed and hierarchical model predictive control: a review. J Process Control. 2009;19(5):723–731.
11. Tatjewski P. Advanced control and on-line process optimization in multilayer structures. Ann Rev Control. 2008;32(1):71–85.
12. Tu MY, Frank TCT, William WGY. Optimizaiton of water distribution and water quality by hybird genetic algorithm. J Water Resour Plan Manage. 2005;131(6):431–440.

Chapter 8
Effects of Uncertain Control in Transport of Water in a River-Wetland System of the Low Magdalena River, Colombia

L. Alfonso and M. Tefferi

Abstract During the 2010 and 2011, extreme flooding events affected the low Magdalena River catchment, Colombia, with devastating consequences. This triggered the urgency of adjusting the new river basing planning framework for the country, in which the generation and use of flood risk maps, was lacking. Recent efforts include the generation of probabilistic flood maps, based on the generation of a hydraulic model and an uncertainty analysis related to the wetland-river connections. Although this effort is a step forward to the definition of design criteria for flood risk prevention measures and for the land-use planning process in general, an integrated vision is still missing. In particular, depending on the hydraulic and hydrological condition of the river-wetland system, the operation of the existing hydraulic structures is sometimes decided illegally by the water users with the strongest economical power and not by the local authority, with the consequent biased water use. The research objective of this study is to analyze the control strategy for the operation of hydraulic structures in the region of the Low Magdalena River, considering uncertain control due to self-operation of the structures by non-official actors. The study includes a literature review on existing methodologies and cases where control structures are significant and where conflicting interests are present. A number of different scenarios are analyzed different control scenarios are tested. The study uses the recently developed 1D–2D model of the region that simulates the Magdalena River Channel with side structures that replicate the river-wetland connections. Conclusions and recommendations of the study are drawn, as well as indications of activities for future research.

L. Alfonso (✉) • M. Tefferi
UNESCO-IHE Institute for Water Education, Delft, The Netherlands
e-mail: l.alfonso@unesco-ihe.org; teffe1@unesco-ihe.org

C. Ocampo-Martinez, R.R. Negenborn (eds.), *Transport of Water versus Transport over Water*, Operations Research/Computer Science Interfaces Series 58,
DOI 10.1007/978-3-319-16133-4_8

8.1 Introduction

Gates and pumping stations and other hydraulic structures are commonly used to control water systems in order to satisfy water quality and quantity demands of different actors. The need to fulfill the interests of different users considering the interactions between subsystems and the external disturbances has increased the requirements for a better control of the systems. The control of water systems aims at achieving their general operational objectives (i.e., supply drinking water, collect and treat sewage, drain rainfall runoff and prevent flooding), in the most cost-efficient manner. In fact, the control of water systems concerns the operation of regulating structures such as pumping stations, weirs and sluices, in order to make the system to meet the demands of the water users as well as possible.

However, in practice, this is not always the case. The Magdalena River, like many other rivers in the world, has diverse water users and interests that are conflicting. Examples are navigation, agriculture and pasture, flood control and fish production. Navigation in the middle and low Magdalena River is important because it is a way to connect important interior cities with the ports of Barranquilla and Cartagena. In consequence, dry periods or sediment deposits imply economic losses for ships that get stuck in bar sands along the river.

The wetlands in the Magdalena River are areas with a very important biodiversity in fauna and flora and with a high potential for fish, forest and crop production [1, 2]. The land is generally owned by a few influential families that develop it for agriculture and cattle [1, 8], who demand more land. Documented experiences [5, 8] show that they generally start land reclamation activities by themselves and decide on the operational status of gates installed for multiple purposes. The disconnections of the streams that link the river and the wetlands have affected the ecology and fish production of the region negatively. This is mainly because of uncontrolled human interventions and the lack of protection policies [9, 12, 13].

Flooding is also a great concern in the lower part of the Magdalena River. In particular, the communities of Sabanagrande, Santo Tomás, and Palmar de Varela in the department of Atlantico, located along a reach of 15 km on the west floodplain and 43 km upstream from the mouth of the Magdalena River into the Caribbean Sea. Several measures have been executed in order to reduce the flood risk in the municipalities of the study area. The main project took place in the year 2000 and comprised the construction of protection dikes around the wetlands. However, due to the conflict of interests existing in the area, the project was not entirely built as designed.

The variety of uses existent in the wetlands causes a complex conflict of interests. On the one hand, farmers and cattle breeders close the sluice gates that connect the wetlands with the river to keep their lands dry when the water level in the river is too high. On the other hand, fishermen open the sluice gates to allow the fishes pass to the wetlands area. There is no operational protocol for such structures and the authorities do not exert any control policy.

The level of income of the local community living in the study area is low due to limited job opportunities and lack of development of sufficient productive work sectors. The poor inhabitants of the towns of the region are engaged in agriculture, fishing and production of hand crafted bricks. Besides, large areas of the wetlands are utilized for producing a wide variety of crops and cattle breeding by investors.

This research focuses on the effects of uncertain control strategies into the landscape of the river-wetland water system in the low Magdalena evaluating different scenarios with modeling tools. By uncertain control strategies we want to take into account the nature of human decisions that are outside the technicalities of control strategies, in particular to the transport of water throughout control structures under extreme events.

This chapter is structured as follows: first, a descriptive section of the case study is presented, which includes the main hydrological features of the region, the characteristics of the flood defense measures and the socio-economical aspects that make control of water a difficult task. Then, a description of the methodology to take into account the uncertainty in the status of control structures on the estimation of flood inundation maps of the area is presented and the resulting maps and the corresponding analysis are reported. Finally, some reflections about the link between transport of and transport over water are made explicit, followed by the discussion of open topics that should be investigated in the future.

8.2 Case Study

The study area is on the lower part of the Magdalena River, and includes the wetlands of Sabanagrande, Santo Tomas, and Palmar de Varela in the department of Atlantico—Colombia (Fig. 8.1). The wetlands are located along a reach of 15 km on the west floodplain and are part of the so called sub-catchment of wetlands of the Magdalena River in the Atlantico department and receive their names from the municipalities where they are located. According to the environmental authority of the region, the study area is located in geomorphologic units that represent stripes of variable width where the river develops curves in the main channel due to the high fluvial dynamics. As a consequence of such dynamic, the stream creates and destroys islands, erodes the riverbank, modifies local flow directions and abandons sections that become wetlands when they are wide enough.

8.2.1 Hydraulics and Hydrology of the Region

Climate in the study area is characterized by warm temperatures all year long, with an average temperature of 27 °C and a high humidity, around 80%. Annual average precipitation is 1,060 mm and three different seasons can be identified throughout the year: rainy season (August–November), when approximately 53% of

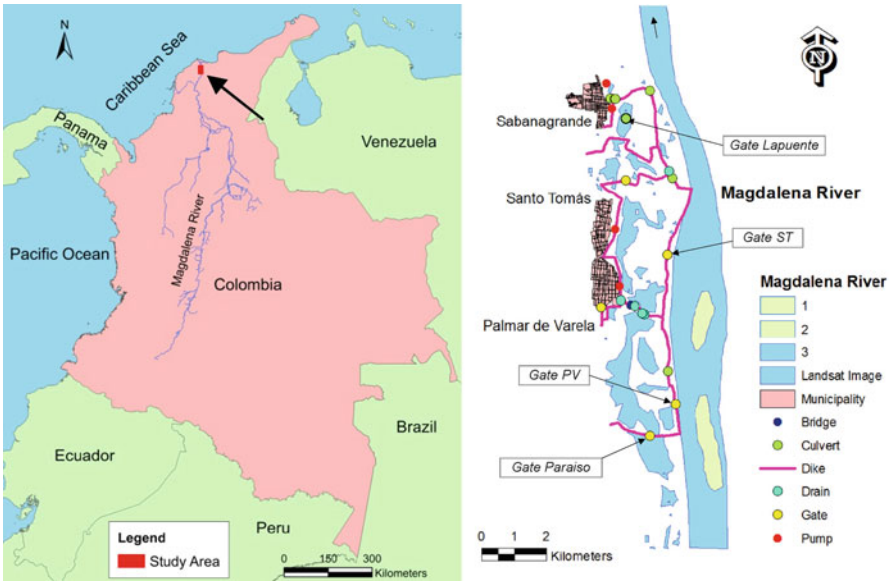

Fig. 8.1 Study area and location of flood defenses and hydraulic structures (adopted from [3])

the total annual precipitation takes place and dry season (December–March), when approximately the 8% of the total annual precipitation takes place, and transitional season, (April–July).

The wetlands of the lower Magdalena River (WLMR) form sub-catchments formed by multiple creeks that drain down to the river. Although this drainage occurs from both sides of the river, we focus the study in the west side along the last 115 km to its mouth in the Caribbean Sea. The system of wetlands can be considered as a subsystem that interacts with the Magdalena River and the runoff contribution from the afferent sub-catchments. The water level is mainly controlled by the fluctuations of the river and by the seasonal runoff that drains the sub-catchments of the system itself. Consequently, during the dry season, vast areas of the wetlands get dry. The sub-catchments that drain to the wetlands of the study area are the ephemeral creeks of Cañafistula and San Martin (Fig. 8.2).

The wetlands are hydraulically connected with the Magdalena River through canals, culverts that pass through the protection dikes, and directly when the river overflows its banks in low areas without dikes. The average annual discharge of the Magdalena River at its mouth is 7,100 m^3/s, typically having peak discharges during the months of June and November, being the latter the highest one.

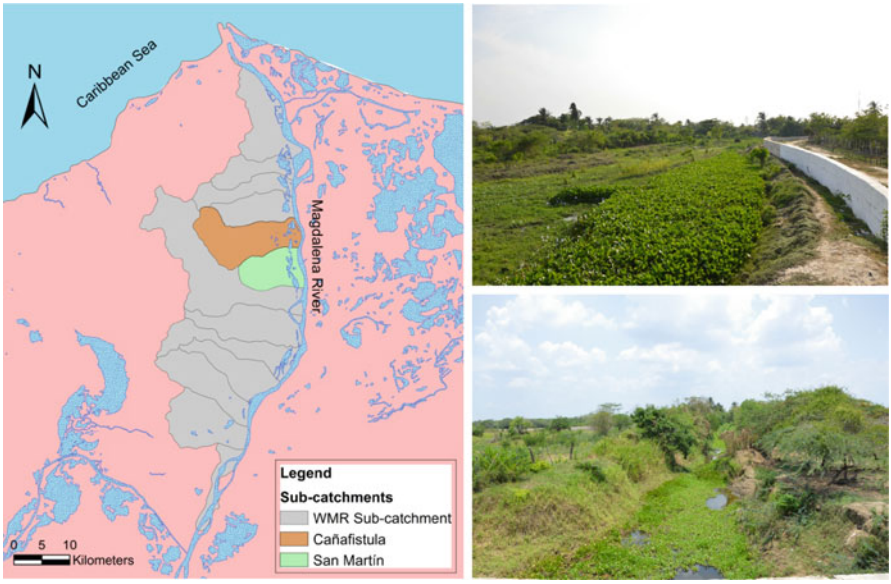

Fig. 8.2 *Left*: sub-catchment of the Magdalena River in the Atlantico department. *Top right*: San Martin Creek. *Bottom right*: canal between the Magdalena River and Santo Tomas wetland (adopted from [3]). *Photos*: Fabio Amador

8.2.2 Flood Defense Measures and Control Structures

Several measures have been executed in order to reduce the flood risk in the municipalities of the study area. The main project took place in the year 2000 and comprised the construction of protection dikes around the wetlands "to confine and regulate the water storage in the wetlands" [16]. However, due to the conflict of interests existing in the area, which is detailed further, the project was not entirely built as designed. To date, an important section of the dike in the municipality of Santo Tomas remains uncompleted.

Multiple hydraulic structures such as culverts, and sluice gates were installed in the dikes between the wetlands and the Magdalena River in order to keep them hydraulically connected, minimizing in this way the ecological impact on the ecosystems (Fig. 8.3). Flood protection measures and control structures affected considerably the hydrodynamic of the wetlands and caused a problem associated to pluvial floods in the towns as the dikes hinder the flow of the runoff to the wetlands.

Activities as agriculture, fishing, and hand-crafted bricks production are carried out in the wetlands as only way of survival for the poorest inhabitants of those towns. Apart from the locals, landowners of vast areas of the wetlands develop extensive crops and cattle breeding. The variety of uses existent in the wetlands causes a complex conflict of interests. On the one hand, farmers and cattle breeders close the sluice gates that connect the wetlands with the river to keep their lands dry when

Fig. 8.3 Example of gates for flood control. *Photo*: Fabio Amador

the water level in the river is too high. On the other hand, fishermen open the sluice gates to allow the fishes pass to the wetlands area. There is no operational protocol for such structures and the authorities do not exert any control policy.

8.3 Methodology and Main Results

Theoretically, well defined control strategies should lead to adequate performance of a water system. However, in practice, there are other aspects that are usually not considered on their initial design and that may impact greatly the system performance. An interesting example is the *control for citizen self-convenience* of the hydraulic structures in our case study, which are operated based on the expediency of a few persons in the community. This implies that the operational status of the structures is not known and therefore they are uncertain at any given time. A general definition of uncertainty in modeling is given by [17]: "any deviation from the unachievable ideal of completely deterministic knowledge of the relevant system". Uncertainty is a relatively new subject in the research field of hydraulic modeling [18]. In particular, we focus here on the effect of uncertain control strategies in flood hazards in the region.

The methodology, explained in detail in [7], consists of producing a set of maps to depict the areas that might be inundated by water under different scenarios, using hydraulic models. Each map is then compared with the observed flood extent and

the models with the best performance are selected. The resulting maps are then integrated into a single one that represents the probability of being flooded given the considered scenarios. These steps are further explained in detail.

The method has been applied to the case study in the evaluation of the effect of the uncertainty in the estimation of the 100-year return period flow in the river [3] and the effects of the uncertainty derived from remote sensing topographical data of the Shouttle Radar Topographical Mission (SRTM-90) [15]. Although flood maps are affected by several other sources such as hydraulic and hydrological data quality, model structure and parameterization [3, 6, 10, 14, 15] uncertainty of control strategies is usually not taken into account. In brief, the method uses a Monte-Carlo procedure to produce a number of models that generate a number of deterministic flood maps for different combinations of operational settings of the control structures.

Models are simplifications of reality, in which processes that are not important are deliberately ignored and those essential of design or operation are implemented. The hydraulic modeling is carried out on a 20 km reach of the lower Magdalena River using the 1D Quasi 2D hydrodynamic SOBEK model. SOBEK is an integrated software package which enables to build complex models by dynamically integrating 1D components from SOBEK-Rural and 2D components from SOBEK Overland Flow. SOBEK 1D solves the De Saint-Venant equations through finite difference scheme.

The result of flood inundation modeling has to be verified by comparing to an existing observed flood extent map of the study area. In the lower Magdalena River, the inundated area obtained from the Landsat image of December 2010 flood event is compared with the model results. The Landsat image is a 3 band (RGB) image obtained from the NASA Landsat program 2010 scene LE70090532010341EDC00 [8]. This image was first classified using Multispec software to identify areas that are flooded from non inundated areas with the aid of supervised classification (Fig. 8.4). Then, the classified Landsat image is compared with the simulated results of SOBEK model using the measure of fit, defined by [10] as given below:

$$F = \left(\frac{A - B}{A + B + C} \right) * 100, \tag{8.1}$$

where A is the size of the flooded/wet area correctly predicted by the model, B is the size of the area predicted as wet by the model but actually is observed as dry/not flooded (over prediction), and C is the size of the area that is predicted as dry by the model but actually is observed as wet (under prediction). The measure of fit is proved to give good results for problems associated to flood inundation modeling and gives the opportunity to compare model predictions against observations [10].

The probabilistic flood inundation maps are then produced using the GLUE method [4], where every individual model is assigned a weight based on how well fits the observed flood extent, based on a Landsat image (Fig. 8.4). The next step is to compute the likelihood L_i weight of each simulation results in the range between 0 and 1. Likelihood is a measure of how well the simulated results obtained from a

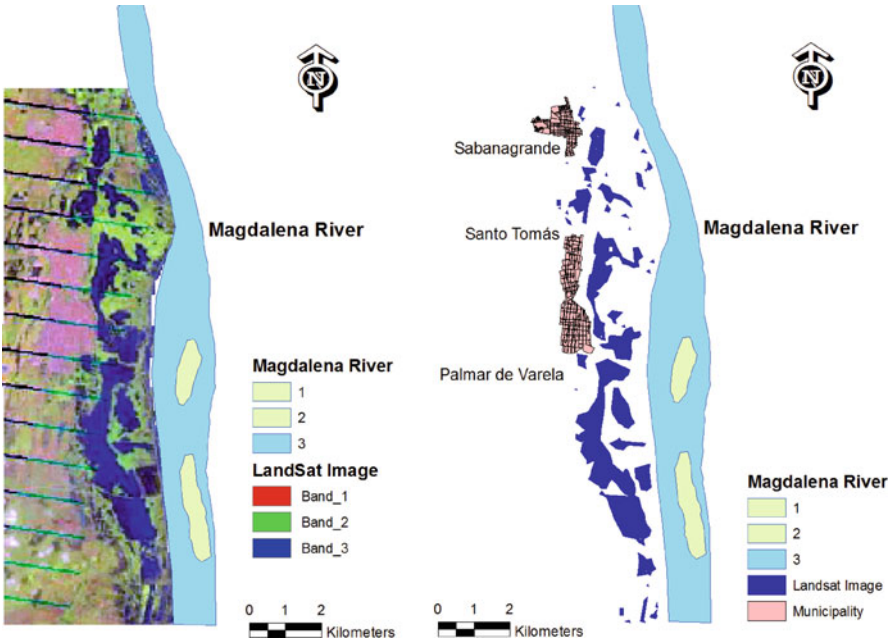

Fig. 8.4 Landsat Image of Dec. 2010 flood event (*left*) and its result after classification (*right*)

given combination of models, parameters and variables fits to the observed data and thus describes their degree of membership of the final acceptable solution. Given the measure of fit of (8.1), L_i is computed as

$$L_i = \frac{F_i - \min_i(F_i)}{\max_i(F_i) - Min_i(F_i)}, \tag{8.2}$$

where $\min_i(F_i)$ and $\max_i(F_i)$ are the minimum and maximum measures of fit found throughout the ensemble simulations. These likelihood values are used for generating uncertain probabilistic flood inundation map. A final model prediction is then generated by the weighted sum of the predictions from each simulation. For instance, given a weight L_i for each simulation i, and the simulation results for the jth model element (e.g., computational cell) of $W_i j = 1$ for wet and $W_{ij} = 0$ for dry, it is possible to develop an uncertain predicted flood inundation map using (8.3).

$$C_j = \frac{\sum_i L_i W_{ij}}{\sum_i L_i}, \tag{8.3}$$

where, C_j stands for a weighted average flood condition of the jth cell of the model [10]. The use of remote sensing data about the extent of inundation is a common practice to validate model-based flood maps. Conceptually, the evaluation of model results derived from an optimal parameter set is straightforward, and the performance measure given in (8.3) may be used.

8.3.1 Results and Discussion

As mentioned above, previous studies evaluated the effect of uncertain flow [3] and topography [15] in the flood maps of the region, including the probabilistic analysis of four topographical data sampling scenarios of 100 simulations each. The best model produced by the scenario with the higher number of behavioral models (those better matching the observed Landsat image in Fig. 8.4) was selected to run the possible 16 combinations of operational statuses of the four existing gates in the area, which can be either closed or opened.

The average inundated area resulting from the 16 maps is 10.7 km^2, with a minimum of 8.5 km^2, a maximum of 13 km^2 and a standard deviation of 2.2 km^2. The resulting probabilistic flood map is presented in Fig. 8.5, which has been build

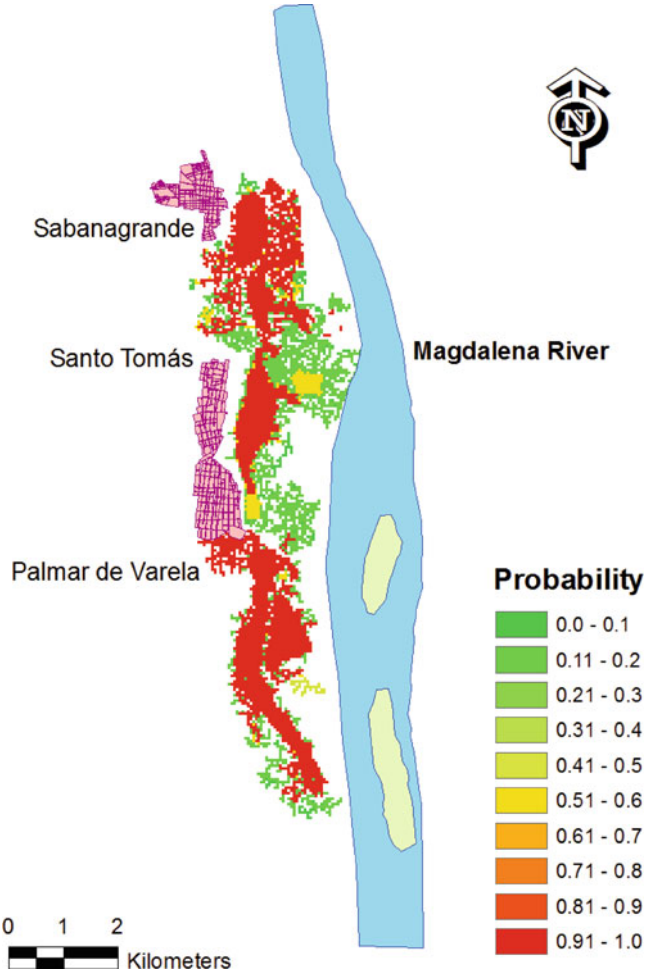

Fig. 8.5 Probabilistic flood map due to uncertain operation of gates

using the best model obtained regarding topographical uncertainty coming from SRTM data. It can be observed that, although the zones with higher probability of flooding largely match those areas in the observed Landsat image, there are important areas that can be flooded due to variations in the operational status of gates.

Another interesting analysis is to consider independent gate opening on the extent of flood inundation area. Results indicate that the inundation area does not change if the gates Lapuente or gate Paraiso (see Fig. 8.1) are operated, and that this is equivalent to the condition when all gates are closed. This leads to the conclusion that the operational state of both gates has no significant effect on the extent of inundation. On the contrary, the opening of gate Santo Tomás (ST) produces a significant increment in the inundation area, of about 5.0 km^2. A similar conclusion can be made for gate Palmar de Varela (PV), which generates an increase in the inundation area of about 3.0 km^2. Table 8.1 shows the total inundation area due to the individual gate opening, keeping the remaining gates closed, compared to the situation when all the gates are closed.

These results are evident when looking at the relative contribution of flooded area for different combinations of gate operation. Figure 8.6 shows the relative incremental flooded area from a number of gates operations combinations. It indicates that opening of either only gate Lapuente or Paraiso does not change the inundation area, which is equivalent to the condition when all gates are closed. This leads to the conclusion that the operational state of both gates does not have significant effect on the extent of inundation. On the contrary, the opening of Santo Tomás (ST) gate produces a dramatic boost in the inundation area. An analysis using different topographical model scenarios shows that this increment is between 3.1 and 5.2 km^2.

In conclusion, based on the results of the simulations, gate ST is the most important one as far as flooding is concerned and hence this particular gate should be closed especially during extreme flood events. This gate appears to be the critical one for fishing activities.

Table 8.1 Simulated inundation areas as a result of local control gate opening scenarios

Scenario	Gate	Status	Inundation area (km^2)
1	Lapuente	Opened	8.6
2	Paraiso	Opened	8.5
3	PV	Opened	8.6
4	ST	Opened	12.5
5	All	Opened	13.0
6	All	Closed	8.5

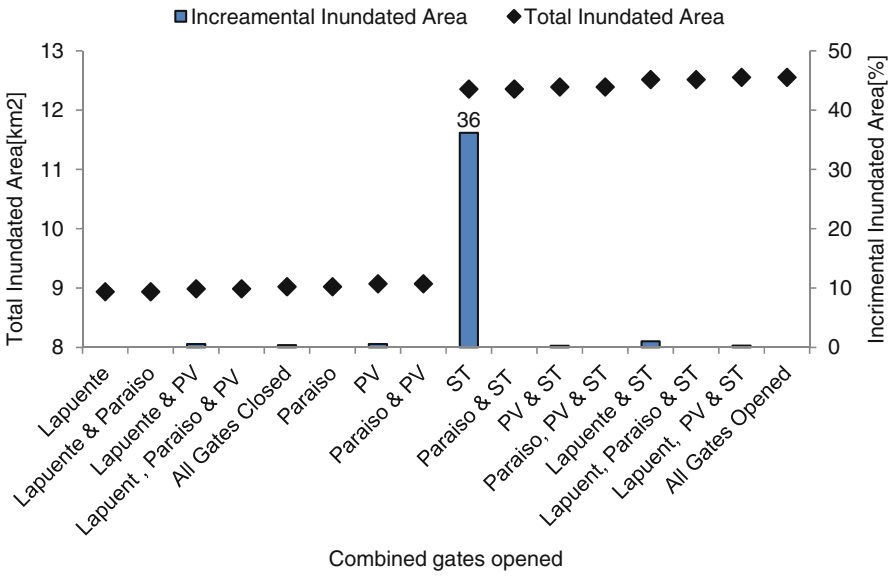

Fig. 8.6 Relative incremental flooded area due to different combinations of gate operations

Table 8.2 Inundation extent at different opening heights of gate ST

Opening height of gate ST (cm)	0	20	40	60	80	100	120	140	160	180	188
Inundation area (km^2)	8.8	9.9	11	11.7	12.2	12.5	12.6	12.7	12.9	13	13
Incremental area (%)	0	13	12	8	6	3	2	1	2	2	0

8.4 Linking Transport of and Transport over Water

All previous analysis have been done considering a binary status of the gate, either fully opened or closed, due to the computational effort required for the 2D model to perform a single simulation. However, the effect of multiple opening states is of interest, in particular because this is a feature of the anthropogenic interference in the status of the control structures by different water users with different water requirements, including transport of and transport over water. To this end, a sensitivity analysis of the status of the gate ST, identified as the most important in the context of flooding, is considered, assuming that the remaining gates are closed.

Table 8.2 and Fig. 8.7 show the flood inundated area as a function of opening height of gate ST at an opening step of 20 cm. As a result, the inundation area consistently increases as the gate opening goes up to 1.0 m. Interestingly, no

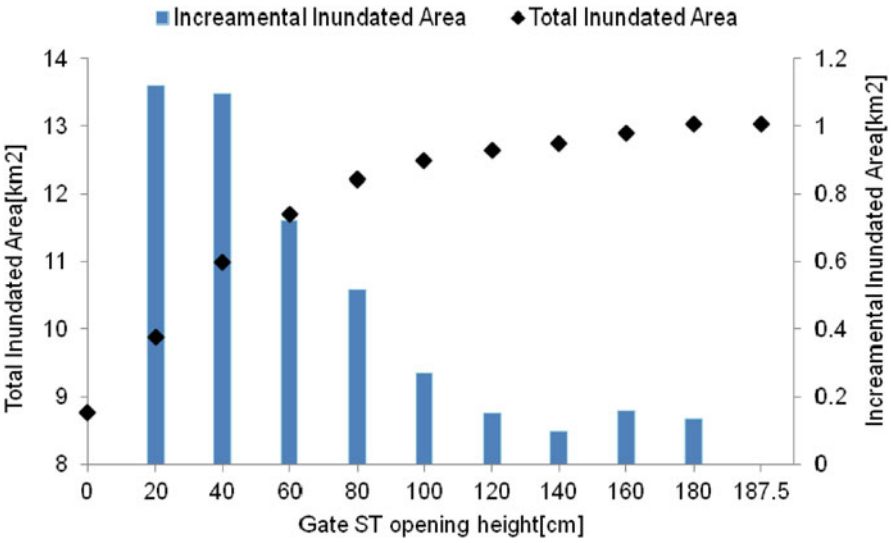

Fig. 8.7 Result of the sensitivity analysis using Gate ST

significant increase of such inundated area is observed beyond that value. In general, the smallest and the largest flood inundation extent are achieved when gate ST is fully closed and fully opened, respectively.

8.5 Open Topics

As demonstrated, uncertainty of social aspects can greatly affect the flood inundation area of controlled, regional and flat water systems. An open question is how to incorporate such a source of uncertainty within an integrated design of control strategies in these cases. Robust optimization could be a possibility, aiming at making the performance of the water system as independent as possible to uncertain variations of control structures.

From the practical perspective, it is well-known that the design of control and real-time control of water systems must take into account all user requirements when defining setpoints at different special and temporal scales and that this is a multi-objective optimization problem [11]. It is also known that robust solutions are obtained if uncertainty is accounted for when solving this kind of problems. In consequence, the use of the concept of robustness could be used as a global performance indicator of transport of/over water systems in further research.

8.6 Conclusions and Future Research

The present study has demonstrated that in a combined framework of control for transport of water and transport over water, different sources of uncertainty must be estimated and analyzed. In particular, sources of uncertainty of anthropogenic nature, such as the one presented, deserve as much attention as those sources that are traditionally taken into account and that normally receive more attention. Probabilistic flood inundation maps can be used to analyze the consequences in terms of transport of water and its implications to other uses, including transport over water, and, in consequence, they can be used as inputs in the design of robust control systems.

This research takes into account water to be transported through the river and through the hydraulic structures to allow for environmental, ecological and social purposes of some stakeholders, in the unusual case in which the stakeholders operate the structures at their convenience. It demonstrates that the current control condition may lead to different situations in terms of flood extension, which affect different water users. Although in the specific case of the WLMR one could argue that a strong implementation of control policies regarding the control of structures would be enough to improve the situation, this is not easy in practice, due to the peculiar social and political situation of the inhabitants of the region. Methodologies from social science are needed to approach the communities and communicate the implications of the current practice and the advantages of collaborative, organized control strategy with clear rules and responsibilities, presumably starting with basic school education.

This research focused on the particular situation of extreme flow conditions on the river. However, it is of interest to further investigate the possible effects of anthropogenic activities on control for the case of normal variations in the river, checking at other criteria beyond flood extension. For example, the effect of uncertain gate operation on the agricultural (transport of water) and fish production (transport over water).

In the context of this book, we can argue that the presented case and the proposed methodology not only addresses transport of water, occurring from the river to the wetland throughout hydraulic structures, but also other aspects, including transport over water. For instance, a fisherman that cannot navigate the wetlands when gates do not allow for water inflow from the river is a common problem in the considered case.

More than a method to bridge the gap between flow and transport, this chapter shows how significant the role of uncertainty is in the performance of control systems, in particular that associated to social aspects. In consequence, management policies aiming at improving these systems should explicitly consider them, in particular in the context of developing countries. We believe this research contributes with new perspectives ultimately leading to a unified management framework.

Acknowledgements This research was carried out for the ColCuencas project, funded by the DGIS (Dutch Development Cooperation)—UNESCO-IHE Programmatic Cooperation (DUPC). The authors would like to thank the Regional Authority of Atlantico CRA for delivering the data and to Fabio Amador, who built the initial hydraulic model of the region.

References

1. Aguilera M. La Mojana: Riqueza natural y potencial económico, In: Documentos de trabajo sobre economîa regional. Banco de la República, Centro de Estudios Económicos Regionales (CEER), ISSN 16923715, 2004;48.
2. Aguilera M. Ciénaga de ayapel: Riqueza en biodiversidad y recursos hídricos. In: Documentos de trabajo sobre economîa regional. Banco de la República, Centro de Estudios Económicos Regionales (CEER), ISSN 16923715, 2009;112.
3. Amador F. Development of a methodology for producing probabilistic flood maps of river-wetland systems: Case study of Magdalena river, Colombia. Master's thesis, UNESCO-IHE, 2013.
4. Beven K, Binley A. The future of distributed models: Model calibration and uncertainty prediction. Hydrol Process. 1992;6(3):279–98.
5. Cormagdalena and ONF Andina. Plan de Manejo de la Cuenca Magdalena Cauca. Informe Final Fase 4. Fluidis, 6003 - I04, 2007.
6. Di Baldassarre G, Montanari A. Uncertainty in river discharge observations: A quantitative analysis. Hydrol Earth Syst Sci. 2009;13(6):913–21.
7. Di Baldassarre G, Schumann G, Bates P, Freer J, Beven K. Flood-plain mapping: A critical discussion of deterministic and probabilistic approaches. Hydrol Sci J. 2010;55(3):364–76.
8. DNP and FAO. Programa de desarrollo sostenible de la región de La Mojana, Departamento Nacional de Planeacion y. Organización de las Naciones Unidas para la Agricultura y la Alimentación, Bogotá, 2002;567.
9. Galvis G, Mojica JI. The Magdalena river fresh water fishes and fisheries. Aquat Ecosyst Health Manage. 2007;10(2):127–39.
10. Horritt MS. A methodology for the validation of uncertain flood inundation models. J Hydrol. 2006;326(1):153–65.
11. Lobbrecht A. Dynamic water-system control: Design and operation of regional water-resources systems. Rotterdam: AA Balkema; 1997.
12. Munera M, Daza JM, Páez VP. Ecología reproductiva y cacería de la tortuga. Rev Biol Trop. 2004;52(1):229–238.
13. Naranjo L, Andrade GI, Ponce E. Humedales interiores de colombia. Bases técnicas para su conservación y uso sostenible. Bogotá: Instituto Humboldt y Ministerio del Medio Ambiente; 1999.
14. Neal J, Keef C, Bates P, Beven K, Leedal D. Probabilistic flood risk mapping including spatial dependence. Hydrol Process. 2013;27(9):1349–63.
15. Tefferi M. Ensemble simulations to estimate uncertainty associated with srtm topography and operation of hydraulic gates in flood inundation mapping: Case study of the lower Magdalena river in Colombia. Master's thesis, UNESCO-IHE, 2014.
16. Urquijo J. Study and design of hydraulic structures in the wetland system of Sabanagrande, Santo Tomás and Palmar de Varela (in spanish), 1997.
17. Walker W, Harremoes P, Rotmans J, van der Sluijs JP, van Asselt MB, Janssen P, von Krauss MP. Defining uncertainty: A conceptual basis for uncertainty management in model-based decision support. Integr Assess. 2003;4(1):5–17.
18. Warmink J. Uncertainty analysis of hydrodynamic river models. University of Twente, Enschede, The Netherlands; 2009.

Chapter 9
Automatic Tuning of PI Controllers for Water Level Regulation of a Multi-pool Open-Channel Hydraulic System

D. Dorchies and P.-O. Malaterre

Abstract The underlining philosophical statement of this chapter is that the promotion of automatic control for open-channel hydraulic systems will be greatly facilitated when simple algorithms and tuning procedures are available and adapted to this type of systems. The objective is therefore to contribute to an "automation for hydraulic systems for dummies" approach. In this chapter, we propose an automatic method to tune a series of distant downstream PI controllers for a cascade of pools. The methodology we present could also be used for local upstream controllers, with minor changes. The method is based on the Auto-Tuned Variation principle (ATV) carrying out a relay experiment. The information obtained from this experiment allows to estimate the parameters of a simplified integrator-delay model of each pool. Finally this allows tuning automatically a series of feedback PI controllers, with given gain and phase robustness margins, and a feedforward controller based on simple time delay. This relay experiment is performed for each pool of the canal or river, in sequence, with automatic activation of the previously tuned PI controllers. Different decoupling configurations, in order to reduce interactions between pools, are evaluated in simulation on the benchmark canal 2 of the ASCE Task Committee on Canal Automation Algorithms.

9.1 Introduction

Transport of water with open-channel hydraulic system has the main objective to convey water from a source (dam, river) to users (agricultural lands, but also industries and cities). Such systems can be very large (several hundreds of kilometers), and varying objectives are assigned to their managers. The main general one is to provide water to the different users at the right moment and in the right quantity, and to guarantee the safety of the infrastructure. Some of these hydraulic

D. Dorchies (✉) • P.-O. Malaterre
UMR G-EAU, Montpellier, France
e-mail: david.dorchies@irstea.fr; pierre-olivier.malaterre@irstea.fr

C. Ocampo-Martinez, R.R. Negenborn (eds.), *Transport of Water versus Transport over Water*, Operations Research/Computer Science Interfaces Series 58,
DOI 10.1007/978-3-319-16133-4_9

systems have also navigation purposes (e.g., Rhône river, Canal du Midi, etc.). In this case, additional constraints on water depth, water level fluctuations, and velocities are also to be satisfied. Long time ago, all hydraulic systems (canal, rivers, sewage systems) were controlled in an upstream control logic [15], since it is the easiest to implement in both manual or automatic approaches. In the case of transport of water, it became internationally recognized that the downstream control logic is hydraulically more efficient, but technically more difficult to design and implement. In the case of pure transport over the water, we could possibly claim that the corresponding classical control objectives could be reached by a simple upstream control logic. But such pure navigation systems are rare, and combined systems are becoming more popular. The development of simple and efficient control algorithms adapted to open-channel hydraulic systems, flexible enough to adapt to local constraints, to upstream or downstream logic configurations, easy to tune and to make evolving, is necessary to continue promoting improvement of the management of such systems through automation.

Most of the technics that have been used so far, for the automation of irrigation canals, are based on PID, Internal Model and Fuzzy Control [13] and are mainly Single-Input Single-Output (SISO) algorithms. Several works on Predictive Control, LQG, $\mathcal{H}_\infty$ or ℓ_1 design methods are also described in the literature, and present the advantage of providing naturally Multiple-Inputs Multiple-Outputs (MIMO) mathematical frameworks. They have been tested on numerical simulators or laboratory canals, and some have applications such as the Predictive Control on the Rhône river since 2000 [7] and on some systems in The Netherlands.

Canal managers or consultant companies designing canals and proposing automatic control rules for their cross-structures, usually prefer simple control technics, that they can tune easily, understand, and transfer onto real systems. It can seem strange that a canal manager needs to understand the controllers applied to the control devices of his canal. But, this is often true, since the dynamics of the canal can change during time (vegetation growth, sedimentation, etc.) or he can be unsatisfied with the behavior of his controllers and may want to change this. This is why, despite possibilities of improvements with more advanced technics, that the well-known PID controllers are still very popular on irrigation canals or rivers. For a single pool, tuning a PI controller can be easy. For a series of pools, with interactions between them, this can become more difficult. The technics based on models and frequency analysis are powerful [6], but far too complicated for civil engineering consultant companies or canal managers. The ATV (Auto-Tuned Variation) is an automatic tuning method first proposed by Aström [1, 2]. An application to the automatic tuning of controllers for irrigation canal pools has been presented by the authors in previous papers on a single pool [9] (for local upstream, local downstream and distant downstream control logic), or on three long pools with little interactions between them [8] (for distant downstream control logic in cascade).

The believe of the authors is that many more applications of automatic control will appear on open-channel systems, for both transport of or over the water, if simple methods can be used. Simple enough to be implemented as standard options in hydraulic softwares (as already done in the SIC^2 software we will use in the

chapter), used by civil or hydraulic engineers designing such systems without any knowledge of automatic control, and understood and accepted by canal or river managers. Methods that could also be tuned directly and automatically on real systems, without the use of any simulation tool, for subsequent tuning for improvement of the original tuning if the manager is not satisfied or if the hydraulic or structural conditions of the canal or river have changed.

This contribution proposes to extend this automatic tuning method to the case of multiple pools irrigation canals or rivers using different decoupling options and a feedforward controller. Results have been checked on the second bench-mark canal proposed by the ASCE Task Committee on Canal Automation Algorithms [4].

9.2 Design of the PI Controller with ATV Tuning Method

9.2.1 Description of ATV Tuning Method

The relay feedback auto-tuning method proposed by [2] was one of the first to be commercialized for tuning of PID controller in industry. It has since remained attractive owing to its simplicity and robustness. The objective of the method is to determine the critical point, from a single experiment, i.e., the process frequency response with a phase lag of $-180°$. It can be shown that under relay control as in Fig. 9.1, the process will oscillate with the period T_u and that the critical gain k_u is approximately given by:

$$k_u = \frac{4d}{\pi a}, \tag{9.1}$$

where d is the relay amplitude and a is the amplitude of the process output [2].

Typical responses are as in Fig. 9.1. The relay is a simple nonlinear element that changes the input to $+d$ when the output error $e = y - r$ becomes negative,

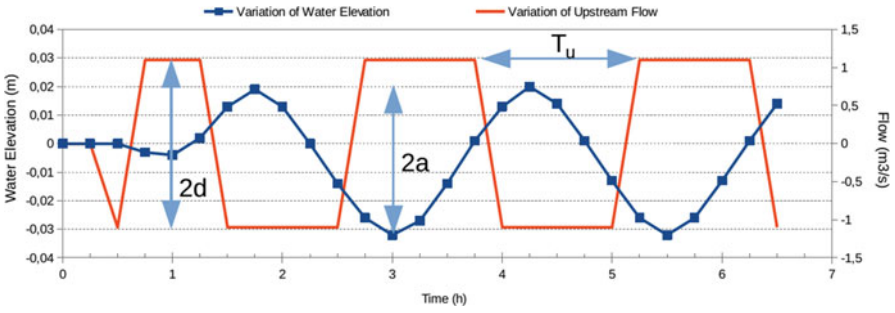

Fig. 9.1 Relay experiment result on the first pool of ASCE test case canal 2

and to $-d$ when the error becomes positive. It is therefore very easy to implement on a real canal, since the gate opening has to be opened or closed of a given value $\pm d$ according to a measured water level y.

9.2.2 Application of ATV Method on One Canal Pool

We will apply the ATV method on a canal pool supposed to be approximated by an Integrator Delay (ID) model proposed by Schuurmans et al. [17]. This simplified model used for the design of water level controllers for irrigation and drainage canals describes the essential characteristics of the processes relevant for canal control (such as water movements and control structures).

This model has two parameters A and τ respectively the inverse of the integrator gain and the delay of the canal pool. The canal pool is then represented, in the frequency domain, by:

$$y = \frac{e^{-\tau s}}{As} u, \tag{9.2}$$

with y the downstream water elevation, u the upstream discharge of the pool and s the Laplace transform variable.

Litrico et al. [9] showed how to compute the ultimate cycle parameters obtained via a relay experiment for an ID model given by (9.2).

Let us examine the system behavior in steady state with persistent limit cycle. We suppose, without loss of generality, that the error becomes negative at $t = 0$. Due to the integrator and since this output error comes from an input negative step of amplitude d, the error is decreasing as a negative ramp of slope $-d/A$. Then, at $t = 0$ the relay leads to a input positive step of amplitude d. At $t = \tau$, this positive step influences the output, which has reached the value $-d \times \tau/A$. Then the output increases as a positive ramp of slope d/A, during a time equal to 2τ. This is depicted in Fig. 9.2. Therefore, the amplitude of the output is equal to

$$a = d \times \frac{\tau}{A}, \tag{9.3}$$

and, using (9.1), the ultimate cycle parameters are given by

$$k_u = \frac{4A}{\pi\tau}, \tag{9.4}$$

and

$$T_u = 4\tau. \tag{9.5}$$

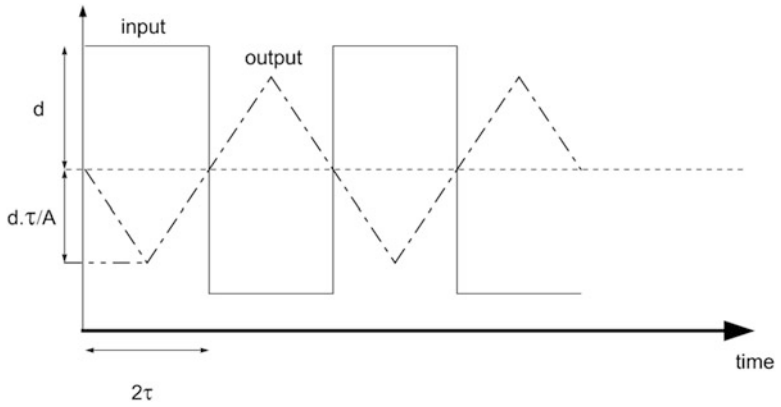

Fig. 9.2 Relay experiment for an ID model

Therefore the relay experiment enables to identify the ID model parameters τ and A

$$\tau = \frac{T_u}{4}, \tag{9.6}$$

$$A = \frac{\pi T_u k_u}{16}. \tag{9.7}$$

9.2.3 Tuning Rule of the PI Controller

Many different rules have been proposed to tune PI or PID controllers from ultimate cycle parameters. Most of them are based on pre-specified rules (such as Ziegler-Nichols rule [19]). Litrico et al. [9] proposed a way to be able to choose the controllers parameters according to time performance and robustness specifications by defining the proportional and the integral parameters, respectively k_p and T_i, from gain and phase margins:

$$k_p = k_u \frac{\pi^2}{8} 10^{-\frac{\Delta G}{20}} \sin\left(\frac{\pi}{180}\Delta\Phi + \frac{\pi}{2}10^{-\frac{\Delta G}{20}}\right), \tag{9.8}$$

$$T_i = \frac{T_u}{2\pi} 10^{\frac{\Delta G}{20}} \tan\left(\frac{\pi}{180}\Delta\Phi + \frac{\pi}{2}10^{-\frac{\Delta G}{20}}\right), \tag{9.9}$$

with ΔG the gain margin in dB and $\Delta\Phi$ the phase margin in degrees.

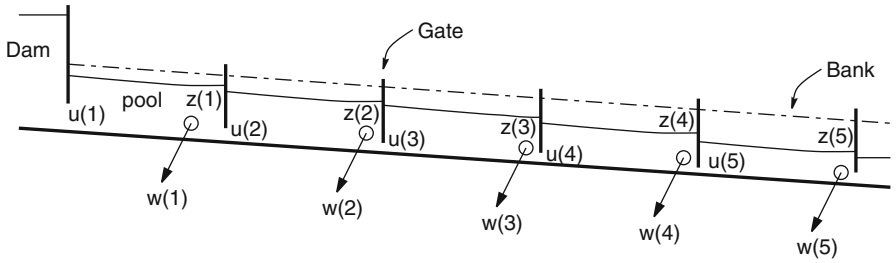

Fig. 9.3 Example of multi-pool canal

9.2.4 Case of Multiple Pools

In the case of multiple pools (cf. Fig. 9.3) controlled with distant downstream PI controllers, one may use a relay experiment to tune successively each pool. This will lead to decentralized PI controllers for the canal pool. However, it is well-known that pool interactions decrease the overall performance of decentralized controllers for an irrigation canal [16]. In a classical decentralized framework, each controller is supposed to be SISO, one control action U aiming at controlling one and only one controlled variable y. This framework is efficient and adapted to situations where indeed each control action U has an influence on only the controlled variable y that it is supposed to control. But in reality, and this is the case in our multi-pool system, each control action U has hydraulic effects on several controlled variables y. This is called coupling effects. There is a mathematical way of assessing the importance of this coupling, using the RGA (Relative Gain Array) index [14]. This coupling effect is becoming stronger when changing from local upstream control logic, to local downstream logic, and even more to distant downstream logic. In our distant downstream control logic, two coupling effects can be denoted:

- If we consider control action variable in term of gate opening W, if gate no. 1 (control action variable U_1) is opened, then water level y_1 will increase after a certain time due to the hydraulic delay in pool no. 1, and since this increase affects the discharge going through gate no. 2, water level y_2 will, in turn, increase.
- If gate no. 2 (control action variable U_2) is opened, then nearby upstream water level y_1 will decrease rapidly.

Several existing decoupling techniques are described in Malaterre and Baume [14] which lead to two strategies for compensating the coupling effects described above.

The first one consists in using discharges Q instead of gate openings W as control action variables (U_i). The direct consequence is that if a given target discharge is maintained through a gate, then the downstream pool is no longer subject to perturbations occurring on the upstream pool.

The second one is the fact that each calculated control action variable U_i, or a portion α of it, is added to the next upstream one U_{i-1}. Hydraulically, this means that if U_i is operated to compensate for a perturbation in its downstream pool i, then we know that this operation will have an interaction effect on y_{i-1}. Of course U_{i-1} will in turn correct the effect of this perturbation (after some delay inherent to the system's characteristics) when its effect is felt on y_{i-1}. But we can anticipate this action by adding directly the correction to U_{i-1}:

$$U_{i-1} = F_{i-1} y_{i-1} + \alpha U_i, \tag{9.10}$$

where F_{i-1} is the transfer function of the PI controller linking y_{i-1} to U_{i-1} and $\alpha \in [0, 1]$. Theoretically α must be equal to 1, but for stability and robustness reasons, it is sometimes reduced close to lower values such as 0.8.

This correction will cancel or at least reduce the effect of U_i on y_{i-1}. This second decoupling technique cannot be as good as the first one proposed above since the delay time on pool $i-1$ implies that the additional correction αU_i at gate $i-1$ will not be felt instantaneously on the controlled variable y_{i-1}.

This decoupler is easy to understand and to design when the control action variable U_i is a discharge Q. In case of a control action variable U_i in terms of gate opening W, it is necessary to use a calculation of the outgoing discharge for calculating the decoupler. Litrico and Malaterre [8] proposes a method using the results of the relay experiment for this purpose. But here, since the experiment described below uses feedforward control which is in term of discharge, discharge conversion into gate opening is required.

9.3 Test Case on ASCE Canal 2

9.3.1 Description of ASCE Canal 2

The ASCE Task Committee on Canal Automation Algorithms (1993–1998) has defined benchmark canals and scenarios for two canals [4]. The aim was to provide researchers with benchmarks that would allow performance comparison between different canal regulation algorithms. Each canal is composed of eight pools separated by cross-gates. The main differences between the two canals are their slopes and in-line volumes. Canal 1 is a steep, fast canal with little storage, and Canal 2 is a flat canal with more storage volume and longer pools. Canal 2 is based on the upstream portion of the Corning canal in California.

Two test scenarios are considered for each canal. For the first one (the tuned test), the control parameters are tuned with the correct canal description, and they are then tested on the same canal system. For the second one (the untuned test), the same control parameters as previously tuned are applied to a canal system with modified Manning and gate discharge coefficients. This second test aims at verifying the robustness of the algorithm.

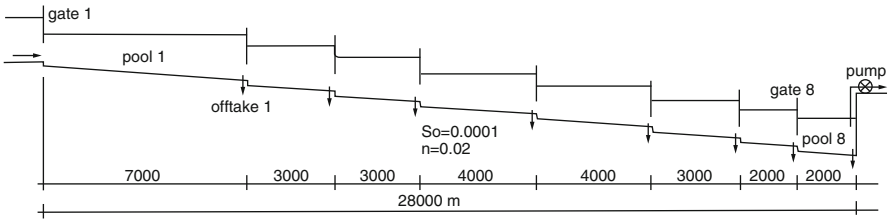

Fig. 9.4 Profile for test canal 2 (taken from [11])

Table 9.1 Hydraulic conditions in the tests 1 and 2 for ASCE test case canal 2

		Offtakes no.								
Test	Period	1	2	3	4	5	6	7	8	Pump
1	Initial withdrawals	1.0	1.0	1.0	1.0	1.0	1.0	1.0	1.0	3.0
	0–12 h	–	–	–	–	+1.5	+1.0	–	–	–
	0–24 h	–	–	–	–	–	−2.0	–	–	–
2	Initial withdrawals	0.2	0.3	0.2	0.3	0.2	0.3	0.2	0.3	0.7
	0–12 h	+1.5	+1.5	+2.5	–	–	+0.5	+1.0	+2.0	+2.0
	0–24 h	−1.5	−1.5	−2.5	–	–	−0.5	−1.0	−2.0	−2.0

In this study, we will focus on the regulation of the eight pools of Canal 2. The control objective is to regulate the downstream level in each canal by modifying upstream discharges and thus the corresponding gate openings. Pools lengths are visible in Fig. 9.4. The bottom width is 7 m, the bottom slope is 0.0001, the Manning's n is 0.02 and the drop at each gate is 0.2 m. Gate movement, between two regulation time steps, is restricted with a minimum gate movement allowed equal to 0.5 % of the gate height.

9.3.2 Description of the Tests

Each test is divided into two parts, 12 h long: 0–12 h (where a feedforward component can be used since the offtake discharge changes are known), and 12–24 h (where the offtake discharge changes are supposed to be unknown and therefore cannot be used by the controller). The time step of the controllers ΔT_r is fixed at 15 min. The first test starts with a heading flow of 11 m^3/s and has a relatively small scheduled flow change at 2 h, followed by a similar unscheduled change at 14 h. The second test represents multiple variations showing dramatic changes with heading flow varying between 2.7 and 13.7 m^3/s. Complete hydraulic conditions of the tests are described in Table 9.1.

For testing the robustness of the controllers, the tests are performed in tuned and untuned conditions. The latter involves unknown changes of some hydraulic parameters of the canal:

- Manning's n value of 0.026 instead of 0.02.
- Check gate discharge is 10 % less than in the tuned conditions.
- Real scheduled offtake discharge changes is 5 % higher than as scheduled.

9.3.3 Performance Indicators

The original objective of the control algorithms for these tests is to keep the water level in the canal constant so that the flow to offtakes will remain constant. Therefore, the main performance criteria proposed by Clemmens et al. [4] are related to maintaining constant water levels at the offtakes, located at the downstream end of each pool. The following indicators are used:

Maximum Absolute Error (MAE)

$$MAE = \frac{\max\left(\left|y(t) - y_{target}\right|\right)}{y_{target}}, \tag{9.11}$$

where $y(t)$ = observed (computed from simulation) water level at time t; and y_{target} = target water level (being the initial water level at time 0).

Integral of Absolute Magnitude of Error (IAE)

$$IAE = \frac{\frac{\Delta t}{T}\sum_{t=0}^{T}\left|y(t) - y_{target}\right|}{y_{target}}, \tag{9.12}$$

where Δt = regulation time step; and T = time period for the test.

Steady-State Error (StE)

$$StE = \frac{\max\left(\left|\bar{y}_{10,12} - y_{target}\right|, \left|\bar{y}_{22,24} - y_{target}\right|\right)}{y_{target}}, \tag{9.13}$$

where $\bar{y}_{h_1,h_2}$ = average water depth between time h_1 and h_2.

Integrated Absolute Discharge Change (IAQ)

$$IAQ = \sum_{t=t_1}^{t_2}\left(\left|Q_t - Q_{t-1}\right|\right) - \left|Q_{t1} - Q_{t2}\right|, \tag{9.14}$$

where Q_t = check gate discharge at time t.

9.3.4 Experimental Design on ATV-PID

The method we will develop in this chapter, combining a series of PID controllers (PI only in our case, to be more precise) tuned by the ATV method will be referred as the ATV-PID method. Several options are possible depending on the type of control action variables, on the feedforward component, on the report from one gate to another, on the order of tuning, etc. The simulations have been performed with SIC^2 version 5.33 developed at Irstea, Montpellier [3]. This software is specially well adapted to the simulation of the automatic control of an open-channel system, and includes a library of preprogrammed algorithms such as the ATV, the PID, the combined ATV-PID that we will use in this chapter and much more. It also offers open interfaces with Matlab, Scilab, WDLangage and Fortran that we will also use for advanced options. At the same time, Scilab [18] was used for driving automatically in batch mode all the simulations and calculating the performance indicators. Simulations use a calculation time step ΔT and a gate movement duration ΔT_o of 1 min. This choice was made for:

- representing a realistic duration of a gate movement,
- reproducing faithfully high frequency waves occurring after a gate movement.

The control time step for the ATV relay experiment is also fixed at 1 min in order to accurately determine the period and the amplitude of the process outputs.

Considering the different issues on coupling effects described in Sect. 9.2.4, the authors propose to analyze the performance of the ATV method on tests 1 and 2 of the ASCE test case canal 2 with different decoupling options.

The first option is the choice of the control action variable at the check gates:

- the flow with check gates acting as pumps hereafter noted option P. This choice allows to verify if the ID model could be representative of the dynamic flow in this case study. Indeed, in the case of pumps, the assumptions underlying the integral-delay model are satisfied.
- the flow with discharge inversion for calculating the opening of the check gates at each control time step hereafter noted option Q. For this purpose, we use here the method of the characteristics used by Litrico et al. [10]. This method takes into account the deviations of the upstream and downstream water levels and their impacts on the gate discharge due to change of hydraulic conditions at the gate due to its movements.
- the gates opening W (except for the head of the canal where the flow Q is used) hereafter noted option W.

For configurations using control action variables Q and W, gate movements are restricted by the minimum gate movements described in Sect. 9.3.1, as imposed by the benchmark specifications. The idea of this minimum gate movement is twofold. First, the actuators do not have an infinite precision. Second, in order to limit the number of operations of the gates and the solicitation of the motors, if the gate movement required by the controller is less than this minimum value, then the

gate will not be moved. For the control action variables P, we did not impose an equivalent minimum discharge change, since this P option is more seen as a reference option for comparison, rather than a realistic option. But, for this P pump option we observed that the canal pools could be dried at some moments due to the very important discharge changes that can be applied at the control structures, contrary to the options where a gate opening is applied. This is why, for this P option, we added a security threshold preventing from drying the pools. When a water level upstream of a pump is dropping to much, below half of the corresponding target water depth, then the downstream pump is stopped during at least 5 min.

The second option is related to the use of the decoupler transferring the value of the control action variable of one structure to the next upstream control structures using (9.10). Several coefficients α are tested: 0, 0.8, and 1.

The last option is related to the way the ATV-PID method is applied on a multiple-pool canal. Each PI controller of a pool is tuned one after the other, but there are many possibilities for the order in which this is done. Just after a PI controller of a pool is tuned, this one is switched into automatic PI mode and regulates the water level at the downstream end of this pool. Therefore, due to coupling issues, it is easy to understand that the order used for tuning the controllers of each pool can change the result of this tuning. The dynamic of a pool with or without the adjacent pools in PI mode is not the same, except for the pump option P, where the coupling effects are completely removed. Two possibilities are then explored: tuning from downstream to upstream (hereafter denoted $Dn \rightarrow Up$), and tuning from upstream to downstream (hereafter denoted $Up \rightarrow Dn$). For taking into account the possible change of dynamics involved when all the PI controllers are activated, compared to the case when some are not, we choose to test an option with so-called *meta-cycles*. In the first meta-cycle, the PI controllers are activated, one after the other, after their first ATV tuning, in a given order ($Dn \rightarrow Up$ or $Up \rightarrow Dn$). The PI controllers not tuned yet are not set to PI mode and therefore the corresponding gates are not moved during the tuning procedure. In the second meta-cycle, ATV tuning is performed again for each pool, one after the other (in the same order than during the first meta-cycle) with all the other PI controllers activated. These PI controllers have first the parameters calculated in the first meta-cycle and are progressively updated by the parameters calculated during the second meta-cycle. We observed, in our example, that the parameters obtained with only one meta-cycle, or with two, are almost the same, at least for the best options that we will select. This is probably due to the satisfactory way of handling the coupling effects. This validates the approach proposed in this chapter, both for an initial tuning when no PI has been tuned yet, and for subsequent tuning procedures, in real field conditions when some or all PI have already been tuned and activated.

Auto-tuning experiments are performed on the ASCE test-case canal 2 with steady conditions corresponding to the beginning of both tests and for tuned conditions as described in Sect. 9.3.2. Litrico et al. [9] advised to use a relay included in the range 10–20 % of the initial discharge. The relay chosen for the test 1 is equal to 10 % of the initial discharge on each check gates (a bigger value

carrying too large oscillations in the pools), and for test 2, it is equal to 15 % of the initial discharge (Lower values resulting in impossibilities to perform the relay experiment because of the minimum gate movement).

Considering the choice of the gain and phase margins used for tuning the PI controllers, Litrico et al. [9] had tested a range of ΔG between 6 and 14 dB with keeping a constant phase margin ratio $\Delta\Phi/\Delta\Phi_{max} = 0.7$ with $\Delta\Phi_{max}$ determined by the formula $\Delta\Phi_{max} = 90(1 - 10^{\frac{\Delta G}{20}})$. For both control action variable P and Q configurations, different values have been tested for the gain margin and we used each time the formula above for calculating the phase margin. Starting from $\Delta G = 10$ dB, we increased this value with a step of 5 dB until the ATV experiment does not lead to oscillating or unstable controllers (e.g., PI controllers with long-lasting oscillations). Finally, the gain and phase margin were respectively 20 dB and 56.7° for configurations with control action variable P and Q, and 15 dB and 51.8° for configurations with control action variable W.

Combining decoupling options and hydraulic conditions, the experiment totals 36 sets of PI parameters. The simulations of the hydraulic behavior and the regulation algorithms are performed under SIC^2 where the ATV-PID method used here is fully implemented. The first decoupler (i.e., use of the characteristics method for discharge inversion calculation for the gate opening) is also available in SIC^2. For the second decoupler, a module written in Windev script language (called WDLangage) is used inside SIC^2 (see Fig. 9.5 for an overview of SIC^2 interface showing the canal and the controllers). For the control action variable W, the SIC^2-Scilab interface was used for calculating discharge conversions used by the second decoupler.

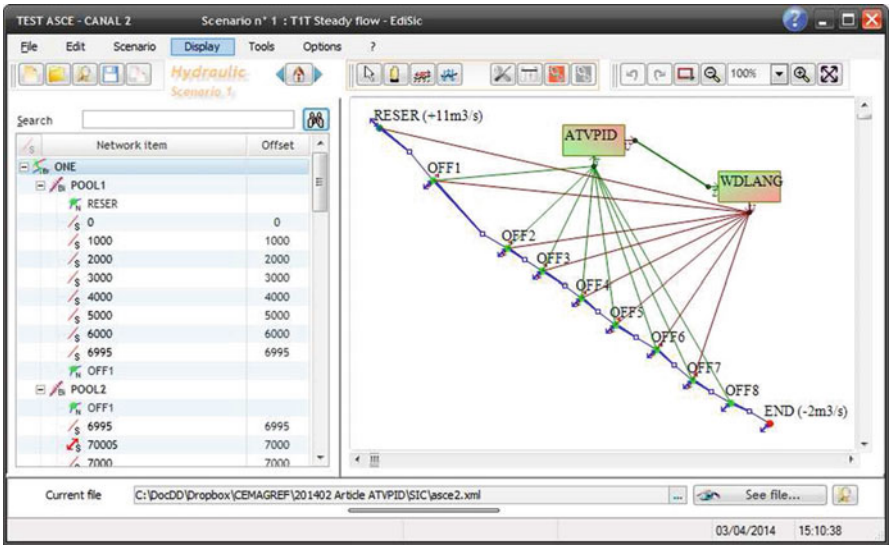

Fig. 9.5 Implementation of ATV-PID experiment within SIC^2

9.3.5 Performing the Tests

The tests are performed for a period of 24 h with a 1 min ΔT simulation time step and 15 min ΔT_r regulation time step. The scheduled flow change at time $t = 2$ h requires the use of a feedforward controller. Keeping in mind the philosophy of simplicity of use, we choose to use a pure delay controller calibrated from the parameters τ (pure delay) and A (backwater area) of the Integrator Delay models identified by the ATV relay experiment with (9.6) and (9.7).

When a discharge variation ΔQ occurs at the downstream end of a reach, a variation of the water level ΔY_c is expected. This variation can be estimated by the characteristic method which corresponds to the equation:

$$\Delta Y_c = -\frac{\Delta Q}{T(C - V)}. \tag{9.15}$$

With T, the top width of the canal, C the wave celerity, and V the mean velocity. Considering that the water level at the downstream end of the reach is equal or close to the target level, T and C remain almost constant and V only depends on the local scheduled discharge Q.

In order to counterbalance this water level variation, one can use the Integrator Delay model to calculate the delay we have to use for the anticipation feedforward action to get an opposite water level variation before the discharge variation occurs at the downstream end of the reach. The link between the delay and the water level variation is shown in Fig. 9.6. The anticipation to apply at the upstream check gate for the feedforward controller is then equal to $\tau + \Delta t_{ff}$, where Δt_{ff} if given by

$$\Delta t_{ff} = \frac{A.\Delta Y_c}{q}, \tag{9.16}$$

with A the integrator parameter of the ID model, q the downstream discharge change ($q = \Delta Q$ for a classical 100 % feedforward loop) and ΔY_c the anticipated water level change calculated with (9.15). That means that if a flow change ΔQ_i is scheduled at time t at the offtake located at the downstream end of the pool i, ΔQ_i will be applied at the upstream check structure at time $t - (\tau + \Delta t_{ff})$.

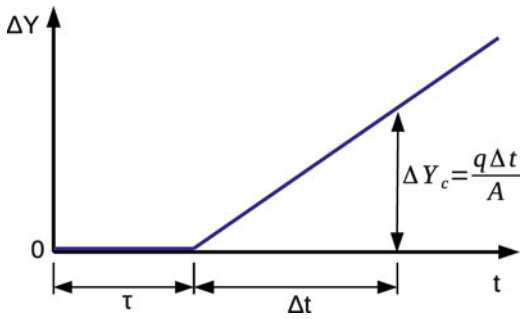

Fig. 9.6 Link between the Integrator Delay model and the water level variation ΔY_c

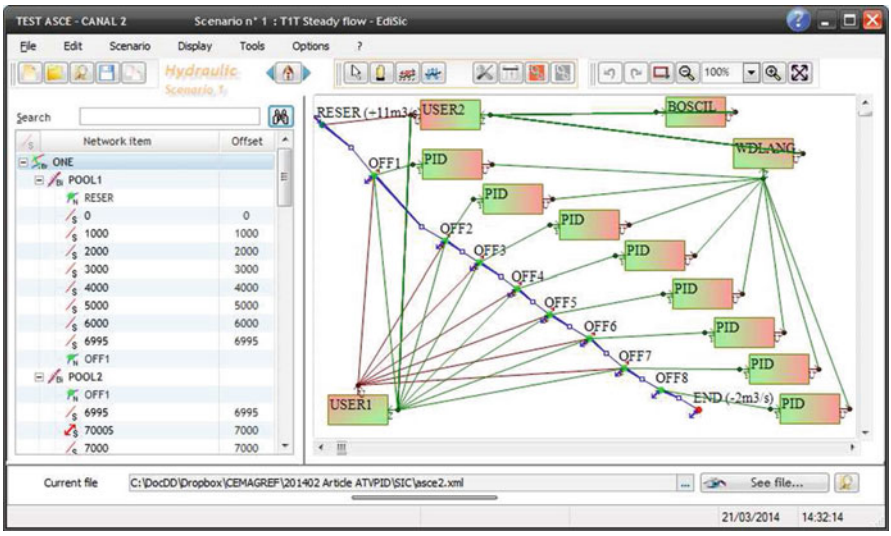

Fig. 9.7 Implementation of PI tests within SIC^2

The feedforward controller is calculated offline in Scilab and applied into SIC^2 with the so-called BOSCIL method which allows to use an open loop controller reading the control variables in file containing a matrix in Scilab format. In addition, we develop specific regulation modules in Fortran in order to be able to use the inversion discharge calculation embedded in SIC^2 but with changing the discharge coefficient to take into account the untuned conditions. See Fig. 9.7 for an overview of the regulation framework interfaces in SIC^2.

On one side, the tests in tuned conditions are performed with the PI set of parameters obtained in tuned conditions. On the other side, the tests in untuned conditions are performed with the same set of parameters obtained in tuned conditions.

9.3.6 Results

Performance indicators have been calculated for the four tests (tests 1 and 2 in tuned, and untuned conditions), for the 18 combinations of decoupler configuration, and for each 12-h period of the tests. For each indicator, maximum and average value of the indicators encountered in the eight pools of the canal are calculated.

All these indicators has been sorted and compared to results of other controllers which have been tested on the ASCE benchmark test-case on Canal 2. These references are:

- PILOTE: A Linear Quadratic Gaussian optimal controller using gate opening as control action variable [12].
- PIR: This controller is based on Dynamic Regulation coupled with a PI controller using a Smith Predictor and the second decoupler used herein. To simplify the coupling of reaches, the discharges to be adjusted at the check gates are used as control action variables [5].
- CLIS based on an inverse solution method of the Saint Venant equations [11].

The current experiments show that the results are very sensitive to the time taken for the operations at the check gates and at the offtakes. A given gate opening at a given regulation time t can be done in an operation time duration ΔT_o of 10 s or of 5 min for example. To simplify, we decided to take this time ΔT_o equal to the numerical simulation time step ΔT. These times steps ΔT_o and ΔT are not specified in the benchmark conditions. Only the regulation time step ΔT_r is specified, meaning the frequency at which a new gate operation can be done. For this benchmark on ASCE Canal 2 it is equal to 15 min. A long numerical simulation time step ΔT will not be able to reproduce high frequencies waves occurring after a gate movement. Especially, we observe in case of the use of Q control action variable that the error between the desired and obtained discharge considerably increases during the ΔT_r time step as the simulation time step ΔT decreases. Since results for PILOTE and CLIS has been produced respectively with a 15 min and 5 min simulation time step ΔT and the one of PIR is not defined, the comparison with these reference should be taken with caution. The tests using a 1 min simulation time step ΔT correspond to more stringent conditions with regards to the performance indicators and also to a more realistic field situation considering that the changes in gate opening or discharge last 1 min.

Detailed Results on Test 1

In Test 1 with tuned or untuned conditions (see Figs. 9.8 and 9.9), PILOTE, CLIS, PIR, and configurations with P as control action variable are often at a good position in the rankings of MAE, IAE, and StE performance indicators. In untuned conditions configurations with W as control action variable are also well ranked for MAE or IAQ indicators. In the rankings of the Integrated Absolute Discharge Change (IAQ), the best configurations are the ones that are generally at the bottom end on the others indicators. It can be explained by the fact that IAQ is an indicator relative to the wear and tear of the check gates and then the best configurations in IAQ are under-reacting controllers.

On the scheduled period (0–12 h), there is no significant differences between configurations using different values of α for the upstream report. We see here that the feedforward controller does most of the job on the scheduled period by bringing the necessary volume of water at the good time. The feedback controller only has to adjust the water level without the need to communicate such big changes in water discharge to the upstream check structures. On the contrary, on the unscheduled

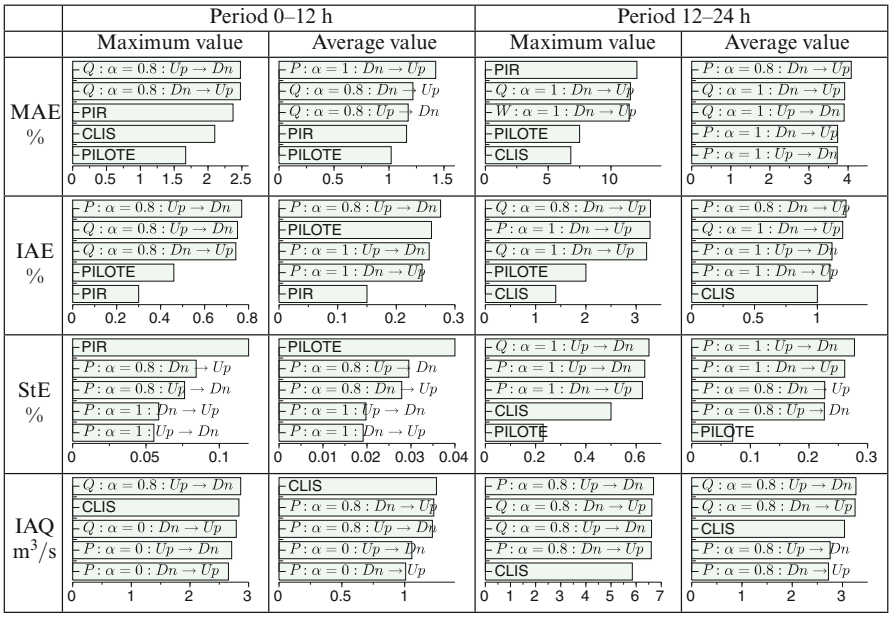

Fig. 9.8 Benchmarking of performance indicators for test 1 in tuned conditions

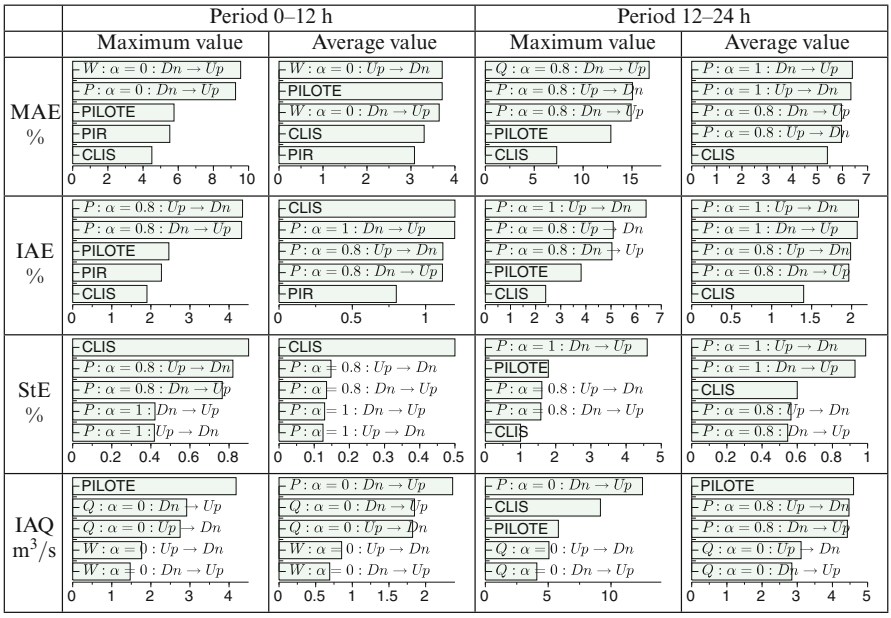

Fig. 9.9 Benchmarking of performance indicators for test 1 in untuned conditions

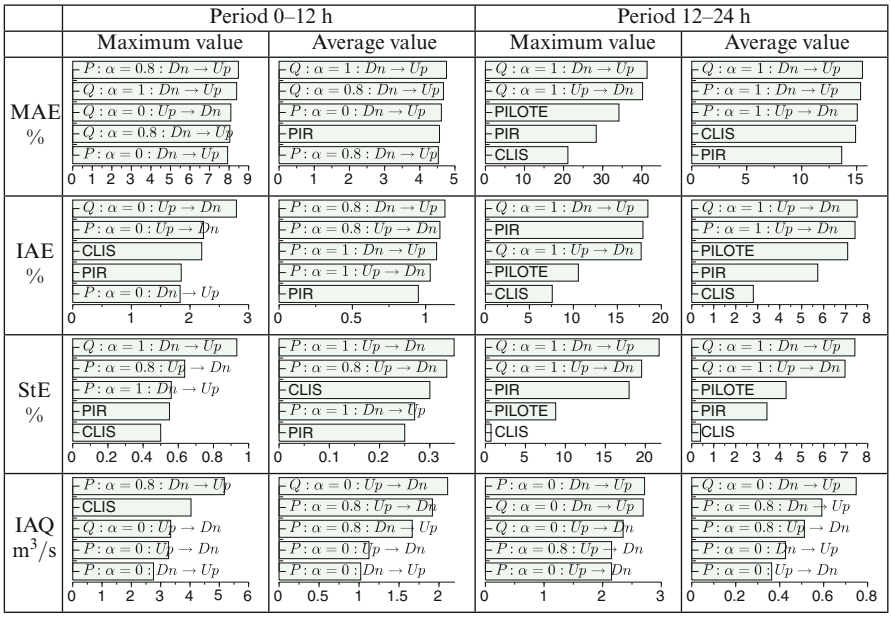

Fig. 9.10 Benchmarking of performance indicators for test 2 in tuned conditions

period (12–24 h), only upstream report with α equal to 0.8 or 1 are on the hit list for MAE, IAE, and StE showing that big deviations in water discharges caused by the feedback controller need to be communicated to the upstream check structures in order to perform well.

Detailed Results on Test 2

The Test 2 offers much larger variations in flow changes. In this test (see Figs. 9.10 and 9.11), one can notice the good reliability of the configurations P and Q both in tuned and untuned conditions on the scheduled period (0–12 h) whatever the upstream report α is. That validate the fact that most of the performance here is due to the feedforward controller which is independent from the upstream report.

Global Ranking

Given the multitude of different results, it is difficult to distinguish which configuration to use in order to maximize most of the performance indicators. For that purpose, we choose to use a scoring method on each of the 64 calculated performance indicators. The first ranked configuration gets 10 points and the worst configuration gets 0 points while the score of all the others configurations

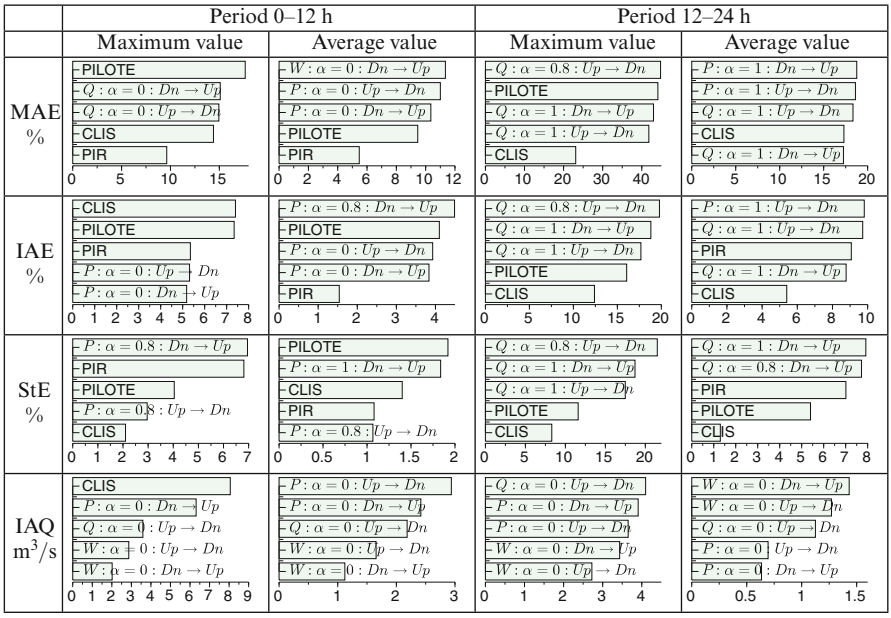

Fig. 9.11 Benchmarking of performance indicators for test 2 in untuned conditions

is calculated proportionally between these two extremes given there respective indicator values. Finally, scores are summed in order to get the global score and the global ranking. The results for the tested configurations is given in Table 9.2.

At first sight, ATV-PID is a controller that under-performs compared to more sophisticated controllers such as CLIS, PILOTE and PIR. Regarding control action variable, P is the best choice, followed by Q and W. That proves the relevance of the ID model used in the ATV method to synthesize the PI controller in the P option, when the hypothesis underlying the ID model are fully valid. The more there exists a deviation between the required discharge change and the obtained one at a gate, the more the controller under-performs.

Regarding upstream report, $\alpha = 0.8$ configurations are at the top-ranking for P and Q configurations, confirming that $\alpha = 1$ configurations raise oscillatory issues. This aspect can be explained by the over-reaction due to the PI controller. For example, if an increase of discharge is done on a check gate, this increase is entirely transmitted to the upstream check gate that will deliver the necessary discharge to fill the gap at the downstream part of the reach. But, because of the delay this gap is not fulfill instantaneously, and the PI controller will aim at compensating for the decrease of water level by increasing the discharge as well. Without surprise, configurations with no upstream report is at the rear of the pack except for W configurations where the solution used here to perform the upstream report does not seem to be efficient. This point will be further investigated in future works.

Table 9.2 Global scores of tested decoupler configurations

Rank	Control action variable	Upstream control transfer	ATV direction	Score
1	CLIS			578
2	PILOTE			544
3	Discharge in Pump mode (P)	$\alpha = 0.8$	Down to up	524
4	Discharge in Pump mode (P)	$\alpha = 0.8$	Up to down	518
5	PIR			509
6	Discharge in Pump mode (P)	$\alpha = 1$	Down to up	492
7	Discharge (Q)	$\alpha = 0.8$	Down to up	484
8	Discharge (Q)	$\alpha = 0.8$	Up to down	481
9	Discharge in Pump mode (P)	$\alpha = 1$	Up to down	481
10	Discharge (Q)	$\alpha = 1$	Down to up	469
11	Discharge (Q)	$\alpha = 1$	Up to down	464
12	Discharge in Pump mode (P)	$\alpha = 0$	Up to down	416
13	Discharge in Pump mode (P)	$\alpha = 0$	Down to up	401
14	Discharge (Q)	$\alpha = 0$	Up to down	366
15	Discharge (Q)	$\alpha = 0$	Down to up	355
16	Opening (W)	$\alpha = 0$	Down to up	262
17	Opening (W)	$\alpha = 0$	Up to down	247
18	Opening (W)	$\alpha = 0.8$	Down to up	236
19	Opening (W)	$\alpha = 1$	Down to up	222
20	Opening (W)	$\alpha = 0.8$	Up to down	216
21	Opening (W)	$\alpha = 1$	Up to down	171

Results for $Dn \rightarrow Up$ and $Up \rightarrow Dn$ configurations generally show no significant differences in the performances indicators but there is always a little advantage for $Dn \rightarrow Up$ configurations with upstream report $\alpha \neq 0$.

Except for StE indicators where the minimum gate movement is in cause, P compared to Q control action variable configurations shows that even with the use of the characteristics method, there could be still scope for improvement in the method used to calculate the gate opening from the discharge equation.

The results can also be examined in relation to the sensibility of the controllers to untuned conditions. In order to asset this issue, we have calculated the average evolution of all the performance indicators for each controller configuration. Results for Test 1, Test 2 and both tests detailed for scheduled and unscheduled periods are presented in Table 9.3.

One can notice that performance indicators downgrading is largely less important in the scheduled period (0–12 h) than in the unscheduled one (12–24 h) for all configuration. That shows that feedforward controllers are more robust to changes of hydraulic conditions. Nevertheless the underestimation of 5 % of scheduled offtakes in untuned condition tested here could not be considered as a hard test of robustness. The less sensitive configurations are the ones with W as control action variable with no upstream discharge reporting ($\alpha = 0$). But this configuration cannot be

Table 9.3 Average evolution of performance indicators between tuned and untuned conditions

	Test 1		Test 2		All tests	
Configuration	0–12 h	12–24 h	0–12 h	12–24 h	0–12 h	12–24 h
CLIS	+63 %	+87 %	+36 %	+132 %	+49 %	+110 %
PILOTE	+154 %	+273 %	+51 %	+68 %	+103 %	+171 %
$P : \alpha = 0.8 : Dn \rightarrow Up$	+185 %	+219 %	+112 %	+146 %	+149 %	+183 %
$P : \alpha = 0.8 : Up \rightarrow Dn$	+185 %	+220 %	+86 %	+142 %	+136 %	+181 %
PIR	+111 %	+315 %	+40 %	+105 %	+75 %	+210 %
$P : \alpha = 1 : Dn \rightarrow Up$	+208 %	+280 %	+76 %	+153 %	+142 %	+217 %
$Q : \alpha = 0.8 : Dn \rightarrow Up$	+227 %	+311 %	+77 %	+152 %	+152 %	+231 %
$Q : \alpha = 0.8 : Up \rightarrow Dn$	+231 %	+317 %	+69 %	+132 %	+150 %	+224 %
$P : \alpha = 1 : Up \rightarrow Dn$	+202 %	+275 %	+89 %	+153 %	+145 %	+214 %
$Q : \alpha = 1 : Dn \rightarrow Up$	+246 %	+338 %	+73 %	+150 %	+159 %	+244 %
$Q : \alpha = 1 : Up \rightarrow Dn$	+245 %	+333 %	+66 %	+132 %	+155 %	+233 %
$P : \alpha = 0 : Up \rightarrow Dn$	+128 %	+138 %	+83 %	+85 %	+105 %	+112 %
$P : \alpha = 0 : Dn \rightarrow Up$	+124 %	+137 %	+82 %	+96 %	+103 %	+116 %
$Q : \alpha = 0 : Up \rightarrow Dn$	+84 %	+148 %	+66 %	+137 %	+75 %	+143 %
$Q : \alpha = 0 : Dn \rightarrow Up$	+87 %	+150 %	+43 %	+78 %	+65 %	+114 %
$W : \alpha = 0 : Dn \rightarrow Up$	−3 %	+4 %	−7 %	+18 %	−5 %	+11 %
$W : \alpha = 0 : Up \rightarrow Dn$	−20 %	−13 %	−12 %	+7 %	−16 %	−3 %
$W : \alpha = 0.8 : Dn \rightarrow Up$	+91 %	+126 %	+27 %	+34 %	+59 %	+80 %
$W : \alpha = 1 : Dn \rightarrow Up$	+150 %	+193 %	+41 %	+46 %	+95 %	+120 %
$W : \alpha = 0.8 : Up \rightarrow Dn$	+73 %	+104 %	+22 %	+26 %	+48 %	+65 %
$W : \alpha = 1 : Up \rightarrow Dn$	+109 %	+112 %	+33 %	+32 %	+71 %	+72 %

considered as robust regarding the poorness of its results in tuned conditions. Best tested configurations are more sensitive to untuned conditions than CLIS, PILOTE and PIR but this conclusion should be nuanced by the fact that the simulation time step used here ($\Delta T_o = \Delta T = 1\,mn$) corresponds to a priori more difficult conditions.

9.4 Linking Transport of and Transport over Water

Main issues in transport of water are to deliver the requested amount of water at the good locations, at the good moment and in the good quantity while, at the same time, minimizing water losses at canal downstream end. Distant downstream control is a very efficient way to reach these objectives because it has the ability to control the discharge delivered from the upstream cross devices and therefore to reduce water losses directly from the source.

The ATV method presented here was applied to this distant downstream control logic. It is easy to implement on a real canal [8]. The combination of this method

with the two decouplers using gate equation inversion with the characteristics method (Q) and upstream discharge reporting ($\alpha = 0.8$) shows in the study that the performances are respectable and robust compared to other more complicated controllers.

Since this regulation method used for transport of water consists in keeping constant water level at the downstream end of the pools, it is also of interest when considering transport over water. Usually in transport over water systems such as navigable rivers, the upstream discharge is not under control and the regulation is done by using a local upstream controllers at each check structure which could be a regulated gate or a simple weir. In these systems, major perturbations are caused by locks when boats move from one pool to another.

It is also possible to use ATV-PID design and tuning method for performing upstream local control but the interest of this in front of a large static weir which will be able to perform a robust control is not obvious. Except if the targeted water level is changing over the time, due to flow or navigation conditions. On the opposite, in the case of the existence of a reservoir at the upstream end of the canal, a distant downstream control should be an efficient solution for both transport of and over water with a good efficiency on saving the water reservoir. ATV-PID will be then specially appropriate on systems where physical parameters (such as bed geometry or roughness) are not well-known or where they can significantly change. Indeed, even if the results show a relative low robustness of the controller compared to more sophisticated controllers, the advantage of the ATV-PID controller is that it can be easily re-calibrated whenever the manager observes a performance loss.

9.5 Conclusions and Future Research

This chapter considered the use of an auto-tuned PI controller (ATV-PID) on a multi-pool open channel system where the PI controller is tuned from an Integrator Delay model determined by a relay experiment on each pool. A feedforward controller has also been calibrated from this relay experiment and use the parameters of the identified ID model to counterbalance the water level variation expected by the discharge variation at the downstream end of the pool and calculated from the characteristics method.

Different decoupling options have been explored to tackle interactions between pools which consist in the use of discharge as control action variable instead of gate opening and the use of a report of discharge variation occurring at one check gate to the next upstream check gates. Different combination of decoupling configuration have been tested on the test canal 2 proposed by the ASCE Task Committee on Canal Automation Algorithms. Four tests separated in a scheduled and unscheduled periods have been performed representing different hydraulic conditions and unknown changes in physical parameters in order to assess the robustness of the controller. All configurations have been assessed with performance indicators and have been compared with results from previous researches.

Results show that ATV-PID method can lead to comparable performance as other more sophisticated such as PIR with a determinant advantage that ATV-PID only need a minimum of information concerning the system to be directly implemented on the field and have the ability to be recalibrated as often as necessary. The best results have been obtained with configuration using discharge (pump mode P) as control action variable and an upstream report of 80 % of the discharge. This option is not very realistic. The main issue is therefore how to get, with a real gate, the closest discharge to the one asked by the controller. The method Q offers a good alternative, inverting the gate equations and anticipating with water level fluctuations generated by the corresponding gate movement using a simple formula obtained from the method of characteristics. This option proved to provide good results close to the ones obtained with the P mode and with more sophisticated MIMO methods, when combined with a 80 % upstream report and a feedforward loop. This method is easy to implement, both on a simulation software for testing and validation, and also on SCADA or RTU units for field use. This therefore fits the objectives we were assigning to the control algorithms and strategy to tune them in the introduction section. It will always be possible in a second step to switch to more advanced methods, when the manager are already convinced by this first simple and performant enough approach. All the equipments (sensors, actuators, RTU, SCADA) used for this series of PI controllers will be able to support the implementation of any other method by just changing some source code lines in the SCADA software.

References

1. Aström KJ, Hägglund T. Automatic tuning of PID controllers. Research Triangle Park: Instrument Society of America; 1988.
2. Aström KJ, Hägglund T. PID controllers: Theory, design, and tuning. Research Triangle Park: Instrument Society of America; 1995.
3. Baume J-P, Malaterre P-O, Belaud G, Le Guennec B. SIC: A 1D hydrodynamic model for river and irrigation canal modeling and regulation. In: Métodos numéricos em recursos hidricos, vol. 7. Associacao Brasileira de Recursos Hídricos; 2005. p. 1–81.
4. Clemmens AJ, Kacerek TF, Grawitz B, Schuurmans W. Test cases for canal control algorithms. J Irrig Drain Eng. 1998;124(1):23–30.
5. Deltour J-L, Sanfilippo F. Introduction of smith predictor into dynamic regulation. J Irrig Drain Eng. 1998;124(1):47–52.
6. Ho WK, Hang CC, Cao LS. Tuning of PI controllers based on gain and phase margin specifications. In: Proceedings of the IEEE international symposium on industrial electronics, 1992, vol. 2, May 1992. p. 879–82.
7. Jean-Baptiste N, Malaterre P-O, Dorée C, Sau J. Data assimilation for real-time estimation of hydraulic states and unmeasured perturbations in a 1D hydrodynamic model. Math Comput Simul. 2011;81(10):2201–14.
8. Litrico X, Malaterre P-O. Test of auto-tuned automatic downstream controllers on gignac canal. In: USCID conference on SCADA, editor. USCID conference on SCADA, Denver, 2007.
9. Litrico X, Malaterre P-O, Baume J-P, Vion P-Y, Ribot-Bruno J. Automatic tuning of PI controllers for an irrigation canal pool. J Irrig Drain Eng. 2007;133:27–37.

10. Litrico X, Malaterre P-O, Baume J-P, Ribot-Bruno J. Conversion from discharge to gate opening for the control of irrigation canals. J Irrig Drain Eng. 2008;134(3):305–14.
11. Liu F, Feyen J, Malaterre P-O, Baume J-P, Kosuth P. Development and evaluation of canal automation algorithm CLIS. J Irrig Drain Eng. 1998;124(1):40–6.
12. Malaterre P-O. PILOTE: Linear quadratic optimal controller for irrigation canals. J Irrig Drain Eng. 1998;124(4):187–94.
13. Malaterre P-O. Control of irrigation canals: Why and how? In: Proceedings of the international workshop on numerical modelling of hydrodynamics for water resources - numerical modelling of hydrodynamics for water resources, Zaragoza, 2007. p. 271–92.
14. Malaterre P-O, Baume J-P. Optimum choice of control action variables and linked algorithms: Comparison of different alternatives. In: Proceedings of the 1999 USCID workshop on modernization of irrigation water delivery systems, 1999. p. 387–405.
15. Malaterre, P-O, Rogers DC, Schuurmans, J. Classification of canal control algorithms. J Irrig Drain Eng. 1998; 124(1):3–10.
16. Schuurmans J. Control of water levels in open-channels. Ph.D. thesis, Delft University of Technology, 1997.
17. Schuurmans J, Bosgra OH, Brouwer R. Open-channel flow model approximation for controller design. Appl Math Model. 1995;19(9):525–30.
18. Scilab Enterprises. Scilab: Free and open source software for numerical computation. Orsay: Scilab Enterprises; 2012.
19. Ziegler JG, Nichols NB. Optimum settings for automatic controllers. Trans ASME 1942;64(11):220–222.

Chapter 10
Hierarchical MPC-Based Control of an Irrigation Canal

A. Sadowska, P.J. van Overloop, C. Burt, and B. De Schutter

Abstract We discuss the problem of controlling an irrigation canal to accommodate fast changes in the canal state in response to events such as offtakes announced with no time lag or sudden weather changes. Our proposed approach comprises a hierarchical controller consisting of two layers with decentralized PI controllers in the lower layer and a centralized MPC-based event-driven controller in the higher layer. By incorporating the hierarchical controller structure we achieve a better performance than with the PI controllers only as currently in use in the real world, while barely increasing the communication requirements and remaining robust to temporary communication link breakdowns as the lower layer can work independently of the higher layer when the links are being restored. The operation of the higher-layer controller relies on controlling the head gate and modifying the settings of the local controllers. This way, an acceleration of water transporting is attained as the controller allows for rapid reactions to the need for more water or less water at a location. Specifically, when there is a sudden need for water, the storage in some of the pools is used to temporarily borrow water. Alternatively, when there is too much water at a location, it can be stored for some time in upstream or downstream pools before the PI controllers manage to remove the water.

A. Sadowska (✉) • B. De Schutter
Delft Center for Systems and Control, Delft University of Technology, Delft, The Netherlands
e-mail: a.d.sadowska@tudelft.nl; b.deschutter@tudelft.nl

P.J. van Overloop
Water Resources Management, Delft University of Technology, Delft, The Netherlands
e-mail: P.J.A.T.M.vanOverloop@tudelft.nl

C. Burt
Irrigation Training and Research Center (ITRC), California Polytechnic State University, San Luis Obispo, CA, USA
e-mail: CBurt@calpoly.edu

C. Ocampo-Martinez, R.R. Negenborn (eds.), *Transport of Water versus Transport over Water*, Operations Research/Computer Science Interfaces Series 58,
DOI 10.1007/978-3-319-16133-4_10

10.1 Introduction

10.1.1 Motivation and Contributions

One of the prominent control problems encountered in the area of water management is to control water flows in an irrigation canal swiftly and with little resources involved. This is prompted by the fact that with diminishing world resources of fresh water, it is of a great importance to manage the remaining water supplies in a way that minimizes potential water losses. In terms of control of irrigation canals, it calls for the gates connecting canal pools being operated in an intelligent way, so there are no spills and water is not wasted, but is used for the purpose of crop irrigation as intended. As a matter of fact, fresh water use for agriculture amounts to over 90 % [17] of the overall fresh water use worldwide. Such a large share is undoubtedly partly due to the old equipment that is still widely used in agriculture as any modernizations would need to be most likely paid by the farmers and thus tend to be not well accepted. Consequently, the control schemes that rely on the immoderate utilization of the vulnerable equipment are unfavorable. For instance, as the communication links that are present in the field are often not reliable enough to be used in a continuous control loop, control schemes that depend excessively on communication may fail to be realizable in practice. Nevertheless, despite such limitations, undoubtedly there is a need for efficient, accurate and resource-conscious water management schemes to meet the aforementioned operational criteria.

All this makes some of the existing methods proposed in the literature for controlling an irrigation canal potentially problematic in reality when adverse practical conditions are present. In that respect, the distributed control strategies introduced in, e.g., [1, 5, 9, 15] as well as the centralized control strategies introduced in, e.g., [22, 27, 28] may turn out to rely too heavily on the communication links, thus being rendered impracticable for a real-life application. This is caused by the requirement of these controllers to communicate in every control step during their operation either with each other in case of distributed control, or with a control center in case of centralized control. The other extreme solution broadly used in practice is the application of decentralized PI controllers installed at each gate along the canal [10, 11, 16, 27]. The decentralized PI controllers, while they do not add up to the communication burden as such controllers require only local information from a pool, may be unable to produce a good enough overall performance. In response to such practical restrictions while not compromising on the performance attained, we propose in this chapter a hierarchical control algorithm. The lower control layer is constituted by the existing local PI controllers and as such there is no need for any additional equipment to be installed on top of the one already present in the field. On the other hand, the higher control layer is formed by a centralized controller, designed using principles of Model Predictive Control (MPC) [4, 12] and activated on an event-driven basis, i.e., only when new events occur, e.g., a water delivery request in one of the delivery points along the canal or a heavy

rainfall. In such circumstances, the higher-layer controller is activated and modifies the head gate settings as well as the setpoints of the local PI controllers. Therefore, in normal operating conditions, the PI controllers take full care of the canal. However, even when there is an event, the additional communication required is limited as the higher-layer controller is designed to communicate to each local PI controller only once per activation to convey all required changes. The changes take form of stepwise setpoint changes: once each setpoint is modified from its original value and then it is set back to the normal operating level. This makes the scheme robust to temporary communication losses as in face of the communication links being down temporarily, the PI controllers still autonomously control the canal.

The hierarchical controller discussed in this chapter has been analyzed earlier on in [18] in which differences in system performance when the higher-layer controller is invoked at every control step or in response to events only were studied. Also [19] considers the hierarchical controller, and specifically the controller there is adopted to fit the Central California Irrigation District Main Canal with ramp-shaped setpoint changes ordered by the higher-layer controller as opposed to stepwise setpoint changes discussed here. In that view, the current chapter contributes in a threefold manner. First, we give an improved and unified account of the previous work. Second, we extend the permissible class of the input profiles. Third, we alter the parameters of the lower-layers controllers too, i.e., the control gains of the PI controllers are found through an optimization routine.

10.1.2 Control Problem Description

We now state the particular control problem under consideration. The aim is to control an irrigation canal to allow swift changes, e.g., new deliveries or flow changes in existing offtakes with no time lag between the moments they are announced and start. However, this has to be done ensuring a certain performance level, i.e., not disturbing excessively the normal canal operation. This means, e.g., that the control actions found by the controller should not result in drying out of the canal or water overtopping the canal embankments. If needed, also stricter constraints may be posed with water levels maintained within a tighter range.

To fulfill the control objectives, a two-layer control strategy is introduced. The lower layer consists of the PI controllers, and the higher layer works by altering the head gate settings and by modifying the settings of the local controllers, and is derived in accordance with MPC techniques.[1] The local controllers are influenced

[1]MPC is a model-based control technique that uses predictions of the state and forecasts of the external inputs to determine optimal future control actions for the system. At every step, the control sequence is found through solving an optimization problem in a receding horizon manner. We refer to [4, 12] for a detailed description of MPC.

by the higher-layer controller by their setpoints being altered in a stepwise manner and by the P and I gains being changed. We consider two possibilities for how the changes are handled.

A) The proportional and integral gains are found beforehand as a first stage, and stay fixed thereafter.
B) The algorithm starts with preexisting proportional and integral gains (chosen by the designer). Then, whenever the higher-layer controller is activated, on top of temporary setpoint changes, the gains are also altered pro tem and afterwards return to their original values.

We now briefly discuss what control inputs are required to be found by the higher-layer controller in cases A) and B) above. More details on how the control inputs specifically influence the controllers in the lower layer will be given in Sect. 10.2.2.

In both cases, the head gate settings are altered by the higher-layer controller, i.e., the variable $M_{\text{head gate}} \in \mathbb{R}$ denoting the position of the head gate is changed. This is done with the help of an N_{p}-element sequence

$$\tilde{M}^{\text{control}}_{\text{head gate}} = (M^{\text{control}}_{\text{head gate}}(0), \ldots, M^{\text{control}}_{\text{head gate,}}(N_{\text{p}} - 1))^T, \tag{10.1}$$

where, as per the principles of MPC, N_{p} is the length of the prediction horizon. Also in both cases A) and B) above, the stepwise setpoint modifications of the local PI controllers are assumed and are found using Time Instant Optimization Model Predictive Control (TIO-MPC) [8, 18, 24, 25]. In a nutshell, while in the standard MPC, the N_{p}-element sequence of each control variable is to be found, in TIO-MPC for a prespecified number of control variable changes in a given prediction window of length N_{p}, the optimization routine returns the time instants when the control variable should change and to what value. In that spirit, to characterize stepwise changes of the setpoints, three quantities are needed: the time instant $t_i^{\text{on}} \in \mathbb{R}$ when the setpoint in pool i should diverge from its predefined level $h_i^{\text{ref, normal}}$, the altered value $h_i^{\text{ref, delivery}} \in \mathbb{R}$ of the setpoint, and the time instant $t_i^{\text{off}} \in \mathbb{R}$ when the setpoint should return to the normal operating value $h_i^{\text{ref, normal}}$. For all pools $i = 1, \ldots, N$ we collect the three values in vectors

$$\begin{aligned} H^{\text{ref, delivery}} &= [h_1^{\text{ref, delivery}}, \ldots, h_N^{\text{ref, delivery}}]^T, \\ T^{\text{on}} &= [t_1^{\text{on}}, \ldots, t_N^{\text{on}}]^T, \\ T^{\text{off}} &= [t_1^{\text{off}}, \ldots, t_N^{\text{off}}]^T. \end{aligned} \tag{10.2}$$

Note that by modifying the setpoints using TIO-MPC in the specific way that each setpoint is changed twice, i.e., once to modify the setpoint from its normal levels to deal with an event and the second time to return to the prespecified value, we limit the amount of interference of the higher-layer controller with the local controllers, which results in diminished communication requirements. As explained earlier, in the alternative formulation of the problem using the standard MPC, direct optimization of the setpoints $h_i^{\text{ref}}(j)$ for the whole prediction horizon could be done. However, to impose exactly two changes of the setpoints, integer constraints

would need to be added [2], resulting in an escalation of the computational burden. In contrast, by using TIO-MPC, the problem is not posed as a mixed integer programming problem but as a real-valued optimization problem and thus the computational requirements are also reduced.

In contrast to $\tilde{M}^{\text{control}}_{\text{head gate}}$, $H^{\text{ref, delivery}}$, T^{on} and T^{off}, the proportional and integral gains are changed differently for the two cases. A common part is a preliminary calibration step done by the designer to choose initial values of the gains. In case A) these values are kept later on with no modifications. Conversely, in a steady-state operation in case B), the predefined values are used whereas when the higher-layer controller is activated to deal with an event, the gains are changed in a stepwise manner similarly to the setpoint, and can be different for each event. Therefore, the controller needs to provide modified values of the gains $K_{\text{P},i}$ and $K_{\text{I},i}$, i.e., to find $K^{\text{temp}}_{\text{P},i}$ and $K^{\text{temp}}_{\text{I},i}$, and to determine the time instants $T^{\text{on,gains}}$ when to switch to the modified values and the time instants $T^{\text{off,gains}}$ when to switch back to the predefined values.

10.1.3 Outline

The outline of this chapter in as follows. In Sect. 10.2 we first describe the dynamical model of a canal in general and for the specific case study; next the proposed solution is discussed, i.e., the improved and extended hierarchical control approach is introduced. Further, in Sect. 10.3 we illustrate how the control approach works in a simulation based case study involving the Central California Irrigation District Main Canal. In Sect. 10.4 we discuss how the proposed strategy for transport of water can be combined with a complementary strategy for transport over water. To finish the chapter, our conclusions together with possible future work are given in Sect. 10.5.

10.2 Main Results

In this section we first discuss the canal dynamics assumed in the chapter. Then, we introduce our method for accelerating transport of water in a canal.

10.2.1 Preliminaries

Canal Dynamics

The canal dynamics are modelled by the so-called Saint Venant's equations [6, 14, 26]

$$\frac{\partial Q}{\partial x}+\frac{\partial A}{\partial t}=q_{\text{lat}},\qquad \frac{\partial Q}{\partial t}+\frac{\partial}{\partial x}\left(\frac{Q}{A}\right)^2+gA\frac{\partial h}{\partial x}+\frac{gQ|Q|}{C^2RA}=0, \tag{10.3}$$

where A is the cross-section area of the canal, q_{lat} is the lateral unitary net inflow, g is the gravitational acceleration, R is the hydraulic radius, and C is the Chézy constant. Water levels h and flows Q for the whole canal can be obtained from (10.3) when each pool is discretized longways into small section and (10.3) is integrated numerically for each section, assuming given flows through gates along the canal, yielding a precise model. That precise model is associated with high computational requirements and thus is not suited for use in a real-time controller design. Therefore, a simplified (linear) model of the canal can be obtained by a more coarse discretization of (10.3) into a water balance of each pool and a delay time in series [13, 20, 21, 27]:

$$h_i(k+1)=h_i(k)+\frac{T_{\text{m}}}{A_{\text{s},i}}(u_{i-1}(k-k_{\text{d}i})-u_i(k)+d_i(k)), \tag{10.4}$$

in which h_i is the water level at the downstream end of a pool, just before gate i, $k_{\text{d}i}$ is the time delay (in sampling steps) before an inflow from the upstream gate $i-1$ affects $h_i(k)$, T_{m} is the model sampling time (equal for all pools), $A_{\text{s},i}$ is the average surface area of pool i, d_i is the net inflow to pool i due to, e.g., an offtake ($d_i<0$) or rainfall ($d_i>0$), and u_i denotes the flow through gate i, with $u_0=Q_{\text{S}}$ denoting the inflow from the head gate. The flows $u_i(k)$, $i=1,\ldots,N$, are determined by the PI controllers installed at each gate according to the formula

$$u_i(k)=\max\left(u_i(k-1)+K_{\text{P},i}\left(e_i(k)-e_i(k-1)\right)+K_{\text{I},i}e_i(k),0\right), \tag{10.5}$$

in which $e_i=h_i(k)-h_i^{\text{ref}}(k)$ denotes the setpoint tracking error with $h_i^{\text{ref}}(k)$ being the value of a setpoint at sample step k, and $K_{\text{P},i}>0$ and $K_{\text{I},i}>0$ are the proportional and integral gains, respectively.

Illustrative Example: Characterization of CCID Main Canal

In this section we revisit the dynamical model of a canal given in Sect. 10.2.1 specifically for the representative example used later in the chapter to illustrate the functioning of the controller developed in the chapter. The representative example is the Central California Irrigation District Main Canal, which is a trapezoidal, gravity-flow channel, consisting of ten pools and ten control structures. To describe the canal in the case study, two models are used. The first one, which is the process model, is exactly the model (10.3) integrated using a longitudinal grid of 1 m, resulting in a very accurate model of the process. In that model, the standard PI controller as described earlier is enhanced to include a first-order low-pass filter as well. This means that to evaluate formula (10.5), we calculate the setpoint tracking errors $e_i(k)$ as $e_i(k)=h_i^{\text{filtered}}(k)-h_i^{\text{ref}}(k)$, where $h_i^{\text{filtered}}(k)=K_{\text{F},i}h_i^{\text{filtered}}(k-1)+(1-K_{\text{F},i})$

$h_i(k)$ with $K_{\mathrm{F},i} \in [0, 1)$. The flows through consecutive gates that are used as boundary conditions in model (10.3) obtained from formula (10.5) are further checked against physical restrictions of a gate (e.g., the maximum opening/width $\bar{\varphi}_i$ such that $0 \leq \varphi_i(k) \leq \bar{\varphi}_i$, and the maximum change rate $|\varphi_i(k) - \varphi_i(k-1)| \leq \Delta_{\max,\varphi,i}$), where $\varphi_i(k)$ denotes the position of gate i at step k. The resulting gate positions are given as

$$\varphi_i(k) = \begin{cases} \hat{\varphi}_i(k) & \text{if } \hat{\varphi}_i(k) \geq -\Delta_{\max,\varphi,i} + \varphi_i(k-1) \\ & \quad \text{and } \hat{\varphi}_i(k) \leq \Delta_{\max,\varphi,i} + \varphi_i(k-1), \\ \Delta_{\varphi,i} + \varphi_i(k-1) & \text{if } \hat{\varphi}_i(k) > \Delta_{\max,\varphi,i} + \varphi_i(k-1), \\ -\Delta_{\varphi,i} + \varphi_i(k-1) & \text{if } \hat{\varphi}_i(k) < -\Delta_{\max,\varphi,i} + \varphi_i(k-1), \end{cases} \tag{10.6}$$

in which $\hat{\varphi}_i(k) = \min\left(\max\left(\varphi_i(k), 0\right), \bar{\varphi}_i\right)$. Then, the flows u_i follow from [3]:

$$u_i(k) = c_i w_i \mu_i \varphi_i(k) \sqrt{2g(h_{i,\mathrm{up}}(k) - h_i^{\mathrm{crest}} - 1/2\varphi_i(k))}, \tag{10.7}$$

$$u_i(k) = c_i w_i \mu_i \sqrt{2g(h_{i,\mathrm{up}}(k) - h_{i,\mathrm{down}}(k))}, \tag{10.8}$$

$$u_i(k) = \frac{2}{3} c_i w_i \mu_i \sqrt{2/3g} \left(h_{i,\mathrm{up}}(k) - \varphi_i(k)\right)^{\frac{3}{2}}, \tag{10.9}$$

for a free-flowing undershot gate, a submerged undershot gate, and an overshot gate, respectively, where c_i denotes a calibration coefficient, w_i is the gate's width, μ_i is the contraction coefficient, and h_i^{crest} is the crest level (see [19] for extra details).

Next to the process model, which stems immediately from (10.3), we also consider a prediction model, which is a simplification of the process model. The simplification is done to relax the computational requirements that would otherwise be inordinate when the complex model (10.3) were used to derive the controller. As explained in Sect. 10.2.1, model (10.3) is linearized and the consequent model takes the form (10.4). This model is linear with the exception of the head gate settings $M_{\text{head gate}}$ that nonlinearly relate to the resulting flows Q_{S} [3].

We have now presented the prerequisites that form a foundation for the content of the further parts of the chapter. Subsequently, we give the main result communicated in the chapter: the derivation of the hierarchical controller used to accelerate transport of water in an irrigation channel.

10.2.2 Proposed Solution: Design of a Delivery Accelerating Hierarchical Controller

We now discuss the hierarchical controller proposed in the chapter. As mentioned earlier, the controller consists of two layers. The lower layer consists of local PI controllers, which operate continuously, and the higher layer includes a centralized

controller designed to work on an event-driven basis. This means that it is activated when there are events that require special actions to be taken on top of the control provided by the lower layer.

Denote by k_c the control step counter associated with the higher-layer controller, and similarly let T_c be the duration of the control cycle of the higher-layer controller, which is an integer multiple of the sampling time of the model T_m. In other words, $A_c = T_c/T_m \in \mathbb{N}$.

We split the derivation of the controller into two parts. First, we discuss the design assuming that only a single activation occurs and that the higher-layer controller may only be reactivated after the steady state is restored, see Sect. 10.2.2. Then, we elaborate on the necessary extensions to enable multiple concurrent active periods of the higher layer, see Sect. 10.2.2.

Concept Description: Single Activation

In this section we introduce the basic ideas regarding the hierarchical controller, where we assume, for the sake of simplifying the message, that only a single activation of the higher layer of the hierarchical controller takes place. At the beginning, before the hierarchical controller is ready to work, a design step needs to be performed, in which initial proportional and integral parameters of the PI controllers are selected. Various methods can be used for this, e.g., a manual tuning, Ziegler-Nichols tuning method [29], lambda tuning method [7], or optimization-based tuning. Here, we briefly explore the last option, i.e., we propose to find the gains through the minimization of a cost function accounting for deviations in the water levels with respect to their setpoints and immoderate fluctuations in water levels and flows, assuming an input consisting of a selection of representative subscenarios with a certain number of flow changes in the pools and changes to the head gate:

$$J_{\text{pre}} = \sum_{i=1}^{N} \sum_{j=1}^{N_{\text{tot}}} \left(w_e e_i(j) + w_{\Delta h}(h_i(j) - h_i(j-1)) + w_{\Delta u}(u_i(j-1) - u_i(j-2)) \right), \tag{10.10}$$

in which $u_i(-1)$ is assumed as a given initial condition describing past flows, and N_{tot} is the length of the prediction horizon in the preliminary step, which can differ from the length of the prediction horizon N_p used by the higher-layer controller in its regular operation mode. In the preliminary step, the cost function J_{pre} is minimized with respect to the proportional and integral gains of the PI controllers, which means that the preliminary optimization problem can be stated as

$$(K_{P,i}^*, K_{I,i}^*) = \min_{K_{P,i}, K_{I,i}} J_{\text{pre}}, \quad \text{subject to } K_{v,i}^{\min} \le K_{v,i} \le K_{v,i}^{\max}, \text{ (10.4)}, \text{ (10.5)}, \tag{10.11}$$

where $\nu \in \{\mathrm{P}, \mathrm{I}\}$, $K_{\nu,i}^{\min} > 0$ are small constants ensuring all gains are strictly positive, and $K_{\nu,i}^{\max} > K_{\nu,i}^{\min}$ is an upper bound for the gains. After solving (10.11), values $K_{\mathrm{P},i}^{*}$ and $K_{\mathrm{I},i}^{*}$ are used later on by the PI controllers.

Now, suppose that the activation of the higher-layer controller takes place at sampling step $k_{\text{activation}}$. Then, the movement of the head gate for the next $N_{\mathrm{p}} A_{\mathrm{c}}$ steps can be found using (10.1) according to the relation

$$M_{\text{head gate}}(k_{\text{activation}} + jA_{\mathrm{c}} + \ell) = M_{\text{head gate}}^{\text{control}}(j), \text{ for } \begin{array}{l} \ell = 0, \ldots, A_{\mathrm{c}} - 1, \\ j = 0, \ldots, N_{\mathrm{p}} - 1 \end{array} \tag{10.12}$$

for $k = k_{\text{activation}}, k_{\text{activation}} + 1, \ldots, k_{\text{activation}} + N_{\mathrm{p}} A_{\mathrm{c}} - 1$ and

$$M_{\text{head gate}}(k) = M_{\text{head gate}}^{\text{steady state}} = M_{\text{head gate}}^{\text{control}}(N_{\mathrm{p}} - 1),$$

for $k > k_{\text{activation}} + N_{\mathrm{p}} A_{\mathrm{c}} - 1$. As can be seen above, after $N_{\mathrm{p}} A_{\mathrm{c}}$ steps, the head gate settings are set to a new steady-state level

$$M_{\text{head gate}}^{\text{steady state}} = M_{\text{head gate}}^{\text{control}}(N_{\mathrm{p}} - 1)$$

afterwards.

In contrast to the head gate settings, which may end up with a different steady-state value after the activation, the setpoints of the local controllers are only changed temporarily to enable speedy flow changes and afterwards return to their predefined levels. Specifically, after the activation, the setpoints of the local controllers change using the triple $(H^{\text{ref, delivery}}, T^{\text{on}}, T^{\text{off}})$ (10.2). For each pool $i = 1, \ldots, N$, the setpoints are found as

$$h_i^{\text{ref}}(k) = \begin{cases} h_i^{\text{ref, delivery}} & \text{if } k_i^{\text{on}} \le k \le k_i^{\text{off}}, \\ h_i^{\text{ref, normal}} & \text{otherwise,} \end{cases} \tag{10.13}$$

in which $k_i^{\text{on}} = \left\lceil \frac{t_i^{\text{on}}}{T_{\mathrm{m}}} \right\rceil$ and $k_i^{\text{off}} = \left\lceil \frac{t_i^{\text{off}}}{T_{\mathrm{m}}} \right\rceil$. Expression (10.13) ensures that stepwise setpoint modifications are executed.

We now discuss what is different in cases A) and B).

A) In this case, the hierarchical controller is directly ready for normal operation. For each activation of the higher-layer controller during its regular operation, the control input that needs to be found is the quadruple

$$\mathcal{U}_{\mathrm{A}} = \left(\tilde{M}_{\text{head gate}}^{\text{control}}, H^{\text{ref, delivery}}, T^{\text{on}}, T^{\text{off}} \right). \tag{10.14}$$

B) Now, in addition to modifying the head gate settings and the setpoints, also the gains of the PI controllers are temporarily changed using a quadruple

$(K_{\mathrm{P}}^{\mathrm{temp}}, K_{\mathrm{I}}^{\mathrm{temp}}, T^{\mathrm{on,gains}}, T^{\mathrm{off,gains}})$. The gains are then changed in the system in a stepwise manner, very much similar to how the setpoints are changed:

$$K_{\nu,i}(k) = \begin{cases} K_{\nu,i}^{\mathrm{temp}} & \text{if } k_i^{\mathrm{on,gains}} \leq k \leq k_i^{\mathrm{off,gains}}, \\ K_{\nu,i}^{\mathrm{normal}} & \text{otherwise,} \end{cases} \tag{10.15}$$

where $\nu \in \{\mathrm{P}, \mathrm{I}\}$ and $k_i^{\mathrm{on,gains}} = \left\lceil \frac{t_i^{\mathrm{on,gains}}}{T_{\mathrm{m}}} \right\rceil$ and $k_i^{\mathrm{off,gains}} = \left\lceil \frac{t_i^{\mathrm{off,gains}}}{T_{\mathrm{m}}} \right\rceil$. The overall control input to be found in case B) is denoted with $\mathcal{U}_{\mathrm{B}}$, which is a tuple defined as

$$\mathcal{U}_{\mathrm{B}} = \left(\tilde{M}_{\mathrm{head\,gate}}^{\mathrm{control}}, H^{\mathrm{ref,\,delivery}}, T^{\mathrm{on}}, T^{\mathrm{off}}, K_{\mathrm{P}}^{\mathrm{temp}}, K_{\mathrm{I}}^{\mathrm{temp}}, T^{\mathrm{on,gains}}, T^{\mathrm{off,gains}} \right). \tag{10.16}$$

With the control inputs $\mathcal{U}_{\mathrm{A}}$ and $\mathcal{U}_{\mathrm{B}}$ defined for cases A) and B), respectively, we may now move forward to defining the cost function that is to be minimized. According to the objectives mentioned in short in Sect. 10.1.2, we define the cost function as follows

$$\begin{aligned} J = {} & \alpha \sum_{j=1}^{A_{\mathrm{c}} N_{\mathrm{p}}} \left(u_N \left(k_{\mathrm{activation}} + j - 1 \right) - Q_{\mathrm{S,\,base}} \right)^2 \\ & + \beta \sum_{i=1}^{N} \sum_{j=1}^{A_{\mathrm{c}} N_{\mathrm{p}}} \left(h_i \left(k_{\mathrm{activation}} + j \right) - h_i^{\mathrm{ref}} \left(k_{\mathrm{activation}} + j \right) \right)^2 \\ & + \mu \sum_{i=1}^{N} \left(t_i^{\mathrm{off}} - t_i^{\mathrm{on}} \right)^2 + \zeta \sum_{i=1}^{N} \left(\Delta h_i^{\mathrm{ref}} \right)^2 + \lambda_\xi \sum_{i=1}^{N} \left(t_i^{\mathrm{off,gain}} - t_i^{\mathrm{on,gain}} \right)^2, \end{aligned} \tag{10.17}$$

where α, β, γ_1, γ_2, μ and ζ are positive weighting coefficients, $\xi \in \{\mathrm{A}, \mathrm{B}\}$, $\lambda_{\mathrm{A}} = 0$, $\lambda_{\mathrm{B}} > 0$, and $\Delta h_i^{\mathrm{ref}} = h_i^{\mathrm{ref,\,delivery}} - h_i^{\mathrm{ref,\,normal}}$. The form of the cost function is chosen in such a specific way to capture the objectives of the controller. In particular, the smaller the first term of J in (10.17) is, the less disruption is for the further downstream users beyond the stretch of the canal under consideration with N pools, as the inflow to that further part is closer to the ordained base flow $Q_{\mathrm{S,\,base}}$. Furthermore, the second term (10.17) penalizes the setpoint tracking errors in order to refrain from selecting control actions resulting in undue deviations in the water levels with respect to their respective setpoints. Thirdly, terms in (10.17) facilitate switching the setpoints and the PI gains in case B) promptly back to their normal levels to bring the system to the normal operating conditions after an activation apace.

To ensure adequate operation of the controller, the following hard constraints need to be satisfied for all $i \in \{1, \ldots, N\}$:

$$h_i^{\min} \leq h_i(k_{\text{activation}} + j) \leq h_i^{\max}, \qquad j = 1, \ldots, N_\text{p} A_\text{c}, \tag{10.18}$$

$$h_i^{\min} \leq h_i^{\text{ref}}(k_{\text{activation}} + j) \leq h_i^{\max}, \qquad j = 1, \ldots, N_\text{p} A_\text{c}, \tag{10.19}$$

$$t_i^{\text{off}} \geq t_i^{\text{on}} + T_\text{m}, \tag{10.20}$$

$$t_i^{\text{on}} \geq k_{\text{activation}} T_\text{m}, \tag{10.21}$$

$$t_i^{\text{off,gain}} \geq t_i^{\text{on,gain}} + T_\text{m}, \tag{10.22}$$

$$t_i^{\text{on,gain}} \geq k_{\text{activation}} T_\text{m}, \tag{10.23}$$

$$M_{\text{head gate}}^{\min} \leq M_{\text{head gate}}(k_{\text{activation}} + j) \leq M_{\text{head gate}}^{\max}, \; j = 0, \ldots, N_\text{p} A_\text{c} - 1, \tag{10.24}$$

$$|M_{\text{head gate}}(k_{\text{activation}} + j) - M_{\text{head gate}}(k_{\text{activation}} + j - 1)| \leq \Delta M_{\text{head gate}}^{\max}, \tag{10.25}$$

$$j = 0, \ldots, N_\text{p} A_\text{c} - 1,$$

$$K_{\nu,i}^{\min} \leq K_{\nu,i} \leq K_{\nu,i}^{\max}, \tag{10.26}$$

$$t_i^{\text{off}} \leq k_{\text{activation}} T_\text{m} + T_\text{c} N_\text{c}, \tag{10.27}$$

$$t_i^{\text{off,gains}} \leq k_{\text{activation}} T_\text{m} + T_\text{c} N_\text{c}, \tag{10.28}$$

$$M_{\text{head gate}}^{\text{control}}(k_{\text{activation}} + j) = M_{\text{head gate}}^{\text{control}}(N_\text{c} - 1), \qquad j = N_\text{c}, \ldots, N_\text{p} - 1, \tag{10.29}$$

$$M_{\text{head gate}}(k_{\text{activation}} + jA_\text{c}) = M_{\text{head gate}}^{\text{control}}(N_\text{p} - 1), \; j > N_\text{p} - 1, \tag{10.30}$$

in which $N_\text{c} \leq N_\text{p}$ is the control horizon. Constraints (10.18) and (10.19) correspond to the physical constraints of the depth of the canal. Constraints (10.20) and (10.21) ensure that the first switch of the setpoint t_i^{on} occurs after the activation moment of the higher-layer controller and the second moment t_i^{off} occurs at least one sampling step after the first one. Constraints (10.22) and (10.23) work similarly but for the PI gains. Clearly, they only apply in case B). Furthermore, constraints (10.24) and (10.25) make sure that the movements of the head gate are compliant with its minimum and maximum position and its maximum change rate, respectively, and constraint (10.26) deals with the upper and lower bounds for the proportional and integral gains. This latter constraint yet again is valid in case B) only. Next, constraints (10.27)–(10.29) enforce all changes to be executed within the control horizon, and, lastly, constraint (10.30) introduces new steady-state head gate settings after the activation to be equal to the last component of $\tilde{M}_{\text{head gate}}^{\text{control}}$, i.e., $M_{\text{head gate}}^{\text{control}}(N_\text{p} - 1)$.

Extension: Multiple Activations

So far, we have discussed the design of the hierarchical controller for a single active period at a time, and a re-activation only allowed after the steady-state has been restored after a preceding activation. Here, we give a broad overview of how the event-driven controller design needs to be extended to enable multiple concurrent active periods.

First, we discuss how the higher-layer controller is allowed to be activated. We introduce two options: the synchronous one and the asynchronous one. In the synchronous case, see Fig. 10.1, the activation can only occur at a multiple of the control step k_c. If there are events in between two control steps k_c and $k_c + 1$, they are grouped together and sent jointly to the higher-layer controller. In contrast, in the asynchronous case, see Fig. 10.2, the activation can occur at any sample step k. Here, we propose to introduce a short time window δ in which individual events occurring within δ time units after a first one in a round are grouped and conveyed to the higher-layer controller together. δ is a design parameter to be selected by the operator of the canal enabling events happening soon after each other being rendered as a single event and swiftly sent to the higher layer controller. We also impose a minimal reactivation time of T_c time units so that the activations do not occur too frequently.

Now, we analyze how the setpoints are permitted to change. Denote by $s \in \mathbb{Z}$ the activation counter, which is initiated with 0 and is incremented every time a new activation takes place. Two options to change the setpoints are the block-modifying strategy and the block-adding strategy. The block-modifying strategy is illustrated in Fig. 10.3 and rely on the principle that once a setpoint block is started

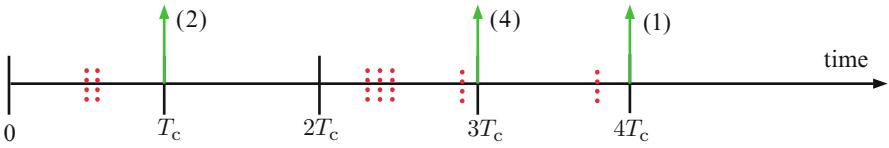

Fig. 10.1 Activation of the higher-layer controller in the synchronous case. All individual events are denoted with *dotted bars*. *Arrows* are used to indicate when the activation occurs with a label representing how many events are dealt with during each activation

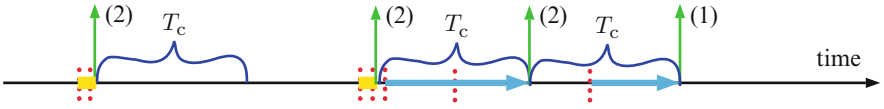

Fig. 10.2 Activation of the higher-layer controller in the asynchronous case. All individual events are denoted with *dotted bars*. *Vertical arrows* are used to indicate when an activation occurs with a label representing how many events are dealt with during each activation. *Horizontal arrows* show the delays with activation of the higher-layer controller for individual requests because of the minimum interval between activations of T_c. *Horizontal bars* indicate the length of the time window δ used to accumulate events occurring soon after each other

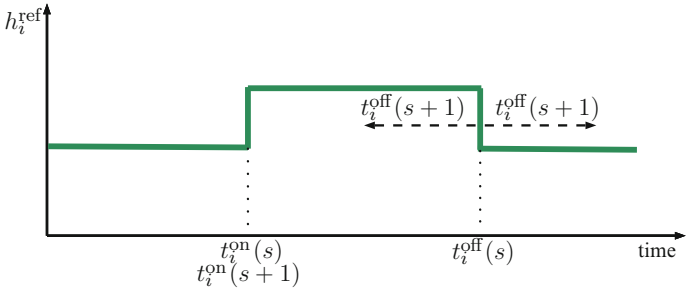

Fig. 10.3 Possible setpoint profiles using block-modifying formulation

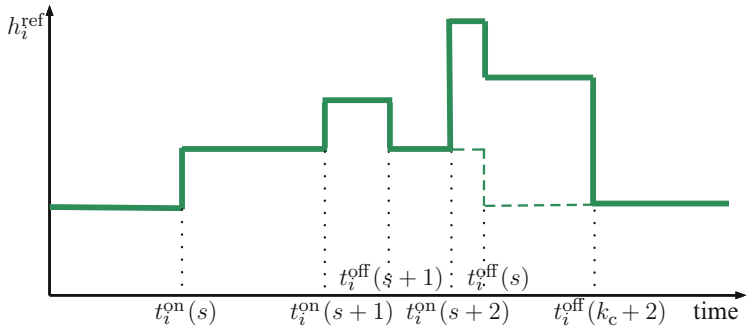

Fig. 10.4 Possible setpoint profiles using block-adding formulation

for activation s, it may only be changed in activation $s+1$ by changing its length, i.e., by modifying $t_i^{\mathrm{off}}(s) = t_i^{\mathrm{off}}(s+1)$. So the overall setpoint profiles, when the block-modifying strategy is implemented, consist of blocks next to one another: when one block finishes, a new one can start. Conversely, in the block-adding strategy, in every new activation new blocks are added on top of the preexisting ones. This is depicted in Fig. 10.4.

In a similar way also the proportional and integral gains of the local controllers may be changed in case B) using block-adding or block-modifying formulations. We leave out the details here for the sake of page limitations.

Next, we discuss how the head gate is controlled by the higher-layer controller for multiple concurrent active periods of the higher-layer controller. A major factor that determines the functioning of the head gate is that when the s^{th} activation of the higher-layer controller takes place at sample step $k_{\mathrm{activation},s}$, the profile of the head gate found for the previous activation is to be updated and a new profile is found and executed. In doing so, the higher-layer controller is of course also aware of the events occurring before the present activation s and the new profile also accounts for them. We illustrate this in Fig. 10.5, where four activations are shown and depicted with the arrows. Observe that once an activation s takes place, the previously found head gate profile $\tilde{M}_{\mathrm{head\,gate}}^{\mathrm{control}}(s-1)$ is no longer valid and the new profile $\tilde{M}_{\mathrm{head\,gate}}^{\mathrm{control}}(s)$

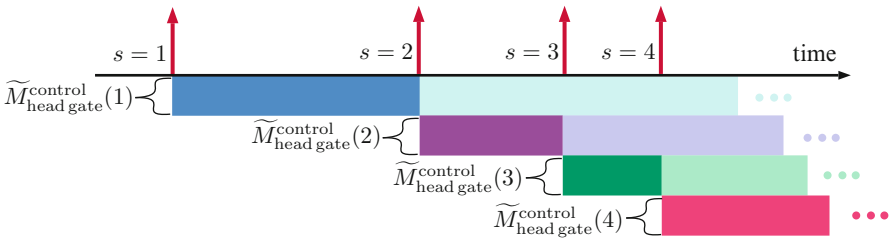

Fig. 10.5 Control of the head gate settings as administrated by the higher-layer controller in face of multiple concurrent activations. Four activations are shown and indicated with the *arrows* and the corresponding profiles for the head gate settings $\tilde{M}^{\text{control}}_{\text{head gate}}(s)$

is applied. This profile is executed until another activation $s + 1$ of the higher-layer controller occurs, at which point the profile of the head gate settings $\tilde{M}^{\text{control}}_{\text{head gate}}(s)$ is again updated with the newly found profile $\tilde{M}^{\text{control}}_{\text{head gate}}(s + 1)$.

The above discussion presents the implementation principles of the hierarchical controller presented in the chapter. The main alterations that need to be accounted for in the multiple-activation case with respect to the single activation is how to deal with modifying setpoints and changing PI gains in case B). This needs to be decided in a design phase, based on the performance requirements of a specific application. The controller then works generally as follows: when there is a need for an activation, the higher-layer controller is triggered and the changes are applied to the system. Then, whenever T_c time units of the reactivation time has passed and new events occur, the controller can be re-activated, and so on.

10.3 Illustrative Example: Results

In this section we discuss the application of the proposed controller on an accurate numerical model of Central California Irrigation District Main Canal. We validate the prediction model used in the controller design in Sect. 10.3.1. Then in Sect. 10.3.2 we present the results obtained by applying the controller to CCID Main Canal and analyze the performance obtained.

10.3.1 Validation of the Prediction Model

We validate pool by pool the prediction model (10.4) with for the parameters given in Table 10.1, where $k_{\text{d}i}$ is given in sampling steps, $A_{\text{s},i}$ in m^2, and T_{m} is 1 min. For each pool $i = 1, \ldots, N$ individually, we apply a step increase of $1.5\,\text{m}^3/\text{s}$ in the

Table 10.1 Parameters of the prediction model (10.4)

i	1	2	3	4	5	6	7	8	9	10
$k_{\mathrm{d}i}$	13	26	21	25	13	11	44	57	15	36
$A_{\mathrm{s},i}$	154842	132722	121181	154842	73346	58066	163951	139358	67979	154842

Table 10.2 VAF for the responses of the process model and the prediction model

i	1	2	3	4	5	6	7	8	9	10
VAF	94%	88%	91%	88%	97%	97%	93%	87%	96%	86%

upstream inflow u_{i-1} with the outflow u_i from the pool at the downstream end kept constant, and with a base flow of $Q_{\mathrm{S,base}} = 7.14\,\mathrm{m}^3/\mathrm{s}$. We apply the same stimuli both for the prediction model and the precise numerical model of the canal. The resulting water levels h_i are measured and compared using the variance-accounted-for criterion:

$$\mathrm{VAF}(m,n) = \left(1 - \frac{\mathrm{var}(m-n)}{\mathrm{var}(m)}\right) \cdot 100\,\%, \tag{10.31}$$

where signal n is obtained from the accurate simulator and signal m from the prediction model. We give the corresponding VAF values for each pool in Table 10.2. It is concluded that the prediction model closely matches the accurate process model and so it is deemed to be suitable for the purpose of the derivation of the controller.

10.3.2 Control Results

We now illustrate the functioning of the proposed control approach in a simulation-based case study. We study here a representative example of a single flow change in pool 10 of magnitude $2.5\,\mathrm{m}^3/\mathrm{s}$ with a base flow of $Q_{\mathrm{S,base}} = 7.14\,\mathrm{m}^3/\mathrm{s}$. The flow change occurs at step $k_{\mathrm{known}} = 180$ and is not announced beforehand. The two cases A) and B) are shown and compared with each other and with a standard method[2] currently used in the field. Using the standard method in the aforementioned circumstances introduces a big disturbance in outflow from pool 10 as in face of the increased offtake outflow from pool 10, the water levels in pool 10 start to decrease and so the PI controller in that pool decreases the outflow to maintain the water level at its desired setpoint. As explained in Sect. 10.2.2, this is an undesirable situation, which is accounted for in the objective function (10.17) of

[2]The standard method works by increasing inflow from the head gate at the time when an offtake is announced to provide extra water needed for the additional offtake and letting the PI controllers transport that water through subsequent pools to the offtake point. This method relies on the PI controllers only with the higher-layer controller being absent.

the hierarchical controller. Therefore, we expect that the situation can be improved when employing the hierarchical controller introduced in this chapter.

To compare the performance when different control methods are applied, we introduce an a posteriori cost function defined as

$$J_{\text{post}} = \alpha \sum_{j=k_{\text{known}}}^{N_{\text{F}}} \left(u_N\left(j-1\right) - Q_{\text{S, base}}\right)^2 + \beta \sum_{i=1}^{N} \sum_{j=k_{\text{known}}}^{N_{\text{F}}} e_i^2\left(j\right), \tag{10.32}$$

where $N_{\text{F}} = 780$ marks the duration of the simulation and the weighting parameters are the same as in the cost function J (10.17) used to derive the controller. These parameters are $\alpha = 5$, $\beta = 10$, $\gamma = 1$, $\mu = 1$, $\zeta = 1$, and $\lambda_B = 1$. Moreover, we use $T_{\text{m}} = 1\,\text{min}$, $A_{\text{c}} = 15$, $N_{\text{c}} = 16$ (corresponding to 240 sample steps), and $N_{\text{p}} = 36$ (i.e., 540 sample steps). In addition, the upper bounds for the proportional gains in the design stage of the hierarchical controller as well as in the normal operation in case B) are determined through stability analysis and subsequently $K_{\text{P},i}^{\max}$ for $i = 1, \ldots, N$ is 89.17, 314.16, 285.47, 363.50, 177.71, 141.57, 416.09, 336.24, 159.90, and 363.50 respectively. The upper bounds for the integral gains are selected as $K_{\text{I},i}^{\max} = K_{\text{P},i}^{\max}$ and the lower bounds for both the proportional and integral gains are $K_{\text{P},i}^{\min} = K_{\text{I},i}^{\min} = 0.01$.

In the design stage, the weighting parameters are chosen to be $w_{\text{e}} = 0.001$, $w_{\Delta h} = 250$ and $w_{\Delta u} = 500$, and the prediction horizon is chosen to be equal to the prediction horizon in the normal operation of the higher-layer controller, i.e., $N_{\text{tot}} = N_{\text{p}} = 540$ sample steps. The scenario considered to determine the gains in the design step consists of five changes in offtakes along the canal and five changes to the head gate to compensate for the offtakes. The resulting gains $K_{\text{P},i}^{*}$ and $K_{\text{I},i}^{*}$ used later on throughout the simulation are given in Table 10.3. Note that in the standard method different gains are used (see $K_{\text{P},i}^{\text{standard}}$ and $K_{\text{I},i}^{\text{standard}}$ in Table 10.3) and these are the gains currently implemented in the real CCID Main Canal.

The results obtained are given in Table 10.4, which lists the values of the a posteriori cost function J_{post} for the three control approaches considered: the standard method, the new hierarchical controller for case A), and the new hierarchical controller for case B). It can be immediately seen that the standard method performs inferiorly in comparison to the new hierarchical controller. The corresponding value

Table 10.3 Proportional and integral gains

	1	2	3	4	5	6	7	8	9	10
$K_{\text{P},i}^{*}$	47.29	207.05	273.25	262.83	71.31	117.79	56.12	20.30	13.68	59.32
$K_{\text{I},i}^{*}$	8.30	2.42	2.98	4.06	4.41	20.26	5.68	0.41	0.28	14.39
$K_{\text{P},i}^{\text{temp}}$	43.58	156.40	80.15	132.43	38.60	25.77	70.52	31.16	19.20	35.59
$K_{\text{I},i}^{\text{temp}}$	9.36	1.38	3.64	3.56	1.39	0.69	2.74	0.47	0.24	3.18
$K_{\text{P},i}^{\text{standard}}$	186	157	143	182	190	152	208	168	165	182
$K_{\text{I},i}^{\text{standard}}$	0.5	0.6	0.6	0.7	1.0	1.1	0.9	1.0	1.8	1.8

Table 10.4 Comparison between the values of J_{post} obtained with the standard method and with the hierarchical controller

	Standard method	Proposed method—case A)	Proposed method—case B)
J_{post}	10800.1	3457.9	1964.5

of the a posteriori cost function is $J_{\text{post}} = 10{,}800.1$. When the new hierarchical controller is applied for case A), a better performance is achieved with the value of the a posteriori cost function being over three times smaller, i.e., $J_{\text{post}} = 3{,}457.9$. This is because the hierarchical controller explicitly takes into account the objectives of the control design and works in a way to minimize the deviation of the system behavior against the desired behavior described using the cost function. The best performance, though, is obtained with the new hierarchical controller for case B), with the a posteriori cost function $J_{\text{post}} = 1{,}964.5$ equating to less than a fifth of the cost function achieved with the standard method. The difference in performance of the controller in cases A) and B) is due to the fact that in case A) the gains of the local PI controllers are fixed and are not selected nor updated for the specific behavior of the system with setpoint changes etc. Conversely, in case B) the controller has the extra freedom to modify the proportional and integral gains on the spot for the purpose of meeting the objectives defined in the cost function. Consequently, in the transient time of dealing with the sudden offtake in pool 10, the PI gains are changed (mostly lowered) to ensure a gentler reaction of the PI controllers to the changed setpoints and thus smoother flows through gates are obtained.

10.4 Linking Transport *of* Water with Transport *over* Water

In the work presented here we explicitly work towards methods for transport *of* water to be delivered to farmers through an irrigation canal. However, the proposed solution also implicitly enhances transport *over* water through maintaining water levels in waterways within a certain range so that ships can operate safely. As such the control strategy proposed in Sect. 10.2.2 can also ensure transport over water. To that end, a number of aspects have to taken care of. In particular, the constraints on the maximum and minimum allowable water levels in (10.18) and (10.19) need to be assigned accordingly.

In future work, the link between the transport-of-water component, as examined in the chapter, and transport over water could be further explored and studied more explicitly. One possible approach to introduce an explicit treatment of transport over water within the presented framework could be to explore a multi-objective approach including the objective of transport of water and the objective of transport over water. The unified control scheme could be formulated in a centralized or distributed fashion (cf. [23] where different objectives are associated with different agents) so as to enable both transport *of* water and transport *over* water.

10.5 Conclusions and Future Research

This chapter has presented a hierarchical controller for the purpose of accelerating transport of water in an irrigation canal. The transport is accelerated in the sense that flow changes along the canal can occur more rapidly, thus more efficient control performance is obtained. The hierarchical controller consists of two layers. In the lower layer, local decentralized PI controllers take care of the canal in its normal operation. In contrast, the higher layer is invoked in response to events only and comprises a centralized predictive controller. This controller works by providing the head gate with an updated profile to account for the event as well as by transiently altering the settings of the local PI controllers. This introduces extra buffer where water can be temporarily stored or can be borrowed from for a speedy delivery to the location where water is needed. We have given in the chapter an in-depth description of the controller design, which includes basic operational concepts and the necessary extensions for continuous operation with multiple events activating the higher-layer controller. The performance of the hierarchical control approach has been demonstrated in a simulation-based case study, which shows that the hierarchical controller outperforms the standard method.

In addition to extending the current work by combining explicitly transport of water with transport over water, further open topics include robustness analysis and robust design in face of uncertainties or unmeasured disturbances. Moreover, an analysis of computational requirements of the proposed control approach to make sure that the scheme can be employed in a real-time operation remains to be studied.

Acknowledgements Research supported by the European Union Seventh Framework Programme [FP7/2007–2013] under grant agreement no. 257462 HYCON2 Network of Excellence.

References

1. Álvarez A, Ridao M, Ramirez D, Sánchez L. Constrained predictive control of an irrigation canal. J Irrig Drain Eng. 2013;139(10):841–854.
2. Bemporad A, Morari M. Control of systems integrating logic, dynamics, and constraints. Automatica 1999;35(3):407–427.
3. Bos G. Discharge measurement structures. In: International Institute for Land Reclamation and Improvement, Publication 20. ILRI; 1976.
4. Camacho EF, Bordons C. Model predictive control. Berlin Heidelberg: Springer; 1999.
5. Cantoni M, Weyer E, Li Y, Ooi SK, Mareels I, Ryan M. Control of large-scale irrigation networks. In: Proc IEEE. 2007;95(1):75–91.
6. Chow VT (1959) Open-channel hydraulics. McGraw-Hill civil engineering. London: McGraw-Hill; 1959.
7. Dahlin EB. Designing and tuning digital controllers. Instrum Control Syst. 1968;41(6):77–83.
8. De Schutter B, De Moor B. Optimal traffic light control for a single intersection. Eur J Control. 1998;4(3):260–276.
9. Li Y, Cantoni M (2008) Distributed controller design for open water channels. In: Proceedings of the 17th IFAC World Congress, Seoul; 2008. pp. 10033–10038

10. Litrico X, Fromion V, Baume J-P, Rijo M. Modelling and PI controller design for an irrigation canal. In: Proceedings of the 2003 European Control Conference, Cambridge; 2003.
11. Litrico X, Malaterre P-O, Baume J-P, Vion P-Y, Ribot-Bruno J. Automatic tuning of PI controllers for an irrigation canal pool. J Irrig Drain Eng ASCE. 2007;133:27–37.
12. Maciejowski JM. Predictive control with constraints. Essex: Prentice Hall; 2002.
13. Malaterre P-O. Control of irrigation canals: why and how? In: Proceedings of the international workshop on numerical modelling of hydrodynamics for water resources, Zaragoza; 2007. pp. 271–293.
14. Malaterre P-O, Baume JP. Modeling and regulation of irrigation canals: existing applications and ongoing researches. In: Proceedings of the 1998 IEEE International Conference on Systems, Man, and Cybernetics, vol. 4, San Diego; 1998. pp 3850–3855.
15. Negenborn RR, van Overloop P-J, Keviczky T, De Schutter B. Distributed model predictive control for irrigation canals. Netw Heterog Media. 2009;4(2):359–380.
16. Ooi SK, Weyer E. Control design for an irrigation channel from physical data. Control Eng Pract. 2008;16(9):1132–1150.
17. Perkins S. Is agriculture sucking fresh water dry? Science NOW, online. Published 13 Feb 2012.
18. Sadowska A, De Schutter B, van Overloop P-J. Delivery-oriented hierarchical predictive control of an irrigation canal: event-driven versus time-driven approaches. IEEE Trans Control Syst Technol. 2015, doi: 10.1109/TCST.2014.2381600
19. Sadowska A, van Overloop P-J, Burt C, De Schutter B. Hierarchical operation of water level controllers: formal analysis and application on a large scale irrigation canal. Water Resour Manag. 2014;28(14):4999–5019
20. Schuurmans J, Clemmens A, Dijkstra S, Hof A, Brouwer R. Modeling of irrigation and drainage canals for controller design. J Irrig Drain Eng. 1999;125(6):338–344.
21. Schuurmans J, Hof A, Dijkstra S, Bosgra O, Brouwer R. Simple water level controller for irrigation and drainage canals. J Irrig Drain Eng. 1999;125(4):189–195.
22. Silva P, Botto MA, Figueiredo J, Rijo M. Model predictive control of an experimental water canal. In: Proceedings of the 2007 European Control Conference, Kos; 2007. pp. 2977–2984.
23. Tian X, Maestre JM, van Overloop PJ, Negenborn RR. Distributed model predictive control for multi-objective water system management. In: Proceedings of the 10th International Conference on Hydroinformatics, Hamburg, July 2012. Paper 175.
24. van Ekeren H, Negenborn RR, van Overloop PJ, De Schutter B. Hybrid model predictive control using time-instant optimization for the Rhine-Meuse delta. In: Proceedings of the 2011 IEEE International Conference on Networking, Sensing and Control, Barcelona; 2011. pp. 216–221.
25. van Ekeren H, Negenborn RR, van Overloop PJ, De Schutter B. Time-instant optimization for hybrid model predictive control of the Rhine-Meuse Delta. J. Hydroinformatics. 2013;15(2):271–292.
26. van Overloop PJ, Clemmens AJ, Strand RJ, Wagemaker RMJ. Real-time implementation of model predictive control on MSIDD's WM canal. J Irrig Drain Eng ASCE. 2010;136(11): 747–756.
27. van Overloop PJ, Schuurmans J, Brouwer R, Burt C. Multiple-model optimization of proportional integral controllers on canals. J Irrig Drain Eng ASCE. 2005;131(2):190–196.
28. Xu M, Negenborn RR, van Overloop PJ, van de Giesen NC. De Saint-Venant equations-based model predictive control of open channel flow. Adv Water Res. 2012;49:37–45.
29. Ziegler JG, Nichols NB. Optimum Settings for Automatic Controllers. Trans ASME. 1942;64:759–768.

Part II
Transport over Water

Chapter 11
Model Predictive Control for Incorporating Transport of Water and Transport over Water in the Dry Season

X. Tian, R.R. Negenborn, P.J. van Overloop, J.M. Maestre, and E. Mostert

Abstract The Netherlands lies in the delta area, which is formed by the Rivers Rhine, Meuse and Scheldt. Being a low-lying country, dikes and other water-retaining structures have been constructed for the purposes of flood protection (transport of water), water supply (transport of water), and navigation (transport over water). All of these objectives are important within the total operational water management. In order to achieve these objectives and make them explicit, we propose a water management approach in which each goal is addressed specifically by a term in a cost function. We assume one centralized Model Predictive Controller, which can determine the balance among the different objectives, as the control strategy for determining which actions to take when controlling the Dutch water system, especially in droughts. Simulation experiments are used to illustrate the potential of this approach under different scenarios in the dry season.

11.1 Introduction

This study focuses on the operational water management in the Netherlands during droughts. Even though droughts may happen once every 25 years in the Netherlands [1, 6], they often last for weeks or even months and result in significant damages. Due to the climate change, they tend to occur more frequently

X. Tian (✉) • P.J. van Overloop • E. Mostert
Department of Water Management, Delft University of Technology, Delft, The Netherlands
e-mail: x.tian@tudelft.nl; p.j.vanoverloop@tudelft.nl; e.mostert@tudelft.nl

R.R. Negenborn
Department of Maritime and Transport Technology, Delft University of Technology, Delft, The Netherlands
e-mail: r.r.negenborn@tudelft.nl

J.M. Maestre
Department of Engineering of Systems and Automatics, University of Seville, Seville, Spain
e-mail: pepemaestre@us.es

C. Ocampo-Martinez, R.R. Negenborn (eds.), *Transport of Water versus Transport over Water*, Operations Research/Computer Science Interfaces Series 58,
DOI 10.1007/978-3-319-16133-4_11

and intensively. The direct consequences are navigable immobilization, sea water intrusion and insufficient water supply for all uses. Moreover, a potential water shortage in the Dutch water system is a shortage for flushing the low-lying polder areas in the west in order to keep the salinity low for agriculture.

Because the country is situated in the delta area formed by the Rivers Rhine, Meuse and Scheldt, a drought tends to take place when very little water flows into the delta area, especially in the summer. The last exceptional drought happened in the Netherlands in 1976. It was caused by a severe lack of rainfall and extremely low inflow from the Rhine River, which was less than 1,250 m^3/s in later June and July. This long water shortage not only directly jeopardized agricultural activities, navigation and polder flushing, but also threatened the stability of dikes, dams and water-related infrastructures. Thus, it is important to investigate how to operationally manage the system so that the damage and loss can be reduced to the greatest extent. This is getting more important, given that climate change studies indicate that extreme droughts will occur more often in the future [6].

The northern and central Netherlands are the focus of this study (see Fig. 11.1), as these are the regions hardest struck by droughts. The study area is located in

Fig. 11.1 Study area

the northern part of the Netherlands and comprises two lakes: Lake IJssel and Lake Marker, three rivers: the River IJssel, the River Nederrijn and the River Lek, as well as the North Sea Canal and the New Waterway (see Fig. 11.1). In this system, the River IJssel is a navigable waterway linking Lake IJssel and Arnhem and the Rivers Nederrijn and Lek both function as waterways linking Rotterdam and Arnhem, and also as a main source of water supply for users in the west, mainly for power supply, polder flushing and agriculture.

Two aspects of water management are included in this study. One is water quantity management during droughts, which is referred to as transport of water. This topic includes water supply and distribution for various purposes, such as drinking water production, agricultural water supply and polder flushing. The other one is navigation, which is referred to as transport over water. Navigation is an economic mainstay in certain regions, for instance, the watershed of the River IJssel. These two aspects were typically investigated separately in previous studies, since they do not have too many conflicts under normal circumstances when enough water is available. However, during droughts, the conflicts appear due to insufficient water. Hence, a decision has to be made on which management goal needs to be met with higher priority, or in other words, how the water flow distributions have to be weighted.

The Dutch water management authorities have formulated a sequence of priorities [1] for water distribution during droughts (see Fig. 11.2). This priority order is set up in a strict manner, which means that when a drought occurs, the categories with lower priorities cannot be satisfied until the ones with higher priorities have been fully satisfied. Water is distributed to regions according to this priority order. For water supply in the Dutch water system, a minimal flow of 25 m^3/s has to be maintained over the River Nederrijn and a setpoint of 285 m^3/s is set on the flow into the River IJssel. Having lower flows than the setpoint means that vessels can only carry limited load so that more vessels are required and waiting time at sluices increases.

Actually, vessels navigate more frequently during the daytime than at night. Moreover, water distribution requires a more subtle, dynamic approach than just working with fixed priorities and turning off certain water flows completely and give full priority to others. This is because some regions mainly require fresh water supply for drinking water and agriculture, such as the western Netherlands, while other regions only require water for navigation during the day time, such as the River IJssel. This inspires us to consider putting the priority in a dynamical and operational order.

In general, both the Rivers Nederrijn and IJssel require water during droughts. The River IJssel has a demand of 285 m^3/s during the daytime and relatively low demands during the night. However in the River Nederrijn, more incoming water can benefit more cities, industries and agriculture, but at least 25 m^3/s has to be maintained. Therefore in this chapter we study the possibility of applying different segmented setpoints. It is then natural that a setpoint (25 m^3/s) is set on the flow into the River Nederrijn during the daytime while a higher setpoint, can be set at night

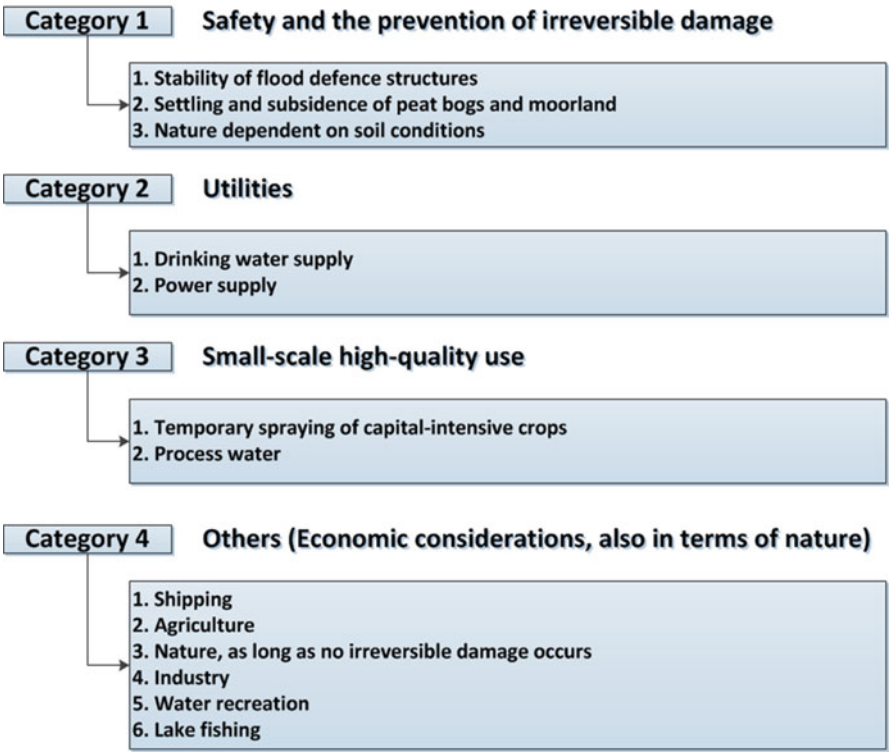

Fig. 11.2 The sequence of priorities in Dutch water management

when the River IJssel does not need so much water for navigation. It is assumed that the area in the west needs 75 m^3/s extra to deal with climate change issues in the future, so a value of 100 m^3/s is used as the setpoint during the night.

Involving and handling predictions also needs to be considered in the future water management of the Netherlands. Water needs to be stored in advance if a water shortage is predicted. All and all, an advanced operational water management method is required that can take these required functionalities into account when controlling the flow in the country. Model Predictive Control (MPC) is utilized in this study, which is a state-of-the-art control technique showing the best performance for the kind of problems that include predicted disturbances and setpoints [2, 4]. Besides that, constraints, delay times and uncertainties can be explicitly taken into account in MPC [5, 9, 10].

This chapter is organized as follows: Sect. 11.2 describes the model of the Dutch water system and the water-related structures. Section 11.3 introduces the management objectives and the MPC controller for solving the problem. Results and a detailed model assessment follow in Sect. 11.4. Section 11.5 gives a general discussion about the topics of transport of water and transport over water. Section 11.6 ends with conclusions and recommendations.

11.2 System Dynamics

11.2.1 System Dynamics of the Water System

A dynamic model of the system needs to be built for describing the relation between water levels and flows in the rivers and canals. A generally accepted way to describe such a system is using the De Saint Venant equations [7, 11, 13]:

$$\frac{\partial Q}{\partial x} + \frac{\partial A_\mathrm{f}}{\partial t} = q_\mathrm{l}, \tag{11.1}$$

$$\frac{\partial Q}{\partial t} + \frac{\partial}{\partial t}\left(\frac{Q^2}{A_\mathrm{f}}\right) + gA_\mathrm{f}\frac{\partial h}{\partial x} + \frac{gQ|Q|}{C^2 R_\mathrm{f} A_\mathrm{f}} = 0, \tag{11.2}$$

where Q is the flow (m^3/s), h is the water level (m), A_f is the wetted area of the flow (m^2), q_l is the lateral inflow (m^3/s), g is the gravitational acceleration (m^2/s), C is the Chezy friction coefficient ($\mathrm{m}^{1/2}/\mathrm{s}$), R_f is hydraulic radius (m), and P_f is the wetted perimeter (m). To use the De Saint Venant in a numerical way, a robust wind-up method is utilized to discretize (11.1) and (11.2) in this study [7, 12]:

$$\frac{dA_\mathrm{f}}{dt} = \frac{Q_{i-1/2} - Q_{i+1/2}}{\Delta x} + q_{\mathrm{l},i}, \tag{11.3}$$

$$\frac{dv_{i+1/2}}{dt} + \frac{1}{A_{\mathrm{f},i+1/2}}\left(\frac{(Q_{i+1/2} + Q_{i+3/2})\cdot v_{i+1} - (Q_{i+1/2} + Q_{i-1/2})\cdot v_i}{2\Delta x}\right.$$
$$\left. - v_{i+1/2}\frac{Q_{i+3/2} - Q_{i-1/2}}{2\Delta x}\right), + g\frac{h_{i+1} - h_i}{\Delta x} + g\frac{v_{i+1/2}|v_{i+1/2}|}{C^2 \cdot R_\mathrm{f}} = 0, \tag{11.4}$$

where the subscripts i, $i + 1/2$ and $i - 1/2$ denote the parameters or variables at staggered grid points i, $i + 1/2$ and $i - 1/2$ respectively.

11.2.2 Water-Related Infrastructures

At Arnhem, the flow from the River Rhine bifurcates into the Rivers IJssel and Nederrijn. The ratio of flows over these two branches is manipulated by a gate at Driel (Fig. 11.3), which is the most important structure for keeping the balance between water supply to the west and navigation in the River IJssel in dry periods. Besides that, five outlets of water into the North Sea in the estuary of the delta, as shown in Fig. 11.1, are the Lorentz Gate and Stevin Gate, the IJmuiden Pump and Gate and the Maeslant Barrier. Three other gates—the Krabbersgat Gate,

Fig. 11.3 The gate constructed at Driel for drought management (*source*: flickr.com\jasja_dekker)

Table 11.1 The main structures used in this study

Structure	Type	Width or maximum capacity
Driel	Gate	108 (m)
Stevin	Gate	180 (m)
Krabbersgat	Gate	36 (m)
Houtrib	Gate	108 (m)
Schellingwoude	Gate	9.8 (m)
IJmuiden	Pump	260 (m^3/s)
IJmuiden	Gate	36.8 (m)
Maeslant	Barrier	360 (m)
Lorentz	Gate	120 (m)

the Houtrib Gate and the Schellingwoude Gate—are operated by Rijkwaterstraat to manipulate the water exchange between the large lakes and the North Sea Canal. All structures, with their parameters, are listed in Table 11.1.

The gates listed in Table 11.1 are all undershot gates that are lowered into water from the top down. The flows via the structures follow (11.5) when the structure flow is free flowing (if the gate position is higher than the downstream water level) or follow (11.6) when the structure is submerged (if the gate position is lower than the downstream water level) [11],

In particular, the structure flow via a free flowing undershot gate is given by:

$$Q(k) = C_g \cdot W_g \cdot \mu_g \cdot \left(h_g(k) - h_{cr}\right) \cdot \sqrt{2 \cdot g \cdot \left(h_1(k) - h_{cr} - \mu \left(h_g(k) - h_{cr}\right)\right)}, \tag{11.5}$$

and the structure flow via a submerged undershot gate is given by:

$$Q(k) = C_g \cdot W_g \cdot \mu_g \cdot \left(h_g(k) - h_{cr}\right) \cdot \sqrt{2 \cdot g \cdot (h_1(k) - h_2(k))}, \tag{11.6}$$

where Q is the flow through the gate (m^3/s), k is time step (s), C_g is the calibration coefficient, W_g is the width of the gate (m), μ is the contraction coefficient, h_g is the gate height (m), h_1 is the upstream water level (m), h_2 is the downstream water level (m) and h_{cr} is the crest level (m). Note that in the case of multiple gates in parallel, the total width can be taken together and the gates can be considered as moving in a synchronized way.

In order to reduce the calculation complexity and be able to use the De Saint Venant in a linear model, both (11.5) and (11.6) need to be linearized by applying the first-order Taylor expansion [11].

This results in the linearized structure flow via a free flowing undershot gate:

$$\begin{aligned} Q(k+1) = {} & Q(k) + f(k) \cdot (h_{up}(k+1) - h_{up}(k)) \\ & + \left(\frac{2 \cdot \left(h_1(k) - h_{cr} - \mu \left(h_g(k) - h_{cr}\right)\right)}{\left(h_g(k) - h_{cr}\right)} + 1 \right) \\ & \cdot f(k) \cdot (h_g(k+1) - h_g(k)), \end{aligned} \tag{11.7}$$

where

$$f(k) = \frac{g \cdot C_g \cdot W_g \cdot \mu_g \cdot \left(h_g(k) - h_{cr}\right)}{\sqrt{2 \cdot g \cdot \left(h_{up}(k) - h_{cr} - \mu \left(h_g(k) - h_{cr}\right)\right)}}, \tag{11.8}$$

and the linearized structure flow via a submerged undershot gate:

$$\begin{aligned} Q(k+1) = {} & Q(k) + f(k) \cdot (h_{up}(k+1) - h_{up}(k)) \\ & - f(k) \cdot (h_{down}(k+1) - h_{down}(k)) \\ & + \frac{2 \cdot \left(h_{up}(k) - h_{down}(k)\right)}{\left(h_g(k) - h_{cr}\right)} \cdot f(k) \cdot (h_g(k+1) - h_g(k)), \end{aligned} \tag{11.9}$$

where

$$f(k) = \frac{g \cdot C_g \cdot W_g \cdot \mu_g \cdot \left(h_g(k) - h_{cr}\right)}{\sqrt{2 \cdot g \cdot \left(h_{up}(k) - h_{down}(k)\right)}}. \tag{11.10}$$

11.3 MPC Control Design for Drought Management

11.3.1 Standard MPC Scheme and the Objective Function

MPC is a model-based control technique, which uses a state-space model to predict future states of the system and then solves an optimization problem using an objective function under constraints on control actions and system outputs over a certain prediction horizon [2]. In this chapter, the states of the proposed MPC scheme include the water levels and structure flows. A linear time-invariant state-space model is built up in MPC to describe and predict these states over the prediction horizon. The state-space equation for each single river-reach can be written as [8, 11]:

$$h(k+1) = h(k) + \frac{Q_s(k)\Delta T + \Delta Q_s(k)\Delta T}{A_s} + \frac{Q_d(k)\Delta T}{A_s}, \tag{11.11}$$

$$\Delta Q_s(k) = Q_s(k+1) - Q_s(k), \tag{11.12}$$

where k is the discrete time step index, ΔT (s) is the time step length, A_s (m^2) is the surface area, Q_s (m^3/s) is the flow through the structure, ΔQ_s (m^3/s) is the change of structure flow and Q_d (m^3/s) is the sum of disturbances and other flows not related to structures, such as rainfall runoff and water abstractions. Note that flows over rivers and canals are not included in the states since they can be calculated by the discretized De Saint Venant Equations (11.3) and (11.4) with the known states or estimated by the stage-discharge fitting curve.

An objective function is built up to formalize the goal of the water management, i.e., in this study to find the optimal solution for water distribution in dry periods. The MPC problem is built up at any step k as a quadratic function with linear constraints [11]:

$$\min_{\Delta Q_s} J(k) = \sum_{j=1}^{N_P} \sum_{l=1}^{L} r_l \Delta Q_{s,l}{}^2(k+j) + \sum_{j=1}^{N_P} \sum_{i=1}^{M_2} s_i Q_i(k+j), \tag{11.13}$$

subject to

$$h_{\min,i} \le h_i(k+j) \le h_{\max,i}, \forall i \in \{1,2,\ldots,M_1\}, \forall j \in \{1,2,\ldots,N_p\},$$

$$Q_{\min,l} \le Q_{s,l}(k+j) \le Q_{\max,l}, \forall l \in \{1,2,\ldots,L\}, \forall j \in \{1,2,\ldots,N_p\},$$

$$h(k+1) = h(k) + \frac{Q_s(k)\Delta T + \Delta Q_s(k)\Delta T}{A_s} + \frac{Q_d(k)\Delta T}{A_s},$$

$$\Delta Q_s(k) = Q_s(k+1) - Q_s(k),$$

where N_P is the prediction horizon, M_2 is the number of reaches, L is the number of controlled structures, $h_{\min,i}$ and $h_{\max,i}$ are the minimum and maximum allowed

water level of the node i. $Q_{\min,l}$ and $Q_{\max,l}$ are the minimum and maximum allowed flow through the structure l, r and s are so-called penalties which are chosen according to a maximum allowed value estimate [11].

11.3.2 Segmented Setpoint Setting in MPC

To achieve the goal that water can be diverted into the River IJssel for navigation during the daytime and into the River Nederrijn during the night, segmented setpoints are set on states in the MPC scheme, as shown in Fig. 11.4.

The segmented setpoints on the water levels and structure flows can be expressed as:

$$\tilde{h}(k) = h(k) - h_r(k), \tag{11.14}$$

$$\tilde{h}_{\min}(k) = h_{\min}(k) - h_r(k), \tag{11.15}$$

$$\tilde{h}_{\max}(k) = h_{\max}(k) - h_r(k), \tag{11.16}$$

$$\tilde{Q}(k) = Q(k) - Q_r(k), \tag{11.17}$$

where

$$h_r(k) = \begin{cases} h_{r,0}, k \in T_0, \\ h_{r,1}, k \notin T_0, \end{cases}$$

$$Q_r(k) = \begin{cases} Q_{r,0}, k \in T_0, \\ Q_{r,1}, k \notin T_0, \end{cases}$$

and T_0 is a set of a certain time period, $h_{r,0}$ and $h_{r,1}$ are reference water levels depending on whether k is within the set T_0, $Q_{r,0}$ and $Q_{r,1}$ are reference flows,

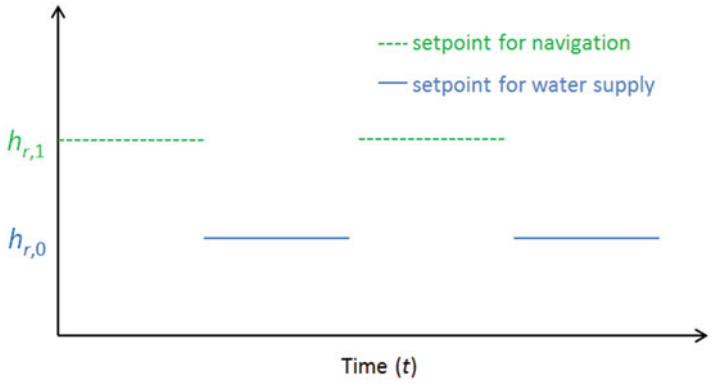

Fig. 11.4 Segmented setpoints on different objectives

$\tilde{h}$ (m) is the deviation between the actual water level h and the reference water level h_r, $\tilde{h}_{min}$ and $\tilde{h}_{max}$ are the deviation between the minimum or maximum allowed water level and reference level and $\tilde{Q}$ is the deviation between the actual flow Q and the reference water flow Q_r (m^3/s).

Therefore, the state space station (11.11) becomes:

$$\tilde{h}(k+1) = \tilde{h}(k) + \frac{Q_s(k)\Delta T + \Delta Q_s(k)\Delta T}{A_s} + \frac{Q_d(k)\Delta T}{A_s}, \quad (11.18)$$

$$\Delta Q_s(k) = \tilde{Q}_s(k+1) - \tilde{Q}_s(k), \quad (11.19)$$

and the quadratic and linear terms of the setpoints are added into the objective function:

$$\min_{\Delta Q_s} J(k) = \sum_{j=1}^{N_p}\sum_{i=1}^{M_1} q_i \tilde{h}_i^2(k+j) + \sum_{j=1}^{N_p}\sum_{l=1}^{L} r_l \Delta Q_{s,l}{}^2(k+j) \quad (11.20)$$

$$+ \sum_{j=1}^{N_P}\sum_{l=1}^{L} t_l(\tilde{Q}_{s,l}^2(k+j)) + \sum_{j=1}^{N_P}\sum_{i=1}^{M_1} p_i \tilde{h}_i(k+j) + \sum_{j=1}^{N_P}\sum_{i=1}^{M_2} s_i Q_i(k+j),$$

subject to

$$\tilde{h}_{\min,i} \le \tilde{h}_i(k+j) \le \tilde{h}_{\max,i}, \forall i \in \{1,2,\ldots,M_1\}, \forall j \in \{1,2,\ldots,N_P\},$$

$$Q_{\min,l} \le Q_{s,l}(k+j) \le Q_{\max,l}, \forall l \in \{1,2,\ldots,L\}, \forall j \in \{1,2,\ldots,N_P\},$$

$$h_r(k) = \begin{cases} h_{r,0}, k \in T_0, \\ h_{r,1}, k \notin T_0, \end{cases}$$

$$Q_r(k) = \begin{cases} Q_{r,0}, k \in T_0, \\ Q_{r,1}, k \notin T_0, \end{cases}$$

where M_1 is the number of nodes, t, q and p are the penalties on $\tilde{Q}$ and $\tilde{h}$. This optimization problem can be solved using CPLEX [3].

11.4 Simulation and Results

11.4.1 Simulation Setup

The extreme drought that happened in the summer of 1976 is chosen in this study for showing the performance of the proposed MPC controller. Figure 11.5 shows the flow of the River Rhine at Lobith in June and July of 1976. The flow which is gauged at Lobith is regarded as the entrance of the River Rhine into the Netherlands. The period that the flow was lower than 1250 m^3/s lasted over 40 days in late June and July and the lowest flow was only 785 m^3/s on July 13, 1976.

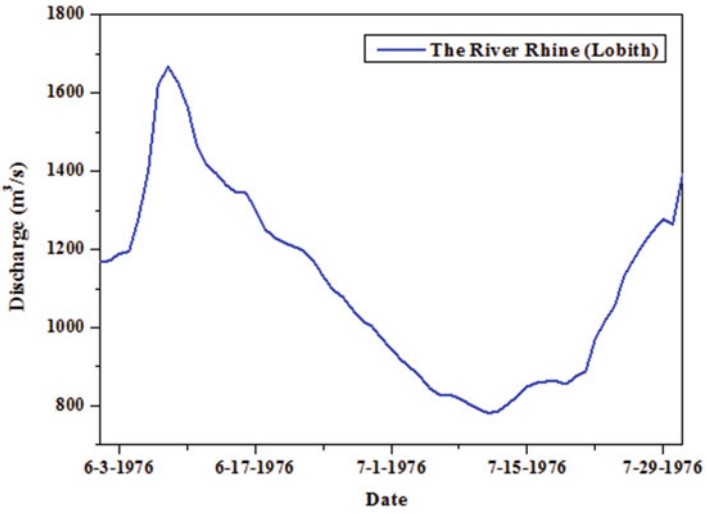

Fig. 11.5 The flow of the River Rhine at Lobith

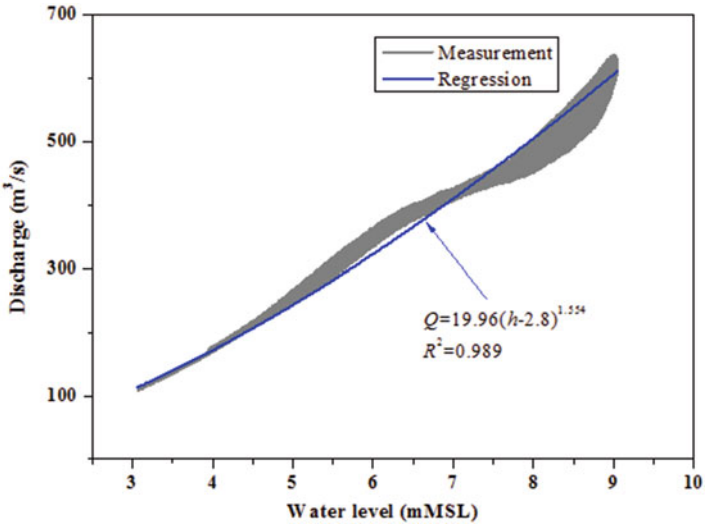

Fig. 11.6 The stage-discharge fitting curve of the River IJssel at Arnhem

A flow of 285 m^3/s is an optimal value for the appropriate navigation over the River IJssel. More vessels and more waiting time to pass locks is required if the flow is lower than the setpoint while the operations on drawbridges are more frequent if the flow is higher than the setpoint. As a result, a flow of 285 m^3/s over the River IJssel is set up as the setpoint. The stage-discharge rating curve (Fig. 11.6) between the water level and flow in the River IJssel is established as:

$$Q = 19.96 \cdot (h - 2.8)^{1.554}. \tag{11.21}$$

Note that the water level is used as a state in the proposed MPC scheme. Therefore, the flow setpoint of 285 m^3/s corresponds to the water level setpoint of 8.3 mMSL at Arnhem.

To meet the requirements of water supply for the users in the west, a day and night segmented setpoint scheme is set up. Between 7 a.m. and 6 p.m., a setpoint of 25 m^3/s is applied at the structure flow via the Driel Gate, while 100 m^3/s is applied otherwise.

Three simulation experiments, one without using setpoints, one using a high penalty on the setpoint with respective to navigation and one using a high penalty on the setpoint with respective to water supply to the west are performed to evaluate the sensitivity of the proposed controller and the day and night setpoint setting. Table 11.2 presents all the parameters used in these scenarios. Note that the coefficients in (11.20) are set to be zero if they are not mentioned in the Table 11.2.

Table 11.2 Simulation parameters

Parameters	Symbol	Value
Storage area of Lake IJssel	$A_{s,1}$	1.2e+9 (m^2)
Storage area of Lake Marker	$A_{s,2}$	7.4e+8 (m^2)
Storage area of North Sea Canal	$A_{s,3}$	3.1e+7 (m^2)
Control time step	N_c	1 (h)
Prediction time step	N_p	1 (h)
4 Simulation horizon	N_T	2,160 (h)
Prediction horizon	N_1	48 (h)
Quadratic penalty on ΔQ via the Lorentz Gate	r_1	1/8,000
Quadratic penalty on ΔQ via the Stevin Gate	r_2	1/2,000
Quadratic penalty on ΔQ via the Krabbersgat Gate	r_3	1/2,000
Quadratic penalty on ΔQ via the Houtrib Gate	r_4	1/3,000
Quadratic penalty on ΔQ via the Schellingwoude Gate	r_5	1/200
Quadratic penalty on ΔQ via the IJmuiden Gate	r_6	1/1,000
Quadratic penalty on ΔQ via the IJmuiden Pump	r_7	1/260
Quadratic penalty on ΔQ via the Driel Gate	r_8	1/100
Linear penalty on Q via the IJmuiden Pump	s_8	1/260
Linear penalty on the h at HollandschDiep	p_{26}	1/100
$\tilde{Q}$ of the Driel Gate (7 a.m.–6 p.m.) (scenario 1 & 2)	$Q_{sr,8}$	25 (m^3/s)
$\tilde{Q}$ of the Driel Gate (6 p.m.–7 a.m.) (scenario 1 & 2)	$Q_{sr,8}$	100 (m^3/s)
$\tilde{h}$ Setpoint on h at Arnhem (scenario 1 & 2)	Q_{14}	8.33 (m)
Quadratic penalty on $\tilde{Q}$ of the Driel Gate (scenario 1)	t_8	1/1,000
Quadratic penalty on $\tilde{h}$ at Arnhem (scenario 1)	q_{14}	1/20
Quadratic penalty on $\tilde{Q}$ of the Driel Gate (scenario 2)	t_8	1/50
Quadratic penalty on $\tilde{h}$ at Arnhem (scenario 2)	q_{14}	1/1,000

11.4.2 Scenario 1: No Setpoint Setting

In Scenario 1, a reference simulation is run to demonstrate the advantage of using the segmented setpoint setting in next two simulations. This scenario fully depends on the current regulations (see Fig. 11.2). In this scenario, no setpoints are set up on the structure flow via the Driel Gate or the water level of the River IJssel. Only a minimal value of 25 m^3/s is required on the structure flow via the Driel Gate. As shown in Fig. 11.7, without any setpoint setting, most water goes into the west. As a result, available riverine depth in the River IJssel for navigation is really limited (Fig. 11.8). As shown in Table 11.3, the total amount of water during the whole period is large. However, the western country obtained less water between July 1st and July 22nd in Scenario 1, when water for navigation during the night is not so necessary.

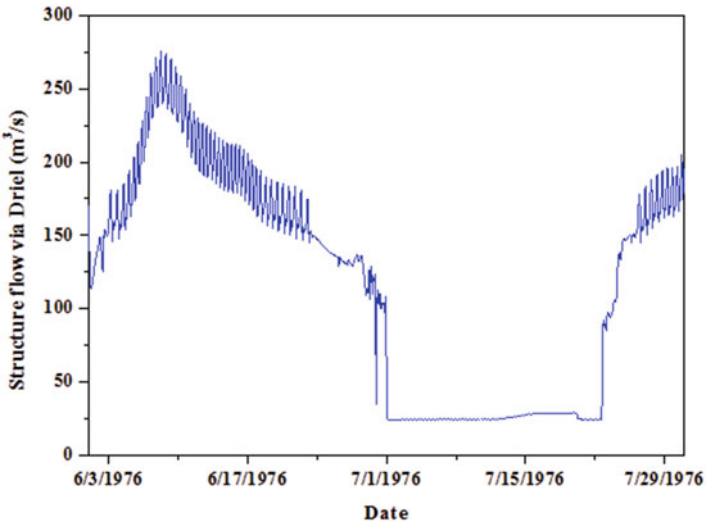

Fig. 11.7 Structure flow via the gate at Driel in Scenario 1

Table 11.3 The amount of the water supply

Flux (m^3/s)	Jun 1–Jul 31	Jul 1–Jul 22
Scenario 1	170,345	13,856
Scenario 2	78,337	24,535
Scenario 3	15,197	208

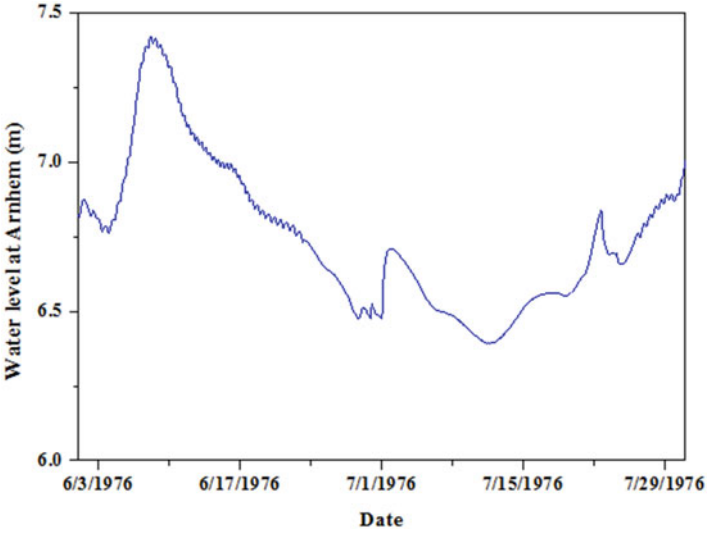

Fig. 11.8 Water level at Arnhem in Scenario 1

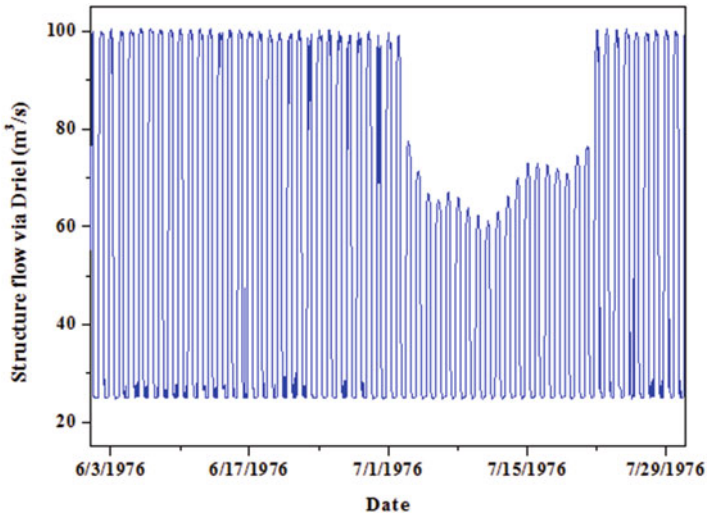

Fig. 11.9 The structure flow via the gate at Driel in Scenario 2

11.4.3 Scenario 2: Low Penalty on Water Supply

In scenario 2, the penalty on the structure flow via the Driel Gate is lower than the penalty on the water level at Arnhem. This means that the water supply for the users in the west is assumed more important than the navigation in the River IJssel. Figure 11.9 shows the water supply towards the west. The minimal demand

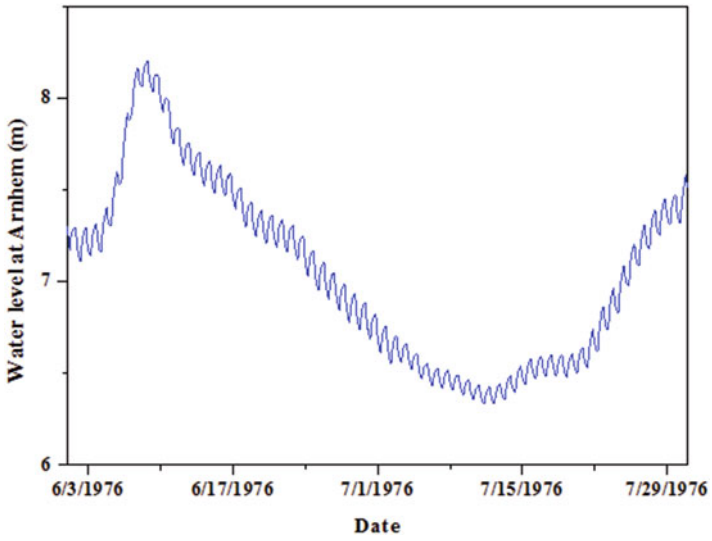

Fig. 11.10 The water level at Arnhem in Scenario 2

of 25 m^3/s during the night can always be satisfied, while during the daytime, the required demand of 100 m^3/s can not always be satisfied. In the middle of July, the discharge of the River Rhine is lower than 1,000 m^3/s so that those water supplies towards the west and for navigation are both extremely limited. That is the reason that the structure flow though the Driel Gate is lower than 80 m^3/s and can not reach the expected amount in the middle of July. Also the water level at Arnhem, as shown in Fig. 11.10, dropped as low as 6.5 m on the 14th July. These limited depths may result in vessels bringing fewer loads and postponing navigation in this dry period. The water level of Lake IJssel increases from −0.2 m to 0.1 m (Fig. 11.11). It is due to the reason that the structure flows via the Stevin Gate and Lorentz Gate are very low (Fig. 11.12). This can slightly benefit the navigation of the River IJssel in the situation that there is not too much water flowing over the River IJssel. In total, the amount of water supply for the users in the west is 78,337 m^3 in June and July and 24,535 m^3 during the serious period between July 1 and July 22 (Table 11.3).

11.4.4 Scenario 3: Low Penalty on Navigation

In Scenario 3, the penalty on the water level at Arnhem is lower than the one on the structure flow via the Driel gate, giving more priority to navigation. Considered here that water supply for the west is relatively less important than navigation, Fig. 11.13 shows that water is diverted towards the River Nederrijn mostly during the night and the expected 100 m^3/s can not be satisfied at all. However, the River IJssel gained

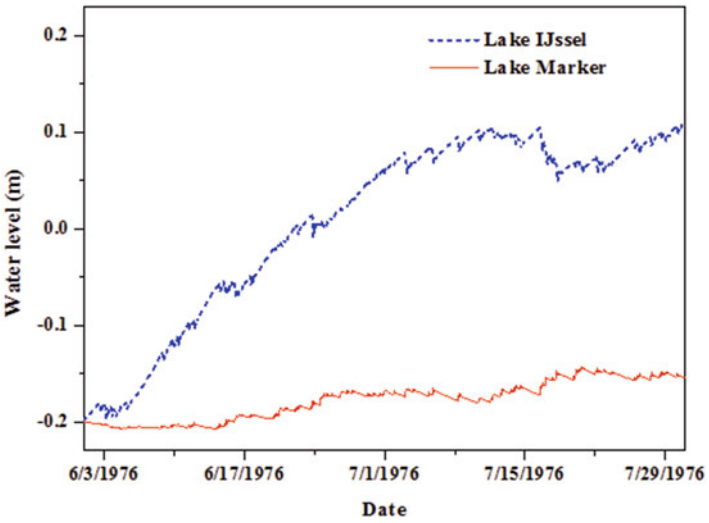

Fig. 11.11 The water levels of Lake IJssel and Lake Marker in Scenario 2

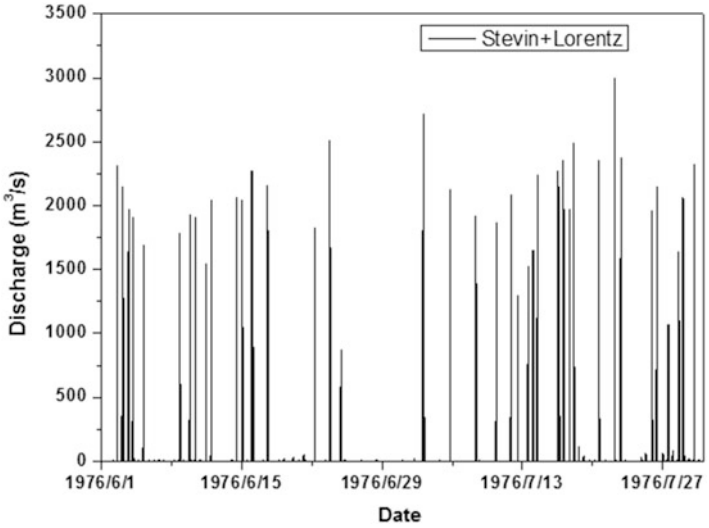

Fig. 11.12 The sum of structure flows via the gates at Stevin and Lorentz in Scenario 2

more water for navigation (Fig. 11.14). Actually, the water level at Arnhem is nearly 1 m higher than the one in Scenario 1. Moreover, day and night navigation is both available in this scenario. In order to benefit the navigation of the River IJssel more, all structures between Lake IJssel and Lake Marker as well as between Lake IJssel and the North Sea are completely shut off. Thus, all water from the River IJssel is stored in Lake IJssel and the water level of Lake IJssel could reach up to 0.4 m in the

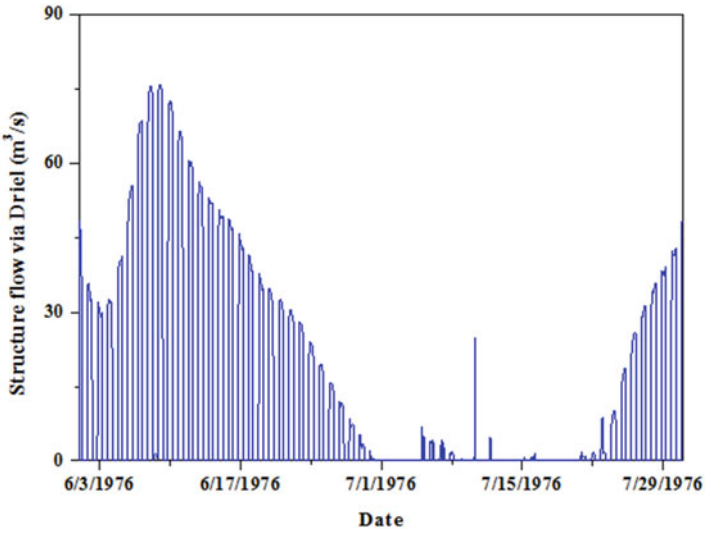

Fig. 11.13 Structure flow via the gate at Driel in Scenario 3

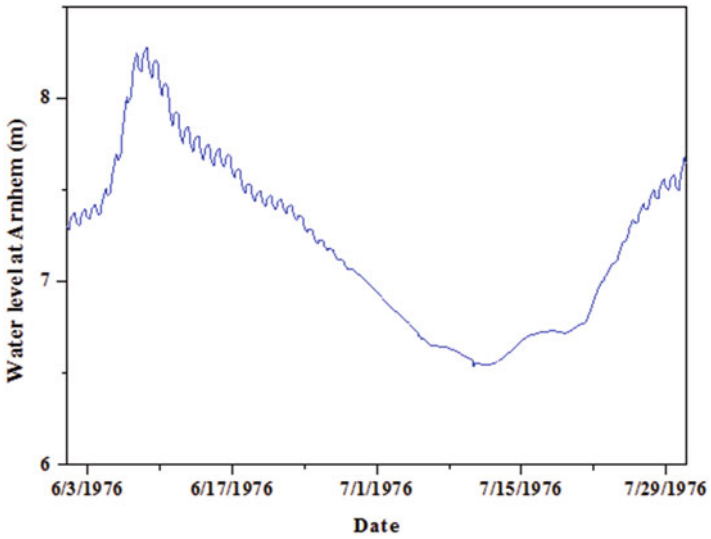

Fig. 11.14 Water level at Arnhem in Scenario 3

middle of July (see Fig. 11.15), which increases the capacity of the navigation in the River IJssel. Compared to Scenario 1, only 15,197 m^3 of water is diverted into the River Nederrijn in June and July and as low as 208 m^3 between July 1 and July 22.

Which one of the scenarios needs to be applied, or which of the stakes are more important, is up to the decision makers. In this study we demonstrate that, when

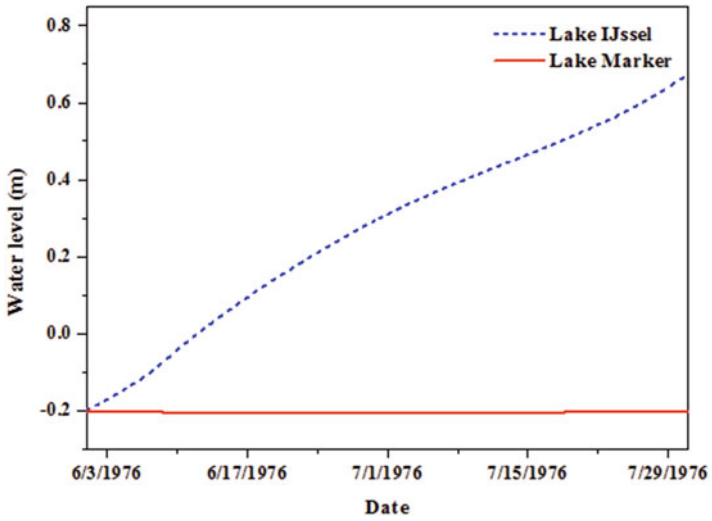

Fig. 11.15 The water levels of Lake IJssel and Lake Marker in Scenario 3

weights of priority are given, the operational system can smoothly implement this choice and is an alternative to the rigid prioritization during droughts, which is common in the present operational water management of the country.

11.5 Discussion on Transport of Water and Transport Over Water

The topic, transport of water, is mainly concerned with the issue of water quantity transport, which is actually comprised of a wide range of water resources management problems, e.g., flood defense, drought management, water supply. To satisfy requirements of transport of water, a right amount of water has to be transported to a right user or a right location at a right time. On the other hand, the topic of transport over water is specifically referred to navigation. The requirement of transport over water is relatively simply, i.e., keeping the water level of the canal close to a predefined reference level. More barges are needed to carry goods if the water level is too low while the bridge has be operated more frequently if the water level is too high.

In previous studies, these two aspects were typically investigated separately since they do not have too many conflicts under normal circumstances when enough water is available. However, during droughts, the conflicts appear due to insufficient water. In order to link transport of water and transport over water, controlling the water level is an intermediary way to balance both benefits. By controlling the water level

of the canal, this chapter simulates a scenario of a drought to illustrate the possibility to include the topics of transport over water and transport of water in the same water management plan.

11.6 Conclusions and Future Research

This chapter focuses on two integrated subjects—transport of water and transport over water in the Dutch water system. They do not conflict with each other until a drought occurs. During droughts, the control problem becomes how to operationally distribute water for different purposes and how much water each purpose can obtain. In this study, three scenarios were chosen to illustrate how MPC dealt with the conflicts between transport of water and transport over water during a drought. In Scenario 2, instead of rigidly diverting a certain amount of water for the users in the west, segmented day-night setpoints were set up on the structure flow via the Driel Gate. Therefore, navigable capability in the River IJssel could benefit during the daytime, while water demand in the west could also be met owing to the compensation at night. Scenario 3 demonstrates the situation that the navigation was considered more important than the water supply. In the present regulations, the navigation is at a lower priority than the water supply. However, for the purpose of scientific research, we have also taken this situation into account and examined how the ratio of the penalties can influence operations on sub-objectives. These two scenarios give two extremes that indicate to what extent the sub-objectives can be achieved by choosing different penalties on them. In future research, with economic losses during droughts taken into consideration, the ratio of penalties will be chosen based on the losses of each sub-objective.

Acknowledgements This research is supported by the China Scholarship Council under Grant 2011614097, the VENI project "Intelligent multi-agent control for flexible coordination of transport hubs" (project 11210) and the Maritime Project "ShipDrive: A Novel Methodology for Integrated Modeling, Control, and Optimization of Hybrid Ship Systems" (project 13276) of the Dutch Technology Foundation STW.

References

1. Arnold G, Bos H, Doef R, Goud R, Kielen N, van Luijn F, Rijkswaterstaat, editors. Water management in the Netherlands, 2nd ed. The Hague: Netherlands Hydrological Society (NHV); 2011.
2. Camacho E, Bordons C. Model predictive control. Sevilla: Spinger ;1999.
3. Holmstrom K, Goran AO, Edvall MM. User's guide for Tomlab, vol. 7. Sweden: TOMLAB Optimization; 2010.
4. Maciejowski JM. Predictive control: with constraints. Harlow: Pearson Education; 2002.
5. Maestre JM, Raso L, van Overloop PJ, De Schutter B. Distributed tree-based model predictive control on a drainage water system. J Hydroinform. 2013;15(2):335.

6. RIZA (Institute for Inland Water Management and Waste Water Treatment). The Netherlands Drought Study (Final report), 2003. http://www.droogtestudie.nl
7. Stelling GS, Duinmeijer SPA. A staggered conservative scheme for every Froude number in rapidly varied shallow water flows. Int J Numer Methods Fluids. 2003;43(12):1329–1354.
8. Tian X, Negenborn RR, van Overloop PJ, Mostert E. Model predictive control of water management using the adaptive prediction accuracy. In: 11th international conference on hydroinformatics, New York, 2014.
9. Tian X, van Overloop PJ, Negenborn RR, Maestre JM. Incorporating transport over water in the multi-objective water management of the Lake IJssel area in The Netherlands. In: Proceedings of 10th IEEE international conference on networking, sensing and control (ICNSC). Piscataway: IEEE; 2013. p. 649–654.
10. van Ekeren H, Negenborn RR, van Overloop PJ, De Schutter B. Hybrid model predictive control using time-instant optimization for the Rhine-Meuse delta. In 2011 international conference on networking, sensing and control. Delft: IEEE; 2011. p. 215–220
11. van Overloop PJ. Model predictive control on open water systems. Ph.D. thesis, Delft University of Technology, 2006.
12. Xu M. Real-time control of combined water quantity & quality in open channels. Ph.D. thesis, Delft University of Technology, Delft, The Netherlands, 2013.
13. Xu M, Negenborn RR, van Overloop PJ, van de Giesen NC. De Saint-Venant equations-based model assessment in model predictive control of open channel flow. Adv Water Resour. 2012;49:37–45.

Chapter 12
Enhancing Inland Navigation by Model Predictive Control of Water Levels: The Cuinchy-Fontinettes Case

K. Horváth, L. Rajaoarisoa, E. Duviella, J. Blesa, M. Petreczky, and K. Chuquet

Abstract Navigation canals are used for transport purposes. In order to allow safe navigation the water level should be kept in a certain range around the Normal Navigation Level (NNL). The water level is disturbed by known and unknown inputs, like tributaries, municipal water flows, rain, etc. Some of these inputs can be used to control the water level. If the geometry requires it, canal reaches are connected by locks. The operation of these locks sometimes can disturb the water level, if the difference between the upstream and downstream water level is large. The objective is to minimize the disturbances caused by these lock operations on the water level in order to maintain the NNL. In this work the global management of the canal reach is discussed and an option to maintain the NNL by active control is introduced. Some inputs to the system, such as other confluences or gates on the side of the locks, can be controlled automatically to react to the disturbances caused by the lock operations using model predictive control to maintain the desired water level.

K. Horváth (✉) • L. Rajaoarisoa • E. Duviella • M. Petreczky
Institut Mines Telecom, Mines Douai, Doaui, France
e-mail: hklau85@gmail.com; lala.rajaoarisoa@mines-douai.fr; eric.duviella@mines-douai.fr; mihaly.petreczky@mines-douai.fr

J. Blesa
Technical University of Catalonia, Institut de Robòtica i Informàtica Industrial (CSIC-UPC), Barcelona, Spain
e-mail: joaquim.blesa@upc.edu

K. Chuquet
Voies Navigables de France, Lille, France
e-mail: karine.chuquet@vnf.fr

C. Ocampo-Martinez, R.R. Negenborn (eds.), *Transport of Water versus Transport over Water*, Operations Research/Computer Science Interfaces Series 58,
DOI 10.1007/978-3-319-16133-4_12

12.1 Introduction

Transport over water has considerable economical and ecological benefits [32, 34]. Navigation offers a more efficient, quieter, safer option for transport of goods. The transport over water consist of sea transport and inland navigation. In the following the latter will be analyzed.

In order to ensure navigation in inland canals the water level should be kept in a range around a reference level, the so called Normal Navigation Level (NNL). The water level has to be maintained in the navigation range in order for the reach to be operable.

The European Union encourages the development of the inland navigation network, especially by using ICT technologies [16]. Tele-controlled sensors and actuators can be installed in order to establish constant on-line monitoring of the system [17, 42] by using SCADA (Supervisory Control and Data Acquisition) systems. The collected historical data can be used to study the navigation reach. There are SCADA systems specially developed for inland navigation [8, 52]. The navigation system can benefit from the use of the SCADA from the maintenance and also from the security point of view [2]. Additionally, there are simulation tools specially developed for inland navigation systems [1].

Another big challenge for the inland navigation networks in the future is handling the effects of the climate change. These networks are very vulnerable to the climate change [6]. Different climate models are available from 10 to 100 years in the literature [36]. Some of these models include also effects like farming [19] or social and economic aspects [11]. The effects of climate change are also studied regionally, for example in the French river basins [5, 12], Mediterranean basin [18], basins in U.K. [3, 7], China [51] and the U.S. [35]. The different studies share some possible effects: global rise of mean sea level, increase in the occurrence of extreme weather events, increase in the surface temperature of the water and changes in river morphology. These events cause changes in water supply and quality that can lead to stronger constraints for inland navigation.

On some navigation systems the effect of climate change has already been studied. In the great lakes the climate change can result in lower water levels and shorter ice cover, e.g., on Lake Ontario. While due to the first factor the vessel load should be reduced (negative effect) due to the second the navigation period can be extended (positive effect). As to adaptive measures intensified dredging and shift of transport to rail is predicted [35]. In Northern Europe studies also describe the decrease in water level. As adaptation similar measures are proposed, but only a modest modal shift to rail is mentioned [24]. The ECCONET European projects studied the effect of climate change on the Middle Rhine, Upper Danube and the Rhine-Main-Danube corridor. For the middle of the twenty-first century the frequency of low flow situations is likely to increase only in the Upper Danube, however, for the distant future low flow situations will become more frequent in all studied areas. They emphasize the regional differences of the behavior [6].

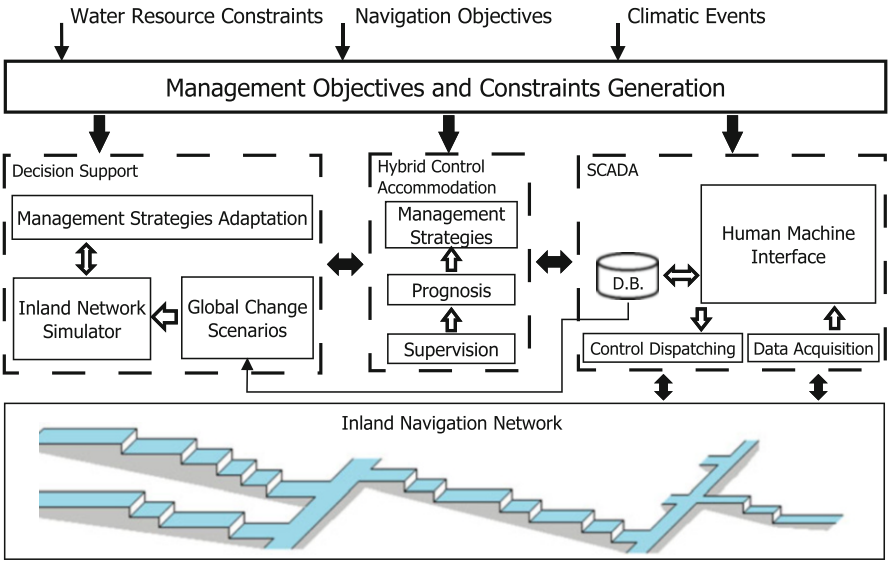

Fig. 12.1 The schematics of the global modeling approach

From these conclusions it can be seen that each system is different, as the regional effects of the climate change also differ to a great extent.

The GEPET-Eau project [13] addresses the adaptive and predictive management strategies for inland navigation networks. The global management architecture is shown in Fig. 12.1 [15]. This architecture is based on a SCADA (Supervisory Control And Data Acquisition) system which allows the tele-management of the network. The management rules and the constraints on the water uses are regrouped in the Management Objectives and Constraints Generation module. Depending on these rules, the Hybrid Control Accommodation module allows the determination of the setpoints that have to be sent to the actuators of the system according to its current state and the forecast of the flood events and the drought periods. The management strategies are adapted taking into account new extreme events. Thus, the long term control objective is to make navigation possible in different external conditions: in case of floods when there is excess of water and the water system should be operated in a way to let the flood wave pass without inundating the neighboring cities. In case of drought, there is a lack of water. Water should be supplied first to priority purposes (like drinking water) and then to navigation. By modeling the global system and extending the controls strategy the final goal of the project is to give solutions for navigation for different scenarios in a global change context. Therefore the goal of the GEPET-Eau project is to study the effect and the adaption to climate change of the navigation network of the north of France.

In order to understand and predict or control the system, modeling is needed. The open channel flow is governed by a pair of hyperbolic partial differential equations, the Saint-Venant (SV) equations. These equations have no analytical

solution for every case, therefore in practice numerical solutions are used. Due to the nonlinearity of these equations, for controller development simplified versions of the SV equations [44] or simple models deduced from these equations are used [29, 30, 40].

Model predictive control (MPC) is commonly used to control different type of water systems, and [37–39, 49]. Using an internal model it is able to incorporate the response characteristics of the system to the control actions, and most importantly it is able to deal with constraints on the control of controlled variables. This ability is especially useful when MPC is applied to navigation systems. The goal for navigation systems is to maintain the water level as close as possible to a certain level, but definitely stay within a certain range. To achieve this hard constraints of MPC can be used. Often there are constraints on the input: the artificial navigation reaches are filled from natural resources, whose availability is restricted. The Cuinchy-Fontinettes Reach (CFR) case study is an example that will be in this chapter investigated further.

A large-scale model of the CFR is developed based on physical rules and system identification approaches [15]. A smaller time and space scale gray box model has been developed in [14] and improved in [22]. This model has been used for controlling the water level in the reach [4] and also for sensor [27] and actuator [26] fault detection.

The goal of this work is by using ICT and control techniques to obtain the best performance of the transport of a canal reach bounded by locks. There is a dynamic connection between the water and the transport system and this connection is bidirectional. The main goal of the study of the transport of water is to allow the transport over water. The water movement should be modeled and controlled in order to maintain the normal navigation level to allow the boats safely navigating. The connection also exists in the other direction: in order to allow navigation lock operations are carried out, that is water is transported (Fig. 12.2).

As in case of a canal reach bounded by locks, lock operations control the transport flow and also the water flow. In this work, lock operations are not controlled, the water flow is only controlled through the surrounding hydraulic structures and the lock operations are treated as disturbance. The control of inflow influences the transport flow: if the water level is not maintained high enough the lock operations would cause a disturbance in the water level out of the range of the allowed water level. Therefore the control of the hydraulic structures and water levels control the interactions between water and transport flow and hence indirectly the transport flow.

This chapter is structured as follows: first the general modeling is described then the case study introduced. After the application of the model to the case study is presented, the results are shown. Then the impact of this work within the framework of transport of and over water is explained. Finally, conclusions are drawn and some open questions are raised.

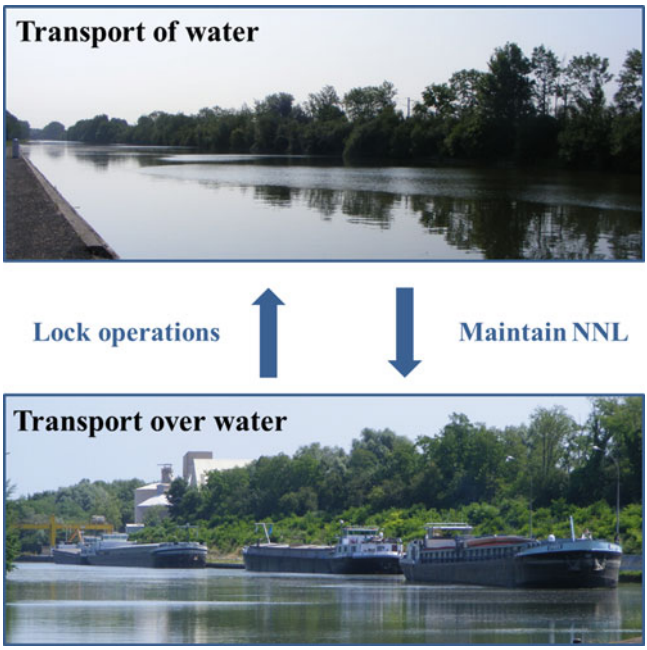

Fig. 12.2 The interaction between transport of water and transport over water in the case of navigation canals

12.2 Methodology: Modeling the Reach for Control Purposes

In order to model the canal reach for control purposes the Integrator Delay Zero (IDZ) model [29] is used. The model is an extension of the Integrator Delay (ID) model [40], that is commonly used in MPC [46, 50].

The ID model captures two governing phenomena of a canal reach: the low frequency integrator behavior and the time delay. The IDZ model includes a zero in order to approximate better the high frequency behavior.

At low frequencies the canal reach behaves like a tank: the water volume is the integral value of the difference between the inflow and the outflow. The water level is proportional to the water volume and the constant of this proportion is the water surface, often called the backwater area, A_s (of course, supposing it to be constant is a simplification of the geometry):

$$A_s^0 = B^0 L, \tag{12.1}$$

where B is the average cross sectional width in m (for rectangular canals) and L is the length of the canal reach in m. The upper case zero indicates that the variables are calculated for a certain steady state regime.

The time delay expresses the time between a change occurring at one extreme of the canal reach and this change can be observed in the other extreme. It depends mainly on the velocity of a traveling wave (celerity) and the length of the canal reach. It is slightly different in the upstream (τ_u) and in the downstream direction (τ_d) and it can be obtained as:

$$\tau_u^0 = \frac{L}{C^0 - V^0}, \tag{12.2}$$

and

$$\tau_d^0 = \frac{L}{C^0 + V^0}, \tag{12.3}$$

where V is the velocity in m/s and C is the celerity in m/s:

$$C^0 = \sqrt{gH^0}, \tag{12.4}$$

and

$$V^0 = \frac{Q^0}{H^0 B^0}, \tag{12.5}$$

where g is the acceleration of gravity in m/s^2, H is the water depth in m.

A zero is added to the ID model in order to account for the high frequency behavior. When a change occurs, (e.g., a discharge step) the first fast increase in water level is modeled very well with the IDZ model due to the presence of the zero. The IDZ model can be obtained from the geometrical characteristics of the canal reach. Details about the calculation of the model parameters can be found in [29] and [28]. The model is a linear model, therefore the quantities to calculate the model should be linearized around an equilibrium regime. This variables of the equilibrium regime are indicated with an uppercase zero.

The final structure of the IDZ model is the following:

$$G(s) = \frac{q_{in}}{h} = \frac{p_1^0 s + 1}{A_s^0 s} e^{-\tau^0 s}, \tag{12.6}$$

where q_{in} is the input discharge, h is the controlled water level, the parameter p_1 accounts for the zero and τ can be τ_u in the upstream direction and τ_d in the downstream direction. $G(s)$ is the transfer function between the input discharge (upstream or downstream) and the water level (upstream or downstream). In order to model a network using the IDZ model, each water level to be controlled can be expressed using the input discharges and transfer functions of the form (12.6). As all

the presented variables are relative to a steady state around which the system was linearized, the system is at the NNL when $h = 0$, so the control objective is to keep h at zero. Then h can be expressed as:

$$h = G_1(s)q_{in1} + G_2(s)q_{in2}, \tag{12.7}$$

where G_1 and G_2 are transfer functions belonging to the different input discharges q_{in1} and q_{in2}.

12.3 Case Study

The navigation system of the north of France allows the transport of goods from Paris to the port of Dunkerque and to Belgium (Fig. 12.3). The system consists of three watersheds: the Aa, the Lys and the Scarpe. Due to the changes in the relief, the canal reaches are connected with locks to overcome the difference in altitude (Fig. 12.4). The Cuinchy-Fontinettes reach (CFR) is located in the centre of the network. The water flows feeding the reach are shown in Fig. 12.5. The upstream part between Cuinchy to Aire-sur-la-Lys is 28.7 km long and called Canal d'Aire, the downstream part between Aire-sur-la-Lys to Saint-Omer is 13.6 km long and called Canal de Neuffossé. The overall length is 42.3 km and the CFR is bounded by the lock of Cuinhy (upstream) and the lock of Fontinettes (downstream).

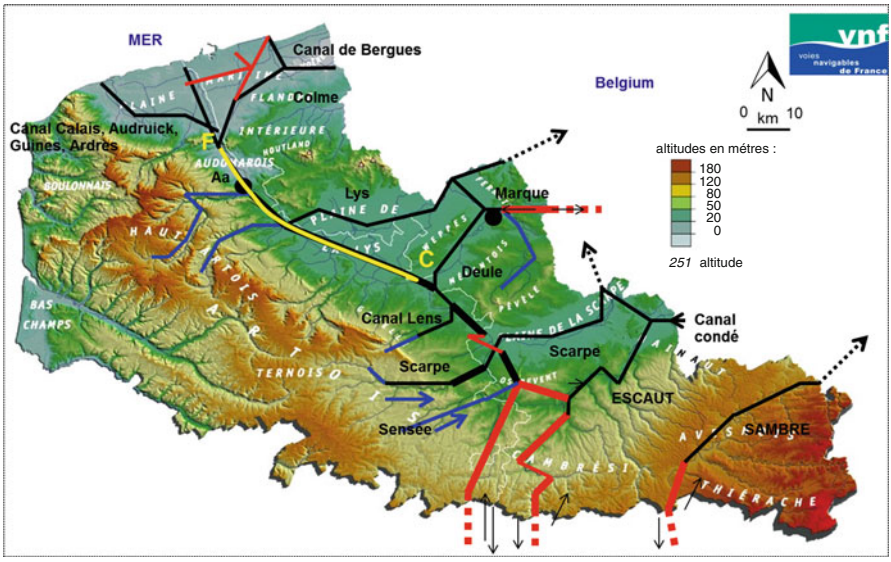

Fig. 12.3 Navigation canal system of the north of France, the CFR is highlighted with *yellow* and the location of the locks is indicated with *yellow*, the *yellow C* shows the location of lock Cuinchy, and the F of the location of lock Fontinettes

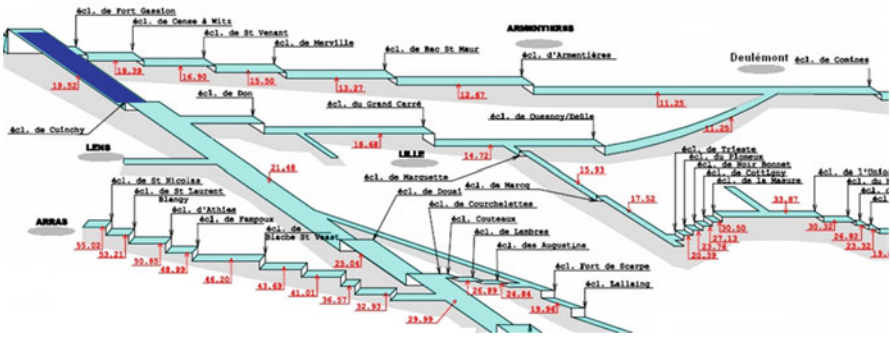

Fig. 12.4 The Normal Navigation Levels of the canal system (*red color*) and the corresponding locks (*black color*), the CFR is highlighted with *dark blue*

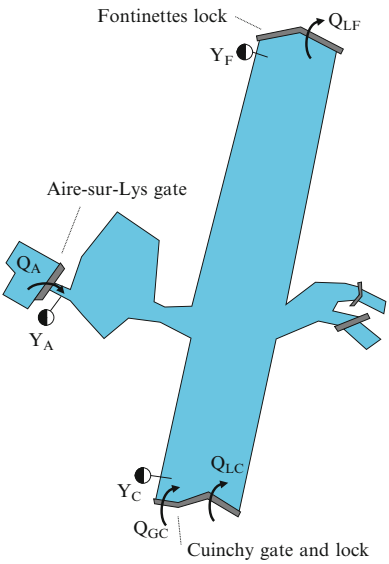

Fig. 12.5 The Cuninchy-Fontinettes reach, Q_{LC} is the discharge of lock Cuinchy, Q_{GC} is the discharge of the gate of Cuinchy, Q_A is the discharge of the gate of Aire and Q_F is the discharge of lock Fontinettes. Y indicates the corresponding water levels

Table 12.1 Physical data of the CFR

Length (m)	Width (m)	Depth (m)	Manning's c. (-)	Discharge (m^3/s)
42,300	52	3.8	0.035	0.6

At Aire-sur-la-Lys there is the confluence of the river Lys divided by a sluice gate from the CFR. The CFR is approximately 52 m wide, it is entirely artificial without considerable slope. The CFR is perpendicular to the natural runoff of the watersheds. The geometry of the reach and the chosen steady state regime for linearization are summarized in Table 12.1.

The lock of Cuinchy overcomes a difference of 2 m between the upstream and downstream water levels, its volume is 3,700 m^3. The maximum discharge that supplies or empties the lock chamber is 11 m^3/s. The lock of Fontinettes has several

times bigger volume, 25,000 m^3, as it overcomes 13 m of water level difference. The maximum discharge it supplies is 28 m^3/s. When a lock is operated the chamber is supplied from the upstream reach and emptied downstream. Hence the operation of lock Cuinchy supplies the CFR with water and the operation of Fontinettes empties it.

The main control objective is to ensure navigation, that is maintain the water level in a range around the Normal Navigation Level (NNL). In case of the CFR, it is NNL=19.52 m NGF (Nivellement Général de la France, i.e., altitude landmark in France). When lock operations occur, in order to maintain the NNL hydraulic structures are operated to counterbalance the effect of the lock operation to the water level. These structures are remotely controlled, usually manually, using the water level and discharge measurements.

There are three locations with control structures in the CFR (Fig. 12.5):

- At Cuinchy: a lock and a gate which are located side by side,
- At Aire-sur-la-Lys: the gate called Porte de Garde,
- At Fontinettes: a lock.

The water level fluctuation is basically caused by the lock operations. Figure 12.6 shows the measured water levels at the lock of Cuinchy and at the lock of Fontinettes and at Aire. Though the time of the lock operations was not documented, there can be seen several drops of more than 20 cm in the water level for example at 15 min, at 2.5 h, at 3.25h and at 4 h. This valleys might be caused by the operation of lock Fontinettes. With gray dashed lines the minimum of the future navigation range is shown. It can be seen that the water level crosses several times the water level limit assigned for the future. Therefore, the control of water level should be

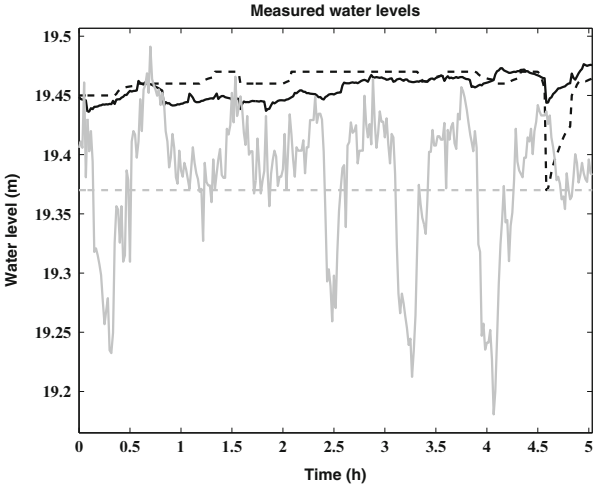

Fig. 12.6 Measured water levels; Cuinchy: *black dashed line*, Aire: *black continuous line*, Fontinettes: *gray continuous line*

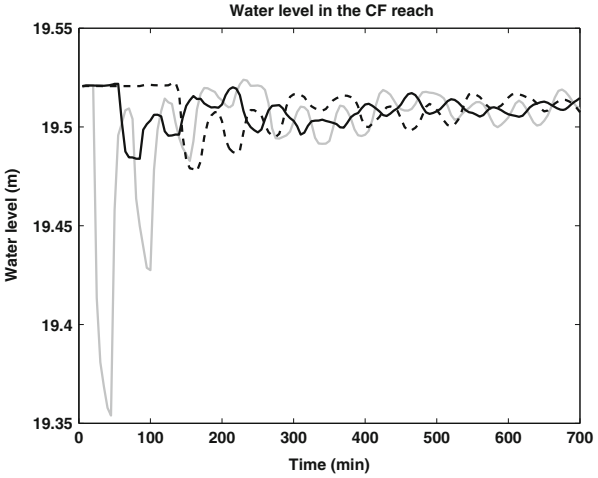

Fig. 12.7 Simulation of one lock operation of Fontinettes; Cuinchy: *black dashed line*, Aire: *black continuous line*, Fontinettes: *gray continuous line*

improved. A wave caused by a lock operation can travel back and forth between the upstream and downstream locks several times before it attenuates; this is seen by the smaller secondary valleys coming back in approximately 4 h after a lock operation ("big valley"). Figure 12.7 shows the water levels after only one lock operation of Fontinettes (numerical simulation). It can be seen that after the first drop of 17 cm the negative wave comes back in 4 h and causes a drop of 10 cm, and in every 4 h causing consecutive drops in the water level at Fontinettes (with gray). The drops can be seen in the other water levels measured at Cuinchy and Aire—at Cuinchy (with black) the negative wave appears after 2 h, this is the time delay of the system. This phenomenon is called resonance and it is first described in [41] and [45], and later studied in depth in [48] and [47].

These waves without control can cause the water levels go out of the allowed range of navigation. In order to maintain the reach in a condition to be possible to navigate the lock operations should be changed or the hydraulic structures should be operated in a way to counterbalance the act of the waves generated by the locks. In this work the second option is addressed with the help of MPC. By implementing an MPC controller to the hydraulic structures and controlling the water supply of the navigation reach it could be possible to maintain the water levels within the navigation range.

12.3.1 Application of the IDZ Model to the CFR

The CFR system has two inputs (flows) and three outputs (water levels). Also, there are two disturbance flows (lock operations), that are not modeled in this case. As it is shown in Fig. 12.5 the water levels are measured and to be controlled at

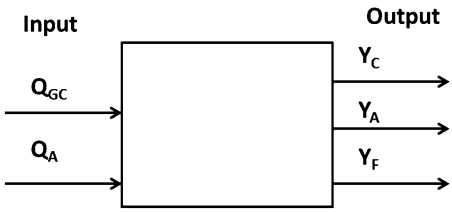

Fig. 12.8 The schematics of the CFR system

three locations: at upstream—at Cuinchy (Y_C), in the middle of the reach—at Aire (Y_A) and at downstream—at Fontinettes (Y_F). These water levels are disturbed by the lock operations upstream by the lock Cuincy—Q_{LC} and downstream by lock Fontinettes (Q_{LF}). These lock operations are unknown to the controller.

If both locks are operated in the same frequency a considerable amount of water is removed from the system since the volume of the lock of Fontinettes is five times bigger than the volume of the lock of Cuinchy. In order to maintain the water level the water volume should be added. It is possible from two control points: upstream, from the gate of Cuinchy (Q_{GC}) and in the middle of the reach, from the gate of Aire (Q_A). Both of these flows have physical constraints: at Cuinchy the maximum flow is $10\,\mathrm{m}^3/\mathrm{s}$ and no negative flow is possible, while at Aire the flow can fluctuate between -7 and $+7\,\mathrm{m}^3/\mathrm{s}$. MPC can handle very well such constrained systems. Each transfer function of the CFR system is modelled by the IDZ model. The scheme of the system is shown in Fig. 12.8. There are three controlled water levels and two control inputs. In order to control these water levels, they should be expressed in terms of the inputs. As both of the inputs are affecting the three controlled outputs, altogether we need to find six transfer functions. All transfer functions are obtained by linearization around an equilibrium point: $Q_A^0 = 0.6\,\mathrm{m}^3/\mathrm{s}$, $Q_{GC}^0 = 0.6\,\mathrm{m}^3/\mathrm{s}$ and $Y_A^0 = Y_C^0 = Y_F^0 = NNL = 19.52\,\mathrm{m}$, that approximation corresponds to a water depth (H) of 3.8 m all around the reach due to the zero slope (see also in Table 12.1). The transfer function of the linearized system is then can be described by a matrix containing six transfer functions:

$$G_{CFR} = \begin{pmatrix} G_{CC} & G_{AC} \\ G_{CA} & G_{AA} \\ G_{CF} & G_{AF} \end{pmatrix}, \tag{12.8}$$

where transfer functions $G_{CC}, G_{AC}, G_{CA}, G_{AA}, G_{CF}, G_{AF}$ have the IDZ structure as in (12.6). The values of the parameters are summarized in Table 12.2.

12.3.2 Controller Development

MPC was developed based on [9] and [45]. The detailed controller development can be found in [23]. Below we follow the presentation of [23]. That is, the

Table 12.2 Properties of the three reaches

Name	Backwater surface (m^2)	τ (s)	p_1 (-)
G_{CC}	1,492 $\times 10^3$	0	9,401
G_{AC}	1,492 $\times 10^3$	4,703	4,618
G_{CA}	1,492 $\times 10^3$	4,698	4,618
G_{AA}	1,492 $\times 10^3$	0	9,238
G_{CF}	2,100 $\times 10^3$	6,925	6,749
G_{AF}	707 $\times 10^3$	2,226	2,209

control objective is to keep the outputs (Y_C, Y_A and Y_F) close to set-point, while disturbances occur (Q_{LC} and Q_{LF}). This is achieved by controlling the two inputs (Q_{GC} and Q_A), while ensuring that the discharge and Cuinchy and Aire satisfy the physical flow constraints of the system (12.9) and (12.10):

$$0 \leq Q_{GC}(t) \leq 10\,(\mathrm{m}^3/\mathrm{s}) \tag{12.9}$$

and

$$-7 \leq Q_A(t) \leq 7 \quad (\mathrm{m}^3/\mathrm{s}). \tag{12.10}$$

for all $t \in [0, +\infty)$. The transfer function presented in Sect. 12.2 expresses the relation between the water level and the input/output discharges. In order to be able to apply MPC, we carried out the following steps:

1. We transform the continuous-time transfer function from (12.8) to a discrete-time one for discrete time controller development.
2. Instead of using the upstream discharge as input, we use the *change of the discharge* as control input. This is incorporated into the discrete-time transfer functions by composing it with an integrator. The reason for the change is that it is easier to express the MPC cost function for this new input than for the original one, with other words the change is discharge can directly be penalized.
3. We compute the minimal state-space representation of the thus obtained discrete-time transfer function.
4. Since MPC yields a state feedback, while the full state of the system is not measurable, we constructed an observer. The controller is then obtained by combining the state feedback provided by MPC with this observer.

The controller is tested by simulating its interconnection with a detailed nonlinear model of the plant. The plant model was implemented in SIC (Simulation of Irrigation Canals) [31]. The model is based on Saint-Venant equations, and it is widely accepted as a fairly accurate representation of physical reality. In particular, it models several non-linear phenomena like advection which are ignored by IDZ type models.

Below we describe the steps mentioned above one by one.

Sampling the Linearized Model

The transfer function G_{CFR} is transformed to a discrete-time transfer function G^d_{CFR} using the zero order hold with sampling time $T_s = 300\,\mathrm{s}$. Hence, if we define the discrete time signals $e(k) = E(kT_s)$ and $Q^d(k) = Q(kT_s)$, $k = 0, 1, 2, \ldots$ and we denote their z-transforms by $\hat{e}$ and $\hat{Q}^d$, respectively, then

$$\hat{e} = G^d_{CFR}\hat{Q}^d \tag{12.11}$$

holds, where $\hat{e}$ denotes the z-transform of the discrete-time signal e and $\hat{Q}^d$ denotes the z-transform of the discrete-time signal $\hat{Q}^d$.

Setting the Rate of Change of the Discharge as Input

The discrete-time transfer functions are multiplied by an integrator $\frac{1}{z-1}$, i.e., we define the transfer matrix

$$H(z) = G^d_{FCR}(z)\frac{1}{z-1}. \tag{12.12}$$

This is done in order to be able to use the differences between discharges as inputs, as opposed to the discharge. That is, the control input used for MPC control synthesis is the discrete-time signal u, with $u(0) = 0$ and

$$u(k) = Q^d(k) - Q^d(k-1).$$

It then follows that with the transfer function $H(z)$ from (12.12), $\hat{e} = H\hat{u}$, where $\hat{u}, \hat{e}$ denote the z-transforms of u and e respectively.

Constructing a State-Space Model

Using standard MATLAB functions, we compute a minimal state-space representation

$$\begin{aligned} x(k+1) &= Ax(k) + Bu(k), \\ e(k) &= Cx(k), \end{aligned} \tag{12.13}$$

of the transfer matrix H. In order to formalize the physical constraints on $Q^d(k)$, we extend the state-space of (12.13) by a new state which represents Q^d. The resulting model is as follows:

$$\begin{aligned} z(k+1) &= \tilde{A}z(k) + \tilde{B}u(k), \\ e(k) &= \tilde{C}z(k), \end{aligned} \tag{12.14}$$

where $z(k) = \left[x^T(k),\ Q^d(k)\right]^T$ and

$$\tilde{A} = \begin{bmatrix} A & 0 \\ 0 & I_2 \end{bmatrix} \quad \tilde{B} = \begin{bmatrix} B \\ I_2 \end{bmatrix},$$
$$\tilde{C} = \begin{bmatrix} C & 0 \end{bmatrix},$$

where I_2 denotes the 2×2 identity matrix.

MPC State Feedback

In order to compute the control law, we use MPC, applied to the state-space representation (12.14). The resulting state feedback $u(k) = w(z(k))$. The map w is obtained as follows. Set $\lambda = 40$ and define the matrices $R = 40.000 I_2$ and $P = 40.000 I_3$, where I_2 and I_3 are the 2×2 and 3×3 identity matrices. The matrices R and P are weights, and λ is the prediction horizon. Define

$$w(z) = u^*(k \mid k), \tag{12.15}$$

where $u^* = (u^*(k \mid k), u^*(k+1 \mid k), \ldots, u^*(k+\lambda-1 \mid k))$ is the solution of the following constrained optimization problem:

$$\begin{aligned} &\min_{u=(u(k|k),u(k+1|k),\ldots,u(k+\lambda-1|k))\in\mathbb{R}^{2\lambda}} J(z,u) \\ &J(z,u) = \sum_{j=1}^{\lambda} e\,(k+j\,|k\,)^T\, Pe\,(k+j\,|k\,) \\ &\qquad + \sum_{j=0}^{\lambda-1} u\,(k+j\,|k\,)^T\, Ru\,(k+j\,|k\,), \\ &\text{subject to the following constraints:} \\ &z(k \mid k) = z, \\ &\forall j = 1, \ldots, \lambda : \\ &z(k+j+1 \mid k) = \hat{A}z(k+j \mid k) + \hat{B}u(k+j \mid k), \\ &e(k+j \mid k) = \hat{C}z(k+j \mid k), \\ &0 \le z_{n+1}(k+j \mid k) \le 10, \\ &-7 \le z_{n+2}(k+j \mid k) \le 7. \end{aligned} \tag{12.16}$$

Here n denotes the size of the state-space of (12.13), and $z_i(k+j \mid k)$ denote the ith entry of $z(k+j \mid k)$. The inequalities (12.9)–(12.10) represent physical constraints on the inputs.

In order to solve this optimization problem, we used the built in MATLAB function [33].

Constructing the Observer

Applying MPC to (12.14) requires the knowledge of the full state $z(k)$ at every step k. However, in practice, the full state is not measured. To address this problem, we used an observer to estimate the state $z(k)$. Since the component $Q^d(k)$ is clearly observable, we used the following reduced order observer

$$\begin{aligned} \hat{x}(k+1) &= A\hat{x}(k) + Bu(k) + L(e(k) - C\hat{x}(k)), \quad \hat{x}(0) = 0, \\ \hat{Q}^d(k+1) &= \hat{Q}^d(k) + u(k), \quad \hat{Q}_d(0) = 0, \end{aligned} \tag{12.17}$$

where the matrices A,B,C are the same as in (12.13) and L is computed as according to synthesis algorithms for minimax observers [10, 20, 25]. More precisely, we consider a noisy state-space representation

$$\begin{aligned} x(k+1) &= Ax(k) + Bu(k) + \eta(k) \\ e(k) &= Cx(k) + \nu(k), \end{aligned} \tag{12.18}$$

where η and ν are deterministic noise processes satisfying

$$\sum_{k=0}^{\infty} (\eta^T(k) W_1 \eta(k) + \nu^T(k) W_2 \nu(k)) \leq 1, \tag{12.19}$$

with $W_1 = (1,000 I_n + 5,000 e_1 e_1^T)^{-1}$, $W_2 = I_3$, n is the dimension of the state-space of (12.13), I_n,I_2 are the $n \times n$ and 2×2 identity matrices, $e_1 = (1, 0, \ldots, 0)^T \in \mathbb{R}^n$. The matrices W_1 and W_2 represent our assumptions on the energy of the disturbances η and ν. The larger these matrices are, the smaller the assumed energy of the disturbance. A minimax observer for (12.18) is a system of the form

$$\hat{x}(k+1) = A\hat{x}(k) + Bu(k) + L(e(k) - C\hat{x}(k)), \tag{12.20}$$

such that the worst case estimation error $\limsup_{k\to\infty} \sup_{\nu,\eta} |l^T(x(k) - \hat{x}(k))|$ is minimal for any vector $l \in \mathbb{R}^n$, where the supremum is taken over all signals ν and η which satisfy (12.19). The gain matrix L is obtained following [10, 20, 25]. That is, we consider the dual LQR control problem

$$\begin{aligned} &\min_{v} \sum_{k=0}^{\infty} (s(k)^T W_1^{-1} s(k) + v^T(k) W_2^{-1} v(k)) \\ &s(k+1) = A^T s(k) + C^T v(k). \end{aligned} \tag{12.21}$$

Note that due to minimality of (12.13), (C, A) is an observable pair, and hence (A^T, C^T) is a controllable pair. From this it then follows that the LQR control problem (12.21) has a solution of the form $v = -Ks$. In addition, the matrix $(A^T - C^T K)$ of the close-loop system is stable. We then set $L = K^T$ to be the gain of the minimax observer (12.20).

Note that if the linear model H had been accurate and the disturbances had not been significant, then any choice of L such that $(A - LC)$ is stable could have been considered. In fact, we tried to use pole placement to obtain such an L. However, when interconnected with the nonlinear numerical model of the system, the observers obtained in such a way showed worse performance than the minimax observer. This is probably due to the fact that our model is just a crude approximation of the underlying physical process, moreover, it does not explicitly include all the disturbances which act on the system.

Control Architecture

The MPC controller is connected with the observer (12.17): when computing the next control input $u(k)$, the estimates $\hat{x}(k)$ and $\hat{Q}^d(k)$ of the observer (12.17) were used instead of $z(k)$. Due to our modeling choices, the true control input which is ought to be applied to the physical system is not $u(k)$, but $Q^d(k) + Q^0$, where $Q^0 = (Q^0_{GC}, Q^0_A) = (0.6, 0.6)^T$ is the stead-state input corresponding the set point $(NNL, NNL, NNL)^T$. Likewise, the actual measurements are the values $Y_C(kT_s)$, $Y_A(kT_s)$ and $Y_F(sT_s)$, not the error signal $e(k)$. The latter can be obtained from the former by subtracting the value of NNL.

To sum up, if we denote by

$$y(k) = \left[Y_C(kT_s),\ Y_A(kT_s)\ Y_F(kT_s)\right]^T \quad \forall k = 0, 1, \ldots$$

the sampled measurement signals, then the equations of the controller can be summarized as follows:

$$\begin{aligned} e(k) &= y(k) - \left[NNL,\ NNL,\ NNL\right], \\ u(k) &= w(\left[\hat{x}^T(k)\ \hat{Q}^d(k)\right]^T), \\ \hat{x}(k+1) &= A\hat{x}(k) + Bu(k) + L(e(k) - C\hat{x}(k))\ \ \hat{x}(0) = 0, \\ \hat{Q}^d(k+1) &= \hat{Q}^d(k) + u(k)\ \ \hat{Q}_d(0) = 0, \\ Q^d(k) &= \hat{Q}^d(k) + u(k) + Q^0, \end{aligned} \tag{12.22}$$

where w is the same as define in (12.15), the gain L is as in (12.17), the matrices A, B, C are from (12.13).

Evaluation of the Performance

The performance of the controller is evaluated as follows. The controller (with partial observations) was tested by connecting it with the nonlinear model of SIC and carrying out simulations. Note that SIC simulates the behavior of the system in continuous time, so we had to perform time sampling of the output and input signals: while performing the simulation, $y(k)$ was set to be the output of the simulation at the kth sampling time, and the control input was taken to be constant between the sampling times.

12.4 Results and Discussion

The developed controllers are tested on a numerical model, solving the complete set of non-linear Saint-Venant equations using a finite differences scheme. The solution is implemented by the SIC software. The controllers are developed in Matlab [33] environment. The SIC calls the control algorithm and sends the measurements to it at control time step and executes its commands.

The MPC is tested using the following scenario: 20 lock operations of lock of Cuinchy and lock of Fontinettes (Fig. 12.9). This is more difficult than the actual scenario: nowadays there is navigation only during the day. However, the future

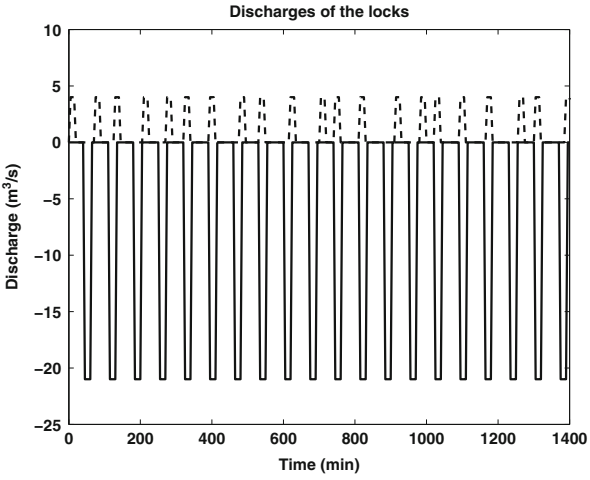

Fig. 12.9 The discharges of the lock operations during a day with 20 min operations, *dashed line* lock Cuinchy with *black line* Fontinettes

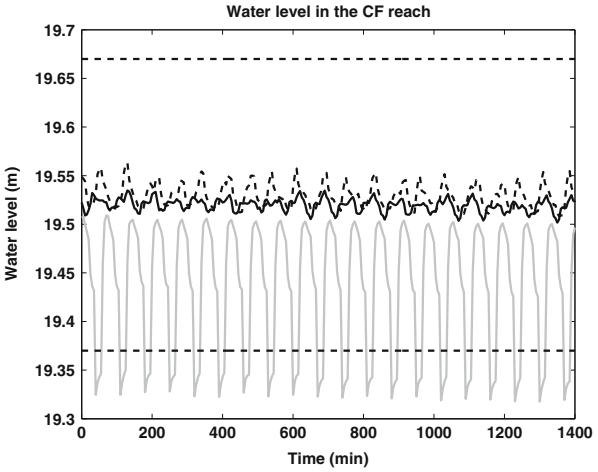

Fig. 12.10 Simulation of 20 lock operations of Fontinettes and Cuinchy: Cuinchy: *black dashed line*, Aire: *black continuous line*, Fontinettes: *gray continuous line*

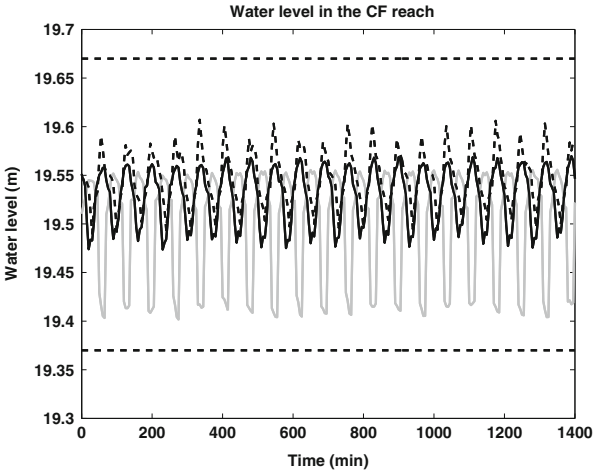

Fig. 12.11 Controlled levels with MPC, with *gray*: Fontinettes, with *black*: Aire and with *dashed line* Cuinchy, *horizontal dashed black line*: sea-worthiness condition

plan of the management is to extend the navigation period. The water levels resulting from the lock operations without using any control action (constant input discharges at the gate of Cuinchy and gate of Aire) are shown in Fig. 12.10. It can be seen that the water levels are not kept in the allowed range for navigation.

For the same scenario MPC is applied. Figure 12.11 shows that all the three water levels are within the navigation range, thus the controller accomplished its objective.

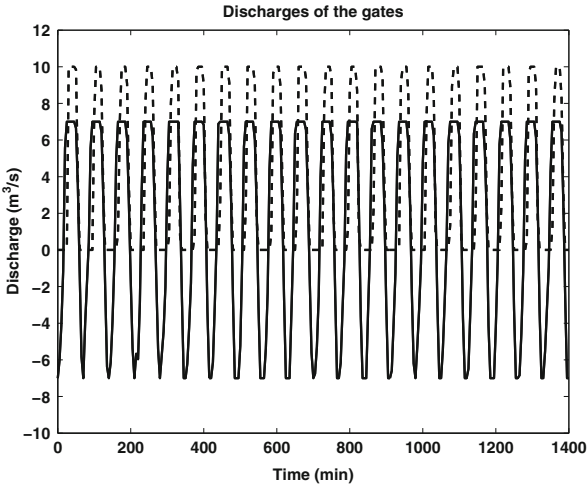

Fig. 12.12 The control flows with MPC, *black line*: gate of Aire, *dashed line*: gate of Cuinchy

Figure 12.12 shows the control actions. It is seen that the control flow at Cuinchy is between 0 and $10\,m^3/s$ and the control flow of Aire fluctuates between $-7\,m^3/s$ and $+7\,m^3/s$. Both of them are in the allowed range. The fluctuation might seem high frequency leading to wear and tear, however, in fact the time of one gate opening or closing is 25 min. The operations are needed to maintain the water levels. A compromise might be found between the extent of the movement of the hydraulic structures and the desired water level difference between the actual and the desired one.

12.5 Linking Transport of and Transport over Water

Large and small scale water transport models are introduced above. In a navigation reach, the transport of water, both the inputs and the outputs, are completely controlled. The quantity of the runoff arriving directly is often smaller compared to the water released the lock operations. Hence, therefore all main inputs are locks and the tributaries: connected by hydraulic structures and the operation of the locks. The main transport of water is hence determined by the navigation: by the operation of the locks. The other inputs and outputs are controlled in a way to maintain constant volume (that is constant water level). The more lock operations are carried out per day the bigger amount of water has to be transported by the canal reach. However, in case of risk of flood the safety, i.e., flood protection overrules the navigation goals. In this case water is transported, distributed through the system in order to avoid the flood in the cities located near to canal reaches. The nearby river can be evacuated into the navigation canal, and the flood wave can be sent to the sea. In this case the lock operation and hence the traffic is restricted.

The transport over water in this work is presented by the lock operations. The number of daily lock operations correspond to the daily transport of boats. In one lock operation one or two boats can go simultaneously. When a boat is crossing the reach it involves two lock operations: upstream, that results in an increase (for Cuinchy it is 3,700 m^3) of water volume and the downstream operation that results in an offtake (for Fontinettes it is 25,000 m^3). Due to the difference between these volumes any pair of lock operations should be compensated by additional inflows in order to keep the water level constant.

Due to the above described two directional connection between transport of and over water the only way to study the system is the combined framework.

A global modeling and optimization of the operation of the system is beneficial for both the water body (for the cities around this area) and for the users of the canal for transport.

Better global management improves the flood protection of the area. With the help of a global model in case of flood, the flood wave can be distributed in the system and the flooding of the neighboring cities can be avoided. With a better flood protocol and faster response to the floods also the navigation period can be extended.

By better management and control of the water level more lock operations can be carried out while the water level is maintained around NNL. More lock operations allow bigger traffic, that is economical benefit for the operators and also a general ecological benefit as more overland traffic is diverted to navigation.

12.6 Open Topics and Possible Future Research Lines

The developed MPC can be improved by modeling directly the resonance phenomenon [21, 49]. In this way the controller can directly act on the resonance waves and this might improve the performance. Another possibility to improve the controller performance is to treat the lock operations as known disturbances. That is, if the schedule of the lock operations is known beforehand the controller can act in advance.

By modeling the lock operation the transport is modeled. However, the direct quantitative benefit from the increase of the transport is not modeled yet. Similar models are published [6] for general cases. The cost of lock operations, pumping and the benefit from the transport can be modeled. With the help of this model the effects of the climate change can be directly quantified with relation to the navigation system. Similar calculations have been carried out in the project ECCONET [6].

Extending further this line, the cost of each lock operation can be determined based on the economic model. The constantly changing prices and conditions can also be communicated on-line to the stake holders as an addition to the already existing on-line communication about the state of the network and the water levels [43].

Next to the economic perspective the ecologic aspect can also be investigated. Though the navigation network is manly artificial water body, its operation affects

the environment and the nearby (confluences) natural water bodies. The effect of the increasing transport to the water quality of the tributaries and to the surrounding flora and fauna can be studied.

As started in this work, the fault detection study can be extended. Not only sensor but also actuator faults should be easily detected. Also the resilience of the system to faults should be investigated and backup plans for sensor faults should be developed.

12.7 Conclusions and Future Research

The management of navigation canal system can highly benefit of ICT. In order to accomplish the multi-objective goals large and small scale optimization can be applied. Dynamic models can be built being able to predict the reaction of the system of the changes in the future either in operation of the system or of changes of external factors, like climate change. In this work a navigation reach is modelled and based on that MPC is developed to control the water levels in order to keep the water levels in a range to allow navigation. A global volume model of the system is introduced in order to be predict the effects of the long term changes. For different purposes different scale models can be used. Finally by connecting the multi-level models a global model for global management optimization can be achieved. Further research is to include more factors in the optimization like ecology and economy. By modeling the transport (the boats and the lock operation) a model for transport over water can be obtained. By linking the two models, the economical factors can be more directly modeled and predicted.

Acknowledgements This work is a contribution to the GEPET-Eau project which is granted by the French ministry MEDDE—GICC, the French institution ORNERC and the DGITM.

References

1. Almaz OA, Altiok T. Simulation modeling of the vessel traffic in Delaware River: Impact of deepening on port performance. Simul Model Pract Theory. 2012;22:146–165.
2. Amin S, Litrico X, Sastry S, Bayen AM. Cyber security of water SCADA systems - Part I: Analysis and experimentation of stealthy deception attacks. IEEE Trans Control Syst Technol. 2013;21(5):1963–1970.
3. Arkell BP, Darch GJC. Impact of climate change on London's transport network. Proc ICE Munic Eng. 2006;159(4):231–237.
4. Blesa J,Duviella E, Sayed-Mouchaweh M, Puig V, Chuquet K. Automatic control to improve the seaworthiness conditions in inland navigation networks. J Marit Res. 2012;9(3):61–66.
5. Boé J, Terray L, Martin E, Habets F. Projected changes in components of the hydrological cycle in French river basins during the 21st century. Water Resour Res. 2009;45(8):231–237.
6. Breemersch T, Heyndrickx C (2012) Effects of climate change on inland waterway transport networks. In: Second Nordic international conference on climate change adaptation, Helsinki, August 2012.

7. Brooke J, White I. Climate change mitigation and adaptation. implications for inland waterways in England and Wales. Technical report, Inland Waterways Advisory Council, 2009.
8. Bugarski V, Bačkalić T, Kuzmanov U. Fuzzy decision support system for ship lock control. Expert Syst Appl 2013;40(10):3953–3960.
9. Camacho EF, Bordons Alba C. Model predictive control. London: Springer; 1998.
10. Cernusko FL. State estimation for dynamic systems. Boca Raton: CRC Press; 1994.
11. Davies EGR, Simonovic SP. Global water resources modeling with an integrated model of the social–economic–environmental system. Adv Water Res. 2011;34(6):684–700.
12. Ducharne A, Habets F, Pagé C, Sauquet E, Viennot P, Déqué M, Gascoin S, Hachour A, Martin E, Oudin L. Climate change impacts on water resources and hydrological extremes in northern France. In: Proceedings of XVIII international conference on water resources, Barcelona; 2010.
13. Duviella E. The GEPET-Eau project http://gepeteau.wordpress.com/bcf/. http://gepeteau.wordpress.com/bcf/, January 2014.
14. Duviella E, Blesa J, Bako L, Bolea Y, Sayed-Mouchaweh M, Puig V, Chuquet K. Inland navigation channel model: Application to the Cuinchy-Fontinettes reach. In: The 10th IEEE international conference on networking, sensing and control, Paris, 10–12 April 2013.
15. Duviella E, Rajaoarisoa L, Blesa J, Chuquet K. Adaptive and predictive control architecture of inland navigation networks in a global change context: application to the Cuinchy-Fontinettes reach. In: IFAC conference on manufacturing modelling, management, and control, Saint Petersburg, 19–21 June 19–21.
16. European Parliament and Council of the European Union. Directive 2005/44/EC, 2005.
17. Fastenbauer M, Sattler M, Schilk G. River information services for commercial users in the inland waterway sector. In: LINDI 2007. International symposium on logistics and industrial informatics, 2007; 2007. pp. 31–36
18. García-Ruiz JM, López-Moreno JI, Vicente-Serrano SM, Lasanta-Martínez T, Beguería S. Mediterranean water resources in a global change scenario. Earth Sci Rev. 2011;105(3–4):121–139.
19. Graveline N, Loubier S, Gleyses G, Rinaudo J-D. Impact of farming on water resources: Assessing uncertainty with monte carlo simulations in a global change context. Agric Syst. 2012;108:29–41.
20. Green M, Limebeer DJN. Linear robust control. DoverPublications.com, 2012.
21. Horváth K. Model predictive control of resonance sensitive irrigation canals. PhD thesis, Technical University of Catalonia, Barcelona; 2013.
22. Horváth K, Duviella E, Blesa J, Rajaoarisoa L, Bolea Y, Puig V, Chuquet K. Gray-box model of inland navigation channel: Application to the Cuinchy-Fontinettes reach. J Intell Syst. 2014;23(2):183–199.
23. Horváth K, Petreczky M, Rajaoarisoa L, Duviella E, Chuquet K. MPC control of water level in a navigation canal the Cuinchy–Fontinettes case study. In: 13th European Control Conference (ECC), 2014.
24. Jonkeren O, Rietveld P, van Ommeren J, te Linde A. Climate change and economic consequences for inland waterway transport in europe. Reg Environ Change. 2013;14:953–965.
25. Krener AJ. Kalman-bucy and minimax filtering. IEEE Trans Autom Control. 1980;25(2):291–292
26. Le Pocher O, Duviella E, Bako L, Chuquet K. Sensor fault detection of a real undershot/overshot gate based on physical and nonlinear black-box models. In: SAFEPROCESS - 8th IFAC international symposium on fault detection, supervision and safety for technical purposes, Mexico City, 29–31 August 2012.
27. Le Pocher O, Duviella E, Chuquet K. Sensor fault detection in a real hydraulic system using classification approach. In: 11th International Conference on Informatics in Control, Automation and Robotics (ICINCO), Nordwijkerhout, 28–31 July 2011.
28. Litrico X, Fromion V. Analytical approximation of open-channel flow for controller design. App Math Model. 2004;28(7):677–695.

29. Litrico X, Fromion V. Simplified modeling of irrigation canals for controller design. J Irrig Drain Eng. 2004;130(5):373–383.
30. Litrico X, Georges D. Robust continuous-time and discrete-time flow control of a dam-river system. (i) modelling. Appl Math Model 1999;23(11):809–827.
31. Malaterre P-O, Baume JP. SIC 3.0, a simulation model for canal automation design. In: Mokhlisse A, editor. International workshop on regulation of irrigation canals: State of art of research and applications, vol. I. L.A.A.A.-C.N.R.S.; 1997. pp. 68–75.
32. Mallidis I, Dekker R, Vlachos D. The impact of greening on supply chain design and cost: a case for a developing region. J Transp Geogr. 2012;22:118–128.
33. MATLAB. version 7.10.0 (R2010a). Natick: The MathWorks Inc.; 2010.
34. Mihic S, Golusin M, Mihajlovic M. Policy and promotion of sustainable inland waterway transport in Europe – Danube River. Renew Sustain Energy Rev. 2011;15(4):1801–1809.
35. Millerd F. Global climate change and great lakes international shipping. Technical report, Wilfrid Laurier University, Waterloo, Ontario; 2007.
36. Murray SJ, Foster PN, Prentice IC. Future global water resources with respect to climate change and water withdrawals as estimated by a dynamic global vegetation model. J Hydrol. 2012;448–449:14–29.
37. Negenborn RR, van Overloop P-J, Keviczky T, De Schutter B. Distributed model predictive control of irrigation canals. Netw Heterog Media. 2009;4(2):359–380.
38. Ocampo-Martinez C. Model predictive control of wastewater systems. Advances in industrial control. London: Springer; 2010.
39. Puig V, Romera J, Quevedo J, Cardona CM, Salterain A, Ayesa E, Irizar I, Castro A, Lujan M, Charbonnaud P, Chiron P, Trouvat J-L. Optimal predictive control of water transport systems: Arrêt-Darré/Arros case study. Water Sci Technol. 2009;60(8):2125–2133.
40. Schuurmans J. Open-channel flow model approximation for controller design. Appl Math Model. 1995;19(9):525–530.
41. Schuurmans J. Control of water levels in open channels. PhD thesis, Delft University of Technology, Delft; 1997.
42. ten Broeke IAA, Willems CPM, Glansdorp CC. River information services: a joint European effort to enhance safety and usability of the inland waterway. In: Intelligent transportation systems, 2001. Proceedings. 2001 IEEE; 2001. pp. 1108–1115.
43. The Ministry of Ecology, Sustainable Development and Energy, France. Vigicrues : Information sur la vigilance “crues”. http://www.vigicrues.gouv.fr/, 1999.
44. M. Xu, P.J. van Overloop, N.C. van de Giesen, On the study of control effectiveness and computational efficiency of reduced Saint-Venant model in model predictive control of open channel flow. Adv Water Resour 2011;34(2):282–290.
45. van Overloop P-J. Model predictive control on open water systems. PhD thesis, Delft University of Technology, Delft; 2006.
46. van Overloop, P., Clemmens, A., Strand, R., Wagemaker, R., and Bautista, E. Real-time implementation of model predictive control on Maricopa-Stanfield irrigation and drainage district’s WM canal. J Irrig Drain Eng. 2010;136(11):747–756.
47. van Overloop P-J, Bombois X. Identification of properties of open water channels for controller design. In: Proceedings of the 16th IFAC symposium on system identification; 2012. pp. 1019–1024.
48. van Overloop P-J, Miltenburg IJ, Bombois X, Clemmens AJ, Strand R, van de Giesen N. Identification of resonance waves in open water channels. Control Eng Pract. 2010;18(8):863–872.
49. van Overloop P-J, Negenborn RR, De Schutter B, van de Giesen NC. Predictive control for national water flow optimization in The Netherlands. In: Negenborn RR, Lukszo Z, Hellendoorn H, editors. Intelligent infrastructures. Intelligent systems, control and automation: Science and engineering, chapter 17, vol. 42. Dordrecht: Springer; 2010. pp. 439–461.

50. van Overloop P-J, Weijs S, Dijkstra S. Multiple model predictive control on a drainage canal system. Control Eng Pract. 2008;16(5):531–540.
51. Wang S, Kang S, Zhang L, Li F. Modelling hydrological response to different land-use and climate change scenarios in the Zamu River basin of northwest China. Hydrol Process. 2008;22(14):2502–2510.
52. White I. Report for the inland waterways advisory council information and communication technology for the UK's inland waterways. Technical Report MSU-CSE-00-2, Inland Waterways Advisory Council Information and Communication Technology, 2008.

Chapter 13
Effects of Water Flow on Energy Consumption and Travel Times of Micro-Ferries for Energy-Efficient Transport over Water

M. Burger and B. De Schutter

Abstract Controlling the transport *of* water by adjusting water flows in rivers and canals, inevitably will have an effect on the transport *over* water by vessels as well. We will discuss the effect of flowing water on scheduling micro-ferries (small autonomous water-taxis) using the least amount of energy, while aiming at satisfying customer demands with respect to pick-up times. This trade-off will be made by optimizing the assignment of micro-ferries to customers in a specific order, and by searching for the best travel speeds.

The interplay between controlling transport of water and scheduling transport over water will become clear by the explicit relation between the speed of the water (influenced by water management) on travel times and energy consumption, derived in this chapter. It is shown that on average the travel times (and thereby the energy consumption) will increase with increasing magnitudes of the current. Hence, decisions made on water management have a direct effect on the performance of the transport system, and the interests of both parties should be taken into account to obtain a well-functioning water transport system.

13.1 Introduction

In this chapter the problem of scheduling pick-ups and deliveries of people with water-taxis is discussed, where—besides the common issue of scheduling within time-windows—we take into account varying speeds of vessels and water flows and their effects on travel times and energy consumption. As such it is a problem involving *transport over water* (of people using water-taxis) when influenced by *transport of water* (via varying speeds of the water flows).

M. Burger (✉)
TBA, Delft, The Netherlands
e-mail: mernout.burger@tba.nl

B. De Schutter
Delft University of Technology, Delft, The Netherlands
e-mail: b.deschutter@tudelft.nl

C. Ocampo-Martinez, R.R. Negenborn (eds.), *Transport of Water versus Transport over Water*, Operations Research/Computer Science Interfaces Series 58,
DOI 10.1007/978-3-319-16133-4_13

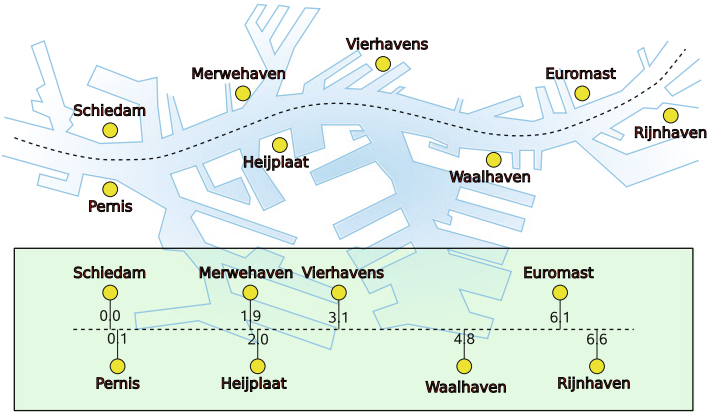

Fig. 13.1 The micro-ferry scheduling problem for the Rotterdam harbor: find an energy-efficient schedule for transporting people between stations along the river. The distances (km) of the stations along the river are indicated in the lower plot

13.1.1 Micro-Ferry Scheduling

We consider the transport of people using small, autonomous water-taxis that travel between several stations along a river in a city. These water-taxis will pickup customers on-demand, and are envisioned to be powered electrically to reduce emissions and noise (although fuel tanks or a hybrid system could also be used). There is a fixed number of stations (see Fig. 13.1) where customers can (dis)embark the vessels and where the batteries can be charged. We will refer to this kind of water-taxi as *micro-ferries*.

Work Related to the Micro-Ferry Scheduling Problem

The problem consists in finding a route for each individual micro-ferry that ensures that each transport request is handled at minimum cost, similar to the (multi-depot) *traveling salesman problem* [2, 14]. Often, variants of the traveling salesman problem—such as the *vehicle routing problem* [13, 18] and the *pick-up and delivery problem* [16]—are concerned with minimizing the travel time or distance. However, these problems do not take into account that the vehicles will have a limited driving range, and hence they might need to charge in between jobs.

Recently, some papers have appeared on energy consumption within scheduling problems. An extension to the vehicle routing problem with (constant speeds and) energy consumption (defined as the multiplication of the vehicle load and the travel distance) is presented in [12]. In the *pollution routing problem* [1] a trade-off is made between minimizing travel distances, travel times, transport costs, and greenhouse emissions. The emissions are related to the energy consumption, which is dependent

on both the speed and the load of a vehicle. A vehicle routing problem with fuel cost minimization is proposed in [19], where the fuel costs are defined as the product of unit fuel costs, fuel consumption rates, and road lengths.

Previous Results on Micro-Ferry Scheduling by the Authors

The *micro-ferry scheduling problem* consists in finding routes that minimize the total *energy consumption*, while satisfying the desired pick-up times as much as possible by using *soft time windows* [8]. By considering the *vehicle speeds* as optimization variables, both the energy consumption and travel times will be variable.

Since reducing the energy consumption is our main focus, the vessels should be light-weight (i.e., a small vehicle load) and hence the batteries (or fuel tanks) shall be small. Therefore, recharging of the batteries (or alternatively refueling of the tank) will be needed during operation. These *recharging times* therefore take a non-negligible amount of time with respect to the travel times, and we took them into account in the scheduling problem in [7].

The energy consumption will be a non-linear function of the vehicle speed, but a (computationally faster) linear function can be used by approximating the energy consumption by a piece-wise affine function.[1] This approach was used in the above-mentioned work, but due to the extra decision variables that were needed to formulate the piece-wise affine functions, only very small (in terms of fleet size and number of requests) problems could be solved efficiently. Exploiting the fact that the non-linear energy consumption function is *convex*, we proposed an alternative formulation of the *function approximation using linear constraints* only [6]. This modeling method greatly reduced the computation times.

For calm water the discussed work would be sufficient, but for *flowing water* one cannot use the same formulations any more. Both the energy consumption and travel times are dependent on the speed of the flowing water; disregarding this fact could result in schedules where micro-ferries run out of energy while transporting customers, and the calculated pick-up times would become incorrect. While the first side-effect is obviously worse than the second, both can be seen as a degradation of the service. To ensure correct pick-up times and to avoid empty batteries a reformulation of the micro-ferry scheduling problem for flowing water was presented in [5]. Since both the pick-up times and the energy consumption are non-linear functions in both the vehicle speed and the water flow speed, it was decided to consider the vehicle speed as a constant in that work to reduce the complexity.

[1] Actually in [6] we showed that the energy consumption is linear in the speed u and pace w (the reciprocal of speed [10]), and there we approximated the function $u = \frac{1}{w}$ by a piece-wise affine function.

13.1.2 Contributions

This chapter will consist of a complete overview of the previous results discussed above, extended with the introduction of *variable speeds for flowing water*. The theoretical results will be provided first, followed by a discussion of the modeling aspects of the micro-ferry scheduling problem.

Theory

The micro-ferry scheduling problem can be seen as an extension of the *multi-depot vehicle routing problem*, where the addition of variable speeds and environmental disturbances results in *convex constraints*. To the best of our knowledge, the authors' work has introduced two topics into the field of operations research, namely

- **reformulation**: modeling of the multi-depot traveling salesmen/vehicle routing problem using the same amount of decision variables as the single-depot variants
- **disturbances**: inclusion of environmental disturbances (e.g., water flows or wind) in scheduling problems

Reformulation of Multi-Depot Traveling Salesman Problems

The multi-depot traveling salesman problem (and its variants) can be stated using the following mixed-integer linear program with 3-index binary variables [2, 18]:

$$\min \quad \sum_{i\in\mathcal{R}}\sum_{j\in\mathcal{R}}\sum_{k\in\mathcal{M}} \mathrm{c}_{ij}\, x_{ijk} \tag{13.1}$$

$$\text{s.t.} \quad \sum_{j\in\mathcal{R}}\sum_{k\in\mathcal{M}} x_{ijk} = 1, \qquad \sum_{h\in\mathcal{R}}\sum_{k\in\mathcal{M}} x_{hik} = 1 \quad \forall\, i \in \mathcal{R} \tag{13.2}$$

$$\{\textit{subtour elimination constraints}\}, \tag{13.3}$$

where $\mathcal{M} = \{1, \ldots, \mathrm{M}\}$ denotes the set of M depots, $\mathcal{N} = \{\mathrm{M}+1, \ldots, \mathrm{M}+\mathrm{N}\}$ denotes the set of N customers, and $\mathcal{R} = \mathcal{M} \cup \mathcal{N} = \{1, \ldots, \mathrm{R}\}$ is the set of $\mathrm{R} = \mathrm{M} + \mathrm{N}$ locations in the problem.

Theorem 1. *The mixed-integer linear program with 2-index binary variables* x_{ij}

$$\min \quad \sum_{i\in\mathcal{R}}\sum_{j\in\mathcal{R}} \mathrm{c}_{ij}\, x_{ij} \tag{13.4}$$

$$\text{s.t.} \quad \sum_{j\in\mathcal{R}} x_{ij} = 1, \qquad \sum_{h\in\mathcal{R}} x_{hi} = 1 \quad \forall\, i \in \mathcal{R}, \tag{13.5}$$

$$k_m = m \quad \forall\, m \in \mathcal{M}, \tag{13.6}$$

$$k_i - k_j + (\mathrm{M}-1)(x_{ij} + x_{ji}) \leq (\mathrm{M}-1) \quad \forall\, i, j \in \mathcal{R}, \tag{13.7}$$

$$\{\textit{subtour elimination constraints}\} \tag{13.8}$$

$$x_{ij} \in \{0, 1\}, \quad k_i \in [1, \mathrm{M}] \quad \forall\, i, j \in \mathcal{R}, \tag{13.9}$$

is equivalent to the mixed-integer linear program (13.1)–(13.3).

A proof for this theorem can be found in [4]. In this formulation the continuous variables k_i can be seen as *node currents*, which are the dual to the *node potentials* in the Miller-Tucker-Zemlin subtour elimination constraints [15].

Figure 13.2 shows an example solution to the above-mentioned formulation for $\mathrm{M} = 5$ depots (shown in the inner circle) and $\mathrm{N} = 40$ customers (shown in the outer circle). By (13.6) each depot gets a unique index number (represented as a unique color). When a variable $x_{ij} = 1$ it means that the trip from location i to j is part of the selected tour, where the direction of the tour is indicated by the arrows in the figure. Along the path the index number will be assigned to the customers through (13.7), resulting in exactly M cycles in the set of $\mathrm{R} = \mathrm{M} + \mathrm{N}$ nodes, each originating from another depot.

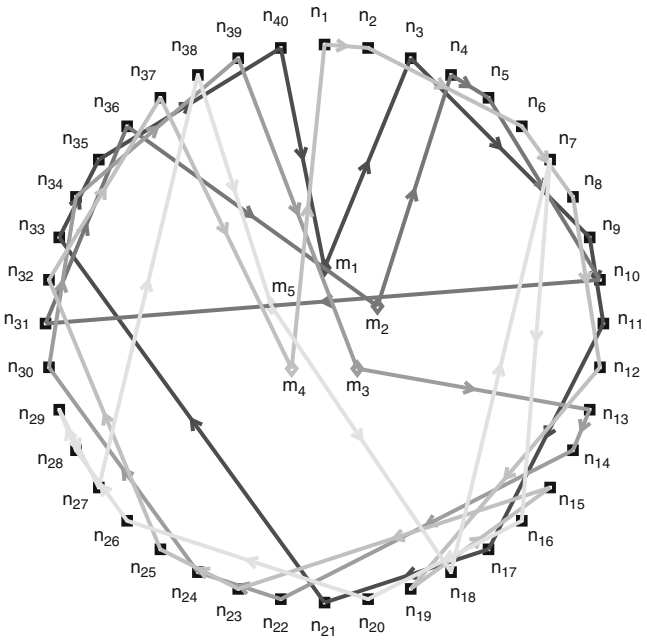

Fig. 13.2 Assignment of new requests to micro-ferries. Each micro-ferry has a unique color, and the requests are ordered with increasing desired pick-up times

The Mean Travel Time Increases with Increasing Disturbances

In the case study that is presented later on in this chapter—where the current flows in parallel to the riverbed—the travel times depend on the water flow. The effect of the magnitude of the flow on the travel times can be stated as follows.

Theorem 2. *The travel time for a round-trip (from one location to another and back) will increase with increasing water flow magnitudes, and therefore both the mean travel time and total energy consumption will increase with increasing magnitudes.*

A formal proof will be provided in Sect. 13.2.1, after introducing the necessary variables and equations. The difference in travel times for going one way or the other is to be expected from experience, but the increase in times for round-trips is less intuitive. Since the micro-ferries will be traveling in both upstream and downstream direction, this means that the total travel time for handling all transport requests will increase with increasing flows, and hence the mean travel times will be higher when the current is stronger. Due to the longer travel times also the energy consumption will increase with the water flow magnitude.

Application

With the extension to variable speeds for flowing water, the variant of the micro-ferry problem as discussed in this chapter provides a complete modeling framework for scheduling vehicles with variable speeds under environmental disturbances. The model takes the following aspects into account:

- **(soft) time windows**: each customer is picked up at the desired time (if possible)
- **varying speeds**: the micro-ferries can travel within a given speed range
- **energy consumption**: the schedules are energy-efficient through minimization of the total energy consumption of the micro-ferry fleet
- **charging**: empty batteries on the water are avoided by keeping track of energy levels and by recharging
- **flowing water**: the effect of currents on travel times and energy consumption is taken into account

13.2 Micro-Ferry Scheduling Problem for Flowing Water

The research on micro-ferry scheduling originated as a fictitious (but realizable) case study for the city of Rotterdam, the Netherlands. With the creation of new container terminals at Maasvlakte II the current harbor activity near the city center is expected to partially move towards the sea. This leaves space for redesigning the

riversides and for creating new housing and offices. To avoid more traffic by car via the already busy roads, alternative transport over the river is a viable option.

Envisioned is a personal transport system with small, autonomous vessels, which we will refer to as micro-ferries. Customers can embark and disembark the ferries at specific locations along the river, and transport requests can be (pre)ordered. To avoid empty batteries while on the river, which is inconvenient on a lake but dangerous when drifting towards a harbor with large container ships and oil tankers, the energy levels are taken into account in the scheduling and a recharge is planned when necessary.

This section starts with a description of the effects of flowing water on travel times and energy consumption, followed by a mathematical formulation of the problem. This formulation is then used to compute a transport schedule in a case study example.

13.2.1 Effects of Flowing Water

With respect to the scheduling problem for micro-ferries, the velocity of the micro-ferry has an effect on two distinct properties; both the travel time and the energy consumption of the micro-ferries change when changing the velocity. The *travel time* will depend on the velocity *relative to the land*, whereas the *energy consumption* will depend on the velocity *relative to the water*. For calm water these two velocities will be equal, but for flowing water one can no longer use a single notion of velocity.

To obtain schedules that take into account the effects of water flows within reasonable computation times, some assumptions are made for modeling the problem:

A1: *The water flow is uniform and time-invariant over the scheduling horizon (in the order of a few hours),*
A2: *Side-slip of the micro-ferries can be neglected,*
A3: *The acceleration and deceleration close to the stations can be neglected, as well as the changes of the water flows near the stations,*
A4: *The water flow is slower than the speed of the micro-ferries.*

Assumption A1 states that the water flow will not change over time nor depends on the location on the river, which means that the water flow is constant. Assumption A2 will hold for reasonable speeds and accelerations (i.e., no sharp turns), which is expected to be valid due to safety reasons. Assumption A3 is valid if the traveled distances are long enough to neglect differences in vessel speeds and water flow speeds at the start and end of a traveled path. Finally, assumption A4 ensures controlability of the micro-vessel on the water by always being able to move forwards relative to the water flow.

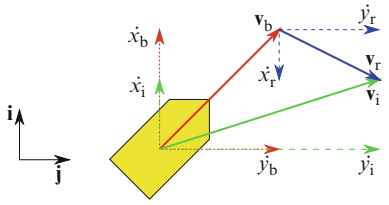

Fig. 13.3 The velocity $\mathbf{v}_i$ with respect to the land is the sum of the velocity $\mathbf{v}_b$ of the micro-ferry plus the velocity $\mathbf{v}_r$ of the water

Velocities and Paths

The flow velocity of a river will influence the perception of speed both on a vessel and of a vessel with respect to the shore. When a vessel travels upstream, it will travel faster relative to the water than relative to the land. This effect can conveniently be described by using three different velocity vectors:

$\mathbf{v}_b$: vessel velocity relative to the water,
$\mathbf{v}_i$: vessel velocity relative to the land,
$\mathbf{v}_r$: water velocity relative to the land.

As shown in Fig. 13.3 these three velocities relate to each other as

$$\mathbf{v}_i = \mathbf{v}_r + \mathbf{v}_b. \tag{13.10}$$

The velocities can be decomposed into the speed components in the x and y direction of the inertial reference frame; for each $* \in \{b, i, w\}$ we have

$$\mathbf{v}_* = \dot{x}_* \mathbf{i} + \dot{y}_* \mathbf{j}, \tag{13.11}$$

where $\dot{x}_*$ and $\dot{y}_*$ denote the speeds in the x_i and y_i direction respectively, whereas $\mathbf{i}$ and $\mathbf{j}$ denote the unit vector in the x_i and y_i direction of the inertial reference frame[2] respectively. The speed u_* associated with a velocity $\mathbf{v}_*$ can be determined as

$$u_* = |\mathbf{v}_*| = \sqrt{\dot{x}_*^2 + \dot{y}_*^2}. \tag{13.12}$$

Paths of a micro-ferry are defined as displacements over time in a certain reference frame. Due to assumptions A1 and A3, we can model a river as a straight waterway (i.e., like a canal), and the micro-ferries will travel in straight-line paths from one location to another. Hence, the path of a micro-ferry can be modeled by a vector with the same direction as its associated velocity. We define the paths $\mathbf{p}_i$, $\mathbf{p}_b$, and $\mathbf{p}_r$ associated with the velocities discussed above. A displacement $\mathbf{p}_*$ can be decomposed as

$$\mathbf{p}_* = x_* \mathbf{i} + y_* \mathbf{j}, \tag{13.13}$$

[2]The inertial reference frame is the reference frame that is fixed with respect to the land.

with the associated path length

$$l_* = |\mathbf{p}_*| = \sqrt{{x_*}^2 + {y_*}^2}. \tag{13.14}$$

Based on these definitions of velocities and paths, we can now analyze the effects of flowing water on the micro-ferry scheduling problem.

Effect on Travel Times

For a vessel that travels with a constant velocity relative to the water, it will take longer to travel from some location a to another location z in upstream direction than from z to a in downstream direction. This section explains how the currents affect the travel times.

Calculation of Travel Times

The travel time of a micro-ferry equals the distance traveled divided by the travel speed; more specifically it is the time it takes to travel from one station to the next. The path $\mathbf{p}_\mathrm{i}$ from one location to the other will not change with the water flow, but the path $\mathbf{p}_\mathrm{b}$ of the micro-ferry relative to the water will be dependent on the velocity $\mathbf{v}_\mathrm{r}$ of the water relative to the land, and the travel time T. Note that for a micro-ferry traveling with a velocity $\mathbf{v}_\mathrm{i}$ relative to the land, the travel time T and the traveled path $\mathbf{p}_\mathrm{i}$ are related as

$$\mathbf{p}_\mathrm{i} = T\,\mathbf{v}_\mathrm{i}. \tag{13.15}$$

Combined with the relation between the different velocities as given in (13.10), the velocity of the micro-ferry relative to the water can be written as (see Fig. 13.4)

$$\mathbf{v}_\mathrm{b} = \frac{1}{T}\mathbf{p}_\mathrm{b} = \frac{1}{T}\left(\mathbf{p}_\mathrm{i} - \mathbf{p}_\mathrm{r}\right) = \frac{1}{T}\mathbf{p}_\mathrm{i} - \mathbf{v}_\mathrm{r}. \tag{13.16}$$

Both $\mathbf{p}_\mathrm{i}$ and $\mathbf{v}_\mathrm{r}$ are constants, and the velocity of the micro-ferry through the water therefore only varies with the travel time T. The speed u_b is related to the water flow and the displacement by

$$\begin{aligned} {u_\mathrm{b}}^2 = |\mathbf{v}_\mathrm{b}|^2 &= \dot{x}_\mathrm{b}^2 + \dot{y}_\mathrm{b}^2 = \left(\frac{x_\mathrm{i}}{T} - \dot{x}_\mathrm{r}\right)^2 + \left(\frac{y_\mathrm{i}}{T} - \dot{y}_\mathrm{r}\right)^2 \\ &= \left(\dot{x}_\mathrm{r}^2 + \dot{y}_\mathrm{r}^2\right) - 2\left(x_\mathrm{i}\dot{x}_\mathrm{r} + y_\mathrm{i}\dot{y}_\mathrm{r}\right)\frac{1}{T} + \left({x_\mathrm{i}}^2 + {y_\mathrm{i}}^2\right)\frac{1}{T^2} \\ &= {u_\mathrm{r}}^2 - 2\left(x_\mathrm{i}\dot{x}_\mathrm{r} + y_\mathrm{i}\dot{y}_\mathrm{r}\right)\frac{1}{T} + {l_\mathrm{i}}^2\frac{1}{T^2}, \end{aligned} \tag{13.17}$$

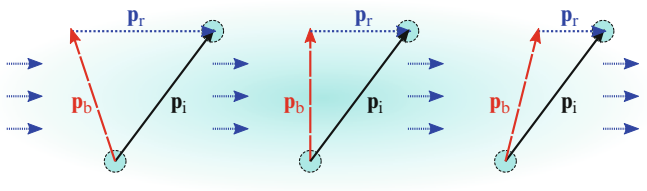

Fig. 13.4 The same path $\mathbf{p}_\mathrm{i}$ in the inertial frame can be accomplished at different velocities, resulting in different paths $\mathbf{p}_\mathrm{b}$ in the body frame

where l_i is the traveled distance of the micro-ferry with respect to the land (i.e., the distance between two locations). Since the traveled distance of the micro-ferry with respect to the water equals $l_\mathrm{b} = u_\mathrm{b} T$ by (13.12), (13.14) and $\mathbf{p}_\mathrm{b} = \mathbf{v}_\mathrm{b} T$, we have

$$l_\mathrm{b}{}^2 = u_\mathrm{b}{}^2 T^2 = u_\mathrm{r}{}^2 T^2 - 2\left(x_\mathrm{i}\dot{x}_\mathrm{r} + y_\mathrm{i}\dot{y}_\mathrm{r}\right) T + l_\mathrm{i}{}^2, \tag{13.18}$$

which is a quadratic equation of the form $\alpha T^2 + \beta T + \gamma = 0$ with

$$\alpha = u_\mathrm{r}{}^2 - u_\mathrm{b}{}^2, \quad \beta = -2\left(x_\mathrm{i}\dot{x}_\mathrm{r} + y_\mathrm{i}\dot{y}_\mathrm{r}\right), \quad \gamma = l_\mathrm{i}{}^2. \tag{13.19}$$

We have $\alpha < 0$ since—by assumption A4—the speed of the micro-ferry u_b will be larger than the speed of the water u_r to ensure controlability of the vessel. Furthermore, $\gamma > 0$ since it represents the distance between two stations. Therefore, using the variables defined in (13.19) the discriminant of (13.18) satisfies

$$\Delta = \beta^2 - 4\alpha\gamma > \beta^2 > 0. \tag{13.20}$$

The second inequality shows that there are two distinct real-valued solutions for T, whereas the first inequality shows that

$$-\beta + \sqrt{\Delta} > -\beta + |\beta| \geq 0, \quad -\beta - \sqrt{\Delta} < -\beta - |\beta| \leq 0. \tag{13.21}$$

Since $\alpha < 0$, positive travel times T can be found by

$$\begin{aligned} T &= \frac{-\beta - \sqrt{\beta^2 - 4\alpha\gamma}}{2\alpha} = \frac{-\frac{1}{2}\beta - \sqrt{\frac{1}{4}\beta^2 - \alpha\gamma}}{\alpha} \\ &= \frac{\left(x_\mathrm{i}\dot{x}_\mathrm{r} + y_\mathrm{i}\dot{y}_\mathrm{r}\right) - \sqrt{\left(x_\mathrm{i}\dot{x}_\mathrm{r} + y_\mathrm{i}\dot{y}_\mathrm{r}\right)^2 - \left(u_\mathrm{r}{}^2 - u_\mathrm{b}{}^2\right) l_\mathrm{i}{}^2}}{u_\mathrm{r}{}^2 - u_\mathrm{b}{}^2}. \end{aligned} \tag{13.22}$$

Note that the water flow-related coefficients $\dot{x}_\mathrm{r}, \dot{x}_\mathrm{r}, u_\mathrm{r}$ are constant for all possible trajectories between the stations, whereas the coefficients $x_\mathrm{i}, y_\mathrm{i}, l_\mathrm{i}$ depend on the start and end location a and z for a certain trip. As opposed to the work in [6], here

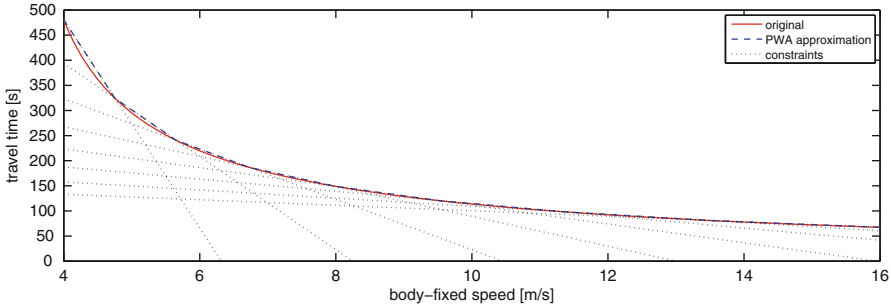

Fig. 13.5 Travel times at different speeds. The convex function can be approximated using constraints

we will treat the speed u_b of the micro-ferry in the water as an optimization variable. Therefore, the travel time T_{az} from location a to z will depend on the chosen speed u_b, as can be seen in the plot of (13.22) in Fig. 13.5.

Linear Approximation for Travel Times

Equation (13.22) is non-linear in the micro-ferry speed u_b. Analysis of the function in (13.22) shows that it is a strictly decreasing, convex function in u_b, for which we can obtain an accurate approximation using a continuous piece-wise affine function

$$\hat{T}_{a,z}(u_\mathrm{b}) = \begin{cases} \mathrm{a}^1_{a,z} u_\mathrm{b} + \mathrm{b}^1_{a,z}, & \mathrm{u}_0 \leq u_\mathrm{b} \leq \mathrm{u}_1, \\ \qquad\vdots & \\ \mathrm{a}^\mathrm{P}_{a,z} u_\mathrm{b} + \mathrm{b}^\mathrm{P}_{a,z}, & \mathrm{u}_{\mathrm{P}-1} \leq u_\mathrm{b} \leq \mathrm{u}_\mathrm{P}. \end{cases} \tag{13.23}$$

Note that by increasing the number of segment P one can increase the accuracy of the approximation at the cost of increasing the computational effort. Since the function $T_{a,z}$ is convex in u_b, we will have $\mathrm{a}^i_{a,z} < \mathrm{a}^j_{a,z}$ for $i < j$, and the function can be written as the maximum of a set of lines

$$\hat{T}_{a,z}(u_\mathrm{b}) = \max_{i=1,\ldots,\mathrm{P}} \left(\mathrm{a}^i_{a,z} u_\mathrm{b} + \mathrm{b}^i_{a,z} \right). \tag{13.24}$$

For such a function the value of $\hat{T}_{a,z}(u_\mathrm{b})$ can be found using the linear program [3]

$$\min \quad T \tag{13.25}$$

$$\text{s.t.} \quad \mathrm{a}^i_{a,z} u_\mathrm{b} + \mathrm{b}^i_{a,z} \leq T \quad \forall\, i \in \{1, \ldots, \mathrm{P}\}, \tag{13.26}$$

where the optimal value T^* will equal the travel time approximation $\hat{T}_{a,z}(u_\mathrm{b})$. An example of the relation (13.22) between the travel time and the travel speed is shown

in Fig. 13.5 as the continuous, red line. The blue, dashed lines show the continuous piece-wise affine approximation $\hat{T}_{a,z}(u_\mathrm{b})$ from (13.23), and the black, dotted lines show the constraints used to approximate the travel time in (13.26).

Effect on Energy Consumption

Due to the flowing water the micro-ferries might need more or less energy to travel from one location to another as compared to still water, depending on whether or not they are traveling against the current. This section explains how the currents affect the energy consumption.

Calculation of Energy Consumption

The dynamics of a vessel can be modelled using the vectorial representation [11]

$$\mathrm{M}\dot{\boldsymbol{\nu}} + \mathrm{C}\boldsymbol{\nu} + \mathrm{D}\boldsymbol{\nu} + \boldsymbol{\tau}_\mathrm{e} = \boldsymbol{\tau}_\mathrm{c}, \tag{13.27}$$

where $\boldsymbol{\nu} = [u, v, r]^\top$ is the velocity vector consisting of the surge speed u, the sway speed v, and the rotational speed r, M is a symmetric, positive definite mass matrix, C is a skew-symmetric Coriolis and centripetal forces matrix, D is a symmetric, positive definite damping matrix, $\boldsymbol{\tau}_\mathrm{e}$ is a force vector representing external disturbances (e.g., wind and currents), and $\boldsymbol{\tau}_\mathrm{c}$ is the control vector representing the forces exerted by the actuators. Using the force balance (13.27) we can write the kinetic energy of a surface vessel as

$$E_\mathrm{kin} = \frac{1}{2}\boldsymbol{\nu}^\top \mathrm{M}\boldsymbol{\nu}, \tag{13.28}$$

and the associated power (due to movement) becomes the quadratic function

$$\begin{aligned} P_\mathrm{kin} &= \frac{d}{dt}E_\mathrm{kin} = \frac{1}{2}\left[\dot{\boldsymbol{\nu}}^\top \mathrm{M}\boldsymbol{\nu} + \boldsymbol{\nu}^\top \mathrm{M}\dot{\boldsymbol{\nu}}\right] = \boldsymbol{\nu}^\top \mathrm{M}\dot{\boldsymbol{\nu}} \\ &= \boldsymbol{\nu}^\top\left[-\mathrm{C}\boldsymbol{\nu} - \mathrm{D}\boldsymbol{\nu} + \boldsymbol{\tau}_\mathrm{c} - \boldsymbol{\tau}_\mathrm{e}\right] = \left[\boldsymbol{\tau}_\mathrm{c} - \boldsymbol{\tau}_\mathrm{e}\right]^\top \boldsymbol{\nu} - \boldsymbol{\nu}^\top \mathrm{D}\boldsymbol{\nu}. \end{aligned} \tag{13.29}$$

In order to take the energy consumption of the micro-ferries into account, we use a simplified expression for the power based on the along-path speed u only. Besides the quadratic and linear terms of (13.29) due to the kinetic energy, we also add a constant term to include the energy losses due to a running motor when the micro-ferries are not moving. Therefore, the power of the micro-ferries will be a quadratic function of the speed, written as [8]

$$P = \pi_2 u^2 + \pi_1 u + \pi_0. \tag{13.30}$$

The energy consumption will depend on the speed u_b relative to the water, and it is kept constant during a trip but used as a variable in the optimization problem. Then, the energy consumption from a to z becomes

$$E_{a,z}(u_\mathrm{b}) = P(u_\mathrm{b})T_{a,z}(u_\mathrm{b}) = \left(\pi_2 {u_\mathrm{b}}^2 + \pi_1 u_\mathrm{b} + \pi_0\right) T_{a,z}(u_\mathrm{b}) \tag{13.31}$$

which is a non-linear equation in the variables u_b representing vessel speed; the travel time T_{az} is a non-linear function in the vessel speed u_b as given by (13.22).

Linear Approximation of the Energy Consumption

Equation (13.31) is non-linear in the micro-ferry speed u_b. Analysis of the function shows that it is a convex function in u_b; hence also this function can be approximated accurately using a continuous piece-wise affine function[3]

$$\hat{E}_{a,z}(u_\mathrm{b}) = \begin{cases} \mathrm{c}^1_{a,z} u_\mathrm{b} + \mathrm{d}^1_{a,z}, & \mathrm{u}_0 \leq u_\mathrm{b} \leq \mathrm{u}_1, \\ \vdots & \\ \mathrm{c}^\mathrm{P}_{a,z} u_\mathrm{b} + \mathrm{d}^\mathrm{P}_{a,z}, & \mathrm{u}_{\mathrm{P}-1} \leq u_\mathrm{b} \leq \mathrm{u}_\mathrm{P}, \end{cases} \tag{13.32}$$

Since the function $E_{a,z}$ is convex in u_b, the value of $\hat{E}_{a,z}(u_\mathrm{b})$ can be found using [3]

$$\min \quad E \tag{13.33}$$

$$\text{s.t.} \quad \mathrm{c}^i_{a,z} u_\mathrm{b} + \mathrm{d}^i_{a,z} \leq E \quad \forall\, i \in \{1, \ldots, \mathrm{P}\}, \tag{13.34}$$

where the optimal value E^* will equal the energy consumption approximation $\hat{E}_{a,z}(u_\mathrm{b})$. An example of the relation (13.31) between the energy consumption and the travel speed is shown in Fig. 13.6 as the continuous, red line. The blue, dashed lines show the continuous piece-wise affine approximation $\hat{E}_{a,z}(u_\mathrm{b})$ from (13.32), and the black, dotted lines show the constraints used to approximate the travel time in (13.34).

Proof of Theorem 2

With the equations for the travel times and energy consumption derived above, we can now prove the statement of Theorem 2. We consider a uniform and time-invariant current, which—without loss of generality[4]—flows along the x-axis of the

[3] Actually, neither the number of partitions P nor the speeds $\mathrm{u}_0, \ldots, \mathrm{u}_\mathrm{P}$ need to be the same for the travel time approximation (13.23) and the energy consumption approximation (13.32).

[4] The inertial reference frame can always be chosen to be aligned with the water flow.

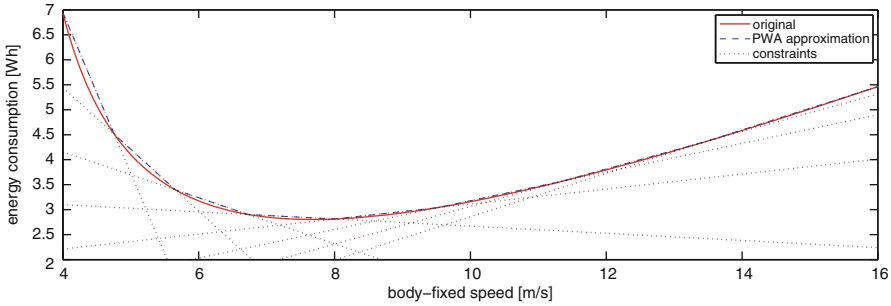

Fig. 13.6 Energy consumption at different speeds. The energy consumption is a convex function of the speed, and can efficiently be approximated using linear constraints

inertial reference frame. Hence, the relative velocity becomes $\mathrm{v_r} = (\dot{x}_\mathrm{r}, \dot{y}_\mathrm{r}) = (u_\mathrm{r}, 0)$ such that the travel time defined in (13.22) becomes

$$T = \frac{\sqrt{(x_\mathrm{i}\dot{x}_\mathrm{r})^2 + ({u_\mathrm{b}}^2 - {u_\mathrm{r}}^2){l_\mathrm{i}}^2} - x_\mathrm{i}\dot{x}_\mathrm{r}}{{u_\mathrm{b}}^2 - {u_\mathrm{r}}^2}.$$

The travel time T_{az} from location a to z can be found by considering the displacement $\mathbf{p}_{\mathrm{i},az} = (x_{\mathrm{i},az}, y_{\mathrm{i},az})$ in the inertial reference frame. Then the return trip from z to a is given by $\mathbf{p}_{\mathrm{i},za} = -\mathbf{p}_{\mathrm{i},az} = (-x_{\mathrm{i},az}, -y_{\mathrm{i},az})$, such that by (13.14) we have $l_{\mathrm{i},az} = l_{\mathrm{i},za}$. When[5] ${u_\mathrm{b}}^2 - {u_\mathrm{r}}^2 > 0$ the difference in travel time $\Delta_T = T_{az} - T_{za}$ of going one way or the other between arbitrary locations a and z is

$$\begin{aligned}\Delta_T &= \frac{\sqrt{(x_\mathrm{i}\dot{x}_\mathrm{r})^2 + ({u_\mathrm{b}}^2 - {u_\mathrm{r}}^2){l_\mathrm{i}}^2} - x_\mathrm{i}\dot{x}_\mathrm{r}}{({u_\mathrm{b}}^2 - {u_\mathrm{r}}^2)} - \frac{\sqrt{(-x_\mathrm{i}\dot{x}_\mathrm{r})^2 + ({u_\mathrm{b}}^2 - {u_\mathrm{r}}^2){l_\mathrm{i}}^2} + x_\mathrm{i}\dot{x}_\mathrm{r}}{({u_\mathrm{b}}^2 - {u_\mathrm{r}}^2)} \\ &= \frac{-2x_\mathrm{i}\dot{x}_\mathrm{r}}{\sqrt{{u_\mathrm{b}}^2 - {u_\mathrm{r}}^2}}. \end{aligned} \tag{13.35}$$

This shows that the travel times are different if there is a current (that is for $\dot{x}_\mathrm{r} \neq 0$), as could be expected; if we travel against the current from a to z (such that $x_\mathrm{i} > 0$ and $\dot{x}_\mathrm{r} < 0$) then $T_{az} > T_{za}$ and indeed $\Delta_T > 0$.

Perhaps less obvious is the fact that the travel time $\Sigma_T = T_{az} + T_{za}$ for a round trip (from a to z and back to a) has a larger travel time when the current's magnitude $u_\mathrm{r} = |\dot{x}_\mathrm{r}|$ increases:

[5] This holds for $|u_\mathrm{b}| > |u_\mathrm{r}|$, which is a necessary condition to be able to move forwards under all circumstances, as desired under normal operations and stated as assumption A4.

$$\Sigma_T = \frac{\sqrt{(x_\mathrm{i}\dot{x}_\mathrm{r})^2 + ({u_\mathrm{b}}^2 - {u_\mathrm{r}}^2){l_\mathrm{i}}^2} - x_\mathrm{i}\dot{x}_\mathrm{r}}{({u_\mathrm{b}}^2 - {u_\mathrm{r}}^2)} + \frac{\sqrt{(-x_\mathrm{i}\dot{x}_\mathrm{r})^2 + ({u_\mathrm{b}}^2 - {u_\mathrm{r}}^2){l_\mathrm{i}}^2} + x_\mathrm{i}\dot{x}_\mathrm{r}}{({u_\mathrm{b}}^2 - {u_\mathrm{r}}^2)}$$
$$= \frac{2\sqrt{(x_\mathrm{i}\dot{x}_\mathrm{r})^2 + ({u_\mathrm{b}}^2 - {u_\mathrm{r}}^2)\,{l_\mathrm{i}}^2}}{{u_\mathrm{b}}^2 - {u_\mathrm{r}}^2}, \tag{13.36}$$

which has a minimum

$$\Sigma_{T,\min} = 2\frac{l_\mathrm{i}}{\sqrt{{u_\mathrm{b}}^2 - {u_\mathrm{r}}^2}}, \tag{13.37}$$

for $\dot{x}_\mathrm{r} = 0$, and Σ_T increases for larger currents. Hence, the larger $|\dot{x}_\mathrm{r}|$, the larger the travel times within the micro-ferry network, and—by (13.31)—the larger the energy consumption needed to handle the requests.

13.2.2 Problem Definition

To formulate the micro-ferry scheduling problem, several optimization variables will be used. First, an overview of these variables is given, followed by a detailed explanation of the relations between them. This will lead to a mixed-integer linear program for finding the transport schedule of the micro-ferries, as shown in the example provided at the end of this section.

Optimization Variables

The optimization variables used for the micro-ferry scheduling problem are summarized next, separated by type. The variables are defined per *request*, which consists of the transport of a customer from one location to another within a certain time window, and the possible relocation, charging and waiting that are associated to the specific transport. The set of non-negative scalars is defined as $\mathbb{R}_+$.

Decision variables:

- $x_{ij} \in \{0, 1\}$: binary variable representing whether ($x_{ij} = 1$) or not ($x_{ij} = 0$) request j succeeds request i,
- $y_j \in \{0, 1\}$: binary variable representing whether ($y_j = 1$) or not ($y_j = 0$) the micro-ferry is recharged after request j,
- $k_j \in [1, \mathrm{M}]$: continuous variable[6] representing the index number of the micro-ferry that handles the request.

[6] Although this variable is continuous, due to the constraints it will always attain an integer value.

Energy variables:

- $e_j \in [0, \mathrm{E}]$: energy level after completion of transport j,
- $f_j \in \mathbb{R}_+$: energy increase (by recharging or refueling) during request j,
- $g_j \in \mathbb{R}_+$: energy consumed during the relocation phase of request j,
- $h_j \in \mathbb{R}_+$: energy consumed during the transportation phase of request j.

Time variables:

- $p_j \in \mathbb{R}_+$: pick-up time for the passengers of request j,
- $q_j \in \mathbb{R}_+$: charging time after handling request j,
- $r_j \in \mathbb{R}_+$: relocation time for request j,
- $s_j \in \mathbb{R}_+$: time window mismatch for request j,
- $t_j \in \mathbb{R}_+$: transportation time for request j.

Speed variables:

- $u_j \in [\underline{\mathrm{u}}, \overline{\mathrm{u}}]$: speed of the micro-ferry during the relocation phase of request j,
- $v_j \in [\underline{\mathrm{v}}, \overline{\mathrm{v}}]$: speed of the micro-ferry during the transportation phase of request j.

Phases of a Request

A transportation of passengers associated with request j (preceded by request i) consists of the following phases (see Fig. 13.7):

- a micro-ferry should (optionally) *relocate* from delivery location δ_i towards the pick-up location π_j for request j,
- the micro-ferry will *transport* the customer(s) from pick-up location π_j to the delivery location δ_j,
- the micro-ferry will (optionally) charge after the transportation at location δ_j,
- when charged the micro-ferry will (optionally) wait until it can handle the next request.

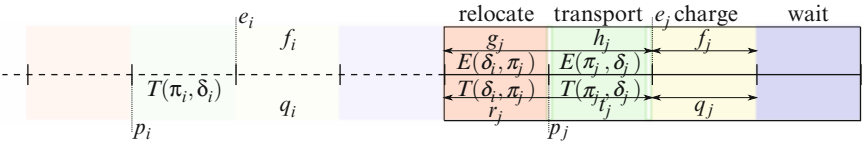

Fig. 13.7 The four phases of a request consist of relocating, transporting, charging, and waiting. The associated energy (*top*) and time (*bottom*) variables show the relations between energy levels e and pick-up times p for successive requests

Each of these four steps takes time and alters the energy level, which should be accounted for in the scheduling of the pick-up times p_j and the charging actions for increasing the energy levels e_j.

Time Variables

For embarking and disembarking the micro-ferries a (combined) duration $\mathrm{t_d}$ can be chosen by the operator, which will be a trade-off between giving the customers enough time to safely enter and exit the micro-ferry, and not wasting time at the station. Furthermore, the time it takes to couple and decouple the ferry to the power source when charging is represented by $\mathrm{t_c}$, and the rate at which the batteries are charged is given by $\mathrm{r_c}$.

The duration for the relocation of the micro-ferry from the delivery station of request i towards the pick-up location of station j is given by the travel time $T(\delta_i, \pi_j)$ calculated using (13.22), where δ_i and π_j denote the index number of the delivery station of request i and the index number of the pick-up station of request j respectively. The duration for the transportation of the customers from pick-up station π_j to delivery station δ_j is given by the travel time $T(\pi_j, \delta_j)$ in (13.22), where π_j and δ_j denote the index number of the pick-up and delivery station of request j respectively.

Let $\hat{T}(a, z)$ denote the continuous piece-wise affine approximation travel time $T(a, z)$ from location a to z, given by (13.23). Using the parameters $\mathrm{a}^p_{a,z}$ and $\mathrm{b}^p_{a,z}$ (which can be determined a priori) the *relocation time* r_j of request j from location $a = \delta_i$ to location $z = \pi_j$ can be determined by the linear program

$$\begin{aligned} \min \quad & r_j && (13.38)\\ \text{s.t.} \quad & \mathrm{a}^p_{\delta_i,\pi_j} u_j + \mathrm{b}^p_{\delta_i,\pi_j} \leq r_j \quad \forall\, p \in \{1, \ldots, \mathrm{P}\}, && (13.39) \end{aligned}$$

where $u_\mathrm{b} = u_j$ is the travel speed during the relocation. Similarly, the *transportation time* t_j of request j from location $a = \pi_j$ to location $z = \delta_j$ can be determined using

$$\begin{aligned} \min \quad & t_j && (13.40)\\ \text{s.t.} \quad & \mathrm{a}^p_{\pi_j,\delta_j} v_j + \mathrm{b}^p_{\pi_j,\delta_j} \leq t_j \quad \forall\, p \in \{1, \ldots, \mathrm{P}\}, && (13.41) \end{aligned}$$

where $u_\mathrm{b} = v_j$ is the travel speed during the transportation. Note that these constraints are defined on the entire domain of u_j and v_j; due to convexity of the original function the optimal value r_j^* / t_j^* will always lie on the line segment associated to the speed domain in the piece-wise affine approximation associated with the optimal speed u_j^* / v_j^* (see Fig. 13.5).

Energy Variables

For the energy consumption during the relocation phase and the transportation phase we will use the continuous piece-wise affine approximation (13.32). The *relocation energy* g_j can then be found by solving the linear program

$$\begin{aligned} \min \quad & g_j && (13.42)\\ \text{s.t.} \quad & \mathrm{c}^p_{\delta_i,\pi_j} u_j + \mathrm{d}^p_{\delta_i,\pi_j} \leq g_j \quad \forall\, p \in \{1,\ldots,\mathrm{P}\}, && (13.43) \end{aligned}$$

where $u_\mathrm{b} = u_j$ is the travel speed during the relocation. Similarly, the *transportation energy* h_j of request j from location $a = \pi_j$ to location $z = \delta_j$ can be determined by the linear program

$$\begin{aligned} \min \quad & h_j && (13.44)\\ \text{s.t.} \quad & \mathrm{c}^p_{\pi_j,\delta_j} v_j + \mathrm{d}^p_{\pi_j,\delta_j} \leq h_j \quad \forall\, p \in \{1,\ldots,\mathrm{P}\}, && (13.45) \end{aligned}$$

where $u_\mathrm{b} = v_j$ is the travel speed during the transportation. Note that these constraints are defined on the entire domain of u_j and v_j; due to convexity of the original function the optimal value g_j^* / h_j^* will always lie on the line segment associated to the speed domain in the piece-wise affine approximation associated with the optimal speed u_j^* / v_j^* (see Fig. 13.6).

Micro-Ferries and Requests

Consider a fleet of M micro-ferries that could be either traveling or waiting at a station. These ferries will already have a pick-up time $p_{\mathrm{o},j}$, an energy level $e_{\mathrm{o},j}$, and a micro-ferry index number $k_{\mathrm{o},j}$. Besides the M current requests (which might be handled when a micro-ferry is docked at a station) there will be N new requests to schedule, resulting in a total of $\mathrm{R} = \mathrm{M} + \mathrm{N}$ requests. The sets

$$\mathcal{M} = \{1,\ldots,\mathrm{M}\}, \quad \mathcal{N} = \{\mathrm{M}+1,\ldots,\mathrm{R}\}, \quad \mathcal{R} = \mathcal{M} \cup \mathcal{N} \tag{13.46}$$

denote the set of current requests, new requests, and all requests respectively. These sets can be seen as the set of depots $\mathcal{M}$, the set of customers $\mathcal{N}$, and the total set of locations $\mathcal{R}$, as used in vehicle routing problems.

Mixed-Integer Linear Programming Formulation

The micro-ferry scheduling problem for flowing water and variable speeds can be solved using the following mixed-integer linear program.

$$\min \sum_{i\in\mathcal{R}} (g_i + \alpha h_i + \gamma s_i - \eta e_i + \rho r_i + \theta t_i) \tag{13.47}$$

$$\text{s.t.} \quad \sum_{i\in\mathcal{R}} x_{ij} = 1; \quad \sum_{i\in\mathcal{R}} x_{ji} = 1 \qquad \forall\, j \in \mathcal{R}, \tag{13.48}$$

$$k_i - k_j \le (M-1)(1 - x_{ij} - x_{ji}) \qquad \forall\, i, j \in \mathcal{R}, \tag{13.49}$$

$$\mathrm{a}^k_{\delta_i,\pi_j} u_j + \mathrm{b}^k_{\delta_i,\pi_j} \le r_j + \mathrm{T}(1 - x_{ij}) \qquad \forall\, i \in \mathcal{R}, j \in \mathcal{N}, k \in \mathcal{P}, \tag{13.50}$$

$$\mathrm{a}^k_{\pi_j,\delta_j} v_j + \mathrm{b}^k_{\pi_j,\delta_j} \le t_j + \mathrm{T}(1 - x_{ij}) \qquad \forall\, i \in \mathcal{R}, j \in \mathcal{N}, k \in \mathcal{P}, \tag{13.51}$$

$$p_i + t_i + q_i + r_j + \mathrm{t_d} \le p_j + \mathrm{T}(1 - x_{ij}) \quad \forall\, i \in \mathcal{R}, j \in \mathcal{N}, \tag{13.52}$$

$$\mathrm{p}_{\mathrm{a},j} - p_j \le s_j; \quad p_j - \mathrm{p}_{\mathrm{b},j} \le s_j \qquad \forall\, j \in \mathcal{R}, \tag{13.53}$$

$$\mathrm{t_c}\, y_j \le q_j \qquad \forall\, j \in \mathcal{R}, \tag{13.54}$$

$$f_j = \mathrm{r_c}\left(q_j - \mathrm{t_c}\, y_j\right) \qquad \forall\, j \in \mathcal{R}, \tag{13.55}$$

$$f_j \le \mathrm{E}\, y_j \qquad \forall\, j \in \mathcal{R}, \tag{13.56}$$

$$e_j + f_j \le \mathrm{E} \qquad \forall\, j \in \mathcal{R}, \tag{13.57}$$

$$\mathrm{c}^k_{\delta_i,\pi_j} u_j + \mathrm{d}^k_{\pi_j,\delta_j} \le g_j + \mathrm{E}(1 - x_{ij}) \qquad \forall\, i \in \mathcal{R}, j \in \mathcal{N}, k \in \mathcal{P}, \tag{13.58}$$

$$\mathrm{c}^k_{\pi_j,\delta_j} v_j + \mathrm{d}^k_{\pi_j,\delta_j} \le h_j + \mathrm{E}(1 - x_{ij}) \qquad \forall\, i \in \mathcal{R}, j \in \mathcal{N}, k \in \mathcal{P}, \tag{13.59}$$

$$\left|e_i - h_i + f_i - g_j - e_j\right| \le \mathrm{E}(1 - x_{ij}) \qquad \forall\, i \in \mathcal{R}, j \in \mathcal{N}, \tag{13.60}$$

$$p_j = \mathrm{p}_{\mathrm{o},j}; \quad e_j = \mathrm{e}_{\mathrm{o},j}; \quad k_j = \mathrm{k}_{\mathrm{o},j} \qquad \forall\, j \in \mathcal{M}, \tag{13.61}$$

$$x_{ij} \in \{0,1\}, \quad y_j \in \{0,1\} \qquad \forall\, i, j \in \mathcal{R}, \tag{13.62}$$

where E is the upper bound on the energy levels e_j, and T should be chosen larger than the latest expected pick-up time (conform to the big-M method [17]).

The objective function (13.47) consists of the total energy consumption during relocation (first term) and transportation (second term), the total time window misfit (third term), it puts a penalty on low energy levels (fourth term), and ensures correct estimation of the travel times (fifth term). A trade-off between using less energy, assigning less pick-up times outside the desired time windows, and keeping the batteries charged can be made by changing the weights $\alpha > 0$, $\gamma > 0$, and $\eta > 0$. The weights $\rho > 0$ and $\theta > 0$ can be used to reduce travel times, but when chosen small the energy consumption is minimized while ensuring correct travel times.

Equalities (13.48) are the assignment constraints ensuring that every request is handled once and only once, and (13.49) assigns the micro-ferry index numbers to the requests. Relocation times and transportation times are determined

using (13.50) and (13.51) respectively; variables r_j and t_j are minimized indirectly through (13.52). When request j proceeds i, (13.52) ensures that the pick-up time for request j is later than the pick-up time for request i, plus the transportation time, charging time, and relocation time (see Fig. 13.7). The time window mismatch s_j will be zero if the pick-up time p_j is scheduled within the desired time window $[\mathrm{p}_{\mathrm{a},j}, \mathrm{p}_{\mathrm{b},j}]$ through (13.53); otherwise, it will be equal to the time outside the time window.

With (13.54) we ensure that when the micro-ferry will charge, the charging time is at least equal to the (dis)connection time t_c. Furthermore, (13.55) couples the charged energy to the charging time, (13.56) ensures that the energy level will not increase when the micro-ferry will not charge, and (13.57) avoids overcharging of the batteries.

The energy consumed during the relocation phase and transportation phase are set using (13.58) and (13.59) respectively; the variables g_j and h_j are minimized directly through (13.47). Unlike the pick-up times (where time can pass while waiting), the energy level of request j is exactly equal to the energy level of request i minus the transportation and relocation energy consumption plus the charged energy, when request i precedes j (see Fig. 13.7). This conditional equality is enforced using the inequality constraints (13.60).

Finally, constraints (13.61) will set the initial conditions for the pick-up times, energy levels, and index numbers of the micro-ferries, and (13.62) are the integrality constraints for the binary variables used in this formulation.

Case Study Example

As a case study we use the Rotterdam harbor example as shown in Fig. 13.1, with $\mathrm{M} = 5$ micro-ferries and $\mathrm{N} = 40$ new requests. The water flow has a speed of 3 (m/s), and the micro-ferries are allowed to travel at speed between 4 and 16 (m/s).

The energy levels are given in percentages, with $\mathrm{E} = 100$ (%) indicating a fully charged battery. The coefficients in expression (13.30) for the power are chosen as $\mathrm{p}_0 = 0.1, \mathrm{p}_1 = -0.02, \mathrm{p}_2 = 0.002$, resulting in a minimum power consumption of 0.05 (%/s) at the optimal speed of 5 (m/s), resulting in a radius of 10 (km). The time for (dis)embarking the micro-ferries is set to $\mathrm{t_d} = 60$ (s), and charging can be done with a fixed setup time $\mathrm{t_c} = 60$ (s) at a rate of $\mathrm{r_c} = 0.1$ (%/s). At the optimal speed it will take 22 min to travel the largest distance of 6.6 (km) (from the station at Schiedam to the station at Rijnhaven).

An example schedule resulting from a randomly generated test case is shown in Figs. 13.2 and 13.8. Pick-up times are determined such that on average there will be 5 min in between consecutive requests per micro-ferry, and pick-up and delivery locations are chosen randomly (but not equal to each other). All micro-ferries start at a (randomly chosen) station with an energy level between 0 and 100 %.

Figure 13.2 shows the assignment of the $\mathrm{N} = 40$ new requests to the $\mathrm{M} = 5$ micro-ferries. Starting from the micro-ferry node, the arrows indicate the order in which the requests will be handled. The requests are sorted based on their desired

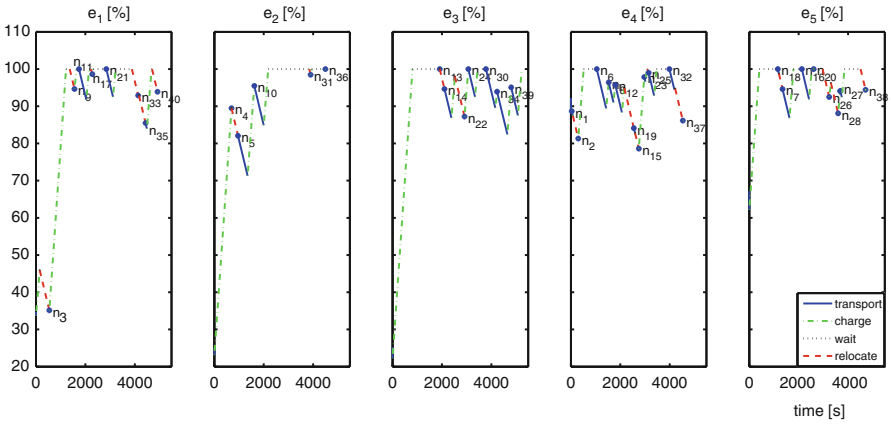

Fig. 13.8 Energy levels over time. Micro-ferries will charge when possible (*dash-dotted green lines*) to avoid empty batteries

pick-up time p_a, and all time windows $[p_{a,j}, p_{b,j}]$ are 60 (s) long. As can be seen the order of the pick-ups is not always consistent with the desired pick-up times, indicating that it was more efficient (in terms of the objective function (13.47)) to change the order.

In Fig. 13.8 the energy levels are shown over time. The different phases of a request are indicated using different line types: red-dashed lines are relocations, continuous blue lines are transportations, dash-dotted green lines indicates charging, and the black-dotted are associated with waiting. The blue stars indicate the pick-up times of the requests. As can be seen the micro-ferries will charge when possible.

13.3 Linking Transport of Water and Transport over Water

13.3.1 Transport over Water

The micro-ferry scheduling problem discussed in this chapter is an example of transport over water. Based on transport requests of customers along a river, the proposed optimization problem (13.47)–(13.62) provides an energy-efficient schedule for transporting customers over the flowing water. The formulation ensures that the micro-ferries will not run out of energy while traveling on the water; the energy level is not allowed to become too low, and charging of the micro-ferries is taken into account in the schedule. Taking into account the velocity of the current is crucial to ensure punctuality and correct predictions of energy levels.

13.3.2 Transport of Water

As discussed in this chapter—and formalized in Theorem 2—the influence of flowing water on the travel times and energy consumption is important for transport over water. Stronger currents result in larger mean travel times, and overall the energy consumption will increase. Since the transport of water will influence the strength of the currents in the rivers and canals, this effect should be considered when managing the water network.

13.3.3 Contribution to a Unified Framework

The micro-ferry scheduling problem can be seen as a transportation problem over water, which is influenced by the transport of water via the strength of the currents in the water network. For the short time-horizon of this problem (a few hours at most) the current can be seen as a constant, and due to the narrow time windows for the pick-up times there is little flexibility in handling the requests during more suitable water flow conditions. Nonetheless, the analysis of this problem shows that there is a direct relation between the strength of the current and the energy consumption.

This work could be extended to transport over water on a larger scale (e.g., between a harbor and the hinter land), such that people or freight will be transported within a large water network with distances of several hundred km, and the time-scale will be in days. In this case the expected water flows—due to transport of water—can be taken into account in the scheduling of the transport of goods. With freight the time windows are usually much larger, thereby creating more flexibility in planning the barges at times that the energy consumption would be low (i.e., when the current is relatively weak).

On the other hand, when given a freight transportation schedule, one can determine how the water network should be managed such that the objectives for the transport of water are met while also reducing the energy consumption for the barges. Eventually, this might lead to a combined optimization problem for both transport of and over water.

13.3.4 Global Performance Measurement

The performance measures for the transport over water as presented here are the total energy consumption of the vessels, and the time window misfit for picking up the customers. Both values should be as small as possible. When combining this problem with transport over water, performance measures such as minimum deviations from target water levels (combined with constraints on minimum and maximum levels) and energy consumption (e.g., for pumping water) can be taken into account in one large optimization problem.

13.4 Open Topics

The mixed-integer linear program (13.47)–(13.62) can be solved with standard hardware and software for small instances, but when considering many requests at once the computation times become too large to be useful in practice. To reduce computation times one could solve the problem over a limited time horizon, and recompute the optimal schedule periodically, hence using a rolling horizon approach. Furthermore decomposition methods [9] can be used to exploit the structure of the problem.

13.5 Conclusions and Future Research

13.5.1 Conclusions

In this chapter we have discussed a modeling framework for transport over water. Autonomous micro-ferries are used to transport customers over the water between different stations. A trade-off is made between energy consumption and picking up the customers on time, and charging of the micro-ferries is scheduled to avoid empty batteries. The speeds of the micro-ferries are also taken as optimization variables to increase the flexibility in scheduling the transport requests.

The micro-ferry scheduling problem can be seen as a variant of the multi-depot vehicle routing problem, and a mixed-integer linear program with 2-index decision variables has been presented to find appropriate schedules. This scheduling problem contains soft time windows, variable speeds, energy levels, and takes into account the effect of water flows. The effect of water flow speeds on both travel times and energy consumption is derived, and we conclude that the mean travel times and total energy consumption will increase with increasing magnitudes of the water flow.

13.5.2 Future Research

The micro-ferry scheduling problem consists in finding a transport schedule with times in the order of minutes, and with travel distances within a city. On this time-scale the water flow is expected to be almost constant. For future research one could consider long-distance transport over water (e.g., from the harbor to the hinterland) where both distances and time scales will be larger. In this case the water flow can no longer be considered a constant, and the influence of the (planned) transport of water becomes even more important.

Acknowledgements This work is supported by the European Union 7th Framework Program [FP7/2007-2013] under grant agreement no. 257462 HYCON2 Network of Excellence, and TUD COST Action TU1102 Towards Autonomic Road Transport Support Systems (ARTS).

References

1. Bektaş T, Laporte G. The pollution-routing problem. Transp Res B Methodol. 2011;45(8):1232–50.
2. Bektas T. The multiple traveling salesman problem: an overview of formulations and solution procedures. Omega 2006;34(3):209–19.
3. Boyd SP, Vandenberghe L. Convex optimization. 8th ed. United Kingdom: Cambridge University Press; 2010.
4. Burger M. Exact and compact formulation of the fixed-destination travelling salesman problem by cycle imposement through node currents. In: Proceedings of the 2013 international conference on operations research, Rotterdam, the Netherlands, Sept 2013. New York: Springer.
5. Burger M, De Schutter B. Energy-efficient transportation over flowing water. In: Proceedings of the 10th IEEE international conference on networking, sensing and control, Evry, France, Apr 2013. IEEE. pp. 226–31.
6. Burger M, De Schutter B, Hellendoorn H. An improved method for solving micro-ferry scheduling problems. In: Proceedings of the 1st European symposium on quantitative methods in transportation systems, Lausanne, Switzerland, Sept 2012. pp. 164–71.
7. Burger M, De Schutter B, Hellendoorn H. Micro-ferry scheduling problem with charging and embarking times. In:Proceedings of the 13th IFAC symposium on control in transportation systems, Sofia, Bulgaria, Sept 2012.
8. Burger M, De Schutter B, Hellendoorn H. Micro-ferry scheduling problem with time windows. In: Proceedings of the 2012 American control conference, Montréal, Canada, June 2012. IEEE. pp. 3998–4003.
9. Conejo AJ, Castillo E, Mínguez R, García-Bertrand R. Decomposition techniques in mathematical programming. 1st ed. Berlin, Germany: Springer; 2006.
10. Daganzo CF. Fundamentals of transportation and traffic operations. 3rd ed. United Kingdom: Pergamon Press; 1997.
11. Fossen TI. Marine control systems - guidance, navigation and control of ships, rigs and underwater vehicles. 1st ed. Trondheim, Norway: Marine Cybernetics; 2002.
12. Kara I, Kara BY, Yetis MK. Energy minimizing vehicle routing problem. In: Dress A, Xu Y, Zhu B, editors. Combinatorial optimization and applications. Lecture notes in computer science, vol. 4616. Berlin/Heidelberg: Springer; 2007. pp. 62–71.
13. Kulkarni RV, Bhave PR. Integer programming formulations of vehicle routing problems. Eur J Oper Res. 1985; 20(1):58–67.
14. Laporte G. The traveling salesman problem: an overview of exact and approximate algorithms. Eur J Oper Res. 1992;59(2):231–47.
15. Miller CE, Tucker AW, Zemlin RA. Integer programming formulation of traveling salesman problems. J ACM. 1960;7(4):326–29.
16. Savelsbergh MWP, Sol M. The general pickup and delivery problem. Transp Sci. 1995;29(1):17–29.
17. Taha HA. Operations research: an introduction. 4th ed. New York: Macmillan Publishing Company; 1987.
18. Toth P, Vigo D, editors. The vehicle routing problem. Monographs on discrete mathematics and applications. Philadelphia: SIAM; 2002.
19. Xiao Y, Zhao Q, Kaku I, Xu Y. Development of a fuel consumption optimization model for the capacitated vehicle routing problem. Comput Oper Res. 2012;39(7):1419–31.

Chapter 14
Potential Fields in Modeling Transport over Water

E. Osekowska, S. Axelsson, and B. Carlsson

Abstract Without an explicit road-like regulation, following the proper sailing routes and practices is still a challenge mostly addressed using seamen's know-how and experience. This chapter focuses on the problem of modeling ship movements over water with the aim to extract and represent this kind of knowledge. The purpose of the developed modeling method, inspired by the theory of potential fields, is to capture the process of navigation and piloting through the observation of ship behaviors in transport over water on narrow waterways. When successfully modeled, that knowledge can be subsequently used for various purposes. Here, the models of typical ship movements and behaviors are used to provide a visual insight into the actual normal traffic properties (maritime situational awareness) and to warn about potentially dangerous traffic behaviors (anomaly detection). A traffic modeling and anomaly detection prototype system STRAND implements the potential field based method for a collected set of AIS data. A quantitative case study is taken out to evaluate the applicability and performance of the implemented modeling method. The case study focuses on quantifying the detections for varying geographical resolution of the detection process. The potential fields extract and visualize the actual behavior patterns, such as right-hand sailing rule and speed limits, without any prior assumptions or information introduced in advance. The display of patterns of correct (normal) behavior aids the choice of an optimal path, in contrast to the anomaly detection which notifies about possible traffic incidents. A tool visualizing the potential fields may aid traffic surveillance and incident response, help recognize traffic regulation and legislative issues, and facilitate the process of waterways development and maintenance.

E. Osekowska (✉) • S. Axelsson • B. Carlsson
Blekinge Institute of Technology, Valhallavägen, 371 41 Karlskrona, Sweden
e-mail: ewa.osekowska@bth.se; stefan.axelsson@bth.se; bengt.carlsson@bth.se

C. Ocampo-Martinez, R.R. Negenborn (eds.), *Transport of Water versus Transport over Water*, Operations Research/Computer Science Interfaces Series 58,
DOI 10.1007/978-3-319-16133-4_14

14.1 Introduction

Flowing and static bodies of water are vital for shipping—the movement of goods and passengers—and as a source of food. Less critical, but still not insubstantial, is the recreational value (swimming, diving, boating, etc.) of seas, lakes and rivers. Thus ensuring maritime security and safety is an important concern for any nation, especially with coastal borders.

In order to safeguard the water, authorities such as the coast guard monitor the waters for signs of activity that could threaten these values. The variety of threats includes smuggling, piracy, accidents (collisions, sinking) and oil spills (accidental or intentional).

Nowadays, ships usually navigate using tools such as GPS, charts and radar in combination with ordinary piloting skills. In narrow waterways, such as a river or an estuary, piloting becomes more important. The seamen need skills in estimating the changing current and topography which depend on different water conditions such as the state of the tide, water level management, or rain fall. The route the ship follows is dependent on both the flow of the water and the piloting skills of the navigator (and any assistant tugs etc.). The contribution of piloting to navigation is difficult to observe and study, as it depends on cognitive skills distributed among the individual crew members [5].

Since 2002 more and more ships are equipped with AIS (Automatic Identification System) navigational equipment that sends and receives position data and other relevant parameters such as course, speed, daytime, type of ship, etc., to give ships and other interested parties a real time view of the shipping in an area [6]. Currently, the use of onboard AIS transceivers on international waters is enforced by the International Convention for the Safety of Life at Sea (SOLAS), and the measurement precision as well as the receiving coverage is constantly increasing. By recording AIS data it is possible to observe precise ship movements even in a narrow waterway and, hence, to get an indirect view of the process of piloting. This enables studying and modeling the actual effect that movement of water has on movement over water, and with sufficient feedback, also the reverse process.

This study uses a method based on potential fields applied to ship movement tracking data (AIS), gathered over a period of time. The potential fields are meant to represent the traffic, its specific properties and intensity in a discretized form, susceptible to visualization. Other existing path plotting solutions are capable of displaying the exact past paths of ships or providing a general statistic overview of the traffic. This study takes a step further in order to accommodate various vessel behavior properties (position, course, speed, daytime), as well as generalize over the data to provide an abstract traffic model.

To that end, all AIS ship tracking data are represented by abstract charge units. Each ship position reported by AIS generates a single charge (dropped by a ship) with values describing the ship's behavior at the reported longitude and latitude. The collection of all charges distributed over a geographical grid give rise to a potential field, which, when visualized, resembles an approximate plot of all the

commonly traveled waterways [6]. Unlike a plot, the potential fields has no linear representation, but a smoothened, heat-map-like representation, where stronger potentials are more desirable and locations with absence of potential should be avoided. Here, due to the limitations of the grayscale printing, potential fields are represented by shades of gray: from nearly white (weakest) to nearly black (strongest). In the original implementation, the colors are analogous to the actual heat map displays: from green being the least intensive traffic, through yellow, to red being the most intensive traffic. Contrary to a chart, which warns for rocks, reefs and shorelines, the extracted pattern shows preferred positions and routes, where deviations are shown as anomalies.

An additional benefit of the method is the decay effect allowing constant model retraining. Namely, over time the accumulated charges are affected by a decay factor, which weakens them the older they become. It allows for the unfrequented and closed waterways to expire, and be removed from the normal traffic model, thus keeping the model up to date. New and more frequented waterways are easier to establish, as the newly deposited charges are the strongest.

To investigate the applicability of modeling AIS traffic records using potential fields, we present an anomaly detection prototype system called STRAND (Seafaring TRansportation ANomaly Detection), which implements the traffic modeling for the collected AIS data. The system functionality is demonstrated here in a complex water system scenario (narrow navigation space, heavy traffic, complicated route).

The following section of this chapter presents the domain background and related research (Sect. 14.2). The in-depth description of the method design can be found in Sect. 14.3. It is followed by a case study in Sect. 14.4 and analysis in Sect. 14.5. Sect. 14.6 encompasses the inspection of study outcomes along with a transdisciplinary discussion into the unified framework and reflections about related open topics. The chapter is ended by concluding remarks and projection of possible future work in Sect. 14.7.

14.2 Background

In general, to aid the kind of monitoring performed in the scope of this study, many sources of data collection could be used, e.g., shore based radar, AIS, visual observations from, e.g., Coast Guard Cutters or civilian traffic. The data is augmented with data from databases, e.g., detailing ownership of ships, their particular properties, photographs and description, or weather forecasts. However, as previously mentioned, the focus is on the AIS system as a source of input, as AIS data are open, freely available and provide a variety of essential information about current vessels' state.

A problem here is the sheer amount of data that has to be processed. In other security domains (such as computer and network security, monitoring of nuclear material, etc.) traffic and behavior modeling as well as anomaly detection (the automatic detection of deviations from normal behavior) has proven useful in handling

comparable amounts of data and providing operators with indications of wrongdoing [1]. Such solutions comprise of advanced, self learning, modeling and anomaly detection systems that, given a mass of historical data, pick out patterns of normal (and abnormal) behavior, and apply this knowledge to the situation at hand. The systems continually appraise the situation and alert the operators about incidents that merit further investigation.

Data modeling and knowledge discovery systems are typically built on some form of machine learning. Machine learning is the study of algorithms that learn in some sense [11]. That is, these algorithms are not programmed in the normal sense of the word. Instead the algorithm is presented with a set of input data and builds a model of the input data domain. This model can then be used, for instance, to classify new input data (in case of anomaly detection typically into two classes: anomalous or normal) and predict how a modeled system will behave in the future. Subsequently, the operator can extract information about the model to gain insight into the modeled domain.

The evaluation of a modeling method's quality and performance is often a challenge. The correctness of a model is frequently shown or demonstrated by various non-numerical visualizations and displays [8–10, 14, 15]. Nevertheless, the ultimate way of assessing or comparing performance of a data modeling method requires a quantitative approach. In this case the applicability of the developed method is quantified by applying the acquired potential field based models to perform anomaly detection. In this study, the process of anomaly detection simply examines whether the currently observed ships are behaving in a way that conforms to the normal model. The definition of an anomaly in this study aligns with that of Chandola, Banerjee and Kumar [3]. Anomaly detection (or outlier detection) is the identification of items, events or observations which do not conform to an expected pattern or common behavior in a dataset. Where the terms anomaly (used here) and outlier are sometimes used interchangeably. Therefore, there is no specific definition of an anomaly and its properties, other that not fitting the normal model (i.e., model describing all possible behaviors considered normal).

Returning to machine learning, on a technical level there are two paradigms that are suitable for the purpose of developing this type of self-learning modeling and anomaly detection systems: unsupervised and supervised learning [17]. Which type is used, is typically based on the sort of input data one has access to. If the historical data (the input) is labeled with correct classifications or predictions (the output), it is possible to apply supervised learning algorithms to generalize from data with known classifications. If, on the other hand, the historical data does not include any associated predictions or classifications, there is a need to use unsupervised learning techniques instead of, e.g., clustering [17]. Consequently, the unsupervised approach is to learn from observations of input data without quantifiable evaluation of the output accuracy. Thus, for a classification problem, an unsupervised learning algorithm automatically partitions the data into groups, while a supervised learning algorithm instead generalizes from data which has already been partitioned into groups. In actual cases the distinction between these two

approaches is not necessarily as clear. In particular, in the AIS case investigated here, while the amount of data that can be classified as normal is large, there are no known (labeled) incidents occurring in the observed time frame. As a consequence, there is an overwhelming majority of benign over malicious event examples, i.e., examples of dangerous or unwanted behavior. Therefore, the approach in this investigation (as is often the case in anomaly detection) is somewhere in between supervised and unsupervised learning, with the classifier learning normal behavior from given examples, but having no well formed idea about unwanted behavior as such.

This work uses artificial potential fields as the machine learning algorithm. Potential fields were first developed in the AI community as a navigation and decision making mechanism, mainly for the development of game AI. The idea behind potential fields, used in that respect is, analogously to, e.g., electrostatic potential, to assign an attractive potential to a desirable position and repelling potential to undesirable positions [4]. This enables, e.g., a simulated unit in a computer game to find optimal positions and paths, by hill climbing in the resulting potential field.

In this work, that technique is used in the reversed manner, by using the idea of artificial potential fields as a learning algorithm, instead of using it for movement generation. The ship movements are used to create charges that ultimately define potential fields representing the patterns of normal behaviors, but also commonly occurring unwanted behaviors (e.g., sailing too near a coast line). By selecting the strength of the potentials and the functions that define how this potential decays with time and dissipates with the distance from the source, the performance of the navigation algorithm can be optimized. To our best knowledge this approach to machine learning, with the potential field defining what the system learns, is novel.

Regardless of the machine learning approach used, a common problem with anomaly detection systems is that they tend to overwhelm the operator with false alarms, i.e., alerts that are not connected to any notable malicious situation [3]. A majority of the commonly applied machine learning algorithms are designed with the main objective of generating the most accurate classification models, where accuracy is defined as the ratio of true classifications (both positive and negative) to all classifications. Accuracy is indeed an important factor to consider, when determining the suitability of an anomaly detection system. However, the fact that one system is proven to be more accurate than other systems does not necessarily imply that it raises fewer false alarms. In fact, it might very well do the opposite. Furthermore, even if there are techniques to address the false alarm problem at its root, for many real-world problems, it is still not possible to completely eradicate the existence of false positives.

Consequently, there is a need for complementary techniques to handle the remaining false alarms in a suitable way. Self learning systems are often opaque, i.e., not transparent in their structure or not intuitive to use. Thus it is difficult, not to say impossible, for the operator to develop a feel for exactly what the system has learned, and hence, to evaluate the correctness of the system. Does it, for instance, have enough background data pertaining to the situation at hand, to make an informed decision, or is it drawing far reaching conclusions based on a too

limited data set? In order to overcome this issue, and to address the remaining false positives, information visualization is applied to the problem of bridging the gap between the operator and the system [12].

Information visualization in the form of the heat-mapped [16] presentation of the potential fields, that make up the learned behavioral model, is used to put the operator in the loop. This way the instances of overfitting (where the detector has drawn too specific lessons from the available data), under training (where the detector instead draws too far reaching conclusions from the little data that is available) can be detected. The latter type of model fitting error often manifests itself in traditional systems as a detector that delivers its results with perfect assuredness, but is in fact wrong. Making the detector more transparent to the operator so that these and other situations can be detected and fixed is a major part of this research. Heat mapping is simply the visual representation of the field strength by color, where, e.g., the weaker (less desirable) field strengths are light gray to white and more intensive (and desirable) ones are dark shades to black. We demonstrate and discuss the actual use of visual pattern representation in the STRAND prototype in more detail in the sections to follow.

14.3 Potential Fields

The idea in using potential fields in maritime traffic modeling is to characterize a collection of an illegible mass of traffic data as an abstract structure that can be easily and intuitively perceived. The concepts of a magnetic field surrounding a magnet, an electrostatic field surrounding an electric charge or a gravitational field surrounding a celestial body, are common knowledge, and, as common, omnipresent phenomena observed every day, can greatly contribute to comprehension if used as an analogy.

Conceptually, each AIS trace (ship movement trace) assigns a charge to a specific location passed by a ship. A collection of charges distributed over an area generates a potential field. The strength of the local field also depends on the surrounding charges (i.e., their density and strength). The three main concepts, introduced by the potential field based method, are:

- the total strength of a local charge,
- the decay of potential fields, and
- the distribution of a potential field around its charged source[12].

Each vessel tracked by AIS is characterized by a collection of n numerical and textual properties. Those properties include the vessel's static parameters, (e.g., name, flag, type), as well as the current state of its dynamic behavior (e.g., speed, course, location), and are either inherently nominal or discretized to a nominal scale. A single vessel carries a set of charges of equal strength, representing its state and behavior projected onto these coordinates. For each AIS report, the set of charges c that a vessel carries is assigned to a location characterized by geographical position coordinates. Mathematically this can be expressed by a vector c_{lat_k,lon_k} with n components

$$c_{lat_k,lon_k} = \langle c^1_{lat_k,lon_k}, c^2_{lat_k,lon_k}, \ldots, c^n_{lat_k,lon_k} \rangle, \tag{14.1}$$

where $c^1_{lat_k,lon_k}$ to $c^n_{lat_k,lon_k}$ are the component charges reflecting reported vessel properties: speed, course, etc.; and lat_k, lon_k are the geographical latitude and longitude coordinates at point k. A vessel traveling in the evening hours (e.g., 21:20) with a northerly course (with a maximal deviation of $\pm$ 22°30') at a speed of 4 knots could for instance drop charges expressed by the following vector c_{lat_k,lon_k} at the passed location k:

Charge	Course				Speed [knot]				Daytime [h]			
	N	NE	…	NW	0–1	1–7	…	>60	6–12	12–18	18–0	0–6
$c_{lat_k,lon_k} = \langle$	1,	0,	…	0,	0,	1,	…	0,	0,	0,	1,	0 $\rangle$

The total charge C at a location is calculated as the sum of all local charges c. In electrostatics the greater an electric charge is, the stronger the electric potential field that surrounds it. Analogously, the more vessel visits are reported at a location, the higher potential builds up in and around it. Hence the aggregate charge C_{lat_k,lon_k} accumulated at a location k, over a time period τ is computed as:

$$C_{lat_k,lon_k} = \sum_{t=0}^{\tau} c_{lat_k,lon_k}. \tag{14.2}$$

The potential field formed by a single charge is most intensive at the location of the charge, and attenuates with (radial) distance. Areas where a potential is very strong represent a traffic pattern and belong to the model of the normal behavior. Areas where a potential is very weak or nonexistent, signal absence of normal behavior—an anomaly. In this study, the anomaly levels are determined using minimal potential thresholds. The total potential at location k is the superposed potential generated by all surrounding charges in location i, decreased by the distance between these locations. Here the potential distribution P is described by two-dimensional Gaussian smoothing, using Euclidean distance for measuring the radial distance between two points:

$$P_{lat_k,lon_k}(t) = \sum_i \frac{1}{2\pi\sigma^2} e^{-\frac{(lat_k - lat_i)^2 + (lon_k - lon_i)^2}{2\sigma^2}} C_{lat_i,lon_i}, \tag{14.3}$$

where σ is the standard deviation of the Gaussian distribution. This use of two-dimensional smoothing draws an analogy to the smoothing of gravitational sensor readings [7].

These equations assume no loss of charge over time. Continuous data collection, defined in that manner, would allow charges to accumulate without an upper bound. This is undesirable, as it would undermine the ability to compare and follow changing trends of the maritime traffic behaviors over time. E.g., once established

real-world traffic patterns may be abandoned as time passes. Therefore, it is desirable for the potential fields that model maritime traffic, to evolve over time to reflect such changes in patterns.

Researchers presenting different approaches often address the problem of real time continuity by applying constructs such as a sliding time frame or a data window [2, 13]. Potential field theory offers an alternative construct of potential decay. Adding a decay factor enables the continuous updating and retraining of the model, by representing charge at a location as a function of time:

$$C_{lat_k,lon_k}(t) = \sum_{t=0}^{\tau} d(t) c_{lat_k,lon_k}, \tag{14.4}$$

where $d(t)$ is a non-increasing decay function with limit at zero, describing the decrease of a local charge over time.

14.4 Case Study Setup

Figure 14.1 demonstrates the general idea of a normal model of vessel behaviors in traffic over water. The map-based representation displays a section of the Polish northern coast and the Gdansk Bay. The overlay, ranging (here grey scale) in shades from almost white to almost black, represents the potential field. In this case, the field expresses all vessel traffic without a specific parameter (such as a course, speed range or certain daytime). It becomes instantly apparent where the ports and harbors, as well as where all the regularly traveled waterways are. Nevertheless, most of the map remains without a visible potential overlay. It does not mean that these waters are closed or restricted, but only that transport in those areas is very infrequent or non-existent.

On the other hand, Fig. 14.2 displays a specific traffic sub-pattern. It is a potential field representing all traffic with course reported as N (northerly). The potential field is visibly sparser and only intensifies in specific areas. There is a clearly visible, regularly traveled, waterway between the port of Gdynia and Jastarnia within the Puck Bay. Both major ports in the region: Gdynia and Gdansk also generate visible amounts of traffic with a northerly course. A portion of the traffic on route from the Gdansk and Puck Bays also needs to pass close by the Hel Peninsula, therefore a local northerly traffic potential field can also be observed in near proximity to the eastern end of the peninsula. The further away from the ports, the more pale and scattered the northerly potential field becomes, which indicates, that this course is not frequently followed. This figure also demonstrates an example of detection. The captured anomalies, represented by larger gray arrows, picture ships violating the displayed northerly potential field. Two of them are observed in Zalew Wislany, where no prior vessel traffic has been seen whatsoever. Whereas the two other detections visible towards the north of the bay, appear to

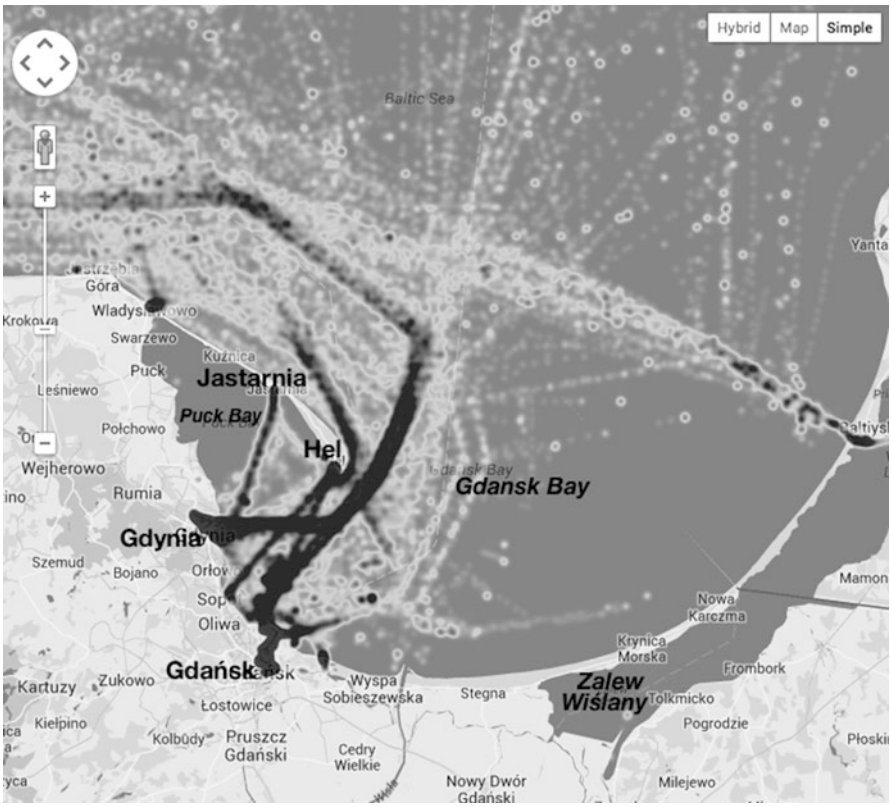

Fig. 14.1 Potential field representing an overall view of the traffic in the Gdansk Bay

be following a vaguely visible, but not well defined northerly potential, which is too weak to recognize their behavior as being normal. In the example from Fig. 14.2, the observed detection indications are supported by a display of the violated potential field, which provides instant insight into the situation, allowing to further minimize the incident reaction time.

14.4.1 Grid Size Versus Display Resolution and Detection Sensitivity

The collected AIS system records consist of packages of current data from each active vessel, downloaded every 90s. Each AIS report contains numeric and textual properties including vessel's static parameters (identification number, call sign and name) as well as current state of its dynamic behavior (time of day, speed, course, location). The tracking data updates are limited to one every 90s, which means that

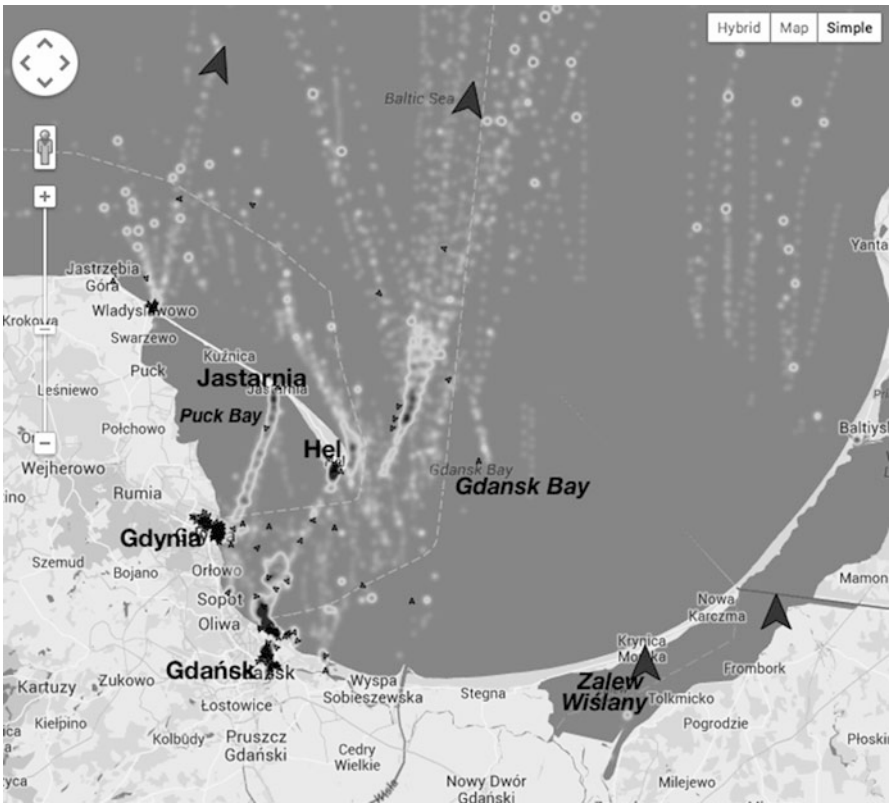

Fig. 14.2 A sub-pattern of traffic for course N, and examples of detections (potential violations)

every time a snapshot of the state of maritime traffic is acquired, it takes another 90s to acquire the next one. The potential field based method, expressed by the STRAND system, requires the setting of different parameters including the grid resolution, the optimization of which is essential for efficient pattern extraction and accurate detection.

The grid resolution in particular is a parameter defining the maximal geographic precision of the model. The linear domain of geographic latitude and longitude is discretized for the computations. In effect the map is represented in form of a grid. All AIS reports recorded within one grid point contribute to the charge of that grid node, therefore the grid size (or density) defines firstly, how dense or sparse the grid will appear when visualized, and secondly, what the maximal sensitivity of the anomaly detection is in terms of physical distance. A smaller size (or denser) grid results in more detailed visualization and higher detection sensitivity. A larger (sparser) grid provides a smoother visualization but lowers the sensitivity of the anomaly detection. Logically, the larger grid sizes are more applicable in locations where the charges (AIS ship position reports) are expected to be more distant from

one another. That occurs when ships travel at higher speeds and through less strictly defined paths, which is mostly the case on the open sea. On the other hand, in constrained conditions, where vessels follow the same paths and need to either remain static or strictly limit their speed, it is logical to expect to receive many AIS reports from very close locations. In the latter situation, where traffic incidents occur in narrower spaces and smaller distances, an increased density of the grid (smaller grid size), implying an increased visualization resolution and detection sensitivity, would be more applicable.

River systems, basin areas and water canal networks are characterized by narrow passages and often heavy traffic due to the limited space available for vessels traversing them. Depending on the time of day and specific location, this means more or less limited speed and narrow room for maneuver for the involved vessels. The experiment performed in this study focuses on such an area, and compares it with less restricted harbor setting. Traffic recorded over the same time period (20 days) from these two areas is modeled using the STRAND system. The selected harbor area includes the two major Polish ports of Gdynia and Gdansk, in the Gdansk bay and the bay of Puck, along with a stretch of the coast and a fragment of the Hel peninsula (see Figs. 14.1 and 14.2). The approximate coordinates are 54.3–54.7°N, and 18.4–18.9°E. The river area studied in the experiment is the Piast Canal connecting the Oder Lagoon with the Baltic Sea. It allows the eastern part of the natural Swina River to be bypassed, providing a more convenient north-south connection for large ships between the Baltic Sea and Stettin. The canal is approximately 12 km long and 10 m deep. In particular the investigation focuses on a narrow stretch of coast near the estuary limited by the approximate coordinates: 53.89–53.93°N, and 14.24–14.29°E (see Figs. 14.3 and 14.4). During a period of 20 days worth of data 2,263 MMSI (Maritime Mobile Service Identity) numbers, identifying one individual vessel each, were registered in the southern Baltic area containing both of the areas investigated in the case study. At the time point selected for demonstrating and analyzing the anomaly detection, in total 654 vessels were present in the southern Baltic basin, from which 120 were within the Gdansk Bay area, and 36—in the river area.

The investigation involved modeling traffic and performing anomaly detection in both of those waterways with grid sizes changing from 10 m to 2,000 m. The results acquired for all types of anomalies (i.e., course anomaly, speed, daytime and waypoint—the general anomaly type) were then stored as the ratio of the detection count to the total number of all examined vessels. With a grid size ranging from 10–100 m, the experiment was performed for each 10 m, in the range 100–1,000 m—for each 100 m, and additionally for 1,500 m and 2,000 m.

Generally speaking, the number of suspected waypoint anomalies decreases when the grid size is enlarged. The disadvantage is that a bigger grid size may also cause failures to recognize real anomalies. Consequently, there is a need to find a reasonable ratio, minimizing the amount of false anomalies without overlooking any actual incidents, in order to balance the trade-off between benefits and disadvantages of more general and more specific parameter settings. A locally optimal grid size (specific for a particular traffic case), would minimize the general type of anomalies

Fig. 14.3 Traffic pattern for course SW

(i.e., violations of traffic patterns for all types of potential fields), and present locally stable ratio between specific attribute detections (course, speed and daytime). If the optimum for specific detection rates correlates with a low count of the general (waypoint) detection type, a possible optimal grid size candidate is found.

Intuitively, an area of open sea should have a sparser grid than a harbor or river area grid. On the open sea traffic is typically faster, i.e., vessels pass longer distances between sending each two AIS reports; and it is sparser, with ships more distant from each other. Therefore, for a group of grid units to meaningfully represent a traffic pattern on the open sea, the grid ought to be relatively larger. For the case of the open sea the acceptable grid sizes range from 300 m to 1,000 m for course and speed, where the anomaly detection count stabilizes. The anomaly rate of waypoint detections is steadily decreasing until 2,000 m [12]. A comparison with the harbor and river traffic cases accentuates the influence of grid size and its relation to the traffic type.

Fig. 14.4 Traffic pattern for course NE

One property common to the traffic scenarios with close proximity between vessels and land or other obstacles, is the limited speed. A vessel moving with the speed of 2–5 knots, which is usual for narrow and heavily traveled passages in inland waters, will change its position by approximately 90–230 m during 90 s. Therefore, coarse grids, suitable for the open sea, are probably suboptimal in these areas.

14.5 Analysis of Obtained Results

The applicability of the potential field based method is demonstrated in practice by the STRAND system. The Piast Canal and the Gdansk bay areas, chosen for the case study, are constrained by factors such as the proximity of land, water flow (rate and direction) and maritime navigation rules. The visualizations of the patterns extracted using STRAND enable the observation of distinctive behaviors and learning about particular properties of the traffic.

14.5.1 Potential Fields as Traffic Patterns for Courses SW and NE

Figures 14.3 and 14.4 show patterns specific to the SW and NE courses, where the shades going from white, through grays to black, (in the original version, colors: green through yellow to red) represents gradually increasing traffic. In Fig. 14.3 the traffic following a south-westerly course seems mostly regulated: it intensifies mostly at the north-western bank of the river, while very sparse on the other side of the river. Still, it does get less regulated to the south, where ships seem to get closer to the opposite riverbank either to dock or "cut the turn". On the other hand, the north-easterly traffic in Fig. 14.4 seems to keep to the right bank in the south, but gets somewhat diffused towards the mouth of the river. The distribution of the potential also allows the observation of a probable reason for that NE traffic diffusing. A point at the western riverbank in the middle of both figures appears to be a frequent destination for tracked vessels, some of which seem to display a disregard for traffic rules when departing in north-easterly direction. That behavior occurred often enough to build up a relatively strong traffic pattern, and if repeated—it would be concerned normal, from a course-specific point of view. If speed, daytime and type of ship are evaluated, new anomalies may be discovered.

14.5.2 River and Harbor Case Comparison

The plots in Figs. 14.5 and 14.6 represent the numbers of detections of types: waypoint, course, speed and daytime. The total is the sum of all anomalies, (i.e., positive detections) regardless of type. Course and speed are stored with precision

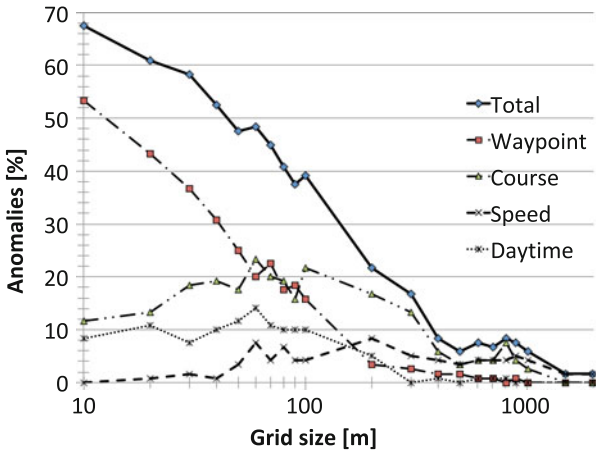

Fig. 14.5 Positive detections percentage in the harbor area as a function of grid size

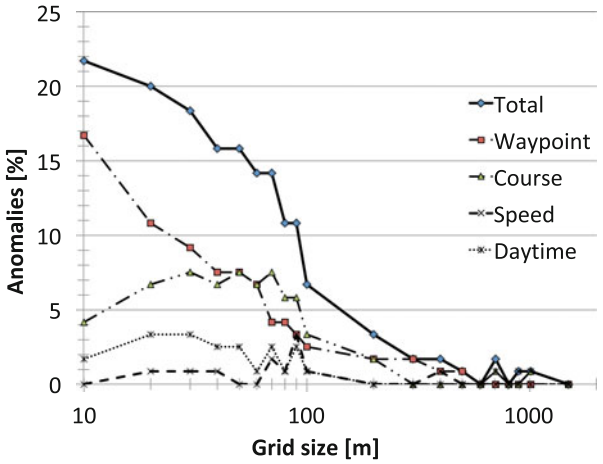

Fig. 14.6 Detections percentage in the river area as a function of grid size

0.1° and 0.1 knot respectively, but for practical reasons are grouped by range. Course is divided into 8 equal 45° intervals: N, NE, E, SE, S, SW, W, and NW. Speed ranges correspond to a speed division levels common for maritime traffic (in knots): Static (0–1), Very slow (1–7), Slow (7–14), Medium (14–22), Fast (22–30), Very fast (30–45), Ultra fast (45–60), and Beyond 60.

The course, speed and daytime are detections made based on an observation of a time of day, course or speed, with which the ship travels, and which is unusual for the ship's present location. It is important to note that these detections may overlap, e.g., a ship may travel with anomalous course and time of day, but at a speed that is normal for its current location. The waypoint detection signalizes the most severely anomalous behavior, and is triggered when a vessel is observed in an area in which no prior visit of any other vessel was ever observed. As a consequence this type of anomaly also indicates anomalous speed, course and daytime, increasing the detection count.

For the harbor area there is a range between 60 m and 200 m where an increased number of course and speed anomalies are found. At the same time the number of waypoint anomalies decreases and flattens out after 200 m grid size. Also the total percentage of anomalies are quite high in this range, up to 25 %.

For the river area the active grid size is even smaller. Starting at 30 m and until 100 m there is an optima for course anomalies. Waypoint, speed and daytime stabilizes at a low anomaly level (below 3 %) at a 100 m grid size, making the total anomalies appear slightly below 3 % of all observations.

14.5.3 Analysis of the Speed and Course Range Binning

Added experimental data sets for course and speed are produced by performing detection on data with altered speed and course. One of the data sets is computed for the real course (say NE) altered as if the ship was traveling with a course slightly more to the left (the altered course is N). In the second data set, the course is altered to the next bin right (e.g., S to SW). In the case of speed the next lower and next higher speeds are tested.

The diagram in Fig. 14.7 plots the results of detections performed on the traffic tracking data with the real speed and course, and with their altered (increased and decreased) values. It is immediately apparent that the amount of detections for the true observed speed and course is lower than for their altered values. The plotted results for altered courses are larger than for the real course. The observed distance between the real course plot and the altered courses shows that there are significantly fewer positive detections for the true 45° interval of vessels' courses, i.e., if the observed vessels were sailing a course set more to the left or to the right, approximately 3three times more of them would be marked as anomalous. This finding suggests that the course scale binning succeeds in differentiating the correct and faulty vessel courses. The lower speed is consistently only slightly greater than the true speed, while the higher speed plot shows much higher initial values and a substantial decrease after.

The patterns for the different parameters are similar, in Fig. 14.7 and 14.8, with high speed at the top and low speed at the bottom (but still above the general speed parameter). Left and right directions are above the general course parameter, with a left turn causing more anomalies compared to a right turn.

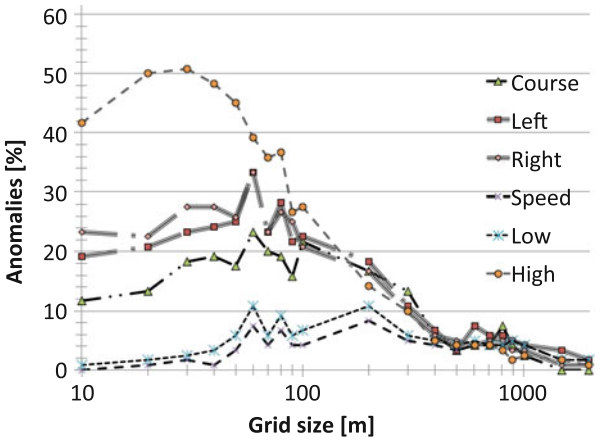

Fig. 14.7 Course and speed binning comparison for the harbor area

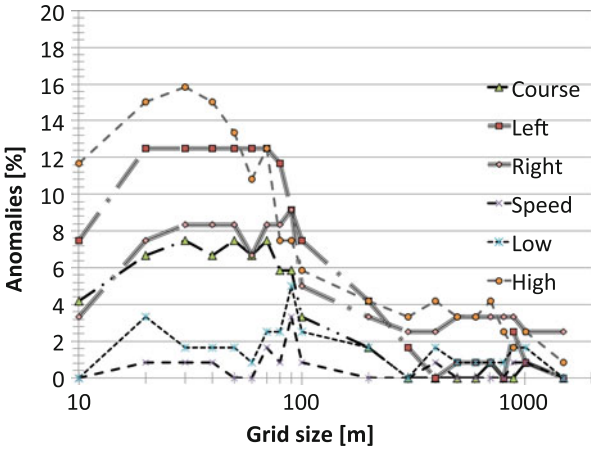

Fig. 14.8 Course and speed binning comparison for the river area

14.6 Open Issues and Interdisciplinary Discussion

Unlike the land, where for the sake of the transport roads need to be built, water is readily available for the transport over even the longest distances. The nearly omnipresent navigable waters do, however, require adjustments in key areas. Usually the changes made to waterways are focused where the most desirable itinerary destinations are, be it trade centers, naval bases, shipyards or leisure centers. The modifications include deepening the riverbed, or less frequently the seabed, to accommodate the draughts of all vessels sailing to that particular destination. Natural river systems may also require widening, to allow passage for broad vessels, traffic in both directions, or for multiple vessels to pass each other.

A larger scale of interference with the natural distribution of waterways is creating new ones, where they previously did not exist. Waterways of this kind are usually built in the most crucial transit locations, not necessarily being destinations on their own. Best known and most impressive examples include the Panama Canal linking the Pacific and Atlantic Oceans, the Suez Canal cutting the distance between Europe and the Far East, and the Welland Canal linking Lake Ontario with Lake Erie (and the St. Lawrence Seaway), avoiding the Niagara Falls by lifting vessels over the height of nearly 100 m. All this to expand the navigable waterways and connect basins for the purpose of water transport.

Such large scale changes may induce direct alterations as well as indirectly impact the natural or previously created waterways. Man-made water reservoirs cause abrupt breaks in the traffic, and may cause damaging alterations to the transport conditions downstream the dam, as well as the balance of the sweet water fauna and flora. To mitigate this kind of negative impact, a lock chamber is often used to open new waterways or substitute natural ones. Nevertheless, it still may prevent fish from migrating if it does not provide an alternative upstream fish-way,

which guarantees a sufficient flow of water. Enhancing waterways by straightening a meandering riverbed often results in changed and intensified sedimentation, thus indirectly changing the conditions for shipping. Such conditions may vary over time and be monitored using the potential fields, through their impact on vessels' behaviors.

These changes to nature are made because of the presence of a land barrier and too shallow or too narrow passages limiting the throughput, freedom, convenience etc. of the transport over water. The need for them, for centuries, was either a common knowledge based on the experience of those privy to the secrets of the seas, ranging from sailors through world traders, to trade and transport strategists. In the current age of digital water traffic registration, computing techniques are able to aid that process. The method based on potential fields, described, demonstrated and analyzed in this study, provides insights into vessel traffic that could be used as an aid or base for projecting maintenance needs and future needs for development of waterways.

The visualized potential fields show the intensity, type, and the time, course and speed related behaviors occurring in the traffic. The selective potentials display very distinctive patterns, which allow the observation of the specifics of the traffic. Thanks to the decay factor, the method also enables the observation and analysis of the changes in traffic trends over time. Such observations may result in the identification of undesired or unexplained behaviors in the traffic, as well as new trends that need to be accommodated. A simple example could be, where vessels commonly change their paths to avoid an unknown obstacle (e.g., a recently sunken ship), which should be removed or properly marked. It is possible to spot increases and decreases in traffic intensity, and examine their underlying causes using more specific potential field views. Another possibility is to observe the changes in speed. A common slowdown in traffic may indicate the presence of obstacles, degradation of the waterway, intensified traffic or a "jam", common violations of the law, etc., which can be made visible and susceptible to analysis by the use of potential fields.

As mentioned, some changes in traffic may be desirable or inevitable, and need to be taken into account. One such change may be the emergence of a new anchorage area, implying insufficient capacity of legitimate docking and anchorage areas. The observation of such behavior is also possible using the potential field based method. The answers to this kind of traffic issues may be, e.g., to increase the proper anchorage area capacity, or to regulate the new anchorage area in an organizational and legislative manner. If the newly emerged behavior is highly undesirable, there may be a need to strengthen the local law enforcement and introduce penalties for violating traffic rules. All along, the changes to traffic patterns, the emergence and decay of water transport trends, can be observed using potential fields. In that way, the STRAND tool can be of great use for waterway development and maintenance.

Furthermore, the adjustable resolution of the traffic modeling and anomaly detection have the potential to provide insights into traffic over water on a very detailed scale. It is possible to notice the symptoms of inefficient, insufficient or improperly used infrastructure. In ports with a large cargo flows the efficiency of docking, loading and unloading, as well as arrivals and departures is crucial for the

proper functioning of the port. Unwanted behaviors spotted either as new trends modeled by the potential fields, or as specific anomalies detected using the normal traffic model, may merit immediate reactions. Therefore our method may be of value for port authorities as well.

In river systems, harbor areas and open canal networks, the transport of water often varies either unconditionally or predetermined depending on local regulations, heavy rainfalls or temperature shift. Traffic conditions are also affected by topographical conditions, windy weather, or time of day. All of these conditions are not visible on a sea chart or by plotting the AIS data. Instead, the skills of the sailors involve both: handling navigational instruments, and making informed, knowledge-based decisions. For the transport over water we investigate three different benefits of using potential fields: visualizing navigational skills, acquiring an overview of actual frequented waterways, and detecting anomalous behavior.

An extended analysis of ship navigation and its actual practice aboard large ships in a naval setting has been the subject of Hutchins' study [5]. The observations in his study involve distributed ship navigation composed of multiple crew members, navigational instruments, water and environmental conditions. Cognitive skills observed in the actual practice aboard, referred to by Hutchins as cognition in the wild, constitute the human knowledge.

The ultimate outcome of the efforts of a crew, i.e., how their ship makes its way, is reflected by its AIS positions. Navigational skills are monitored and visualized by the concept of potential fields. Therefore, distributed cognitive processes in a ship may partly be described by potential fields, because of the effects of cognitive skills embedded in the AIS. The visualization takes into account strength and distribution of the potential field during a specific period of time. A decay function guarantee a flexibility over time; varying long term conditions affect the result by favoring newer measurements over older. In that interpretation, the developed method corresponds very closely with Hutchins view on learning, paraphrased here:

> I look at learning or conceptual change as a kind of local adaptation in a larger dynamic system of coordinations of representational media.

Current tools that visualize the AIS system give an overview of vessels encountered in a given area, including, e.g., type of ship, speed and position but also the previous route and destination. A disclaimer is that some of the data must be inserted manually and the AIS equipment may deliberately or accidentally be out of service. So a perfect overview of the actual traffic cannot be guaranteed. Adding visualization of the potential fields as a complement to the current AIS tools will improve the overview because it takes into account data of past experiences.

Potential fields may act as a way of planning the actual route to a destination. Waypoints may deviate and a certain velocity may be preferred depending on time of day, weekday and time of the year. One obvious way of detecting anomalies is to follow deviations from the route and the course of the ship. By plotting transmitted waypoints it is possible to detect previous positions and the proportion of vessels that visited the same waypoints in the past. In the same way, by plotting courses and speed it is possible to detect more volatile changes in the positions done by

the vessels. By adjusting the grid size to the specific conditions of transport in river and open canal networks, it should be possible to fine tune the anomaly detection facilities. We found preferred grid sizes varying from 300–1,000 m in the open sea, 60–200 m in the harbor case to 30–100 m in the investigated river case. Also, the number of proposed anomalies decreases to about 10 % of all observations or less, compared to about 15 % in the open sea and about 25 % in the harbor case.

For both harbor and river cases high speed generates a fivefold or more increase in the number of anomalies compared to low speed. In the harbor case, turning left or right has about the same amount of anomalies for the investigated grid size. In the river case, turning left causes around 50 % more anomalies than turning right. Traveling along a river is similar to traveling on a motorway, the driver needs to follow traffic rules, especially the right-side traffic rule and speed limits. The generated potential fields discover these rules automatically. For both cases: avoid traveling too fast because of heavy traffic and narrow passages. For the river case: avoid shifting towards oncoming traffic, i.e., turning left.

Although real incidents, i.e., requiring the reaction of the authorities, represent a vanishingly small percentage of all alarms, the potential fields monitor the actual behaviors, without any knowledge introduced in advance, i.e., are able to detect anomalous incidents in advance. Even though there will be a lot of false alarms (and most likely some real incidents will go undetected), for a supervisor, monitoring the actual traffic, introducing a tool for visualizing the potential fields would still facilitate traffic surveillance.

The AIS is an open system for the automatic identification of all marine traffic (as well as airplanes) live and in a real world setting. In the majority of marine traffic visualization tools available online, traffic is by default displayed as the plot of markers representing vessel positions symbolically marked on a two-dimensional map. Many of those pages enable viewing most recent position history for specific vessels, but none visualizes data of previous vessels no longer present at the sea chart. Therefore, the majority of visualization of AIS and other positioning equipment data, offer at best the viewing of the current state of the global fleet. The STRAND tool, computing and visualizing the potential fields, starts with a blank sheet, and fills it with accumulated traffic data recorded by AIS. The most frequented waterways become visible as lines and spots of intensive potential. The contours of the river banks or quays in the stream become visible as the lack of data instead of a pre-drawn template. All unexpected events, such as entering a not previously visited position or sailing with an unusual course, are regarded as anomalies.

The introduced anomaly detection tool, STRAND, should be regarded as a visualization tool for a human expert, introducing some novel skills compared to traditional equipments like radar and GPS. There are various potential benefits and practical applications of the method, depending on the user. From a ship navigator point of view, the display of patterns of correct or normal behavior, in this simple and clear form, aids the choice of the safest and most optimal path. From a traffic safeguarding perspective, the anomaly detection based on potential fields may help quickly and comprehensively inspecting possible traffic incidents. Finally, from

the authorities' point of view, the clear overview of traffic may help recognize traffic regulation and legislation issues, as well as aiding the process of waterways development and maintenance.

The investigation results suggest that it is possible to optimize routes using potential fields as a way of planning the actual route to destination, i.e., based on past experiences. Waypoints may deviate and a certain velocity may be preferred depending on time of day, weekday and time of the year. This may act as a planning tool subject to direct observations.

14.7 Conclusions and Future Work

This chapter described the successfully implemented method based on potential fields. The STRAND prototype system allowed to demonstrate the modeling capabilities of the method and optimize the detection performance. In two investigated study cases, the system has been shown to successfully model traffic and perform anomaly detection with results dependent on the geographical grid resolution. The visualization of the potential fields displayed a comprehensive representation of various traffic patterns, which allowed for an observation of trends in traffic flow and its regulation. The analysis of detection outcomes led to identifying the optimal grid sizes for each of the cases, and furthermore, resulted in an observation of the asymmetry in course-based detection, suggesting a right-hand sailing rule.

The visual and quantitative analysis based on the STRAND system demonstrated the applicability of the potential field based method. Nevertheless, many research goals remain to be addressed in future work. A major challenge is to conduct a valid quantitative study analyzing the detection performance of the method and its implementation. In the face of the lack of labeled AIS or radar data sets, and maritime anomaly detection benchmarks, an interesting performance study could be based on a combination of real AIS traffic data and information about incidents (e.g., from coast guards incident reports or IMO marine incidents database), which would be treated as labeled anomalies. Another challenge is to define and publish a first proper labeled data set with maritime traffic anomalies, to enable reliable comparative performance studies.

Another research direction left for possible future work is addressing the need for different modeling resolution (grid size) in different areas, depending on the intensity of the traffic and complexity of the waterways. A related issue is the distance represented by a unit of longitude, cosinusoidally decreasing with the increase of latitudes from the equator to the poles. In the examined case, the precision of longitude units is approximately halved (cosine at the latitude of ca. 55°), in order to prevent the latitude-longitude inequality in detection sensitivity.

There are various potential benefits and practical applications of the potential field based traffic modeling method, depending on the user domain, ranging from ship navigation, through traffic safeguarding and waterway maintenance, to legislation. When thoroughly examined, tested and optimized, the method and

its implementation could be used as an object of a user study, and deployed as a real-life application, either addressing a specific user group characteristics and requirements, or as a generic maritime information system, supporting the maritime domain awareness in a broader sense.

References

1. Axelsson S, Sands D. Understanding intrusion detection through visualization. In: Advances in information security. vol. 24. Heidelberg: Springer; 2006.
2. Brax C, Karlsson A, Andler SF, Johansson R, Niklasson L. Evaluating precise and imprecise state-based anomaly detectors for maritime surveillance. In: Proceedings of the 13th conference on information fusion (FUSION). 2010.
3. Chandola V, Banerjee A, Kumar V. Anomaly detection: A survey. ACM Comput Surv. 2009;41(3):1–58.
4. Hagelbäck J. Multi-agent potential field based architectures for real-time strategy game bots. PhD Thesis, Blekinge Institute of Technology. Sweden: Karlskrona/Blekinge; 2012.
5. Hutchins E. Cognition in the wild. Cambridge: MIT Press; 1995.
6. International Maritime Organization: Guidelines for the onboard operational use of shipborne automatic identification systems. 2002.
7. Jekeli C. Alternative methods to smooth the earth's gravity field. In: Reports of the Department of Geodetic Science and Surveying, Report 327, Ohio State University, Columbus. 1981.
8. Kazemi S, Abghari S, Lavesson N, Johnson H, Ryman P. Open data for anomaly detection in maritime surveillance. Expert Syst Appl. 2013;40(14):5719–29.
9. Laxhammar R, Falkman G. Sequential conformal anomaly detection in trajectories based on hausdorff distance. In: Proceedings of the 14th international conference on information fusion (FUSION). 2011.
10. Laxhammar R, Falkman G, Sviestins E. Anomaly detection in sea traffic - a comparison of the gaussian mixture model and the kernel density estimator. In: Proceedings of the 12th international conference on information fusion. 2009.
11. Mitchell TM. Machine learning. New York: McGraw-Hill; 1997.
12. Osekowska E, Axelsson S, Carlsson B. Potential fields in maritime anomaly detection. In: Proceedings of the 3rd international conference on models and technologies for intelligent transport systems. 2013.
13. Ristic B, La Scala B, Morelande M, Gordon N. Statistical analysis of motion patterns in ais data: Anomaly detection and motion prediction. In: Proceedings of the 11th international conference on information fusion. 2008.
14. Riveiro M, Falkman G. Interactive visualization of normal behavioral models and expert rules for maritime anomaly detection. In: Proceedings of the sixth international conference on computer graphics, imaging and visualization. 2009.
15. Riveiro M, Falkman G, Ziemke T. Visual analytics for the detection of anomalous maritime behavior. In: Proceedings of the 12th international conference information visualisation. 2008.
16. Tufte ER. The visual display of quantitative information. 2nd ed. Cheshire: Graphics Press; 2001.
17. Witten IH, Eibe F. Data mining: practical machine learning tools and techniques. Morgan Kaufmann Series in data management systems. 3rd ed. Burlington: Morgan Kaufmann; 2011.

Chapter 15
Safe and Efficient Port Approach by Vessel Traffic Management in Waterways

J. Froese

Abstract The vast majority of global transports are managed by waterborne transport and continuous trade increase calls for always more productive transport means and methods. Port approaches and waterways cannot become increased along with the increase of vessel size, especially in the container trade, and limits cannot become experienced by trial and error. Navigation errors may result in ship accidents with catastrophic consequences for man, material and environment. Therefore scientific methods are required to amend navigational expertise in order to enable management of waterborne traffic by exhausting the available infrastructure capacity without violating risk boundaries. Navigational requirements and conditions depend on manifold parameters which all must be taken into account when establishing an effective traffic management system as a further development of the existing vessel traffic service (VTS) systems. The paper elucidates the multidisciplinary views and contributions and provides an outlook into the current research path based on comprehensive experience from VTS-operations and the availability of advanced information and communication technologies.

15.1 Introduction

World trade continuously increases, fostered by free trade agreements allowing for commodities, capital and labor to flow freely. Global exchange of goods is dependent on effective and efficient transport systems in which the majority is moved by ships. The invention of a standardized transport units, the container, in the fifties of the last century, boosted global transport dramatically by lowering costs per unit. Nowadays there is a fierce competition between shipping lines resulting in the continuous effort to gain competitive advantage by economies of scale, means to deploy always bigger container vessels.

J. Froese (✉)
Jacobs University Bremen GmbH, 28759 Bremen, Germany
e-mail: j.froese@jacobs-university.de

C. Ocampo-Martinez, R.R. Negenborn (eds.), *Transport of Water versus Transport over Water*, Operations Research/Computer Science Interfaces Series 58,
DOI 10.1007/978-3-319-16133-4_15

As waterway dimensions cannot become increased with the same speed as vessel dimensions do, margins of safety of navigation are being increasingly exhausted because ports want to keep pace with ship development to not lose business. The big challenge is to enhance existing vessel traffic management systems to meet future requirements of ports with restricted navigational access without jeopardizing traffic safety. A vessel accident during a port approach, either by collision or grounding, may have disastrous results by polluting the environment by bunker oil or hazardous cargo.

Vessel traffic service (VTS) as provided by coastal states to surveil and assist vessel traffic is both, a technical system and a methodology. European VTS as most other similar services in the world follow the principle of "minimum interference with traffic". With respect to port approaches usually the "first come, first serve"-principle applies. This, however, results in suboptimal traffic flows.

The research work, jointly conducted with the German Shipping and Waterway Administration aims at identification of conditions and circumstances to be taken into account for optimum traffic flows, risk considerations and development of traffic guidance procedures to fully exploit waterway capacities without putting safety at stake.

The outline of this chapter is as follows. In Sect. 15.2, the main chapter discussion is presented, where the navigation conditions are explicitly stated, the relation of this research with transport of and over water is given, research objectives around the safe navigation are determined and several research project examples around this topic are listed and briefly discussed. In Sect. 15.3, the open topics of research in this field are proposed and discussed. Finally, the main conclusions of the chapter are drawn in Sect. 15.4.

15.2 Main Discussion

15.2.1 Navigational Requirements and Conditions When Navigating a River or Channel Fairway

Transport over water provides by far the highest transport capacity from all modes including road, rail, air and waterborne and both, global and national transport depend on it. As margins of safety on waterways are continuously shrinking upon the increasing size of the ships, traffic procedures must compensate to maintain an acceptable risk level.

Waterway traffic management depends on the relevant components of the ship-waterway-environment system are briefly elucidated below. The following system modules need to be considered (see Fig. 15.1).

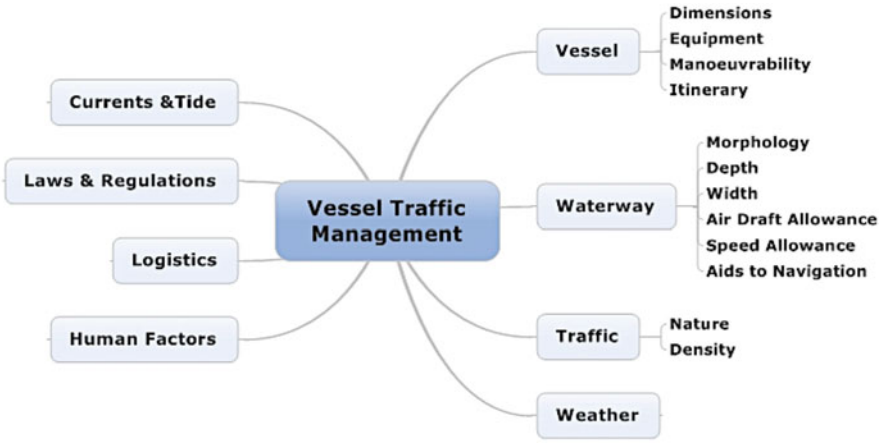

Fig. 15.1 Most relevant components of the ship-waterway-environment system

Vessel

Dimensions: The biggest container vessels currently (2015) in operation [15] measure

- Length 400 m
- Beam 59 m
- Draft 16,0 m
- Height 73 m
- Carriage capacity 19,100 TEU[1]

This, however, is not the end of development in carriage capacity and hence in size [14]. It is estimated that port and cargo-handling limitations, will allow for container vessels up to 24,000 TEU resulting in a length of about 450 m whereas the beam and the draft will stay relatively constant. These big vessels are not only a challenge for the ports but even more for the fairways leading to ports. There can be approach restrictions by

- navigable water depth
- fairway width
- sharp bends
- passage height under bridges

Equipment: Generally accurate navigation in coastal areas and port approaches is feasible assumed the availability of

[1]Twenty Foot Equivalent Unit, measurement unit to determine capacity and volumes in container transport, based on a standard container size of 20 × 8 × 8.

- two-axis speed sensor measuring both, speed through the water and over ground,
- heading indicator (gyro),
- rate of turn indicator (ROT),
- differential global positioning system (DGPS) providing a position accuracy within decimetre range,
- high resolution echo sounder,
- electronic chart display and information system (ECDIS), the maritime geographical information system [10],
- Radar,
- automated identification system (AIS) allowing identification and tracking of vessels [12],
- communication to other vessels and shore-based services.

These minimum requirements to safely conn a large vessel in confined waters are not always satisfactorily met, therefore portable pilot units (PPU) have been invented. A ruggedized laptop provides the processing and display platform to operate tools as ECDIS, AIS and individual pilot information. As rate of turn is very important, PPUs are frequently combined with two DGPS sensors temporarily mounted on the ship bridge, thus providing ship speed and ROT independent from vessel equipment. In case there is a pilot-plug available on the bridge to link a PPU to the vessel information system, the full range of vessel movement information will also be displayed.

Manoeuvrability: The track-keeping ability of a vessel depends on propulsion and steering means. The basic configuration provides a propeller and a rudder. Both can become combined when providing propulsion and steering by azimuth drives. Additionally bow thrusters can further improve manoeuvrability. In case of insufficient manoeuvrability, tugs can assist and provide external propulsion and steering forces. Under adverse wind and/or current conditions a vessel must maintain a minimum speed to compensate drift and to keep the intended track. This "safe minimum steering speed" of a vessel depends on vessel attributes, such as the lateral area under and over water and its distribution over the ship length causing both, a lateral drift and a turning momentum. Of course the safe minimum steering speed also depends on wind direction and force and ship heading. For a container vessel sailing under 7–8 Bft abeam wind,[2] the safe minimum steering speed will be around seven knots. Such a speed may already cause squat problems in areas of small under-keel clearance and the vessel command must solve the conflict between safe minimum steering speed and squat effects (increased immersion caused by dynamic pressure effects).

Itinerary: A big vessel may not just sail up a fairway and berth at a terminal. There must be a berth available and assistance services, such as pilotage, tug assistance and mooring teams, prepared to support. Of course liner ships sail according to

[2]Bft: Beaufort, a measure for wind speed provided in knots.

an itinerary but adverse weather conditions and delays in prior ports often result in a change of the estimated time of arrival (ETA) complicating the performance of the complex processes around a vessel's port arrival.

Waterway

Morphology: Appropriate fairway width and depth is a pre-requisite of safe navigation but besides an artificial channel with a constant symmetric profile, waterways including dredged channels provide an irregular morphology resulting in sometimes fast changing hydrodynamic forces upon the ship's hull. As hydrodynamic effects depend on the vessel speed, morphologic conditions may require reduced speed.

Depth: Required minimum water depth for safe navigation must take the following factors into account:

- immersion of ship hull (draft)
- water density depending on salinity and temperature
- trim, i.e., the difference between forward and aft draft
- list, i.e., heeling angle
- tide height including wind impact on water level
- uncertainties of tide prediction, soundings and charting

not only for static conditions, e.g., alongside a berth but also for dynamic conditions by hydraulic-hydrodynamic interaction when underway. A heeling angle will not only be caused by distribution of load and ballast but also by abeam wind or by rudder momentum in a turn. If not in calm waters possible rolling, heaving and pitching, increasing the draft, must be considered. Ship's draft in shallow water also is increased by squat (increased immersion caused by dynamic pressure effects) depending on speed.

The margin of safety in navigable water depth is called *under-keel clearance* and shall take into account all factors listed above. Hence the under-keel clearance is not a fixed value but depends on actual conditions as expected tide, wind speed and direction and manoeuvre speed. It is common under normal conditions to determine the under-keel clearance by 10 % of the vessel's draft. A vessel sailing at 14.5 m draft then requires a water depth of minimum 16 m for safe navigation. Under tight conditions when the under-keel clearance is already exhausted and tide effects the approach of big ships, larger uncertainties in tide predictions are not acceptable. Those ports where large vessel traffic depends on the tide usually have a very accurate tide prediction service based on hydrographical and meteorological conditions. Radio-equipped tide gauges then allow continuous assessment of actual tide conditions.

Benefiting from raised sea level by tide impact works well when sailing upstream a river towards a port as the ship speed usually allows keeping pace with the tide progress from the open sea towards the port. When departing from same port, aiming at the open sea it becomes more complicated as the low tide travels

from the sea towards the port and the vessel can only benefit a brief period from the raised water level. Therefore for tidal ports the departure time window is narrower than the arrival time window. Accurate calculation of exploitable time windows therefore is essential.

Width: Fairways are marked by buoys but this does not mean that the maximum draft allowance is valid for the whole fairway as there are often channels dredged providing less width than the fairway. Dredging of fairways is very costly and waterway authorities therefore try to minimize efforts resulting in a channel within the waterway just meeting vessel navigational requirements. Big ships can only use parts of the buoyed fairways and therefore are dependent on highly accurate navigation as there can be on special marking of the dredged channel which would hinder all other traffic. When assessing the navigability of fairways also the dynamic conditions must be taken into account:

- Bank effect, asymmetric water flow caused by the proximity to the channel bank, results in a suction effect towards the bank and a turning momentum away from the bank which in the worst case may result in loss of ship's controllability
- Ship-to-ship interaction, when ships overtake each other or meet, high and low pressure areas of both ships are adding up to pushing off, suction and turning effects with risk of collision; the same effects between a vessel moored and a passing vessel may result in breaking the moorings of the vessel berthed.
- When passing a channel bend a vessel must turn resulting in a drift angle increasing the effective ship's *footprint* width.

A channel width of 300 m is common for dredged channels and when considering a vessel beam of around 50 m in an encountering situation with a vessel of the same size, results in a passing distance of only 100 m when both ships maintain 50 m distance from the channel border. With regards to possible ship-to-ship interaction this must be considered as an absolute minimum and is only possible in a straight channel without any bends, at moderate speed conducted by competent navigators.

Air Draft Allowance: If a port approach requires passing of a bridge, the maximum air draft allowance must be taken into account. When most bridges were constructed nobody estimated the big size of today container vessels resulting in a maximum air draft of about 60 m, depending on the vessel's immersion (draft). A deep draft vessel requiring tidal support to maintain a safe under-keel clearance might then have problems to pass a bridge.

Speed Allowance: Vessels navigating in a fairway cause swell waves. Depending on the fairway width these waves may have an impact on shore-based constructions, natural environment or persons at the strand. For narrow waterways therefore speed restrictions apply.

Aids to Navigation: Visual aids to navigation such as buoys and lighthouses are valuable cross references when determining a vessel's position but advanced navigation widely relies on electronic aids to navigation, mainly satellite-based

GPS and the more accurate DGPS[3] where a shore-based reference station within the same area corrects the GPS signal.

Traffic

Nature of Traffic: The composition of ship types and carried cargoes within a traffic pattern has an impact on traffic organization as, e.g., passing distances and tug escorts. Traffic hindrances as underwater works, divers and vessels restricted in manoeuvrability also must be considered.

Traffic Density: Traffic density as nature of traffic is a risk factor. The higher the density the more probable a casualty occur.

Weather

Meteorological conditions include sea state, wind, rain- or snowfall, visibility and ice. Besides the wind impact on the tracking keeping ability of a vessel, also heavy rain, snowfall and fog may restrict visibility and require reduced speed.

Currents and Tide

Current may either impede a vessel's track keeping ability, when causing a drift, or influence speed over ground or both. As tidal currents and heights are time-dependent navigational conditions may considerably change once the length of a fairway results in long exposition time of a vessel. There are European waterways requiring up to 8 h sailing time from the open sea to the port.

Laws and Regulations

- National laws as far as possible are compatible to international laws, however, national conditions usually require some modifications.
- Regional/local regulations cover peculiarities.

Logistics

Logistics here refers to the flow of cargo to and from a port and terminal is related to vessels arrivals. Containers are usually delivered and picked up within 3 days

[3]Differential global positioning system providing correction of satellite-based position by land-based reference stations.

before arrival and departure of a vessel. Ultra large container vessels, carrying almost 20,000 TEU and hence causing between 6,000 and 10,000 moves (container handling) per terminal provide a challenge not only to the terminal logistics but also to road traffic management, where haulage trucks can cause huge traffic jams. The estimated time of arrival (ETA) of such big vessels therefore is the key trigger of all related processes far beyond mere navigation.

Human Factors

Vessel traffic in coastal areas and port approaches is well regulated but neither can regulations cover all potential situations nor do they provide detailed performance guidance. The effectiveness and safety of a port approach therefore also depends on the skills, the knowledge and the attitudes of the operators managing all processes from pilots conning the vessels to the mooring man, berthing it. Education, training and experience must mirror technical and operational opportunities and risks to allow for most adequate decision making and performance.

Vessel Traffic Management

A vessel traffic service (VTS) [11, 13] is a shore-based service provided by a shipping administration (competent authority) to support safe and efficient vessel movements in coastal waters (territorial sea, usually 12 nautical miles off coast). The traffic image is generated from radar detection and individual vessels and their sailing plans are captured by VHF-communication,[4] AIS and VHF direction finders exploiting VHF communication transmissions. A VTS needs reliable and comprehensive traffic image and vessel sailing plans to provide

- information service providing traffic, weather and navigational information to support on-board decision making delivered at regular time intervals, event-driven or upon vessel request,
- traffic organization service, advising or, in case the VTS-operator is accordingly empowered, instructing vessels to mitigate navigational risks,
- navigational assistance service upon request of individual vessels, in case of extraordinary vessel passages (tug and tows, deep draft vessels or vessels otherwise restricted in manoeuvrability or posing a higher navigational risk) supporting the vessel command including the pilot aboard or sometimes even replacing the pilot (remote or distant pilotage), e.g., in case of adverse weather, not allowing a pilot to board a vessel,
- enforcement of laws and regulations.

[4]VHF: Very high frequency, the marine mobile band covers the frequencies between 156.0 and 162.025 MHz.

A VTS service is commonly being considered an advice to the vessel based on information available in the shore-based traffic centre and the interpretation ability and general competence of the VTS-operator. The final decision making must take place on the vessel's bridge as a traffic situation may locally be different than according to a displayed image. Frequently VTS authorities, depending on the national regulations, are empowered to intervene as a shipping police authority, e.g., to slow down, halt or deviate traffic in case of an accident. Even when available techniques and technologies would allow for a stronger position of a VTS to direct ships rather to only provide advice, authorities are reluctant to change their operation to not transfer navigational responsibility from ship to shore and hence liability.

15.2.2 Link to Transport of and over Water

Ships traffic in a specific waterway environment cannot become increased unlimited. Besides physical restrictions as, e.g., fairway dimensions, the traffic may not result in unsafe situations resulting in unacceptable risks. The governing research question therefore is to develop methods and tools to exploit a waterway to its maximum traffic capacity without violating risk boundaries. As the composition of waterborne traffic in relation to all possible vessel collectives and the navigable geometry can be extremely multifaceted, this requires a research solution embracing all potential configurations and conditions.

15.2.3 Research Objectives

Port approaches which are not adjacent to the open sea resulting in longer waterways to be navigated very seldom have the capacity to allow for free flow of vessel traffic. There are sections of waterways where large ships may neither overtake nor encounter each other. Some narrow waterways only allow for one-way traffic or provide encountering and overtaking *boxes* in wider sections. This calls for a stringent traffic management providing sailing plans to vessels and guide them accordingly, continuously tracking position and speed, intervening once pre-planning traffic pattern is not maintained.

However, there is still a navigational principle reading "first come, first serve", a reluctance of shipping authorities to intervene and no satisfactory tools to pre-plan and manage complex traffic conditions. Even a long waterway was easy to manage as long as there were only very few big ships per high tide to consider. Encounterings and overtakings could be managed on short notice either by the vessels command alone or assisted by the vessel traffic service. The number of large vessels meanwhile increased dramatically and is further increasing so that the optimum flow of traffic is difficult to determine.

Optimization goal must be the total throughput of traffic not the easiness of an individual vessel. This can of course result in waiting times for some vessels. The research objective then is to develop a model, allowing for computer-based traffic prediction and management and to support decision making within a system of increasing complexity.

The above described components of a waterway result in a large amount of information. It is not long that in traffic and logistics lack of information was an issue and often caused disturbances. The triumphal procession of information and communication technology (ICT) meanwhile resulted in the contrary, information overflow, making it very difficult to identify the significant information. Successful future vessel traffic management therefore will widely depend on computer-based support tools for interpretation of traffic pattern and for appropriate decision making.

15.2.4 Research Examples

ISIMAT

In 2002 there was already evidence that the percentage of very large vessels will continuously increase and pose a problem for managing the waterway traffic. The German Ministry of Education and Research therefore awarded a research contract to a consortium composed of Atlas Elektronik GmbH (VTS Manufacturer), Institute of Ship Operation, Sea Transport and Simulation ISSUS and BLG Consult. The project duration was from 2003 to 2005 and the research part "interactive vessel traffic management tool" was conducted by ISSUS [5]. Goodwin [7] and Toyoda et al [16] had developed vessel domain models indicating the "effective area around a ship which a navigator would like to keep free with respect to other ships and stationary objects" as defined by Goodwin. The domain model however was developed for area traffic rather than line traffic. Area traffic allows ships to sail in almost all directions, resulting in crossing of ship trajectories, whereas line traffic allows only bi-directional traffic with encounters and overtaking but no crossings. Traffic in waterways is line traffic and hence the domain model had to be adapted.

The relationship between all traffic vessels, other floating and fixed objects and the waterway was described by cells. A single cell of defined dimensions can be occupied by various objects to be considered by a vessel navigating along the waterway. Attributes can become awarded to cells as wells as to objectives. Cell attributes are, among others, dimensions and alignment of dredged channel and traffic rules to restrict, e.g., encounters. Attributes of objectives are for instance vessel type and cargo (e.g., hazardous cargo), dimensions, position and track and speed. Ship attributes include the three-dimensional vessel domain, speed, acceleration/deceleration and all parameters relevant for safe navigation. Attributes can be static, as, e.g., object and cell dimensions are, or dynamic as vessel movement, meteorological and tidal conditions. This classical entity relationship

model (ER-model) approach must allow the definition of relationships not only between entities (objects) but also between attributes as in case of strong wind, e.g., the attributes *direction of wind and force*, *ship heading* and *stability* must provide the input data to calculate the increase of the ship's draft by wind-caused heeling.

ISIMAT considerations are ship-focused, not traffic focused, i.e., the view from own ship to all traffic to become encountered during the whole waterway passage. The domain geometry was specified according to the input of ship masters which resulted in particulars more relevant for the open sea than for waterways. In any case the ISIMAT domain model provides a workable platform for further research and development.

SafePort

The SafePort project [2] was co-funded by the European Commission and conducted from 2010 to 2011. The consortium consisted of BMT Group Ltd, Dublin Port, Kongsberg Norcontrol, Universities of Glasgow and Stratclyde, Marimatech, NEXT Ingegneria dei Sistemi SpA, Istituto Superiore Mario Boella and Port Authority of Gijon.

The objectives of SafePort were to develop and demonstrate a vessel traffic management and information system (VTMIS) to foster safe navigation and port efficiency and to develop a pilot aid (SafePilot) to support the realization of a sailing plan provided by the VTMIS. Accuracy of positioning was of emphasized by using EGNOS[5] functionalities. In order to achieve these objectives, the accuracy, reliability and safety of life aspects of EGNOS are critical. Additionally, the implementation of authentication mechanisms to support identification and safe recognition of assets, cargo, ships, etc. is essential for safety-related operations.

PRISE

The Port of Hamburg can only be reached by Europe's longest sea port waterway. The distance from the pilot boarding station at the mouth of the River Elbe to Hamburg is about 78 nautical miles (about 144 km). Large container vessels must match their sailing plan to the course of tide to safely navigate up and down the river. For the Port of Hamburg accessibility is a sensitive issue to maintain the position as a global hub port.

In the view of the increasing number of large vessels, resulting in complex traffic processes along the waterway, it was decided to develop an IT-platform to optimize sequencing and arrival of mega-ships on the river Elbe and at the Port of Hamburg,

[5]European Geostationary Navigation Overlay Service, a European DGPS to augment satellite-navigation for increased accuracy.

Fig. 15.2 Port River Information System Elbe (PRISE). Adapted from PRISE/DAKOSY

the Port River Information System ELBE, in brief PRISE [8], see Fig. 15.2. The project consortium under the leadership of DAKOSY was composed of the terminal operators HHLA and Eurogate, the Elbe Pilot Association and Hamburg Port Authority. The work commenced in 2011 and was concluded in 2013, then followed by a 1 year test bed and finally the operational system launched in March 2014. The project was financed by the terminal operators HHLA and Eurogate as well as the operative platform.

PRISE allows the terminals to plan ahead, to react on changes of ETA on short notice and to apply optimized cooperative resource planning. Of course there has been more research, test beds and case studies, however, the general tendency is to improve current traffic management without re-thinking the whole system and benefiting from new technologies or go even one step further to first provide a vision and then driving development into this direction. ISIMAT was found the only research project attempting some new trend-setting by providing the basis for a decision support system assisting both, VTS operators and vessel commands, to significantly increase the time window for traffic planning and manage extremely complex traffic systems. Since the project had been concluded, technology has been further advanced and nowadays provides the toolbox for solutions allowing to maximum exploit existing infrastructure to foster more but still safe and efficient traffic without extending current infrastructure. Many waterways are reaching a limit not allowing for further deepening and/or widening for ecological but also financial reasons. A more intelligent use of existing waterways and ports then is the only way to grow economically.

15.2.5 Multidisciplinary

A safe and efficient port call of a large vessel navigating along narrow waterways requires an interplay of various disciplines such as those listed below (among other):

- Naval architecture regarding vessel design and hydrodynamics
- Shipbuilding
- Navigation providing manoeuvring requirements
- Hydrography capturing and describing navigable waters including tidal effects and charting it
- Hydraulics to provide knowledge of water transport
- Meteorology capturing and describing weather phenomena
- Civil engineering to allow appropriate construction of shipping infrastructure
- Information and communication technology providing the vital platform for information exchange and processing
- Logistics providing the commercial framework of ship operation
- Assistances services to provide pilotage, tugs and mooring
- Shipping administrations offering vessel traffic service and establishing the regulatory framework

Assumed that the existing infrastructure and shipping services allow safe and efficient navigation and the vessels dimensions and manoeuvrability stays within feasible margins, traffic operations must become adapted to the dynamic waterway conditions. Waterway traffic of course needs to be efficient to meet logistics commercial goals but it also must be extremely safe applying a zero-accident policy as the consequences of a collision or grounding within a waterway can be really disastrous from the point of environmental pollution. Risk assessment and mitigation therefore must be an inherent part of all planning and operation. The large vessel sizes force to exploit the system boundaries until the very edge and hence the determination of minimum margins of safety is essential based on sound risk assessment. This however is only possible once detailed and up-to-date information of all relevant aspects is accessible and can be processed to produce an estimated traffic image of high accuracy and within a time frame to allow for timely traffic organisation when required.

For many waterways there are commonly hydraulic and tidal models available. Individual vessels manoeuvring behaviour as well as a whole traffic patterns can be simulated. Research aims therefore should be set at developing a cluster simulation model allowing determining optimum traffic organisation (sequencing, sailing plan, speed profiles) sufficiently advanced to actual navigation to manage traffic accordingly. Jointly with the German Shipping and Waterway Administration the current national vessel traffic management system is scrutinized to identify needs and opportunities for enhancement.

15.2.6 Research Concept

By combining state of the art conning techniques and technologies aboard of prudently navigated vessel on-board intelligence can be generated which will allow widely autonomous traffic behaviour (compare *free flight concept of air traffic control* [3]).

The on-board system may consist of a repository of all vessel-related information amended by the necessary up-to-date local knowledge transmitted from the VTS. The local/regional methods, regulations, rules, tools, databanks etc. finally contribute to compose a powerful decision support system communicating with the VTS as governing authority, other vessels, filtering the relevant ones, tracking those, simulating path and manoeuvre prediction in relation to traffic and fairway and displaying conning information to allow the navigator to follow and confirm manoeuvres. In tidal waters radio-gauges in combination with tidal models will allow to manage small under-keel clearances in real time taking all governing conditions into account.

The recently developed 3D-ECDIS [1, 4] will allow much more precise navigation according to actual morphology. Decision-support systems (DSS), some years ago developed from artificial intelligence systems have not been very successful in applications with a high share of uncertainties, solved by inference engines and heuristic methods and tools (*learning from experience*). In navigation, heuristics is a questionable concept for decision making in critical situations but this seems not necessary when basing on advanced but proven techniques and technologies. Almost all decision making in navigation can become deterministic assumed necessary information can be retrieved. A difficult issue, however, remains risk mitigation but not because of the DSS deficiencies but because of currently not satisfying risk assessment methods (additional research required).

There are indicators that multi-agent system (MAS) technology can provide a solution to improve autonomous navigation in congested waters. A MAS consists of *agents* and the *environment*. Usually agents in MAS are software agents but also can be widely autonomous acting intelligent entities (active cognitive agents) as it is the case in traffic management where the vessels represent the agents.

The advantage of applying MAS to support vessel traffic management is that it must not be switched from *conventional* to MAS but can be gradually invented and tested. Thus no undefined risk must be taken. Similar to the free flight concept in air traffic control [3], the role of a VTS will change from a continuously provided service, currently still by verbal communication, to a supervising and on-demand advising service, only intervening upon request or system alerts indicating unclear or risky situations and conditions.

15.3 Open Topics

Whatever new systems and operations will emerge from on-going and planned activities, one current basic principle of vessel traffic management needs to be jettisoned: *first come, first serve* can no longer become applied once the total traffic system is the subject of optimization. Organizing large vessel traffic in narrow waterways requires sequencing of vessel in such order that encountering and overtaking conflicts are avoided or at least minimized.

An accurate picture of the navigable underwater morphology is of utmost importance. The current electronic sea-chart, a particular type of an Electronic Chart Display and Information System (ECDIS), is based on a so-called landscape model representing the morphology in two dimensions. Depth areas are planes of same minimum depth and significant soundings are embedded sounding objects. For precise navigation and for prediction of hydrodynamic effects as squat and bank effects, a high-resolution 3D-chart is required (3D terrain model). The technology has been developed within the EU project EFFORTS [1, 4] and in principle is available.

There are currently no methods for reliable assessment of navigational risks. This is because risk, defined as the multiplication product from probability of event by average consequence costs, is a probability-based approach. Different from road traffic, sea traffic does not deliver a sufficient number of accidents to determine probabilities. Accumulation over time (considering many years) is no solution because conditions, mainly by invention of new technologies, changes. Trustworthy risk assessment, however, is an indispensable pre-requisite of decision making in vessel traffic management. Therefore further research is required searching for another approach. The functional resonance analysis method, to analyse complex socio-technical systems, extended by the environmental component, seems to be worth-while for investigation [6, 9].

15.4 Conclusions and Future Research

Well established systems with convincing success records are not prone for easy changes. Thus it is much easier to modify established vessel traffic management services and system gradually than to come up with a widely new concept. Going for something new must not follow the *the newer, the better* principle but a sound cost-benefit analysis. What does it cost to not optimum exploit existing waterways or port clients swooping ports because of delays or risk of accidents? Which are the benefits of a new concept and what does it cost? How can a solution become validated and verified? How getting all involved party in the same boat? Political issues are usually much more difficult to become solved than any technical problem.

Future research should follow the a.m. path but of course can be questioned and argued. A constructive think tank activity will then hopefully set the scene.

Own concepts have been disclosed knowing that science is at least as competitive as commerce but all experts will immediately understand that no single entity or small consortium can solve all problems within an acceptable time frame, therefore a distributed research approach is required involving several disciplines.

References

1. Bailey T. All in the detail, ports & harbours; 2009.
2. European Commission. Safeport. http://www.safeportproject.com/.
3. European Commission/Eurocontrol. Sesar - the future of flying. http://www.airtrafficmanagement.net/2012/11/handing-over/.
4. Froese J. Effective operations in ports. In: Port Technology International, number 41; 2011. http://www.porttechnology.org/technical_papers/.
5. Froese J, Hoyer S, Töter S. ISIMAT - Interaktives Schiffsverkehrsmanagement-Tool, Teilprojekt 2: Strukturen, Schnittstellen, Domänenstrategie: Endbericht zum Forschungs- und Entwicklungsvorhaben. TUHH ISSUS, Maritime Logistics; 2006.
6. Frost B, PT. Mo J. System hazard analysis of a complex socio-technical system: The functional resonance analysis method in hazard identification. Technical Report, School of Aerospace, Mechanical and Manufacturing Engineering, Royal Melbourne Institute of Technology; 2014.
7. Goodwin EM. A statistical study of ship domains. J Navig. 1973;26:130–130.
8. Hamburg D. Port river information system elbe (prise). http://www.dakosy.de/en/solutions/port-community-system/prise/.
9. Hollnagel E. FRAM, the functional resonance analysis method: modelling complex socio-technical systems. England: Ashgate; 2012.
10. International Maritime Organisation (IMO). Performance standards for electronic charts, 1995. Adopted in 1995, by resolution A.817(19)), amended in 1996 by resolution MSC.64 (67) and by resolution MSC 86 (70).
11. International Maritime Organisation (IMO). Guidelines for vessel traffic services; 1997. Resolution A.857 (20).
12. International Maritime Organisation (IMO). Guidelines for the installation of a shipborne automatic identification system, 2003. http://www.imo.org/OurWork/Safety/Navigation/Pages/AIS.aspx.
13. International Association of Marine Aids to Navigation and Lighthouse Authorities (IALA). Vessel traffic services manual. 5th ed; 2012.
14. Lowry N, Porter J. Scorpio sets sights on 20,000 TEU titans. Technical Report; 2014.
15. Maersk. http://www.maersktechnology.com/stories/stories/pages/triple-evessels.aspx.
16. Toyoda S, Fujii Y. Marine traffic engineering. J Navig. 1971;24:24–34.

Chapter 16
Technological Challenges and Developments in European Inland Waterway Transport

R.G. Hekkenberg

Abstract In many parts of the world, vast quantities of goods are transported over rivers and canals by means of ships and pushed convoys. This makes these waterways important transport corridors. Of all modes of transport, inland waterway transport has the strongest interaction between infrastructure and the vessels/vehicles that perform the transport. Locks, bridges and waterway depth limit the dimensions of vessels that are used in all directions, while the water depth, fairway cross-section and flow speed of the water have a significant impact on the speed and fuel consumption of these vessels. This in turn influences the cost of transport and thereby the economic viability of transport over water. In this chapter, the interaction between ship and waterway and its impact on the economic viability of inland shipping is highlighted, followed by a discussion of the recent and ongoing efforts to innovate the design of inland ships with the aim of minimizing transport cost and emissions. This is followed by a case study in which the dimensions of inland tank ships that are intended for operation on the river Rhine are optimized, taking into account the properties of the waterway and the boundary conditions that are imposed by the transport chain in which the ship operates. Finally, on the basis of this case study and the discussion of recent and ongoing innovations, possible approaches for optimization of inland waterway transport and inland ships are discussed.

16.1 On the Interaction Between Ship and Waterway

The interaction between a ship and the waterway on which it sails is a crucial factor in the economic viability of operating this ship and, therefore, in the viability of inland waterway transport on a given waterway. This section will elaborate on which factors influence the competitiveness of inland shipping and how these factors are affected by the interaction between ship and waterway.

R.G. Hekkenberg (✉)
Delft University of Technology, Delft, The Netherlands
e-mail: r.g.hekkenberg@tudelft.nl

C. Ocampo-Martinez, R.R. Negenborn (eds.), *Transport of Water versus Transport over Water*, Operations Research/Computer Science Interfaces Series 58,
DOI 10.1007/978-3-319-16133-4_16

Table 16.1 Cost breakdown for a large Rhine vessel [1]

Labor	42 %
Capital cost	30 %
Fuel	14 %
Repair and maintenance	3 %
Other	11 %

In a market such as that of intra-continental transport of goods in Europe, direct transport costs are a crucial decision driver for shippers [9, 11]. Often whoever can transport goods at the lowest price will be commissioned to do so, as long as certain boundary conditions regarding service schedule, transport time and cargo carrying capacity of the vessel or vehicle are met. Furthermore, in a highly competitive market, over a longer period of time cost and price of transport will be close together [5]. Since the European inland waterway transport markets for containers, dry bulk and liquid bulk are all highly competitive, lower transport cost per unit of cargo implies a better competitive position of a shipping company. A large part of all inland shipping companies in Europe are owner-operators with a single ship, no office ashore and no administrative staff. E.g., in the Netherlands owner-operators with a single ship account for 89 % of all inland shipping companies [2]. Therefore, the cost of transport is very strongly related to the ship and its operation. As an example, Beelen [1] provides an indicative cost breakdown, as shown in Table 16.1, for a large Rhine vessel, i.e., a dry bulk vessel with a length of 110 m and a beam of 11.40 m, one of the most common vessels in western Europe:

The cost elements in Table 16.1 will be discussed below in order to create a further understanding of the influence that the properties of a waterway have on the viability of inland waterway transport.

Labor costs are strongly dependent on the crew requirement of a ship, which in western Europe is prescribed by regulations by the CCNR [3]. According to these regulations, the number of crew members and their job description are dependent on the operational profile of the ship (14, 18 or 24 h per day, represented by the codes A1, A2 and B), the length of the ship, the level of equipment on board (coded S1 or S2) and whether or not any barges are pushed. A small part of these regulations, for ships not pushing barges, is shown in Table 16.2.

Since the crew requirement is partly determined by the size of the ship, but is not linearly dependent on its cargo carrying capacity, ships of different sizes will have different labor cost per ton of cargo carrying capacity. As a rule, the larger the ship, the lower the labor cost per ton of cargo carrying capacity will be. Since the maximum size of a ship is typically determined by the length and width of the locks in its intended area of operation, the depth of the fairway and/or regulatory limits that are associated with the properties of the waterway itself, there is a strong link between these waterway properties and the labor cost of transport by inland ship. What the maximum size of ship is that is allowed to sail on various European waterways, is clarified by means of a classification system that is developed by CEMT [7]. Table 16.3 shows a part of this classification system.

Table 16.2 Crew regulations

Class	Crew	A1		A2		B	
		S1	S2	S1	S2	S1	S2
L ≤70 m	Captain	1		2		2	2
	Helmsman	–		–		–	–
	Full sailor	–		–		–	–
	Ordinary sailor	1		–		1	–
	Basic sailor	–		–		1*	2*,***
70 <L ≤86 m	Captain	1 or 1	1	2		2	2
	Helmsman	– or –	–	–		–	–
	Full sailor	1 or –	–	–		–	–
	Ordinary sailor	– or 1	1	–		2	1
	Basic sailor	– or 1	1	1*		–	1
L >86 m	Captain	1 or 1	1	2	2	2 or 2	2
	Helmsman	1 or 1	1	–	–	1 or 1**	1
	Full sailor	– or –	–	–	–	–	–
	Ordinary sailor	1 or –	–	1	–	2 or 1	1
	Basic sailor	– or 2	1	1*	2*	– or –	1

*The basic sailor or one of the basic seamen may be replaced by a deckhand
**The helmsman needs to be in possession of the patent required by the Rhine patent rules
***One of the basic sailors must be over 18 years of age

Table 16.3 CEMT classes and ship dimensions (partial)

Waterway class	Maximum length (m)	Maximum beam (m)	Maximum draught (m)
I (West of Elbe)	38.5	5.05	1.8–2.2
II (West of Elbe)	50–55	6.6	2.5
III (West of Elbe)	67–80	8.2	2.5
IV (West of Elbe)	80–85	9.5	2.5
Va (West of Elbe)	95–110	11.4	1.8–2.5–2.8
⋮			

In practice, the dimensions of the majority of ships that are built are just below these maximum dimensions or the length at which the crew complement needs to be increased, as shown in Table 16.2.

The second major cost component in Table 16.1 is capital cost. Like with labor cost, capital cost of a ship is not linearly dependent on its cargo carrying capacity. EICB [6] provide some figures: a ship with a cargo carrying capacity of 450 tons costs around 1.2 million Euro, while a 1,500 ton ship costs around 2.5 million Euro and a 3,000 ton ship costs around 3.5 million Euro. Since these figures imply lower capital cost per ton of cargo carrying capacity for larger ships, this again demonstrates that larger ships, which require larger waterways, have a definite cost advantage over smaller ships.

The third major cost component from Table 16.1 is fuel consumption, the prediction of which is still one of the main scientific challenges in inland waterway transport. The actual fuel consumption of an inland ship is strongly dependent on many factors. When water is wide and deep, for instance in oceans, the relation between the speed and fuel consumption of a ship is roughly quadratic: if a ship sails twice as fast, it will require roughly four times as much fuel to get from A to B. How much fuel that is, in turn depends on the size of the ship, its shape and the properties of its propeller(s) and drive train. It, however, also depends on other factors that are not part of the design of the ship itself such as the wind, waves and current that the ship encounters and the amount of marine growth on the hull (i.e., barnacles, algae, etc.).

When the water in which a ship sails gets shallow and/or confined, for instance on a river, there is further interaction between the waterway and the ship. Shallow water will limit the maximum speed of the ships to roughly the root of the gravity constant multiplied by the water depth: $v = (gh)^{0.5}$. When the ship's speed approaches this speed, its resistance rises rapidly. As a result of this, in practice inland cargo ships will not sail faster than 70 % of this speed, which is usually much slower than the normal speed of seagoing ships. This in turn limits the number of trips that a ship can make and thereby limits the amount of cargo that a ship can transport in a given amount of time. When a waterway is not only shallow, but also has a limited width, fuel consumption at a given speed is increased further. In this case, the ship will basically act as a blockage that is moved through the waterway. Since the remaining waterway cross-section at the position of the ship will be smaller than the cross-section in front of the ship and behind it, the flow speed of water along the ship's hull will increase. As a result of this, more power and fuel are needed to propel a ship at a given speed than when it would sail in unrestricted water.

Methods to correct a ship's speed or propulsion power for shallow water effects were developed as early as 1932 by Schlichting [13] and improved in 1963 by Lackenby [10]. Since then several more methods have been developed, but according to Raven [12] "there are doubts on their validity and accuracy", especially in the extremely shallow and confined conditions posed by inland waterways. Furthermore, there are no adequate empirical methods available to assess the impact of some of the specific features of inland ship hulls, such as the tunnels at the aftship or the bow shape, which may be very different from that of seagoing ships. This leaves only model testing or CFD calculations as acceptable ways of predicting a ship's fuel consumption, and in practice this is often considered to be too expensive for Inland ships. Furthermore, these methods also have their limitations and inaccuracies. As a result, it seems safe to conclude that there is often significant room for improvement regarding both the prediction of an inland ship's fuel consumption and the fuel consumption itself.

Apart from the difficulty of assessing the fuel consumption of a given ship in a waterway with a known cross-section and depth, as discussed above, there is the additional complication that these properties are not easily determined. Especially in free-flowing rivers, water depth as well as cross-section will change both in time and in space: The waterway slowly erodes while the current will carry sediment

to different locations, thus changing the water depth locally. At the same time, rainfall and/or melting of snow will influence the amount of water that flows through the river at any given time, thereby changing both cross-section and depth. Geographically the waterway cross-section will increase as more tributaries join the river and the cross-section's shape will differ strongly from place to place due to the natural shape of the river and due to manmade obstacles such as groynes.

Summarizing the above, around 90 % of an inland ship's cost is influenced by the properties of waterway on which it sails. This makes inland waterway transport a mode that interacts much stronger with the infrastructure it uses than road and rail. There is, however, still a lot of room for improvement regarding the analysis of this interaction.

In the next section, it is elaborated what ship operators are currently doing to improve the economic and environmental performance of their ships and operations, taking into account the limitations of the waterways. Section 16.3 will discuss a case study on the optimization of ship dimensions, which will put the ongoing scale enlargement of European inland ships in perspective. Section 16.4 discusses the link between transport over water and transport of water. In Sect. 16.5, conclusions are drawn and relevant future research is discussed.

16.2 Recent Developments in Inland Ship Design

There appear to be two major drivers for innovation in inland ship design in the European inland shipping sector: innovations are either focused on reducing costs or on reducing emissions. Both will be discussed in the following sections, starting with the reduction of costs and followed by the reduction of emissions.

16.2.1 Developments with the Goal of Reducing Costs

Especially in Western Europe, the dimensions of inland ships have always been closely related to the limiting dimensions of infrastructure like locks. In practice, many ships have dimensions that are close to the maximum dimensions of the CEMT classes that are shown in Table 16.3. There is, however, a trend towards larger ships, thereby increasing economies of scale. In the last decades, only very few ships are built for class I to III waterways, while more and more ships have main dimensions that are larger than class Va, which essentially limits their operational area to the larger rivers. Figure 16.1, taken from the PhD thesis of Hekkenberg [8] shows a clear increase in the average deadweight of newbuild vessels in the period 1996–2008. This trend is also identified by TNO [14], who on the basis of trend line analysis predict an average increase in cargo carrying capacity of roughly 2 % per year between 2008 and 2020. Furthermore, in 2011, the 147 m long tank ship VT

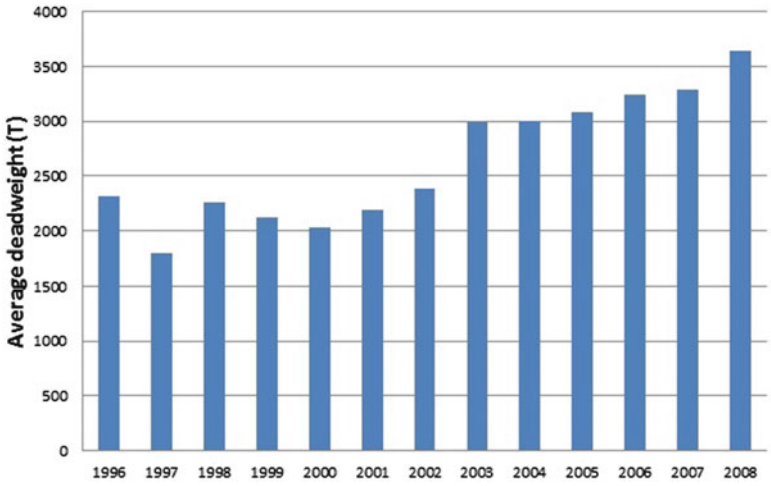

Fig. 16.1 Average deadweight of newbuild ships

Vorstenbosch entered service. This made it the first inland ship in Europe to exceed the length limit for indivisible ships of 135 m imposed by the Central Commission for Navigation of the Rhine (CCNR).

In order to maximize economies of scale for small ships, the Dutch Barge Truck and Q-barge projects looked into the development of small coupled units or push convoys with self-propelled barges, that are able to sail independently on small waterways and can be joined on larger waterways. In Belgium, a similar approach was studied by Van Hassel [16] within the INLANAV project. Thus far this has however not resulted in a significant market uptake of such concepts.

Other efforts to reduce costs through modifications to the ship are mainly found in the field of ship resistance and propulsion. There has been extensive research into the possibility of reducing drag through air lubrication of the hull, e.g., in the PELS and PELS II projects, while more efficient, bio-inspired, alternatives for the ship's propeller have been investigated in the form of the whale tail wheel in the 1990s [15] and, more recently, through a similar concept by O-foil who have built a full-scale system on a 40 m long inland ship in 2013. A different concept, the Futura Carrier, featuring distributed propulsion by means of two steerable propellers at the stern and two at the bow, was developed around 2007. Several vessels of this type were built, but there appears to have been no further market uptake of the concept.

There are also attempts to reduce costs through a more efficient drive train. Diesel-electric and hybrid alternatives to conventional diesel direct drives have been implemented on several vessels such as diesel-electric tank ship Amulet, built in 2010, and hybrid dry bulk ship Semper Fi, built in 2012. Despite claims of significant fuel savings, such vessels, however, remain exceptions and the majority of the newbuild fleet is still diesel-direct driven.

Apart from the scale enlargement discussed earlier, the main innovation that actually appears to get a foothold in the sector is the use of LNG as a fuel. The benefits that are attributed to LNG are that it is cheaper than gasoil and that it leads to lower emissions. Despite difficulties like the absence of bunker stations for this fuel and regulations that forbid its use on board inland ships, the first LNG-driven inland ship, tank ship Argonon, entered service in 2011. Since then, work is done to develop bunker points for LNG and to develop suitable regulations for its application as a fuel for inland ships. Meanwhile several more vessels that are fueled by LNG have been built, several shipyards have developed concepts for such vessels and in 2014, coupled unit Eiger-Nordwand was retrofitted with an LNG installation. However, price development of LNG as a fuel for inland ships remains highly uncertain and as a result, so does the future development of LNG-powered inland ships.

16.2.2 Developments with the Goal of Reducing Emissions

Traditionally, inland shipping is known as a very fuel-efficient and, therefore, environment friendly mode of transport. However, with the introduction of the EURO emission standards for truck engines, inland shipping's main competitor, road transport, has managed to drastically reduce its emissions of NOx and PM (particulate matter). This development, together with the fact that inland ships emitted much more SOx than trucks due to the much higher sulphur content of inland shipping fuel, led to the situation that in the first decade of the twenty-first century, inland shipping in many cases no longer outperformed road transport in terms of environmental performance. Following the development of the EURO standards for trucks, the CCNR I and II standards were developed for inland ships. At the time of writing of this chapter (i.e., 2014), however, the emission limits for these standards are much less strict than those of the latest EURO standards. Nonetheless, there have been several incentive schemes for clean ships, as a result of which a number of catalysts and particulate matter (PM) filters have been installed on board of inland ships, thereby drastically reducing their emissions of NOx and PM. Meanwhile, the emission of SOx has been virtually eliminated because in 2011, the sector switched from the "original" fuel to sulphur free diesel that is also used in trucks, called EN590. The major downside of filters and catalysts is that thus far, they are not profitable investments and there is no outlook that this will change in the future. The investment cost, maintenance cost and, in case of catalysts, price of consumed urea outweigh any potential fuel savings. Therefore, unless external incentives or more strict emission regulations are developed, it seems unlikely that there will be a large scale market uptake of these technologies. There have been a host of projects trying to reduce the emissions, including project CREATING in FP6 (the European 6th framework research programme) and project MoVe IT! in FP7, but thus far, this has not led to generic solutions that have been applied widely.

An alternative to reduction of emissions from diesel engines is the use of other sources of energy. Since solar energy requires large surfaces of solar cells to generate any significant amount of energy and using wind energy is impractical on confined waterways with many (low) bridges, these technologies have not gained a foothold in inland waterway transport. There have been several projects that investigated the potential of hydrogen as a fuel, but they have not been applied to inland ships on a larger scale than river ferries and small passenger boats. For cargo ships, there are too many obstacles like the required volume of the hydrogen tanks, the absence of bunkering facilities and the high price of fuel cells. The only alternative energy source that appears to be really breaking through is LNG, as was discussed in the previous section. It offers an outlook of reduced cost as well as reduced emissions, although the actual costs are still highly uncertain as a result of the uncertainty of the price development of LNG at bunker stations.

16.3 Transport Cost Minimization for Inland Ships: A Case Study

In the previous sections, it was discussed that there are several ways in which the European inland shipping sector has tried, and still tries, to reduce costs and/or emissions. It was also discussed that only a few of these developments are actually taken up by the market. The development that has thus far impacted the market most is scale enlargement. Therefore in this section, a case study is presented to assess how large the benefits of further scale enlargement can be for tank ships on the river Rhine. The details of this study, as well as similar studies for dry bulk and container ships and a description of the models underlying the case study may be found in previous work by the author [8].

16.3.1 Case Setting

In this case, the transport of gasoil from the oil terminals in Rotterdam that are located in close vicinity to the Dintelhaven port basin to Dordrecht (45 km), Nijmegen (136 km), Duisburg (247 km) and Koblenz (430 km) is studied, see Fig. 16.2. The route to each of these locations is free of locks, thereby allowing large ships to reach them. Furthermore, this route is located on the busiest inland waterway stretch in Europe.

To assess to which extent an increase in the dimensions of inland ships will lead to benefits in terms of cost reduction, it is assessed what the out-of-pocket cost of transport, i.e., the amount of money that the shipper will have to pay to the transport operator to transport his goods, will be as a function of the dimensions of the ship that is used. It is also assessed how a shipper's total logistical costs, which includes

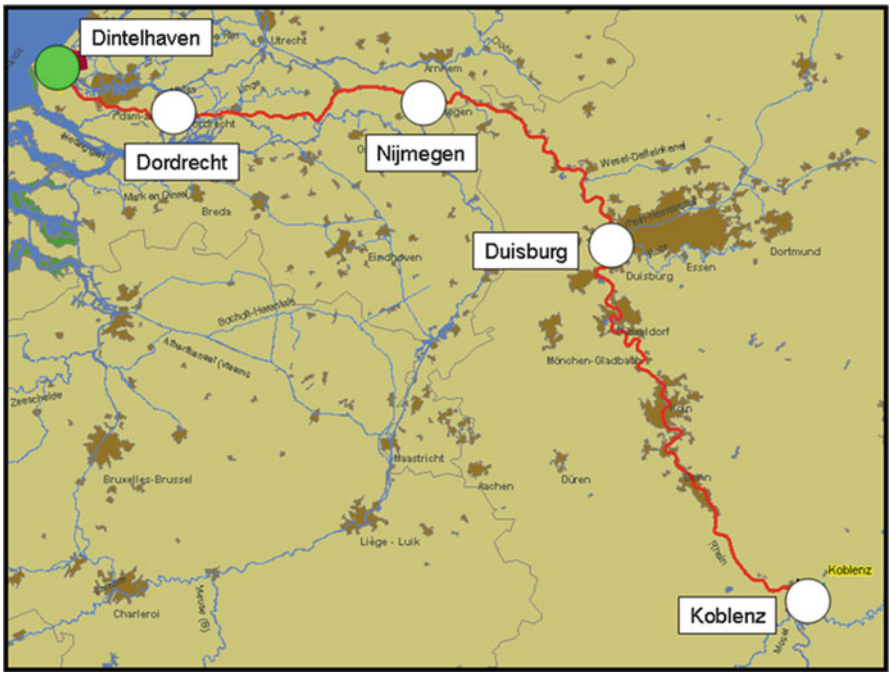

Fig. 16.2 Origin and destinations of the case study, taken from [8]

Table 16.4 Lengths and beams of ship designs

Ship lengths (m)	40	50	60	70	80	95	110	135	160	185
Ship beams (m)	5	6.5	8	9.5	11	12.5	15	17.5	20	25

holding cost of stock, is affected by the use of ships with different main dimensions. Earlier on in this chapter, it was stated that for a market like the European inland waterway transport sector, in the long run the price of transport will be very close to the transport operator's costs. Therefore, in this case the shipper's out-of-pocket costs of transport are assumed to be identical to the transport operator's costs.

For the purpose of this analysis, a series of 518 ship designs with systematically varied length, beam and draught is created. The lengths and beams of the designs are as given in Table 16.4.

Design draughts of the ship range from 1.5 to 4.5 m with 0.5 m intervals, while length to beam ratios of 4 and 20 are used as boundary conditions. This leads to the matrix of designs as shown in Fig. 16.3, in which the smallest ship has dimensions that are close to those of the smallest inland ships that are commercially operated in Europe, while the largest ship has dimensions that are very close to the largest possible dimensions on the investigated route.

To this matrix, a series of additional designs with a length of 86 m are added as well as a series of designs with a beam of 11.45 m, thus including the typical

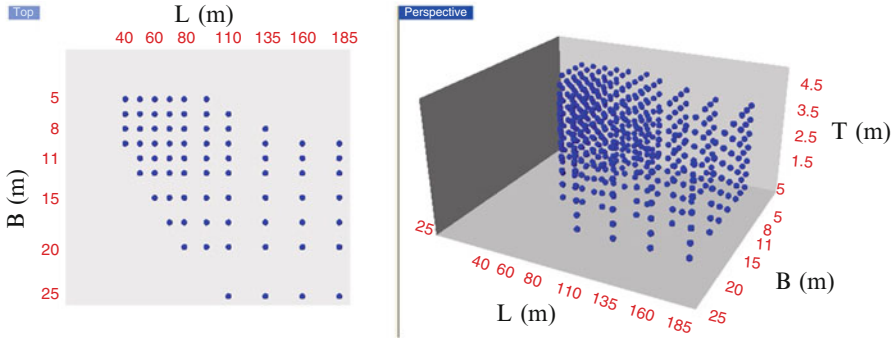

Fig. 16.3 Top down and 3D view of length, beam and draught of developed designs, taken from [8]

length and beam of common European inland ships. For each of the ships in this design set, performance on each of the routes is determined, assuming it sails upstream with as much cargo as possible and returns empty. This performance is determined by a combination of a cost model and a voyage time calculation model. For a given ship design, the voyage model determines the time that is required to make a round trip between two destinations and the amount of cargo that that ship can carry on a waterway with a given water depth. This leads to the number of tons of cargo that can be transported per year. The cost model determines the cost per ton of transported cargo by dividing the sum of annual crew cost, fuel cost, interest cost, depreciation, maintenance cost, insurance cost by the number of tons that are transported annually. These models include several assumptions and choices regarding sailing times, loading and unloading times, crew cost, fuel prices etcetera. These will not be discussed here, but may be found in [8], together with an elaborate description of the models themselves.

As was discussed earlier on in this chapter, the water depth in a river varies over time as well as geographically and is often unknown. Therefore, several water depth scenarios are included in the analysis: in the first scenario, it is assumed that the water depth is large enough to allow all ships to be loaded to their design draught. In the second scenario, the guaranteed water depth of 3.3 m between Rotterdam and Duisburg and of 3.0 m between Duisburg and Koblenz, as described in [4], are used, leading to maximum draughts (Tmax) of 2.8 and 2.5 m respectively. In practice, for a large part of the year, the actual water depth will lie somewhere between the values of these two scenarios. Finally a third scenario where ships have a maximum draught of 1.75 m, representing a period of drought, is added.

Table 16.5 Optimal ship dimensions Rotterdam–Dordrecht

Dordrecht	Tmax = 4.5 m	Tmax = 2.8 m	Tmax = 1.75 m
Optimal dimensions (m)	110 × 20 × 4.5	135 × 17.5 × 3	135 × 25 × 2
Cost percentage			
Optimal (%)	100	100	100
Standard 135 m vessel (%)	114	118	149
Standard 110 m vessel (%)	127	132	170
Standard 86 m vessel (%)	165	126	143

Table 16.6 Optimal ship dimensions Rotterdam–Koblenz

Dordrecht	Tmax = 4.5 m	Tmax = 2.8 m	Tmax = 1.75 m
Optimal dimensions (m)	135 × 25 × 4.5	135 × 25 × 2.5	135 × 25 × 2
Cost percentage			
Optimal (%)	100	100	100
Standard 135 m vessel (%)	124	132	153
Standard 110 m vessel (%)	156	167	196
Standard 86 m vessel (%)	212	152	178

16.3.2 Outcomes of the Case: Out-of-pocket Costs

The first analysis is based on the out-of-pocket costs of transport. For all above mentioned scenarios, the out of pocket costs of transport per ton of transported cargo are calculated for each of the designs using the model that is elaborately described in [8] and the design that leads to the lowest costs is identified. In Tables 16.5 and 16.6, the length, beam and draught of these optimal designs are presented for destinations Dordrecht and Koblenz. Furthermore the performance of these designs, i.e., percentage of incurred out of pocket cost per ton of transported cargo compared to the performance of common vessels with a length of 86 and 110 m, is presented.

From the second row in Table 16.5, it can be observed that in all cases the optimal length is 110 or 135 m and that the width of optimal ship, which is 20–25 m, is significantly larger than the width of common 110 meter long ships which is typically 11.45 m. It is, however, quite close to the dimensions of the largest tank ships that operate on the Rhine. Considering the fact that the largest ship designs in the matrix are 185 m long, it also becomes clear that there are limits to scale enlargement since these very long ships do not emerge as optimal solutions. What also becomes apparent is that it is beneficial to adapt the design draught of a ship to the depth of the waterway, especially if that depth frequently leads to a low maximum draught. In these cases, the cases where the maximum draught is 1.75 m, the cost difference between the optimal ship and standard 110 and 135 m with typical design draughts between 3 and 3.5 m is significantly larger than in cases where the maximum draught is closer to these draughts.

For the much longer route to Koblenz, results are presented in Table 16.6. What becomes apparent from a comparison of Tables 16.5 and 16.6 is that the optimal dimensions do not change much as a function of the distance, but that the difference in cost of the optimal solution compared to standard ships does become larger.

For the intermediate distances, in all cases, the optimal length is 135 m, the optimal beam is 20 or 25 m and the optimal design draught is equal to or slightly larger than the maximum possible draught. Altogether, this case implies that the existing length limit of 135 m for indivisible ships as prescribed by the CCNR does not impede the use of efficient and competitive tank ships. At the same time, it implies that maximizing ship length to this limit, maximizing the beam of the ship and matching design draught to the maximum possible draught can lead to significant transport cost reductions compared to the most common ships. Further analysis, not included in this chapter, shows that these conclusions are hardly sensitive to variations in crew cost, sailing schedule (14, 18 or 24 h per day) or depreciation time of the ship. Therefore the results and conclusions drawn from them are considered to be stable. It is, however, important to realize that these conclusions cannot be extrapolated to container ships and dry bulk ships, because of the different building cost and cargo carrying capacity they have at the same main dimensions. For conclusions on these ships, the reader is again referred to [8].

16.3.3 Outcomes of the Case: Total logistical Costs

For a shipper, not only the out-of-pocket costs of transport are important. He cares (or should care) about his total logistical costs, thus including among other things holding cost of stock, i.e., depreciation of goods, interest on the capital tied up in the goods, warehousing cost and insurance cost. Of all of these items, for bulk goods the interest on capital is the only one that is significantly influenced by the dimensions of the ship, since it determines the batch size in which goods are delivered. The batch size is assumed to be equal to the ship's cargo carrying capacity. Therefore, in the second part of this study, it is also assessed how the combination of out-of-pocket transport costs and interest costs change as a function of the ship's dimensions, assuming that the value of the cargo, gasoil, is 700 Euro per ton, the interest rate is 4 % and the customer's demand is 10,000, 25,000, 50,000 or 100,000 tons per year. Here, out of pocket costs are determined in the same way as in the previous case, while interest costs are determined using the above mentioned value of the goods, the interest rate and the average time that a unit of cargo will be in stock. This average time is based on the shipment size, i.e., the cargo carrying capacity of the ship, and the customer's annual demand. Again, cost calculations, the full details of the case and similar cases for the transport of coal and iron ore may be found in [8].

For the case Rotterdam–Dordrecht, the change of optimal dimensions compared to the case where only out-of-pocket cost is included is shown in Table 16.7. The original optimum mentioned in the table refers to the optimal dimensions on the basis of out-of-pocket costs alone, as described in the previous section.

Table 16.7 Optimal ship dimensions Rotterdam–Dordrecht

	Original optimum (m)	New optimum (m)	New optimum (m)
Rotterdam–Dordrecht		Annual demand 10,000 T	Annual demand 25,000 T
Tmax = 4.5 m	110 × 20 × 4.5	50 × 9.5 × 3	70 × 12.5 × 3.5
Tmax = 2.8 m	135 × 17.5 × 3	70 × 9.5 × 2	70 × 12.5 × 2.5
Tmax = 1.75 m	135 × 25 × 2	70 × 9.5 × 2	80 × 17.5 × 2
Rotterdam–Dordrecht		Annual demand 50,000 T	Annual demand 100,000 T
Tmax = 4.5 m	110 × 20 × 4.5	60 × 11.45 × 4.5	70 × 12.5 × 4.5
Tmax = 2.8 m	135 × 17.5 × 3	110 × 11 × 2.5	110 × 11 × 2.5
Tmax = 1.75 m	135 × 25 × 2	80 × 17.5 × 2	110 × 17.5 × 2

Table 16.8 Optimal ship dimensions Rotterdam–Nijmegen

	Original optimum (m)	New optimum (m)	New optimum (m)
Rotterdam–Nijmegen		Annual demand 10,000 T	Annual demand 25,000 T
Tmax = 4.5 m	110 × 20 × 4.5	60 × 9.5 × 3.5	70 × 12.5 × 3.5
Tmax = 2.8 m	135 × 25 × 3	70 × 12.5 × 2.5	110 × 11 × 2.5
Tmax = 1.75 m	135 × 25 × 2	70 × 12.5 × 2	110 × 15 × 2
Rotterdam–Nijmegen		Annual demand 50,000 T	Annual demand 100,000 T
Tmax = 4.5 m	110 × 20 × 4.5	70 × 12.5 × 4.5	80 × 20 × 4.5
Tmax = 2.8 m	135 × 25 × 3	110 × 11 × 2.5 m	110 × 11 × 2.5
Tmax = 1.75 m	135 × 25 × 2	110 × 15 × 2 m	**135 × 25 × 2**

What immediately becomes clear from Table 16.7 is that in case of a short transport distance like the 45 km from Rotterdam to Dordrecht, holding cost becomes an important factor: in order to keep stocks low, small batches (and therefore small ships) are preferred over large ships with low transport costs.

For the case Rotterdam to Nijmegen, where transport cost is significantly higher than for the trip to Dordrecht, it becomes clear from Table 16.8 that the optimal ship size increases and that it is even identical to that of the base case for the low water scenario with an annual demand of 100,000 tons. Cases where the optimal ship dimensions do not deviate from those of the original case are printed bold in tables 16.7 to 16.10.

In case of transport to Duisburg, in Table 16.9, it can be seen that this effect becomes stronger. Ship sizes increase further and are identical to original optimum more often.

When the transport distance increases further, it becomes clear from a comparison between Tables 16.9 and 16.10 that this does not lead to any major changes in ship dimensions. Apparently, the increase in transport costs for different ships is not large enough to have a significant effect on their ranking.

From the above, it becomes clear that scale enlargement to a length of 20–25 m is possible and beneficial, but that further lengthening of the ships beyond the current maximum length of 135 m does not lead to a clear improvement. These dimensions are in fact quite close to those of the largest tank ships that are currently in operation

Table 16.9 Optimal ship dimensions Rotterdam–Duisburg

	Original optimum (m)	New optimum (m)	New optimum (m)
Rotterdam–Duisburg		Annual demand 10,000 T	Annual demand 25,000 T
Tmax = 4.5 m	135 × 25 × 4.5	70 × 12.5 × 3.5	60 × 15 × 4.5
Tmax = 2.8 m	135 × 25 × 3	60 × 15 × 2.5	80 × 17.5 × 3
Tmax = 1.75 m	135 × 25 × 2	80 × 17.5 × 2	**135 × 25 × 2**
Rotterdam–Duisburg		Annual demand 50,000 T	Annual demand 100,000 T
Tmax = 4.5 m	135 × 25 × 4.5	80 × 20 × 4.5	80 × 20 × 4.5
Tmax = 2.8 m	135 × 25 × 3	135 × 17.5 × 3	**135 × 25 × 3**
Tmax = 1.75 m	135 × 25 × 2	**135 × 25 × 2**	**135 × 25 × 2**

Table 16.10 Optimal ship dimensions Rotterdam–Koblenz

	Original optimum (m)	New optimum (m)	New optimum (m)
Rotterdam–Koblenz		Annual demand 10,000 T	Annual demand 25,000 T
Tmax = 4.5 m	135 × 25 × 4.5	70 × 12.5 × 3.5	60 × 15 × 4.5
Tmax = 2.5 m	135 × 25 × 2.5	70 × 15 × 2.5	86 × 15 × 2.5
Tmax = 1.75 m	135 × 25 × 2	135 × 15 × 2	**135 × 25 × 2**
Rotterdam–Koblenz		Annual demand 50,000 T	Annual demand 100,000 T
Tmax = 4.5 m	135 × 25 × 4.5	80 × 20 × 4.5	80 × 20 × 4.5
Tmax = 2.5 m	135 × 25 × 2.5	**135 × 25 × 2.5**	**135 × 25 × 2.5**
Tmax = 1.75 m	135 × 25 × 2	**135 × 25 × 2**	**135 × 25 × 2**

on the Rhine. What also becomes apparent is that the optimal ship dimensions are not only dependent on the properties of ship and waterway, but also on the volume of goods that is required by a customer. Customers with a limited demand of relatively valuable goods have no benefit from transport by large ships, unless the batches of goods that are delivered to them can be significantly smaller than the cargo carrying capacity of this ship.

16.4 Transdisciplinary Discussion

In this chapter, the optimization of inland ships is discussed. This is part of the optimization of transport over water, but does not explicitly take the transport of water into account. The two topics are, however, closely linked since inland waterways exist only because water is transported from inland locations to the seas and/or oceans. Implicitly, the link between the two topics is incorporated in this chapter through the exploration of the effect of different water depths on the optimal dimensions of inland ships: The more water is transported through a given channel, the higher the water level will be. In practice, it can often be observed that if not enough water is transported through a channel, either permanently or seasonally, measures are taken to ensure that transport over water is still possible by building of

dams and locks. This way, a sufficiently high water depth for economically viable waterborne transport of goods is guaranteed at all times.

Especially for free flowing rivers, a unified framework where transport of water and transport over water are more closely linked would be beneficial. As was discussed earlier in this chapter, the dynamics of the water flow through a river lead to ever-changing morphology of the river bed and to different water depths and waterway cross-sections in both time and space. When transport over water is assessed independently of the transport of water, the logical consequence is that water depth and cross-section are assumed static or, at best, quasi-static. In the end, this leads to an inability to properly adapt ships to the actual conditions of the waterway and, therefore, to suboptimal ships. This phenomenon can be observed in the development of inland ships in Europe in the past decade: more and more large-draught ships are built. These ships perform well when water levels are high, but perform poorly when they are low. As long as transport over water and transport of water continue to be analyzed separately, it will remain unclear what the optimal solution for the transport of goods over water is. In a unified framework, optimizing inland waterway transport from a ship-technology point-of-view does become a possibility.

In the research presented in this chapter, several steps have been taken that can be useful in such a unified framework: an approach for the calculation of transport cost for specific transport scenarios, which include water depth, was presented and, more importantly, the technical properties and building costs of inland ships with a wide range of main dimensions have been established. Without this knowledge, it is possible to establish how changes in the transport of water affect transport over water by state-of-the-art ships, but it remains impossible to re-optimize transport over water when the transport of water, i.e., water depth, changes significantly for a given waterway.

16.5 Conclusions and Future Research

In this chapter, it has been clarified that there is a strong interaction between the economic viability of operating an inland ship and the properties of the waterway on which it sails. For a case in western Europe, it was also shown that if the waterway allows it, the use of larger, wider, ships than those that are currently common in Europe can be beneficial. However, further scale enlargement beyond the dimensions of the largest tank ships that operate on the Rhine is unlikely to be beneficial. At the same time, it is concluded that it is not only the properties of waterway and ship that determine the optimum dimensions of a ship. There also needs to be a match between the amount of cargo that is delivered to a customer and that customer's demand in order to limit the cost of stock.

Regarding innovation in the sector, there have been numerous initiatives to improve the economic and environmental performance of inland ships, but only scale enlargement has actually achieved a significant market uptake. LNG might become the next big breakthrough, but this depends heavily on the development of

the price of LNG. Furthermore, many of the developments in the sector are practical in nature, while only a few are based on thorough scientific research.

Anyone who attempts to improve inland waterway transport within Europe should keep in mind that cost is a major decision driver and therefore, any proposal for a perceived improvement that leads to higher costs should include sound argumentation why the perceived benefits of this improvement outweigh the higher costs. It should also be kept in mind that the out-of-pocket costs of transport are only a part of the total logistic costs and therefore that minimization of out-of-pocket costs of transport alone may lead to a false conclusion regarding the optimal dimensions of the ship to be used. This is mainly an issue if a proposed improvement affects the cargo carrying capacity of the ship or, to a lesser extent, the transport time.

A reduction of the out-of-pocket costs of transport can be achieved in several ways, including but certainly not limited to the technological aspects discussed in this chapter. When limiting oneself, however, to these technological aspects, the most striking shortcoming in current knowledge is related to the interaction between ship and waterway: In many cases, the details of water depth and waterway cross-section are unknown, even though they have a significant impact on a ship's speed, fuel consumption at that speed and the cost of transport. Furthermore, even if these conditions are known, there is a lack of good methods to predict speed and fuel consumption for a given ship. This in turn makes it hard to optimize elements of a ship that are related to the hydrodynamics and/or drive train, while also making it hard to predict the benefits of proposed improvements.

To solve these shortcomings, several projects have recently been initiated in the Netherlands. The COVADEM project aims at mapping the waterway through cooperative depth measurements using many cargo ships, while the Top Ships project focuses on powering prediction for inland ships. These projects provide a step in the right direction, but further research on the topic is certainly required. Further ship technology-related topics include the operation of coupled units, i.e., cargo ships pushing one or more barges and the maneuverability of inland ships.

Future research topics that are not related to the technical properties of include the development of more knowledge about the decision drivers of shippers that use inland shipping, the annual volumes of goods that each shipper requires and their geographical locations. Further data on lingering times in ports is also desirable, since this influences the amount of time as ship can actually spend sailing. This in turn has a strong influence its annual transport capacity.

References

1. Beelen M. Structuring and modelling decision making in the inland navigation sector. PhD thesis, Universiteit Antwerpen, Antwerp, Belgium; 2009.
2. CBS and AVV. Nederland en de scheepvaart op de binnenwateren. Technical Report, Centraal Bureau voor de Statistiek and Ministerie van Verkeer en Waterstaat Directoraat-generaal Rijkswaterstaat Adviesdienst Verkeer en Vervoer; 2003.

3. Central Commission for Navigation on the Rhine. Rheinschiffsuntersuchungsordnung 1995, ausgabe 2007. Technical Report, Central Commission for Navigation on the Rhine; 2007.
4. Central Commission for Navigation on the Rhine. Navigation channel clearances of the rhine. Technical Report, Central Commission for Navigation on the Rhine, Strasbourg, France; 2011.
5. de Baere P, Blauwens G, van de Voorde E. Transport economics. 4th ed. De Boeck, Berchem, Belgium; 2008.
6. EICB. Plan van aanpak klein schip, hoofdrapport. Technical Report, EICB; 2011.
7. European Conference of Ministers of Transport. Resolution no. 92/2 on new classification of inland waterways. Technical Report, European Conference of Ministers of Transport; 1992.
8. Hekkenberg RG. Inland ships for efficient transport chains. PhD thesis, Delft University of Technology, Delft, The Netherlands; 2013.
9. Kreutzeberger ED. Distance and time in intermodal goods transport networks in europe: a generic approach. Transp Res A. 2008;42:973–93.
10. Lackenby H. The effect of shallow water on ship speed. In: Shipbuilder and marine engine builder. London: Shipbuilder Press; 1963. vol. 70, p. 446–50.
11. Platz TE. The efficient integration of inland shipping into continental intermodal transport chains, measures and decisive factors. PhD thesis, Radboud Universiteit Nijmegen, Nijmegen, the Netherlands; August 2009.
12. Raven HC. A computational study of shallow-water effects on ship viscous resistance. In: Proceedings of the 29th symposium on naval hydrodynamics; 2012.
13. Schlichting O. Schiffswiderstand auf beschränkter wassertiefe—widerstand von seeschiffen auf flachem wasser. STG Jahrbuch, 35;1934.
14. TNO. Vlootontwikkeling binnenvaart. Technical Report, TNO; 2010.
15. van den Berg W. The whale tail wheel. Workshop on unconventional propulsion, ITTC 1996; 1996.
16. van Hassel E. Developing a small Barge convoy system to reactivate the use of the small inland waterway network. PhD thesis, Univeristeit Antwerpen, Antwerp, Belgium; 2011.

Chapter 17
Wave Filtering and Dynamic Positioning of Marine Vessels Using a Linear Design Model: Theory and Experiments

V. Hassani and A.M. Pascoal

Abstract This chapter describes a procedure to obtain an improved design model of ships subjected to the influence of currents and sea waves. The model structure is at the heart of the application of new techniques in control and estimation theory to the problem of Dynamic Positioning (DP) and wave filtering of marine vessels. The model proposed captures the physics of the problem at hand in an effective manner and includes the sea state as an uncertain parameter. This allows for the design of advanced control and estimation algorithms to solve the DP and wave filtering problems under different sea conditions. Numerical simulations, carried out using a high fidelity nonlinear DP system simulator, illustrate the performance improvement in wave filtering as a result of the use of the proposed model. Furthermore, using Monte-Carlo simulations the performance of three DP controllers, designed based on the plant model developed, is evaluated for different sea conditions. The first controller is a nonlinear multivariable PID controller with a passive observer. The second controller is of the Linear Quadratic Gaussian type and the third controller builds on $\mathcal{H}_\infty$ control techniques using the mixed-μ synthesis methodology. The theoretical results are experimentally verified and the performance of wave filtering in DP systems operated with the controllers designed for different sea conditions are further examined by model testing a DP operated ship, the Cybership III, in a towing tank equipped with a hydraulic wavemaker.

V. Hassani (✉)
Department of Marine Technology, Norwegian Marine Technology Research Institute (MARINTEK) and Centre for Autonomous Marine Operations and Systems (AMOS), Norwegian University of Science and Technology, Trondheim, Norway
e-mail: Vahid.Hassani@ntnu.no

A.M. Pascoal
Laboratory of Robotics and Systems in Engineering and Science, Instituto Superior Técnico, University of Lisbon, Lisbon, Portugal
e-mail: Antonio@isr.ist.utl.pt

C. Ocampo-Martinez, R.R. Negenborn (eds.), *Transport of Water versus Transport over Water*, Operations Research/Computer Science Interfaces Series 58,
DOI 10.1007/978-3-319-16133-4_17

17.1 Introduction

The first step in the design of a control system or observer for a marine vessel, transporting and operating over water, is the development of a model describing the dynamic behavior of the ship and its interaction with the environment that captures the influence of waves and currents. An appropriate control design model should be simple enough and yet reflect the main physical characteristics of the plant at hand. A controller designed using a model of this type will inherit structural information about the physical properties of the plant and has the potential to achieve good performance and robustness properties, if at all possible. This chapter is devoted to derive such a control design model that satisfies the above properties and can therefore be used for efficient design of Dynamic Positioning (DP) systems. The latter started to appear in the 1960s for offshore drilling applications, due to the need to drill in deep waters and the realization that Jack-up barges and anchoring systems could not be used economically at such depths. Nowadays, many types of marine vessels such as drilling, pipe laying, crane, supply, passenger, and cruise vessels are equipped with a DP systems [27]. Early DP systems were implemented using PID controllers. In order to restrain thruster trembling caused by the wave-induced motion components, notch filters in cascade with low pass filters were used with the controllers [6]. However, notch filters restrict the performance of closed-loop systems because they introduce phase lag about the crossover frequency, which in turn tends to decrease phase margin. An improvement in the performance obtained with DP controllers was achieved by exploiting more advanced control techniques based on optimal control and Kalman filter theory, see [1]. These techniques were later modified and extended in [2, 3, 5, 10–13, 25, 28, 30, 32]. For a survey of DP control systems, see for example [27] and the references therein.

One of the most fruitful concepts introduced in the course of the body of work referred above is that of wave filtering, together with the strategy of modeling the total vessel motion as the superposition of low-frequency (LF) and wave-frequency (WF) vessel motions. It was further recognized that in order to reduce the mechanical wear and tear of the propulsion system components, in small to high sea states, the estimates entering the DP control feedback loop should be filtered by using a so-called wave filtering technique so as to prevent excessive control activity in response to WF components. In practice, position and heading measurements are corrupted with sensor noise. Furthermore, measured position and heading reflect the impact of external disturbances such as waves and ocean currents acting on the vessel. The need therefore arises for an observer to achieve wave filtering and "separate" the LF and WF position and heading estimates (see [6] for details). In extreme seas or swell with very long wave periods, wave filtering is turned off as described in [17, 21, 27].

In [28], WF filtering was done by exploiting the use of Kalman filter theory under the assumption that the kinematic equations of the ship's motion can be linearized about a set of predefined constant yaw angles (36 operating points in steps

of 10°, covering the whole heading envelope); this is necessary when applying linear Kalman filter theory and gain scheduling techniques. However, global exponential stability of the complete system cannot be guaranteed. In [9], a nonlinear observer with wave filtering capabilities and bias estimation was designed using passivity methods. An extension of this observer with adaptive wave filtering was described in [31]. Gain-scheduled wave filtering was introduced in [32].

To the best of our knowledge, in the wave filtering techniques described in the above mentioned references the WF components of marine vessel motion are computed in a earth-fixed frame (also denoted as North-East-Down frame), while the hydrodynamic forces and torques acting on the vessel are naturally given (via the corresponding hydrodynamic coefficients) in terms of variables that are best measured in body-axis (because they capture the influence between the vessel and the environment locally, no matter what the attitude of the vessel is, in inertial coordinates). Assuming a stationary wave pattern, this suggests that the WF motions should be modeled in a hydrodynamic frame (or body frame) rather than in a North-East-Down frame. This observation is at the root of the new linear model adopted in this Chapter both for control and wave filtering purposes.

From a practical standpoint, this chapter is strongly motivated by the need to develop high performance Dynamic Positioning (DP) systems. The latter have traditionally been for low-speed applications, where the basic DP functionality is either to keep a fixed position and heading of a ship, or to move it slowly from one location to another. In this work, using a low speed assumption, a linear model of a vessel is developed that captures practical aspects and plays a central role in the design of control and estimation algorithms for DP and wave filtering of marine vessels in presence of sea waves and disturbances. The main emphasis of the chapter is on the new linear model proposed; to show the usefulness of the model, two wave filters are designed, one based on the model proposed and the other on a commonly used model, after which their performance is compared. The new model can also be used for control systems design. This is illustrated with the design and the evaluation of three classes of DP controllers operating under four different sea conditions: calm, moderate, high, and extreme seas. The first class of controllers is a nonlinear multivariable PID (designed based on a nonlinear plant model). In this setup, a nonlinear passive observer is used for wave filtering. The observer provides estimates of the LF components of position and velocity of the vessel that are used in the controller. Four different nonlinear PID controllers are designed, covering the sea conditions from calm to extreme seas. The remaining two types of controllers are designed based on the new linear model presented. The second class of controllers is of the Linear Quadratic Gaussian (LQG) type. It consists of a steady state Kalman filter and a linear quadratic (state-feedback) controller. As in the previous case, four different LQG controllers are designed covering different sea conditions. The third class of controllers builds on $\mathcal{H}_\infty$ control techniques; four $\mathcal{H}_\infty$ robust controllers are designed for different sea conditions.

The performance of the controllers derived is evaluated with the help of Monte Carlo simulations performed under different environmental conditions, from calm to

extreme seas, using the Marine Cybernetics Simulator (MCSim) [29]. Experimental model tests are also carried out using the Cybership III model vessel of the Marine Cybernetics Laboratory (MCLab) [20].

The structure of the chapter is as follows. Section 17.2 is a brief introduction to important issues that arise in the design of DP systems, followed by the presentation of a new linear vessel model that will be used for filter and control systems design purposes. A brief description of three selected DP control laws (where two of them are designed using the newly proposed vessel model) is given in Sect. 17.2.2. Section 17.3 describes the Marine Cybernetics Simulator and contains the results of numerical Monte-Carlo simulations with stochastic signals that illustrate the performance of the DP controllers and associated estimators under calm to extreme sea conditions. In Sect. 17.4, a short description of the model-test vessel, Cybership III, and experimental results obtained with it are presented. Conclusions and suggestions for future research are summarized in Sect. 17.6.

17.2 Dynamic Positioning, Wave Filtering and Ship Modeling

In DP systems, the key objective is to maintain the vessel's heading and position within desired limits. Central to their implementation is the availability of good heading and position estimates, provided by properly designed filters. In general, measurements of the vessel velocities are not available and measurements of position and heading are corrupted with different types of noise. Consequently, the estimates of the velocities must be computed from corrupted measurements of position and heading through a state observer. Furthermore, only the slowly-varying disturbances should be counteracted by the propulsion system, whereas the oscillatory motion induced by the waves (1st-order wave induced loads) should not enter the feedback control loop to prevent excessive control activity in response to WF components of motion. To this effect, DP control systems should be designed so as to react to the LF forces imparted to the vessel only. As mentioned before, wave filtering techniques are exploited to separate the position and heading measurements into LF and WF position and heading estimates. Figure 17.1 illustrates this concept graphically. It was this interesting set of ideas that motivated the work reported in the present chapter on the development of a linear design model for marine vessels with a view to DP and wave filtering applications. In what follows, for the sake of clarity, the vessel model described in [9, 26, 32] is described first. The model admits the realization

$$\dot{\xi}_\omega = A_\omega(\omega_0)\xi_\omega + E_\omega w_\omega, \tag{17.1}$$

$$\eta_\omega = C_\omega \xi_\omega, \tag{17.2}$$

$$\dot{b} = -T^{-1}b + E_b w_b, \tag{17.3}$$

$$\dot{\eta}_L = R(\psi_L)\nu_L, \tag{17.4}$$

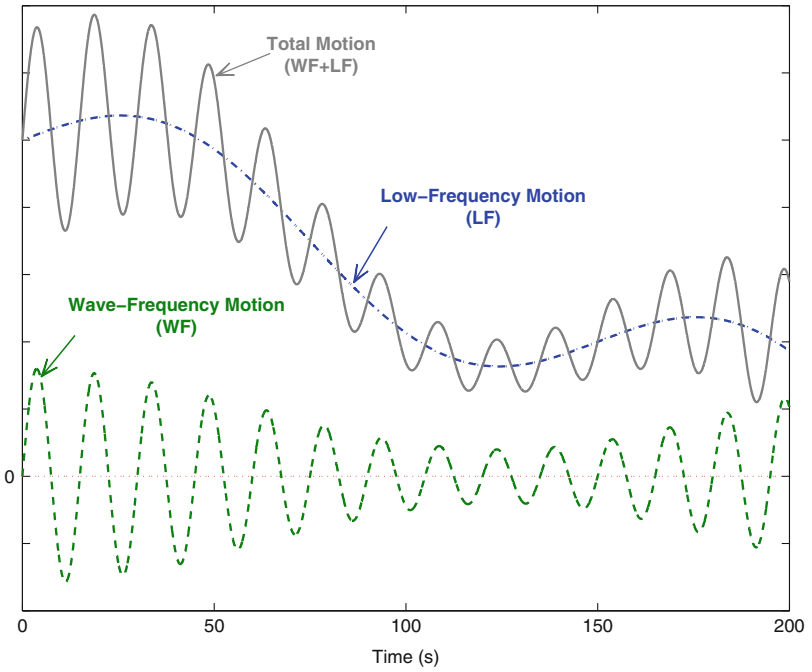

Fig. 17.1 The total motion of a ship is modeled as a LF response with the WF motion added as an output disturbance (adapted from [9, 26])

$$M\dot{\nu}_L + D\nu_L = \tau + R^T(\psi_{tot})b, \tag{17.5}$$

$$\eta_{tot} = \eta_L + \eta_\omega, \tag{17.6}$$

$$\eta_y = \eta_{tot} + \upsilon, \tag{17.7}$$

where (17.1) and (17.2) capture the 1st-order wave induced motion in surge, sway, and yaw; (17.3) represents a low order Markov process approximating the slowly varying bias forces (in surge and sway) and torques (in yaw) due to waves (2nd order wave induced loads) and currents, where the latter are given in earth fixed coordinates but later expressed in body-axis in (17.5). Vector $\eta_\omega \in \mathbb{R}^3$ captures the vessel's WF motion due to 1st-order wave-induced disturbances, consisting of WF position (x_W, y_W) and WF heading ψ_W of the vessel; $w_\omega \in \mathbb{R}^3$ and $w_b \in \mathbb{R}^3$ are zero mean Gaussian white noise vectors, and

$$A_\omega = \begin{bmatrix} 0_{3\times3} & I_{3\times3} \\ -\Omega_{3\times3} & -\Lambda_{3\times3} \end{bmatrix}, \qquad E_\omega = \begin{bmatrix} 0_{3\times1} \\ I_{3\times1} \end{bmatrix},$$

$$C_\omega = \begin{bmatrix} 0_{3\times3} & I_{3\times3} \end{bmatrix},$$

with

$$\Omega = \text{diag}\{\omega_{01}^2, \omega_{02}^2, \omega_{03}^2\},$$
$$\Lambda = \text{diag}\{2\zeta_1\omega_{01}, 2\zeta_2\omega_{02}, 2\zeta_3\omega_{03}\},$$

where ω_{0i} and ζ_i are the dominant WF and relative damping ratio, respectively. Matrix $T = \text{diag}(T_x, T_y, T_\psi)$ is a diagonal matrix of positive bias time constants and $E_b \in \mathbb{R}^{3\times3}$ is a diagonal scaling matrix. Vector $\eta_L \in \mathbb{R}^3$ consists of low frequency, earth-fixed position (x_L, y_L) and LF heading ψ_L of the vessel relative to an earth-fixed frame, $\nu_L \in \mathbb{R}^3$ represents the translational and rotational velocities expressed in a vessel-fixed reference frame, and $R(\psi_L)$ denotes a homogeneous transformation given by

$$R(\psi_L) = \begin{bmatrix} \cos(\psi_L) & -\sin(\psi_L) & 0 \\ \sin(\psi_L) & \cos(\psi_L) & 0 \\ 0 & 0 & 1 \end{bmatrix}.$$

Equation (17.5) describes the vessels's LF motion at low speed (see [6]), where $M \in \mathbb{R}^{3\times3}$ is the generalized system inertia matrix including zero frequency added mass components, $D \in \mathbb{R}^{3\times3}$ is a linear damping matrix, and $\tau \in \mathbb{R}^3$ is a control vector of generalized forces generated by the propulsion system, which can produce surge and sway forces as well as a yaw moment. Vector $\eta_{tot} \in \mathbb{R}^3$ represents the vessel's total motion, consisting of total position (x_{tot}, y_{tot}) and total heading ψ_{tot} of the vessel. Finally, (17.7) represents the position and heading measurement equation, where $v \in \mathbb{R}^3$ is zero-mean Gaussian white measurement noise.

Clearly, in the model described in (17.1)–(17.7) the evolution of the WF components of motion, given by (17.1), (17.2) and (17.7), are modeled as a 2nd-order linear time invariant system, driven by Gaussian white noise, in earth-fixed frame.

It is commonly accepted in station keeping operations, assuming small motions about the coordinates η_d (x_d, y_d, and ψ_d), that the coupled equations of WF motions can be formulated in a hydrodynamic frame as[1]

$$M(w)\ddot{\eta}_{R\omega} + D_p(w)\dot{\eta}_{R\omega} = \tau_{\text{wave1}}, \tag{17.8}$$
$$\dot{\eta}_\omega = R(\psi)\dot{\eta}_{R\omega}, \tag{17.9}$$

[1]In six degrees-of-freedom dynamics, (17.8) is written as $M(w)\ddot{\eta}_{R\omega} + D_p(w)\dot{\eta}_{R\omega} + G\eta_{R\omega} = \tau_{\text{wave1}}$, where $G \in \mathbb{R}^{6\times6}$ is the linearized restoring coefficient matrix due to the gravity and buoyancy affecting heave, roll, and pitch only (see [26] for more details). Throughout this chapter a three degrees-of-freedom dynamics is used for the design purposes, while a six degrees-of-freedom dynamics is used in the simulation.

where $\eta_{R\omega} \in \mathbb{R}^3$ is the WF motion vector in the hydrodynamic frame, $\eta_\omega \in \mathbb{R}^3$ is the WF motion vector in the Earth-fixed frame, and $\tau_{\text{wave1}} \in \mathbb{R}^3$ is the first order wave excitation vector, which depends on the vessel's heading relative to the incident wave direction. In the above, $M(w) \in \mathbb{R}^{3\times3}$ is the system inertia matrix containing frequency dependent added mass coefficients in addition to the vessel's mass and moment of inertia and $D_p(w) \in \mathbb{R}^{3\times3}$ is the wave radiation (potential) damping matrix. Here, it is assumed that the mooring lines, if any, will not affect the WF motion [33].[2]

The above indicate that the WF motion should be computed in the hydrodynamic frame. We now recall that the problem of modeling the hydrodynamic forces applied to a vessel in regular waves is solved as two sub-problems: "wave reaction" and "wave excitation"; the forces calculated in each of these sub-problems can be added together to give the total hydrodynamic forces [4]. Potential theory is assumed, neglecting viscous effects. The following effects are important:

Wave Reaction, i.e., forces and moments on the vessel when the vessel is forced to oscillate with the wave excitation frequency. The hydrodynamic loads are identified as added mass and wave radiation damping terms.

Wave Excitation, i.e., forces and moments on the vessel when the vessel is restrained from oscillating and there are incident waves. This gives the wave excitation loads which are composed of so-called Froude-Kriloff (forces and moments due to the undisturbed pressure field as if the vessel were not present) and diffraction forces and moments (forces and moments due to the presence of the vessel changes the pressure field).

Results from model tests and computer programs for vessel response analysis often come in the form of transfer functions or tables of coefficients. Similar tools can be applied to study linear wave-induced motions, 2nd-order wave drift, and slowly varying motions. To a large extent, linear theory is sufficient to describe wave-induced motions and loads on vessels. This is especially true for small to moderate sea states.

To this effect, a frequency spectrum $S(\omega)$ is usually selected to describe the energy distribution of the wind generated sea waves and swell over different frequencies, with the integral over all frequencies representing the total energy of the sea state. Common frequency spectra are the Pierson-Moskowitz spectrum, the ISSC spectrum (or modified Pierson-Moskowitz spectrum recommended by International Towing Tank Conference for fully developed sea), the Joint North Sea Wave Project (JONSWAP) spectrum [18], and the more recent doubly peaked spectrum introduced by Torsethaugen (see [6, 26] and the references therein for details). Linear approximations of the wave spectra are studied in the literature; in particular, 2nd-order wave transfer function approximations have been used extensively, see [2, 3, 5, 10–13, 21, 25, 28, 30, 32].

[2]It is worth to mention that the evolution of the WF components of motion, given by (17.1) and (17.2), are in fact a simplification of (17.8) and (17.9).

In this work we also consider a 2nd-order wave transfer function approximation and we propose a modified model for the WF components of motion as follows:

$$\dot{\xi}_\omega = A_\omega(\omega_0)\xi_\omega + E_\omega w_\omega, \tag{17.10}$$

$$\eta_\omega = R(\psi_L)C_\omega\xi_\omega, \tag{17.11}$$

$$\dot{b} = -T^{-1}b + E_b w_b, \tag{17.12}$$

$$\dot{\eta}_L = R(\psi_L)\nu_L, \tag{17.13}$$

$$M\dot{\nu}_L + D\nu_L = \tau + R^T(\psi_{tot})b, \tag{17.14}$$

$$\eta_{tot} = \eta_L + \eta_\omega, \tag{17.15}$$

$$\eta_y = \eta_{tot} + v, \tag{17.16}$$

where all the variables are as defined in (17.1)–(17.7). At this point we would like to highlight the difference between (17.2) and (17.11). As mentioned before, the evolution of the WF components of motion in (17.1), (17.2) and (17.7), are modeled as a 2nd-order linear time invariant system, driven by Gaussian white noise, in earth-fixed frame, while (17.8) suggests that the WF motions be modeled in a body frame. From a physical point of view, it is obvious that the WF motions depend on the angle between the heading of the vessel and the direction of the wave. Assuming stationary waves,[3] one can assume that a linear approximation can be used to described wave-induced motions in the body frame. This justifies the modification applied in (17.11). Modeling the WF motions in earth-fixed frame means that every time a new command for a desired heading is issued, the WF motion dynamic should be updated. By modeling the WF motion dynamics in the body frame this is avoided entirely.

17.2.1 A New Linear Design Model

For low speed DP and wave filtering applications, the following assumptions can be made (these assumptions are widely used in the literature, see [5, 19, 30–32]):

Assumption 1. Position and heading sensor noise are neglected, that is $v = 0$, since the measurement error induced by measurement noise is negligible compared to the wave-induced motion.

Assumption 2. The amplitude of the wave-induced yaw motion ψ_ω is assumed to be small, that is, less than 2–3° during normal operation of the vessel and less than 5°

[3] In long-crested irregular sea, the sea elevation can be assumed statistically stable. See [26] for details and differences between long- and short-crested seas.

in extreme weather conditions. Hence, $R(\psi_L) \approx R(\psi_L + \psi_W)$. From Assumption 1 it follows that $R(\psi_L) \approx R(\psi_y)$, where $\psi_y \cong \psi_L + \psi_W$ denotes the measured heading.

Assumption 3. The time-derivative of the total heading $\dot{\psi}_{tot}$ is small and close to zero (low speed assumption).

We will also exploit the model property that the bias time constant in the x and y directions are equal, i.e., $T_x = T_y$.

At this point, to represent the dynamics of the vessel in a linear form, it is convenient to introduce a new system of vessel parallel coordinates as described in [6, 7, 26]. Vessel parallel coordinates are defined in a reference frame fixed to the vessel, with axes parallel to the earth-fixed frame. In what follows, they will be denote by the upper script p; vector $\eta_L^p \in \mathbb{R}^3$ consists of the LF position (x_L^p, y_L^p) and LF heading ψ_L^p of the vessel expressed in body coordinates, defined as

$$\eta_L^p = R^T(\psi_{tot})\eta_L. \tag{17.17}$$

Computing its derivative with respect to time yields

$$\begin{aligned} \dot{\eta}_L^p &= \dot{R}^T(\psi_{tot})\eta_L + R^T(\psi_{tot})\dot{\eta}_L \\ &= \dot{R}^T(\psi_{tot})R(\psi_{tot})\eta_L^p + R^T(\psi_{tot})R(\psi_L)\nu_L. \end{aligned} \tag{17.18}$$

Using a Taylor series to expand $R^T(\psi_{tot})$ about ψ_L and neglecting the higher order terms, it follows that

$$R^T(\psi_{tot})R(\psi_L) \cong I + \psi_W S, \tag{17.19}$$

where

$$S = \begin{bmatrix} 0 & 1 & 0 \\ -1 & 0 & 0 \\ 0 & 0 & 0 \end{bmatrix}.$$

Simple algebraic manipulations yield

$$\dot{R}^T(\psi_{tot})R(\psi_{tot}) = \dot{\psi}_{tot} S. \tag{17.20}$$

From (17.18)–(17.20) it can be concluded that

$$\dot{\eta}_L^p \approx \dot{\psi}_{tot} S \eta_L^p + \nu_L + \psi_W S \nu_L. \tag{17.21}$$

We now study the time evolution of the slowly varying bias forces, b, expressed in the vessel parallel coordinates as

$$b^p = R^T(\psi_{tot})b. \tag{17.22}$$

Clearly,

$$b = R(\psi_{tot})b^p, \tag{17.23}$$

and differentiating both sides yields

$$\dot{b} = \dot{R}(\psi_{tot})b^p + R(\psi_{tot})\dot{b}^p. \tag{17.24}$$

From (17.12), (17.23) and (17.24) it follows that

$$\dot{R}(\psi_{tot})b^p + R(\psi_{tot})\dot{b}^p = -T^{-1}R(\psi_{tot})b^p + E_b w_b. \tag{17.25}$$

Reordering (17.25) and multiplying both sides by $R^T(\psi_{tot})$ gives

$$\begin{aligned}\dot{b}^p = &-R^T(\psi_{tot})T^{-1}R(\psi_{tot})b^p - R^T(\psi_{tot})\dot{R}(\psi_{tot})b^p \\ &+ R^T(\psi_{tot})E_b w_b.\end{aligned} \tag{17.26}$$

Using the assumption that $T_x = T_y$, it can be shown that $R^T(\psi_{tot})T = TR^T(\psi_{tot})$; simple algebra also shows that $R^T(\psi_{tot})\dot{R}(\psi_{tot}) = -\dot{\psi}_{tot}S$.

Equation (17.26) can be rewritten as

$$\dot{b}^p = -T^{-1}b^p + \dot{\psi}_{tot}Sb^p + R^T(\psi_{tot})E_b w_b. \tag{17.27}$$

Summarizing the equations above yields

$$\dot{\xi}_\omega = A_\omega(\omega_0)\xi_\omega + E_\omega w_\omega, \tag{17.28}$$

$$\eta_\omega = R(\psi_L)C_\omega \xi_\omega, \tag{17.29}$$

$$\dot{b}^p = -T^{-1}b^p + \dot{\psi}_{tot}Sb^p + R^T(\psi_{tot})E_b w_b, \tag{17.30}$$

$$\dot{\eta}_L^p = \dot{\psi}_{tot}S\eta_L^p + \nu_L + \psi_W S\nu_L, \tag{17.31}$$

$$M\dot{\nu}_L + D\nu_L = \tau + b^p. \tag{17.32}$$

Moreover, using Assumptions 1, 2 and 3 a ***linear model*** is obtained that is given by

$$\dot{\xi}_\omega = A_\omega(\omega_0)\xi_\omega + E_\omega w_\omega, \tag{17.33}$$

$$\eta_\omega^b = C_\omega \xi_\omega, \tag{17.34}$$

$$\dot{b}^p = -T^{-1}b^p + w_b^f, \tag{17.35}$$

$$\dot{\eta}_L^p = \nu_L, \tag{17.36}$$

$$M\dot{\nu}_L + D\nu_L = \tau + b^p, \tag{17.37}$$

$$\eta_y^f = \eta_L^p + \eta_\omega^b, \tag{17.38}$$

where η_ω^b are WF components of motion in body-coordinate axis, and w_b^f and η_y^f consists of a new modified disturbance and a modified measurement defined by $w_b^f = R^T(\psi_y)E_b w_b$ and $\eta_y^f = R^T(\psi_y)\eta_y$, respectively.[4]

17.2.2 A Brief Review of Three DP Controllers

In what follows we give a short description of three types of controllers used in the current chapter. The first type of controller consists of a nonlinear multivariable PID coupled with a nonlinear passive observer. Passive observers were introduced in the late 1990s; the main motivation for their development was the need to overcome the difficulty of tuning a relatively large number of parameters (through experimental testing of the vessel) in other commonly used approaches such as back-stepping and Kalman filtering, see [5, 30, 31]. In fact, the tuning procedure is simplified significantly using passivity arguments [31]. Moreover, in the absence of measurement noise passive observers satisfy satisfy the property of global convergence, that is, all estimation errors converge to zero. Another interesting property of passive observers is that the wave filtering parameters (filter gains) are functions of the dominating wave frequency, thus making them appropriate candidates for adaptive wave filtering when the sea state and dominating wave frequency are unknown.

In this type of controller, the observer provides estimates of the LF components of the position and the velocity of the vessel which are used in the nonlinear multivariable controller structure. To cover the different sea conditions from calm to extreme seas, we have designed four different controllers and observers based on different values of the dominant wave frequency. For further details on controller design the reader is referred to [21, 26].

The second class of controllers is of the LQG type. It consists of a steady state Kalman filter and a linear quadratic (state-feedback) controller. In order to design the LQG controller, we used the linear model of the vessel presented in (17.33)–(17.38). As in the previous case, four different LQG controllers were designed,

[4]When designing observers for wave filtering in dynamic positioning, since the controller regulates the heading of the vessel, the designer can assign a new intensity to w_b^f; however, assigning the intensity of the noise in practice requires considerable expertise.

based on four different dominant wave frequency values, covering different sea conditions from calm to extreme. Details on the design of the LQG DP controllers can be found in [17].

The third type of controller is a robust DP controller designed using $\mathcal{H}_\infty$ and mixed-μ control techniques. In this set-up, the practical assumptions are exploited in order to obtain a linear design model with parametric uncertainties describing the dynamics of the vessel. Appropriate frequency weighting functions are selected to capture the required performance specifications at the controller design phase. The proposed model and weighting functions are then used to design robust controllers. The problem of wave filtering is also addressed during the process of modeling and controller design. As in the previous cases, four $\mathcal{H}_\infty$ robust controllers were designed for different sea conditions. For details on the development of the vessel's model with parametric uncertainty, as well as the procedure adopted for robust DP controller design, the reader is referred to [15, 16].

17.3 Wave Filtering and Control: Numerical Solutions

In what follows we summarize the results of Monte Carlo simulations of wave filtering and dynamic positioning systems. The simulations were carried out using the MCSim. After a short description of the simulator, we evaluate the improvements obtained with the changes in our proposed modified design model. This being done, the DP controllers introduced in Sect. 17.2.2 are evaluated using the simulator.

17.3.1 Overview of the Simulator

The MCSim is a modular, multi-disciplinary simulator based on Matlab/Simulink developed at the Centre for Ships and Ocean Structures, Dept. of Marine Technology, Norwegian Univ. of Science and Technology. The MCSim incorporates high fidelity models, denoted as process plant models or simulation models in [26], at all levels (plants and actuators). It is composed of different modules that include the following:

1. **Environmental module**, containing different wave models, surface current models, and wind models.
2. **Vessel dynamics module**, consisting of a LF and a WF model. The LF model is based on the standard six degrees-of-freedom vessel dynamics, whose inputs are the environmental loads and the interaction forces from thrusters and the external connected systems.
3. **Thruster and shaft module**, containing thrust allocation routine for non-rotating thrusters, thruster dynamics, and local thruster control. It may also include advanced thrust loss models for extreme seas, in which case detailed information about waves, current and vessel motion is required.

4. **Vessel control module**, consisting of different controllers, including nonlinear multivariable PID controllers, for DP.

Details on the MCSim can be found in [8, 22, 23, 29].

In what follows, the results of Monte-Carlo simulations performed with the MCSim are shown to illustrate and assess the performance of a number of different types of observers and controllers for an offshore vessel with DP system. To this effect, in the next section two types of observers based on the two distinct models described by (17.1)–(17.7) and (17.10)–(17.15) are introduced. Their performance is evaluated comparatively under different environmental conditions, from calm to high seas. In the simulations, the environmental conditions are simulated using the JONSWAP spectrum [18]. The study shows the usefulness of the new linear design model adopted. This is followed by a section where the performance obtained with the three types of controllers defined before is also assessed in simulation.

17.3.2 A Comparison of the Modified and Classical Design Models

In this section, in order to compare the usefulness of the two design models described by (17.1)–(17.7) and (17.10)–(17.15), we start by designing a Luenberger-like observer for the model presented by (17.1)–(17.7). After tuning the observer gains (for the best estimation performance), we use the same gains and design another Luenberger-like observer based on the model described by (17.10)–(17.15). The two observers share the same structure (except for the proposed modification) and have the same gains.[5] We compare the estimation results of the two above mentioned observers and reason that better performance with one of the observers reflects the superiority of the model adopted for its design.

To design the observer and optimize the gains we follow the procedure of designing nonlinear passive observer for marine vessels. Passive observers were introduced in [9, 30, 31]. The structure of passive observers for a DP vessel model described by (17.1)–(17.7) is given by

$$\dot{\hat{\xi}}_\omega = A_\omega(\omega_0)\hat{\xi}_\omega + K_1\tilde{\eta}_y, \tag{17.39}$$

$$\hat{\eta}_\omega = C_\omega\hat{\xi}_\omega, \tag{17.40}$$

$$\dot{\hat{b}} = -T^{-1}\hat{b} + K_2\tilde{\eta}_y, \tag{17.41}$$

[5]All the gains are optimally tuned for the observer designed using the model described in (17.1)–(17.7). Such a selection favors the old DP model; however, a comparison of the results of simulations shows that the observer designed using the newly proposed model yields better performance.

$$\dot{\hat{\eta}}_L = R(\psi_y)\hat{v}_L + K_3\tilde{\eta}_y, \tag{17.42}$$

$$M\dot{\hat{v}}_L + D\hat{v}_L = \tau + R^T(\psi_y)\hat{b} + R^T(\psi_y)K_4\tilde{\eta}_y, \tag{17.43}$$

$$\hat{\eta}_y = \hat{\eta}_L + \hat{\eta}_\omega. \tag{17.44}$$

For details on nonlinear passive observers and the selection of the observer gains, i.e., $K_i, i = 1 \ldots 4$, the reader is referred to [5, 6, 9, 19, 26, 30–32].

The structure of the second observer for a DP vessel model described by (17.10)–(17.15) (i.e., observer based on the new proposed DP model) is adopted from the one in (17.39)–(17.44) except for the WF motion that is now expressed in body coordinates as

$$\hat{\eta}_\omega = R(\psi_y)C_\omega\hat{\xi}_\omega. \tag{17.45}$$

In conclusion, throughout this section we use the same set of gains in order to ascertain the impact of the design model on the performance obtained with the observers. Three different environment conditions from calm to high seas are considered, and for each one a separate observer is designed. Table 17.1 shows the definition of the sea condition associated with a particular model of supply vessel that is used in the MCSim.

For simulation purposes, the nominal values for the dominant wave frequency are selected as $\{0.48, 0.63, 0.92\}$ (rad/s). Figures 17.2 and 17.3 show the time evolution of total motion and the LF component of the motion and their estimates by two passive observers [one based on the model (17.1)–(17.7) and the other based on the modified model (17.10)–(17.15)] in a high sea state condition. The simulation is done in a station keeping scenario where a nonlinear multivariable PID controller regulates the position and heading of the vessel about zero. It is seen that even with wave filtering, some of the 1st-order wave frequency components are present in the LF estimates.[6] However, the simulations support the conclusion that the observer proposed in this chapter yields very good performance when compared with that obtained with the passive observer described in [9]. To quantify the potential performance improvement of our modified observer over the passive observer of [9], we introduce "percentage comparison" figure of merit given by

$$\%E = \frac{|\mathrm{VAR}_{\tilde{p}_L^{old}}| - |\mathrm{VAR}_{\tilde{p}_L^{new}}|}{|\mathrm{VAR}_{\tilde{p}_L^{new}}|} \times 100, \tag{17.46}$$

[6] At this point, we should emphasize that the observers are designed according to the simple model of (17.10)–(17.15) [and (17.1)–(17.7)] while they are tested in the MCSim using a high fidelity model which captures hydrodynamic effects, generalized coriolis and centripetal accelerations, nonlinear damping and current forces, and generalized restoring forces. Moreover, in the MCSim the JONSWAP wave spectrum is used to simulate the waves while the observers are designed using a linear second order approximation of the spectrum.

Table 17.1 Definition of sea states from [24]

Sea state	Dominant wave frequency ω_0 (rad/s)	Significant wave height H_s (m)
Calm seas	>1.11	<0.1
Moderate seas	[0.74 1.11]	[0.1 1.69]
High seas	[0.53 0.74]	[1.69 6.0]
Extreme seas	<0.53	>6.0

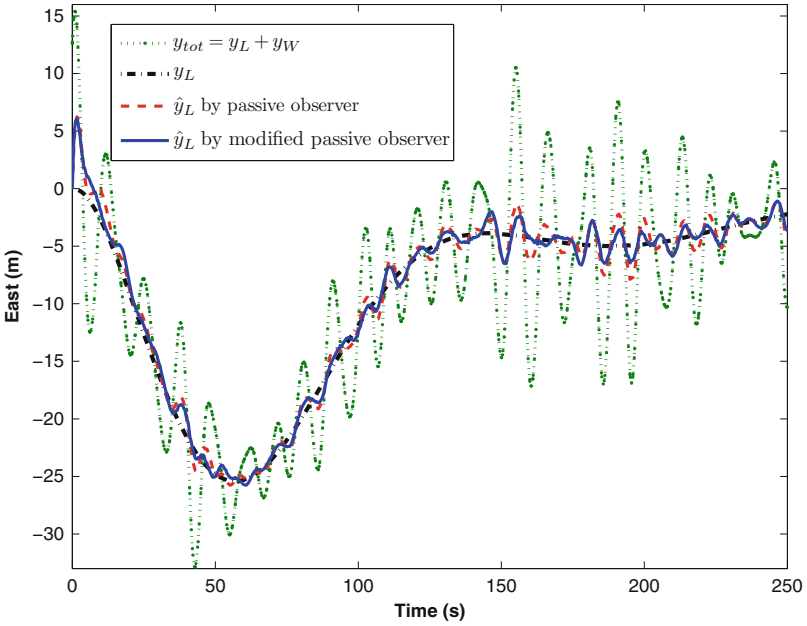

Fig. 17.2 Total motion, LF component of a (typical 100 m long) DP vessel (only sway), and its estimates

where $\text{VAR}_{\tilde{p}}$ is the variance of $\tilde{p}$, $\tilde{p}_L^{old}$ and $\tilde{p}_L^{new}$ are the estimation error of p_L with the passive observer of [9] and our modified observer, respectively, and finally p_L is the LF component of the motion in surge, sway or yaw.

Table 17.2 summarizes the result of Monte-Carlo simulations with different environment conditions from calm to high seas where a nonlinear multivariable PID controller regulates the position of the ship at origin. We have computed the performance improvement of our modified observer over that described in [9].

Table 17.3 shows similar results when the vessel position was commanded to change 300 m forward in surge and sway while keeping the heading at zero; this simple maneuver was executed with the nonlinear multivariable PID control law referred to above. As Tables 17.2 and 17.3 show, as the sea condition changes from calm to high seas, there is significant performance improvement with the use of the new proposed observer, when compared with that of the passive observer in [9].

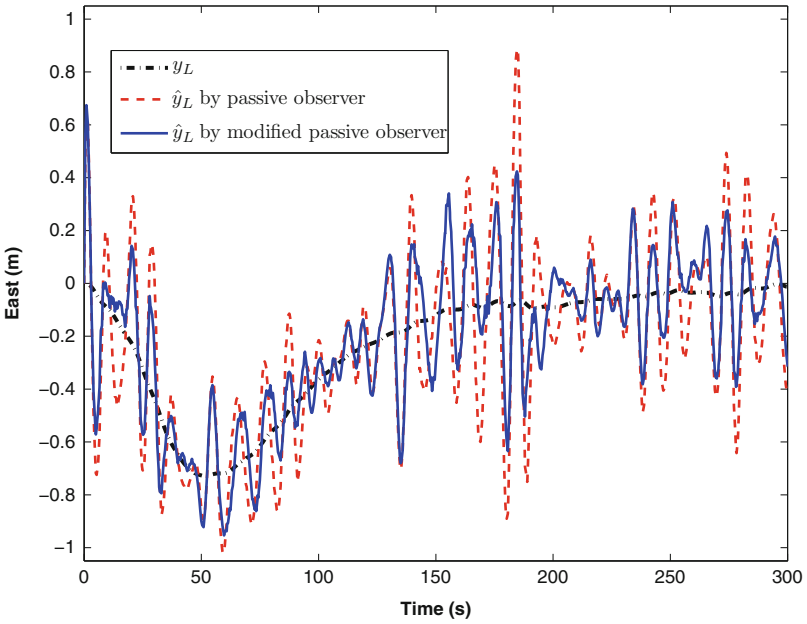

Fig. 17.3 LF component of a (typical 100 m long) DP vessel (only sway), and its estimates

Table 17.2 Performance improvements of new observer (station keeping)

	Calm seas	Moderate seas	High seas
%E in surge	16 %	18 %	78 %
%E in sway	22 %	25 %	115 %
%E in yaw	−9 %	51 %	93 %

Table 17.3 Performance improvements of new observer (Manoeuvering)

	Calm seas	Moderate seas	High seas
%E in surge	17 %	18.5 %	80 %
%E in sway	24 %	27 %	115 %
%E in yaw	−8 %	51 %	94 %

The reason for this behavior is the violation of Assumption 2 with the observer in [9]. In fact, when shifting from calm sea to moderate and high sea conditions, the amplitude of the wave-induced yaw motion becomes larger and neglecting this term causes performance degradation. This problem is alleviated in our proposed observer (by modeling the WF motion in the body frame).

Now that the efficacy of the newly proposed design model has been shown we will continue, in what follows, by presenting the result of numerical simulations with three different types of DP controllers designed based on the new model.

17.3.3 Numerical Simulations with Three Types of DP Controllers

This section summarizes the results of Monte-Carlo simulations aimed at assessing the performance achievable with the three types of controllers described before. In parallel, we study the performance of the wave filters designed using the newly proposed model, when used in conjunction with the first and second controllers of Sect. 17.2.2. In the simulations, the different environment conditions from calm to extreme seas were simulated using the JONSWAP spectrum [18]. Notice that in addition to the three environment conditions (calm, moderate, and high sea) used in Sect. 17.3.2 we also consider the extreme sea state, see Table 17.1.

We start by comparing the estimation-performance of the wave filters when run together with the first two controllers.[7] At this point in the simulation, the nominal values for the dominant wave frequency were selected as $\{0.48, 0.63, 0.92, 1.18\}$ (rad/s). Figure 17.4 shows the vessel's total and low frequency motion components using a passive-like observer (that is run with a nonlinear PID controller) and a Kalman filter (inserted in an LQG observer/controller structure) in a calm sea state. The simulation is done in a station keeping scenario where a nonlinear multivariable PID controller (in conjunction with a passive observer) and a LQG controller (which includes a Kalman filter in its structure) regulate the position and heading of the vessel about zero. To allow for a better estimation-performance comparison, in Fig. 17.5 we only show the LF component of the motion and its estimates by the passive observer and a Kalman filter in calm sea state (for the same simulation as the one shown in Fig. 17.4). It is seen that the Kalman filter is better (in terms of estimating the LF components of motion) than the passive observer. Figures 17.6 and 17.7 show the results of similar simulations for moderate and high seas. The results support the observation that the Kalman filter has better wave filtering properties (estimation of the LF part of the motion) when compared to the passive observer. Moreover, it is also seen that even with wave filtering, some of the 1st-order wave frequency components are seen in the LF estimates. Figures 17.8, 17.9, and 17.10 focus on the motion control capabilities, and illustrate the performance obtained with the DP controllers mentioned before, under different sea conditions.[8] Here we should highlight that in Figs. 17.8, 17.9, 17.10, and 17.11 we present only the LF components of motion. These simulations suggest that the LQG has the best performance in terms of regulating the LF components of motion and the robust controller has the worst performance overall. Notice that the robust controller does not include any observer to estimate the LF motions and the controllers are fed with the total position (LF+WF). However, if the comparison is done in terms of total vessel motion (LF+WF), the robust controller exhibits superior dynamic

[7] Wave filtering in the robust DP controller is not implemented explicitly, see [15, 16] for details.

[8] All the results are presented in full scale. During the testing phase care was taken to ensure that all controllers were tuned to their best performance, so as to allow for a fair comparative study.

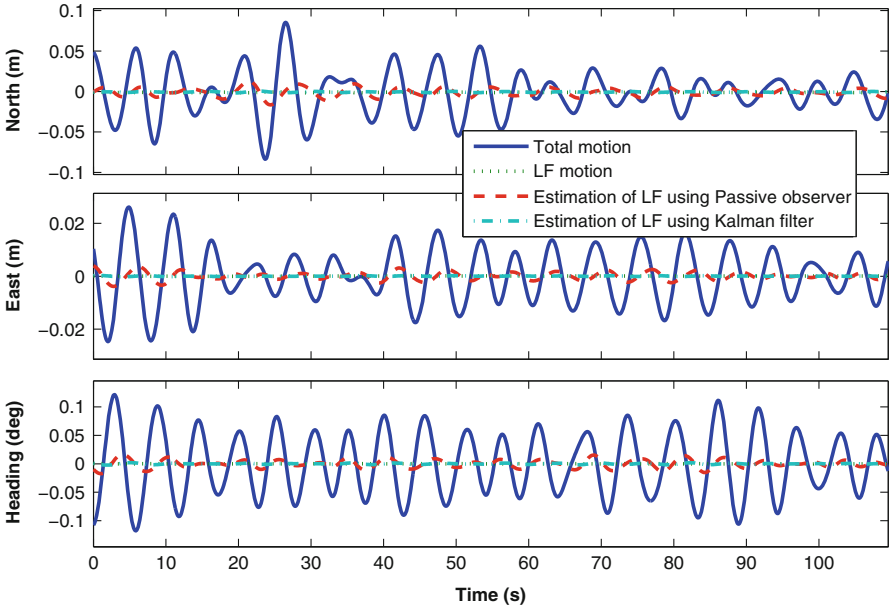

Fig. 17.4 Numerical simulations (calm sea): total motion of the vessel, LF components of motion, and estimation of the LF motion with a passive observer and a Kalman filter

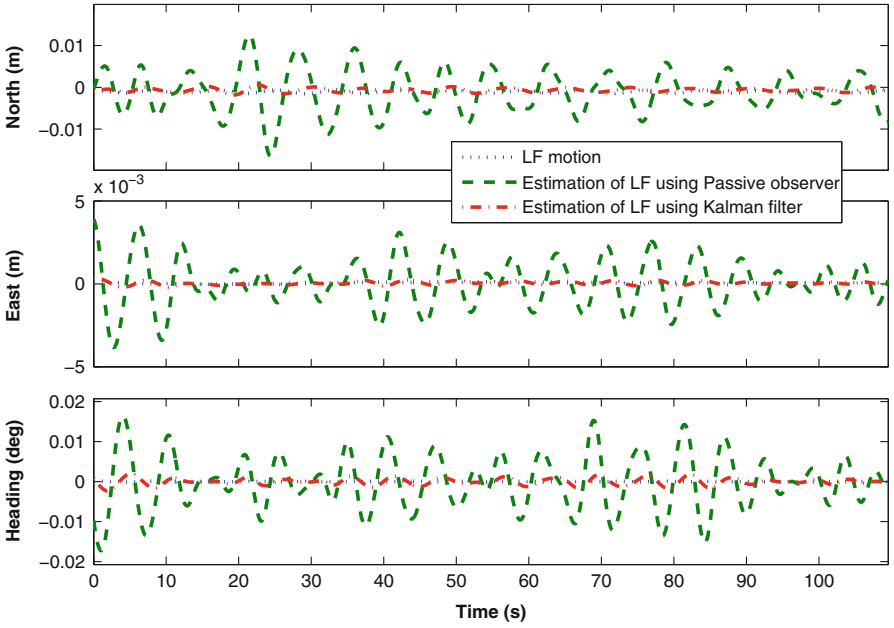

Fig. 17.5 Numerical simulations (calm sea): LF components of motion and estimation of the LF motion with a passive observer and a Kalman filter (a zoom in on Fig. 17.4)

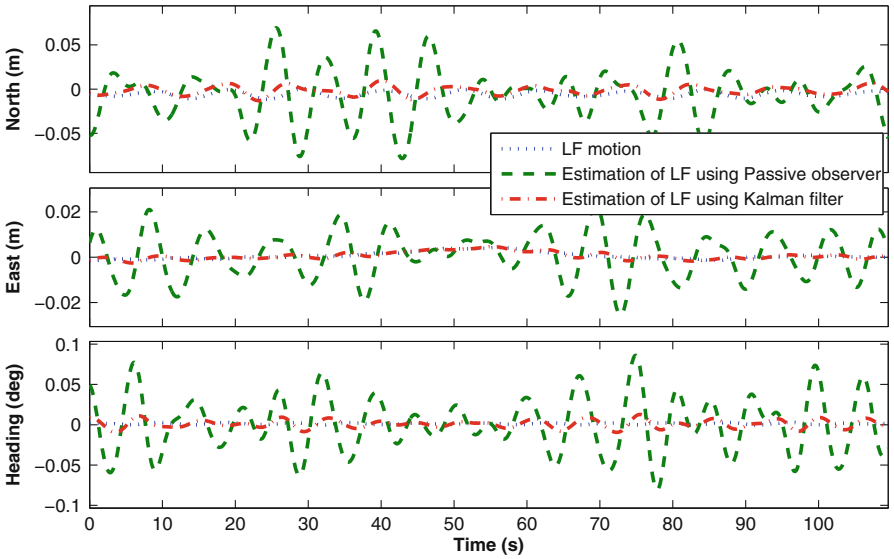

Fig. 17.6 Numerical simulations (moderate sea): LF components of motion and estimation of the LF motion with a passive observer and a Kalman filter

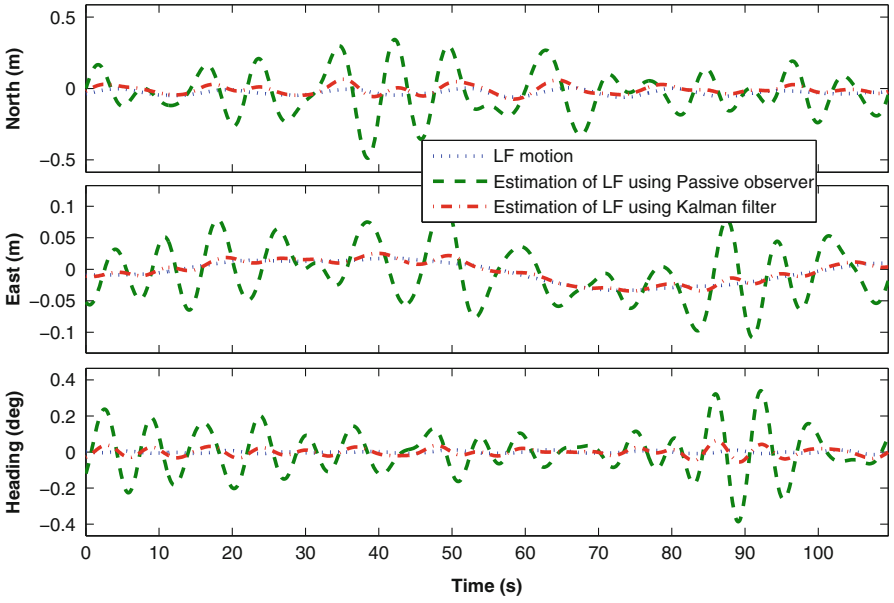

Fig. 17.7 Numerical simulations (high sea): LF components of motion and estimation of the LF motion with a passive observer and a Kalman filter

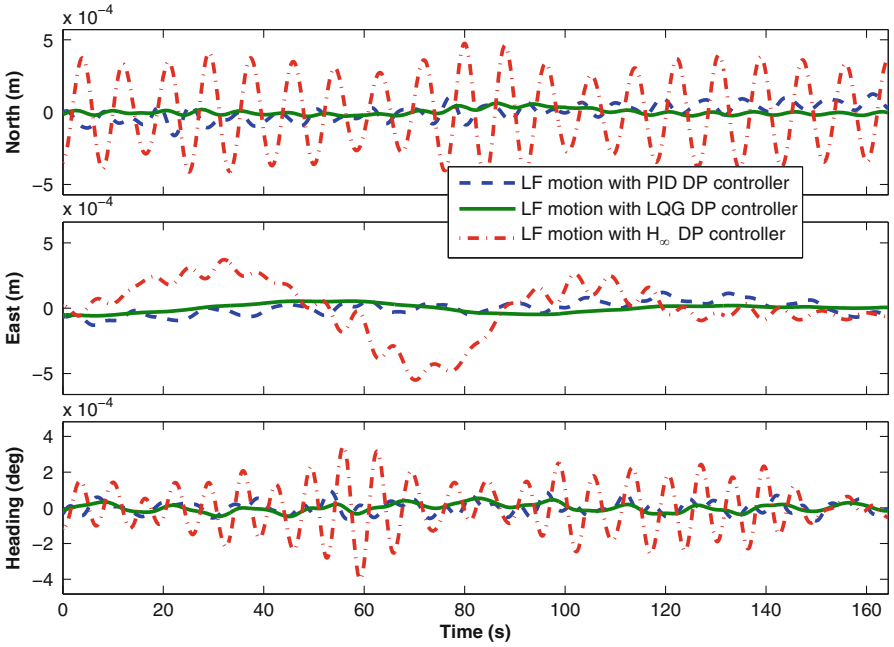

Fig. 17.8 Numerical simulations (calm sea): LF components of motion of the vessel operating with different DP controllers

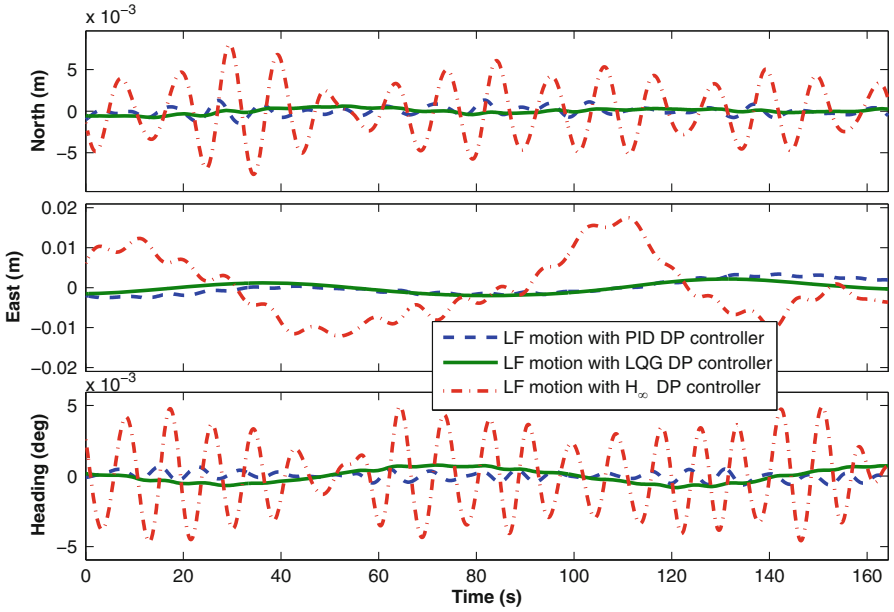

Fig. 17.9 Numerical simulations (moderate sea): LF components of motion of the vessel operating with different DP controllers

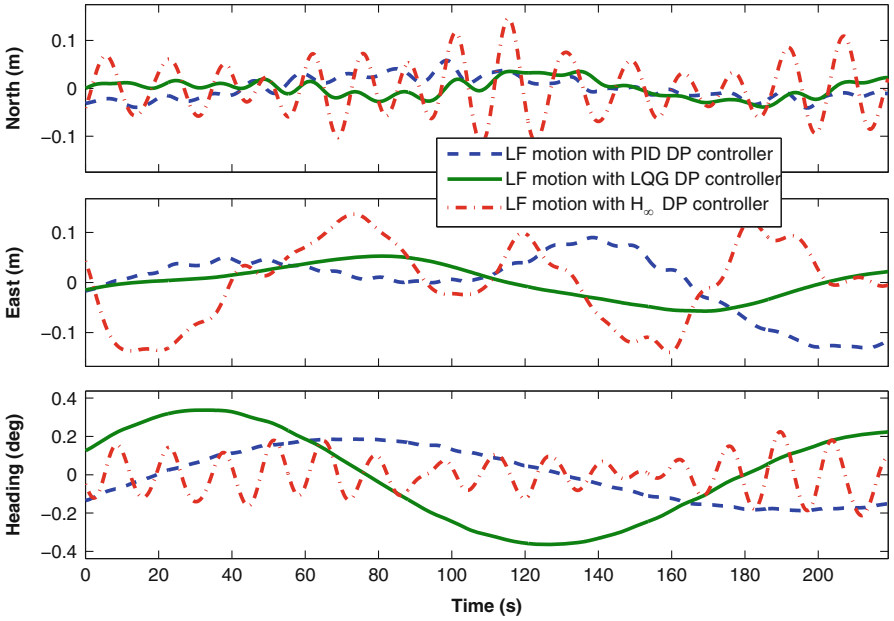

Fig. 17.10 Numerical simulations (high sea): LF components of motion of the vessel operating with different DP controllers

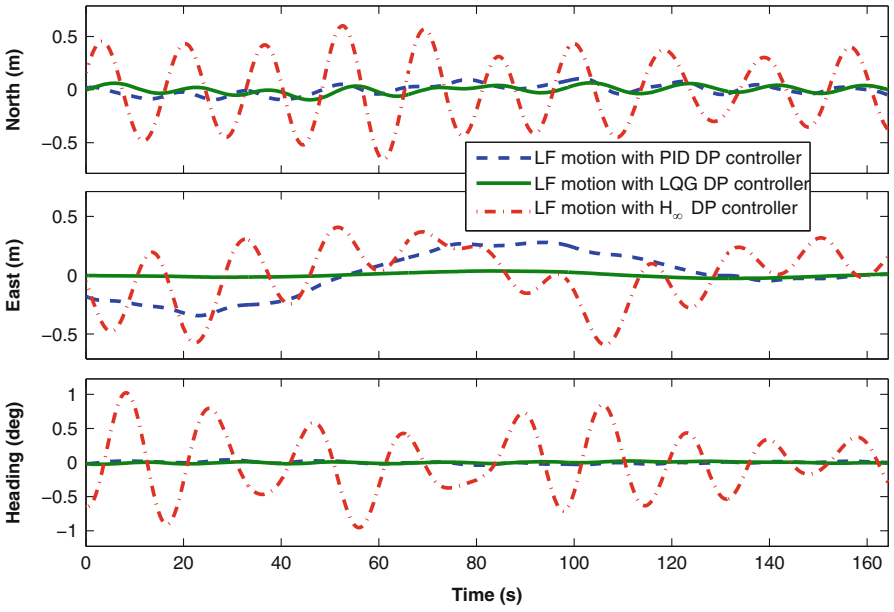

Fig. 17.11 Numerical simulations (extreme sea): LF components of motion of the vessel operating with different DP controllers

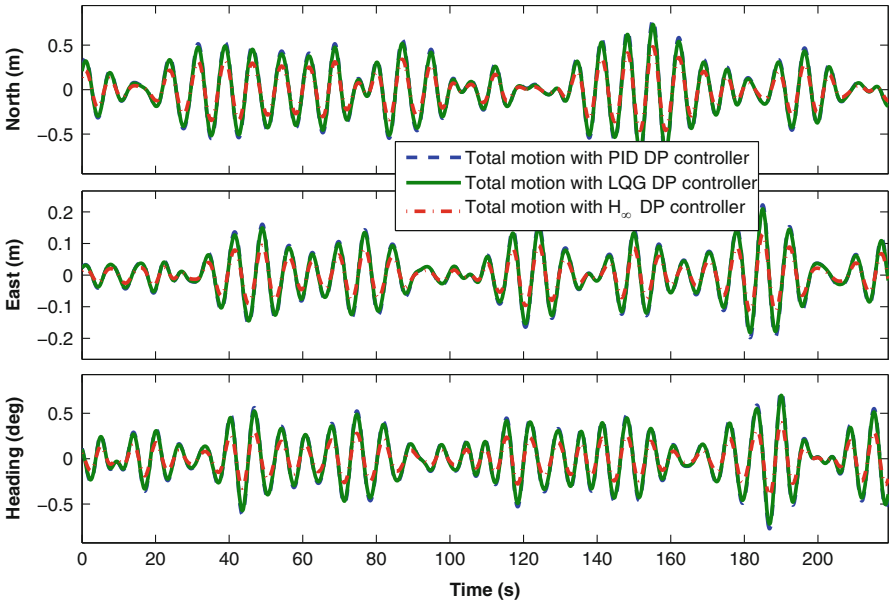

Fig. 17.12 Numerical simulations (moderate sea): total motion of the vessel with different DP controllers

positioning with respect to that obtained with the other two types of controllers (that show similar performance), see Figs. 17.12 and 17.13. This is due to the poor wave filtering of the robust controllers and the fact that the robust controllers (without an explicit wave filter) try to regulate all the motions of the vessel (and not only the LF part). Notice that in extreme seas or swell with very long wave periods, wave filtering is turned off as described in [17, 21, 27] and the DP controllers should regulate the total motion of the vessel (and not only the LF part), and hence, robust controllers will be favorable in extremes seas.

17.4 Experimental Model Testing Results

This section bridges the gap between theory and practice. To this effect, we assess the performance of the three types of controllers described before using an experimental set-up consisting of the Cybership III model vessel of the Marine

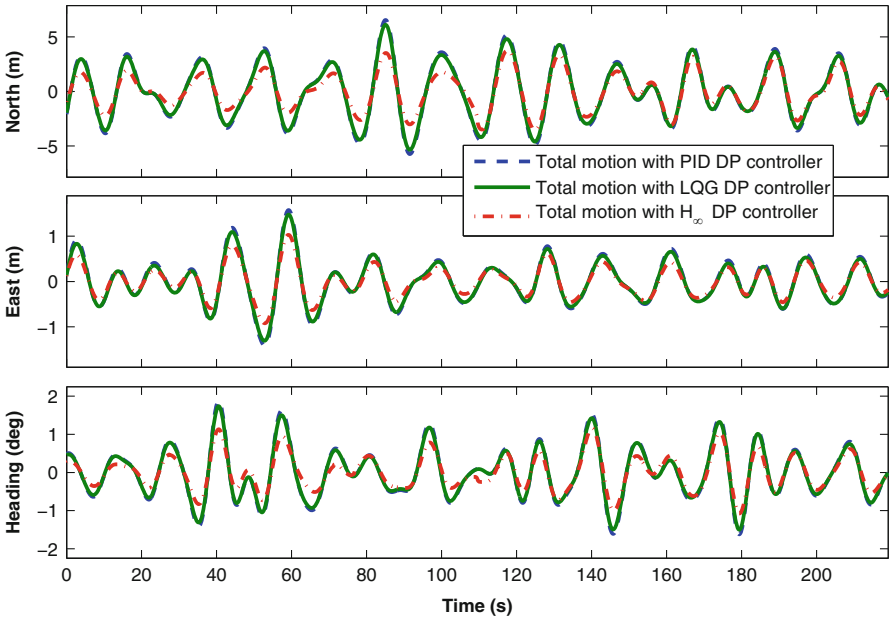

Fig. 17.13 Numerical simulations (extreme sea): total motion of the vessel with different DP controllers

Cybernetics Laboratory (MCLab), Department of Marine Technology, Norwegian University of Science and Technology (NTNU). During the tests, different sea conditions were emulated using a hydraulic wave maker.

17.4.1 Overview of the Cybership III

Cybership III is a 1:30 scaled model of an offshore vessel operating in the North Sea. Table 17.4 presents the main parameters of both the model and the full scale vessel.

Cybership III is equipped with two pods located at the aft. A tunnel thruster and an azimuth thruster are installed at the bow.[9] The vessel has mass $m = 75\,kg$, length $L = 2.27\,m$ and breadth $B = 0.4\,m$. The main parameters of the model are presented in Table 17.4. The internal hardware architecture is controlled by an onboard computer that communicates with the onshore PC through a WLAN. The PC onboard the ship uses QNX real-time operating system (target PC). The control system is developed on a PC in the control room (host PC) under Simulink/Opal and downloaded to the target PC using automatic C-code generation and wireless

[9]For technical reasons in this experiment the tunnel thruster was deactivated.

Table 17.4 Model main parameters

	Model	Full scale
Overall length	2.275 m	68.28 m
Length between perpendiculars	1.971 m	59.13 m
Breadth	0.437 m	13.11 m
Breadth at water line	0.437 m	13.11 m
Draught	0.153 m	4.59 m
Draught front perpendicular	0.153 m	4.59 m
Draught aft. perpendicular	0.153 m	4.59 m
Depth to main deck	0.203 m	6.10 m
Weight (hull)	17.5 kg	Unknown
Weight (normal load)	74.2 kg	22.62 tons
Longitudinal center of gravity	100 cm	30 m
Vertical center of gravity	19.56 cm	5.87 m
Propulsion motors max shaft power (6 % gear loss)	81 W	3200 HP
Tunnel thruster max shaft power (6 % gear loss)	27 W	550 HP
Maximum speed	Unknown	11 knots

Ethernet. The motion capture unit, installed in the MCLab, provides Earth-fixed position and heading of the vessel. The motion capture unit consists of onshore 3-cameras mounted on the towing carriage and a marker mounted on the vessel. The cameras emit infrared light and receive the light reflected from the marker.

To emulate the sea conditions, a hydraulic wave maker system is used. It consists of a single flap covering the whole breadth of the basin, and a computer controlled motor, moving the flap. The device can produce regular and irregular waves with different spectrums. We have used the JONSWAP spectrum to simulate the different sea conditions for our experiments, see [18].

17.4.2 Model Testing Results

Figure 17.14 shows the vessel position and heading in a moderate sea condition. The results of the model test are in agreement with the ones obtain in the numerical simulation study, showing satisfactory performance of wave filtering (estimating the LF part of the motion) for both the passive observer and the Kalman filter. However, the Kalman filter yields a smoother estimate of the LF vessel motion, as shown in Fig. 17.15 that is a zoom-in on Fig. 17.14 (we omit the total motion in Fig. 17.15 for the sake of a better comparison). It is seen that the Kalman filter provides smoother estimation of the LF part of motion.

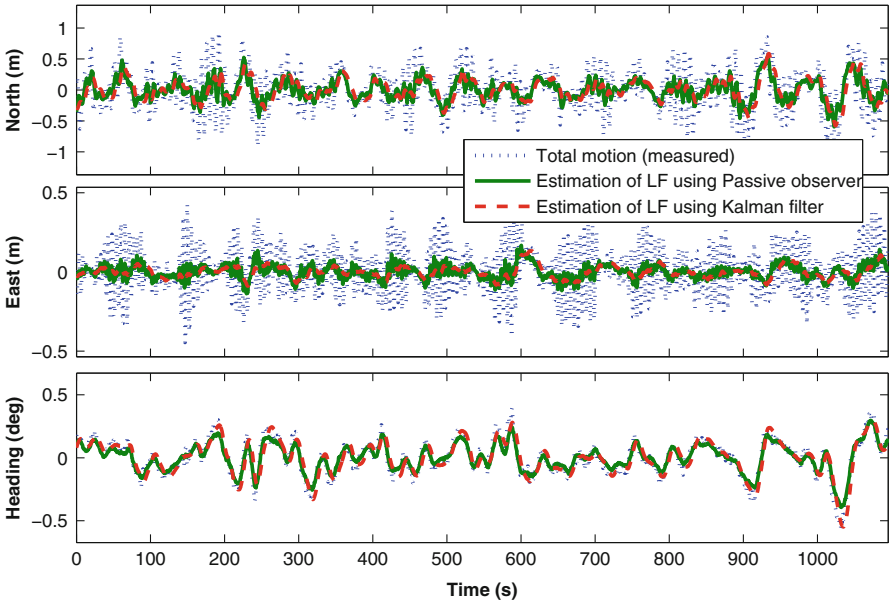

Fig. 17.14 Experimental results (moderate sea): total motion of the vessel and estimation of the LF components of motion with a passive observer and a Kalman filter

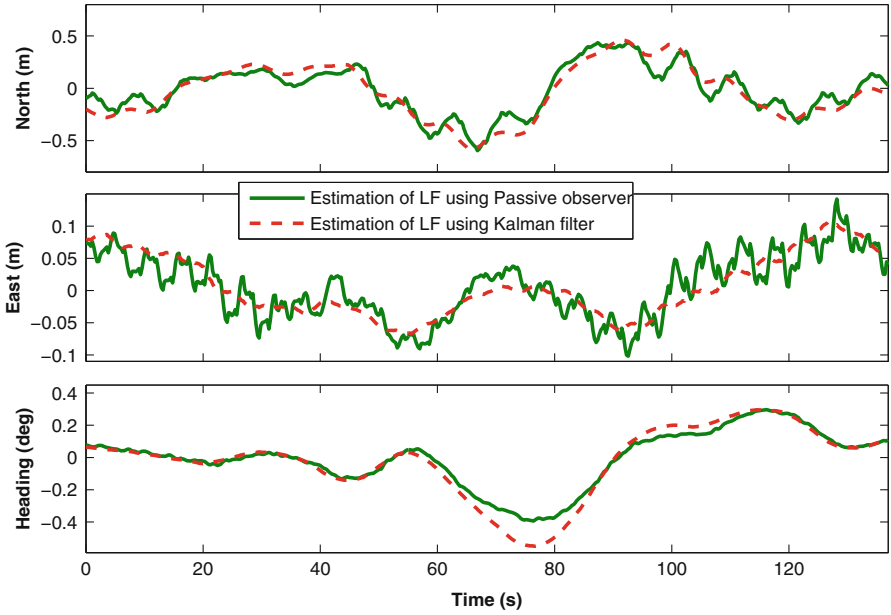

Fig. 17.15 Experimental results (moderate sea): estimation of the LF components of motion with a passive observer and a Kalman filter (zoom in of Fig. 17.14)

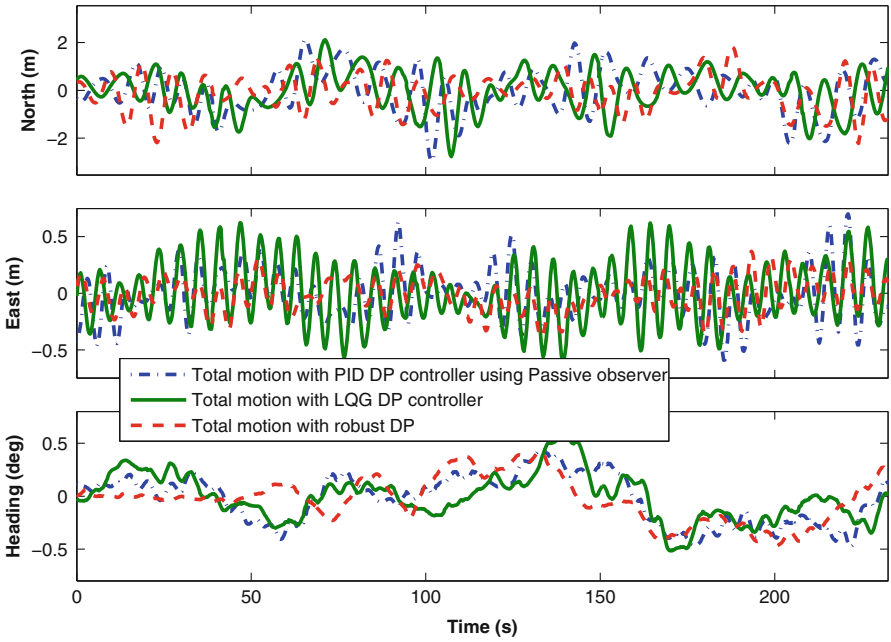

Fig. 17.16 Experimental results (high sea): total motion of the vessel with different DP controllers

Table 17.5 Experimental results (high sea): calculated covariance of total motion of the vessel (average of three experiments)

	x (m)	y (m)	ψ (deg)
PID with a passive observer	0.80	0.03	0.05
LQG controller	0.74	0.07	0.04
robust controller	0.62	0.02	0.09

Figure 17.16 shows the comparison of the total motion of the vessel in high sea, working under different DP systems; notice that the robust DP controller has a (slightly) better performance in the regulation of the vessel and the two other controllers have similar performance. Table 17.5 shows the mean covariance of three station keeping experiments with the above mentioned controllers. The table also shows that the robust DP controller has better performance (in terms of x_{tot} and y_{tot} regulation, but not in ψ_{tot}) in the station keeping scenario, when compared with the other two controllers.

17.5 Combined Framework in Transport of Water and Transport over Water

This chapter is focused on the development of a new linear model of marine vessels subjected to currents and sea waves. This is a key step in devising solutions to the problem of dynamic positioning and wave filtering of vessels for scientific and

commercial operations. The model proposed captures the influence of forces and moments due to currents and sea waves. The effect of sea waves includes two terms: (a) oscillatory forces and moments and (b) slowly varying forces and moments (modeled together with the forces and moment due to currents). Notwithstanding the simplicity of the model, it captures the physics of the problem at hand in an effective manner. Hence, it is at the heart of the application of new techniques in control and estimation theory to the design of wave filters and controllers for DP systems. Most marine vessels equipped with DP systems operate in open seas where flow control is impossible. However, some passenger, cruise, and commercial vessels with DP systems also travel in open channels where transport of water and flow control are clearly feasible. Should the need arise for the use of DP systems in such circumstances, the information received from the control system that regulates transport of water in open canal networks can in principle be used to update the proposed model to use higher fidelity models of currents to best capture the effect of the latter on the vessel. This combined framework of transport of and over water could potentially improve the performance of DP systems and speed up their initialization process.[10]

17.6 Conclusions and Future Research

This chapter proposed a new linear design model for marine vessels subjected to ocean waves and currents, with application to wave filtering and dynamic positioning. Its key contribution was the development of a modified linear model that captures the physics of the vessel in a simple, yet effective manner. Numerical simulations, carried out using a high fidelity nonlinear dynamic positioning (DP) simulator, showed the performance improvement in wave filtering due to the use of the modified model in comparison with commonly used models. The proposed model is instrumental in applying new techniques in control and estimation theories to the problem of DP as shown in [14–17] for simulation and model testing. The chapter offered also a comprehensive evaluation of the performance obtained with a set of three DP controllers designed for different sea conditions, for a representative vessel model. The evaluation included Monte-Carlo simulations, as well as model-test experiments with a vessel in a towing tank equipped with a wave making system. The results obtained confirmed that Kalman filter exhibits superior performance in wave filtering. Moreover, they also showed that robust DP controller has better performance in the regulation of the total motion of the vessel (LF+WF). However, a PID controller equipped with a passive observer was the simplest controller to design and tune. Future work will include the application of the methodologies developed to the design of DP controllers for a real vessel.

[10]Before a DP system is functional, the state estimate of the filter in the DP system should converge to its steady state performance; this initialization may take tens of minutes.

Acknowledgements We thank our colleagues Asgeir J. Sørensen, A. Pedro Aguiar, N.T. Dong, and Thor I. Fossen for many discussions on wave filtering and adaptive estimation. We would also like to thank T. Wahl, M. Etemaddar, E. Peymani, M. Shapouri, and B. Ommani for their invaluable assistance during the model tests at MCLab. This work has been carried out at the Centre for Autonomous Marine Operations and Systems (AMOS) in collaboration with the Norwegian Marine Technology Research Institute (MARINTEK). The Norwegian Research Council is acknowledged as the main sponsor of AMOS. This work was supported by the Research Council of Norway through the Centres of Excellence funding scheme, Project number 223254—AMOS.

References

1. Balchen J, Jenssen NA, Sælid S. Dynamic positioning using Kalman filtering and optimal control theory. In: The IFAC/IFIP symposium on automation in offshore oil field operation, Bergen, 1976. p. 183–6.
2. Balchen J, Jenssen NA, Sælid S. Dynamic positioning of floating vessels based on Kalman filtering and optimal control. In: Proceedings of the 19th IEEE conference on decision and control, New York, 1980. p. 852–64.
3. Balchen J, Jenssen NA, Sælid S. A dynamic positioning system based on Kalman filtering and optimal control. Modeling, Identification and Control (MIC). 1980;1(3):135–63.
4. Faltinsen OM. Sea loads on ships and offshore structures. Cambridge: Cambridge University Press; 1990.
5. Fossen TI. Nonlinear passive control and observer design for ships. Modeling, Identification and Control (MIC). 2000;21(3):129–84.
6. Fossen TI. Handbook of marine craft hydrodynamics and motion control. Chichester: Wiley; 2011.
7. Fossen TI, Perez T. Kalman filtering for positioning and heading control of ships and offshore rigs. IEEE Control Syst Mag. 2009;29(6):32–46.
8. Fossen TI, Perez T. Marine systems simulator (MSS). 2009. http://www.marinecontrol.org/.
9. Fossen TI, Strand JP. Passive nonlinear observer design for ships using lyapunov methods: Full-scale experiments with a supply vessel. Automatica. 1999;35:3–16.
10. Fossen TI, Sagatun SI, Sørensen AJ. Identification of dynamically positioned ships. J Control Eng Pract. 1996;4(3):369–76.
11. Grimble MJ, Patton RJ, Wise DA. The design of dynamic ship positioning control systems using stochastic optimal control theory. Optim Control Appl Methods. 1980;1:167–202.
12. Grimble MJ, Patton RJ, Wise DA. The design of dynamic ship positioning control systems using stochastic optimal control theory. IEE Proc. 1980;127(3):93–102.
13. Grøvlen Å, Fossen TI. Nonlinear control of dynamic positioned ships using only position feedback: An observer backstepping approach. In: Proceedings of the IEEE conference on decision and control (CDC'96), Kobe, 1996.
14. Hassani V, Sørensen AJ, Pascoal AM. Evaluation of three dynamic ship positioning controllers: from calm to extreme conditions. In: Proceedings of the NGCUV'12 - IFAC workshop on navigation, guidance and control of underwater vehicles, Porto, 2012.
15. Hassani V, Sørensen AJ, Pascoal AM. Robust dynamic positioning of offshore vessels using mixed-μ synthesis. Part I: Designing process. In: Proceedings of ACOOG'12 - IFAC workshop on automatic control in offshore oil and gas production, Trondheim, 2012.
16. Hassani V, Sørensen AJ, Pascoal AM. Robust dynamic positioning of offshore vessels using mixed-μ synthesis. Part II: Simulation and experimental results. In: Proceedings of ACOOG'12 - IFAC workshop on automatic control in offshore oil and gas production, Trondheim, 2012.

17. Hassani V, Sørensen AJ, Pascoal AM, Pedro Aguiar A. Multiple model adaptive wave filtering for dynamic positioning of marine vessels. In: Proceedings of ACC'12 - American control conference, Montreal, 2012.
18. Hasselmann K, Barnett TP, Bouws E, Carlson H, Cartwright DE, Enke K, Ewing JA, Gienapp H, Hasselmann DE, Kruseman P, Meerburg A, Müller P, Olbers DJ, Richter K, Sell W, Walden H. Measurements of wind-wave growth and swell decay during the joint north sea wave project (JONSWAP). Ergnzungsheft zur Deutschen Hydrographischen Zeitschrift Reihe. 1973;8(12):1–95.
19. Loria A, Fossen TI, Panteley E. A separation principle for dynamic positioning of ships: theoretical and experimental results. IEEE Trans. on Contr. Syst. and Tech. 2000;8(2): 332–43.
20. MARINTEK. Marine cybernetics laboratory. 2014. http://www.sintef.no/home/MARINTEK/Laboratories/Marine-Cybernetics-Laboratory/. Accessed 31 July 2014 [Online].
21. Nguyen TD, Sørensen AJ, Quek ST. Design of hybrid controller for dynamic positioning from calm to extreme sea conditions. Automatica. 2007;43(5):768–85.
22. Perez T, Smogeli ØN, Fossen TI, Sørensen AJ. An overview of marine systems simulator (MSS): A simulink toolbox for marine control systems. In: Proceedings of Scandinavian conference on simulation and modeling (SIMS'05), Trondheim, 2005.
23. Perez T, Sørensen AJ, Blanke M. Marine vessel models in changing operational conditions – a tutorial. In: 14th IFAC symposium on system identification (SYSID'06), Newcastle, 2006.
24. Price WG, Bishop RED. Probabilistic theory of ship dynamics. London: Chapman and Hall; 1974.
25. Sælid S, Jenssen NA, Balchen J. Design and analysis of a dynamic positioning system based on Kalman filtering and optimal control. IEEE Transactions on Automatic Control. 1983;28(3):331–9.
26. Sørensen AJ. Lecture notes on marine control systems. Technical Report UK-11-76, Norwegian University of Science and Technology, 2011.
27. Sørensen AJ. A survey of dynamic positioning control systems. Annual Reviews in Control. 2011;35:123–36.
28. Sørensen AJ, Sagatun SI, Fossen TI. Design of a dynamic positioning system using model-based control. J Control Eng Pract. 1996;4(3):359–68.
29. Sørensen AJ, Pedersen E, Smogeli Ø. Simulation-based design and testing of dynamically positioned marine vessels. In: Proceedings of international conference on marine simulation and ship maneuverability (MARSIM'03), Kanazawa, 2003.
30. Strand JP. Nonlinear position control systems design for marine vessels. Ph.D. thesis, Dept. of Eng. Cybernetics, Norwegian University of Science and Technology, Trondheim, 1999.
31. Strand JP, Fossen TI. Nonlinear passive observer for ships with adaptive wave filtering. In: Nijmeijer H, Fossen TI, editors. New directions in nonlinear observer design. London: Springer; 1999. p. 113–34.
32. Torsetnes G, Jouffroy J, Fossen TI. Nonlinear dynamic positioning of ships with gain-scheduled wave filtering. In: Proceedings of the IEEE conference on decision and control (CDC'04), Paradise Iceland, 2004.
33. Triantafyllou MS. Cable mechanics for moored floating systems. In: Proceedings of 7th international conference on the behaviour of offshore structures at sea (BOSS'94), Cambridge, 1994. p. 57–77.

Chapter 18
Closed-Loop Identification and Control of Inland Vessels

A. Padilla, R. Bittner, and J.I. Yuz

Abstract Extensive research has been conducted on a navigation system for inland vessels at the University of Stuttgart and at the Max Planck Institute for Dynamics of Complex Technical Systems, Magdeburg (Focus Max Planck Gesellschaft, Computer at the helm, http://www.mpg.de/942027). As part of this navigation system, a model-based track-keeping controller has been developed. A high performance controller is required because of the reduced space available on rivers and canals. The control structure consists of two components, a feedback and a feedforward block, where the former is provided by a linear quadratic gaussian controller. Both components require the ship dynamics model and thus, the parameter estimation of the underlying model is a key issue to achieve high performance. In this chapter, we firstly consider Monte Carlo simulations to generate data of the closed-loop system and then the parameters of a continuous-time steering dynamics model are identified. The parameter estimation problem is solved applying an instrumental variable method, which takes into account the control structure. Parameter identification using real closed-loop experiments is also considered. Additionally, we evaluate the experiments for parameter estimation through a sensitivity analysis.

18.1 Introduction

In the 1970s at the University of Stuttgart started a project whose aim was to develop a navigation system for inland vessels. Afterwards, in the late 1990s, the Max Planck Institute for Dynamics of Complex Technical Systems in Magdeburg

A. Padilla (✉)
Universidad de La Frontera, Temuco, Chile
e-mail: arturo.padilla@ufrontera.cl

R. Bittner
Max Planck Institute for Dynamics of Complex Technical Systems, Magdeburg, Germany
e-mail: ralph.bittner@ieee.org

J.I. Yuz
Universidad Técnica Federico Santa María, Valparaiso, Chile
e-mail: juan.yuz@usm.cl

C. Ocampo-Martinez, R.R. Negenborn (eds.), *Transport of Water versus Transport over Water*, Operations Research/Computer Science Interfaces Series 58,
DOI 10.1007/978-3-319-16133-4_18

joined the project. During all these years, different track-keeping controllers for inland navigation have been proposed (see, for instance, [4, 6, 21, 22, 32]). In this study, we consider a model-based approach, which requires a ship dynamics model that is both accurate and simple. In particular, we are interested in a ship model of the steering dynamics, which depends on parameters related to hydrodynamic forces. Different methods are available to determine these parameters [11]. In this chapter, the parameters are identified from collected data as it was done in [2].

Experiments like zig-zag maneuvers [29], spiral maneuvers, and multi-frequency binary tests [8] can be used to identify the parameters of ship dynamics models. This kind of experiments are performed in open-loop, in contrast to closed-loop experiments that are done using a controller. In [35], closed-loop identification was performed using a pseudo random binary sequence (PRBS) as an excitation signal external to the control system. In this chapter, closed-loop experiments using the model-based track-keeping controller are considered. First we use a PRBS experiment in Monte Carlo simulations. Then, for real data we consider navigation where the desired track resembles a sine function.

Wind and stream are two important disturbance for inland navigation on a river. Of course, such disturbances make the parameter identification of ship models hard. Thus, data collected in experiments on a canal (without stream) is preferred but not always possible. Additionally, the reduced space available in waterways act as a constraint on the input signal of the ship dynamics, which is the rudder. That is, significant rudder excitation is important for the parameter estimation process, but it requires more navigation space.

The parameter estimation of ship models subject to wind and stream disturbances has been shown a challenging task. Using open-loop experiments, continuous-time (CT) identification methods have been successfully tested in [29] to cope with this issue. Nevertheless, some drawbacks of open-loop identification of inland vessels have been reported in [35], namely, the identification experiments can not be automated, and the rudder excitation might depend strongly on the skipper. We consider here closed-loop identification, whose main difficulty is due to the correlation between the disturbances and the control input signal induced by the feedback mechanism. Different parameter estimation approaches can be used to solve this problem [24]. In this chapter, we consider an instrumental variable scheme for closed-loop CT identification. Instrumental variable methods for closed-loop identification of discrete-time (DT) systems have been topic of research in the literature, both for linear time-invariant (LTI) [15–17, 19], and linear parameter varying (LPV) systems [31]. On the other hand, closed-loop continuous-time model identification has been treated in [13, 14, 18, 33]. The refined instrumental variable (RIV) method is one of the most well known approaches for CT identification and it has been shown that provides good results in simulation [34]. The closed-loop version for CT systems (CLRIVC) is presented in detail in [18] for single-input single-output systems. We here apply the CLRIVC for single-input multi-output systems. This approach is compared with a standard identification scheme based on optimization.

The aim in a parameter identification problem solved through an optimization-based approach is to minimize the objective function, which measures the accuracy of the estimated model to reproduce the data. Sometimes, such a parameter identification problem is not well defined, in the sense that different combinations of parameters lead to similar objective function values. Process noise, measurement noise, and/or structural model uncertainties might explain such phenomenon. In this study, this parameter accuracy problem is evaluated through a sensitivity analysis, as in [29].

The chapter is organised as follows: In Sect. 18.2, we present the steering dynamics model of a ship. Next, in Sect. 18.3, we describe the basics of the track-keeping controller that is used in the closed-loop identification. Section 18.4 presents the optimization-based identification approach and the CLRIVC, which are afterwards tested through Monte Carlo simulations. A sensitivity analysis and a parameter identification of a ship dynamics model using real data are considered in Sects. 18.5 and 18.6 respectively. Finally, conclusions are drawn in Sect. 18.8.

18.2 Ship Dynamics

In this section we present the ship dynamics model that has been developed for inland navigation. The motion of a ship has six degrees of freedom, namely three motions in the planes and three rotations. The motions in the planes are called surge, sway and heave and correspond to the longitudinal, sideways and vertical motions, respectively. The rotations are called yaw, roll and pitch, and are related to the vertical, longitudinal and transverse rotation axes, respectively. For the ships and navigation conditions considered in this study, the roll, pitch and heave are negligible [35] due to the lack of waves on inland waterways. Complex ship models with several parameters, like the Abkowitz model [12], can be used to thoroughly represent the ship dynamics. However, parameter identification from real data of such models have not delivered so far satisfactory results [35]. Therefore we use models with few parameters and accurate enough for control applications. They also consider explicitly the current, which is essential in inland navigation.

Figure 18.1 shows the variables related to the steering dynamics of a ship and how they are obtained: some of them are directly measured (d.m.), and the others are computed using measurements (c.u.m.) from algebraic relations.

The steering dynamics model is composed of the yaw and the drift dynamics. The former is defined through the so called Nomoto model [28] and the latter is derived in [7] (see more in [4, 29]). The steering dynamics is then defined by

$$\dot{r} = -\rho_1^N v_\mathrm{r} r + \rho_2^N v_\mathrm{r}^2 \delta, \tag{18.1}$$

$$\dot{\beta} = -\rho_3^N \frac{v_\mathrm{r}^2}{v_\mathrm{abs}}(\beta - \beta_\mathrm{w}) + \rho_4^N r + \rho_5^N \frac{v_\mathrm{r}^2}{v_\mathrm{abs}}\delta, \tag{18.2}$$

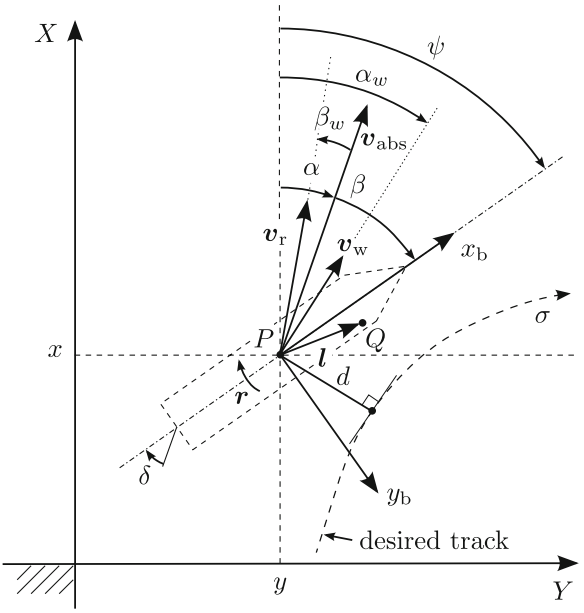

Variable	Physical quantity	How is obtained
$\boldsymbol{r}$	Turning or yaw rate	d.m. (output)
$\boldsymbol{v}_{\text{abs}}$	Absolute velocity	c.u.m. (scheduling variable)
$\boldsymbol{v}_{\text{w}}$	Velocity (over ground) of the water current	$v_{\text{w}} \approx$ constant
$\boldsymbol{v}_{\text{r}}$	Relative velocity	c.u.m.
α	Course angle	c.u.m.
α_{w}	Current direction	$\alpha_{\text{w}} \approx \alpha_{\text{GL}}$
β	Drift angle	c.u.m. (output)
β_{w}	Drift angle correction due to current	c.u.m.
ψ	Heading or yaw angle	d.m.
δ	Rudder angle	d.m. (input)
d	Distance to desired-track	c.u.m.
x	X-axis position coordinate	c.u.m.
y	Y-axis position coordinate	c.u.m.

Fig. 18.1 Variables of the system. d.m.: directly measured, c.u.m.: computed (from kinematic, trigonometric, and geometrical equations) using measurements

$$\beta_{\text{w}} = \frac{v_{\text{w}}}{v_{\text{r}}} \sin(\alpha - \alpha_{\text{w}}), \tag{18.3}$$

$$v_{\text{r}} \approx v_{\text{abs}} \pm v_{\text{w}}, \tag{18.4}$$

where δ is the input. r and β are the outputs of the model and they are related by the following kinematic expressions

$$\dot{\psi} = r, \tag{18.5}$$

$$\beta = \psi - \alpha. \tag{18.6}$$

Equation (18.4) is an approximation of the relative velocity v_{r}, where $+$ is for upstream navigation and $-$ is for downstream navigation. Assuming that the velocity of the river current v_{w} is a known constant depending on the river, the scheduling variable of the steering dynamics model (18.1)–(18.4) is then the absolute velocity v_{abs}.

Hereafter we consider that for the drift model, the contribution of the rudder force is negligible, as in [7], i.e., $\rho_5^N = 0$. Thus, the parameter vector to be estimated is

$$\boldsymbol{\rho}^N = \begin{bmatrix} , \boldsymbol{\rho}_r^N \\ \boldsymbol{\rho}_\beta^N , \end{bmatrix} \tag{18.7}$$

where

$$\boldsymbol{\rho}_r^N = \begin{bmatrix} \rho_1^N & \rho_2^N \end{bmatrix}^T, \tag{18.8}$$

$$\boldsymbol{\rho}_\beta^N = \begin{bmatrix} \rho_3^N & \rho_4^N \end{bmatrix}^T. \tag{18.9}$$

The superscript N is used to denote normalized parameters (i.e., parameters that do not depend on the velocities v_{r} and v_{abs}). Of course, when v_{r} and v_{abs} are constant, a linear time-invariant model is obtained:

$$\dot{r} = -\rho_1 r + \rho_2 \delta, \tag{18.10}$$

$$\dot{\beta} = -\rho_3(\beta - \beta_{\mathrm{w}}) + \rho_4 r. \tag{18.11}$$

All the components of the parameter vector $\boldsymbol{\rho}^N$ are (physically) constrained to be positive. Moreover, the parameter ρ_4^N is defined [7] as

$$\rho_4^N = \frac{m - C_{ml}}{m - C_{mq}} \tag{18.12}$$

where C_{ml} and C_{mq} are added mass terms, and m is the ship total mass. From strip theory, according to [11], the added masses can be roughly approximated by:

$$-1.00m \leq C_{mq} \leq -0.70\,\mathrm{m}, \tag{18.13}$$

$$-0.10m \leq C_{ml} \leq -0.05\,\mathrm{m}, \tag{18.14}$$

and therefore

$$0.52 \leq \rho_4^N \leq 0.65. \tag{18.15}$$

In Fig. 18.1, some of the system variables are directly measured (d.m.) and others are computed from kinematic and trigonometric equations using measurements (c.u.m.). For the yaw dynamics, r and δ are d.m., and v_{abs} is c.u.m. as follows: the absolute speed at point Q, $\boldsymbol{v}_{\text{abs}_Q}$, (see Fig. 18.1) is defined by two measurements, its magnitude and course angle at point Q. From kinematic, we obtain the absolute velocity $\boldsymbol{v}_{\text{abs}}$ at the center of gravity of the ship, P, as follows:

$$\boldsymbol{v}_{\text{abs}_Q} = \boldsymbol{v}_{\text{abs}} + \boldsymbol{r} \times \boldsymbol{l}, \tag{18.16}$$

where $\boldsymbol{r}$ is the yaw rate vector and $\boldsymbol{l}$ is the vector that defines the position of point Q with respect to the center of gravity P.

Regarding the measurements of the drift dynamics, it can be noticed that the course angle α is directly obtained from $\boldsymbol{v}_{\text{abs}}$, which is computed using (18.16). To compute β, we consider a body-fixed reference frame $x_{\text{b}} y_{\text{b}} z_{\text{b}}$ (see Fig. 18.1), which is fixed to the vessel. Then β is computed using the components of $\boldsymbol{v}_{\text{abs}}$ in the axes x_{b} and y_{b}. On the other hand, the course of the water α_{w} can be approximated by the tangential direction of the guiding line α_{GL} (see more in [22]), i.e.,

$$\alpha_{\text{w}} \approx \alpha_{\text{GL}}. \tag{18.17}$$

In electronic charts for navigation systems, the guiding line is an a-priori given reference line, which is nearly parallel to the course of the river. This guiding line is used for automatic track-keeping. Thus, from (18.3), (18.4), and (18.17), we obtain an approximation of β_{w}.

18.3 Track-Keeping Controller for Inland Vessels

The evolution of the track-keeping controller, which is shown in Fig. 18.2, is presented in detail in [4–6, 9, 21, 22, 26, 32]. In this chapter, we limit ourselves to give the basics for the purpose of this study.

The track-keeping system in Fig. 18.2 consists of a feedforward and a feedback controller. The latter corresponds to a linear quadratic Gaussian controller [1], that is, it consists of a linear quadratic regulator (LQR) and a Kalman filter as an observer.

The aim of the controller is to minimize d (see Fig. 18.1), which is the distance between the control reference point (for instance, the center of gravity P of the ship) and the desired track. The abovementioned guiding line is defined through a certain course angle α_{GL}, curvature κ_{GL} and derivative of the curvature κ'_{GL} with respect to the arc length σ. The desired track is based on this guiding line. Sometimes the ship

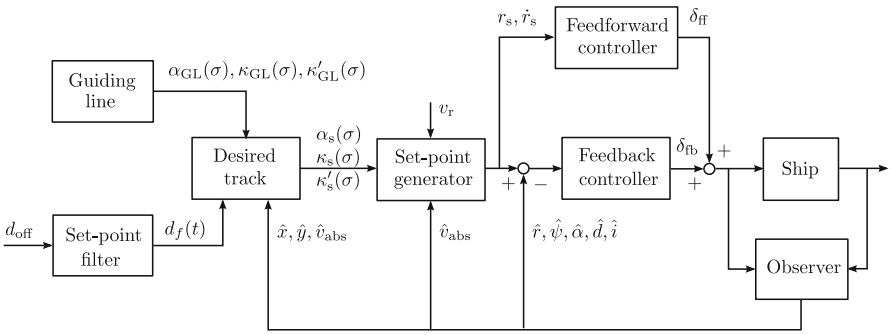

Fig. 18.2 Track-keeping controller

must move away from the guiding line, for instance, in order to overtake another vessel. Then, the skipper sets with a joystick an offset to the guiding line, giving rise to a shifted navigation reference line, which is parallel at an arbitrarily distance d_{off} to the guiding line. To achieve a smooth transition from the guiding line to the new reference line, a set-point filter is used to generate d_f. The information of the guiding line and the set-point filter is then combined in the *desired track* block. Then, given the desired course angle α_s, desired curvature κ_s, and desired curvature derivative κ'_s in σ, the set-point generator, based on the inverse drift dynamics model, computes the desired state variables $\boldsymbol{x}_s$ in time domain [4, 6, 22],

$$\boldsymbol{x}_s = \left[r_s \ \psi_s \ \alpha_s \ d_s \ i_s \right]^T, \tag{18.18}$$

where i_s is given by

$$i_s = \int_{t_0}^{t} d_s \, \mathrm{d}\tau. \tag{18.19}$$

As the aim is to keep the control reference point on the desired track, then $d_s = i_s = 0$. Additionally, the set-point generator delivers the inputs of the *feedforward* block, i.e., the desired yaw rate r_s and desired yaw acceleration $\dot{r}_s$.

The control input is the rudder angle $\delta = \delta_{ff} + \delta_{fb}$, where δ_{ff} is provided by the feedforward and δ_{fb} by the feedback controller. The former can be considered since the navigation path is a-priori known and it is implemented through the inversion of the Nomoto model [6]. To compensate model errors and disturbances an LQR is used as a feedback. The feedback component of the rudder angle is defined by:

$$\delta_{fb} = -\boldsymbol{K}(\boldsymbol{x}_s - \hat{\boldsymbol{x}}), \tag{18.20}$$

where $\boldsymbol{x}_s$ is given in (18.18), $\boldsymbol{K}$ is a gain vector,

$$\boldsymbol{K} = \left[k_r \ k_\psi \ k_\alpha \ k_d \ k_i \right], \tag{18.21}$$

and $\hat{\boldsymbol{x}}$ is the estimated state vector,

$$\hat{\boldsymbol{x}} = \left[\hat{r} \ \hat{\psi} \ \hat{\alpha} \ \hat{d} \ \hat{i} \right]^T. \tag{18.22}$$

The distance d is defined by [32]

$$d(\sigma_P) = \frac{1}{\sqrt{x_s'(\sigma_P)^2 + y_s'(\sigma_P)^2}} (-y_s'(\sigma_P)(x - x_s(\sigma_P)) + x_s'(\sigma_P)(y - y_s(\sigma_P))), \tag{18.23}$$

where x and y are the location coordinates of the ship, and x_s and y_s the desired location coordinates. σ_P is the value of σ that gives the minimum distance d and it is defined implicitly by the orthogonality condition

$$0 = x_s'(\sigma_P)(x - x_s(\sigma_P)) + y_s'(\sigma_P)(y - y_s(\sigma_P)). \tag{18.24}$$

For the design of the controller gain $\boldsymbol{K}$, we have to build a linear time-invariant model of the control error dynamics $\boldsymbol{x}_s - \hat{\boldsymbol{x}}$. Basically, considering (18.1)–(18.3), (18.5), (18.6), (18.23), and a linearization process, we arrive at the following state-space representation to design the LQR (see [4, 9]),

$$\frac{\mathrm{d}}{\mathrm{d}t} \begin{pmatrix} r_s - \hat{r} \\ \psi_s - \hat{\psi} \\ \alpha_s - \hat{\alpha} \\ \hat{d} \\ \hat{i} \end{pmatrix} = \begin{pmatrix} -\rho_1 & 0 & 0 & 0 & 0 \\ 1 & 0 & 0 & 0 & 0 \\ 1 - \rho_4 & \rho_3 & -\rho_3(1 + v_w/v_r) & 0 & 0 \\ 0 & 0 & -v_{abs} & 0 & 0 \\ 0 & 0 & 0 & 1 & 0 \end{pmatrix} \begin{pmatrix} r_s - \hat{r} \\ \psi_s - \hat{\psi} \\ \alpha_s - \hat{\alpha} \\ \hat{d} \\ \hat{i} \end{pmatrix} + \begin{pmatrix} \rho_2 \\ 0 \\ 0 \\ 0 \\ 0 \end{pmatrix} \delta_{fb}, \tag{18.25}$$

where the state $\hat{i}$ is used to define an integral component of the control input that guarantee us zero offset in case of disturbances. Notice that we are interested in estimating ρ_1, ρ_2, ρ_3 and ρ_4 in model (18.25) from data, as shown in the next section. The velocities v_{abs} and v_r are computed using measurements (c.u.m.), and v_w is assumed to be a known constant.

18.4 Continuous-Time Identification Methods

In this section we present two approaches for estimating the parameters of the ship dynamics model given by (18.1)–(18.4): identification as an optimization problem and the refined instrumental variable method for closed-loop systems.

Since the yaw model and drift model are independently parametrized, we can estimate the parameters of them independently (see more in [29]). Next we define the identification of the drift model. The identification of the yaw model is treated analogously.

18.4.1 Identification as an Optimization Problem

The drift angle observations β_t can be written as

$$\beta_t = \hat{\beta}_t + e_t, \tag{18.26}$$

where the subscript $_t$ is the time from 1 to n. Under the assumption that the error e_t between output observations β_t and simulated model output $\hat{\beta}_t$ is independent and has a Gaussian or normal distribution, the parameter identification might be defined as

$$\boldsymbol{\rho}_\beta^N = \arg \min_{\boldsymbol{\rho}_\beta^N \in \mathrm{R}} \; V_\beta, \tag{18.27}$$

where $\boldsymbol{\rho}_\beta^N$ is the parameter vector defined in (18.9) and the cost function is

$$V_\beta = \sum_{t=1}^{n} (\beta_t - \hat{\beta}_t(\boldsymbol{\rho}_\beta^N))^2. \tag{18.28}$$

The minimization of (18.28) is performed applying a numerical search algorithm. We use the MATLAB function fmincon, which offers the possibility to work with different algorithms. In this study, we use the interior-point algorithm (see more in [29]). In the following, we will refer to the optimization-based identification approach as OPT.

18.4.2 Instrumental Variable Method

The closed-loop refined instrumental variable method for continuous-time systems CLRIVC is presented in detail in [18]. In that study, LTI single-input single-output models are considered. In this study we treat LTI models with a single input and multiple outputs.

The feedforward block of the track-keeping controller, presented in Sect. 18.3, generates the signal δ_{ff}, which is correlated to the disturbances. In order to meet ideal conditions to apply this instrumental variable approach, we simplify the track-keeping controller by not considering the feedforward part. Moreover, we do not consider the observer, that is, we assume that the state variables are directly available from measurements. Figure 18.3 shows the assumed closed-loop configuration, which is relevant for the following explanations.

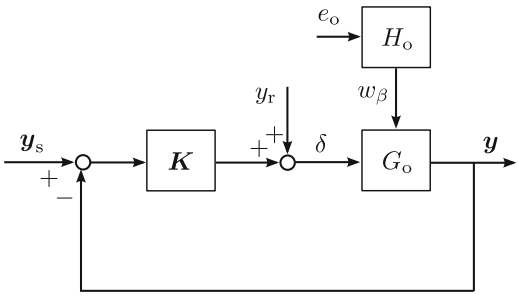

Fig. 18.3 Closed-loop system with a linear quadratic regulator

The data generating system is defined as

$$\dot{r} = -\rho_1^o r + \rho_2^o \delta, \tag{18.29}$$

$$\dot{\psi} = r, \tag{18.30}$$

$$\dot{\beta} = -\rho_3^o(\beta - \beta_w) + \rho_4^o r + w_\beta, \tag{18.31}$$

$$\dot{x} = v_{abs} \cos\alpha, \tag{18.32}$$

$$\dot{y} = v_{abs} \sin\alpha, \tag{18.33}$$

$$\beta_w = \frac{v_w}{v_r} \sin(\alpha - \alpha_w), \tag{18.34}$$

$$v_r \approx v_{abs} \pm v_w, \tag{18.35}$$

$$\alpha = \psi - \beta, \tag{18.36}$$

$$0 = x_s'(\sigma_P)(x - x_s(\sigma_P)) + y_s'(\sigma_P)(y - y_s(\sigma_P)), \tag{18.37}$$

$$d(\sigma_P) = \frac{1}{\sqrt{x_s'(\sigma_P)^2 + y_s'(\sigma_P)^2}}(-y_s'(\sigma_P)(x - x_s(\sigma_P)) + x_s'(\sigma_P)(y - y_s(\sigma_P))), \tag{18.38}$$

$$i = \int_{t_0}^{t} d \, \mathrm{d}\tau, \tag{18.39}$$

where the input is the rudder angle δ and the output is

$$\boldsymbol{y} = \begin{bmatrix} r & \psi & \alpha & d & i \end{bmatrix}^T. \tag{18.40}$$

Equations (18.29)–(18.36) correspond to the ship dynamics model presented in Sect. 18.2 and (18.37)–(18.39) are related to the control task defined in Sect. 18.3. Notice that in the representation (18.29)–(18.39) we consider that the speeds v_{abs}, v_w and thus v_r are constant. The variables $\boldsymbol{y}_s$ and y_r are external signals that are assumed to be uncorrelated with e_o. The external signal $\boldsymbol{y}_s$ corresponds to the desired output, which is equal to the desired state variables $\boldsymbol{x}_s$ defined in (18.18), i.e.,

$$\boldsymbol{y}_s = \boldsymbol{x}_s = \begin{bmatrix} r_s & \psi_s & \alpha_s & 0 & 0 \end{bmatrix}^T. \tag{18.41}$$

The signal w_β is a colored noise and it is generated using the linear filter H_o in Fig. 18.3. This term w_β is included to represent the effect of the wind, which may be modeled as an additive term in the differential equations that describes the ship dynamics [4, 9, 12]. Additionally, w_β could represent problems in the approximation of α_w (see (18.17)), that corresponds to the current direction.

The model of the system given in (18.29)–(18.39) is defined as follows:

$$\dot{r} = -\rho_1 r + \rho_2 \delta, \tag{18.42}$$

$$\dot{\psi} = r, \tag{18.43}$$

$$\dot{\beta} = -\rho_3(\beta - \beta_w) + \rho_4 r, \tag{18.44}$$

$$\dot{x} = v_{abs} \cos\alpha, \tag{18.45}$$

$$\dot{y} = v_{abs} \sin\alpha, \tag{18.46}$$

$$\beta_w = \frac{v_w}{v_r} \sin(\alpha - \alpha_w), \tag{18.47}$$

$$v_r \approx v_{abs} \pm v_w \tag{18.48}$$

$$\alpha = \psi - \beta, \tag{18.49}$$

$$0 = x_s'(\sigma_P)(x - x_s(\sigma_P)) + y_s'(\sigma_P)(y - y_s(\sigma_P)), \tag{18.50}$$

$$d(\sigma_P) = \frac{1}{\sqrt{x_s'(\sigma_P)^2 + y_s'(\sigma_P)^2}} (-y_s'(\sigma_P)(x - x_s(\sigma_P)) + x_s'(\sigma_P)(y - y_s(\sigma_P))), \tag{18.51}$$

$$i = \int_{t_0}^{t} d \, \mathrm{d}\tau. \tag{18.52}$$

Our aim here is to estimate the parameters of the drift dynamics model (18.44) that we extend by considering a discrete-time noise model, that is,

$$\beta(t_k) = \sum_{i=1}^{2} G_i(p, \boldsymbol{\rho}_\beta) u_i(t_k) + H(q, \boldsymbol{\eta}_\beta) e(t_k), \tag{18.53}$$

where p is the time-derivative operator ($p = d/dt$), and

$$G_i(p, \boldsymbol{\rho}_\beta) = \frac{B_i(\boldsymbol{\rho}_\beta)}{F(p, \boldsymbol{\rho}_\beta)}, \tag{18.54}$$

with

$$F = p + \rho_3, \tag{18.55}$$

$$B_1 = \rho_3 \qquad B_2 = \rho_4, \tag{18.56}$$

where u_1 and u_2 are β_w and r, respectively.

The noise model $H(q, \boldsymbol{\eta}_\beta)$ is a discrete-time autoregressive moving-average (ARMA) model

$$H(q, \boldsymbol{\eta}_\beta) = \frac{1 + c_1 q^{-1} + \cdots + c_{n_c} q^{-n_c}}{1 + d_1 q^{-1} + \cdots + d_{n_d} q^{-n_d}}, \tag{18.57}$$

where q is the shift operator. Thus, we have a Box-Jenkins hybrid model, which is composed of a CT process model and a DT noise model. Notice that the noise model does not match the true noise source.

The parameter vector of the process model is

$$\boldsymbol{\rho}_\beta = \begin{bmatrix} \rho_3 & \rho_4 \end{bmatrix}^T, \tag{18.58}$$

and the parameter vector of the noise model is

$$\boldsymbol{\eta}_\beta = \begin{bmatrix} d_1 & \ldots & d_{n_d} & c_1 & \ldots & c_{n_c} \end{bmatrix}^T. \tag{18.59}$$

Therefore the parameter vector of the hybrid model (18.53) is

$$\boldsymbol{\theta}_\beta = \begin{bmatrix} \boldsymbol{\rho}_\beta \\ \boldsymbol{\eta}_\beta \end{bmatrix}. \tag{18.60}$$

The regulator in Fig. 18.3 consists of a gain vector K (see (18.21)). Hence, the controller feedback output δ_{fb} is given by

$$\delta_{\text{fb}} = \boldsymbol{K}(\boldsymbol{y}_{\text{s}} - \boldsymbol{y}). \tag{18.61}$$

To build the instrumental variables we have to generate a noise-free output $\mathring{\boldsymbol{y}}$ and a noise-free input $\mathring{\delta}$. The former is computed from (18.42)–(18.52), and the latter from

$$\mathring{\delta} = \boldsymbol{K}(\boldsymbol{y}_{\text{s}} - \mathring{\boldsymbol{y}}) + y_{\text{r}}. \tag{18.62}$$

Equation (18.53) can be written as a linear regression in time instance $t = t_k$, i.e.,

$$\beta^{(1)}(t_k) = \boldsymbol{\varphi}^T(t_k)\boldsymbol{\rho}_\beta + \tilde{v}(t_k), \tag{18.63}$$

where the superscript$^{(1)}$ represents the first time-derivative, $\boldsymbol{\rho}_\beta$ is the parameter vector, and

$$\boldsymbol{\varphi}^T(t_k) = \begin{bmatrix} -(\beta(t_k) - \beta_{\text{w}}(t_k)) & r(t_k) \end{bmatrix}. \tag{18.64}$$

$$\tilde{v}(t_k) = F(p, \boldsymbol{\rho}_\beta) H(q, \boldsymbol{\eta}_\beta) e(t_k). \tag{18.65}$$

From the formulation of the one-step-ahead prediction error, filtered variables are defined. These filtered variables, denoted by the subscript $_{\mathrm{f}}$, are used later in the parameter identification process. For instance, the filtered output is obtained by

$$\beta_{\mathrm{f}}(t_k) = Q_{\mathrm{d}}(q, \boldsymbol{\eta}_\beta)[(Q_{\mathrm{c}}(p, \boldsymbol{\rho}_\beta)\beta)(t_k)], \tag{18.66}$$

where $Q_{\mathrm{c}}(p, \boldsymbol{\rho}_\beta)$ and $Q_{\mathrm{d}}(q, \boldsymbol{\eta}_\beta)$ correspond to the CT and DT filters, respectively:

$$Q_{\mathrm{c}}(p, \boldsymbol{\rho}_\beta) = \frac{1}{F(p, \boldsymbol{\rho}_\beta)} \qquad Q_{\mathrm{d}}(q, \boldsymbol{\eta}_\beta) = \frac{D(q, \boldsymbol{\eta}_\beta)}{C(q, \boldsymbol{\eta}_\beta)}. \tag{18.67}$$

Details on how to compute these filters can be found in [34]. Then, analogously to (18.63), we can write the filtered output as

$$\beta_{\mathrm{f}}^{(1)}(t_k) = \boldsymbol{\varphi}_{\mathrm{f}}^T(t_k)\boldsymbol{\rho}_\beta + \tilde{v}_{\mathrm{f}}(t_k), \tag{18.68}$$

where

$$\boldsymbol{\varphi}_{\mathrm{f}}(t_k) = \left[-(\beta_{\mathrm{f}} - \beta_{\mathrm{w,f}})\ r_{\mathrm{f}}\right]^T, \tag{18.69}$$

$$\tilde{v}_{\mathrm{f}}(t_k) = Q_{\mathrm{d}}(q, \boldsymbol{\eta}_\beta)Q_{\mathrm{c}}(p, \boldsymbol{\rho}_\beta)v(t_k) = e(t_k). \tag{18.70}$$

The CLRIVC method is an iterative scheme thoroughly presented in [18]. It can be initialized with the closed-loop simplified RIVC method presented in [18]. In this study, we apply the algorithm changing only the initialization step, which is defined as follows:

- Estimate the parameter vectors $\boldsymbol{\rho}_r$ and $\boldsymbol{\rho}_\beta$ to define the controller gain vector $\boldsymbol{K}$ using (18.25). The parameter vectors are independently obtained by the least-squares method from continuous-time ARX models. These ARX models are built using the generalized Poisson moment functional (GPMF) approach (see [3] for a discussion about the design parameters of this approach).
- Use the *Two-Step* algorithm of [18] using the GPMF approach to get a second estimate of $\boldsymbol{\rho}_\beta$.

18.4.3 Monte Carlo Simulations

In order to evaluate the CLRIVC method presented in Sect. 18.4.2, 100 Monte Carlo simulations are performed to generate data, that corresponds to the steering dynamics of a ship guided by a track-keeping controller. The parameters are identified and then the performance is measured using the fit proposed in [25]. For the drift model, the fit is given by

$$\text{fit} = 1 - \frac{\text{norm}(\mathring{\beta}(t) - \beta(t))}{\text{norm}(\beta(t) - \text{mean}[\beta(t)])}, \tag{18.71}$$

where β is the noise-free drift and $\mathring{\beta}$ is the noise-free simulated output. Notice that since we are dealing with a Monte Carlo simulation, the noise-free drift is available to compute the fit (18.71).

The artificial measurements correspond to a closed-loop experiment, where, using the feedback mechanism in Fig. 18.3, we consider y_r as a Pseudo-Random Binary Sequence (PRBS) as shown in Fig. 18.4a. It is assumed that the desired track is the X-axis (see Fig. 18.1). Thus, the distance d is equal to the y-coordinate [32], i.e.,

$$\dot{d} = \dot{y} = v_\text{abs} \sin\alpha. \tag{18.72}$$

Since the desired track is the X-axis, the desired output (18.41) is equal to the null vector at any time instance.

The ship navigates downstream in a straight river, i.e., $\alpha_\text{w} = 0$. The artificial measurements are generated using (18.29)–(18.40). The drift model (18.31) with the disturbance term w_β leads to a CT ARARMAX model. As it was mentioned in Sect. 18.4.2, the term w_β could represent the effect of the wind or other disturbances. This makes the parameter identification of the drift model harder than the one of the yaw model, as it is usually the case in practice. Thus, from these Monte Carlo simulations we only identify the parameters of the drift model ρ_3^N, and ρ_4^N. We modeled w_β as a colored noise process of the following form

$$w_\beta(s) = \frac{1.0 \cdot 10^{-3}}{s + 1.0 \cdot 10^{-3}} w(s), \tag{18.73}$$

where $w(s)$ is a zero-mean white noise signal with a constant spectral density equal to 0.15.

The noise-free data is shown in Fig. 18.4b–d. We additionally show the influence of w_β for the case where the worst fit was obtained using OPT. The ship absolute speed v_abs is 3.0 m/s and the stream speed v_w is 1 m/s. Each data batch has a length of 6 min and is generated using a sampling time of 0.3 s. The true parameter vector is:

$$\boldsymbol{\rho}^{\text{o},N} = \begin{bmatrix} 1/12 \\ 7.7 \cdot 10^{-3} \\ 1/13 \\ 0.6 \end{bmatrix}. \tag{18.74}$$

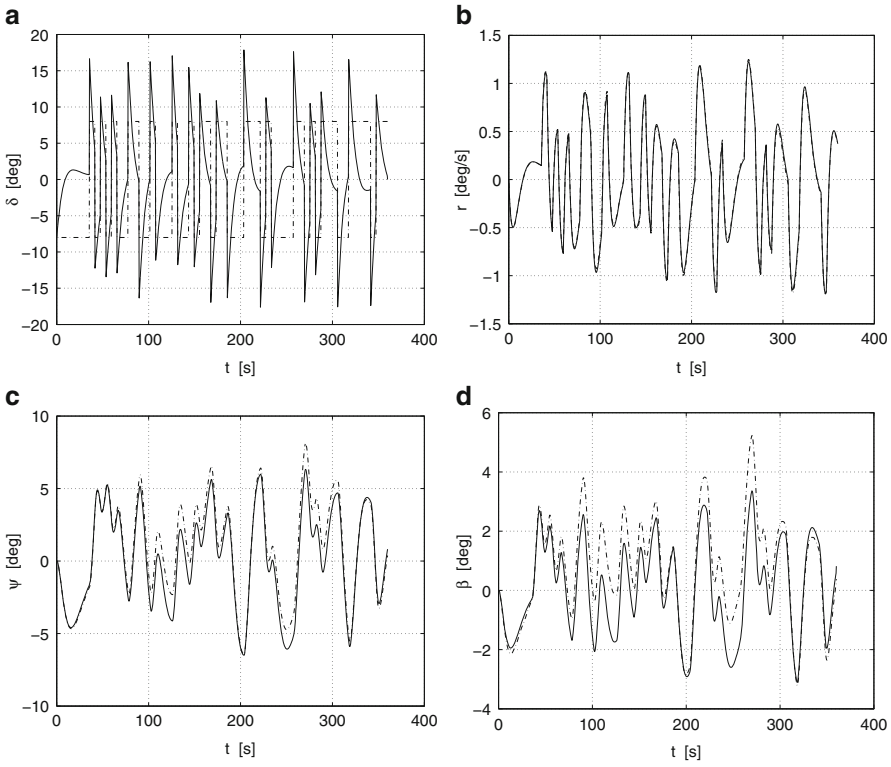

Fig. 18.4 For (**a**), *dash-dotted line*: y_r , *continuous line*: δ. For (**b**)–(**d**), *continuous line*: noise-free data, *dash-dotted line*: disturbed data

Given the speeds v_{abs}, v_{w}, and from (18.25) and (18.74), we define the gain vector

$$\boldsymbol{K}^T = \begin{bmatrix} 5.832 \\ 1.287 \\ 5.223 \cdot 10^{-1} \\ 2.942 \cdot 10^{-2} \\ 2.236 \cdot 10^{-4} \end{bmatrix}. \tag{18.75}$$

The CLRIVC method is initialized using the GPMF. To reduce the number of the design parameters we consider a normalized GPMF with certain Poisson filter order l and Poisson filter cut-off frequency λ (details about the design parameters of the GPMF are given in [3]). The parameter l must be equal or greater than the differential equation order and λ is chosen depending on the system bandwidth and the expected behavior of the filter. Since we are dealing with a slow disturbance, we consider λ greater than the approximate system bandwidth, leading to a filter with a dominant derivative behavior [3]. For $l = 3$ and $\lambda = 0.4$ we obtain good estimates. Additionally, for the noise model, the chosen design parameters are $n_c = 1$ and $n_d = 1$.

Table 18.1 Results of the parameter identification

	Mean		Std. deviation	
Method	ρ_3^N [1/m]	ρ_4^N [1]	ρ_3^N [1/m]	ρ_4^N [1]
OPT	1/15.6	0.58	$1.13 \cdot 10^{-2}$	$1.78 \cdot 10^{-2}$
CLRIVC	1/15.3	0.59	$3.48 \cdot 10^{-3}$	$5.09 \cdot 10^{-3}$

Table 18.2 Fits of the parameter identification

	Fit		
Method	Median (%)	Mean (%)	Std. deviation (%)
OPT	95.5	94.7	3.73
CLRIVC	95.7	95.7	1.34

The mean values and the standard deviations of the parameters are shown in Table 18.1 and the fit in Table 18.2. It is important to mention that in some of the simulations OPT fails to give reasonable parameter estimates, which means an unsuitable fit. To take this issue into account, in OPT, the parameter estimates were constrained to (1.0 ± 0.80) times their true value. If the resulting estimate reaches one of these boundaries, we consider the optimization process to have failed, which means that the parameter estimation method is not able to deal with the disturbance level. Even though boundaries are not used for the CLRIVC approach, we also consider the method to fail if the estimates exceed the boundaries. The computations in Tables 18.1 and 18.2 do not take into account failed results. OPT fails 24 times (out of 100), and CLRIVC does not fail. We see that the best results are obtained with the CLRIVC method, although the noise model used in the identification does not match the true noise source.

18.5 Sensitivity Analysis

In this section we present an approach to evaluate the accuracy of the estimates of the model parameters. Different parameter combinations may lead to similar values of the objective function due to the model structure and/or inadequate experiment conditions. The sensitivity analysis offers a way to quantify such a problem. We explain here the main concept of the sensitivity analysis (see [29, 30] for details).

Let us consider a first order differential equation

$$\dot{x} = f(x, \boldsymbol{u}, \boldsymbol{\theta}), \tag{18.76}$$

with the inputs $\boldsymbol{u}$ and a p-dimensional parameter vector $\boldsymbol{\theta}$. To identify the parameters we define the objective function

$$V = \sum_{i=1}^{N} (x_i - \hat{x}_i(\boldsymbol{\theta}))^2, \tag{18.77}$$

where x_i is the measurement and $\hat{x}_i$ is the simulation for a given set of parameters $\boldsymbol{\theta}$. The optimization problem is then defined by

$$\boldsymbol{\theta}_{\text{opt}} = \arg\min_{\boldsymbol{\theta} \in \Re} V, \tag{18.78}$$

where $\boldsymbol{\theta}_{\text{opt}}$ is the optimal or estimated parameter vector. Our goal is to evaluate the accuracy of the estimated parameters applying a sensitivity analysis to the cost functional V with respect to the parameters.

Let us define a certain parameter vector variation as $\boldsymbol{\Delta\theta} = \boldsymbol{\theta} - \boldsymbol{\theta}_{\text{opt}}$. The sensitivity of the objective function to $\boldsymbol{\Delta\theta}$ can be measured through

$$R_V = \frac{V(\boldsymbol{\theta}) - V(\boldsymbol{\theta}_{\text{opt}})}{V(\boldsymbol{\theta}_{\text{opt}})}. \tag{18.79}$$

We are interested in the minimum of R_V for the parameter vector variation $\boldsymbol{\Delta\theta} = \boldsymbol{\theta} - \boldsymbol{\theta}_{\text{opt}}$. The sensitivity of the objective function is then defined through the following indicator:

$$\hat{R}_V = R_V(\boldsymbol{\nu}_{\text{opt}}), \tag{18.80}$$

where $\boldsymbol{\nu}_{\text{opt}}$ is the unitary vector which minimizes R_V, i.e.,

$$\boldsymbol{\nu}_{\text{opt}} = \arg\min_{\|\boldsymbol{\nu}\|=1} R_V. \tag{18.81}$$

A value of $\hat{R}_V$ close to zero means that there are directions where the value of the cost function only slightly changes. As a consequence, a numerical algorithm may fail to find a unique minimum. Therefore, $\hat{R}_V$ should be large in order to ensure accurate parameter estimates when minimizing the cost function.

To circumvent the minimization problem (18.81) we consider an approximation for $\hat{R}_V$ as in [29]. In Sect. 18.6, we only show approximate values of $\hat{R}_V$, which are compared with the exact solutions. Comparisons are not presented, but the approximations are in close agreement with the exact solutions.

18.6 Identification Using Real Data

In this section, the identification approach OPT described in Sect. 18.4.1 is tested with real data from an experiment in closed-loop using the track-keeping controller presented in Sect. 18.3. The CLRIVC method is not applied to real data, as explained next in Sect. 18.6.1. Instead we use the simplified refined instrumental variable method for CT-LPV systems (LPV-SRIVC), which is for open-loop configurations and it has been successfully tested in [29]. To apply the LPV-SRIVC it is necessary

that the system input is uncorrelated with the disturbances. Although this requirement is not fulfilled in this case, the low disturbance level of the considered real data, makes it possible to obtain good estimates.

18.6.1 Parameter Identification Considering CLRIVC

In this section, we briefly discuss the problems that arise when applying the CLRIVC to real data.

As mentioned in Sect. 18.4.2, to build the instrumental variables, we have to make use of (18.42)–(18.52). However, using these equations it is not possible to obtain a good estimate of the distance d and the heading ψ. Modeling errors in the yaw dynamics and/or rudder offsets might explain the prediction errors in d and ψ [35].

Additionally, to build the instrumental variables, we need a model of the absolute speed v_{abs} which is not available in the current setting.

It is important to recall, that to apply the CLRIVC approach, the external signals $\boldsymbol{y}_{\text{s}}$ and y_{r} must be uncorrelated with e_{o} (see Fig. 18.3). For a normal navigation in closed-loop using the track-keeping controller, it can be assumed that δ_{ff} corresponds to y_{r}. Unfortunately, under normal navigation in closed-loop, both δ_{ff} and $\boldsymbol{x}_{\text{s}}$ are in fact correlated with e_{o}. Nevertheless, the authors believe that in general this correlation might be mild. Thus, strictly speaking, the experiments in Sect. 18.6.2 are not suitable for this method. Suitable but not available data, would be the PRBS experiment in a real ship considered in [35].

18.6.2 Parameter Identification Considering OPT and LPV-SRIVC

The collected data is from a research ship called Falke, that has a length of 16 m. Both estimation and validation data corresponds to special maneuvers, where the desired tracks resemble sine functions. The navigation are performed on a canal, i.e., the current speed is 0. The length of the estimation and validation data are 14:16 min and 5:34 min, respectively. In this case, since the estimated parameters are computed to be directly inserted in the controller settings, the output signal of the controller δ_{c}, instead of the rudder angle measurement δ, is used for the identification. In this way, we consider the actuator dynamics, which is not negligible for small ships like the Falke. Part of the estimation data is shown in Fig. 18.5.

The LPV-SRIVC is initialized with the GPMF, whose chosen design parameters are $l = 3$ and $\lambda = 0.4$. In Table 18.3, we show the results of the parameter identification, where the first and second rows correspond to the estimated parameters using OPT and LPV-SRIVC, respectively. The third row corresponds to the parameters

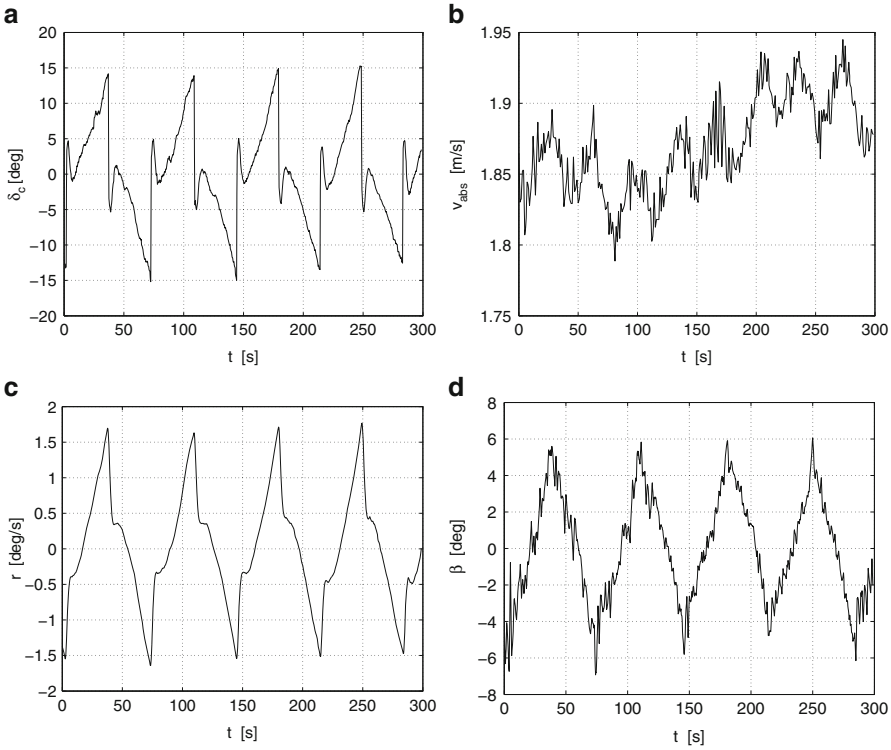

Fig. 18.5 Estimation data

Table 18.3 Results of the parameter identification

Case	ρ_1^N [1/m]	ρ_2^N [1/m^2]	ρ_3^N [1/m]	ρ_4^N [1]
OPT	1/12.0	$6.75 \cdot 10^{-3}$	1/9.8	0.77
LPV-SRIVC	1/12.9	$6.44 \cdot 10^{-3}$	1/10.2	0.76
Controller	1/12.5	$7.70 \cdot 10^{-3}$	1/12.7	0.60

that were already in use in the model-based track-keeping controller. The parameters of the controller have been successfully tested before under different navigation conditions and therefore, they can be taken as a benchmark. The differences in the estimates of the drift model in comparison to the controller parameters, might be explained by a GPS delay.

The values of the root mean square error (RMSE) of the cross-validation are presented in Table 18.4. Figure 18.6 shows a comparison of the real data and the simulations with the parameters obtained from OPT, and the parameters of the controller. The low disturbance level explains the good results that are obtained.

The values of $\hat{R}_V$ from the sensitivity analysis are 33.0 % and 6.4 % for the yaw and drift model, respectively. These results mean that the yaw model is easier to

Table 18.4 Cross-validation

	RMSE	
Case	Yaw (deg/s)	Drift (deg)
OPT	$1.31 \cdot 10^{-1}$	1.00
LPV-SRIVC	$1.29 \cdot 10^{-1}$	1.07
Controller	$1.04 \cdot 10^{-1}$	1.26

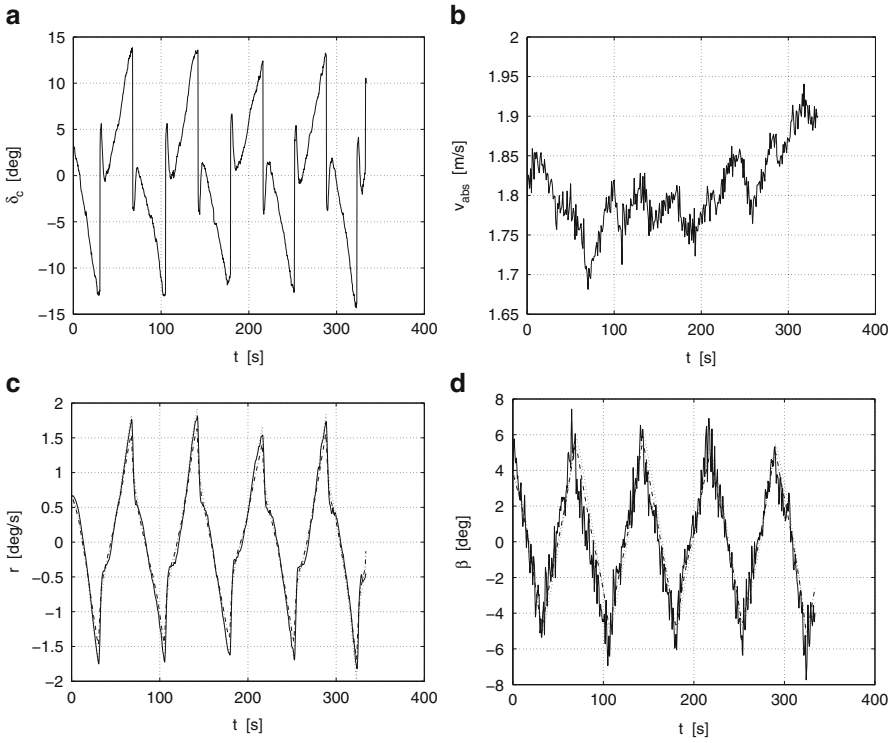

Fig. 18.6 Cross-validation. Comparison between measurements (*continuous line*), simulations with the results of method OPT (*dash-dotted line*) and simulations with the parameters of the controller (*dotted line*)

identify than the drift model, as is usually the case. On the other hand, high values of $\hat{R}_V$ are obtained for both the yaw and drift model, which indicates a low disturbance level in the estimation data.

Finally, we illustrate the performance of the controller in Fig. 18.7. The navigation corresponds to the evaluation data shown in Fig. 18.6. The good match between the rudder angle measurement δ and the rudder feedforward δ_{ff} in Fig. 18.7c shows the good quality of the estimated model.

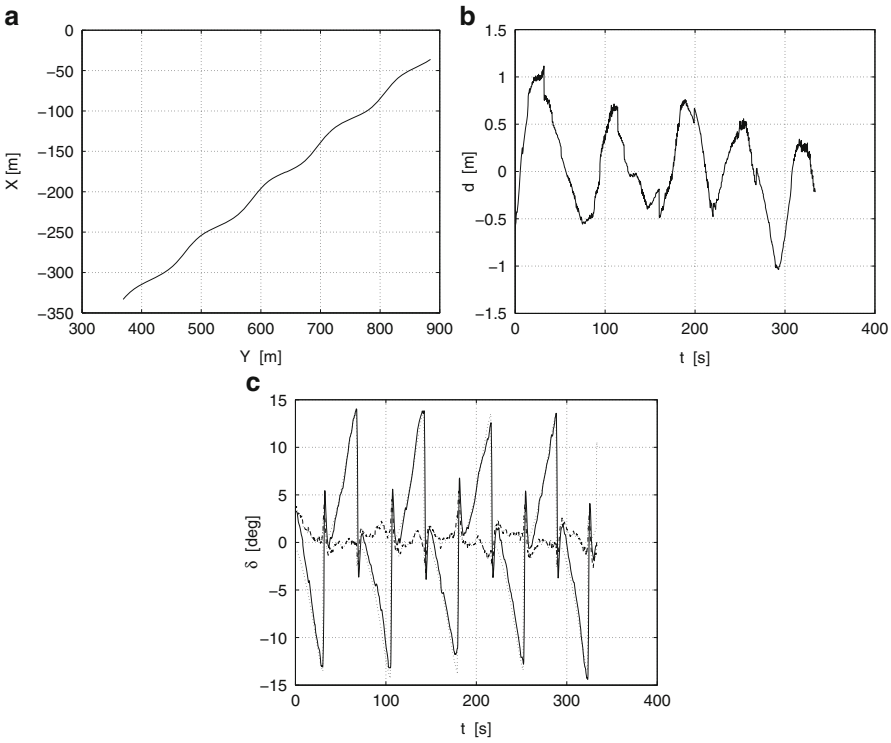

Fig. 18.7 Performance of the track-keeping controller for the ship Falke. (**a**) Real navigation path. (**b**) Distance to desired track d. (**c**) Rudder angle measurement δ (*continuous-line*), rudder feedback δ_{fb} (*dash-dotted line*), and rudder feedforward δ_{ff} (*dotted line*)

18.7 Linking Transport of and Transport over Water

Our study is focused in the transport over water, nevertheless, it is related to the transport of water. The authors are convinced that acceptable results of the track-keeping controller can only be achieved, if the particular conditions for navigation on inland waterways are considered. This makes it necessary to pay attention to the transport of water in the inland waterway, identifying and describing its relevant characteristics and their influence on the ship's behavior.

In contrast to navigation conditions in open sea, inland waterway navigation is restricted to a reduced space. As a consequence of such space problems and the permanent changes of the ship heading imposed by the waterways, it is essential to consider the drift dynamics in the ship maneuverability. Additionally, the ship dynamics is subject to disturbances, namely, tributary streams and forces due to other near passing vessels. Another particular aspect of inland waterways, with respect to the scenario in open sea, is the shallow water navigation condition. The effect of changes in the water depth should be considered in the ship dynamics

for $h/T < 5$, where h is the water depth, and T is the draft of the ship [20]. For $h/T < 5$, we assume that the water depth is constant and therefore, changes in the river bed are treated as disturbances. On the other hand, the vessel speed is considerably affected by the current, and the steering dynamics is quite different upstream from downstream [5]. Regarding the current direction, in inland navigation it can be approximated by the tangential direction of the river axis. In our case, we use the guiding line of the navigation system.

Solutions for the ship dynamics modeling, parameter identification, and track-keeping controller have been proposed and implemented considering the abovementioned particular conditions of inland navigation. These solutions can be used to solve specific transport of water problems. For instance, the developments achieved so far in the modeling can be applied to the inverse problem, that is, the design of the waterway considering the ship dynamics models.

On the other hand, the track-keeping controller could be part of a much more complex hierarchical control system, that manages both water and transport resources, as it is discussed in [26, 27]. In the first automation level of this complex system, we can find a track-keeping controller and a *collision and detection avoidance system*. In the latter, extensive research has been conducted in [26]. Next comes the second automation level, whose aim is to coordinate different ships. As part of the second level, coordination between ships and locks might also be considered. An interesting application related to this field, is the development of a path planing method for lock entering maneuvers in [23]. Finally, there is a third automation level which optimizes the shipping process taking into account locks, loading/unloading facilities, etc.

18.8 Conclusions and Future Research

In this chapter we explore the performance of a closed-loop continuous-time identification method, which is applied to the parameter estimation of an inland vessel model. The identification is a challenging task because the ship is subject to important disturbances, namely wind and stream.

The navigation data that we use to identify the parameters is obtained in a closed-loop setting using a model-based track-keeping controller. The parameter estimation approach that we analyze here is the closed-loop refined instrumental variable method for continuous-time systems (CLRIVC), that takes into account the control structure in the identification process. In Monte Carlo simulations, this instrumental variable scheme shows good results, and as expected it outperforms an optimization-based method (OPT), which in this case does not consider any noise model.

Experiments with a full scale ship are used to identify parameters with OPT. In this study, the CLRIVC cannot be considered so far with real data, as explained in a few paragraphs. Moreover, as far as the authors know, the CLRIVC has only been tested in simulation. Thus, future research will be conducted to see how

this approach performs using real data. Instead of considering the CLRIVC, we apply the open-loop simplified refined instrumental variable method for continuous-time linear parameter varying systems (LPV-SRIVC). Since the real data has a low disturbance level, both the OPT and LPV-SRIVC approaches perform well, as shown by a cross-validation. The accuracy of the estimates is further evaluated through a sensitivity analysis. On the other hand, the performance of the model-based track-keeping controller is briefly illustrated. The good results achieved by the controller are another evidence of the suitability of the estimated model.

Another important topic of research that would involve big efforts, is the development of a complex hierarchical control system, as it was previously mentioned. The track-keeping controller presented here could be part of such a control system, whose task would be to manage both water and transport resources.

Acknowledgements The authors thank Professor Ernst Dieter Gilles and the Max Planck Institute for Dynamics of Complex Technical Systems, Magdeburg-Germany where Arturo Padilla did part of the work presented in this chapter and from where the navigation data was obtained. The presented research on modeling and control was conducted by Ralph Bittner under the direction of Professor Gilles at the Max Planck Institute.

References

1. Anderson BDO, Moore JB. Optimal control: Linear quadratic methods. Englewood Cliffs: Prentice Hall; 1989.
2. Åström KJ, Källström CG. Identification of ship steering dynamics. Automatica. 1976;12: 9–22.
3. Bastogne T, Garnier H, Sibille P. A PMF-based subspace method for continuous-time model identification. Application to a multivariable winding process. Int J Control. 2001;74(2): 118–32.
4. Bittner R. Modellbasierte Bahnführung von Binnenschiffen. Ph.D. dissertation, Otto von Guericke Universität Magdeburg (in preparation).
5. Bittner R, Gilles ED. Automatic track-keeping of inland vessels in flowing waterways. In: 4th international symposium on automatic control, Wismar, September 2005. Hochschule Wismar; 2005.
6. Bittner R, Driescher A, Gilles ED. Entwurf einer Vorsteuerung zur hochgenauen Bahnführung von Binnenschiffen. In: Wismarer Automatisierungssymposium, vol. 3, Wismar, 2002.
7. Bittner R, Driescher A, Gilles ED. Drift dynamics modeling for automatic track-keeping of inland vessels. In: Peshekhonov VG, editor. 10th Saint Petersburg international conference on integrated navigation systems, Saint Petersburg, May 2003. State Research Center of the Russian Federation "Elektropribor"; 2003. p. 218–27.
8. Blanke M, Knudsen M. Optimized experiment design for identification of marine systems. In: 14th IFAC world congress, Beijing, 1999.
9. Bolk S. Entwurf einer lqg-regelung zur bahnführung von binnenschiffen. Diplomarbeit, Universität Stuttgart, 2004.
10. Focus Max Planck Gesellschaft. Computer at the helm. http://www.mpg.de/942027.
11. Fossen TI. Guidance and control of ocean vehicles. New York: Wiley; 1994.
12. Fossen TI. Marine control systems. Marine Cybernetics; 2002.
13. Garnier H, Gilson M, Zheng WX. A bias-eliminated least-squares method for continuous-time model identification of closed-loop systems. Int J Control. 2000;73(1):38–48.

14. Gilson M, Garnier H. Continuous-time model identification of systems operating in closed-loop. In: 13th IFAC symposium on system identification, 2003.
15. Gilson M, Van den Hof P. On the relation between a bias-eliminated least-squares (bels) and an iv estimator in closed-loop identification. Automatica. 2001;37:1593–600.
16. Gilson M, Van den Hof P. IV methods for closed-loop system identification. In: 13th IFAC symposium on system identification, 2003.
17. Gilson M, Van den Hof P. Instrumental variable methods for closed-loop system identification. Automatica. 2005;41:241–49.
18. Gilson M, Garnier H, Young P, Van den Hof P. Instrumental variable methods for closed-loop continuous-time model identification. In: Garnier H, Wang L, editors. Identification of continuous-time models from sampled data. New York: Springer; 2008. p. 133–60.
19. Gilson M, Garnier H, Young P, Van den Hof P. Optimal instrumental variable method for closed-loop identification. IET Control Theory Appl. 2011;5(10):1147–54.
20. Gronarz A. Rechnerische Simulation der Schiffsbewegung beim Manövrieren unter besonderer Berücksichtigung der Abhängigkeit von der Wassertiefe. Ph.D. thesis, Gerhard-Mercator-Universität Gesamthochschule Duisburg, 1997. http://duepublico.uni-duisburg-essen.de/servlets/DerivateServlet/Derivate-5111/inhalt.htm.
21. Herzer B. Die automatische bahnführung von schiffen mit nichtminimalphasiger dynamik. Ph.D. dissertation, Universität Stuttgart (in preparation).
22. Herzer B, Gilles ED. Disturbance estimation for feedforward control of inland vessels. In: 8th IFAC conference on control applications in marine systems, Rostock-Warnemünde, 2010.
23. Lachmeyer A, Herzer B, Gilles ED. Path planning for lock entering maneuvers using nonlinear programming. In: 8th IFAC conference on control applications in marine systems, Rostock-Warnemünde. IFAC; 2010.
24. Ljung L. System identification, theory for the user. 2nd ed. Englewood Cliffs: Prentice Hall; 1999.
25. Ljung L. Experiments with identification of continuous time models. In: 15th IFAC symposium of system identification, Saint-Malo, 2009.
26. Lutz A. Kollisionserkennung und -vermeidung auf Binnenwasserstraßen. Ph.D. thesis, Universität Stuttgart, 2011. http://elib.uni-stuttgart.de/opus/volltexte/2011/6399/.
27. Lutz A, Gilles ED. Opportunities for Automated Inland Navigation. In: Konings R, Priemus H, Nijkamp P, editors. The future of automated freight transport: Concepts, design and implementation. Edward Elgar Publishing; 2005. p. 51–64.
28. Nomoto K, Taguchi T, Honda K, Hirano S. On the steering qualities of ships. Int Shipbuild Prog. 1957;4:354–70.
29. Padilla A, Yuz JI, Herzer B. Continuous-time system identification of the steering dynamics of a ship on a river. Int J Control. 2014 (to appear).
30. Rawlings JB, Ekerdt JG. Chemical reactor analysis and design fundamentals. Nob Hill Publishing; 2002.
31. Tóth R, Laurain V, Gilson M, Garnier H. Instrumental variable scheme for closed-loop lpv model identification. Automatica. 2012;48:2314–20.
32. Wahl A. Einsatz optimaler Regelverfahren zur automatischen Bahnführung. Ph.D. thesis, Universität Stuttgart, 2001.
33. Young PC. Recursive estimation and time-series analysis: An introduction for the student and practitioner. Berlin: Springer; 2011.
34. Young PC, Garnier H, Gilson M. Refined instrumental variable identification of continuous-time hybrid Box-Jenkins models. In: Garnier H, Wang L, editors. Identification of continuous-time models from sampled data. Berlin: Springer; 2008. p. 91–131.
35. Zimmermann R. Repräsentation dynamischer Schiffsmodelle in einem Navigationssystem für die Binnenschiffahrt. Ph.D. thesis, Universität Stuttgart, 2000.

Chapter 19
Nonlinear Iterative Control of Manoeuvring Models for Transport over Water

E. Revestido Herrero, M. Tomás-Rodríguez, and F.J. Velasco

Abstract This chapter addresses the problem of control design and implementation of a nonlinear marine vessel manoeuvring model. The chapter includes a thorough literature review of the current state of the art in the nonlinear control of marine vessels field. Then, the model will be presented; the authors will consider a highly nonlinear vessel 4 DOF model as the basis of the work. The control algorithm will be introduced providing the adequate mathematical description. The control algorithm here proposed consists of a combination of two methodologies: (i) An iteration technique that approximates the original nonlinear model by a sequence of linear time varying equations whose solution converge to the solution of the original nonlinear problem and, (ii) A lead compensation design in which for each of the iterated linear time varying systems generated, the controller is optimized at each time on the interval for better tracking performance. The control designed for the last iteration is then applied to the original nonlinear problem. Simulations and results will be presented and will show an accurate performance of the approximation methodology to the non linear manoeuvring model and also an accurate tracking for certain manoeuvring cases under the control of the designed lead controller. The main characteristics of the nonlinear systems response are the reduction of the settling time and the elimination of the steady state error and overshoot.

19.1 Introduction

One of the basic manoeuvres performed by transport systems over water is the so called course-keeping manoeuvre. In this manoeuvre, an autopilot or a heading controller is needed with the aim of controlling the course angle. This manoeuvre

E.R. Herrero (✉) • F.J. Velasco
Universidad de Cantabria, Santander 39005, Spain
e-mail: revestidoe@unican.es; velascof@unican.es

M. Tomás-Rodríguez
School of Engineering and Mathematical Sciences, City University London, London EC1V 0HB, UK
e-mail: Maria.Tomas-Rodriguez.1@city.ac.uk

C. Ocampo-Martinez, R.R. Negenborn (eds.), *Transport of Water versus Transport over Water*, Operations Research/Computer Science Interfaces Series 58,
DOI 10.1007/978-3-319-16133-4_19

is the basis of a guidance system based on the Line Of Sight (LOS) method [11], which provides satisfactory results in tracking a path defined by waypoints. A good performance of the course-keeping manoeuvre becomes of paramount importance when a vehicle is guided along restricted waters since there is little margin for tracking errors.

The design of autopilots based on PID methods has been in use since 1920s [9] with the help of gyrocompasses which measured the vehicle's heading angle for feedback purposes. The main challenges in the design of ship autopilots are the surrounding environmental uncertainties such as waves, wind, ocean currents and the high nonlinear ship dynamics. In addition to these, the rudder dynamics also present saturation-type nonlinearities on its rate and deflection angle. Several articles deal with the design and implementation of PID based autopilots, in which linearizations for the vessel's manoeuvring model are performed, (i.e., [11, 14, 15, 19, 20, 26]). In most low speed applications, it is acceptable to neglect the nonlinear dynamics on the shipt's manoeuvring model due to linear terms predomination. However, in the case of high speed applications, tight turns, large sideslip angles or in the presence of currents, nonlinear effects become pronounced and thus neglecting them may degrade the controller's performance and robustness. Different nonlinear methods [11] have been presented for course-keeping autopilott's design such as state feedback linearization [9], nonlinear backstepping [2, 34], sliding mode control [17], output feedback [18], H_∞-control [13], particle swarm optimization [28], genetic algorithms [17], fuzzy logic methods [5], etc. For most of these type of applications, nonlinear manoeuvring models in 1 degree of freedom (DOF) are considered, i.e., [21] or [3], therefore, the coupling between variables is not taken into account. Due to the complexity of some of the above cited nonlinear methods, the implementation may be time consuming from the computational point of view. The aim of this chapter is to design a control method for a nonlinear marine vessel manoeuvring model without performing any simplification in the model's nonlinearities or variable's couplings. This chapter proposes a control strategy based on an optimized lead compensation control methodology combined with an iteration technique used to approach the original nonlinear system. This iteration technique was initially presented in [29, 30] and has been used to solve various nonlinear control problems such as optimal control [31], observers design [12], nonlinear optimal tracking [8], etc. One of its advantages is the fact that it maintains the inherent nonlinear characteristics of the system's behavior, providing the grounds for a robust control implementation where modeling uncertainties are removed and no linear approximation is performed. The iteration technique is applied to a 4 DOF nonlinear manoeuvring ship model. This opens the novel possibility of course-keeping autopilot design based on lead compensation methodology applied to a nonlinear model. This approach exists without the limitations of the linear models previously indicated, and keeps the simplicity of the lead compensation design and implementation. Based on a preliminar study, the use of a lead controller instead of a conventional PID is justified. By an appropriate optimization technique, a good compromise between the overshoot and time response is achieved without stationary state error.

The general objective is to design a controller for nonlinear systems of the form:

$$\dot{x} = f(x) = A(x)x(t) + B(x)u_c(t, \theta_c), \quad x(0) = x_0 \tag{19.1}$$

where $u_c(t, \theta_c)$ is the control action, θ_c is the set of controller's parameters, $x(t)$ is the state vector, $A(x)$, $B(x)$ are state dependant matrices of appropriate dimensions and is the vector $x(0)$ of initial conditions.

Replacing the nonlinear system by a sequence of "i" linear time varying (LTV) systems, then a sequence of "i" corresponding feedback laws $u_c^{(i)}(t, \theta_c)$ is generated: for each of them, the closed-loop response for the ith LTV system at each time t of the time interval is controlled by the designed lead controller $u_c^{(i)}(t, \theta_c)$. From the convergence of the sequence of LTV solutions [30], the last of the iterated control laws, $u_c^{(i)}(t, \theta_c)$, (corresponding to the ith iteration), will provide lead controller stability objectives satisfaction when it is applied to the nonlinear system.

19.1.1 Theoretical Contribution

Iteration Technique for Nonlinear Systems

This iteration methodology approaches the solution of nonlinear dynamical problems in a global manner. It replaces the original nonlinear problem by a sequence of linear time varying (LTV) systems whose solutions converge in the space of continuous functions to the solution of the nonlinear system under a mild Lipschitz condition [30]. This section contains the basis on how this technique can be implemented and its convergence theorem.

Any nonlinear system given on the form:

$$\dot{x}(t) = f[x(t)] = A[x(t)]x(t) + B[x(t)]u_c(t), \tag{19.2}$$

where the vector of initial conditions $x(0) = x_0 \in \mathbb{R}^n$, and $A[x(t)] \in \mathbb{R}^{n\text{x}n}$ is locally Lipschitz and state dependant, can be approximated by a sequence of LTV equations where the vector of states $x(t) \in \mathbb{R}^n$, inside the matrices $A[x(t)]$ and $B[x(t)]$ are substituted at each iteration "i" by the states obtained in the previous iteration $x^{(i-1)}(t)$. This is:

$$\begin{aligned} \dot{x}^{(1)}(t) &= A[x(0)]x^{(1)}(t) + B[x(0)]u_c^{(1)}(t), \\ &\vdots \\ \dot{x}^{(i)}(t) &= A[x^{(i-1)}(t)]x^{(i)}(t) + B[x^{(i-1)}(t)]u_c^{(i)}(t), \end{aligned} \tag{19.3}$$

with $x^{(1)}(0) = \cdots = x^{(i)}(0) = x(0)$, for $i \geq 1$ and $\forall t \in [0, \tau]$. The solutions of this sequence of LTV equations, $x^{(i)}(t)$, converge to the solution of the nonlinear system $x(t)$ given in (19.2). For more details on the global convergence Theorem

and its corresponding proof, the reader is referred to [30] and [29]. The application of this technique provides an accurate representation of the nonlinear solution after just a few iterations. Nonlinear systems of the form (19.2), satisfying the local Lipschitz requirement can be now approached by classic linear methods. This, is a very mild assumption since it is an already assumed condition for the uniqueness of the solution.

19.1.2 Application-Based Contribution

The Mathematical Model

The nonlinear dynamical model in here is known as manoeuvring. Manoeuvring deals with the ship's motion in absence of waves excitation (calm water) [23]. The motion results from the action of control devices such as control surfaces (rudders, fins, T-foils) and propulsion units. In manoeuvring theory, the motion of 4 DOF ship models requires from four independent coordinates in order to fully determine the position and orientation of the vehicle, which is considered to be a rigid body. These coordinates represent the longitudinal and lateral positions and speeds as well as and their derivatives along the respective coordinate frames. The four degrees of freedom under consideration in this work describe the ship's motion (surge, sway and yaw) on the horizontal plane and the roll in the vertical plane. Two coordinate frames are used: the n coordinate system (earth-fixed), O_n, is used to define the ship position and the system b, (body-fixed) O_b, helps to define the ship's orientation [23].

The rigid-body equations of motion of the 4 DOF model are given by [24]:

$$\begin{aligned} m[\dot{u} - y_g^b \dot{r} - vr - x_g^b r^2 + z_g^b pr] &= \tau_X \\ m[\dot{v} - z_g^b \dot{p} + x_g^b \dot{r} + ur - y_g^b (r^2 + p^2)] &= \tau_Y \\ I_{xx}\dot{p} - mz_g^b \dot{v} + m[y_g^b vp - z_g^b ur] &= \tau_K \\ I_{zz}\dot{r} + mx_g^b \dot{v} - my_g^b \dot{u} + m[x_g^b ur - y_g^b vr] &= \tau_N \end{aligned} \tag{19.4}$$

The subindex $_g$ refers to the center of gravity and the superindex ^{b} to the b-frame. Details of the parameters included in (19.4) can be found in [24]. These equations of motion are formulated about the b-frame, which is fixed to the point determined by the intersection of the port-starboard plane of symmetry, the waterline plane and the transverse vertical plane at $L_{pp}/2$ (see [24] for hull dimensions). The force terms on the right hand side of (19.4) can be described as the total contribution of the hydrodynamic, propulsion and control forces:

$$\tau = \tau_{hyd} + \tau_p + \tau_c \tag{19.5}$$

Hydrodynamic Forces, τ_{hyd}

The hydrodynamic forces appear due to the motion of the vessel in calm water. The following equations correspond to the model established by [6] that proposed a simplified version of the model in [22], preserving in this way the most important hydrodynamic coefficients so that the model describes a wide variety of manoeuvring regimes in spite of some minor simplifications. Hydrodynamic forces are mainly composed by surge, sway, roll and yaw terms:

- *Surge terms*

$$\tau^b_{Xhyd} = X_{\dot{u}}\dot{u} + X_{vr}vr + X_{u|u|}u|u| \tag{19.6}$$

- *Sway terms*

$$\begin{aligned}\tau^b_{Yhyd} &= Y_{\dot{v}}\dot{v} + Y_{\dot{r}}\dot{r} + Y_{\dot{p}}\dot{p} + Y_{|u|v}|u|v + Y_{ur}ur + Y_{|v|v}|v|v + Y_{|v|r}|v|r + Y_{|r|v}|r|v \\ &+ Y_{\phi|uv|}\phi|uv| + Y_{\phi|ur|}\phi|ur| + Y_{\phi uu}\phi u^2\end{aligned} \tag{19.7}$$

- *Roll terms*

$$\begin{aligned}\tau^b_{Khyd} &= K_{\dot{v}}\dot{v} - K_{\dot{p}}\dot{p} + K_{|u|v}|u|v + K_{ur}ur + K_{|v|v}|v|v + K_{|v|r}|v|r + K_{|r|v}|r|v + K_p p \\ &+ K_{\phi|uv|}\phi|uv| + K_{\phi|ur|}\phi|ur| + K_{\phi|uu|}\phi u^2 + K_{|u|p}|u|p + K_{p|p|}p|p| - K_{\phi\phi\phi}\phi^3 \\ &+ \rho g \nabla GMt\phi\end{aligned} \tag{19.8}$$

- *Yaw terms*

$$\begin{aligned}\tau^b_{Nhyd} &= N_{\dot{v}}\dot{v} + N_{\dot{r}}\dot{r} + N_{|u|v}|u|v + N_{ur}ur + N_{|v|r}|v|r + N_{|r|v}|r|v + N_{\phi|uv|}\phi|uv| \\ &+ N_{\phi u|r|}\phi u|r| + N_{|p|p|}|p|p + N_{|u|p}|u|p + N_{\phi u|u|}\phi u|u| + N_{|v|v}|v|v\end{aligned} \tag{19.9}$$

Note that $\dot{\psi} = r$ and $\dot{\phi} = p$.

Propulsion Forces

The dynamics of the propulsion system are not included in the model as in [24]. It is assumed that the propellers deliver a constant thrust T that compensates the resistance on calm water:

$$T = -X_{u|u|}u^2_{nom}, \quad \tau_p = [T,\ 0,\ 0,\ 0]^T, \tag{19.10}$$

where u_{nom} is the service speed and τ_p the resultant propulsion forces vector.

Control Forces: Rudder

The vessel under study in here is equipped with two rudders which together with the commanding machinery constitute the actuators of the system. In order to obtain the expression of the control forces, some other concepts need to be introduced first. Hydrofoil lift and drag forces [16], are given by the following expressions:

$$L = 1/2\rho V_f^2 A_f \bar{C}_L \alpha_e \tag{19.11}$$

$$D = 1/2\rho V_f^2 A_f (C_{D0} + \frac{(\bar{C}_L \alpha_e)^2}{0.9\pi a}), \tag{19.12}$$

where V_f is the local velocity at the foil, A_f is the area of the foil, α_e is the effective angle of attack in radians, and a is the effective aspect ratio. We can use the following linear approximation to represent the lift coefficient:

$$\bar{C}_L = \frac{\partial C_L}{\partial \alpha_e}|_{\alpha_e=0}. \tag{19.13}$$

Once the stall angle of the hydrofoils is reached, the lift saturates in value. In order to calculate the lift of the rudder, the effective angle of attack, α_e, is approximated by the mechanical angle of the rudder: $\alpha_e \approx \delta_c$, and the local flow velocity at the rudder is considered to be equal to the vessel's total horizontal speed, $V_f = \sqrt{u^2 + v^2}$. Then, a global correction for the lift and drag can be applied [4].

The control forces, τ_c, generated by the rudder in the b-frame are:

$$\tau_c \approx [-D,\ L,\ z_{CP}^b L,\ x_{CP}^b L]^T, \tag{19.14}$$

where x_{CP}^b and z_{CP}^b are the coordinates of the center of pressure of the rudder (CP) with respect to the b-frame. The CP is assumed to be located at the rudder stock and in the middle of the rudder span. The hydraulic machinery moving the rudder is implemented in this work following the model of [33] that considers both a maximum rudder angle and rate. When working in the unsaturated zone, the rudder's dynamics can be represented by a first order system:

$$\dot{\delta}(t) = \frac{1}{T_m}\left[\delta_c(t) - \delta(t)\right], \tag{19.15}$$

where $\delta(t)$ is the rudder angle, $\delta_c(t)$ the commanded rudder angle and T_m is the hydraulic machinery's constant.

Kinematics

The kinematics cover the geometrical aspects of the vessel's displacement without considering mass and forces. The position of the ship is obtained by performing a transformation between the body-fixed ($b-frame$) linear velocities and the time derivative of the positions in the ($n-frame$). This can be expressed for a 4 DOF manoeuvring model as:

$$\begin{aligned} \dot{x}_n &= u \cdot cos(\psi) - v \cdot sin(\psi) cos(\phi), \\ \dot{y}_n &= u \cdot sin(\psi) + v \cdot cos(\psi) cos(\phi). \end{aligned} \tag{19.16}$$

19.1.3 Controller Design

An automatic pilot or a heading controller must fulfil two functions: course-keeping and change of course. In the first case, the control objective is to maintain the trajectory of the vessel following a desired constant heading, ψ_d. In the second case, the objective is to perform heading changes without introducing large response oscillations and within a minimum time. In both cases, the adequate functioning of the system must be independent from the disturbances produced by existing external factors such as wind, waves and currents.

The heading trajectory followed by the vessel, $\psi(t)$, can be obtained by means of a second order reference model:

$$\ddot{\psi}(t) + 2\zeta w_n \dot{\psi}(t) + w_n^2 \psi(t) = w_n^2 \psi_d, \tag{19.17}$$

where w_n is the natural frequency and ζ is the desired damping ratio of the closed loop system. ζ is typically chosen to lie within the interval values ($0.8 \leq \zeta \leq 1$) in order to account for security issues [32]. In restricted waters and for collision avoidance, the course-changing manoeuvre should have a clear start, in order to warn nearby ships of the intention of the manoeuvre and, for that reason, that manoeuvre should preferably be completed with no overshoot.

The following PID control schema is conventionally used for the heading control implementation:

$$U_c(s) = \frac{\delta_c}{E}(s) = \left[k_p + \frac{k_i}{s} + \frac{k_d s}{\alpha T_d s + 1} \right], \tag{19.18}$$

where $k_d = T_d k_p$ and $k_i = k_p / T_i$ being T_d the derivative time, T_i the integral time, $\delta_c(s)$ the Laplace transform of the rudder position and $E(s)$ the Laplace transform of the error, $e(t) = \psi_d - \psi(t)$ and $U_c(s)$ is the Laplace transform of the control signal, $u_c(t, \theta_c)$. The $\psi(t)$ vector is extracted from the states, being $x(t) = [u\ v\ p\ r\check{z}\ \phi\ \psi\ \delta\ x_n\ y_n]^T$ and $x_{(6)}(t) = \psi(t)$.

The noise levels of the onboard standard instrumentation may cause derivative model noise amplification problems. The PID schema (19.18), in which the derivative action is filtered by a first order system $\frac{1}{\alpha T_d s + 1}$, avoids this problem of noise amplification.

It is highly likely that the rudder's deflection angle and rate saturations provoke the windup phenomenon (see [1] for more details) when PID methodology is applied. This is, the PID integral term, $(\frac{k_i}{s})$, may become large and as a consequence, the heading response may show high levels of oscillation. There exist several anti-windup schemes in the literature (see [1] and references therein), but instead of applying one of them, this would make the designed controller more complex, a simpler method is chosen: a modified control structure such as the following first order network controller is used, note that the integral action has been omitted:

$$U_c(s) = \frac{\delta_c}{E}(s) = K\left[\frac{s+z}{s+p}\right], \tag{19.19}$$

where $K > 0$ and $p > z$.

The expression (19.19) represents a lead compensation controller that has a zero located nearer to the s-plane origin than the pole. This dominant zero improves the stability of the system, which is desirable in order to satisfy the objective of obtaining a heading response without overshoot.

Note that (19.18) and (19.19) become equal to each other if the integral term $K_p/(T_i s)$ is zero, being equivalent to a PD controller transfer function.

19.1.4 Tuning the Controller

The tuning task is performed by following the schema on Fig. 19.1, in which the optimization algorithm takes data from the output (vessel's heading angle $\psi(t)$) and from the input (desired heading ψ_d). In the selection of the optimization method the aims of the heading control were taken into account: To minimize both the response's overshoot and the settling time without steady state error. For these reasons, the authors chose the minimax optimization technique, as it minimizes the maximum value of the output. In this way, when the maximum value of the output is reduced, the heading's overshoot is minimized too.

The application of the minimax problem to the heading control, consist on minimizing the maximum value of the output, $\psi(t)$, over the simulation time interval $[t_0, t_f]$. The following constrain is imposed such that $\psi(t)$ is always less or equal than the constant input value ψ_d,

$$\psi(t) \leq \psi_d, \quad t_r \leq t \leq t_f \tag{19.20}$$

being t_r the rise time of the system. By imposing this restriction, a flat response with no overshoot and no stationary error is expected. The value of t_r is determined based on a prior knowledge of the system response. Then, the minimax problem is applied [7, 27]:

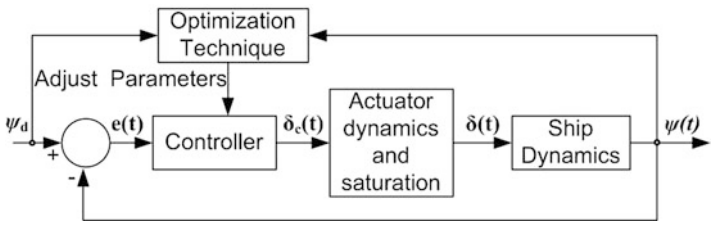

Fig. 19.1 Closed-loop diagram for the optimization process

$$\min_{\theta_c^{(i)}} \max_j \{\psi_j(\theta_c^{(i)})\} \equiv \begin{cases} \psi(t) \leq \psi_d, & t_r \leq t \leq t_f, \\ lb \leq \theta_c^{(i)} \leq ub, \end{cases} \tag{19.21}$$

where $\psi(t)$ is the heading angle, $\theta_c^{(i)}$ are the controller's parameters for the corresponding ith LTV approximation to be optimized , lb is the lower bound of the parameters, ub is the upper bound of the parameters and the subindex j represents one set of multivariable functions.

19.1.5 Implementation Procedure

Based on the theory previously presented, the heading control implementation process can be summarized according to the following steps:

Initialization

Set initial values for the constants and variables involved in the process: $lb, ub, x(0), \theta_c^{(0)}, t_0, t_f, t_r, \psi_d, h, tol_x, tol_{\theta_c}$.

Step 1

The first step to solve system (19.23) is to approximate it by solving the following linear time invariant system:

$$\dot{x}^{(1)}(t) = A[x_0]x^{(1)}(t) + B[x_0]u_c^{(1)}(t, \theta_c^{(1)}), x^{(1)}(0) = x_0.$$

This system represents a linear model and it differs from the nonlinear behavior, not being a good representation; that is the reason why the heading control is not optimized at this step, then we made $\theta_c^{(1)} = \theta_c^{(0)}$.

Step 2

1. Optimize the heading control loop:

$$\min_{\theta_c^{(2)}} \max_j \{\psi_j(\theta_c^{(2)})\} \equiv \begin{cases} \psi(t) \leq \psi_d, & t_r \leq t \leq t_f \\ lb \leq \theta_c^{(2)} \leq ub \end{cases}$$

   for $j = 1, 2, \ldots t_f/h$. The optimization stops when $\|\theta_c^{(2)} - \theta_c^{(1)}\| < tol_{\theta_c}$ is true.

2. With the obtained parameters $\theta_c^{(2)}$, the following LTV system is solved for $x^{(2)}(t)$ by using the designed control action $u_c^{(2)}(t, \theta_c^{(2)})$ and the initial conditions $x^{(2)}(0) = x(0)$:

$$\dot{x}^{(2)}(t) = A[x^{(1)}]x^{(2)}(t) + B[x^{(1)}]u_c^{(2)}(t, \theta_c^{(2)})$$

If $\|x^{(2)} - x^{(1)}\| < tol_x$ is satisfied, the algorithm stops at this point, if not, go to next step.

$$\vdots$$

Step (i)

1. Optimize the heading control loop by:

$$\overset{min}{\theta_c^{(i)}} \overset{max}{j} \{\psi_j(\theta_c^{(i)})\} \equiv \begin{cases} \psi(t) \leq \psi_d, & t_r \leq t \leq t_f \\ lb \leq \theta_c^{(i)} \leq ub \end{cases}$$

   for $j = 1, 2, \ldots t_f/h$. The optimization stops when the condition $\|\theta_c^{(i)} - \theta_c^{(i-1)}\| < tol_{\theta_c}$ is satisfied.

2. With the obtained parameters $\theta_c^{(i)}$, the next step is to solve the following LTV system for initial conditions $x^{(i)}(0) = x(0)$:

$$\dot{x}^{(i)}(t) = A[x^{(i-1)}]x^{(i)}(t) + B[x^{(i-1)}]u_c^{(i)}(t, \theta_c^{(i)}),$$

   When $\|x^{(i)} - x^{(i-1)}\| < tol_x$ is satisfied, the algorithm stops, if not, go to step $i + 1$.

Note that during the optimization process in order to obtain the set of functions $\{\psi_j(\theta_c^{(i)})\}$ it is necessary to solve the corresponding LTV approximation:

$$\dot{x}^{(i)}(t) = A[x^{(i-1)}]x^{(i)}(t) + B[x^{(i-1)}]u_c^{(i)}(t, \theta_c^{(i)}), \tag{19.22}$$

to obtain $x^{(i)}$, as much as needed by the optimization algorithm. The control output $u_c^{(i)}(t, \theta_c^{(i)})$ at each iteration is given by the control structure defined in Sect. 19.1.3 and the initial conditions are $x^{(i)}(0) = x(0)$.

19.1.6 Iteration Technique Approximation for Control Purposes

In this section, the methodology previously introduced is applied to the case of heading control of the vessel model. The equations of motion of this system are highly nonlinear and can be written on the form:

$$\dot{x}(t) = A[x(t)]x(t) + B[x(t)]u_c(t, \theta_c), \quad x(0) = x_0 \in \mathbb{R}^n. \tag{19.23}$$

where $A[x(t)] \in \mathbb{R}^{nxn}$, $B[x(t)] \in \mathbb{R}^{nxm}$, $x(t)$ is the state's vector and the control $u_c(t, \theta_c)$ is designed by using the methodology presented in Sect. 19.1.3. The system (19.23) can be approximated by the following sequence of LTV systems:

$$\begin{aligned} \dot{x}^{(1)}(t) &= A[x(0)]x^{(1)}(t) + B[x(0)]u_c^{(1)}(t, \theta_c^{(1)}), \\ &\vdots \\ \dot{x}^{(i)}(t) &= A[x^{(i-1)}(t)]x^{(i)}(t) + B[x^{(i-1)}]u_c^{(i)}(t, \theta_c^{(i)}), \end{aligned} \tag{19.24}$$

with initial conditions $x^{(1)}(0) = \cdots = x^{(i)}(0) = x(0)$. For each of these "$i$" LTV iterations, a control action signal $u_c^{(i)}(t, \theta_c)$ is designed. Once last iteration is obtained, the sequence of solutions converges to the nonlinear solution, $\lim_{i \to \infty} \left[x^{(i)}(t)\right] \to x(t)$. The last designed control signal will be applied to the original nonlinear problem, achieving control of the states:

$$\dot{x}(t) = A[x(t)]x(t) + B[x(t)]u_c^{(i)}(t, \theta_c^{(i)}), \quad x(0) = x_0 \in \mathbb{R}^n. \tag{19.25}$$

19.2 Specific Case Study Discussion

In this section, the theory previously presented has been implemented in Matlab/Simulink and applied to the particular case study of a full scale coastal patrol vessel. The set of parameters and the main characteristics of the coastal patrol are included in [24]. The coastal patrol is equipped with two rudders and its service speed is $u_{nom} = 15$ knots ($7.71\, m/s$). The simulations were carried out using Matlab/Simulink and the GNC toolbox [10].

The cited case of study of a full scale coastal patrol vessel is evaluated under two different scenarios: firstly, a standard 20–20° zig-zag manoeuvre is considered in order to show the convergence of the iteration methodology presented in the theory and secondly, a 20° course-keeping manoeuvre is presented to show the accuracy of the tracking capabilities of the designed controller when applied to the last of the iterated LTV systems.

19.2.1 Main Results

In this section the authors show the results for the first scenario when it is applied the iteration technique presented in Sect. 19.1.1 to approximate the vessel's nonlinear model given in Sect. 19.1.2 for the particular case of a full scale coastal patrol. The simulation time was $t_f = 200$ sec and the integration step size was set to be $h = 0.1$. As a rule of thumb, the sampling period h is chosen to be in the range of

20–40 samples within the rise time of the fastest degree of freedom. The equations of motion of this system, (19.4)–(19.16), are highly nonlinear and can be written on the form:

$$\dot{x}(t) = A[x(t)]x(t) + B[x(t)]u_c(t), \quad x(0) = x_0 \in \mathbb{R}^9, \tag{19.26}$$

where the systemt's matrix $A[x(t)] \in \mathbb{R}^{9x9}$, $B[x(t)] \in \mathbb{R}^{9x2}$, $u_c(t)$ is the control signal and $x(t)$ is the state vector, $x(t) = [u\ v\ p\ r\check{z}\ \phi\ \psi\ \delta\ x\ y]^T$. u is the surge (longitudinal speed), v is the sway, this is the lateral speed, p is the angular speed of roll, r is the angular speed on yaw, ϕ is the angular displacement in roll, ψ is the angular displacement in yaw, δ is the rudder displacement for direction management purposes and x_n, y_n are the corresponding coordinates for longitudinal and lateral positions expressed in the n-frame.

A standard 20–20° zig-zag manoeuvre (see [16]) is simulated, the reason for choosing such a large amplitude is to excite the vessel's high nonlinear dynamics and to show the good fit of the iteration technique to the nonlinear original system. The control vector to carry out this manoeuvre is $u_c(t) = [\delta_c\ T]^T$, where T was previously defined in (19.10) and δ_c is the rudder's deflection that must follow the zig-zag manoeuvre phases as shown in Fig. 19.2. Despite there is no control methodology design, the zig-zag manoeuvre is in closed loop as the actual value of $\psi(t)$ is measured and until it reaches a determined value the rudder does not change from starboard to port or viceversa (see 2^{nd}, 3^{rd}, 4th, and 5th phase points where the rudder angle of deflection is changed in Fig. 19.2). The zig-zag manoeuvre should be completed with at least five phases.

The initial conditions, $x_0 = [u_{nom}\ 0\ 0\ 0\ 0\ 0\ 0\ 0\ 0]^T$, substitute the states on the first approximated linear system's matrices, $A[x_0]$, $B[x_0]$ and, subsequently, the iteration technique results in a sequence of linear time varying (LTV) systems where 20 iterations were needed to approach the original nonlinear system.

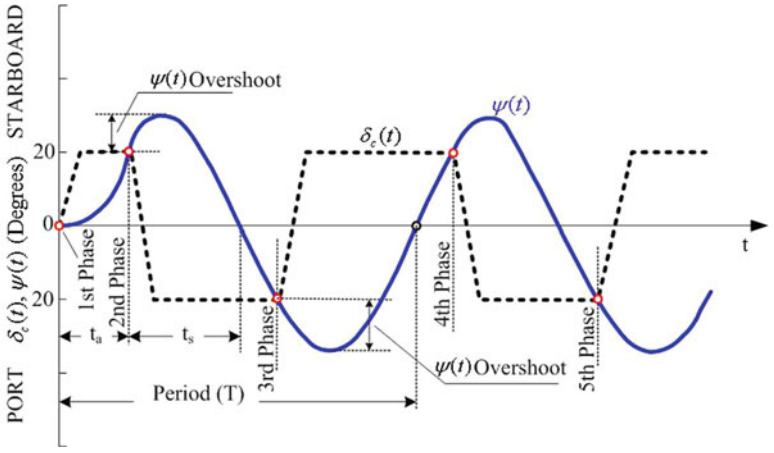

Fig. 19.2 20–20° zig-zag manoeuvre phases and corresponding values of the heading angle $\psi(t)$ represented in *solid blue line* and the rudder's deflection $\delta_c(t)$ represented by *dashed black line*

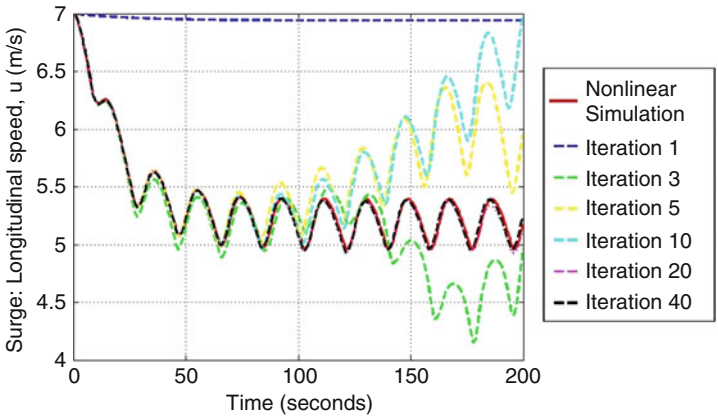

Fig. 19.3 Convergence of $u(t)$ on a 20–20° zig-zag manoeuvre. *Red line* represents the movement of the original nonlinear system. The *pink line* represents the 20th iterated LTV approximation and the *black line* is the 40th iteration

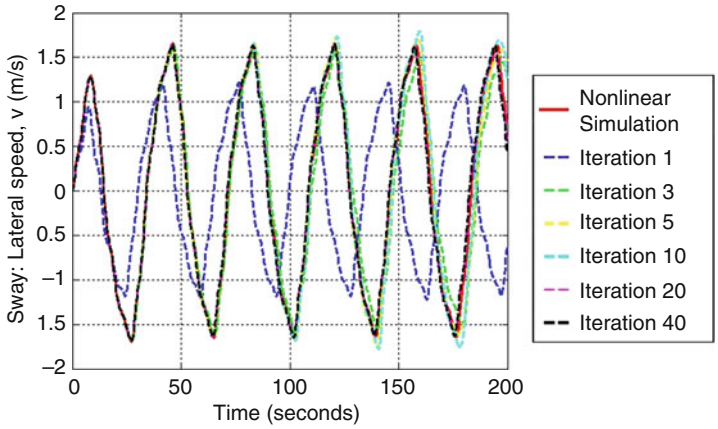

Fig. 19.4 Convergence of $v(t)$ on a 20–20° zig-zag manoeuvre. *Red line* represents the movement of the original nonlinear system. The *pink line* represents the 20th iterated LTV approximation and the *black line* is the 40th iteration

Figures 19.3, 19.4, 19.5, 19.6 show the time history of various states during the 20–20° zig zag manoeuvre for some of the iterations and as well the evolution in time of the states in the nonlinear case (red line), this is done in order to illustrate the convergence of this method. It is shown how the 20th solution is a good representation of the nonlinear system solution, also the 40th solution is shown in order to demonstrate the convergence of the states. After the 20th iterated solution, $x^{(20)}(t)$, the convergence to the nonlinear solution $x(t)$ is clear and also it is shown how the consequent iterations, i.e., $x^{(40)}(t)$ show little variation with respect to it, this is, $\left\| x^{(40)}(t) - x^{(20)}(t) \right\| \to 0$ when $t \to \infty$.

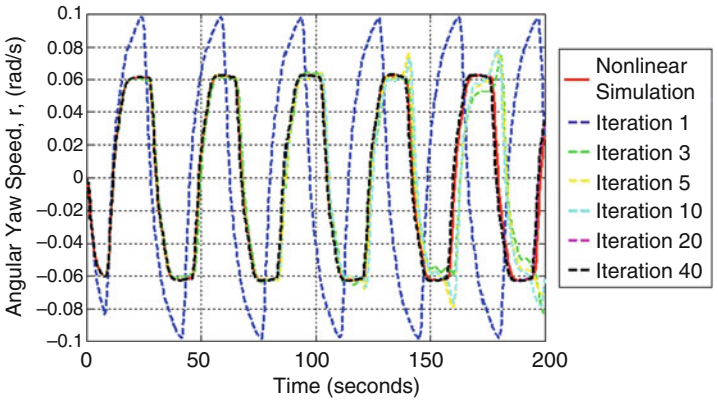

Fig. 19.5 Convergence of $r(t)$ on a 20–20° zig-zag manoeuvre. *Red line* represents the movement of the original nonlinear system. The *pink line* represents the 20th iterated LTV approximation and the *black line* is the 40th iteration

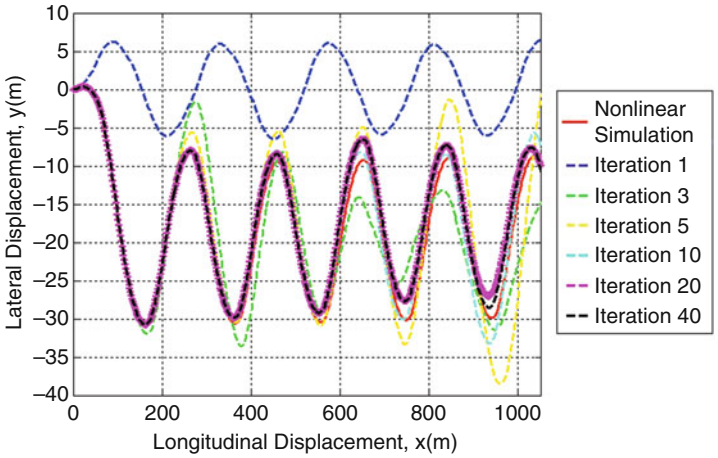

Fig. 19.6 Vessel's position on the plane (x_n, y_n) along this manoeuvre

Figure 19.6 shows the vessel's position on the plane (x_n, y_n) along this manoeuvre; it is clear to see how the 20th iteration (pink line) gives an accurate approximation to the behavior of the original nonlinear system (red line). From the previous figures, it is clear to conclude that when the iteration technique is implemented, after a short number of iterations, the original nonlinear expression for the vessel's dynamics gets a good representation by the last of the linear approximations, 20 in this particular case.

The second simulation scenario is a course keeping manoeuvre of $\psi_d = 20°$ degrees that will validate and test the iterative controller design implemented following the steps given in Sect. 19.1.5. The manoeuvre should be completed satisfying the objectives stated in Sect. 19.1.3.

The vessel's model defined in Sect. 19.1.2 is rearranged on the form $\dot{x} = A(x)x(t) + B(x)u_c(t,\theta_c)$ where $x(t,\theta_c) = [u\ v\ p\ r\check{z}\ \phi\ \psi\ \delta\ x_n\ y_n]^T$ and the control vector is $u_c(t,\theta_c) = [\delta_c\ T]^T$. The initial conditions are taken from [23] as: $x_0 = [u_{nom}\ 0\ 0\ 0\ \ 0\ 0\ 0\ 0\ 0]^T$.

In previous results for the 20° course-keeping manoeuvre case, a PID controller (19.18) was applied and a high value of T_i was obtained by the optimization method. As explained in Sect. 19.1.3, the optimization technique applied for the tuning, in an attempt to reduce the oscillation caused by the integral windup problem, provides a high value of T_i and therefore reduces to the minimum the influence of the integral term. This suggest that the contribution of the integral term k_i/s in the PID controller (19.18) (being $k_i = k_p/Ti$) can be neglected. For all of this reasons, a lead compensation controller (19.19) without integral action is used instead. The constrains of the controller parameters were set to $lb = 0$ and $ub = \infty$, in order to avoid unstable controller behavior. The lead compensation controller initial parameters were selected taking into account that this type of controller must have a dominant zero near to the s-plane origin.

Figures 19.7 and 19.8 show the results for a course keeping 20° (0.349 rad) manoeuvre for each iteration "i". After the 5th iteration, the algorithm converges,

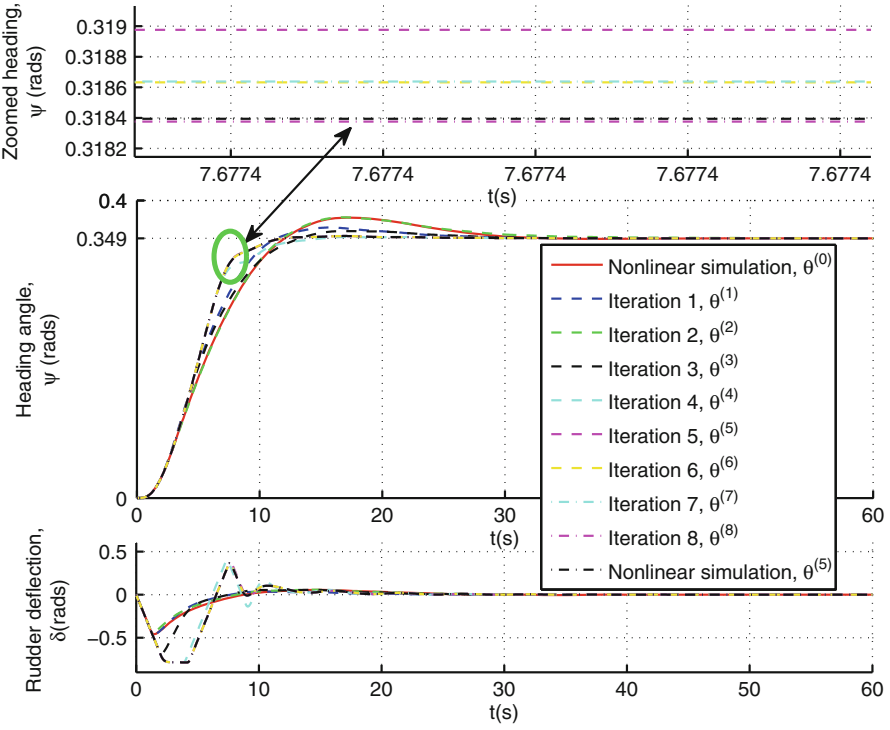

Fig. 19.7 Convergence results of the controlled variable $\psi(t)$ and the actuator's variable, the rudder deflection, $\delta(t)$, for the coastal patrol vessel on a course keeping 20° manoeuvre

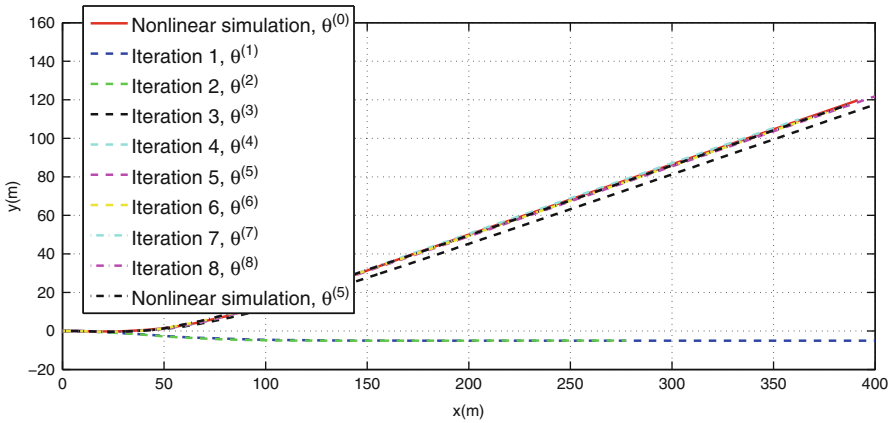

Fig. 19.8 Position convergence results for the coastal patrol vessel for a course keeping 20° manoeuvre

the corresponding control parameters θ_c and the heading response $\psi(t)$ remain almost unchanged. The zoom made for the yaw variable $\psi(t)$ on the top part of Fig. 19.7 for the iterations 5–8 shows that the difference between iterations i and $i-1$, is within the order of $\frac{1}{100}$ of degree, illustrating the convergence properties of the presented algorithm. Figures 19.7 and 19.8 clearly show an accurate approximation for the 5th iteration to the nonlinear model (compare iteration 5 with the simulated data generated with the original nonlinear system and the controller parameters $\theta_c^{(5)}$). At this stage, (i=5), the overshoot is reduced in the heading response $\psi(t)$ and the settling time is reduced with respect to the previous iterations. Furthermore, the steady state error ($e(t) = \psi_d - \psi(t)$) converges to zero after only 30 sec. The bottom part of Fig. 19.7 shows the actuator's displacement, $\delta(t)$, which represents the actual value of the rudder's angle of deflection. There is saturation present in the actuator for the fifth iteration, but with the selected lead compensation controller the windup problem is avoided obtaining a response without overshoot. The lead compensation controller is a simpler solution that an anti-windup scheme for the PID controller.

19.3 Transdisciplinary Discussion Into the Unified Framework

The work proposed in this chapter has a direct significant impact on the design and control of systems for transport over water since we propose a control algorithm that combines two control methodologies in order to implement a navigation system. The results given in the previous section for a course keeping manoeuvre provides a good performance since the proposed algorithm take into account an accurate

representation of the dynamics of the non linear manoeuvring model object of study of this work including all the non linearities. Furthermore, the presented results for the heading response: the elimination of the existing overshoot, the reduction of the settling time and the elimination of the steady state error contribute to the safety in the navigation in restricted waters and also to the energy saving due to the elimination of the response oscillations. In restricted waters and for collision avoidance, the course-changing manoeuvre should have a clear start, in order to warn nearby ships of the intention of the manoeuvre and, for that reason, that manoeuvre should preferably be completed with no overshoot and this aim is managed with the algorithm proposed in this work. For all of these reasons, this work contribute to facilitate the transport over water that constitutes one of the layers of the unified framework.

The other layers of the unified framework treated in this book consist of the water flowing through its infrastructure and the interactions between the water flow and the transport flow. The work proposed in this chapter does not cover the transport of water directly but the application of the iteration technique to approximate the dynamics of non linear manoeuvring models could be applied to water systems, in the same way as in this chapter, since the iteration technique allows an accurate representation of the non linear dynamics with its consequently benefits. Moreover, in the case of a combined framework in which is considered the interaction between the two layers, the iteration technique could be applied as well to approximate a model that would include the interaction between the transport system dynamics and the water dynamics. Then, considering an accurate model with the interactions between the two systems it would improve the performance of the designed controller.

19.4 Open Topics

In the literature there are variety of marine vessel models of motion dynamics that provides an adequate representation of the dynamics for different types of operational conditions [25]. These operational conditions are related to the speed of the vessel, the state of the environment: waves, current and wind, the water depth, the mass distribution, and the vessel condition (intact or damaged). In case that the operational conditions change the structure of the model and the parameters must change. In spite of this, there is a lack in the literature of models than consider the interaction between the water systems and the transport systems. This is still an open topic than in case of being addressed in an accurate way it would provide the possibility of a the design of an appropriate control system. This would be interesting as well in the case of coordinated control of several vehicles where one of the vehicles is the leader and the rest of the vehicles must follow the leader, then, what would be the effect of the interaction among the several vehicles and the water systems.

19.5 Conclusions and Future Research

In this chapter, the authors proposed a control strategy based on an optimized lead compensation controller methodology combined with an iteration technique based on LTV approximations to approach the nonlinear dynamics of a ship. It has been discussed the benefits that the proposed control strategy provides to the transport systems over water. The theory here presented has been implemented in Matlab/Simulink and applied to the particular example of a full scale coastal patrol vessel under two different scenarios: firstly, a standard 20–20° zig-zag manoeuvre is considered in order to show the convergence of the iteration methodology presented in the theory and secondly, a 20° course-keeping manoeuvre is presented to show the accuracy of the tracking capabilities of the designed controller when applied to the last of the iterated LTV systems.

On the first case, the results show that the approximation to the vessel's nonlinear dynamical equations in the 20–20° zig-zag manoeuvre is a good approximation after only a few number of iterations, 20 in this case. By generating this sequence of LTV equations that approximate the original nonlinear dynamics, now linear control techniques can be applied to the last of these iterations (20th). This is a good advantage since linear control methods are usually simpler and computationally cheaper to implement.

On the other hand, for the 20° course-keeping manoeuvre, the proposed control strategy and reference tracking methodology is tested. A high value of T_i obtained with the proposed control strategy in preliminary results, indicates that the rudder's saturation provokes the integral windup problem when PID control is applied. Therefore, it is advisable to use a controller without integral term such as the lead compensation controller. The presented results with the lead compensation controller meet the stated objectives in the heading response: the elimination of the existing overshoot, the reduction of the settling time and the elimination of the steady state error. In addition to this, the lead compensation controller constitutes a simpler solution than an anti-windup scheme for a PID controller.

The authors are currently investigating further possibilities within this area: the control strategy here proposed will be extended to the multivariable control case in order to develop a trajectory control methodology.

Acknowledgements This chapter has been partially supported by the Spanish Ministry of Defense, matching program-1003211003100 and by the MINECO:DPI2011-27990 with FEDER funds.

References

1. Astrom KJ, Hagglund T. Advanced PID control. ISA—the instrumentation, systems, and automation society. Research Triangle Park, NC, 2006.
2. Bateman A, Hull, J, Lin Z. A backstepping-based low-and-high gain design for marine vehicles. Int J Robust Nonlinear Control. 2009;19(4):480–93.

3. Bech MI, Smith LW. Analogue simulation of ship maneuvres. Hy 14, Hydro-Og and Aerodynamics Laboratory, 1969.
4. Bertram V. Practical ship hydrodynamics. 2nd edn. Oxford: Butterworth-Heinemann; 2012.
5. Bhattacharyya SK, Rajesh G, Gupta DK. Fuzzy autopilot for ship maneuvering. Int Shipbuild Prog. 2011;58(4):191–218.
6. Blanke M. Ship Propulsion Losses Related to Automated Steeering and Prime Mover Control. Ph.D. Thesis, The University of Denmark Lyngby, 1981.
7. Brayton RK. Hachtel GD. A new algorithm for statistical circuit design based on quasi-newton methods and function splitting. IEEE Trans Circuits Syst. 1979;CAS-26(9):784–94.
8. Cimen T, Banks SP. Nonlinear optimal tracking control with application to super-tankers for autopilot design. Automatica 2004;40(11):1845–63.
9. Fossen TI. High performance ship autopilot with wave filter. In: Proceedings of the 10th international ship control systems symposium, 1993. p. 2271–85.
10. Fossen TI, Perez T. Marine systems simulator (mss). http://www.marinecontrol.org/, 2004.
11. Fossen TI. A survey on nonlinear ship control: from theory to practice. In: Preprints of the 5th IFAC conference on maneuvering and control of marine craft. Kidlington, UK, 2000. p. 1–16.
12. Hernandez CN, Banks SP, Aldeen M. Observer design for nonlinear systems using linear approximations. IMA J Math Control Inf. 2003;20(3):359–70.
13. Hu SS, Yang PH, Juang JY, Chang BC. Robust nonlinear ship course-keeping control by h i/o linearization and -synthesis. Int J Robust Nonlinear Control. 2003;13(1):55–70.
14. Kallstrom CG. Autopilot and track-keeping algorithms for high-speed craft. Control Eng Pract. 2000;8(2):185–190.
15. Kallstrom CG, Astrom KJ, Thorell NE, Eriksson J, Sten L. Adaptive autopilots for tankers. Automatica. 1979;15(3):241–54.
16. Lewis EV. Principles of naval arquitecture. The society of naval architects and marine engineers, 1989.
17. McGookin EW, Smith DJM, Li Y, Fossen TI. Ship steering control system optimisation using genetic algorithms. Control Eng Pract. 2000;8(4):429–43.
18. Morawski L, Pomiriski J. Ship track-keeping experiments with a physical tanker model. Control Eng Pract. 1998;6(6):763-9.
19. Moreira L, Fossen TI, Soares CG. Path following control system for a tanker ship model. Ocean Eng. 2007;34(14–15):2074–85.
20. Nguyen VC, Le TO, Do TBS, Nguyen MM, Nguyen TM, Dinh TKT, Man TN. Study on an effective adaptive ship autopilot. In: The 8th IEEE International Workshop on Advanced motion control, AMC '04. march 2004. p. 707–10.
21. Norrbin NH. On the design and analysis of the zig-zag test on base of quasi linear frequency response. Technical Report 104-3, The Swedish State Shipbuilding Experimental Tank (SSPA), 1963.
22. Norrbin NH. Theory and observation on the use of a mathematical model for ship manoeuvring in deep and confined waters. In: 8th Symposium on Naval Hydrodynamics, USA, 1970.
23. Pérez T. Ship Motion control Course keeping and roll Stabilisation using rudder and fins. London: Springer; 2005.
24. Perez T, Ross A, Fossen TI. A 4-dof simulink model of a coastal patrol vessel for manoeuvering in waves. In: Proceedings of the conference on manoeuvring and control of marine craft (MCMC 2006), Lisbon, 2006.
25. Perez T, Soerensen AJ, Blanke M. Marine vessel models in changing operational conditions—a tutorial. In: Proceedings of the 16th IFAC symposium on system identification (SYSID 2006). Netherlands: Amsterdam; 2006. p. 6.
26. Reid RE, Mears BC. Design of the steering controlled of a supertanker using linear quadratic control theory: a feasibility study. IEEE Trans Autom Control. 1982;AC-27(4):940–2.
27. Revestido E, Moyano E, Velasco FJ, López E. Tuning heading controllers of an autonomous in-scale fast-ferry model. In: Maritime Transport IV, 2009.
28. Samanta B, Nataraj C. Design of intelligent ship autopilots using particle swarm optimization. In: IEEE Swarm intelligence symposium, 2008 SIS. 2008. p. 1–7.

29. Tomas-Rodriguez M, Banks SP. Linear, Time-varying approximations to nonlinear dynamical systems: with applications in control and optimization. Lecture notes in control and information sciences. vol. 400. London: Springer; 2010.
30. Tomas-Rodriguez M, Banks SP. Linear approximations to nonlinear dynamical systems with applications to stability and spectral theory. IMA J Math Control Inf. 2003;20(1):89–103.
31. Tomas-Rodriguez M, Hernande CN, Banks SP. Parametric approach to optimal nonlinear control problem using orthogonal expansions. In: Proceedings of the IFAC World Congress, vol. 16. Prague, Czech Republic, 2005. p. 556–61.
32. van Amerongen J. Adaptive steering of ships: a model- reference approach to improved manoeuvring and economical course keeping. Ph.D. Thesis, Delft University of Technology, Delft, The Netherlands, 1982.
33. van Amerongen J. Adaptive steering of ships-a model reference approach. Automatica. 1984;20(1):3–14.
34. Witkowska A, Smierzchalski R. Nonlinear backstepping ship course controller. Int J Autom Comput. 2009;6(3):277–84.

Chapter 20
Performance Evaluation of an Inland Pusher

M. Godjevac and M. Drijver

Abstract In order to meet the future exhaust gas emission standards on European inland waterways, ship owners are facing challenges when selecting the optimal power configuration and/or retrofit option. While there are many variations of power configurations for an inland vessel, a typical ship owner is not certain which of those possibilities is the best one. To help tackling these challenges, a comprehensive study has been carried out where various power configurations have been evaluated against the operational profile of an inland pusher on river Rhine. The operational profile was obtained by measuring the fuel rack position and ship speed during the period of 6 months. Comparing the transport efficiency (i.e., fuel consumed versus cargo transported) with the recorded water levels it was shown that the transport efficiency doubles in deep water periods. Furthermore, it was argued that a more flexible power configuration, with an additional shaft line, could contribute to the total efficiency. Based on the operational profile, seven alternative power configurations have been selected. They include: diesel-direct, diesel-electric, gas engine-electric, and a combination of diesel-direct and diesel-electric. Afterwards, an estimate of the total exhaust emissions during one typical voyage was made for all alternative configurations using dynamic models. For the investigated vessel, the diesel direct configuration still is the most efficient configuration regarding the energy consumption. However, regarding NOx and PM the performance of power configurations based on gas engines is superior. As an alternative for NOx reduction, the effect of SCR installation was also considered which appears to be practical solution for retrofitting as well.

M. Godjevac (✉)
Delft University of Technology, Delft, The Netherlands
e-mail: M.Godjevac@tudelft.nl

M. Drijver
CIG Maritime Technology, Groningen, The Netherlands
e-mail: drijvermichiel@gmail.com

C. Ocampo-Martinez, R.R. Negenborn (eds.), *Transport of Water versus Transport over Water*, Operations Research/Computer Science Interfaces Series 58,
DOI 10.1007/978-3-319-16133-4_20

20.1 Introduction

Merchant vessels on European inland waterways are typically around 20 years old and owned by small (family) companies. At the same time, exhaust emission regulations on European inland waterways are becoming more stringent. For a ship owner, this situation raises multiple questions regarding the possible power configurations of inland ships and how to meet the future regulations. In order to tackle this issue, a research project under the title "Modernization of Vessels of Inland Waterway Freight Transport"? (MoVeIT) is running within the European seventh framework program. This chapter presents some outcomes of the MoVeIt project, as well as the investigation presented in [5], and its main focus point is the optimization of the ship's drive and power system in such a way that it is matched to the conditions that the ship will face throughout its life. Questions related to the selection of the fuel type (diesel or natural gas), power transmission (direct or electric), and power generation (number and sizes of engines) are answered in this study with respect to their related exhaust emissions and fuel consumptions. An inland pusher operating on the river Rhine is selected as the case study for this investigation. Firstly, the operational profile measurements are done during 6 months sailing period. Also, emission test cycle measurements are done on board of the vessel. Secondly, a selection of alternative power configurations is made, including: diesel-direct, diesel-electric, gas-electric, and hybrid power configurations. Thirdly, dynamic models of all power configurations are created in the Matlab/Simulink environment. Finally, combining the models with the results of the measurements, the total emissions and fuel consumptions are calculated for each power configuration for one typical journey. Figure 20.1 depicts the process that has been used in this investigation.

In total 2 sets of measurements are used in this study and their results are presented in this document. Further, 10 dynamic models of different power configurations are created to estimate their exhaust emissions (NO_x, SO_x, CO_x, HC, PM). For diesel direct power configurations, a selective catalyst reduction (SCR) is an option to reduce the NO_x emission. The effect of an SCR installation is also considered in this chapter and its urea consumption is calculated as well.

While the title of this book is "Transport of Water Versus Transport Over Water", the focus of this chapter is rather on the transport over water. Here the performance of an inland pusher is analyzed in terms of its exhaust emissions and

Fig. 20.1 Schematic illustration of the research process

Fig. 20.2 Veerhaven X in four barges configuration

fuel consumption during operation. However, the fuel consumption and transport efficiency are closely related to the conditions on the river, namely to the water depth, and the scope of this chapter is actually broader than just the transport over water. As shown in this chapter, the transport efficiency drops significantly during periods of low water due to part load conditions in which the pusher is operating. If the level of water could be somehow increased during periods of low water, for example by the transport of water, then the transport over water would be improved as well, and this illustrates how the transport over water may be affected by the transport of water.

An inland pusher called Veerhaven X (see Fig. 20.2) is selected for the case study. This is one of the biggest pushers operating on the river Rhine and it is considered as state of the art amongst inland pushers. The ship operates mostly between Rotterdam and Duisburg pushing the barges with coal and iron upstream from Rotterdam to Duisburg in 4 or 6 barges configuration, depending on the water level and cargo loaded. After leaving its cargo, the ship picks up the empty barges and goes back downstream to Rotterdam. A typical trip takes about 40 h where an upstream voyage is about 24 h and a downstream voyage is about 12 h.

Figure 20.3 shows the power configuration of Veerhaven X. The ship is equipped with three identical mechanically driven diesel direct propulsion trains and four generator sets for auxiliary power. The total installed propulsion power is 4,080 kW. Each propulsion train is equipped with a fixed pitch propeller with 5 blades and 2.05 m diameter.

This chapter is structured according to the research process illustrated in Fig. 20.1. The results of the long-term measurements conducted on-board of Veerhaven X are presented in Sect. 20.2. These measurements define the operational profile of Veerhaven X. Section 20.2 also presents the transport efficiency of the vessel during the period of the operational profile measurements and in Sect. 20.3 the results of exhaust emission measurements are given. In Sect. 20.4,

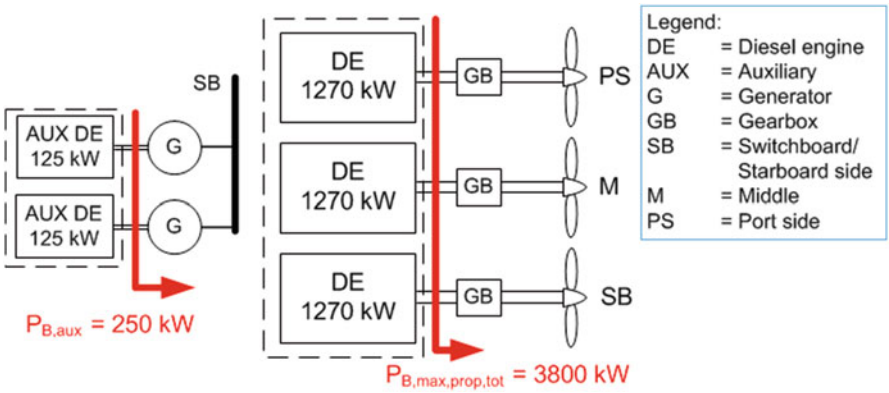

Fig. 20.3 Power configuration of Veerhaven X

alternative power configurations are defined using the operational profile measurements from Sect. 20.2. Subsequently, dynamic models of the selected alternative power configurations are described in Sect. 20.5. The results of the exhaust emission measurements from Sect. 20.3 are then used to calibrate the models in Sect. 20.5. After which the resulting emissions and fuel consumptions from the models of the alternative power configurations are presented in Sect. 20.6. The analysis of the results is given in Sect. 20.7 and the conclusions are presented in Sect. 20.8.

20.2 Operational Profile and Transport Efficiency

To get more insight in the long term performance of the ship and its fuel consumption, the operation of the ship is observed during 6 months by measuring the following parameters:

- Fuel rack position of the starboard, middle, and portside engine
- GPS position and speed over ground

In order to get the operational profile of the vessel (i.e., power versus time) it is necessary to calibrate and convert the measurements of the fuel rack position to the power consumption. The fuel rack position is first converted to the fuel flow, which is then converted to the engine power. Figure 20.4 shows the operational profile of the ship and water level recorded during the measurements. According to its mission profile, the operational profile of Veerhaven X is divided in three operational modes: upstream, downstream, and manoeuvring, which take 59, 31, and 10 % time of the total operational profile, respectively.

Besides the operational profile measurements, the logbook of the ship is used in this study to analyse the transport efficiency. The logbook contains the records of the total amount of cargo transported and total fuel consumed for each journey.

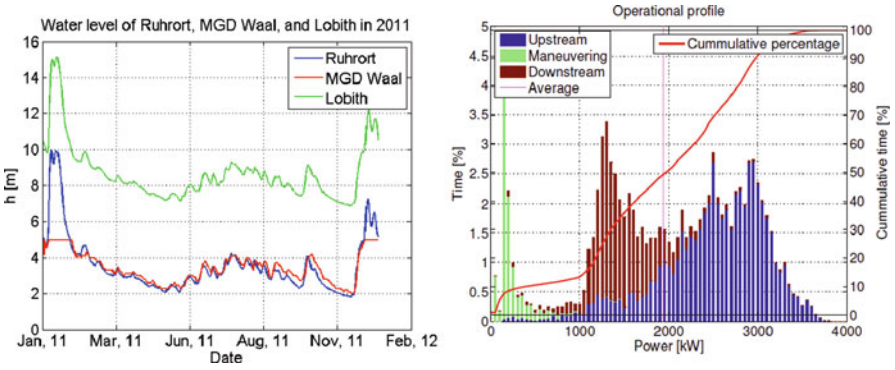

Fig. 20.4 Rhine water levels (*left*), and operational profile of Veerhaven X during 6 months (*right*)

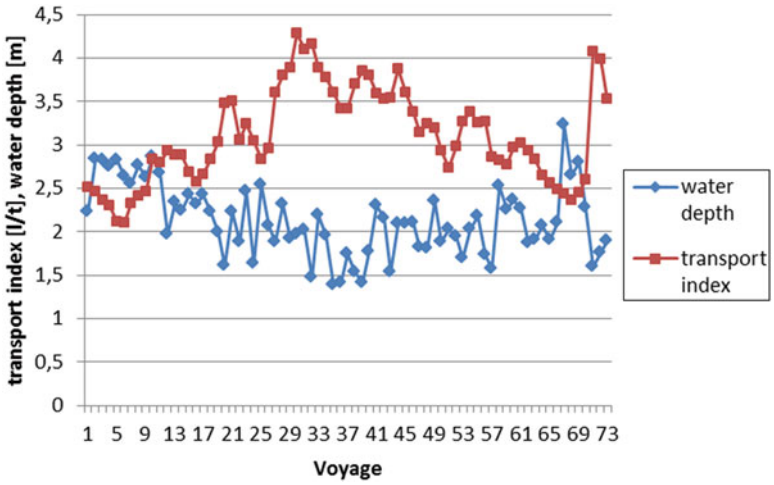

Fig. 20.5 A comparison of the recorded fuel consumptions and cargo transported (l/t) with the water level at river Rhine during 73 voyages of Veerhaven X

By cross-referencing the logbook data with the recorded water levels it is possible to get a link between the water level and transport efficiency. Figure 20.5 shows the transport efficiency together with the recorded water levels, in which the transport efficiency is given as the transport index in terms of the liters of fuel consumed per ton of cargo transported (l/t). Thus, the low values of l/t indicate low fuel consumption and higher efficiency. From Fig. 20.5, it is noticeable how transport efficiency follows the oscillation in water levels. In fact, the transport efficiency can oscillate by a factor two during the recorded 73 journeys.

Based on the operational profile measurements it is possible to further differentiate between the journeys made in four or six barges configuration. Figure 20.6 shows the amount of cargo transported per voyage, in four and six barges configuration,

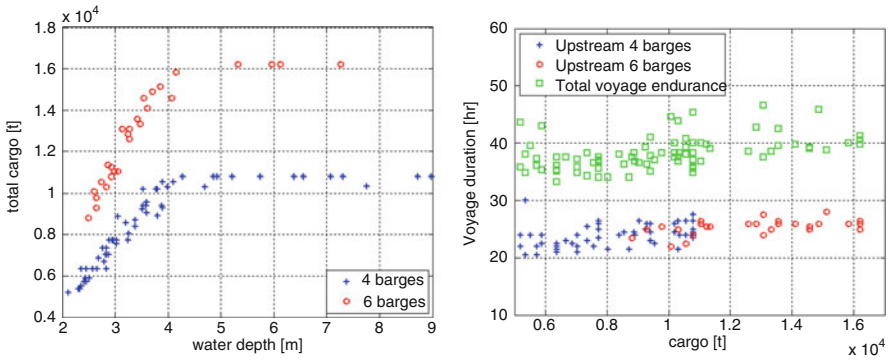

Fig. 20.6 Amount of cargo transported in four and six barges configurations (*left*), and voyage duration (*right*)

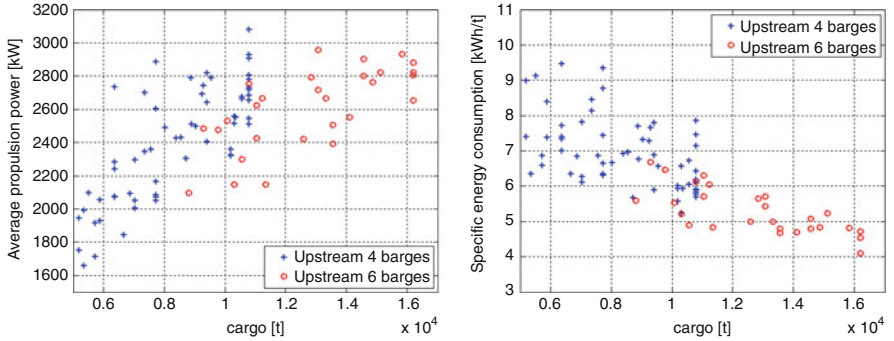

Fig. 20.7 Average power per journey (*left*) and average specific power (*right*)

and the duration of each voyage. Note that the difference in voyage duration seen in Fig. 20.6 (right) was mostly caused by the waiting time and not by the speed variance.

Further, it is possible to calculate the average power during each voyage. Figure 20.7 shows the average power per voyage and specific average power (kWh/t) per voyage as a function of the cargo transported. In Fig. 20.7, it is noticeable that the voyages with more cargo require less specific average power, i.e., they are more efficient. In previous figures it was shown how the duration of the voyages was more or less constant. Since the distance for each voyage is the same, it is possible to conclude that the speed over ground is similar for all investigated journeys. In fact, the only variable in investigated journeys is the cargo transported. Since water levels dictate the maximal draft of the barges, it is possible to relate the water levels to the cargo transported, i.e., barges are always loaded according to the maximal allowable draft. Subsequently, low water levels will cause low load conditions which will cause an engine to operate in a less efficient region of the operating envelope,

i.e., engine load will be less than 50 % (see Fig. 20.13). Besides this, low water depth may cause an increase in hydrodynamic resistance of the ship due to the shallow water effect, which will deteriorate the transport efficiency even further.

20.3 Operational Profile and Transport Efficiency

Besides the operational profile measurements presented in Sect. 20.2, a set of exhaust emission measurements is used in this study as well. The results of the exhaust emission measurements are presented in [8] and they are analyzed in this section. A standard emission measurement test cycle is used (E3 test cycle) to measure the exhaust emissions of the investigated vessel. This is a standard test cycle that applies to propeller law operated main engines and is required by international standards for exhaust emission certification/approval (ISO 8178). Also, legislative requirements are given in weighted cycle average values. As given in Table 20.1, the test cycle consists of four test points where emissions are recorded. For each of the points there is a weight factor and final emission values are weighted average values during the test cycle. Table 20.1 shows the E3 test cycle, with runs at 100, 75, 50, and 25 % of the nominal engine power, and the associated weight factors (WF). In Table 20.1, the engine speed follows from the propeller law and is a function of engine power P_B relative to nominal engine power P_{B0} and nominal engine speed n_{e0}:

$$n_e = n_{e0} \left(\frac{P_B}{P_{B0}} \right)^{1/3}. \tag{20.1}$$

The emission measurements are taken at the steady engine load and the results show average values. The measured emission components are O_2, CO, CO_2, NO as NO_x, HC as C_3H_8, and PM. The emission measurements are given for the dry exhaust which means that the emission measurements represent the values of a fully dried sample. The exhaust emissions are measured in ppmv and mg/m^3 values. Since legislative limitations are related to the specific power, it is necessary to convert the measurements to kg/h and g/kWh values. The original report in [8] gives emission values in terms of g/kWh as well, but it does not explain the conversion method. The conversion of exhaust emissions from ppmv to g/kWh is explained in [10] and it is named as NLDA method in [5]. Table 20.2 shows weighted cycle average values of Veerhaven X according to the methods described in [8] and [10], respectively named as SGS and NLDA calculation method. As can be seen,

Table 20.1 E3 emission measurement test cycle

Run	1	2	3	4
rpm	100 %	91 %	80 %	63 %
Power	100 %	75 %	50 %	25 %
WF	0.2	0.5	0.15	0.15

Table 20.2 Weighted cycle averages of SGS method, NLDA method, and CCNR2 emission regulations

Emission	SGS	NLDA	CCNR2
CO [g/kWh]	0.51	0.54	3.5
HC [g/kWh]	0.78	0.78	1.0
SO_2 [g/kWh]	0.64	0.67	–
NO_x [g/kWh]	8.03	8.48	8.5
PM	0.08	0.09	0.2

Table 20.3 Specific fuel consumption versus engine power for SGS, NLDA, and test bed records

Engine power [kW]	263	591	922	1226
sfc SGS and NLDA [g/kWh]	229	202	196	196
sfc test bed records [g/kWh]	239	208	198	196
Difference [%]	4.2	2.9	1.1	0

the emission values from both methods are comparable. Table 20.2 also gives an overview of the allowable exhaust emissions on Rhine as defined by the Central Commission for the Navigation on Rhine (CCNR2) from which it follows that the emissions of Veerhaven X are within the allowed limits.

Regarding the specific fuel consumption (sfc), the manufacturer gives the sfc values for four working points. Table 20.3 shows a comparison of the sfc values measured by SGS and by the manufacturer. For more details regarding the exhaust emission formation and related fuel consumptions the reader can take a look into [10] and [9].

Results shown in Table 20.3 indicate low discrepancy between the specific fuel consumption presented in [8] and the specific fuel consumption measured by the manufacturer. Since the results from Tables 20.2 and 20.3 are used in Sect. 20.5 to calibrate the dynamic models of different power configurations, it is beneficial that the results are cross checked with the manufacturer data. Furthermore, in Table 20.2 it can be observed that the NLDA conversion method is in line with the results presented in [8].

20.4 Operational Profile and Transport Efficiency

While in previous sections contain information about the operational profile of Veerhaven X, the goal of this section is to define the alternative power configurations which will be dynamically modelled in order to estimate their total emissions and efficiencies. The alternative configurations will be defined according to the operational profile of Veerhaven X and they include different types of fuel, power arrangement, and transmission options. Regarding the fuel types, alternative configurations will investigate engines which use diesel fuel and natural gas. Regarding the power arrangements, alternative configurations will investigate power configurations with different engine sizes and number of engines, for example

2 smaller engines versus one large engine. Regarding the transmission options, alternative configurations will include the diesel-direct, diesel-electric, and hybrid (i.e., a combination of diesel direct and diesel electric) power transmission.

20.4.1 Benchmark Power Configuration

Before defining the alternative power configurations, the benchmark power configuration will be defined first. The benchmark power configuration is based on the power configuration of Veerhaven X but with somewhat altered maximum power. The total power of the benchmark configuration is based on the operational profile shown in Fig. 20.4, where it is noticeable that the maximum recorded total power at the shafts never exceeds 3,800 kW. Also, the recorded auxiliary power never exceeds 250 kW. In order to optimize the benchmark configuration, the benchmark power configuration will have 3,800 kW maximum power delivered at three propeller shafts, and the maximal auxiliary power 250 kW.

20.4.2 Alternative Power Configurations

Because of varying water levels, it is argued that a configuration with four propellers might be more beneficial for the pusher. For draught conditions, it is estimated that the efficiency of four propellers, with a smaller diameter, would be much higher than the efficiency of three propellers with a larger diameter. The hydrodynamic performance of the configuration with four propellers was investigated in [2] and it was decided that all alternative power configurations will have four propellers. Figure 20.8 shows the aft ship arrangement for all alternative power configurations where propeller diameter is 1.80 m.

In order to make a fair comparison amongst different power configurations, it is necessary to ensure that the total power delivered to the shaft is the same for all power configurations. Since diesel electric and gas electric power configurations include additional conversions of energy and additional components, the total installed power for these configurations will be larger in comparison with the diesel direct configuration. Figure 20.9 shows an example of a diesel electric power configuration with undefined number of engines and their sizes. The exact number of engines will be defined later.

For electric configurations, the power delivered to the propeller P_p is a function of the total engine brake power P_B and the efficiencies of the components between the diesel engine and the propeller:

$$P_p = P_B \cdot \eta_{gen} \cdot \eta_{sw} \cdot \eta_{TF} \cdot \eta_{FC} \cdot \eta_{EM} \cdot \eta_{TRM}, \tag{20.2}$$

Fig. 20.8 Aft ship arrangement of alternative power configurations

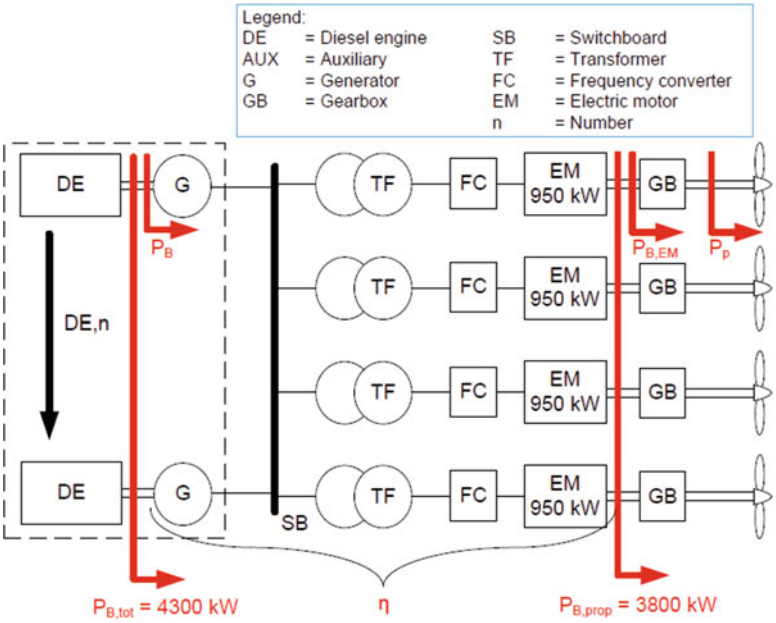

Fig. 20.9 General illustration of diesel-electric power configurations

Table 20.4 Total installed power for: diesel-direct propulsion (DDP), diesel-electric propulsion (DEP), gas-electric propulsion (GEP), hybrid propulsion (HP), and benchmark power configuration

Power [kW]	DDP	DEP/GEP	HP	Benchmark
$P_{B,max,tot,prop}$	3,800	4,175	3,800 to 4,175	3,800
$P_{B,max,tot,aux}$	2*125	125	2*125 to 125	2*125
$P_{B,max,tot}$	4,050	4,300	4,050 to 4,300	40,500

where the efficiencies of the components are defined as:

- Generator efficiency $\eta_{gen} = 0.97$ and electric motor efficiency $\eta_{EM} = 0.97$ as in [6]
- Switchboard efficiency $\eta_{SW} = 0.999$, transformer efficiency $\eta_{TF} = 0.997$, and frequency converter efficiency $\eta_{FC} = 0.97$ as in [1]

In general, electrical power configurations are more suitable for ships with high auxiliary power demands, for example see [3], because of their flexibility of power generation and distribution. As a consequence they need smaller auxiliary engines, and therefore it will be assumed that only one half of the total auxiliary power is needed for the alternative electric power configurations. The other half will be added to the total power installed (PB,tot). Table 20.4 shows the summary of the total maximum installed power for different power configurations.

Since power configurations which use natural gas currently run only in electric power configuration, the total installed power for gas-electric power configurations (GEP) will be the same as for the diesel-electric power configurations (DEP). The hybrid power configuration (HP) will be a combination of diesel-direct and diesel-electric power configuration, and the total installed power for hybrid power configurations could be between the total power needed for diesel-direct power configurations and the total power needed for diesel-electric power configurations. Table 20.5 shows possible alternative configurations with diesel-direct (DDP), DEP and GEP, and HP. In the table, the candidates are given for a combination of maximum engine brake power. The number of different engine sizes ranges from one to three different sizes and the total number of engines installed ranges from one to five engines. In the columns, the number before the asterisk sign, "*", is the number of engines and the number after the asterisk sign is the maximum engine brake power in kW.

20.4.3 Selection of Alternative Power Configurations

The selection of the alternative configurations from the candidate alternatives is based on:

Table 20.5 Candidate alternative configurations

Nr. of engine sizes	Nr. of engines	DDP [kW]	DEP/GEP [kW]	HP [kW]	
				DDP	DEP
1	1	3,800	4,300	–	–
	2	1,900	2,150	2,050	2,050
	3	1,267	1,433	1,380	2*1,380
	4	950	1,075	2*1,020	2*1,020
	5	–	860	2*825	3*825
2	2	3,000+800	1,800+2,500	1,900	2,200
	3	2*950+1,900	2*800+2,700	1,900	2*1,100
	4	2*800+2*1,100	3*800+1,900	2*950	2*1,100
	5	–	4*800+1,100	2*800	3*850
3	3	2,000+1,000+800	2,500+1,000+800	1,900	1,900+1,800
	4	800+900+2*1,050	800+1,000+2*1,250	2*950	900+1,300

- The time percentage that engines run in the optimal fuel consumption region throughout the operational profile.
- Equal load share is assumed amongst the engines.

The optimal fuel consumption region was assumed to be between 50 and 85 % of engine power and Table 20.6 presents the calculated time fractions of the candidate configurations and the power configurations which are selected for further investigation (marked with bold letters). Even though power configurations with three different engine sizes have high time percentage of optimal fuel consumption, it was decided not to include them into further consideration because of the related spare parts and maintenance aspects.

Based on the results shown in Table 20.6, the following power configurations are selected for further investigation:

- Benchmark configuration: diesel-direct power configuration with three shaft lines and three 1,267 kW engines
- DDP 4*950: alternative diesel-direct power configuration with four shaft lines and four 950 kW engines
- DDP 2*950 + 1,900: alternative diesel-direct power configuration with four shaft lines, two 950 kW engines, and one 1,900 kW engine. The larger engine is driving two propellers, and each smaller engine is driving separate propeller.
- DDP 2*800 + 2*1,100: alternative diesel-direct power configuration with four shaft lines, two 800 kW engines, and two 1,100 kW engines. This configuration consists of two father-son drives, where each father-son drive consists of one 800 kW engine, one 1,100 kW engine, father-son gearbox, and two propellers.
- DEP/GEP 5*860: alternative diesel-electric or gas-electric power configuration consisting of five 860 kW generator sets and four shaft lines.

Table 20.6 Cover coefficient of candidate configurations where the selected alternative configurations are bolded

Nr. of engine sizes	Nr. of engines	DDP		DEP/GEP		HP [kW]		
		Power [kW]	t [%]	Power [kW]	t [%]	DDP [kW	DEP [kW]	t [%]
1	1	38,00	55	4,300	57	–	–	–
	2	1,900	83	2,150	83	2,050	2,050	86
	3	**1,267**	**85**	1,433	89	1,380	2*1,380	89
	4	**950**	**94**	1,075	94	2*1,020	2*1,020	94
	5	–	–	**860**	**95**	2*825	3*825	94
2	2	3,000+800	71	1,800+2,500	94	1,900	2,200	93
	3	**2*950+1,900**	**94**	2*800+2,700	94	1,900	2*1,100	94
	4	**2*800+2*1,100**	**95**	**3*800+1,900**	**94**	2*950	2*1,100	94
	5	–	–	**4*800+1,100**	**95**	**2*800**	**3*850**	**95**
3	3	2,000+1,000+800	94	2,500+1,000+800	95	1,900	1,900+1,800	95
	4	800+900+2*1,050	94	800+1,000+2*1,250	95	2*950	900+1,300	95

- DEP/GEP 3*800 + 1,900: alternative diesel-electric, or gas-electric power configuration consisting of three 800 kW generator sets, one 1,900 kW generator set, and four shaft lines.
- DEP/GEP 4*800 + 1,100: alternative diesel-electric, or gas-electric power configuration consisting of four 800 kW generator sets, one 1,100 kW generator set, and four shaft lines.
- HP DDP2*800+DEP3*850: alternative hybrid power configuration with two 860 kW diesel engines driving two propellers, and three (diesel) generator sets of 850 kW driving the other two propellers.

20.5 Dynamic Models

This section describes the dynamic models of the selected power configurations from Table 20.6 in the previous section. The block diagram of the models used in this study is in Fig. 20.10 and it shows the structure of the models. The model in Fig. 20.10 is developed in MatLab/Simulink environment and it will be used to estimate the related emissions ($em_{prop,j}$) and fuel consumptions (fc_{prop}) . The inputs to the model are the operational profile measurements ($P_{prop,up}$) and cargo loaded ($\nabla_{tot,loaded}$). Instead of immediately trying to trace back the measured operational profile to the fuel consumed, an attempt is made to have a realistic simulation of the

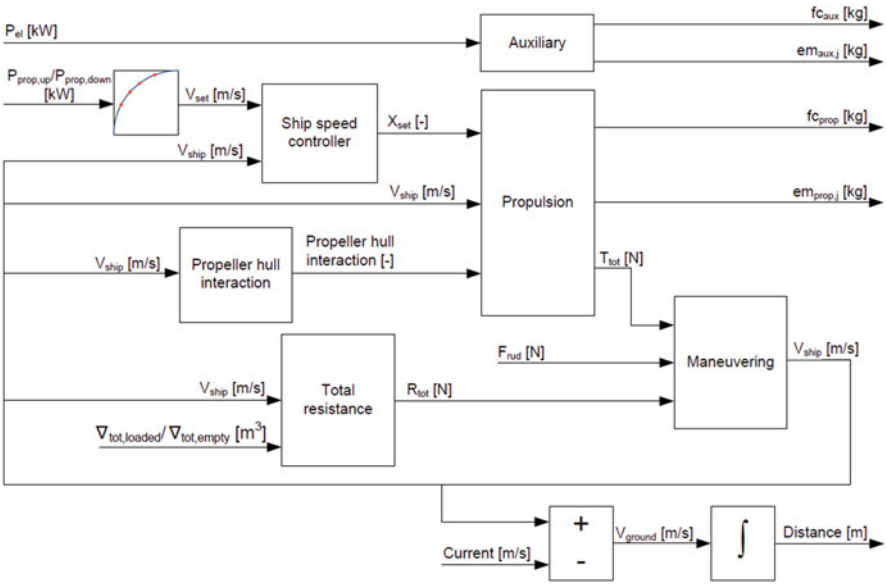

Fig. 20.10 Block diagram of dynamic model used in this investigation

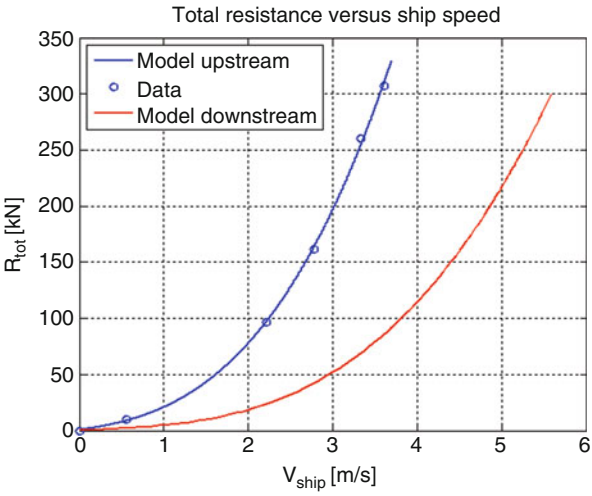

Fig. 20.11 Modelled resistance in upstream and downstream mode, and measurement data as in [2]

voyage with the ship speed controller block imitating the helmsman. In the model, the measured power is converted to the set speed (V_{set}), using the ship resistance curve, which is then converted to the fuel rack setting (X_{set}). Figure 20.11 presents the total resistance of the model in upstream (loaded condition) and downstream mode (empty condition) according to the data provided in [2]. Also, coefficients for the propeller-hull interaction were derived from [2]. In Fig. 20.10, the manoeuvring block has the possibility to include the manoeuvring forces in the rudder to fully simulate the voyage trajectory. The manoeuvring forces are modelled according to [7]. However, the applicability and accuracy of Kijima model for the case of Veerhaven X is not known. Thus, in order to reduce the uncertainties and speed up the computation time, the manoeuvring possibility is switched off and the model assumes a straight line trajectory.

Perhaps the most elaborate part of the model is the propulsion block in Fig. 20.10. The purpose of the propulsion block is to calculate the thrust based on the fuel rack setting. Figure 20.12 shows the structure of the propulsion block. Depending on the specific power configuration, the engine block will contain the diesel and/or the gas engine models. The diesel engine model uses the Seiliger cycle and it is described in [11]. The gas engines are modeled with the "Mossel" engine model which is described in [11] and [10].

Figures 20.13 and 20.14 show matching of fuel consumption characteristics of the modelled diesel and gas engines with the available data for four different engines: two diesel engines and two spark-ignition gas engines. Namely:

- 1,360 kW diesel engine in Fig. 20.13 left was used to match the models of 800, 850, 860, 900, 1,100, and 1,267 kW diesel engines
- 1,900 kW diesel engine in Fig. 20.13 right was used to match the models of 1,900 kW diesel engine
- 1,000 kW and 1,900 kW gas engine in Fig. 20.14 was used to match the models of 800, 860, 1,100, and 1,900 kW gas engines

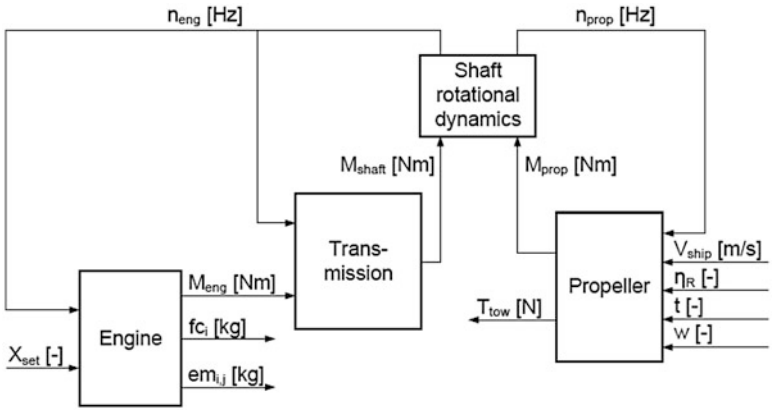

Fig. 20.12 Block diagram of Propulsion block in Fig. 20.10

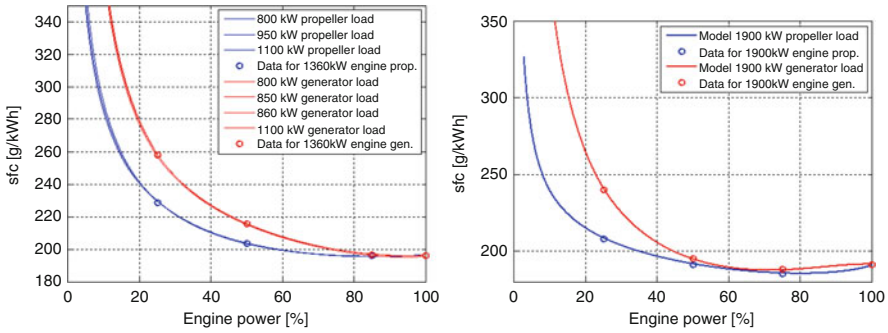

Fig. 20.13 Matching of specific fuel consumptions with the test bed records of 1,360 kW diesel engine (*left*) and 1,900 kW diesel engine (*right*)

Fig. 20.14 Matching of specific fuel consumptions with the test bed records of 1,000 and 1,900 kW gas engine

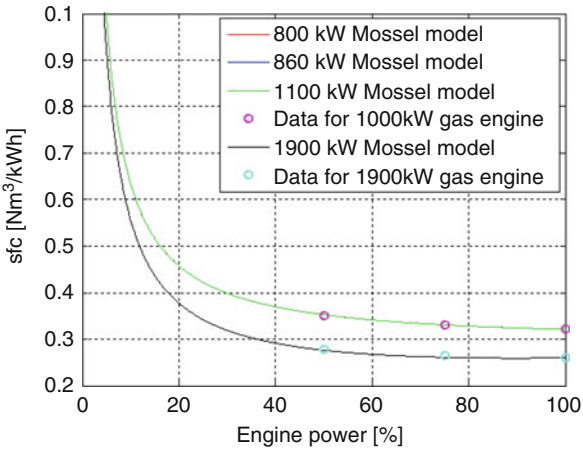

The power transmission block shown in Fig. 20.12 will be different for diesel-direct power configurations and for diesel/gas-electric power configurations. For diesel-direct power configurations the transmission block is a gearbox with the constant gearbox ratio. Only for "DDP 2*800 + 2*1,100?" the gearbox will have the father-son gearbox ratios. For electric power configurations, the transmission block consists of switchboards, frequency converters, and electric motors. The model for electric motors is based on the wound rotor model presented in [4]. For all power configurations some power management system is needed to regulate the number of engines switched on and their loading distribution. The exact rules used to control the number of running engines are based on the operational profile of one typical journey which is presented in the next section.

20.6 Modeled Results

The aforementioned dynamic models are used to calculate the emissions of the alternative power configurations during one typical journey between Rotterdam and Duisburg. Figure 20.15 shows the propulsion power in kW versus voyage duration in %, during the investigated journey. In the model, the total voyage duration is: 24 h upstream, and 13 h downstream. The current is set to 0 m/s in Rotterdam and 1.66 m/s in Duisburg with linear increase during the voyage. The current is negative when sailing from Rotterdam to Duisburg and positive when sailing from Duisburg to Rotterdam. The total cargo transported in the loaded condition is 14,700 tons which is based on the logbook of Veerhaven X.

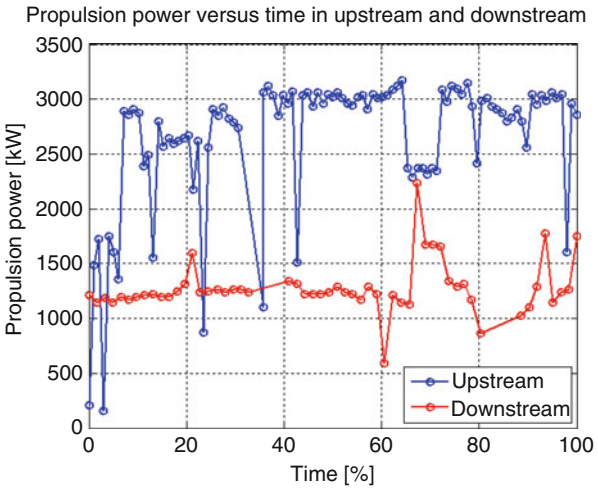

Fig. 20.15 Input propulsion power in upstream and downstream mode of one typical voyage

As mentioned in the previous section, for each configuration it is necessary to decide on the number of engines that are running and the load share amongst the engines. Because of uncertainties related to the performance of the propellers in the trailing shaft conditions, it was assumed that all propellers are always running in both operation modes (upstream and downstream mode). This assumption is also supported from every-day sailing practice. For most of the diesel-direct power configurations this will mean that all engines are always on (for both operation modes). Only for the father-son power configuration (DDP 2*800 + 2*1,100) it is possible to switch off some engines in the downstream mode. For diesel-electric and gas-electric power configurations, especially in the downstream mode, it is not necessary that all engines are always running on. This is especially beneficial for electric configurations with the 1,900 kW engine where the priority was given to the larger engine because of their higher efficiencies. Regarding the number of engines running, general rule is to have engines running between 50 and 85 % of their maximum power (as defined in Figs. 20.13 and 20.14). Regarding the load sharing, equal load share amongst the running engines was assumed for all power configurations, except for the GEP 3*800+1,900 for which the larger engine is more loaded due to its significantly higher efficiency.

Since diesel and natural gas fuel have different lower heating values (LHV), the resulting fuel consumption is represented as the resulting energy consumption. The total energy consumption was the sum of all individual consumptions for each power configuration during the investigated voyage. The energy consumption per engine was calculated according to:

$$E = LHV \cdot \int_{t_{begin}}^{t_{end}} \dot{m}_f \, dt, \tag{20.3}$$

where $\dot{m}_f$ is the fuel flow. For diesel fuel the LHV for diesel is 42.7 and LHV for gas (LNG) is 43.64 was assumed. Figures 20.16 and 20.17 show the resulting energy

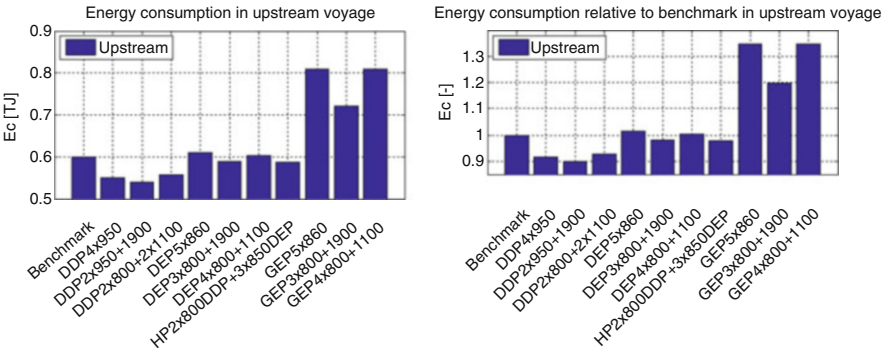

Fig. 20.16 Comparison of energy consumption of Benchmark, diesel-direct, diesel-electric, gas-electric, and hybrid power configurations for upstream part of the voyage

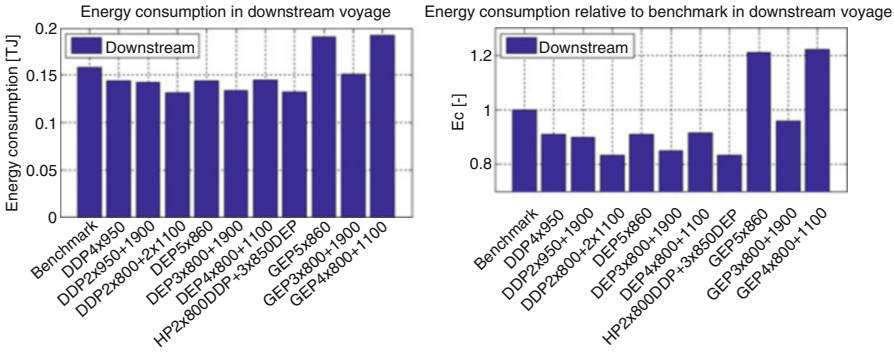

Fig. 20.17 Comparison of energy consumption of Benchmark, diesel-direct, diesel-electric, gas-electric, and hybrid power configurations for downstream part of the voyage

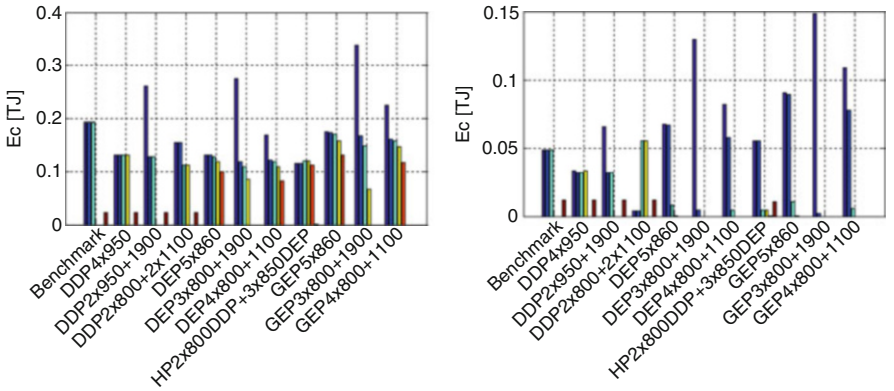

Fig. 20.18 Energy consumption per engine in upstream (*left*) and downstream part of the voyage (*right*)

consumptions of all power configurations for the upstream and downstream part of the investigated journey. Figure 20.18 shows energy consumptions of each engine for all power configurations for the upstream and downstream conditions. Bars in the graphs show energy consumption of each engine in the configuration, where the largest engine is the first bar. For example in DEP 3*800+1,900, first bar is the engine of 1,900 kW and the other three bars are 800 kW.

Figure 20.19 shows the total energy consumption of the entire journey for all power configuration and Fig. 20.20 shows the total emissions of all diesel-direct and diesel-electric power configurations for the entire journey. The figure shows the total emissions of all engines per power configuration. Emissions of gas-electric power configurations are presented separately in Fig. 20.21. The results of the models are discussed in the next section of this chapter.

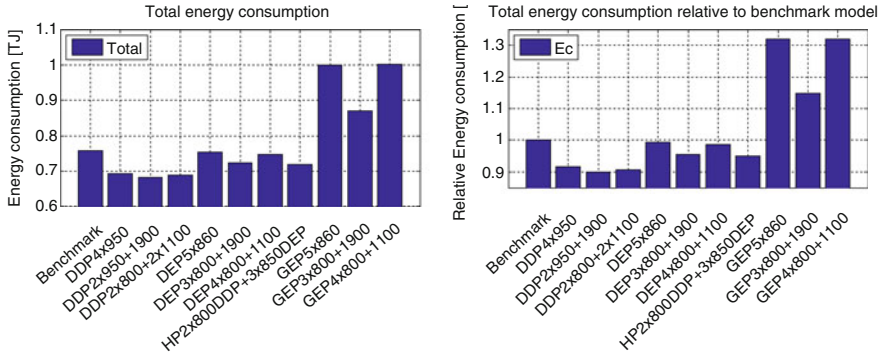

Fig. 20.19 Comparison of energy consumption of Benchmark, diesel-direct, diesel-electric, gas-electric, and hybrid power configurations for the entire voyage

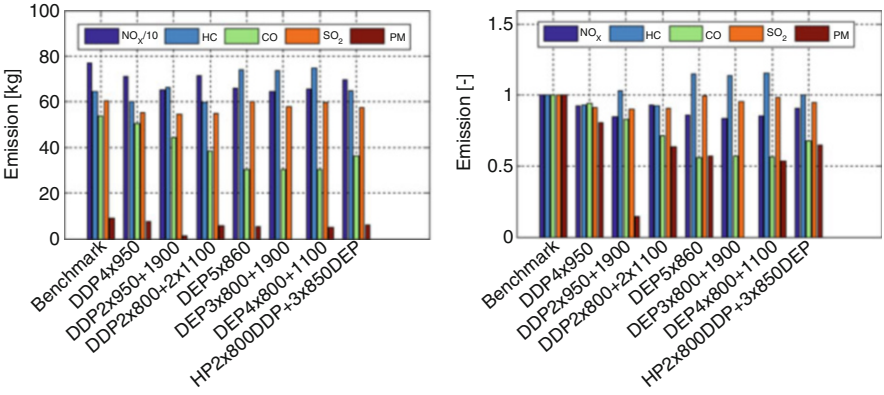

Fig. 20.20 Resulting emissions of diesel-direct and diesel electric power configurations for the investigated voyage

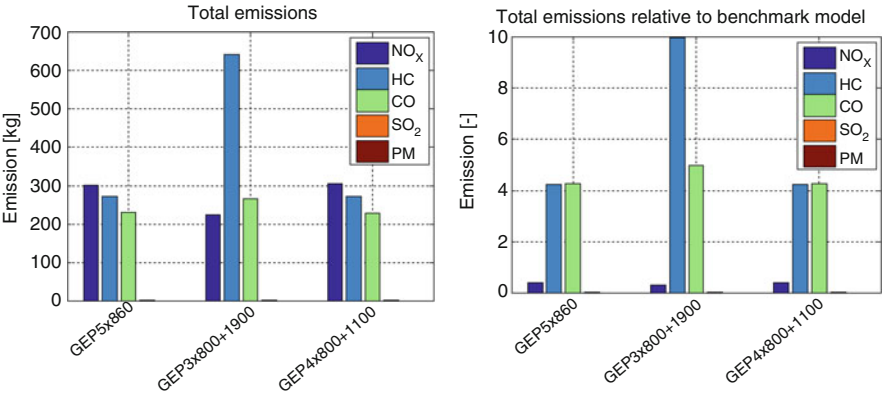

Fig. 20.21 Total emissions of configurations with gas engines (*left*) and their emissions relative to the emissions of the benchmark configuration (*right*)

20.7 Discussion

Before discussing the results of the analysis given in Sect. 20.6, it is useful to compare some of the results with the logbook records of the ship. For the investigated journey, it was recorded that the amount of fuel consumed was 21 ton of diesel while the benchmark model in Fig. 20.19 gives an estimate of 18 tons of diesel. It should be mentioned that the logbook shows the consumptions between 19 and 24 tons for journeys with similar cargos. Since the benchmark model has somewhat smaller and more efficient engines than the real ship, the estimate of the benchmark model seems realistic. Moreover, the correctness of the model has been evaluated against the emissions and fuel consumption measurements.

The difference amongst the fuel consumptions recorded in the logbook results partially from the difference in water levels. A low water level can influence the performance of the ship in several ways: it limits the draft of the barges and the cargo loaded, it increases the resistance due to the shallow water effect, and the propellers might not be fully submerged. Since water levels can vary between 2 and 10 m, it was decided that all alternative configurations have four propellers instead of three. Even though the analysis shows that the alternative configurations have higher efficiency then the benchmark model, it should be noted the effect of low water levels was not fully investigated here. The best way to evaluate the performance of all configurations would be to calculate the related fuel consumptions for the entire operational profile during 1 year. Since this data is not available, and the data related to the performance of the three-shaft configuration in partially submerged conditions is also not available, it was decided to leave this analysis for future work. Nevertheless, the work done in this chapter shows that it is possible to get 10 % improvement in the efficiency just by selecting another power configuration.

Looking at the investigated configurations, the DDP 2*950+1,900 seems to be the most efficient power configuration. Also the total amount of exhaust emissions is favorable with this configuration. There are probably few reasons for this, one is high time percentage of the optimal engine usage presented in Table 20.6 and another reason is better engine efficiency for 1,900 kW diesel engine, presented in Fig. 20.13. Also, the diesel-direct power configurations have advantage over the electric power configurations because of less components and one energy conversion less. However, the diesel-electric power configurations show quite respectable performance, in general even better than the benchmark model. Looking at the gas engine configurations they provide large NO_x reduction but their total energy consumption is higher than for DDP. This is explained by lower combustion efficiency of gas engines, which is expected to be improved in the coming years. Other benefit of gas engines is that they produce less CO_2 in comparison with diesel engines. However, their production of hydrocarbon gasses and carbon monoxide is not favorable in comparison with diesel engines. Again, the gas configuration with the large 1,900 kW engine shows best results amongst gas engine configurations. Here it should be mentioned that further improvement of the results could be achieved for all power configurations if the trailing propeller mode was allowed.

This would improve their performance mainly in the downstream mode. It is estimated that the overall improvement of the efficiency would be around 1 % due to trailing propellers.

20.8 Conclusions and Future Work

The goal of this chapter was to investigate the performance of alternative power configurations of an inland pusher on river Rhine. As in many other performance analysis, this analysis is driven by two motivations. First motivation was an economical motivation, i.e., an attempt was made to estimate the fuel consumption of different power configurations. The second motivation was a legislative motivation, i.e., an attempt was made to estimate which configuration agrees with the current and future exhaust gas limitations. Looking at the current exhaust gas limitations, all investigated power configurations fall below the current exhaust gas limitations set by CCNR. However, it is expected that the future limit for NO_x emissions will be set to 1.8 g/kWh. While for gas engines this limit is ok, for diesel engines the forecasted NO_x limit will be challenging. An option for diesel engine power configurations is to add a selective catalytic reduction (SCR) device which reduces the NO_x emissions. Since SCRs use urea to operate, it is convenient to know how much urea is needed for a modern diesel engine to meet the future NO_x limit. Looking at the equation presented in [12] it is possible to estimate that a ship such as Veerhaven X would use around 15 l of urea per MWh. Based on its performance, an SCR installation seems to be a practical solution for retrofitting of older vessels.

Based on the results for one representative journey, the diesel direct power configuration seems to be the most efficient. However, the gas-electric configurations are superior regarding the NOx emissions. Even though the analysis done above used one specific vessel for the case study, it is possible to draw some general conclusions. Based on the entire analysis, it is possible to conclude that the gas engines (or dual fuel engines) have a lot of potential and probably will be more used in the future. On the other hand, modern diesel engines are still good option for new build vessels and definitely very good option for retrofit of old vessels. In combination with an SCR it is conceivable that diesel engines will remain the main prime movers of inland vessels for coming years. As shown in this chapter, the transport over inland waterways is closely related to the water level. By transporting the water it should be possible to increase the water depth on an inland waterway and increase the transport efficiency during the periods of low water levels. However, the feasibility of this proposal remains to be scrutinized in the future.

Acknowledgements This research has been partially supported by EU-FET granted project: "Modernisation of Vessels for Inland waterway freight Transport MOVE IT!", project reference number: 285405. Authors would like to thank ThyssenKrupp Veerhaven B.V., in particular Mr. Be Boneschansker for his support.

References

1. Adnanes AK. Maritime electrical installations and diesel electric propulsion. ABB, 2003.
2. Bieker K. Future pusher bericht 2072. Internal report, technical report, DST - Development Centre for Ship Technology and Transport Systems, 2012.
3. Buckingham J. Hybrid drives for naval auxiliary vessels. Technical report, Engineers Australia, 2013.
4. de Ryuck K. Simulation of advanced engine room configurations with energy savings concepts. MSc thesis, report nr.: Sdpo.11.020, TU Delft, 2011.
5. Drijver M. Future pusher project. MSc thesis, report nr.:SDPO.13.030, TU Delft, 2013.
6. Frouws JW. Aes decision model. Technical report, TU Delft, 2008.
7. Kijima K, Nakiri Y, Katsuno T, Furukawa Y. On the manoeuvring performance of a ship with the parameter of loading condition. J Soc Nav Archit Jpn. 1990;168:141–8.
8. SGS. Resultaten emissiemetingen van de motoren van duwboten. Internal report, technical report, SGS Nederland B.V., 2010.
9. Shi W. Dynamics of energy system behaviour and emissions of trailing suction hopper dredgers. PhD thesis, TU Delft, 2013.
10. Stapersma D. Diesel engines volume 4: Emission and heat transfer. Lecture notes, TU Delft, 2010.
11. van Deursen EW. Control of hybrid ship drive systems. MSc thesis, report nr.:SDPO.11.022, TU Delft, 2011.
12. Wartsila. Imo tier III solutions for Wartsila 2-stroke engines – selective catalytic reduction (scr). Product brochure, Wartsila, 2011.

Chapter 21
City Logistics by Water: Good Practices and Scope for Expansion

J. Maes, C. Sys, and T. Vanelslander

Abstract Urban freight transport became a specific research topic as the general awareness on the increasing negative effects of these freight delivery activities on the local livability grows. The awareness for external costs (congestion, emissions, noise and road safety) by the public grew. As a result, (local) governments implemented specific policies. Often, these limit the free, flow of traffic, put limits on (un)loading activities and limit urban road capacity. As a result, logistics entrepreneurs innovate their last mile transport operations. An under-investigated opportunity is the use of waterways for urban freight delivery purposes. This chapter lists best practices found in Western Europe. These transport freight towards or in the city. In this chapter, a Dutch concept was translated into a specific case for the Belgian city of Ghent. A cost simulation of an urban delivery concept with an electrically-powered vessel is developed and gives us insight in the actual competitiveness. Based on our own simulation, conclusions are drawn. Further research opportunities are indicated.

21.1 Introduction

The attractiveness of urban city centers is damaged among others by increasing transportation activities. Urban mobility points at the presence of public transport, cars, bikes, etc., while urban distribution entails freight transport: vans, trucks, etc. More road transport on the one hand and more freight transport on the other hand combined with a lack of open space lead to mobility challenges in city centers. This is certainly the case when infrastructure and policy impose more and more limitations to the free movement of freight flows. This observation, and the expectations for the future, cater for sustainable mobility and logistics to be higher on the (inter) national agenda. Various evolutions in the sector and in related policy decisions generate more and more attention for urban logistics

J. Maes • C. Sys • T. Vanelslander (✉)
University of Antwerp, Antwerp, Belgium
e-mail: maes.jochen@gmail.com; christa.sys@uantwerpen.be;
thierry.vanelslander@uantwerpen.be

C. Ocampo-Martinez, R.R. Negenborn (eds.), *Transport of Water versus Transport over Water*, Operations Research/Computer Science Interfaces Series 58,
DOI 10.1007/978-3-319-16133-4_21

challenges. The scope of this chapter is limited to urban freight distribution, a dynamic urban activity. Changes in this sub-sector of logistics come among others from an evolution of society towards a post-industrial society, an ageing population, a worldwide urbanization trend and the increasing attention among the wider public for sustainable developments. Urbanization turns cities more than ever into densely populated areas and nodes of different activities. In 1950, 50 % of the world population lived in cities. In 2000, that share had increased to 77 %, and by 2020, 83 % of the population is expected to live in city centers. To keep cities liveable and attractive, the presence of activities and services is needed. As a result, the largest consumption of goods and services in Western Europe occurs in urban environments. Not only extensive leisure time activities and shopping outlets but also easily accessible office locations increase the attractiveness of urban cores. These different activities increase the demand for efficient mobility and generate a demand for goods. Next to the easy movement of persons towards, from and inside the city, the activities in the central business district also generate various freight flows. The logistics complexity, combined with the societal impact, urges for a change in the practical and technological organization of both urban person mobility and urban freight distribution. Hesse [22], for instance, states that new technologies, organizational structures, a changing demand pattern, other transport strategies and transport costs, a changing labor pattern and spatial division of the urban space have all changed already heavily the logistics operations. More innovation is still needed to decrease the conflict between liveability and mobility. All these activities and related trips occur at a relatively small space. Although the freight flows are vital for an inner core, the city center infrastructure is not always ready to handle them. The European Commission [17] in its Green Paper on A new urban mobility culture took into account the achievements of the CIVITAS'[1] project. It states that an integrated policy is needed for the different urban mobility aspects. Both person and freight transport get attention. More fluent transport, and hence less congestion, is a key issue as it has consequences at economic, social and ecological levels. A next challenge is reducing air pollution. Also intelligent transport systems (ITS) are dealt with. A last topic on the agenda is integrated spatial planning. The findings were confirmed in the European Commission's [18] White Paper on 'A Roadmap to a Single European Transport Area—Toward a competitive and resource efficient transport system'. That White Paper states that cities today are responsible for about a quarter of transport-related CO_2 emissions, and that 69 % of traffic accidents happen in cities. The gradual disappearance of classical combustion vehicles is envisaged, and will contribute strongly according to the EU to a decreased oil-dependence, exhaust gas emissions, and local air pollution and noise hindrance. The White Paper imposes strict and ambitious targets for urban road transport. The number of cars in cities using classical combustion is to be halved by 2030, and to disappear totally by 2050. Urban distribution by 2030 has

[1]CIty VITality Sustainability: the CIVITAS network helps cities in setting up more sustainable, clean and energy-efficient urban transport by integrating and jointly implementing policy measures.

to be handled in a nearly CO_2-free way. Those targets emerge from the European Commission's framing climate policy. The actions with respect to urban logistics range between optimizing the logistics chain and investigating and implementing innovative concepts. For the former, grouping logistics flows at specific locations into larger volumes may increase their chances of fitting transport via alternative transport modes, like inland navigation. For the latter, but related to achieving the former, innovation with impacts both on industrial-economic cost structures and social welfare is supported. New water navigation concepts to be used for distribution in city centers may fit here. Moreover, they can be a good way of getting rid of the old-fashioned image with low flexibility, limited investments and solitary behavior in the logistics chain that alternative transport modes suffer from. The focus in this chapter is on inland waterway transport towards, from and inside city centers. In particular, the attention goes to opportunities that inland waterway concepts offer for alleviating accessibility and viability problems that cities face. The next section defines and delineates the concept of "urban logistics" and the types of flows it involves. Section 21.3 deals with a number of existing inland waterway concepts applied in urban distribution. The central question is whether waterway transport can be a viable alternative for urban distribution. What are long-run successful concepts and where have they been applied? Can critical success factors be discerned in the set of cases? Section 21.4 makes an in-depth analysis of a potential application of inland waterway urban transport in a Flemish case, more in particular in Ghent. The final section wraps up the conclusions and makes a number of considerations on the usefulness of applying a broader framework, including the linkage between transport over water and transport of water.

21.2 Urban Logistics: A Definition and Inland Waterway Markets

Urban logistics is a logistics process whereby goods are collected at one or more addresses, after which they are possibly brought to a distribution center, where transhipment and groupage occur, in order to have them redistributed to one or more delivery addresses. It is a separate logistics discipline, with an own last mile-focused dynamic, that requires a tailored policy. Over time, the spatial composition of cities has changed to an extent that operations like storage and transhipment do not find a space any more within the urban environment [8]. Loading and unloading are the only logistics activities left within city centers. Those activities often meet opposing objectives from the side of policy-makers and inhabitants. First, future market potential for urban waterway transport is defined. The postal or package market is a potential user of inland waterway urban distribution. Research on the topic is rather scarce. A number of cases are known where the concept is actually being applied. Goods are, for instance, transported per truck towards the city border, and then consequently transhipped into a small vessel. Such a small ship then sails a distribution round inside the city center. It may entail a pre-trajectory per truck and a last-mile approach per ship. When the consignee is not located alongside the city

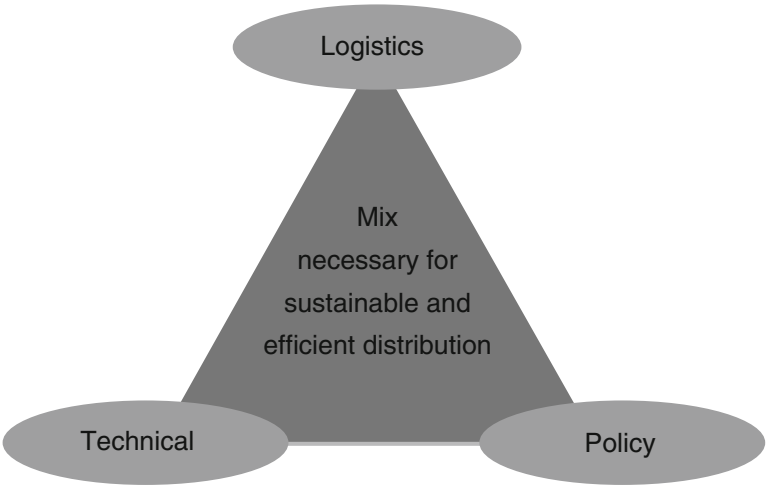

Fig. 21.1 Three solution dimensions of Quak [32]

waters, a short last mile trajectory over land may be needed. Alternatives to road vans or trucks (with classical combustion or electric) are then carts, bicycles or by foot.

Non-container and non-bulk tests were held in Flanders, for instance, for pallet transport of building materials and Fast Moving Consumer Goods [7]. Both commodity types can easily be palletized, which increases the speed and efficiency of transhipment operations. The destination of those goods in most cases are city centers, as the retail shops distributing them are mainly located there. This concept mainly plays for larger volumes. Consolidation decreases the unit transport cost. The real last mile will still require a van or truck solution.

Second, key success factors for logistics innovations need to be met. For an urban logistics solution to have potential to be successful, Quak [32] states that three components are needed (Fig. 21.1): logistics, technical and policy perspectives. Innovative logistics concepts change transport planning and habits but are often supported by technical innovations. Policy makers are then the third actor that needs to support or facilitate the innovation in the start-up phase in order to reach a market-competitive position in the long run.

21.3 Urban Waterway Logistics: Best Practices

This section focuses on a number of innovative applications of urban waterway transport concepts. A distinction is made between transport within cities and transport to and from cities.

21.3.1 Waterway Transport Within Cities

In this subsection, consecutively, the Utrecht Beer Boat, the Amsterdam City Supplier and the DHL Floating Service Center are treated.

The Utrecht Beer Boat

The Utrecht city center is still characterized by many small streets, historical buildings, bridges and waterways. Exactly those generate problems to urban freight distribution. Trucks are too heavy, long or large to get into the city center. Loading and unloading options are limited because of the confined open space. The consequence is that trucks cause road blockage. A first initiative by policy makers was introducing limitations on the vehicle lengths. The heavy traffic also caused road and cellar damage. Hence, a second reply was introducing weight limitations. Shifting towards smaller vans was not a preferable option for the transport actors, as this imposes an additional transhipment cost and moreover worsened environmental performance. Other imposed policy measures were introduced afterwards: time windows, city compartmenting, low-traffic zones and low-emission zones. The historical center of Utrecht features a large number of inner waterways. During the twelfth century, along those waterways, cellars, quays and quay walls were built. Alongside those quays, goods were directly transshipped towards the cellars. But the increasingly cheap and quick road transport made the waterway transport gradually being abandoned. After restoring these quays and quay walls as of 1993, inhabitants requested the renewing of the wharf cellars for freight distribution [35]. Beer Boat's innovative logistics concept uses water transport to deliver freight into the city core. The concept is based on an initially diesel-propelled, and later on fully electricity-propelled inland ship (Fig. 21.2). Since 1996, the latter sails through the city center with drinks and other catering. The ship can transport several rolling containers and is equipped with a hydraulic crane that delivers the goods to the quays. This way of transport prevents damage to the historic quays and does not require additional infrastructure.

After this first Beer Boat, a second vessel was put into service in 2010. This one features an electric engine, that is charged at the end of the working day with green power. It can sail, load and unload a day long on one charge [3]. Locations in the city have charging points, even though not needed for continuous operations. Multi-modal transport concepts grew as, for companies not located alongside water, a co-operation agreement was made between the Beer Boat and Utrecht's Cargo Hopper.[2] The Beer Boat concept is offering services in the inner city of Utrecht. The company does not limit itself there though. Plans exist to further extend the reach of the Beer Boat. The Cleaning and Port Service (RHD) consider an electrical

[2]Cargohopper is an other urban distribution concept in Utrecht, whereby an electric vehicle pulls a number of carts. The vehicle can, no matter the time windows, travel through the inner city.

Fig. 21.2 The historic inner city of Utrecht gets delivered by a Beer Boat

garbage vessel [1]. The vessel was designed in function of the Utrecht canals in order to have a maximum market outreach. RHD, the vessel owner, designed a ship with a loading capacity of 18 tonnes or 40 to 48 rolling containers (corresponding to six vans or two truckloads). The first Beer Boat had a length of 18.80 m, a width of 4.26 m, a draught of 1.10 m and a coaster profile of only 1.65 m [37]. The second Beer Boat went a step further, with a 55 kW synchronous engine, powered by a 480 V battery with a capacity of 86.4 kWh. The vessel also has a backup 83 kW diesel engine. The Beer Boat has a sailing reach of over 80 % of the Utrecht canals. Only the Merwede Canal features two bridges that are too low for the vessel. The Kruisvaart, the Stadsbuitengracht and the Kromme Rijn can only handle a limited load: draught is less than 0.90 m there [10]. Initially designed for providing bars with drinks, the market reach extended to various eateries, pubs and leisure locations, as well as some shops. As of 2005, also a wholesale market was served by the Beer Boat. In 2010, the Beer Boat served 65 customers, among which four breweries. Utrecht hosts about 700 eateries, among which 237 in the inner city. There is also a dense concentration of retail establishments. The Beer Boat also allows transporting fresh, cooled and frozen products, in conditioned containers. Even miscellaneous transport is possible, like, e.g., house removals and building materials. Reverse flows are taken too, for instance, garbage from bars and restaurants. In order to be able to serve all customers, the ship sails twice a day and five times a week [1]. The big advantages of the Beer Boat are its independence from time windows, one-way streets, traffic congestion, weight and length limitations, etc. That increases reliability of deliveries, which reduces road congestion in the city. Furthermore, there is a socio-physical impact: operators can now always load and unload by crane, which leads to less charging and health problems than before. Finally, it is a solution that is more friendly to the environment, with less emissions and less noise produced. Table 21.1 presents the annual CO_2, NO_x and PM_{10} emissions for the Beer Boat versus the van solution. For the Beer Boat, a distinction is made

Table 21.1 Annual CO_2, NO_x and PM_{10} emissions Beer Boat [13]

	PM_{10} kg/year	CO_2 kg/year	NO_x kg/year
Vans	1.88	17,400	32.64
Beer Boat			
Diesel-powered	1	12,789	5
Grey power-driven	0.04	981	0.044
Green power-driven	0.88	4,811	27.7
Van versus Beer Boat—absolute decrease			
Diesel-powered	−0.88	−4,611	−27.7
Grey power-driven	−1.84	−6,952	−32.6
Green power-driven	−1.84	−16,429	−32.6
Van versus Beer Boat—percentage decrease	%	%	%
Diesel-powered	−74	−27	−85
Grey power-driven	−98	−40	−100
Green power-driven	−98	−94	−100

between diesel, grey and green power. Using the electrical Beer Boat reduces annual emissions by 94 %, or an annual reduction of by 16.5 tonnes [19].

Next to the advantages, an the Beer Boat by also has a number of drawbacks. First, using the Beer Boat will require organizational changes, and will lead to a shift in costs (less transport costs per unit of load, higher inventory costs). The Beer Boats furthermore are made available by the city of Utrecht, and rented out to companies that take care of the actual distribution. The emission-free vessel costs about € 800,000, of which € 400,000 was funded by the policy measure ALU (Actieplan Luchtkwaliteit Utrecht) and the European Fund for Regional Development (EFRD). The remaining amount was funded by the exploitation of the first Beer Boat. Operating the ship also requires two staff members, for safe loading and unloading, which leads to high operational expenses. In terms of the solution dimensions of Quak [32], all three of them are present with the Beer Boat solution. The logistics component consists of a shift from road to water of all kinds of commodities. The largest technical improvement lies with the second version, which involves a shift from diesel towards electric propulsion, with a significant emission reduction. Policy-wise, the concept provides a solution since it reinforces the urban distribution policy framework in Utrecht, due to its pragmatism, innovativeness and coherence [10].

The Amsterdam City Supplier

Also in Amsterdam, waterway transport concepts have been tested. Amsterdam features a lot of canals, initiated during the Middle Ages, but further expanded over the years, and used a lot for transporting commodities. Together with the

Fig. 21.3 "Vracht door de gracht" by Mokum Maritiem

canals, warehouses were built where goods were stored. But the Amsterdam canals gradually had to give way to streets and parking space. The urban waterway system was halved, but still covers about a quarter of the urban territory [2]. More recently, initiatives were taken to significantly refurbish the city canals. At the same time, and similarly to Utrecht and also other cities, various limitations were imposed to urban road transport [5]. In 2007, the initiative "Vracht Door De Gracht" (Freight through the canal) was launched by Mokum Mariteam. It is a co-operation agreement between three shipping companies (Rederij't Smidtje, Rederij de Nederlanden and Canal Company), waste processor ICOVA (Inkoop Combinatie van Afvalstoffen) and logistics supplier Koninklijke Saan. Only in September 2010, the first electrically-propelled vessel, shown in Fig. 21.3, was put into service. Via a loading and unloading location outside the city, the goods are transhipped from road vehicles. The last mile in the city center is done by waterway. Reverse flows, comprising organic hotel and restaurant waste, are taken and brought to a processing plant, that transforms the waste into bio fuel. That bio fuel is used for the vessel's diesel engine [31].

The fleet was expanded later on with a second vessel, called "Power Supplier". It is equipped with two cascaded generators of in total 80 KVA for power supply to building operators and leisure events, and its power lasts for 8–10 h. The ship has diesel-electric propulsion of 35 kW. The diesel generators are used for trajectories outside the inner city, and for the eventual recharging of batteries. The ship measures 20 m in length, 4.5 m of width, an average draught of 1.0 m, and a coaster profile of 1.85 m. It has a surface of 15.75 by 3.75 m, a cargo capacity of 85 m^3, and can take up to 56 t of cargo. It has a hydraulic crane. An innovative feature are the automatic, telescopic spuds [19] and [26]. On 23 June 2010, a co-operation agreement was concluded between Mokum Mariteam and the united companies of Food Center Amsterdam. The latter is a wholesale market. Its customers got the opportunity to deliver their goods in a silent, efficient and clean way. Six companies were the launching customers initially. High-volume goods are targeted:

- Fruit and vegetables, meat, fish, game and poultry, etc.
- General foodstuff
- Building materials
- Hotel, hospital and nursery laundry
- Drinks and food for the food service industry
- Underground waste containers for shops
- Books for musea and bookshops
- Cooled and frozen foodstuff
- Supermarket goods

In 2011, Binnenstadservice, a logistics service provider for city retail outlets, signed a co-operation agreement with Mokum Mariteam. The goods are grouped at the city borders. From there, they go via water to the end receiver. The last stretch after unloading can only be 150 m when using an electric puller. In other cases, an electric truck has to be used, but that increases the last mile cost [9]. The concept has similar efficiency and reliability advantages as the Utrecht Beer Boat. At environmental level, the low-noise electrical engine generates a reduction of energy usage and PM_{10} and CO_2 emissions. A supplementary advantage is that the City Supplier's crane, as opposed to that of the Beer Boat, can be operated from a short distance [12]. There are also disadvantages to the concept. Like with the Utrecht Beer Boat, logistics habits will need to be adapted. When extra storage space and equipment is needed, this will have a cost too. Also, for larger distances, when trucks need to be used, costs will increase as compared to the classical road solution. This solution too provides a good mix of the solution dimensions of Quak [32]. The City Supplier helps Mokum Mariteam provide a contribution to better accessibility and viability in Amsterdam's historical city center. The engine is low in noise, which is a clear technological advancement. In terms of policy, the solution contributes to economic efficiency, social and environmental goals the city tries to achieve.

The DHL Floating Service Center

Still in Amsterdam, the DHL Floating Service Center initially was a tourist sailing boat, used on the city canals. The vessel was transformed in 1997 into a package delivery vessel of DHL Worldwide Express. Benches were replaced by postal sorting tables, and walking bridges were installed. The ship has a fixed sailing route through the city center. In the morning, the ship receives its mail to be delivered along the route, while in the evening, the collected return mail is passed on to DHL's classical express network. The concept is connected to nine cycling messengers and two couriers with vans. The latter are used for parcels that are too large or too heavy to be transported by bike [33, 40]. The ship has a length of 17 m and a net transport content of 30 m^3 [28]. It has a large sailing reach. The project was largely financed by DHL itself. The City of Amsterdam took care of financing the project development [14]. The DHL Floating Service Center was launched in the same environment as the City Supplier from the preceding section.

Congestion and an increasing number of limitations to road transportation generated sufficient conditions for this alternative to function. The environmental benefits equally grew. DHL's van fleet was reduced from 10 to two vans. This boils down to an annual reduction by 150,000 km or 12,000 l of fuel [14]. Capacity and flexibility increase as more customers can be served a day than with the classical van solution. Finally, the transport solution brings a positive image to the city and serves as an example to other companies. In this case too, the main solution directions are found in the DHL Floating Service Center. Converting an old tourist boat is a creative technical solution. The combination with cycling messengers makes it a rather unique logistics solution. Equally, the concept allows escaping the policy limitations imposed on road transport [10].

Concluding Observations

The three mentioned Dutch concepts have a number of common characteristics. Utrecht and Amsterdam both feature a historical city center, and used historic city canals. Moreover, due to the historical character, the physical structure of the latter canals cannot be changed and therefore the canals cannot cope with the scale increase in road transport vehicles and operations. Both cities even feature a rather restrictive policy framework with respect to road transport. These all seem ingredients that contribute to the potential for inland waterway transport. The result is largely similar advantages and disadvantages of the three concepts. The characteristics are evaluated in Table 21.2. The largest benefit consists of the external cost reduction (people (less emissions and noise), planet (less emissions) and also profit (less congestion)). A negative point is the operational cost side: the extra transhipment cost is a barrier in being competitive to road transport. The last mile can also cause problems: when the distance is too large, and extra vehicles are needed, the logistics cost increases. One item that was not mentioned yet, is that full-year operations may be hampered in case canals freeze in winter time [36].

21.3.2 Waterway Transport Towards Cities

In this category, the Dutch Distrivaart, car transport, the Paris paper transport and more generic distribution as well as the Lille waste transport are elaborated on. For each of them, critical success factors are determined. These factors may also function as key success factors of inner city distribution solutions.

Dutch Distrivaart

Distrivaart was a Dutch project that consisted of transporting palletized goods via inland navigation. It envisaged a large volume shipped between distributors and retail supermarkets, with 40 ships, 17 distribution centers and 43 million pallets.

Table 21.2 Advantages and disadvantages of the three Dutch concepts

	Beer Boat	Vracht Door De Gracht	DHL Floating Service Center
Advantages			
Low external cost	x	x	x
No time windows	x	x	x
Reverse flows	x	x	x
Disadvantages			
Staffing cost	x	x	
Change of logistics habits	x	x	x
Transhipment cost increases	x	x	
Subsidy needed upon start	x		

A cost reduction of 20 % was aimed at. The inland vessels, measuring 1.20×1.00 m, could handle 520 pallets or 20 truckloads [25]. The development was part of a trend to invest in modified inland vessels. The Netherlands, for instance, invested in the Mercurial-Latistar ship, bringing grain from Wormerveer to Nijmegen [39]. Another example is the Belgian inland vessel that sails between Antwerp and Duisburg for transporting bananas at constant temperature. Also estuary shipping was an important development, with the same vessel sailing on inland waterways and the coast. Different companies like Heineken/Amstel, Bavaria, Grolsch, Coca-Cola, Albert Heijn and Schuitema showed interest. The project started in 2002 with the River Hopper vessel, to test the transport of food products via water. However, in 2005 it was stopped. The technical River Hopper installation featured problems with its loading and unloading system. Moreover, the ship was used for volumes that were too small: critical mass lacked. The system would have been break-even as of six vessels. That never happened. The main reasons are that the supplementary costs of a last mile stretch and longer lead times were underestimated [30]. Groothedde en Rustenburg [21] in their simulation research divided the project in three development phases. First, a limited number of ships had to sail as a transport network. The focus was to be on attracting shippers. A second phase entailed establishing a distribution network. This step required more intensive planning and especially data exchange. The ship was to serve as a cross-docking platform. The third phase was still more intensive. A collaborative network was to be established, for information exchange and chain orchestration to give returns. The ship would then function as a floating warehouse. The project would have become profitable in phase 1 as of 16.3 million pallets, and in phase 2 as of 26.6 million pallets.

Paris Car Transport by Water

One of the most recent urban distribution concepts by water is used in Paris. Inland waterway operator Compagnie Fluviale de Transport (CFT) takes care of a new delivery method of new vehicles along the Seine river. The vehicles are transported via water to the city, and get delivered by road to dealers and rental companies. The new service was called Distri and was developed in view of the increasing restrictions on trucks carrying cars. Trips with more than 8 vehicles per truck would be forbidden by 2016. For the 1,000 car transport trips per week towards and from Paris, this measure has a big impact. The largest car transporters stepped into the project: Gefco, CAT, STVA, TEA and Walon. Also the car producers Renault and Peugeot-Citroën expressed interest. The pilot project showed positive results, but a commercial implementation will not happen before 2016. Theoretically, a service can be scheduled each weekday. This way, more than 30,000 car transport trips per year can be met. This does not include reverse trips [38].

Paper Distribution Paris: Rouen

Since 2006, Paris transports waste paper via inland vessels to a recycling plant of paper producer UPM Kymmene close to Rouen. The sailing distance between Paris and Rouen is 210 km. Since 2008, ships with rolls of recycled paper are shipped as return load to the French capital. The ships supply some five publishers, where the most important newspapers and magazines for the Paris region are printed. The return load materialised through a co-operation agreement between UPM Kymmene, waterway operator Voies Navigables de France and Sytcom. Initially, a ship of 800 tonnes with a crane took care of transporting the waste paper. To enable the return of paper rolls with a width of 2.5 m, UPM shifted to a larger ship (1,800 tonnes) on which modified 45 foot containers are loaded. The company invested for this transport in 70 containers that are 13.7 m large. The vessel ships twice a week 30 such containers from and to Rouen. That reduces traffic on the heavily congested A13 motorway by 4,500 truck trips per year.

Paris Distribution

The Paris center features a changing logistics and mobility policy. The city investigates whether more sustainable multimodal transport can take over part of the road transport. Patier [29] showed that there is potential for waterbound distribution concepts in the Paris region. A multi-criteria analysis showed that non-alcoholic drinks and non-food products for supermarkets can better be transported via water. This type of products has a high weight-volume balance. Transhipment locations in the city center can be used to perform the last mile with truck transport. Ships with own loading and unloading cranes on board fit best. Applying the concept leads to a 55 % CO_2 reduction. In the case of the non-alcoholic drink flows, the bundling would also allow for a € 75,000 of cash savings.

Paris Franprix Inland Waterway Distribution Platform

In France, the Casino Groupe invested in a concept of urban freight distribution by inland waterways to deliver subsidiary Franprix's retail locations. From September 2012 on, Franprix delivers goods to 80 retail locations in the core of Paris via inland waterways. The concept materialised in close cooperation with logistics expert Groupe Norbert Dentressangle, the Ports de Paris and organization Voies Navigables de France. One barge represents 26 containers, or 450 pallets. These are transhipped to the barge at Bonneuil-sur-Marne's port, located at the south of Paris. Then, the barge sails 20 km over the rivers la Marne and the Seine, passing two locks. At the port de la Bourdonnais, on walking distance of the Eifel Tower, trucks leave from the terminal to the final locations, as shown by Fig. 21.4 [6].

Fig. 21.4 Transhipment of Franprix containers at Paris [6]

Every container, transported this way represents a saving of 10,000 km of road transport per year. When 48 containers are transported daily, the concept represents a saving of 450,000 km of road transport annually [6].

Lille Waste Transport

In 1999, the city of Lille, a Northern-France city of 225,000 inhabitants, started transporting urban waste by water to the incineration and recycling plants. Since September 2007, an annual volume of 200,000 tonnes got transported this way [24]. The project is part of a larger project. The 'Centre de Valorization Organique (CVO)' in Sequedin, 10 km away from Lille, processes an annual volume of 100,000 tonnes of household waste into compost or bio-fuel. The investment amounted to € 75 million, borne by the City of Lille, ADEME, the Nord-Pas-de-Calais region, Voies Navigables de France, FEDER and the European Investment Bank. The nearby bus depot uses the bio-gas for about 150 busses [24].

Concluding Observations

First of all, most of the applications of waterway towards city centers are found in France. This may have to do with the fact that national and/or local governments promote this way of transport, and set up co-ordinated approaches for doing so.

Furthermore, it seems that the French applications deal with a wide variety of products: from low-value goods (waste) to high-value products (cars). This means that solutions have the potential to work for a broad product range. Finally, it turns out that all French water transport initiatives towards cities are apparently viable: none failed. This opposed to the Dutch Distrivaart, which in essence is a similar product as the one in Paris where food and drinks are delivered by waterway transport, but which apparently was not viable. One of the reasons may be critical mass.

21.4 Urban Waterway Logistics: An Option for Flemish Cities?

This section makes an empirical analysis of a pure urban transport solution. Similarities were looked for between the concepts defined earlier and the Flemish local situation. The DHL Floating Service Center is expected to have a chance of being successful in a Flemish context. Flanders has several historic city centers with inner city waterways like for example Ghent, Bruges and Mechelen. A theoretical application is made to the city of Ghent. Ghent has a historical city center that is well accessible by water and is densely populated and therefore has a concentrated demand for goods. Additionally, like the previously mentioned Dutch cities of Utrecht and Amsterdam, Ghent features a city structure that is not favorable to road transport: many small streets, no (un-)loading areas, etc. To remedy the negative effects of road transport, the city also implemented measures like maximum axle loads and vehicle height and length. That means that more or less the same critical conditions as mentioned when analyzing the Dutch cities previously seem to be present for allowing for a shift towards waterway transport [41]. This section will analyze whether the mix of critical success factors in Ghent is sufficient for actually allowing for such a shift: are the problems with road transport so big that they provide an incentive to users to shift towards inland waterway transport, is water depth sufficient and the network sufficiently extensive, is the critical customer mass in proximity of the canals reached, etc. The solution will also be evaluated in the framework of Quak [32].

21.4.1 Physical and Waterway Structure of the City of Ghent

The City of Ghent was founded in the seventh century at the confluence of the rivers Scheldt and Leie [34]. The first canals in the city were used for defense but also trading purposes. A connection with the then nearby sea was sought by building extra canals (Brugse Vaart, Coupure and Sasse Vaart). During the twentieth century, the Beltway Canal (Ringvaart) was built [23]. During the 1960s, cars got

a lot more attention, large roadways towards and inside the city were built, and water basins were filled in order to give way to roads and parking areas [11]. In the nineties, Ghent drafted a "Revitalization plan" for it canals, with two components: first, revitalizing the Leie in the historical center, and re-opening the Nederschelde; second, replacing some fixed bridges by movable ones and refurbishing quay walls. Water tourism was the main driver for this. Therefore, today, the region of Ghent holds some 917 km^2 of waterways.

21.4.2 Concerned Actors

In Ghent, two actors are considering introducing a water transport system. The first partner is Max Mobiel, a not-for-profit organization that supports the development and introduction of sustainable initiatives for mobility and employment in the Ghent area. At current, Max Mobiel hosts in Ghent a commuting service between the railway station and company zones, a biking point (bike rental, repair and storage), and a courier service mainly for documents. The courier service functions based on biking messengers combined with light vans [27]. The second partner is Elektroboot. This actor is a not-for-profit organization and has an electricity-propelled motor boat, the "Sidderaal", that initially was used as a free commuting service. The goal was to promote the introduction of environment-friendly and low-noise vessel propulsion techniques. An advantage is that the vessel is fully depreciated, so that the capital cost decreases strongly. In the beginning, the project got support, also financially, from the City of Ghent, the Province of Eastern Flanders and a number of sponsors. These two partners, but also other potentially concerned stakeholders, as well as the roles they may take, are summarized in Fig. 21.5.

The two mentioned parties alone are not sufficient for making the project a success. The parties from Fig. 21.5 are all needed to develop a successful water transport concept. The goal is picking up express shipments (small parcels, mail and light goods) at the city borders, and bring them to the city center via the water with an electrical boat. A small depot outside the historical city center may be needed in order to provide temporary storage. Elektroboot makes available its vessel. Working with the existing vessel is the base scenario. Investment alternatives can be calculated. The latter can imply serious impacts on the last mile cost [4, 10, 20]. A transhipment area or depot would be the starting and ending point of one or more daily rounds. In the first phase, it can be a mere mooring location. Later on, a storage area may be crucial, as goods can then be stored at night in order to be delivered the next morning. Logistics activities may be performed in this premise [10]. The city will need to be involved. It is since 2008 a member of the CIVITAS project, and may support the inland waterway solution as part of CIVITAS. Transporting mail by waterway is a new concept for Ghent. Possibly, a number of infrastructural measures are needed (quay walls, ship fixing points, etc.). The canals may need to be updated too: some locations may feature too shallow water. Waterway operator "Waterwegen en Zeekanaal" needs to be involved

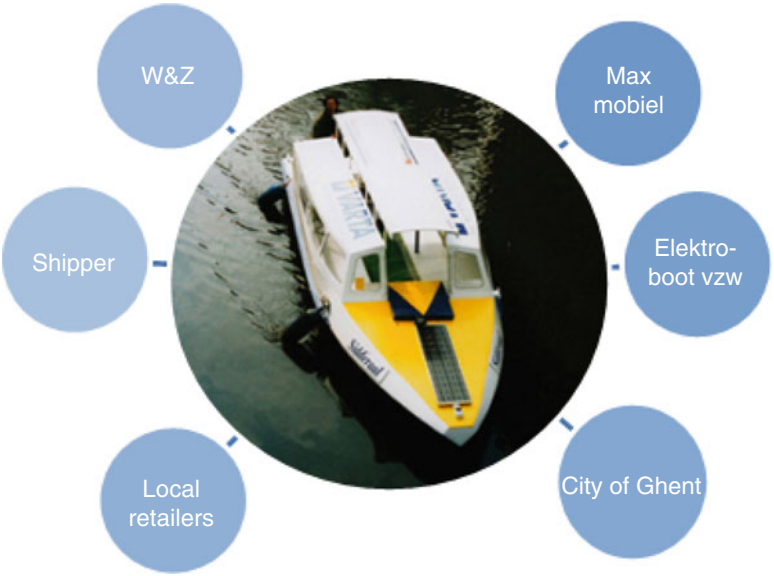

Fig. 21.5 Potential partners Elektroboot project

therefore. Finally, shippers, receivers and logistics operators need to be convinced about the project. To reach them, more exposure will need to be achieved. The city's commercial associations, street managers, etc. need to be involved, so as to make the advantages of the project clear.

21.4.3 Cost-Benefit Analysis

This section trades off costs and benefits of the concept. Consecutively, the sailing reach, the goods types and the customers are dealt with, as well as operational and social costs under a number of operational scenarios.

The Sailing Reach

The sailing reach is largely determined by the dimensions of the vessel. This happens because the existing infrastructure (bridges and locks) and the characteristics of the waterways themselves (width, depth, etc.) can obstruct the vessel. Ghent counts 42 bridges and locks in its inner city. In the first phase, the existing vessel "Sidderaal" can be used. Its characteristics are shown in Table 21.3 [4, 10]. The Sidderaal is propelled by an electrical engine that provides the necessary power for propelling the ship. The ship is equipped with a Solar charge function, which

Table 21.3 Technical characteristics of the Sidderaal [10]

Properties	Dimensions
Length	7.48 m
Width	2.20 m
Coaster profile	1.4 m
Average empty draught	50 cm
Average draught upon full load	55 cm
Net weight	3.5 tonnes
Freight capacity (tonnage)	1.5 tonnes
Electrical engine power	3 kW
Battery sailing hours	8 h
Battery charging time for full charging	4 h

enables it to sail without quay power. Battery packages on board the vessel are charged with solar energy when the ship is not sailing. They provide the necessary energy when the engine requires more energy than provided by the photovoltaic panels on board [15].

Goods and Customers

In a first phase, the Elektroboot can mainly be used for re-enforcing existing deliveries by Max Mobiel. The company caters for deliveries within the Ghent territory (all 9000-postal codes + some sub-municipalities). Volumes are brought in by the partners in this project. The goods then have to be transported by bike from the quay to the end destination, which imposes limitations on allowable weights. In a later phase, the two pulling parties envisage collaboration with logistics service providers like DHL, TNT, B-Post, Taxipost, La Redoute, etc. Max Mobiel will take care of the logistics system, since they can then manage the administration, track the receipt and perform the last mile. Figure 21.6 shows a suggested round trip. The Sidderaal can sail on all indicated waterways. There are no limitations as to length, width or depth. The red line is the approach route. The node between the red line and the blue round trip line is the transhipment location.

Operational Expenses

For the cost-benefit appraisal, operations are assumed to take place 8 h a day, five days per week during 46 labor weeks. This takes into account holidays, the ship not being available due to maintenance and repair, and possible ice formation on the city's canals (6 weeks a year on overage). The main cost parameters are staff cost, maintenance, insurance, administration and communication. As to staff cost, there are possibilities to use social employment. Max Mobiel employs for its cycle messaging services staff under special conditions. As that is always temporary, the calculations in this section take into account the full cost.

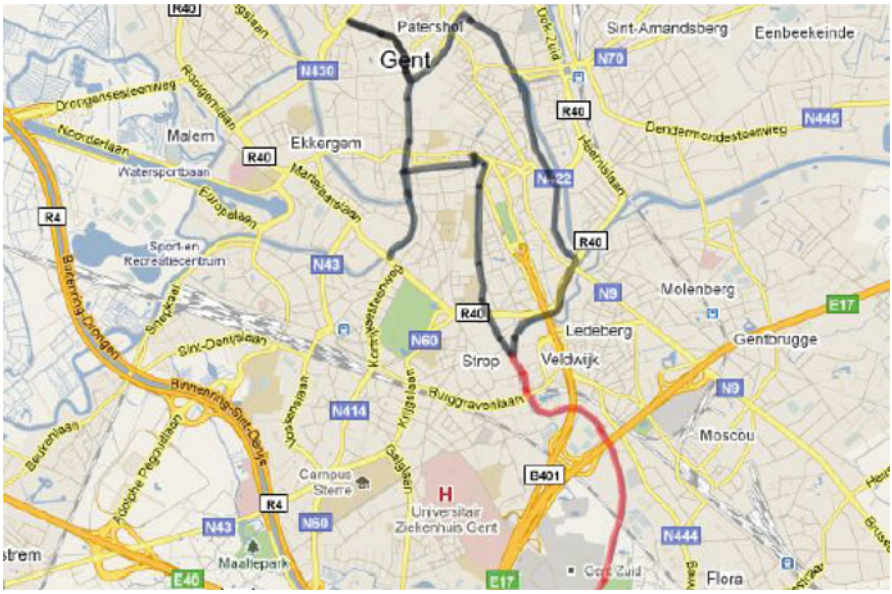

Fig. 21.6 Possible round trip

The cost parameters are quantified in Table 21.4. Staff costs are calculated by multiplying hourly cost figures for the sector with 1.5. The reason is that one full-time steering captain is needed, as well as a half-time cycling messenger for the last mile. Electricity usage is limited, just like port dues. Maintenance amounts to € 22 per day. Other expenses amount to € 40 per day. In sum, assuming 230 working days a year, a total daily cost of € 325.87 is obtained. Each working day allows for two round trips. Reverse flows are not considered.

For calculating the necessary time of a round trip, the following components are considered [16].

- Sailing time: 2 h.
- In the historical heart of Ghent, the maximum allowed sailing speed amounts to 5 km/h. The distance sailed is a bit less than 11 km.
- Mooring and unmooring and delivering shipments to cycling messenger: 1h20.
- Mooring and unmooring is assumed to take 5 min. Delivering the shipment to the cycling messenger takes 1 min, and is to be performed at 13 scheduled mooring locations.
- Lock passage: not applicable.
- Departure and arrival: 30 min.
- Departing and arriving from the depot each are assumed to take 15 min.

The depot is located at about 2.75 km from the city center, located at the bottom of Fig. 21.6. Maximum sailing speed is 12 km per hour. To cover the total trip distance, Elektroboot needs about 4 h. The Sidderaal has a maximum cargo capacity

Table 21.4 Cost parameters Elektroboot concept, when using Sidderaal [4, 10]

Staff cost	Per year	Per day
Persons on the ship for (un-)loading = 1 FTE	60	260.66
Daily staff cost		173.66
0.5 FTE cycling messenger		87.00
Electricity usage (quay power)	1	4.34
Port dues	0	0
Repair and maintenance	5	21.73
Other costs	9	39.11
Insurance	1.5	6.52
Staffing equipment	5	21.73
Communication	2.5	10.86
Ship depreciation	0	0
Exploitation: 8 h per day, 5 days per week, 46 weeks per year		
Total daily cost		€325.87

of 1.5 tonnes. It will be hard to reach full capacity utilization in the beginning. Max Mobiel at current has some 6.26 deliveries per day, with some 10 deliveries per trip, so it can realistically be said that in the base scenario about 62 deliveries can be made with the Sidderaal, or 31 deliveries per round trip. Table 21.5 makes a comparison of three possible operational scenarios, assuming that in the alternatives, an investment in a new ship with and without crane is made. A new ship would cost about € 100,000. A new ship with a crane would even cost € 250,000. Depreciation happens over 10 years. In the case of a crane on the new ship, 2 FTE of staff are needed, and repair and maintenance expenses will be higher. All other parameters are assumed to remain equal.

Figure 21.7 visualizes the cost calculation per scenario, and, as opposed to Table 21.5, includes the depot cost. That implies that in case of own management, capital and interest costs need to be added, as well as depreciation, registration and property expenses, heating/cooling, electricity and all other maintenance costs. The annual depot cost is estimated at some € 7,500. Per delivery, that would mean an additional € 0.53. Transhipment in the depot and staffing are the most important cost categories. A comparison is also made with the classical van scenario. In order for the inland navigation scenario to be competitive with the classical van scenario, for scenario 1, at least 64 deliveries per day are needed, at a cost of about € 5 per delivery. The scenario 2 curve slightly outpaces that of scenario 1. In order for scenario 3 to be competitive with the classical van solution, at least 130 packages per day would be needed.

An element not valued in the above calculations, is the increased reliability: in general, it can be assumed that reliability is higher for the waterway solution than for the classical van solution, due to the absence of congestion, unforeseen road obstacles, etc.

Table 21.5 Cost parameters Elektroboot concept, under three scenarios [4, 10]

	Sidderaal (base scenario)	New ship (scenario 2)	New ship with crane (scenario 3)
Staff	1.5	1.5	2.5
Daily staff cost (1 or 2 FTE)	(1.5) 260.66	(1.5) 260.66	(2.5) 434.43
+ 0.5 FTE cycling messenger (0.5)			
Electricity usage (quay power)	1,000	1,000	4,500
Port dues	0	0	0
Repair and maintenance	5,000	5,000	15,000
Other costs			
Insurance	1,500	1,500	3,000
Staffing equipment	5,000	5,000	7,500
Communication	2,500	2,500	5,000
Ship depreciation	0	10,000	25,000
Total daily cost	325.87	369.35	695.29
Exploitation: 8 h per day, 5 days per week, 46 weeks per year			

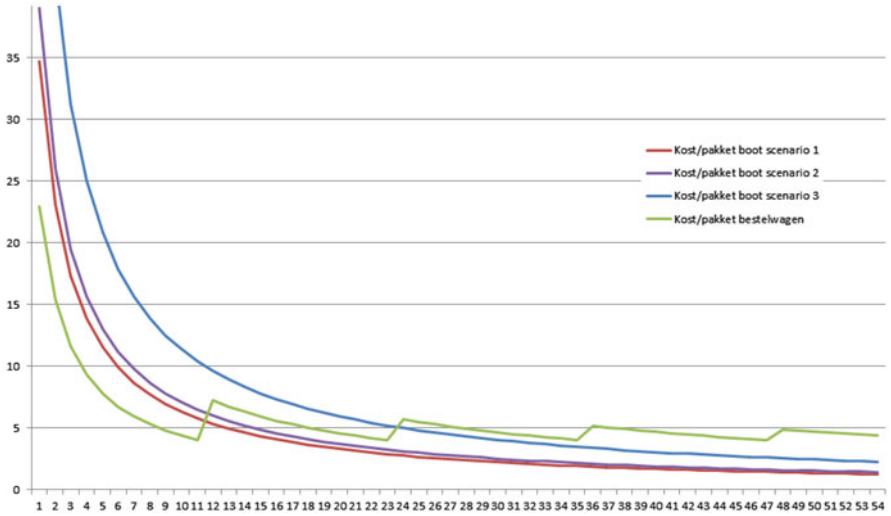

Fig. 21.7 Cost per package ship and van scenarios (including depot cost)

Social Benefits

The appraisal not only experiences operational cost impacts, but it also generates benefits to society. It contributes, in combination with other measures of course, to less congestion, emission and noise hindrance, heritage damage, road damage, accidents, etc. The Elektroboot concept can replace 1.5 van trips per round trip. That amounts to 690 road trips per year. Each van drives on average 30 km per trip. Multiplying by external unit costs per tonnes-km of 0.0241 for Elektroboot

and 3.45 for road transport respectively, results in annual external costs of € 10 for Elektroboot and € 500 for road. These calculations do assume full capacity utilization.

21.5 Transdisciplinary Discussion on Urban Waterway Logistics

The illustrated inland waterway urban distribution concept clearly has a number of benefits, but needs sufficient capacity on the inland waterways and a critical mass of users. Operational capacity is of course limited by existing infrastructure (sailing width, height of bridges and locks, draught, etc.). Waterway capacity may be expanded, but that may raise three other issues: physical limitations, potential safety impacts and potential environmental impacts. First of all, expanding waterways is problematic, as, apart from expanding canals being expensive and difficult in urban circumstances, it requires increasing water volumes. It may not be easy to get those volumes. Urban distribution at that moment is competing with other uses of the same water, for drinking purposes, for instance. Teaming up with urban tourism, which might also benefit from increased water volumes in cities, might be an option. But even if it were possible to achieve increased water volumes, having them present in city centers may increase the risk of floodings. That will require extra infrastructural measures to be taken, which again will be expensive, and those costs will need to be borne by someone. Furthermore, getting more water inside city centers may technically be possible, but not desirable from an environmental point of view: it may lead to a changed water balance over the network, inducing salinity problems in some locations. A better solution than expanding waterway capacity seems to be to expand ship capacity in such a way that no deeper draught nor more height are needed. Length and width of the vessel may be expanded, to the extent that does not hamper the manoeuvring of the vessel. A direct link with transport of water also occurs when the water cannot be transported anymore: in case of frost, for instance, city canals may be frozen, and the urban distribution may be blocked. It was mentioned before that the number of frost weeks in Belgium is rather limited, but that may not be the case in other cities that are potential users of the concept. Also, it should be noted that city environments usually have a micro-climate with temperatures being slightly higher than outside cities.

21.6 Conclusions and Future Research

It is clear from the preceding analysis that transporting certain commodities by water inside cities may deliver benefits. However, the concept was also shown to be conditional. First of all, scale of operations should be sufficiently large, in order

for the project not to be structurally loss-making. Second, and related, to reach that scale, it helps when the city's roads are congested and when the government is taking measures for alleviating road problems and reducing the number of truck or van trips. Third, internalization of external costs throughout the logistics chain would reinforce the case for urban waterway distribution. Fourth, the image of inland waterway transport also needs to be changed. The classical view is that inland barging only applies to bulky goods, and more recently also containers. It was shown in this contribution that it can also be a solution for much smaller unit parcels. It would be interesting now to scientifically verify whether the proposed solution still holds in other circumstances, and under which conditions it does so: changing water levels, physical limitations, urban policies, etc. That would imply a kind of sensitivity analysis. Furthermore, it would be interesting to determine whether a public or rather a private or a combined approach is more suitable. It looks like in order to achieve sufficient volume, most projects would at least require some public subsidy when operated privately. Also best practices of waterway transport towards cities were considered, and show potential. Many of them can be complementary to inner city waterway distribution. Examples of potential application are waste collection. It would be interesting to analyze what the possibilities are, and what operational and social benefits they offer.

References

1. Aanstoot B. Oude binnenstad van utrecht bevoorraad per schip. VAK M, 22–25, 2010.
2. Amsterdam.info. De amsterdamse grachten. http://www.amsterdam.info/nl/grachten/, 2009.
3. Bier D. Welbesteed, 2009.
4. Birnie D. Electroboot founder. various meetings, 2011.
5. Buck Consultants International. Eindrapport: Regionale bevoorrading stadsregio amsterdam. Nijmegen: Stadsregio Amsterdam; 2009.
6. Casino Groupe. Franprix container transhipment paris. http://www.groupe-casino.fr/IMG/jpg/image_3_grand.jpg, 2014.
7. Cornillie I, Macharis C. Pallets on the inland waterways: a river regional distribution concept, 2006.
8. Dablanc L. Goods transport in european cities : Difficult to organize, difficult to modernize. Transp Res A. 2007;41:280–5.
9. De binnenvaartkrant. http://www.debinnenvaartkrant.nl/2/images/uploadkrant/pdf/2005/200503_0102.pdf, 2005.
10. Desclée M. Waterwegen: de oplossing voor binnenstedelijke problemen? toepassing: haalbaarheidsstudie project ŚelektrobootŠ. Master's thesis, Universiteit Antwerpen faculteit toegepaste economische wetenschappen, 2011.
11. Dewilde E. Gent, een stad aan het water. http://users.telenet.be/tundraqueen/belgie.htm, 2008.
12. Dijkhuizen B. Mokum mariteam amsterdam: duurzaam door de grachten. http://www.logistiek.nl/distributie/duurzaamheid-regelgeving/did12891-mokum-mariteam-amsterdam-duurzaam-door-de-grachten.html, 2010.
13. Ecofys. Rapport "emissiebesparing door inzet elektrische bierboot". Ecofys Netherlands, 2008.

14. Eichwald H. Dhl's floating distribution centre. http://wx.toronto.ca/inter/mte/mte.nsf/f2c6f08d57948f1e8525678d004e6755/7283332c182723488525681200 6a1f60?OpenDocument, 1999.
15. Elektrischvaren.info. 2008 het jaar van de zon? http://www.elektrischvaren.info/?nr=318, 2011.
16. Elektroboot vzw. Elektroboot gent ambassadeur sociale economie 2007,. http://www.elektroboot.org/home.html, 2007.
17. European Commission. Groenboek een nieuwe stedelijke mobiliteitscultuur. SEC(2007) 1209, COM(2007) 551, Brussel, September 2007.
18. European Commission. Witboek stappenplan voor een interne europese vervoersruimte Ű werken aan een concurrerend en zuinig vervoerssysteem. SEC(2011) 359, SEC(2011) 358, SEC(2011) 391, COM(2011) 144, Brussel, Maart 2011.
19. Expertise en Innovatie Centrum Binnenvaart (EICB). Mini distrivaart utrecht vervolg. http://www.informatie.binnenvaart.nl/innovatie/technieklogistiek/169-bierboot-utrecht-tweede-vaartuig-.html, 2008.
20. Gevaers R, Van de Voorde E, Vanelslander T. A quantitative assessment of last-mile characteristics in b2c supply chains and urban distribution. In: METRANS: Urban freight conference, Long Beach, USA, 12-14/10/2011, 2011.
21. Groothedde B., Rustenburg M. Distrivaart netwerkontwikkeling de weg naar een volwaardig netwerk in de binnenvaart. Technical report, TNO INRO rapport 2003-014, Delft, 2003.
22. Hesse M. The city as a terminal: the urban context of logistics and freight transport. Alderschot: Ashgate Publishing Limited; 2008.
23. Hesters L. De heropening van de gentse binnenwateren. http://www.watererfgoed.be/Docs/WEV%204%20mei%202010%20-%20Hesters.pdf, 2010.
24. INE/EFIP. Urban transport, september 2008. http://www.inlandnavigation.org/uploads/Brochures/ine_efip_urban_transport.pdf, 2008.
25. Kia M, Shayan E, Ghotb F. Positive impact of distribution centres on the environment. Transp Rev. 2003;23(1):105–22.
26. Mokum Mariteam. Mokum mariteam: Vracht door de gracht. http://mokummariteam.nl/, 2012.
27. Max Mobiel. Max mobiel. uw partner in slimme woon- en werk mobiliteit! http://www.max-mobiel.be, 2012.
28. NCSI. Innovatieve werkplek: Dhl floating service centre. http://www.ncsi.nl/nl/kennis/kennisbank/innovatieve-werkplek--dhl-floating-service-centre/683?q=duurzame%20inzetbaarheid&p=10, 2009.
29. Patier D. The conditions of modal shift in dense urban areas. In: Taniguchi E, Thompson R, editors. Innovations in city logistics. ISBN 978-1-60456-725-0, 2008.
30. Philipsen L, Bosman W. Te vroeg voor initiatieven als distrivaart? http://www.logistiek.nl/archief/id9805-Te_vroeg_voor_initiatieven_als_Distrivaart.html, 2005.
31. Platform voor elektrisch en hybride varen. Doop elektrische city-supplier in amsterdam. http://www.elektrischvaren.info/?nr=454, 2011.
32. Quak H. Sustainability of urban freight transport. retail distribution and local regulations in cities. ERIM, 2008.
33. Schuttevaer. Dhl-pakjesboot heeft zich bewezen in amsterdam. http://www.schuttevaer.nl/nieuws/actueel/nid7749-dhl-pakjesboot-heeft-zich-bewezen-in-amsterdam.html, 2007.
34. Stad Gent. Beknopte geschiedenis van een koppige stad. http://www.visitgent.be/eCache/VGN/2/288.html, 2008.
35. StadsOntwikkeling. Terug van weggeweest: bevoorrading via de werfkelders aan het water. http://www.utrecht.nl/smartsite.dws?id=168424, 2010.
36. Stevenson R. In amsterdam, packages travel via canals, bicycles. http://www.reuters.com/article/2009/07/15/us-dhl-amsterdam-boat-idUSTRE56E2TE20090715, 2009.
37. Stulemeijer F. Bierboot heet voortaan ŚstroombootŠ. http://www.unizo.be/transportcoach/pp_blog.jsp?id=4400, 2010.

38. Todd S. Barges ready to bring new cars into paris. http://www.ifw-net.com/freightpubs/ifw/index/barges-ready-to-bring-new-cars-into-paris/20017903184.htm?source=ezine&utm_source=IFW+Daily+News+Bulletin&utm_campaign=2bdace5ffe-IFW_13_9_119_13_2011&utm_medium=email, 2011.
39. Van Rulo V. Mercurial-latistar en de logistiek van tarwezetmeel. Master's thesis, Hogeschool Rotterdam, 2003.
40. Velthoven A. Dhl pakjesboot tien jaar in de vaart. http://www.ttm.nl/nieuws/id22691-DHL_pakjesboot_tien_jaar_in_de_vaart.html, 2007.
41. Walgraeve V. Stedelijke distributie in beeld via bevoorradingsprofielen: Casestudie gent. Universiteit Gent, 2010.

Chapter 22
Reactivation of the Small Inland Waterway Network

E. van Hassel

Abstract Inland shipping in North Western Europe is a well known transportation mode which can make use of a large and dense inland waterway network. However in the last 50 years no new small inland ships have been built. The reasons why these small inland ships are disappearing are explained. In order to deal with the diminished supply on the small inland waterways a new type of inland navigation system is proposed. A methodology is developed to research this new inland navigation system. In the developed methodology a network design, tug and barge design, transportation costs and competition models are combined into a single model. The main goal of the total model is to determine the profitability, expressed in the Net Present Value (NPV), of the investment in a specific ship and network design. Also the link between transport function of waterway and the actual design of the waterway network is made. Lastly the role of the government is discussed in how it could facilitate the reactivation of the small inland waterway network.

22.1 Introduction

Inland shipping in North Western Europe is a well-known transportation mode that can make use of a large and dense inland waterway network. This network consists of several types of waterways that are either small canals or large rivers. This waterway network has different functions, such as providing a freight transport network for inland ships, or it can be used as a network for leisure ships and it is also used as water management network.

This chapter deals with the freight transport function of the inland waterway network and more in particular the small inland waterways. The inland waterway network has different types of waterways and for each type of waterway an inland ship type is developed. On the small inland waterways, for instance, only ships with a payload up to 600 tonnes can be used (length smaller than 50 m). These small waterways make up 50 % of all the navigable waterways in Flanders (Belgium).

E. van Hassel (✉)
University of Antwerp, Antwerp, Belgium
e-mail: Edwin.vanHassel@UAntwerpen.be

C. Ocampo-Martinez, R.R. Negenborn (eds.), *Transport of Water versus Transport over Water*, Operations Research/Computer Science Interfaces Series 58,
DOI 10.1007/978-3-319-16133-4_22

However, in the last 45 years, no new small dry cargo inland ships have been built. As a result, the small inland fleet is diminishing, and cargo formerly transported by small inland ships risks being shifted to road transportation.

The aim of this chapter is to briefly clarify the reasons behind the reduction of the small inland fleet. The second aim is to show that it is best to develop a new shipping system instead of adjusting the inland waterway infrastructure. In the concept development stage it is important to both consider the technical and the economical aspect. The third aim is to show that it is possible to re-activate the small inland waterways with a developed new inland navigation system that, first of all, can compete with its competitors, primarily road transportation, and also provide a sustainable transport option. Also two different implementation strategies are considered. An application is made for the Flemish small inland waterway network.

Further on, a link will be made between the transport function of the (small) waterways (transport over water) and the inland waterway network itself (transport of water). Next, the role of the government is discussed with respect to the re-activation of the small inland waterways. This chapter will conclude with conclusions and directions of further research.

22.2 Case Study

22.2.1 Introduction

The inland ships that are sailing on the inland waterways provide a sustainable and reliable transportation mode. In the Netherlands, 40 % and in Flanders 11.5 % of the total transported cargo is transported by inland shipping [5]. These inland waterways have a spare capacity, contrary to the already heavily congested roads. Therefore, these inland waterways can play a vital role in dealing with the growing demand for transportation in The Netherlands and Belgium. In Fig. 22.1, an overview of the inland waterways in the Netherlands and Belgium is given.

Figure 22.1 shows that the inland waterways form a dense network that connects the two main ports in the Hamburg-Le Havre range (port of Rotterdam and the port of Antwerp) with its hinterland. There is some difference between the different waterways. There are large rivers (Rhine, Waal, Scheldt and Maas), small rivers, where only small inland ships can sail, and men-built waterways (i.e., canals) (either large or small).

Every waterway has its own characteristics and own maximum type of inland ship capable of sailing on that waterway. All these waterways are categorized into different C.E.M.T. classes. The classes are based on the maximum dimensions of the ships that are capable of sailing on that waterway. An overview of these different waterway classes can be found in Table 22.1.

In this research, small waterways are considered to be of class II and smaller. Waterways of class III and IV are classified as medium sized waterways rather

Fig. 22.1 Inland waterways in the Northwest of Europe [2]

Table 22.1 Overview of the different waterway classes [7]

Class	Length (m)	Width (m)	Draft (m)	Air draft (m)	Payload ship (tonne)
I	38.50	5.05	1.8–2.2	4	250–400
II	50–55	6.6	2.5	4 to 5	400–650
III	67–80	8.2	2.5	5 to 5	650–1,000
IV	80–85	9.5	2.5	5.25–7	1,000–1,500
Va	95–110	11.4	2.5–4.5	5.25–7	1,500–3,000
Vb	172–185	11.4	2.5–4.5	9.1	3,200 (barge convoy 1 × 2 barges in length)
VIa	95–110	22.8	2.5–4.5	7–9.1	3,200–6,000 (barge convoy 1 × 2 barges a breast)
VIb	185–195	22.8	2.5–4.5	7–9.1	6,400–12,000 (Barge convoy 2 × 2 barges)
VIc	193–200	34.2	2.5–4.5	9.1	9,600–18,000 (Barge convoy 2 × 3 barges)
VIIb	195/285	34.2	2.5–4.5	9.1	14,500–27,000 (Barge convoy 3 × 3 barges)

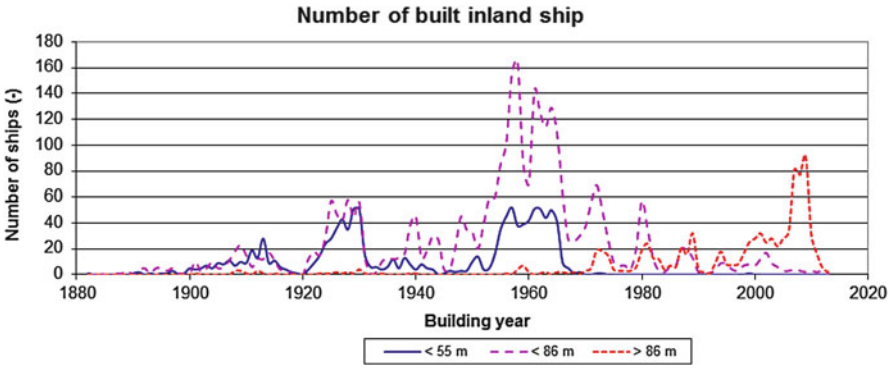

Fig. 22.2 Overview of number of built dry cargo inland ships (own figure based on [14])

than small waterways. The waterways of class V and larger are considered large waterways. The main dimensions of the ships are limited by either dimensions of the smallest locks located on that waterway (length and width) or by the depth of the waterway (draft). The air draft is limited by the height of the bridges crossing the waterway. Therefore, small ships are defined as ships that can sail on those small waterways. It are these small inland ships that are not being built for the last 50 years and, as a result, are disappearing. This is illustrated in Fig. 22.2 where the number of ships built per year are given for three different types of dry cargo inland ships (smaller than 55 m, smaller than 86 m and larger than 86 m).

This will lead to a situation where the small inland waterway infrastructure will not be used at all in the near future by dry cargo inland ships. In this case study, a new concept will be suggested that could be used to reactivate the small inland waterway network. This case study is structured as follows. First, a short explanation will be given of why these small ships are disappearing. Secondly the new concept will be proposed. In order the research this new concept a model has been developed. This model will be explained in Sect. 22.4. In Sect. 22.5 the application of the model will be given.

22.2.2 Reduction of the Number of Small Inland Ships

A lack of new building of small inland ships, the increasing age of the existing small inland navigation fleet and a lack of influx of new captain owners for small ships are the major reasons that, without intervention, in the near future the small inland waterways risk not being used anymore. Due to a shortage of supply on the small waterways, companies that are located at small inland waterways, will use road transport instead of inland navigation or they could relocate their activities.

This section will deal, briefly, with the analysis behind the lack of new small inland ships. In Fig. 22.3, a schematic overview is given of the mechanism that will

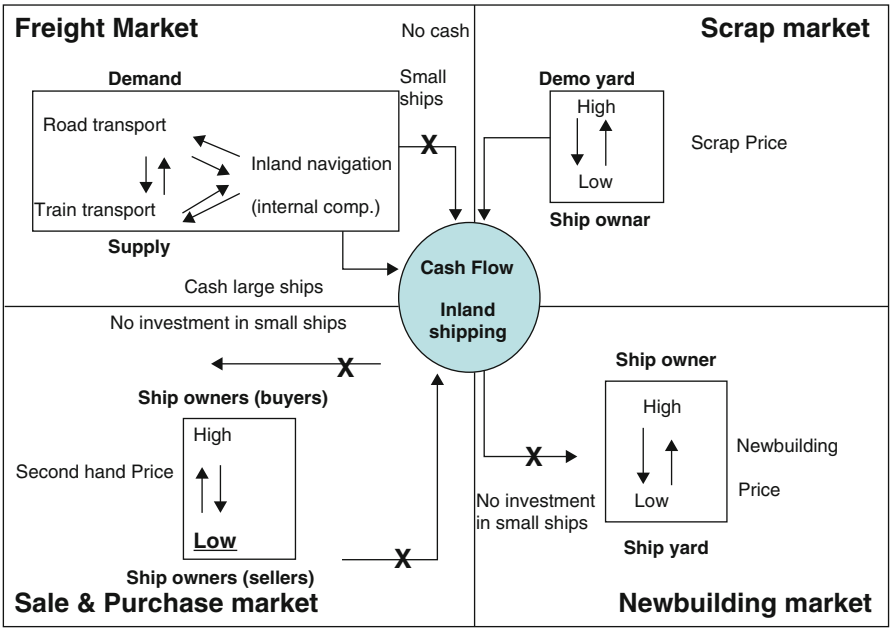

Fig. 22.3 Overview of the cash flow mechanism of inland navigation [10]

lead to the lack of new small inland ships. This lack is explained by the lack of cash available in the sector. The major underlying reasons for the lack of cash and therefore no new construction of small inland ships are the following:

- Competition of other modes of transportation and other inland ships.
- Economies of scale of the inland fleet.
- Banks/investing companies not willing to invest in small ships.
- New ship-owners not willing to operate a small ship.
- Large entry and exist barriers.

In Fig. 22.3, the four different shipping markets are given (freight, sale & purchase, newbuilding and scrap market) [10]. The first market that is described in this figure is the freight market in which the small inland ships have to operate. In this market, the ships have to compete with their main competitors:

- Road transport
- Train transport
- Other inland ships:
  - Large inland ships
  - Small inland ships
- Intermodal transport (combination of barge, train and road transport)

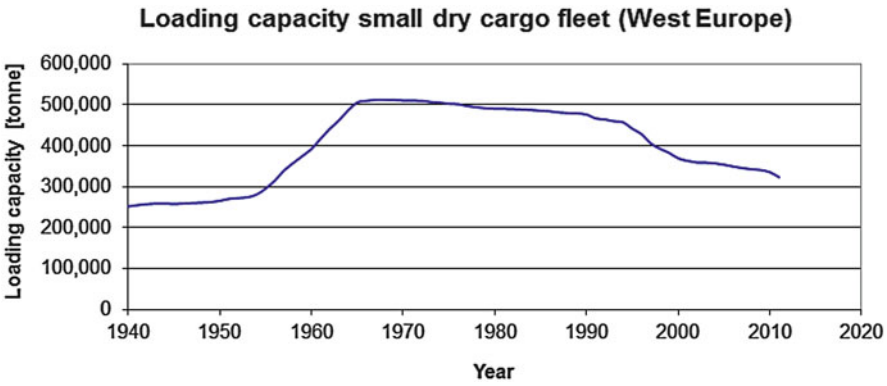

Fig. 22.4 Evolution small dry cargo fleet in Western Europe (own figure based on [14])

Due to the severe competition of road transportation and larger inland ships, small ships do not generate enough money while large ships can.

Due to the lack of cash (own equity and debt financing) not enough money is available to buy second-hand ships and as a result the price of second-hand ships will be reduced. As a result, the second-hand market, i.e., the sale & purchase market, will hardly generate money and no cash will be moved into the small inland shipping (SIS) market. If the second-hand prices drop and the market conditions are bad, no new ships will be ordered. Therefore there will be no new-building market for the small inland ships.

The only cash that will flow into the SIS market will come from the scrap market or the rebuilding market. In the latter case, the ships will be transformed into a living ship for example. As a result, the number of small inland ships will be reduced. This can be observed in Fig. 22.4 where the evolution of the small dry cargo fleet is given.

The supply on the small inland waterway network is diminishing mainly due to too severe competition from road transportation. This has resulted in five main consequences:

- No new small inland ships are being built.
- Technical decline and withdrawal of the existing small inland fleet.
- Limited to no inflow of new young captains for the small inland fleet.
- Reduction of the number of available captains.
- Insufficient maintenance of the small inland waterway infrastructure.

A consequence of the diminishing small inland fleet is the inevitable disappearance of diversity in the total inland fleet. The new ships that are being built are increasing in size and therefore the available sailing area of these ships is reduced because the larger ships can only sail on a limited number of inland waterways. There is consequently a serious risk of being left with only large inland ships, while more than 50 % of the inland waterway network can only be reached with smaller

(smaller then 600 ton) ships. Due to an increasing number of larger ships (and also their respective capacity), an overcapacity in the larger inland shipping segment has occurred [12].

With respect to the small inland waterway infrastructure, the diminishing small inland fleet in Flanders will lead to a shift of 4,000,000 tonnes of cargo from the waterways to the road [13]. Those tonnages are added to the already heavily congested roads. These extra tonnages and the further increase in cargo flows will lead to more investments in expanding the road capacity, while the available infrastructure of the small waterways will not be used at all. This capacity is very much needed to deal with a large part of the total tonnages to be transported. As the waterways are cheaper to maintain than roads and as they are already present, no new infrastructure investments are needed to deal with a large part of the total transported tonnages.

Due to a growing awareness of environmental care and carbon footprint, the EU member states want to stimulate the use of the modes producing the lowest amount of emissions per transported tonne.km. These emissions in transport could be diminished by the reactivation of the small inland waterway network providing transport of part of the cargo flows.

22.2.3 Proposing a Solution

Adjusting the Infrastructure

In order to deal with the previously mentioned problems of increasing congestion on the road network and growing awareness of environmental care, and the diminished supply on the small inland waterways, two main solutions are developed. The first suggested solution is to upgrade the existing small inland waterway network from CEMT II to CEMT IV.

For this the locks on the waterways have to be enlarged and the canal width and depth have to be increased. Besides the previously mentioned adjustments, also a new bottom and side banks have to be installed. This approach is applied in The Netherlands where two small inland waterways in the southern part of the country are upgraded from class II to class IV waterways [6]. This Dutch approach of dealing with the reduced sailing area of the current inland fleet is simulated here for the Flemish small inland waterway network. In [13] it is calculated how much money is needed to execute the required investments. The unit costs of performing the required works are taken from [11]. The calculations have shown that the total costs of upgrading the small waterways in Flanders are at least €1.7 billion. This is quite a large amount of money which will exceed the current budget of upgrading and maintaining the total inland waterways in Flanders by 755 to 1. The total budget for investments in the inland waterway network in Flanders up to 2015 is limited to €2.248 million [3]. Besides the very large costs, also the time needed to complete all the necessary work is very long. It will take years, or even decades,

to complete all the works. It is therefore decided not to focus on the enlargement of the small inland waterway infrastructure but to develop a new inland navigation system that will be adjusted to the existing small inland waterway network.

Adjusting the Shipping Concept

The new concept that is developed can be described as a two-stage tug and barge concept. In the first stage, the tug and barge concept sails in its usual configuration with several barges pushed by a single tug and traveling through large inland waterways from seaports to the entrance of the small inland waterway. In the second stage, at the entrance of a small inland waterway, the convoy is uncoupled and several small barges will sail separately to their different destinations on this waterway.

Push-barge convoys have already been used for a long time on the large waterways in Europe (Rhine trade) and the United States (Mississippi trade). In those push barge convoys, the barges are left behind at the starting point and end point of the trip. These barges can therefore be handled without the presence of a push ship so that the most expensive part of the ship (the main engine(s) and crew members) can be better deployed. At the places where the barges are left behind, a port tug is used to relocate the barges from a clustering point to the terminal. These push barge convoys consist of large push barges.

In the small barge convoy system the barge size will be decreased in order to make such a system applicable for the small inland waterways. The main focus of the concept is to combine economies of scale on large waterways (i.e., tugs and barges together) while the individual barges are small and economically feasible enough to sail on small waterways. In this way the total convoy could compete with road transportation. Figure 22.5 gives an overview of the small barge convoy system.

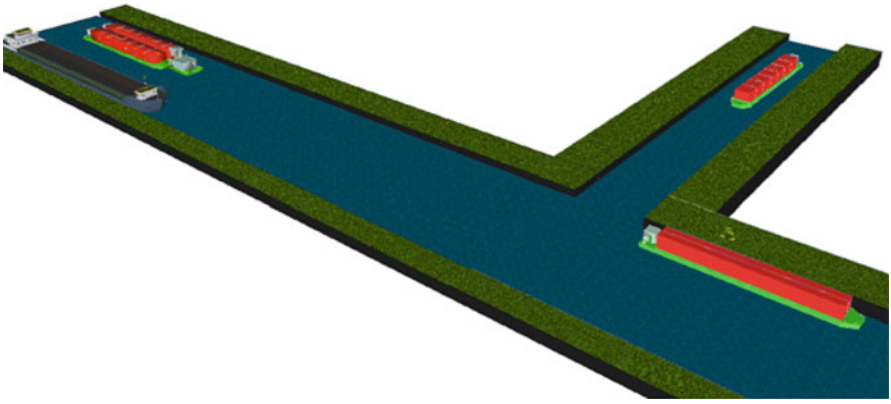

Fig. 22.5 Overview of the small barge convoy system [13]

The concept will have different crews who will operate the tug and the barges. One crew will be operating the tug when the barges are pushed to and from the entrance of the small inland waterways and the seaport. This crew will also deal with the coupling and uncoupling of the barges. This crew will work in a week on/week off regime on the tug so that the crew will not live on board. The next crew will be located in the seaport where they will move the barges from the barge collection point to the terminals in the port. The last crew is a flexible one who will sail the barges, if necessary, on the small inland waterways. This new captain gets on board and sails the barge to the final destination. When the barge is moored, the captains will be brought back to the starting point. These captains will go home when the work is done. It is also possible that people can rotate for instance from seaport-duty to small-river duty or from small-river duty to push-ship duty. This will make the work more diverse.

The barges are "exchanged" at the seaport and at the entrance of the small waterway. The small barge captain does not need to start his sailing activity right at the moment that the tug and barge convoy reaches the entrance of the small waterway. The barges will be left behind at the exchange point and the next day the barge captain can start his work. The barges that have to be sailed back to the seaport only need to be present when the tug and barge convoy reaches the exchange point. Because in the small barge convoy system the barges can sail independently, it is not necessary to have a port tug for the relocation of the barges in the seaport.

For propulsion, the barges use electric engines powered either by a generator set located in the aft of the barge or by batteries located in the double bottom of the barge. Also a combination of the two systems is possible. Several systems could be used to charge the batteries. A power connection to the shore can be used while loading and unloading, preferably using electricity from a grid based on "green" energy such as wind or solar power.

Modeling the Proposed Solution

The aim of the model is to investigate the influence of different network and/or barge and tug design options on the transportation price and hence on the competitiveness of the small barge convoy system.[1] The total model will be built up of three major model components: the new concept, supply of the existing modes and the competition between the new concept and the other modes. In Fig. 22.6, a schematic overview of the model is given.

The upper part of the model, the supply side, is divided into two parts. The first part (Small Barge Convoy System) is the model concerning the developed small barge system.

[1]The transportation price will be based on these transportation cost plus a markup which has to be calculated with an iterative relation.

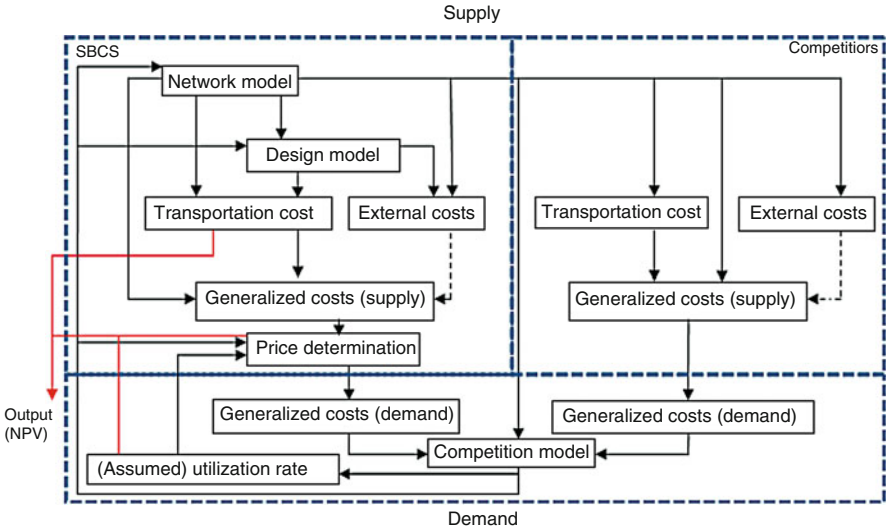

Fig. 22.6 Overview of the different model parts of the modeled concept [13]

First a network configuration in the network model must be selected. Based on this network the design model will design the tug and barges. Based on the network and the design of the tug and barges the cost model will be used to calculate the transportation costs and the external costs.[2] The transportation costs, the external and other non-monetary cost components such as time and reliability will determine the generalized costs.

The final output of the model will be a Net Present Value (NPV) of the investment in the small barge system. The NPV will be based on the total earnings and costs during the total life time of the small barge system (20 years). The earnings are related to the transportation price per TEU (or tonne). The transportation price is determined by the total costs per unit plus a profit margin. This profit margin is a variable that is dependent on the competition of the other modes and it will be determined in such a way that a competitive price can be obtained (see Fig. 22.6). Furthermore, the earnings are also dependent on the occupation rate of the barges. A low occupation rate will therefore lead to lower earnings and therefore a lower free cash flow. These two iterative relations are addressed in the model (see Fig. 22.6).

The NPV is the discounted profit from the investment in the new barge system. The discounting factor is set equal to the weighted average cost of capital (WACC). In the calculations the investment is financed with 20 % equity and 80 % debt. This WACC is an average of the cost of equity (set at 10 %) and the cost of capital (4.6 %).

[2]The external costs are costs caused by a (transportation) firm and for which it does not pay, such as congestion cost, noise, accidents and emissions.

If the NPV is larger than zero it mains that it is worthwhile to invest. But which design option is the best option? Also therefore the NPV method can be used. The main advantage of calculating the NPV of an investment is that it allows comparisons between different design options. The option with the highest NPV is the best option to use. If the investment decision would be based on an internal rate of return (IRR) it has a disadvantage because the IRR does not give insight into the magnitude of the return.[3] Based on the NPV the different design options are ranked and investment decisions will be made.

The second part of the top side of Fig. 22.6, i.e., competitors, represents the modeling of supply of the competitors for the small barge system. From the network model the alternative routes of the competitors are determined and the transportation and external costs are calculated. Also the generalized costs of the competitors are determined. The bottom part of Fig. 22.6 represents the demand side. Here, the competition between the small barge system and its competitors is determined. In this part of the model, the generalized costs of the cargo owners are determined. This demand part of the model will take into account the generalized costs and the transportation price of the small barge system.

Figure 22.6 illustrates that the network model will influence the design of the barges and tug (number of barges pushed, maximum dimensions of the barges, etc.) but also the transportation costs (traveled distance, number of locks that have to passed, etc.). The transportation costs are also influenced by the design (speed of the tug, hull shape, propulsion system, etc.). The transportation price of the small barge system will be determined on the basis of its generalized costs and by the competition from the other modes.

In order to determine the transportation price, the utilization rate of the barges must be known. Because the utilization rate cannot be determined a priori, an iterative approach is applied. This means that an initial utilization rate of the barges (and thus market share) will be assumed. In the competition model, the market share of the small barge system, will be calculated based on the competition of the other modes. This calculated market share will be compared to the initially assumed market share. If the calculated market share is larger than the initially assumed market share, then the latter can be accepted. If not, the assumed initial utilization will be decreased with one percent and the calculation is run again. If no suitable solution can be found the occupation rate will be set at the original assumed value and the price is lowered until the calculated market share is equal to the assumed market share. This means that it is possible that a design option will get a negative NPV. This means that such an option is not a option to invest in.

From the competition model there is also another feedback relation, to the part of the model in which the small barge system is modeled. The competition of the other modes will have a direct influence on the maximum level of the transportation price and the utilization rate of the barges (first iterative relation). The transportation costs

[3] An example is: a 2 % return on €100.000 (€2.000) is preferred over a 10 % return on €10.000 (€1.000).

of the small barge system are influenced by changes in the barge network and/or design changes of the barges and tugs (second iterative relation). Therefore the profitability of the small barge system will be determined by balancing these two iterative relations.

The model has been programmed in the knowledge-based system Quaestor.[4] Quaestor is capable of solving iterative relations which are needed to be solved for the design of the barges and tug. Another advantage of the Quaestor system is that it can be extended with other software programs. In this model it combines Excel (final output) and Rhinoceros[5] (3D output of the design model).

22.2.4 Application of the Model on the Flemish Inland Waterway Network

Potential Demand

The total available market of cargo flows having an origin or destination in the port of Antwerp and an origin or destination at the small waterways in Flanders is given in Fig. 22.7 and Table 22.2. The cargo flows are a summation of the existing cargo

Fig. 22.7 Overview of the different small waterways in Flanders based on [7]

[4]Quaestor is a knowledge management system software tool developed by Qnowledge. It is a development platform, working environment and management tool for engineers, enabling integration of design configurations, calculations and the generation of drawings and graphs [8].

[5]Rhinoceros is a 3D cad package that is used to draw the 3D designs of the barges and the tug [9].

Table 22.2 Cargo flows from the port of Antwerp to the different Flemish waterways [1, 15]

	Route 1	Route 2	Route 3	Route 4
Containers (in)	2.250	7.500	8.140	–
Containers (out)	2.720	12.600	9.950	–
Bulk (in)	233.500	128.000	10.000	231.461
Bulk (out)	–	–	84.000	463.248

flows and the potential cargo flows that are now transported by road. These cargo flows consist of containers and dry bulk cargo. The reason why both types of cargo are takin into account is that both types can be transported in the same convoy. In a convoy a combination of four barges for example, two could be filled with containers, one with sand and one with iron ore. In this case each small barge will have a different final destination at the small waterway.

Determining the Main Features of the Small Barge System

Now that the total potential demand for the small waterways is known, it is possible to insert this data into the model so that it can be used in the competition model. In order to determine the main features of the developed concept the model, which has been described in the previous section, is used to construct several graphs in which the influence of the analyzed parameter is shown. The investigated parameters are expressed in net present value (NPV) of the total tug and barge system. All the different designs of the networks and equipment (barges and tug) are ranked according to the NPV.[6] The main features of the small barge convoy system have been determined by a systematic variation of the different design parameters. The design with the highest NPV was selected as the main design. These main design features are the following:

- The tug and barge convoy should sail in a semi-continuous regime.
- The tug and barge convoy should have a design speed of 3.5 m/s.
- The tug should be equipped with a diesel-direct propulsion system.

From the previous analysis a suitable case can be identified. In this case the tug and barge convoy is sailing on Route 2 (four barges), Route 3 (four barges) and Route 4 (two barges) (see Fig. 22.7). In Fig. 22.8 the Rhino output of the design is given for the situation that the tug is pushing 4 barges.

Dealing with Future Uncertainties

In order to determine whether the small barge convoy system can succeed in a competitive market, a lot of future (exogenous) uncertainties must be taken

[6]For the interested reader the total analysis is extensively described in [13].

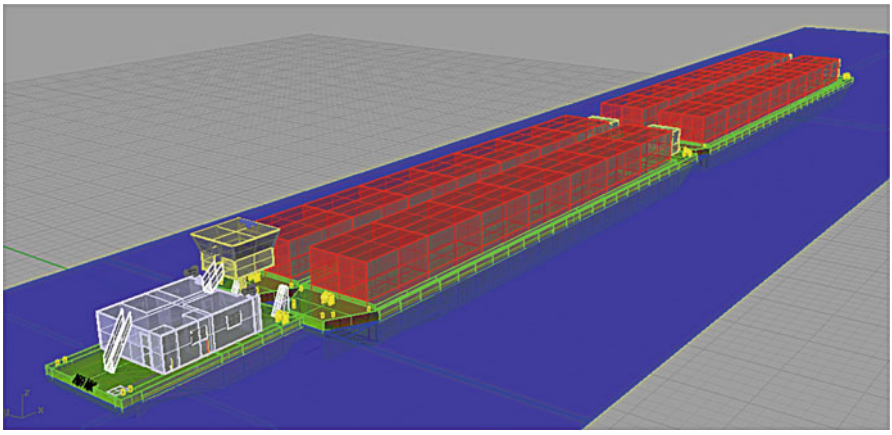

Fig. 22.8 3D design of the first case (4 barges Routes 2 and 3) [13]

Table 22.3 Developed future scenarios [13] (TT is travel time and dim. ships is diminishing ships)

	Scenario 1	Scenario 2	Scenario 3	Scenario 4	Scenario 5	Scenario 6
Infrastructure development						
Road	Enough capacity	Enough capacity	Enough capacity	Enough capacity	Congestion + 10 % TT	Congestion + 10 % TT
Inland waterways	Upgrade infra	Only maintenance	Only maintenance	Only maintenance	Only maintenance	Only maintenance
Inland Nav policy						
Int. Ext costs	No	No	No	No	No	Yes
Adjustment crew rules	No	No	No	Yes	Yes	Yes
Exceptions small ships	Yes	Yes	Yes	Yes	Yes	No
Economic parameters						
Fuel price	€ 900/ton	€ 900/ton	€ 600/ton	€ 600/ton	€ 600/ton	€ 600/ton
Inflation	1,80 %	1,80 %	1,80 %	1,80 %	3 %	3 %
Interest costs	10 %	10 %	4,60 %	4,60 %	4,60 %	4,60 %
Costs of Equity	15 %	15 %	10 %	10 %	10 %	5 %
Existing small inland fleet						
Number of ships	enough ships	dim. Ships	dim. ships	dim. ships	dim. ships	No ships

into account. To deal with those uncertainties, such as fuel price and inflation development and policy changes, different scenarios are developed which are built up of different policy decisions and economic developments that influence the NPV of the small barge system.

In Table 22.3 the different scenarios are presented, where the first scenario is a bad scenario for the small barge convoy system and the sixth is the best theoretical scenario. Scenario 4 is the base scenario which has been used in all the previews calculations. In this base case, the NPV is equal to €4.000.000. All the monetary values are given for the base year 2009.

The first scenario is one in which the government will make the decision to upgrade the small inland waterways to larger waterways, while the barges are dimensioned on the small waterways. Therefore the smaller barges have to compete with larger "normal" inland ships. In this scenario, the crew rules are not adjusted and it is not possible to sail with only one captain on the small waterways. The required standards for inland ships commissioned by the EU will also not be applied to the small ships. In this scenario, it is also very difficult to borrow money: the interest costs will be high and the minimum IRR that the investment company will require will be high.

The last scenario (6th) is the complete opposite of the first scenario. There is no upgrade of the small waterways and due to the economic growth (and therefore the demand for transport) the roads will be more congested. The crew rules are changed in favor for the small barge convoy system, the external costs are internalized and the small ships must comply with the new standards of the EU, so that no small ships are left. Due to this reduction in competition, the risk of implementing the new concept is reduced and the costs of equity will go down, as well as the interest costs of the loan. The scenarios 2 to 5 are gradually built up from the most negative to the best possible scenario. In Fig. 22.8 the results of the calculations are graphically shown.

Figure 22.9 shows that the NPV and IRR of the small-barge convoy system will increase with an increasing scenario number. The increase in NPV can be achieved due to the increase of the transportation prices. The transportation prices can be increased because of increasing transportation prices of the competitors (internalization of external costs) and by a decrease in costs (decrease of costs of equity, fuel price, interest costs). Figure 22.8 may also lead to the conclusion that in the first two scenarios no business case can be made because the IRR is lower than the WACC (NPV smaller then 0). The increase in WACC is due to the increase in costs of equity (10–15 %) and interest costs (4.6–10 %). This is due to the fact

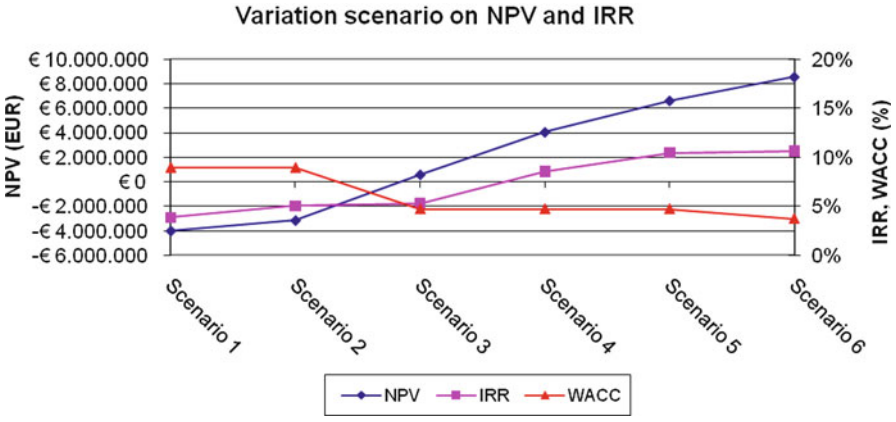

Fig. 22.9 Influence of different scenarios on the NPV and IRR (scenario 4 = base case; 2009 values) [13]

that the fixed costs form an important part of the total cost of the new concept. Therefore if the costs of equity and interest are increased, the profitability of the system decreases.

Another important observation is the large difference between scenario three and four. There is only one difference between the two scenarios, namely the possibility of sailing with only a captain on the small inland waterways instead of a crew with a sailor. The total NPV decreases from €4.000.000 to a mere €200.000 if an additional crew member must be taken into account. So if one wants such a system to be implemented, the reduction of the crew to only one captain on the small inland waterways is needed.

22.2.5 Implementing the Small Barge System

In the previous section business cases were developed that could be used to re-activate the use of the small inland waterways. The developed cases were optimized if the total tug and barge system was fully working. But in order to make this full potential materialize, the small-barge convoy system must be implemented. In this section, two implementation strategies will be further investigated to determine which strategy is best to use.

Two different implementation strategies are developed:

- Building up the small barge system from a small starting position (not all the needed barges are built in the start-up phase)
- Building up the small barge system with all the barges of which some are directly laid-up (i.e., risk of overcapacity at the start, not all barge are deployed directly)

The first implementation strategy is to build up the total tug and barge system by starting from a small start position (limited capacity). The risks involved in building a tug plus 20 barges at once could be too high if not all the potential clients are willing to shift their cargo flows to the small-barge system during the start-up phase. Due to the scepticism of the new technology (electrically-driven barges) or to an alternative logistics system, not all the available cargo flows might be offered to the small-barge system. Then a smaller starting position could be more desirable. In the time that only a few barges are deployed, the barge concept could prove itself and could therefore persuade the cargo owners to shift all the potential cargo flows to the new system.

The second implementation strategy is to start with all the needed barges (sufficient capacity at the start). All the required barges plus the tug are built at once. When the building costs of the barges are low, due to empty order-books of the shipyards and/or low steel prices, the transportation costs could be reduced. The transportation costs of a tug and barge system with a large amount of barges is predominantly determined by fixed costs caused by the newbuilding costs (interest costs, insurance and pay-back of the loan). If, in the start-up phase, not all the barges are needed due to not enough cargo to transport (i.e., overcapacity), some barges are laid up.

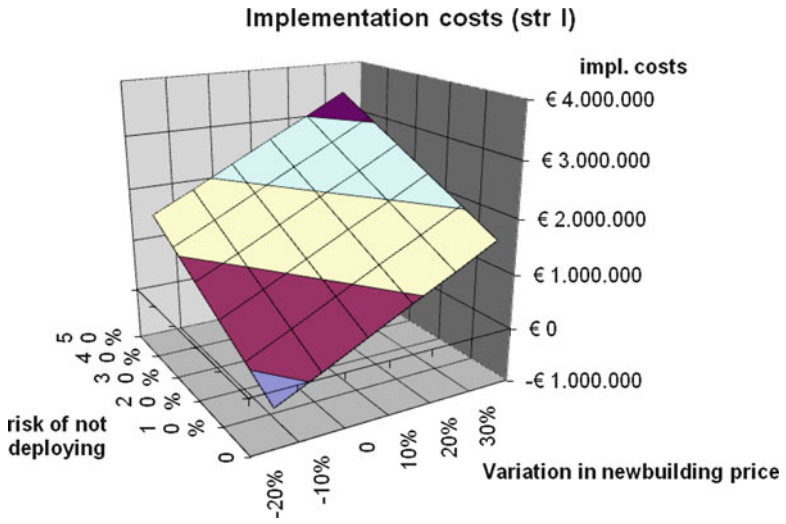

Fig. 22.10 Implementation costs of strategy one (2009 values) [13]

For each of the two strategies the implementation costs are calculated. In the calculations there are two main variables: the variation in newbuilding price of the barges and the risk that not all the barges are going to be used due to insufficient demand. This last aspect takes into account the risk that the small-barge system could fail to expand to the desired optimal situation. In Fig. 22.10 the implementation cost of the first strategy is show.

Only probabilities up to 50 % of not deploying all barges are taken into account because, if the probability is higher than 50 % of not deploying all barges, then that business case should not be considered. It can be concluded that the implementation costs will increase significantly if the risk of not deploying all barges increases.

In Fig. 22.11 the implementation costs of strategy 2 are given. The variation in newbuilding price of the second "package" of barges does not influence the implementation costs of strategy 2. The influence of the increasing risk of not deploying all barges is larger for this strategy than for the first one.

In Table 22.4 an overview is given of which strategy prevails over the other in terms of implementation costs.

From Table 22.4 (and Figs. 22.9 and 22.10) it can be concluded that strategy 2 only prevails when there is no risk of not implementing all the barges (0 %) and if the newbuilding costs of the second "package" of barges are increased by more than 10 %. In all other situations strategy one prevails. It can therefore be concluded that the small barge system should best be implemented starting from a small starting position and further built up in phases.

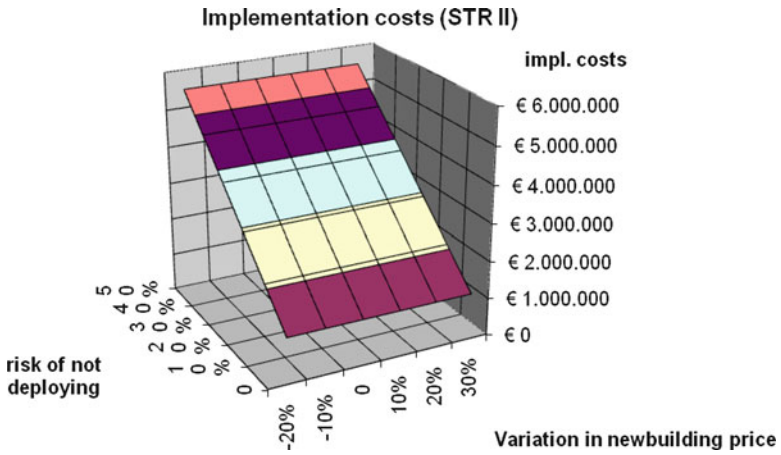

Fig. 22.11 Implementation costs of strategy two (2009 values) [13]

Table 22.4 Overview of prevailing strategies [13]

		Variation in new building price					
		−20 %	−10 %	0	10 %	20 %	30 %
Risk of not deploying	0	1	1	1	1	2	2
	10 %	1	1	1	1	1	1
	20 %	1	1	1	1	1	1
	30 %	1	1	1	1	1	1
	40 %	1	1	1	1	1	1
	50 %	1	1	1	1	1	1

22.3 Discussion of the Unified Framework

This research has a strong focus on the freight transportation function of the waterway network. However, also a link was made between freight transport and the use of the inland waterway network. This waterway network has two main functions:

- a freight transportation network (transport over water)
- a water management network (transport of water)

The function of the freight transport network has already been discussed in the previous chapter. For the water management function, the total waterway network plays a vital role. It is expected that, due to climate change, more heavy rainfalls will occur in combination with longer dry periods. This will result in more "peak" moments where more water has to be transported via the waterways to sea. But the longer dry periods will also result in longer periods where the water level of the waterways will decrease. The payload of a ship is directly related to the water level

of the waterway. If the water level is too high, inland ships cannot pass under a bridge (reduced headway); if the water level is too low a ship cannot be loaded to its design capacity. This will have a large impact on the operational cost of transport over water. This means that for the function of transport over water a more stable water depth is needed, while from a transport of water perspective, the waterway infrastructure needs to deal with extremes in the amount of water that needs to be transported.

In a Delta, such as the Rhine-Scheldt Delta, the waterways are also used to divert excess of water to regions to "store" the water when storm barriers (such as the Oosterschelde kering or the Maeslant kering) are closed. Then the waterway network of rivers and channels is primarily used to transport water and the transport function over water will stop. First of all, the rivers and channels in the first place store water. If water levels become too high, designated areas could be deliberately flooded. The locks on the waterways could be used to "steer" the water in to the right direction. In this situation, the transport over water will stop and the total waterway network will only be used for transport of water. This shows how the two elements are interlinked and need to be integrated when analyzing waterway networks and when a new ship type is developed.

The total network of waterways consists of large variety of either large or small rivers and channels. As already mentioned in the case study the waterway network consist for a large part of small waterways. These (mostly) manmade small waterways have, besides their dimensions, also one additional element in common: they are (very) old. Some examples of these small inland waterways with their date of opening in The Netherlands and Belgium are:

- Leuven–Dijle canal (Flanders/Belgium) (1763)
- Dessel–Turnhout–Schoten (Flanders/Belgium) (1873)
- Bocholt–Herentals (Flanders/Belgium) (1846)
- Zuid Willemsvaart (Netherlands/ Belgium) (1822)
- Wilhelmina-kanaal (Netherlands) (1922)

When those channels where built the main aim was to create a transportation network. The dimensions of the waterway were set at the standards of the those days. This means that the locks on those small waterways are dimensioned at the standards of the ships in the eighteenth and nineteenth century.

Also the function of those canals was different than what they are used for these days. In the eighteenth and nineteenth century, before the introduction of the rail network, canals were also used to transport persons besides transporting cargo. For the transport function the canal was also dimensioned to accommodate seagoing ships that sailed to, for example, Great Britain. An example is the trade of bricks from de Rupel-region near Antwerp to Scotland. It is hard to imagine that seagoing ships (such as a standardized Dutch freight ship called a fluit-ship) in the eighteenth century had a length of 40 m and a width of 5.5 m and a payload of 360 tonnes! In those days one could never imagine that sea going vessels would increase to the immense sizes that are common today. When seagoing ships increased in size and railways entered the European main land, the canals were more used for cargo

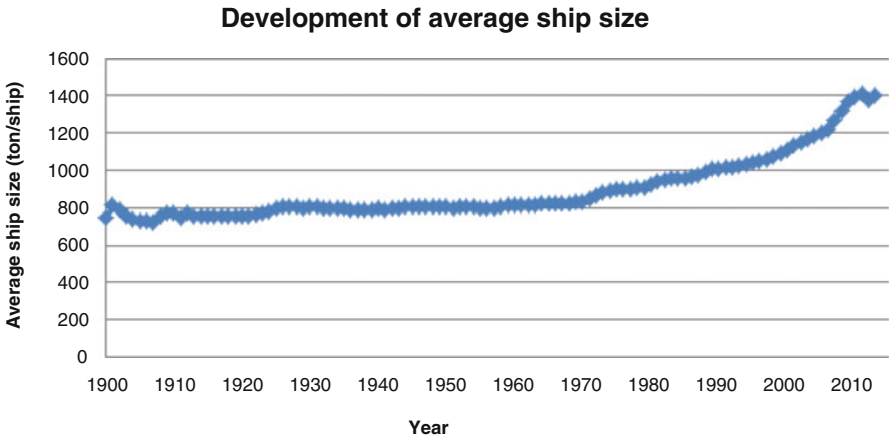

Fig. 22.12 Development of the average ship size of dry cargo inland navigation ships own figure based on [14]

transportation by inland ships. The size of the dry cargo inland ships also started to increase. Figure 22.12 shows that the development of the dry cargo ship size in the inland navigation sector was quite stable until 1960s. As of then, the dry cargo inland navigation fleet has increased in size from an average of 800 ton per ship to 1.400 ton per ship (increase of 75 % in 50 years). This means that the development of the ship size of the dry cargo inland navigation fleet increased at "high" speed while the inland waterway network remained constant.

The examples of the above-mentioned small inland waterways show that when a canal is built, it will have a very long life time. So when a canal has been designed and built, it is very difficult to change the design of the network. Also updating the inland waterway network is not an easy task. The cost to upgrade the infrastructure is high (see also the case study) and the time to complete the works is very long. It can take years of preparations, designing, and planning before such works can take place while the actual works on the canals can also take years. A recent example is the construction of new canal near 's-Hertogenbosch in the Netherlands where a new canal of 5 km is built to re-route the old canal that passes through to the city center. The remaining part of the canal (20 km) is dredged so that the larger ships can sail on that waterway. The first plans to make this upgrade date from the 1980s, while the total project is expected to be completed in 2014–2015. So the time between developing a project and the actual execution takes over 30 years! Given the current government budget cuts in The Netherlands and Belgium it will be even more difficult to get funding for more inland waterway upgrading projects.

This does not mean that the available infrastructure should be abandoned. The available infrastructure should be used more to provide an alternative transportation mode to deal with the increasing problems of congestion and other external costs of freight transportation. In the case study, an alternative approach was developed by changing the inland navigation concept, so changing the ship while the

infrastructure can remain constant. However changing the inland navigation sector can take as long and can be as challenging as changing the inland waterway infrastructure! Inland navigation is quite conservative to say the least and implementing a radical new system is not an easy task. So here we reach an impasse. Could there be a role for the government to get out of this impasse?

22.4 Role of the Government in Reactivating the Small Inland Waterways

As stated in the previous section, it is very difficult to upgrade the small inland waterways and it is also difficult to introduce a new inland navigation system due to the conservative nature of the sector. If the goal is to use more inland navigation and the available infrastructure, the calculations in Sect. 22.2 have shown that it is much more efficient to adjust the inland navigation system than to upgrade the infrastructure. It is very difficult for a government or the E.U. to directly subsidize the inland navigation system, to take away a part of the risk, because then they are interfering in the market. Providing budgets for upgrading or building infrastructure (TEN-T program), which are available for al market players, is allowed even as supporting research and development projects (e.g., Marco Polo).

Therefore the implementation of a new type of inland navigation system will be left to the market. The market will pick up a new type of system if there is shortage of available capacity of small inland ships. Currently the small inland waterways are becoming a niche market of the inland navigation sector. The ships that are used are the old (average age of hull is over 78 years [12]) inland ships. These ships are equipped with engines and other propulsion equipment that are also old (on average 25 years). These old engines will not fulfill the CCR-2 norms of 2015 and the new CCR-4 norms that inland engines have to fulfill in 2020/25. The owners of the small inland ships will have great difficulty to fulfill these new regulations due to the high investment cost of upgrading the engines while the value of the ship itself is low. Therefore there is an ongoing lobby process where an exemption should be created for the small ships. The goal of this lobby is to help the remaining part of the small inland fleet. Having said this, the small inland fleet is still declining in available capacity, reducing the utility of the small inland waterways even further.

If we recap it was stated at the beginning of this chapter that the overall goal (of a government) is that more cargo should be transported via the inland waterways. The small inland waterways can play a vital role in achieving this goal. As already stated in the previous sections of this chapter, re-activating the inland waterways is difficult and direct government intervention, which could take away a part of the implementation risk, is not allowed. What the government, in cooperation with the sector, can do is maintaining the proposed CCR rules for all inland ships. The remaining part of the small inland fleet will be taken from the market and an immediate shortage of small inland ships occurs. In such a situation, the new

concepts can be implemented in the sector, in which these new barges will fulfill to all the highest and latest technical requirements. Besides that, this concept can also be used to re-activate the existing small inland waterway infrastructure without additional investments in the infrastructure.

So there is a clear role for the government and that is that it has to choose for future, for cleaner transport, for a better usage of the small inland waterways. This can be done by maintaining the new CCR-rules forcing out the remaining small inland fleet and let the market pick-up new small barge systems.

22.5 Conclusions and Future Research

With respect to the unified framework, it can be concluded that the design and control system of the inland waterways and that of the inland ships are not in balance. The development of the inland navigation fleet has gone in to the direction of the larger ships (on average an increase of 75 % over the last 50 years) while the inland waterway infrastructure remained almost constant. This means that a large part of the available infrastructure will not be used any more while this infrastructure can play an important role in providing a transport mode with a low carbon footprint and low emissions per performed tonne.km.

The research in the case study has shown what the main reasons are for the disappearance of the small inland ships. Without these small ships, a large part of the available infrastructure will not be used while this infrastructure can be used for the transportation of cargo from the seaports in Belgium and The Netherlands towards their hinterlands.

In order to reactivate the use of the small inland waterways, a new concept has been developed where the infrastructure is taken as a constant. This concept has been further researched in depth to determine the optimal design of both the network and used barges and tug. Within this model the network (logistics), the design of barges (technical) and the transport economics are all equally important.

The application of the developed model showed that a profitable business case can be made. The scenario analysis showed that the profitability will be affected by the different scenarios. Especially when the financial requirements are increased (increase of interest cost or cost of equity) the concept will not have a positive NPV, which will thus result in a negative investment decision. This means that if the risk of implementing this concept is too high (high cost of equity and loan), according to the private market, the concept will not be implemented. In order to deal with this, the risk must be reduced. This can be done by building up the concept from a smaller “starting position” to start up the concept and to build up the concept when it has proven itself.

The new concept (or any other concept) cannot directly be supported by a government due to the fact that the government is directly interfering in the market. Therefore these new systems have to be picked up by the market. The role that the government can play is to maintain the new CCR rules for inland ships, so that

the part of the small inland fleet that does not fulfil these new rules will be forced from the market and so creating a demand for new inland navigation system to reactivate the small inland waterways.

Acknowledgements The research presented in Sect. 22.2 of this chapter was conducted within and funded by the INLANAV-interreg IV project [4].

References

1. Buck Consultants International. WATERSLAG: onderzoek naar de vrachtpotentie en inventaris van de waterweginfrastructuur in Vlaanderen en Zuid-Nederland, 2006. (In Dutch).
2. Bureau voorlichting binnenvaart. http://www.bureauvoorlichtingbinnenvaart.nl/, 2009.
3. Clinckers L, Portugaels E. Infrastructuurmasterplan voor de Vlaamse waterwegen, horizon 2014, 2010. (in Dutch).
4. INLANAV. http://www.inlanav.eu/, 2011. EU interreg IV project (http://www.inlanav.eu).
5. Meersman H, Van de Voorde E, Vanelslander T, Verberght E. Indicatorenboek 2009, Duurzaam goederenvervoer Vlaanderen, 2010. (in Dutch).
6. MIRT. Infrastructure investment program Netherlands. http://mirt2011.mirtprojectenboek.nl/, 2011.
7. Promotie Binnenvaart Vlaanderen. http://www.binnenvaart.be/nl/waterwegen, 2010.
8. Qnowledge. Quaestor. http://www.qnowledge.nl.
9. Rhinoceros. Rhinoceros modeling tools for designers. http://www.Rhino3d.com/.
10. Stopford M. Maritime economics. 3rd ed. London: Routledge; 2008.
11. Technum NV, Resource Analysis, Ecory, Leuven KU. Studie naar de ontwikkelingsmogelijkheden van de kleine waterwegen in Vlaanderen inzake scheepvaart. Antwerp, 2002.
12. Van Hassel E. Structuurverandering in het segment van de grote drogeladingbinnenvaartschepen antwerpen. Working paper University of Antwerp, 2013. (in Dutch).
13. Van Hassel E. Developing a small barge convoy system to reactivate the use of the small inland waterway network. PhD thesis, University of Antwerp, 2011.
14. Vereniging de binnenvaart. Ship data of the West European dry cargo inland fleet, 2013.
15. Waterwegen en Zeekanaal NV and scheepvaart NV. Shipping statistics on the Flemish waterway. Year books, 2007, 2008, 2009.

Chapter 23
Fostering Cooperation in Inland Waterway Networks: A Gaming and Simulation Approach

A.W. Veenstra, J. van Meijeren, J. Harmsen, and A. Verbraeck

Abstract Inland waterway transport is an important economic activity in the Netherlands and in Europe. Especially in the hinterland transport of containers, inland shipping is expected to form the backbone of a multimodal transport system. To support and strengthen the inland waterway industry in the Netherlands, the Dutch Government conducted a stimulus program called Impuls Dynamic Traffic Management Waterways. As part of this stimulus program, research was carried out into the economic structure of the inland waterway transport industry, and the potential for cooperation in certain geographical areas in the hinterland. To support the development of new logistics concepts for inland waterway transport, we developed a simulator, in which market parties can develop new transport and logistics concepts, and investigate the impact of implementing these concepts. Several gaming sessions with industry representatives were conducted for six of the main geographical areas in the Dutch waterway system. From the sessions, we can conclude that further cooperation is possible in certain geographical areas, which can result in a concept that can prove to be beneficial for the partners in the transport network, as well as their customers. A second conclusion is that the combination of simulation and gaming in an interactive workshop setting proved to be a very effective way to stimulate discussions on innovations in the inland waterway transportation sector.

A.W. Veenstra (✉)
Eindhoven Technical University, Eindhoven, the Netherlands
e-mail: a.w.veenstra@tue.nl

J. van Meijeren • J. Harmsen
TNO, Delft, The Netherlands
e-mail: jaco.vanmeijeren@tno.nl; jorrit.harmsen@tno.nl

A. Verbraeck
Delft University of Technology, Delft, The Netherlands
e-mail: a.verbraeck@tudelft.nl

C. Ocampo-Martinez, R.R. Negenborn (eds.), *Transport of Water versus Transport over Water*, Operations Research/Computer Science Interfaces Series 58,
DOI 10.1007/978-3-319-16133-4_23

23.1 Introduction of the Research and Background

Inland shipping is an important mode of transport that facilitates economic activity in the Netherlands and in Europe. Especially in the hinterland transport of containers, inland shipping is expected to form the backbone of a multimodal transport system. To support and strengthen the position inland shipping in the Netherlands, the Dutch Government has conducted a stimulus program in the period 2011–2013, called Impuls Dynamic Traffic Management Waterways (IDVV).

In this stimulus package, research [6] was carried out into both the economic structure of the inland shipping sector and the potential for cooperation between different stakeholders in the Dutch hinterland. While this was not the first time, previous efforts to analyse the inland shipping industry in the Netherlands never had a strong basis in scientific research. Much of the existing literature deals with hinterland networks, see for instance [15] and [4]. The economic structure analysis revealed that inland shipping has a number of important strengths, such as economies of scale and environmental impact—compared to trucking—but that there are also weaknesses.

These weaknesses are the low profitability of shipping companies (leading to a low level of long term investments) and fragmented innovation stimulation and adaptation. In addition, a weakness is the complex and hierarchical interplay of different stakeholders in the value chain. Traditional roles in inland shipping are the single shipowners, inland terminal operators, inland network operators, port authorities, and shippers. However, each of these stakeholders can play multiple roles that are associated with some of the other actors: a terminal operator can also operate ships, or an inland network operator can also operate terminals. In this network of relationships, the single shipowner is the weakest party, that nevertheless represents the largest part of the inland fleet.

As a result of this position, the single shipowner receives a lot of attention by policymakers and representative bodies. This attention overshadows some of the other stakeholders who determine to a much greater extent how cargo flows through the inland shipping system: terminal operators, inland network operators and shippers.

These parties have a vision on the industry, have the funds to invest in innovation, and are usually a stable factor in a specific part of the inland shipping network. Therefore, in the IDVV program, more attention was given by policy makers and other government parties to these other parties.

This chapter deals with the mechanisms that were developed in the IDVV program to foster cooperation between the various parties in the inland shipping system in the Netherlands. Below, we will elaborate on the economic structure analysis of the inland waterway system. The analysis illustrates the partitioning of the system into subsystems, and underpins the rational for facilitation of cooperation. We then introduce a simulation tool and serious game that was developed in the IDVV program to foster cooperation between market parties in the inland shipping system. In the next section, we describe several case studies we conducted on the basis of the game. We finish with a discussion of the link to the theme of this book, and topics for further research.

23.2 Economic Structure Analysis of Inland Shipping

An economic analysis of the Dutch inland shipping container transport [7] revealed that in fact, the inland waterway network can be partitioned into a number of fairly distinct operating, or navigation, areas. These areas are depicted in Fig. 23.1. In these areas, the inland waterway system revolves around one or more inland terminals, that usually control a fleet of owned and chartered inland vessels. The chartered inland vessels are usually owned and operated by single shipowners. In some of the operating areas, larger inland shipping network operators also offer scheduled services, often in cooperation with the local inland terminals.

In the economic analysis of the operating areas, an analysis was conducted into the dominant business models. Five main models were identified [8]:

1. Catchment area perspective: the objective of most parties in an operating area is to connect shippers in the region to international transport networks. The dominant parties are shippers and local inland terminal operators.
2. Hinterland network operator perspective: the objective is to develop dedicated, often multimodal, links between multiple selected inland terminals and deep-sea terminals. Dominant parties are the inland network operators, either inland transport operators or inland terminal groups. These parties operate a larger network including multiple terminals and shipping lines.
3. Deep-sea terminal perspective: the objective is to develop a transport network that is oriented towards providing connectivity for one or more deep-sea terminals.
4. Shipping line perspective: the objective is to develop a transport network that is oriented towards providing connectivity for the benefit of the ocean shipping line.
5. Neutral coordinator perspective: a neutral party can coordinate transport in or into the hinterland, often by using services offered by other parties. The neutral coordinator can be any party, but is often a multimodal transport network operator or freight forwarder.

In each of these operating areas, especially the ones in which more than one inland terminal operator is present, there is a delicate balance between competition and cooperation. This can be seen from Table 23.1 that lists the dominant business model in some of the main operating areas.

Note that four of the five business model perspectives occur in the Dutch hinterland. The occurrence of the neutral coordinator perspective is questionable: some hinterland network operators play a more or less neutral role, but still use their own assets. This negates their neutrality. Due to the different dominant business models, different parties control the main flows and transport movements in each operating area. There are, however, transport operators who operate in multiple areas, and are thus confronted with different power relationships in these different areas.

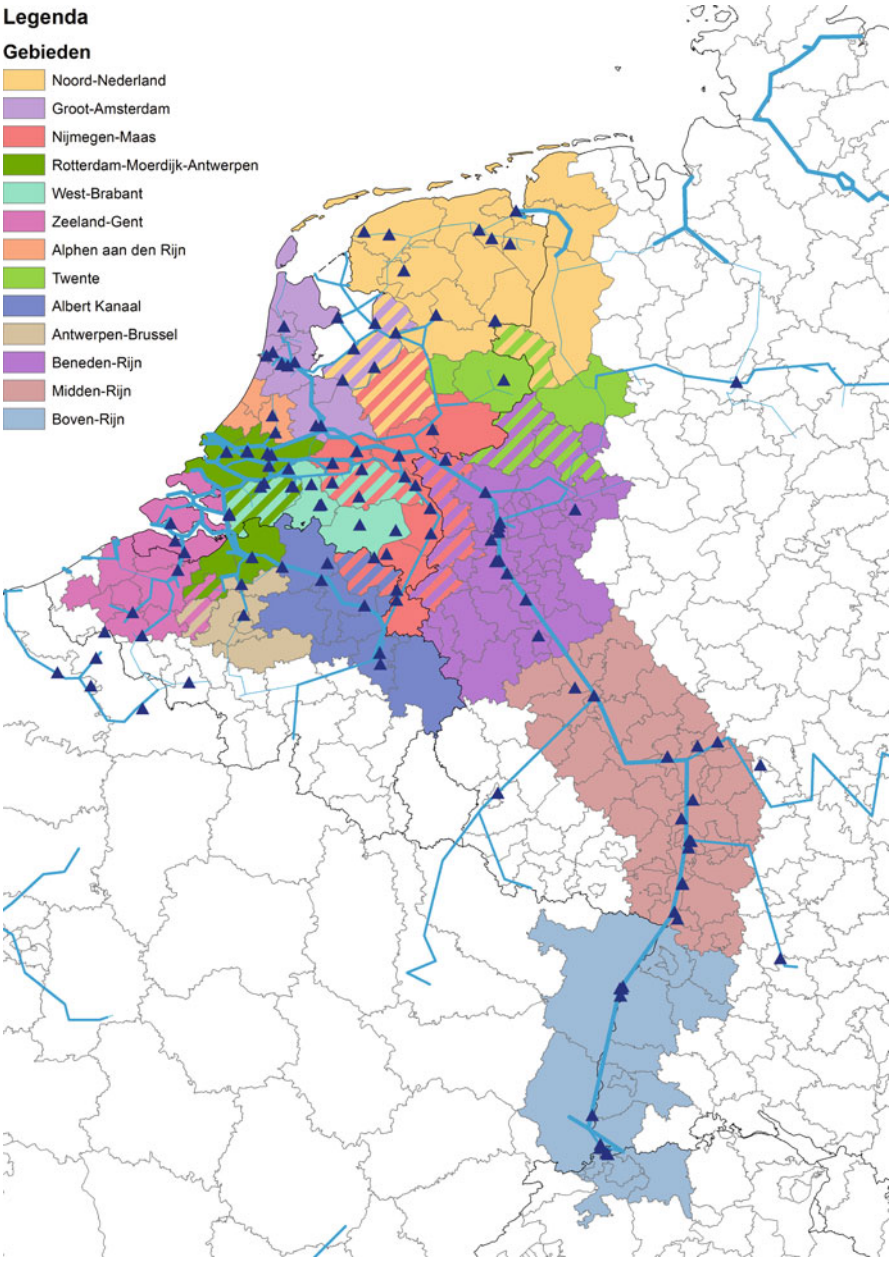

Fig. 23.1 Partitioning of the Dutch/German inland waterway system

Table 23.1 Overview of dominant business models for selected operating areas

Operating area	Dominant business model	Secondary business model
Noord Nederland	Catchment area	
West Brabant	Catchment area	
Nijmegen-Maas	Hinterland network operator	
Groot Amsterdam	Hinterland network operator	Shipping line
Rotterdam Moerdijk Anwerpen	Deep-sea terminal	Shipping line

Two additional factors play an important role in the complexity of relationships between stakeholders in the operating areas: the current overcapacity in the container terminal hinterland network (on average, the throughput is 44 % of the total capacity, although there are some terminals that are much closer to their design capacity) and the overlap or lack of overlap between the catchment areas of some of the inland container terminals [7]. For instance, in West Brabant and Amsterdam, there is considerable overlap. In West Brabant, the four terminals therefore cooperate to a large degree, but this is not the case in Amsterdam. In Noord Nederland, the terminals are far apart, but operate in a thin market, which would also require some cooperation to maintain a viable network service. The two terminal groups in this area compete fiercely, however, for the limited number of large shippers in the area.

In the distant and more recent past, in the Netherlands, many initiatives have been introduced to strengthen inland shipping. These initiatives have been given impetus by external developments such as the extension of the Maasvlakte in the Netherlands, and strong expectations of growth in transshipment volume in the ports. Many of these initiatives introduced new logistics concepts for inland shipping, such as hub and hop concepts. The hub concept is a concept in which one terminal plays a central role in a network of connections between other terminals. The hop concept is a concept in which a ship picks up containers at more terminals, before sailing the main leg to deep sea terminals or a hub terminal. Both concepts are presented schematically in Fig. 23.2. These concepts play an important role in the research in this chapter, but also, for instance, in the initiative Nextlogic (see http://www.nextlogic.nl) that aimed to solve planning problems for inland vessels in the Port of Rotterdam in a centralized way, and the Transumo Approach project [2, 13] that focused on distributed planning concepts for container barges and container terminals in the Port of Rotterdam.

Based on this complex interplay of parties and business models in operating areas, it is not surprising that cooperation between these parties is very difficult to establish. Apart from the few positive examples (such as the West Brabant and the Lower Rhine operating areas), in most operating areas with more than one terminal, all terminals have a hard time keeping their business profitable.

There is therefore a great need to assist these parties in developing constructive plans for further cooperation, even if they have tried this several times already, and failed. The focus of such cooperation should be to develop joint inland shipping

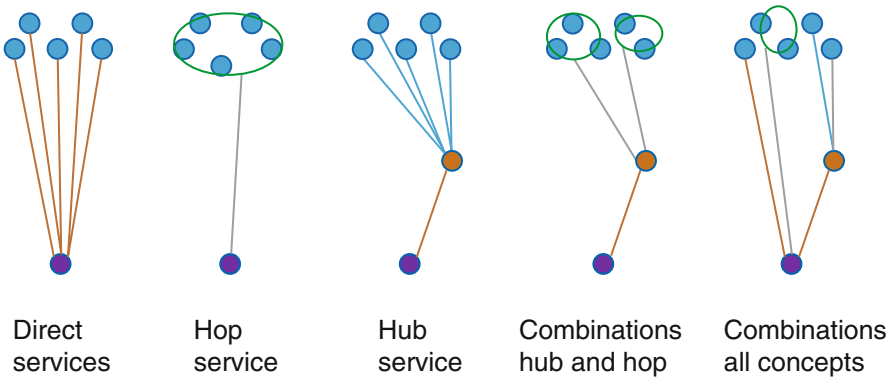

Fig. 23.2 Schematic presentation of a hub and hop concept

concepts that fit with the dominant business model in the operating area. To support the development of these new inland shipping concepts, we developed a simulator, in which market parties can develop new concepts in a neutral way, and investigate the impact of implementing these concepts in their operating area. Simulators have been used sparingly in the inland waterway industry, see for instance [1]. We will present the main structure of the simulator and some case studies in the next section.

23.3 Simulator Development and Gaming Sessions

23.3.1 Simulator Development

Based on the principles of discrete-event simulation [17], a simulator of the entire inland shipping network of the Netherlands was developed. The objective of this simulator was to support the design and evaluation of new inland shipping concepts in specific operating areas, by market parties. For this purpose, a tool with several modules was developed. The basis of the tool is a component-based [16] simulation model of the inland waterway network (rivers, canals, terminals, locks, bridges, ships) that is automatically generated from available data [5]. The simulation library to build the tool was the Distributed Simulation Object Library (DSOL) [11], which is Java-based and enables distributed use and easy integration with other services [12]. As we wanted to invite market parties to jointly think and develop new business concepts, it was key to extend the simulator for interactive use by the market parties. Serious Gaming concepts were used to enable organizations to jointly develop innovations for the barge transportation sector. For the game development, we had to balance reality (the level of realism for the involved organizations), meaning (the ability to develop and evaluate meaningful new transport and logistic concepts), and play (supporting the involvement of the parties in the process) [3]. Additionally,

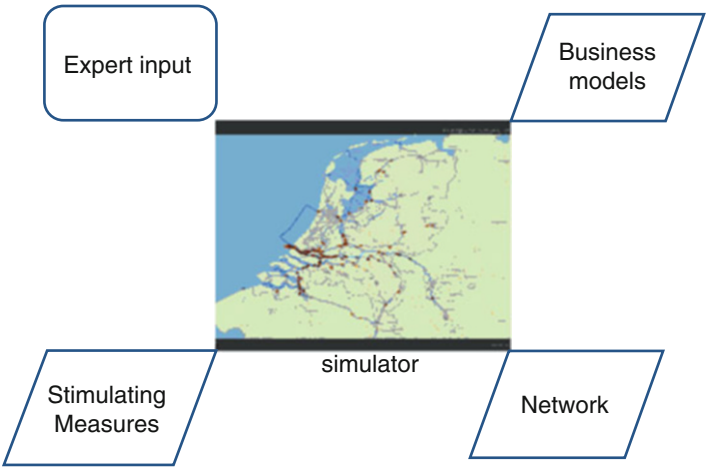

Fig. 23.3 Conceptual structure of the inland waterway network simulator

several other services needed to be included [14] to support visualization during the simulation experiments or game play, and to support the evaluation of simulation or game results (an evaluation module). The data used to drive the simulation built heavily on results gathered in earlier subprojects of the IDVV project such as the waterway network analysis [7], the business model analysis (actors, roles) [6], an analysis of main stimulating policy measures [8], and expert input on certain details of the waterway network. This is depicted in Fig. 23.3.

The core model consists of the following components (see [9] for a more elaborate description of the model):

1. Detailed data on the infrastructure network,
2. Model for terminal operations,
3. Model for ship operations,
4. Model that generates transport demand,
5. Input and configuration module,
6. Planning generator,
7. Output and statistics module,
8. User interface.

23.3.2 Gaming Sessions and Scenario Studies

Six gaming sessions with approximately 70 industry representatives were conducted for the main operating areas in the Dutch waterway system. In these sessions, groups of different stakeholders in the value chain engaged in simulation experiments, and the design and evaluation of new logistics concepts and measures. Partly, these

Table 23.2 Organizations involved in the gaming and simulation sessions

Ocean shipping lines	CMA-CGM, Maersk, MSC, NYK, CSAV
Deep sea terminals	ECT, APMT
Barge operators	Alcotrans, Contargo, Danser, ProLog, MegaBarging, Van Uden Honkoop
Inland terminal operators	Born, BCTN, Beverwijk, BIM, Tilburg, Oosterhout, Moerdijk, Venlo, Markiezaat, Kampen (1 en 2), CTU, HTS, HOV, IMS, MCS
Logistic service providers	CEVA, DHL, Geodis Wilson, MOL Logistics, K&N, Katoen Natie, Kloosterboer
Port authorities	HBR, Zeeland Seaports
Government/other	

sessions were used to fine-tune the model, collect missing market data and test the usefulness of the model. For another part, these sessions were used to explore innovative logistics concepts and gain insight in the advantages and disadvantages of these concepts. The parties involved in the sessions are shown in Table 23.2:

The sessions were designed around four selected concepts:

1. Setting up of a hub terminal,
2. Development of a hop concept, possibly in combination with a hub terminal,
3. Re-use of empty containers in terminals,
4. Development of new functionalities of terminals or closing terminals.

In the gaming sessions, participants were asked to first develop individual scenarios for each of these concepts, in the simulation tool. In the second part of the session, participants were given the possibility to combine their ideas in a new concept that would be evaluated with the simulation model.

At the end of each gaming/simulation session, all stakeholders were asked to reflect on the drivers for successful implementation of the scenarios.

23.3.3 Review of the Main Outcomes of the Gaming Sessions: Hub Concepts

The gaming sessions for the six main operating areas showed different results for the development of hub concepts. In Brabant and Antwerp-Rotterdam a hub concept is not viable, but in the other four areas, Lower Rhine, Maas corridor, Amsterdam and Noord Nederland, development of a hub could lead to benefits, see Fig. 23.4. The substantial distances between inland terminals, and the distance to the Port of Rotterdam are important factors in this. A major issue is the choice of location for the hub. Using existing terminals will often require capacity extension. In addition, the additional handling costs in the hub are a critical factor to consider. These costs can be mitigated if the hub handles enough volume.

Fig. 23.4 Example of a hub concept for Noord Nederland, where in this case Amsterdam is used as a hub location

23.3.4 Review of the Main Outcomes of the Gaming Sessions: Hop Concepts

In some operating areas, the hop concept is already used, for instance in Brabant. In the operating area Antwerp-Rotterdam, a hop concept was not feasible. In the other four areas, a hop concept could be possible, but there are some restrictions. In the Maas corridor, the terminals and operators did not think they had sufficient maturity to manage the complications of a hop concept. In Amsterdam and Noord Nederland, the simulations showed that the choice of terminals that take part in the hop concept is crucial for its viability. Terminals that do not fit into a roundtrip need to continue on their own, and maintain their own services to the mainports. In addition, inland port charges by municipalities can be a bottleneck for this concept. If each municipal port authority charges fees, even when a ship is picking up a small number of containers, hopping quickly becomes too expensive compared to direct transport.

23.3.5 Review of the Main Outcomes of the Gaming Sessions: Re-use of Empty Containers

The re-use of empty containers is already used extensively in the Brabant, and along German ports in the Lower Rhine operating areas. In other areas, the match of import and export flows is not optimal for extensive re-use of containers. In all operating areas, parties would like to centralize the storage of empty containers, in other to facilitate re-use. This depends on the cooperation of the shipping lines, who all have their own container management strategy.

23.3.6 Review of the Main Outcomes of the Gaming Sessions: Terminal Extensions and Closings

Gaming sessions around opening or closing terminals revealed that especially in Amsterdam and Noord Nederland, reduction of the total terminal capacity in the region could be advantageous for the other (remaining) inland shipping and terminal parties. In the other operating areas, terminal capacity is sufficient, and new terminal capacity will only be developed when there is sufficient demand in the market.

The simulation runs with the model focused strongly on the hub and hop concepts, as well as some infrastructural adjustments, such as reduced opening times of bridges and locks. The simulations largely confirm the concepts and scenarios that were developed by the practitioners in the gaming sessions.

The simulation also showed some other interesting developments. These resulted from the way costs and tariffs are calculated in the model. Costs are the sum of fixed and variable costs items in the inland waterway operation, and as such, these costs are sensitive to handling volume. Tariffs are determined, in the model, by allocating fixed market tariffs to various activities, such as a transport, or handling of a container at a terminal. These tariffs do not change with handling volume. Since many of the concepts are based on performing more activities (which results in higher overall tariffs) that generate larger volumes in hub terminals (which results in lower cost per TEU-km), in general the simulations show increasing tariffs against decreasing costs. From a commercial perspective, this sounds positive, but for the logistics concepts to be viable, parties need to focus on the decreasing costs as a basis for marketing these concepts, instead of market tariffs. In practice, this already occurs in the hub concept that is developed around the container terminal of Pernis by Combi Terminal Twente. Pernis is treated as a cost center, and handlings in Pernis are charged based on the cost of handling, not on the market tariff for a handling. As a result of this approach, the concept of transshipping containers in Pernis works.

The simulations show that reductions of opening hours of locks and bridges result in higher uncertainty of the sailing times, and longer waiting lines at the locks/bridges.

The simulations show that, in general, the following results can be achieved for innovative logistics concepts:

- Reduction of waiting times by 50 %,
- Increase of vessel utilization by more than 10 %,
- Reduction of costs by 20 %,
- Doubling the number of sailings per week,
- Reduction of CO_2 emissions by 40 %.

These results depend strongly on the particular concept, operating area, and parties involved.

As a result of these positive findings, many stakeholders became convinced that further cooperation would be beneficial in most of the operating areas. In some areas, this cooperation is already based on a sound footing (Brabant), but in most other areas, parties were just beginning to explore forms of cooperation. As a result of these sessions, innovative logistics concepts based on cooperation are currently being developed in various operating areas: Noord Nederland, Maas corridor (Nijmegen) and Amsterdam.

23.4 Case Study

One further case study was conducted with the simulation model: the decoupling of sailing and terminal operations. This case study will be discussed in more detail in this section. See [10] for more details.

23.4.1 Decoupling Sailing and Terminal Operations

Many of the services in the Dutch inland waterway network are initiated by inland terminals, who maintain a regular transport service to the Port of Rotterdam. As a result, these services are point-to-point, and inland terminal operations are tuned to the arrival and departure of a vessel. These terminals will always attempt to fully utilize their own ships, even if this means delaying transportation of containers that could be transported on someone else's ship. This leads to inefficient transport services, and a tendency to ignore the cooperation potential with other parties.

In this case study, scenarios were developed where terminals relinquish their own services, and rely on independent inland transport operators. This independent operator, or operators, could then rely on hub and hop concepts to offer services that would facilitate multiple terminals in one or more operating areas.

The concept for this case study was explored in the operating area Amsterdam and involved five terminals: IJmuiden, Beverwijk, and three terminals in Amsterdam. The case study contained three steps:

1. Interviews with market parties,
2. Additional cost calculations,
3. Simulation study.

The interviews with market parties in the Amsterdam area revealed that the terminals already use a mix of independent and own transport services. This has as a benefit that they are already familiar with the logistics concept of hopping, because the independent operator already employs this concept. This does not mean they are very positive about hopping. They question the design of a hop concept that would service the entire operating area. Also, they worry about possible competing hop concepts in the region and unforeseen consequences of this situation (unreliable services, unpredictable tariffs, and volume that cannot be moved in time). The general attitude towards hopping is that it is a solution for low volumes that have to be moved outside the regular schedules of the terminals' own schedules. Finally, the market experts feel that the set of terminals around Amsterdam will not have enough volume to maintain a dedicated independent services. Other terminals, from other operating areas, would need to be added to the network. Especially some terminals in Noord Nederland are candidates for such an addition. The selection of the right terminal is important, because there is a balance between adding sailing time, and adding volume to the hop network.

The simulation model is suitable for the analysis of a hop concept, such as the one considered in this case study. In the simulation model, a hop service can be developed, and new ships can be created to perform the transportation in this service.

The additional cost calculations for the decoupling of transport and terminal operations includes a calculation of relevant transport chain costs, and a calculation based on market tariffs. The relevant costs are: pre- and end haulage by truck, costs of all activities at the terminal, costs of transportation by barge, and costs at the deep sea terminal. The tariffs are for activities such as: a land side move, a loading or unloading move, and a sailing tariff. These two calculation approaches lead to different insights in the impact of the hop concept.

For a hop concept, a combination of these two methods needs to be considered: cost calculations for the activities at the terminal and a tariff calculation for the independent transport services. The simulation model shows these three options next to each other in the user output.

In the simulation, the current situation, characterized by direct links between terminals and the Port of Rotterdam, is compared with an independent hop service that serves all terminals. The hop service is not optimized. It is just a feasible solution that moves all containers. It is thus very well possible that further optimization will result in a more effective service.

Simulation runs were performed for three variants:

1. A full hop service, starting in IJmuiden, then Beverwijk, and the other terminals in Amsterdam, and without a hub. A 208 TEU ship type is employed,
2. A hop service as in 1, but without Beverwijk. Beverwijk is served with a point-to-point service,
3. A hop service as in 2, but without IJmuiden. IJmuiden is served with a point-to-point service. A smaller type of ship is employed (90 TEU).

The results show that variant 1. does not offer advantages against the current situation in terms of reliability and cost per TEU km, while there are more sailings, with resulting higher CO_2 output. For individual terminals, the results can differ: some terminals benefit, while others do not, measured in terms of transit time. This holds especially for the first terminal in the hop service (IJmuiden).

Variant 2. shows positive results for both IJmuiden and Beverwijk, in terms of cost per TEU km and CO_2 output. For the other terminals, the results are more or less similar to variant 1. This result confirms an earlier insight that the success of a hop concept depends on the choice of terminals.

In variant 3. the simulation shows that this variant has advantages for all terminals in the hop service. These benefits are not the same for the terminals, however. The costs per TEU km are slightly lower for one terminal, but four times as low for the other two remaining terminals in Amsterdam. In addition, this variant also shows that smaller ships may result in benefits for the hop service.

23.5 Linking Transport over Water

This chapter is about the transport over water. It combines an economic analysis with an engineering design methodology, with which a practical simulation tool was developed that represents the Dutch inland shipping network for containers. We have conducted research through a gaming approach, in which industry representatives developed innovative inland shipping concepts that were subsequently evaluated in our inland waterway network simulator.

The simulator is widely accepted as an important tool to facilitate discussions between practitioners and between practitioners and policymakers. As such, the tool is heavily used in meeting between government and business. There is a link with transport of water. The Dutch waterway network is both a transport network and a water management system. As a result, the water levels in some of the waterway s can be controlled by government agencies, and the management of locks is also dependent on both objective of efficient transport and efficient water management. These two goals sometimes clash.

A recent example is the budget cuts on the operational waterway management staff, as a result of which, opening times of locks in some of the more peripheral regions were cut. This has an immediate impact on the traffic of vessels through those locks. Currently, discussions are ongoing to see how the goals of waterway

management (including the management of water levels) and the goal of an efficient waterway transport system can be better aligned. The solution is to let locks be operated based on transport demand, rather than on scheduled times related to working hours.

23.6 Open Topics

There are several issues that require further work. First of all, the inland network simulator can be extended in various ways. Market parties have indicated that extension of the scope of the network to Germany and Belgium is important for a complete analysis of innovative concepts. In addition, the gaming element, that was introduced through discussion sessions, could be included in the simulator. This could be done, for instance, by introducing a bidding process on transport contracts from shippers in operating areas.

The simulator could be extended to represent a larger part of the inland shipping industry. Currently, it only contains container transport. Other important market segments are dry and liquid bulk transport.

Another extension is to develop the simulator as a testing environment for optimization algorithms for some of the innovative hub and hop concepts that were developed in the gaming sessions.

Finally, the structure of the simulator is also suitable to represent rail transport. The simulator could therefore also be used to develop and evaluate concepts that consider the integration of rail, barge and truck transport into synchromodal concepts.

23.7 Conclusions and Further Research

In this chapter, we have represented our research on the development of a simulation and gaming approach for the Dutch inland shipping system, that fosters further cooperation between market parties.

We have discussed the structural economic analysis of the Dutch inland shipping industry. This analysis explains to a large degree why cooperation in some of the operating areas in the Dutch inland transport system is difficult to establish and often unsuccessful. We have then introduced a simulation model that we used in gaming sessions with market parties and other stakeholders to evaluate a number of specific transport concepts that require cooperation. In addition, we let market parties develop cooperation scenarios that would generate benefits in their particular operating areas. Finally, we present a further case study on the decoupling of sailing and terminal operations in one particular operating area.

We can draw two conclusions from our research. The first is that there is scope for cooperation in certain operating areas, and there a specific mix of partners,

operational activities, and the right market price can result in a concept that can prove to be beneficial for both the partners and their customers. There are, however, specific conditions that need to be met, and this requires more thorough analysis of the concepts and scenarios, as well as building trust, than is often the case in practice. Our tool proved to be very instrumental in facilitating this analysis and the building of trust.

A second conclusion is that our approach—simulation combined with a gaming approach with practitioners—is a very effective way to support innovation in a transport sector such as inland shipping. By practicing with innovative concepts and scenarios on a neutral platform, market practitioners reveal more of their intentions and expectations that they would normally do, and because it is in simulated and playful environment, they feel uninhibited to do so. As a result, real trust and mutual understanding is created nevertheless.

We see interesting extensions of our research in other parts of the transport industry, where similar difficulties to forge partnerships and the need to create innovative concepts based on cooperation exist. One particular industry that springs to mind is rail cargo transport that is faced with some serious long term challenges, that can only be addressed successfully through cooperation.

Acknowledgements This research was funded by the Rijkswaterstaat program Impuls Dynamisch Verkeersmanagement Vaarwegen, Spoor 3. The project, perceel 1, was carried out jointly by TNO, TU Delft, Ab-Ovo, Panteia, Erasmus University Rotterdam, EICB and Modality Software Solutions. We thank Rijkswaterstaat for their kind permission to publish the results of our study.

References

1. Bush A, Biles WE, DePuy GW. Waterway, shipping, and ports: iterative optimization and simulation of barge traffic on an inland waterway. In: Proceedings of the 35th conference on Winter simulation: driving innovation, WSC '03. Winter Simulation Conference, 2003.
2. Douma A. Aligning the operations of barges and terminals through distributed planning. PhD thesis, University of Twente, Enschede, The Netherlands, December 2008.
3. Harteveld C. Triadic game design: balancing reality, meaning and play. Heidelberg, Germany: Springer; 2011.
4. Van Der Horst MR, De Langen PW. Coordination in hinterland transport chains: a major challenge for the seaport community. Marit Econ Logist. 2008;10(1):108–29.
5. Huang Y. Automated simulation model generation. PhD thesis, Delft University of Technology, Delft, The Netherlands, November 2013.
6. IDVV1.5. System renewal inland shipping (in Dutch), Synthesis report, Deliverable 1.5, October 2012. Impuls Dynamisch Verkeersmanagement Vaarwegen, Spoor 3, Cluster 1. Delft, The Netherlands: Rijkswaterstaat; 2012.
7. IDVV3.2. Multimodal international container network (in Dutch). Deliverable 3.2, November 2012. Impuls Dynamisch Verkeersmanagement Vaarwegen, Spoor 3, Cluster 3. Delft, The Netherlands: Rijkswaterstaat; 2012.
8. IDVV3.3. Inventory and global evaluation measures (in Dutch). Deliverable 3.3, March 2013. Impuls Dynamisch Verkeersmanagement Vaarwegen, Spoor 3, Cluster 3. Delft, The Netherlands: Rijkswaterstaat; 2013.

9. IDVV3.4. Simulation and games (in Dutch). Deliverable 3.4, July 2013. Impuls Dynamisch Verkeersmanagement Vaarwegen, Spoor 3, Cluster 3. Delft, The Netherlands: Rijkswaterstaat; 2013.
10. IDVV3.5. Pilots (in Dutch). Deliverable 3.5, July 2013. Impuls Dynamisch Verkeersmanagement Vaarwegen, Spoor 3, Cluster 3. Delft, The Netherlands: Rijkswaterstaat; 2013.
11. Jacobs PHM. The DSOL simulation suite. Enabling multi-formalism simulation in a distributed context. PhD thesis, Delft University of Technology, Delft, The Netherlands, November 2005.
12. Jacobs PHM, Lang NA, Verbraeck A. D-SOL; a distributed Java based discrete event simulation architecture. In: Proceedings of the 34th conference on winter simulation: exploring new frontiers, WSC '02, pages 793–800. Winter Simulation Conference, 2002.
13. Melis M, Miller I, Kentrop M, Van Eck B, Leenaarts M, Schut M, Treur J. Distributed rotation planning for container barges in the Port of Rotterdam. In: Verduijn T, van de Loo B, editors. Intelligent logistics concepts. Delft: Eburon Publishers; 2003. p. 101–116.
14. van Houten SPA. A suite for developing and using business games. PhD thesis, Delft University of Technology, Delft, The Netherlands, November 2007.
15. Veenstra A, Zuidwijk R, van Asperen E. The extended gate concept for container terminals: Expanding the notion of dry ports. Marit Econ Logist. 2012;14(1):14–32.
16. Verbraeck A. Component-based distributed simulations: The way forward? In: Proceedings of the eighteenth workshop on parallel and distributed simulation, PADS '04. New York, NY, USA: ACM; 2004. p. 141–148.
17. Zeigler BP, Praehofer H, Kim TG. Theory of modeling and simulation. 2nd ed. San Diego, USA: Academic Press; 2000.